AD-A040 774 NATIONAL AERONAUTICS AND SPACE ADMINISTRATION GREENB--ETC F/G 14/2
PROCEEDINGS OF THE ANNUAL PRECISE TIME AND TIME INTERVAL (PTTI)--ETC(U)
DEC 75

UNCLASSIFIED NASA-GSFC-X-814-76-45 NL

1 OF 8
ADA040774



AD A040774

X-814-76-45

PROCEEDINGS

OF THE

SEVENTH ANNUAL
PRECISE TIME AND TIME INTERVAL
(PTTI)
APPLICATIONS AND PLANNING MEETING

DECEMBER 2-4, 1975

DDC
RECEIVED
JUN 15 1977
C

DISTRIBUTION STATEMENT A
Approved for public release;
Distribution Unlimited

AD No.
DDC FILE COPY

GODDARD SPACE FLIGHT CENTER
GREENBELT, MARYLAND

For information concerning availability
of this document contact:

Technical Information Division, Code 250
Goddard Space Flight Center
Greenbelt, Maryland 20771

(Telephone 301-982-4488)

"This paper presents the views of the author(s), and does not necessarily reflect the views of the Goddard Space Flight Center, or NASA."

(1) (14) NASA-GSFC-
X-814-76-45

(6)

PROCEEDINGS
OF THE SEVENTH ANNUAL
PRECISE TIME AND TIME INTERVAL
(PTTI)
APPLICATIONS AND PLANNING MEETING (7th)

Held at Goddard Space Flight Center
December 2-4, 1975

(11) 4 Dec 75 (12) 743 p.

Sponsored by

Naval Electronic Systems Command
NASA Goddard Space Flight Center
Naval Observatory
Naval Research Laboratory
Defense Communications Agency

ACCESSION for
NTIS
DDC
UNANNOUNCED
JUSTIFICATION
Letter on file
BY
DISTRIBUTION/AVAILABILITY CODES
Dist. AVAIL. and/or SPECIAL
A

Prepared by
GODDARD SPACE FLIGHT CENTER
Greenbelt, Maryland 20771

DDC
REPRODUCED
JUN 21 1977
A

156 200

4B

OFFICERS AND COMMITTEES

EXECUTIVE COMMITTEE

James A. Cauffman
Naval Electronic Systems Command

Andrew R. Chi
Goddard Space Flight Center

Laura C. Fisher
U.S. Naval Observatory

Andrew C. Johnson
U.S. Naval Observatory

Theodore N. Lieberman
Naval Electronic Systems Command

James A. Murray, Jr.
Naval Research Laboratory

Robert R. Stone, Jr.
Naval Research Laboratory

Schuyler C. Wardrip
Goddard Space Flight Center

GENERAL CHAIRMAN

DR. HARRIS A. STOVER
Defense Communications Agency

TECHNICAL PROGRAM COMMITTEE

DR. FRIEDRICH H. REDER – CHAIRMAN
U. S. Army Electronics Command

D. W. ALLAN
National Bureau of Standards

J. F. BARNABA
Newark Air Force Station

LAURA FISHER
U. S. Naval Observatory

D. C. KAUFMANN
Goddard Space Flight Center

DR. W. J. KLEPCZYNSKI
U.S. Naval Observatory

T. N. LIEBERMAN
Naval Electronic Systems Command

L. J. RUEGER
Applied Physics Laboratory

DR. H. A. STOVER
Defense Communications Agency

S. C. WARDRIP
Goddard Space Flight Center

EDITORIAL COMMITTEE

L. J. RUEGER – CHAIRMAN

D. W. ALLAN
National Bureau of Standards

DR. R. J. COATES
Goddard Space Flight Center

DR. W. J. KLEPCZYNSKI
U.S. Naval Observatory

DR. R. MOORE
Naval Research Laboratory

DR. R. F. VESSOT
Smithsonian Astrophysical Observatory

SECRETARY

JOHN A. BOWMAN
Naval Research Laboratory

SESSION CHAIRMEN

SESSION I
Dr. William J. Klepczynski
U.S. Naval Observatory

SESSION II
David W. Allan
National Bureau of Standards

SESSION III
Dr. Gernot M. R. Winkler
U.S. Naval Observatory

SESSION IV
Dr. Robert F. Vessot
Smithsonian Astrophysical Observatory

SESSION V
Dr. Friedrich H. Reder
U.S. Army Electronics Command

SESSION VI
L. J. Rueger
Applied Physics Laboratory

ARRANGEMENTS

Donald C. Kaufmann, GSFC
Schuyler C. Wardrip, GSFC

FINANCE COMMITTEE

Laura C. Fisher, USNO
Schuyler C. Wardrip, GSFC

PUBLICATIONS

Virginia L. Walker, GSFC
Schuyler C. Wardrip, GSFC

TECHNICAL ASSISTANCE

David Phillips, NRL
Dewey Pritt, NRL
John Bowman, NRL
James C. Perry, Jr., GSFC
Paul J. Kushmeider, GSFC
Donald C. Kaufmann, GSFC
Joseph Soucy, Bendix

RECEPTIONISTS

Marie Nader, GSFC
Dorothy Outlaw, USNO
Julia Larkins, TRACOR
Marilyn Hughes, NRL

ENTERTAINMENT

William H. Hocking, GSFC

BANQUET SPEAKER

Dr. William B. Lenoir, NASA Astronaut
Subject: The Space Shuttle Program

CALL TO SESSION

Dr. Harris A. Stover, DCA

WELCOME ADDRESS

Dr. John F. Clark, GSFC

CONTENTS

Page

SESSION I

PTTI and Its PP&T'S (Problems, Pitfalls and Troubles),
Gernot M. R. Winkler 1

Co-ordinated Universal Time in Australia,
J. McK. Luck and J. R. Woodger 11

PTTI Technology in South Africa and Specific Problems Germane to This Geographic Area,
J. Hers 43

Recent Changes and Future Trends in NBS Time and Frequency Dissemination Services,
R. E. Beehler, D. W. Hanson, and D. D. Davis. 61

SESSION II

Outlook for Precision Frequency Control in the 1980's,
Erich Hafner 101

Clock Time Errors and Time Prediction,
David W. Allan 121

Radiation Effects in Crystal and Atomic Frequency Standards,
T. M. Flanagan and R. E. Leadon 125

A Portable Rubidium Clock for Precision Time Transport,
Helmut Hellwig and A. E. Wainwright 143

Performance and Operation of the NRC Primary Cesium Clock, CsV,
A. G. Mungall, H. Daams, D. Morris,
and C. C. Costain 165

CONTENTS (Continued)

Page

The Millman Effect in Cesium Beam Atomic Frequency Standards,
A. G. Mungall 195

A New Method for Generating Overtone Frequencies in a Quartz Oscillating Circuit,
Harish Bahadur and R. Parshad 215

Demonstration of the Frequency Offset Errors Introduced by an Incorrect Setting of the Zeeman/Magnetic Field Adjustment on the Cisium Beam Frequency Standard,
Donald C. Kaufmann 231

A Study of Hydrogen Maser Resonators and Storage Bulbs for Use in Ground and Satellite Masers*,
Edward M. Mattison, Robert F. C. Vessot, and
Martin W. Levine 243

Frequency Stability Requirements for Two Way Range Rate Tracking,
Victor Reinhardt 265

SESSION III

High Precision Time Transfers in the Field,
W. J. Klepczynski 285

Frequency Converter from 3.58 MHz to 5.0 MHz for Frequency Comparison by Means of TV Color Sub-carrier,
Tadao Inouye and Chikao Takeuchi 297

High Precision Time Transfer Methods,
Kenneth Putkovich 323

International Time Transfer Between USNO and RGO via NTS-1 Satellite,
H. M. Smith, N. P. J. O'Hora, R. Easton,
J. Buisson, T. McCaskill 341

CONTENTS (Continued)

Page

A Two-Way Time Transfer Experiment Using a Synchronous Satellite, A. R. Chi and E. Byron 357

The State Time and Frequency Service in the USSR, V. V. Sajin and V. G. Iljin 377

The USSR State Time and Frequency Standard, V. G. Iljin and V. V. Sajin 383

Subnanosec – Laser-Pulse Time Transfer to an Aircraft to Measure the Gen. Relativ. Altitude Effects on Atomic Clock Rates, C. Alley. 393

SESSION IV

Applications of PTTI Techniques in Communications Systems, Dr. Harris A. Stover 399

An Integrated Communication, Navigation, IFF System, Major J. A. Krupinski 423

VLBI: Past, Present, and Future, Irwin I. Shapiro 425

Precise Time for Very Long Baseline Interferometry at Santiago, Chile and Related Problems Germane to this Geographic Area, F. Noël 429

Radio Interferometric Geodesy using a Rubidium Frequency System, Peter F. MacDoran, J. B. Thomas, K. M. Ong, H. F. Fliegel and D. D. Morabito 439

CONTENTS (Continued)

Page

SESSION V

Path Delay Corrections for Loran Signals,
Ronald G. Roll 457

EM Fields in Nonuniform Multilayered Structures Steady State and Loran C Pulse Excitation,
E. Bahar 475

Test of Low-Cost Omega Navigation Over Alaskan Airways,
Robert Moore 495

Inflight Worldwide VLF Experience Using Global Navigation GNS-500,
William R. Tymczyszyn 521

Geomagnetic Storms and Associated Phase Anomalies of a VLF Radio Wave at Midlatitudes,
Tadayoshi Hara and Koji Horiai 549

Some Aspects of Project Speckled Trout,
W. J. Klepczynski and Major W. L. Bertino, USAF 559

SESSION VI

Satellite-to-Satellite Tracking System and Orbital Error Estimates,
P. E. Schmid, P. D. Argentiero, and F. O. Vonbun 569

NASA Tracking Ship Navigation Systems,
John J. McKenna 601

Analysis of the Impact of Satellite Navigation System Receiver Oscillator Errors on User Navigation Performance*,
Gregory L. Mealy 627

CONTENTS (Concluded)

Page

Precision Satellite Time Determination for Application to GEOS-3 Data, F. M. Boykin and R. F. Dwyer 651

Spaceborne Rubidium Frequency Standard for NAVSTAR GPS, D. E. Ringer, J. Gandy and E. Jechart 671

List of Attendees and Registrants 699

FOREWORD

The Proceedings contain the papers presented at the Seventh Annual Precise Time and Time Interval (PTTI) Applications and Planning Meeting and the edited record of the discussion period following each paper.

This Meeting provided a forum to promote more effective, efficient, economical and skillful applications of PTTI technology to the many problem areas to which PTTI offers solutions. Specifically the purpose of the meeting is to:

a. Disseminate, coordinate, and exchange practical information associated with precise time and frequency;

b. Acquaint systems engineers, technicians and managers with precise time and frequency technology and its applications; and

c. Review present and future requirements for PTTI.

Attendees come from various U.S. Government agencies, private industry and foreign countries to present papers and participate in the meeting in a mutual interchange of information. Papers were presented relative to frequency and time services; frequency and time devices; clock synchronization techniques and PTTI applications to navigation, communications, position location, and interferometry.

These Proceedings, taken together with those of prior meetings provide a good cross-section of the status of PTTI technology and its applications.

Many people contributed to the success of this year's Meeting. On behalf of the Executive Committee, I want to acknowledge the Session Chairmen, Speakers, and Authors, members of the Technical Program Committee and Editorial Committee, and the many others who gave freely of their time.

Additional copies of the 1972, 1973, 1974 and 1975 Proceedings can be obtained by sending $5.00 for each copy desired to:

S. C. Wardrip
Code 814
Goddard Space Flight Center
Greenbelt, Maryland 20771
or Telephone (301) 982-6587

Harris A. Stover
General Chairman

PRECEDING PAGE BLANK-NOT FILMED

CALL TO SESSION

Dr. Harris Stover
Defense Communication Agency

DR. STOVER: I am Harris Stover from the Defense Communications Agency, and it is my pleasure to call to session this Seventh Annual Precise Time, Time Interval Applications and Planning Meeting.

A purpose of the meeting is the exchange of information that will enable us to make better use of PTTI. I think that the Technical Program Committee, under Dr. Reder, has selected an excellent set of papers to initiate that exchange of information. However, we would also like to have your participation in the discussion periods.

I would like to remind you that the sessions are being recorded, so that the discussion periods can appear in the printed proceedings. It would be helpful if you could provide a written report of your contributions to the discussion sessions that would help the editorial committee.

Again this year, we have quite a large foreign participation at this meeting, and that should increase the breadth of the information exchange. It is my pleasure to call on Dr. John F. Clark, the Director of the Goddard Space Flight Center, for the welcoming address.

PRECEDING PAGE BLANK-NOT FILMED

WELCOME ADDRESS

Dr. John F. Clark
Goddard Space Flight Center

DR. CLARK: Some repeat performances are enjoyable. This is certainly one of them. I had the pleasure of welcoming you and encouraging your efforts in 1973 when you last did us the honor of convening at Goddard. I know it's trite to say that it seems like yesterday. And I mention it, of course, only because of your professional interest in the passage of time. However, have you noticed as you grow older that the earth is actually increasing its speed around the sun?

Coupled with that is the other phenomenon, that there aren't enough hours in the day anymore. I would hope that this group could do something about these problems, for the need is great.

It is a pleasure to welcome you back. This will mark the third time that we have hosted a PTTI Meeting. I am in better condition now than when we met in 1973 when I welcomed you after being up most of the night before working with the pictures of Mars which were just coming in from the Mariner flight. The pace has been heavy since that historic event. Many of you have been intimately involved with the scientific, applications, and manned spacecraft launched in the past two years. After the Skylab series, we had a successful joint flight with the Russians. When the Space Shuttle provides the opportunity to resume manned flight (beginning in the 1980s) it will complete the merger of manned flight and scientific efforts.

If the spacecraft which NASA will launch for non-NASA organizations is considered, the pace of the space program in the interim between now and the era of the shuttle will be extremely active. The Delta launch vehicle alone, for example, will be flying at a rate of more than once per month for the next two years. Some of NASA's launches in the interim should be of special interest to your community, such as the Tracking and Data Relay Satellites, the High Energy Astronomy Observatories, and the Laser Geodynamics Satellite (LAGEOS).

Woven through all this activity will be the binding thread of the precision frequency and time community. Many of the scientific measurements that have been made and the information that has been collected could not have been properly interpreted and correlated without precise frequency and time sources. The scientific community as a whole is grateful for what you as a group have been able to achieve in your various laboratories.

PRECEDING PAGE BLANK-NOT FILMED

We presently have on the drafting table the design for a frequency measurements and standards laboratory which we hope to start constructing within the next several months. This facility, which will be one of the finest magnetically shielded and environmentally controlled measurement and test laboratories in the country, will house our primary hydrogen maser frequency standards. We hope to achieve parts in ten to the fifteenth long term frequency stability measurements over 100 days and longer.

The laboratory will also be used to verify the accuracy (to parts in ten to the fourteenth) of primary frequency standards and the precision of calibration of hydrogen masers for long periods of time.

This laboratory is being constructed here at Goddard as a separate structure in a remote location. For those who know the center's geography, it will be beyond our network test and training facility. Its location and design are such that there will be a minimum of shock and vibration. We anticipate construction to be finished by the end of CY 76.

In addition to our NASA commitments to support our various internal programs, we will continue our hydrogen maser support to the scientific community such as those in the fields of VLBI, radio astronomy, geodesy and red shift and relatively measurements areas.

In the precise timing area we presently rely on terrestrial radio transmissions and portable clock trips to achieve ±25 microsecond global clock synchronization at our network tracking stations.

Our future programs will have to do much better. For example, in the geodetic measurements required for the LAGEOS satellite experiments, we will have a need for + or - 1 microsecond world wide clock synchronization. LAGEOS is one of the scientific satellites in the Earth and Ocean Physics Application Program.

A laser tracking network of 8 stations is being brought into existence. It will be portable, with each station housed in a trailer. We will be able to move the trailers to various sites for precise geodetic work. We are building the new timing system needed for precision work with this network. Some proof-of-concept experiments on the world wide satellite time transfer techniques have just been completed. Goddard and NRL worked with the Royal Greenwich Observatory, the Radio Research Laboratory in Tokyo, the U.S. Naval Observatory, and the Australian Division of the National Map Facility at Orroral Valley, Australia. We used the Navy's Navigational Technology Satellite (NTS-1) for these experiments, with encouraging results.

Among our guests today from the Navy is Rear Admiral Julian Lake who heads up the U.S. Naval Electronic Systems Command; Dr. H. Q. North, the Associate Director of Research, the Naval Research Laboratory, and Dr. K. Aa Strand, Scientific Director U.S. Naval Observatory. And I see from the program that many of you are from abroad, and that makes this meeting very valuable. There are few other meetings that I know of which bring together so many scientists and engineers from around the world who work in the PTTI field. Goddard is proud to be a charter member of this community and we look forward to continued cooperation with each of you.

On behalf of NASA, the U.S. Naval Observatory and the U.S. Naval Electronic Systems Command, the three sponsoring agencies, I extend a special welcome to those of you from other countries. Your attendance here attests to the importance of this meeting.

I'll be seeing you at some of the sessions during your three days here, and at the banquet tomorrow night. I wish you a very successful meeting.

PTTI AND ITS PP&T'S
(Problems, Pitfalls and Troubles)

Gernot M. R. Winkler
U.S. Naval Observatory

ABSTRACT

An overview will be given of the main problem areas in practical Time/Frequency (T/F) applications. Specifically the following will be briefly discussed:

Specifications versus realistic clock performances.

Operations - power, reliability, redundancy.

Training of operators.

Repair - maintenance.

Standards - conventions.

Utilization of assets (use all clocks available).

Path and equipment delays - variations.

Management understanding and approval versus decision delaying and decision avoidance techniques.

It appears to me that precise timing systems may be, at least initially, more subject to troubles than other systems of comparable complexity, even though modern precision clocks reach levels of reliability which are excellent. However, our clocks are parts of systems and it is in this overall context that I wish to discuss briefly some problems and pitfalls that I have seen and experienced myself. The two most important single problems stem from the fact that clocks must operate without any interruption; and from frequent misunderstandings and errors in the basic system design, i.e. in the overall balance of the engineering compromise. Fig. 1 is a summary of the main factors in such a balance. As so often

in life, if we are too demanding, we will have to pay dearly, and not only with money, but also in terms of parameters which are usually underestimated at the time of system acquisition, e.g. maintenance, training etc.

We have seen a significant change in doctrine in the overall design of systems in the DoD in the last five years. It has not yet filtered down through the ranks. One used to specify optimum performance of the overall system. This entailed the need for many special developments of subsystems and components - a very costly process by the time everything was debugged and ready for production. A much quicker, less expensive, safer (no breakthroughs required), and operationally much more reliable strategy of systems acquisition is one where a survey of components and subsystems already in production precedes the overall system concept development including its final specification. In our terms of reference, this means that we first should look at what is currently available in the timing area.

Fig. 2 is a short list of what is practical and sufficient for the large majority of users at this time. On the other hand, Fig. 3 shows what I believe could be obtained with systems which exist, but which require a modest further development (several hundred thousand dollars).

An area of frequent misconceptions is the great difference in performance and environmental sensitivity of the various clock types. This is a large and important area which I present in Fig. 4.

In addition to other criteria which limit the choice of a clock type for a particular application, the system noise is often overlooked as a basic limitation of clock utility. Fig. 5 is possibly an oversimplification, but one can see very clearly that towards the right part of the Figure we gain a great margin of safety with less expensive, simpler and more reliable clocks.

I consider it as one of the great injustices in this world that those who select and purchase complex systems usually are not the ones who have to operate them. In fact, no other measure may be as effective in improving technological performance as keeping the noses of our specifiers and procurers on the grindstone of operations after the goods have been delivered. Fig. 6 lists only the most important sources of trouble, lack of redundancy and primary power.

Now let us move to the human side. Fig. 7 points to the need to adhere to standards in our terminology and Fig. 8 sketches my minimum ideas on training.

Maintenance of PTTI equipment (Fig. 9) in my opinion can only be organized with a view to the qualifications of the people on hand. In an environment of frequent transfers, a technician may never see a malfunctioning atomic clock (they have half-life times of 3 to 4 years), so why should we train him extensively in such a sophisticated piece of equipment? In such a case, replacement maintenance is the only economical approach. Many mini-computer users seem to have reached the same conclusion and that is also why the Naval Electronic Systems Command has established its atomic clock logistic support facility (within its Washington Division).

That one should use all assets (Fig. 10) is not a very frequently followed maxim and brings me to my last and most delicate point: Management (Fig. 11).

It is also the most important item because when things go wrong, who else is to be blamed but management? It is strange, however, that we don't do much better in this area, since most of us are managers as well as subordinates to higher management which should give us an excellent opportunity at least to see how not to do things! Since we can hardly tell our superiors how to run their ships, we can only do one thing to improve this world: Learn from the mistakes of others and do it better ourselves.

But there must be one word of caution. Our attention may be so out of focus from some particular examples of pseudo-management that we mistake it for something different. Management is not firefighting, or bookkeeping, or "politics" - it is thinking, planning and motivating. Nothing else will lead to success in science and technology.

Therefore, let us use the opportunities for constructive actions whenever it is up to us to move. In the PTTI area we depend on mutual cooperation if we want to obtain the best performance at least cost with greatest reliability. To make such cooperation work, it is essential to develop a positive attitude which looks at the goals rather than at the procedures and which is more after substance and less after form. To achieve this goal, we must communicate and inform each other of problems and possible solutions; that is the purpose of this conference.

What We Want	and	What We Pay
Stability Infrequent Synchronization		Cost Size Weight Power Consumption Maintenance Costs Reliability Operator Training

Fig. 1. Clocks are Parts of Systems. Engineering is a Compromise Betwixt.

By more than 95% of users

5 μs Time Accuracy
0.2 μs Time Precision
1×10^{-11} *Frequency* Accuracy
1×10^{-12} Frequency Precision

Fig. 2. Practical and Needed, Today

5 ns Accuracy, Locally (PC, TV, μ-Wave)
100 ns Time Accuracy Worldwide
5×10^{-14} Frequency Stability (1d)

Fig. 3. Possible Today

	Additive Noise	Perturbing Noise	Parameter Changes
Atomic Clocks (Rb, Cs) τ range Causes Influenced by	 < 1s Thermal Buffer amps.	 1s to 1 week Shot noise of detector Age	 > 1 week Spontaneous systematic Environment
Quartz Clocks τ range Causes Influenced by	 < 1s Thermal circuits Amount of buffering	 -- Acceleration Vibration	 > 10s Spontaneous diffusion of defects Age, environment, radiation

Fig. 4. Noise Types and Oscillators

Phase Noise	500 ps	10 ns	200 ns	2μ	1 ms
Typical System	VLBI μ-Wave	Loc. TV Ph 3 DSCS Improved NAVSAT	DSCS Loran-C TV Network TRANSIT	VLF Noon OMEGA	HF VLF Ops
Clock of Choice	"H"	Cs 004	Cs	Rb	Xtal
Sigma (1d)	6×10^{-15}	3.5×10^{-14}	2.3×10^{-13}	2×10^{-13}	1×10^{-10}
Required	6×10^{-15}	1.2×10^{-13}	2.3×10^{-12}	2×10^{-11}	1.2×10^{-8}
Safety Margin	0	5 db	10 db	20 db	21 db

Fig. 5. System Noise and the Choice of Clocks. We assume daily re-synchronization.

Reliability Through Real Redundancy
Power, Standby, NO-Breaks
One DC Line Can Also Be Shorted
Project Books for Clocks

Fig. 6. Operations.

Discipline in Terminology
Clock Difference - Signs
Clock Rate, Fast - Slow
Frequency, High - Low

Fig. 7. Standards - Conventions.

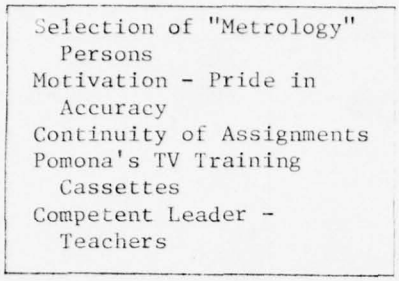


Fig. 8. Training.

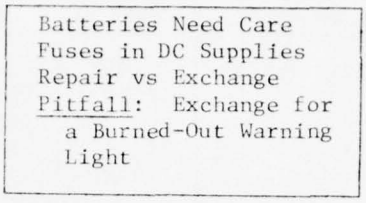


Fig. 9. Maintenance.

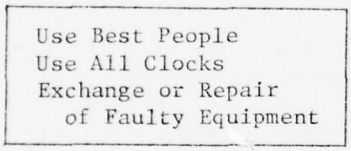


Fig. 10. Use of Assets.

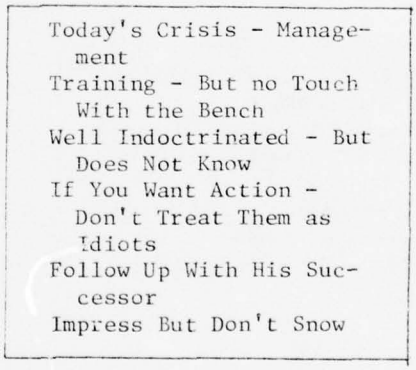


Fig. 11. Management.

REFERENCES

1. Hellwig, H., Frequency Standards and Clocks: A Tutorial Introduction, NBS Technical Note 616, March 1974.

2. Hellwig, H., A Review of Precision Oscillators, NBS Technical Note 662, February 1975.

QUESTION AND ANSWER PERIOD

DR. KLEPCZYNSKI:

Klepczynski, Naval Observatory.

Is today's crisis management or is it crisis management?

DR. WINKLER:

I think the fact that we have crisis management is already a problem. Because management has nothing to do with bookkeeping, and yet, I think that is what everybody thinks it is. It has nothing to do with side effects. I think it has to do with thinking and planning and with motivating, but how can you do that?

MR. LIEBERMAN:

Could we go back to that slide about the VLF? Are you saying synchronization for VLF operation versus VLF noon? Are you suggesting that we go to crystal oscillators for the 1 millisecond timing versus the 2 microseconds for VLF noon timing? Are you talking about the need for timing or are you talking about synchronization of the communications?

DR. WINKLER:

I am talking about the limitation of all your measurements if you use high frequency signals. You are limited to a precision of about 1 millisecond from day to day. If you lose time, you can pick up time, again to 1 millisecond, by listening to a time signal. If you have a daily operation like that, in a system where the 1 millisecond phase noise is your allowed performance limit, I think a quartz crystal oscillator is your oscillator of choice because it gives you a performance about 100 times better than what you need in order to stay within that 1 millisecond from day to day.

MR. LIEBERMAN:

Is that at the transmitter?

DR. WINKLER:

At the transmitter as well as the receiver. It is only

that you want to use, in order to freely utilize the benefits of the time system, you will want to have less frequent re-synchronization than daily and then, of course, here you are immediately using your margin of safety.

And then you may decide you want to put in a higher performing clock, but that is caused by a less frequent than daily re-synchronization, given that phase noise. If you want to stay within 2 microseconds over a period of 100 days, I would even go to the same choice.

So, again, please, I have to apologize in the interest of making a point, somehow one has to start out with oversimplified charts. This is an oversimplification. But, I think it gives you the main ideas, what are the parameters and where can I have payoffs? It brings out another point, of course, and that is that any systems engineer ought to be really bargaining about these various performance parameters. That is a process which I don't think is really carried out.

I have never yet seen people who will turn around and say, look, that is simply asking for too much trouble. But, you can have this. Could you design your system around a great capability here? It is a kind of bargaining and maybe we are not salesmen enough to point out great advantages on the one hand and a high price on the other one. The design of a system, not by first dreaming up a gigantic thing which will do everything and then worrying about what components do we now have to develop. I think that is the wrong approach.

That is what is causing the very high expenditures which we are facing in our modern system. The right approach, I think, is to look around to have a general idea of what we want to do and to look around at what is available today and only use those components. But, I don't think we are doing that.

DR. COSTAIN:

Dr. Winkler, you mentioned for 100 nanosecond worldwide synchronization that it would take about $100,000 or $200,000. Are you referring for installation and are you including any maintenance costs in this?

DR. WINKLER:

I have mentioned several hundred thousand. I don't think you can do it with $100,000. There are two candidates which I think could do that. One is the improved transit satellites about which I hope to hear a little bit more again this session. We had a paper last year about it and what you need to do here is to get several hundred thousand dollars to develop receivers, and the other one is the navigation technology satellite or the navigation development satellite going into the global positioning system.

Here again, to get started with timing receivers will require that kind of funding but after we have started and really have some receivers on the market, I am sure the price will go down. I think such a receiver, in fact, I am reasonably confident, is already under development for the global positioning system.

So, I think that this is within the reach, a couple of hundred thousand dollars will give you, I am quite confident, 200 nanoseconds. In fact, I think last year there was a report by the NRL group, NRL mentioned by Dr. Clark. Some of these experiments which are being carried on, are exactly in that area, and I think they are achieving this kind of performance; 200 nanoseconds.

It is clear that a worldwide coverage can only be achieved by a satellite.

CO-ORDINATED UNIVERSAL TIME IN AUSTRALIA

J. McK. Luck and J. R. Woodger
Division of National Mapping, Australia

ABSTRACT

The Australian co-ordinated time scale UTC(AUS) has been in existence since January 1, 1973 and is based on a small variable ensemble of caesium frequency standards compared regularly by the television method. Due to its distance from Europe and America, this time scale cannot make use of LORAN-C or VLF methods for reliable comparison with other time scales, especially those of the United States Naval Observatory and the Bureau International de l'Heure. Hence it relies for its relation to these time scales on infrequent flying clock visits from USNO, its own stability and the Timation experiment described at previous meetings. UTC(AUS) is a free running time domain scale with a prediction capability of the order of 1 microsecond over a 600 day interval. Considerable problems have been experienced in maintaining the caesium standards and determining TV travel times which have changed due to characteristics of the transmissions and changes in location of the standards; yet careful selection of ensemble constituents and more sophisticated least squares analysis of portable clock trips, together with further Timation Satellite experiments, are expected to lead to an order of magnitude improvement over previous capabilities.

1. INTRODUCTION

Time keeping in Australia is characterised by its isolation from the major time scales of the world, at least at the microsecond level. Accordingly, the co-ordinated universal time scale UTC (AUS) was instituted on 1 January 1973 following a meeting of major interested parties on 6 June 1972. The time scale consists of a small number, usually about five, of Hewlett Packard commercial caesium standards compared daily using a commonly received television transmission from the Australian Broadcasting Commission's networked 1300 local newscast (Miller, 1970). The participating laboratories, and other caesium standards and time services in Australia whether linked by TV or not, are listed in Table I.

To determine TV travel delay times, to compare precisely the relationships between the clocks, and to provide time checks on State time services and remote clocks not receiving the networked television transmissions, National Mapping's portable caesium standard DNM590 has been used on many occasions as typified in Table II. One major activity associated with the DNM590 trips

PRECEDING PAGE BLANK-NOT FILMED

has been taking our best estimates of UTC (USNO MC) to the other establishments, particularly in July 1975 when DNM590 visits were made throughout the eastern half of Australia concurrently with the visits by the United States Naval Observatory portable clock PC 1117/IC-2. The successes of predictions made in June, prior to the visit, are shown in Table III, together with corrected 'predictions' made after the event as the result of the discovery of several anomalies in the TV travel delay times.

The initial relationships of Australian clocks with UTC (USNO MC) were based on the USNO portable clock trips in February and December 1973, and Timation II satellite time transfer experiments in July and September 1973 and January 1974 (Easton et al, 1973, Luck and Morgan, 1974). Subsequently, the relationships were estimated using UTC(AUS) as the indicator of superior clock performance, and only superior clocks were used to maintain the relationships. Specifically, VLF (Swanson and Kugel, 1972), LORAN-C (Potts and Wieder, 1972) and Moonbounce (Higa, 1972) techniques, all of which are available to National Mapping through the good offices of NASA, have not been used in any way. That is, the time scale has been constructed for the support of detailed investigations using precise time and time interval rather than as a by-product of the investigations.

2. TIME AND FREQUENCY USERS

The National Measurement Laboratories (NML) of the Commonwealth Scientific and Industrial Research Organisation (CSIRO) operate under Australian Government legislation (Australian Government Legislation, 1960, 1964) to maintain standards of frequency and time interval. NML in turn has chartered the Division of National Mapping (DNM) and the Australian Telecommunications Commission (ATC), formerly the Australian Post Office, to maintain local standards in support (Australian Government Authorization, 1971). ATC is also responsible under legislation for time dissemination which it does via radio station VNG at Lyndhurst, Victoria on frequencies of 4.5, 7.5 and 12.5 MHz, and by telephone landlines. Both these organisations serve a variety of civil and government users.

National Mapping is charged, under its function statement as a government organisation, with 'maintaining astronomical time scales', which includes the determination of UT1 with its Photographic Zenith Tube on Mount Stromlo and the consequent maintenance of precise time.

Sydney and Perth Observatories and the South Australian Post Office maintain their own local time scales for general public use, for example commercial radio time signals, while CSIRO's

radio observatory at Parkes uses its caesium for frequency calibrations and pulsar timing (McCulloch et al, 1973). Hewlett Packard (Australia) maintains an active caesium for instrument calibration purposes and as a service to its customers who have all benefited considerably by HP's consequent in-house expertise.

There are two groups active in VLF and ionospheric research in Australia who also require precise frequency and time information. The first is headed by Dr. J. Crouchley of the Physics Department, University of Queensland. The second is under Dr. D. Robertson of Weapons Research Establishment, Department of Defence.

Australian defence establishments have a long recognised need for accurate frequency control and precise navigation, as does the Department of Transport, and as space-age navigation becomes a part of everyday Australian life, so does the need for precise time as well as frequency. The Joint Defence Research Facilities have a major investment in caesium standards but, in the past, have tended to remain isolated from the general time and frequency community here.

The NASA space tracking agencies each maintain their own local time scales by such means as LORAN-C skywave, Moonbounce, VLF and satellites, together with regular flying clock visits. Those in the Australian Capital Territory have always co-operated with UTC (AUS) although preferring to remain independent for their own purposes. However, with the current introduction of one microsecond accuracy requirements, they are well placed to play a major role in distributing stable and accurate time throughout Australia.

Finally, some local time services are known to rely on nineteenth century pendulum clocks which are compared audio-visually with radio time signals.

3. NATIONAL MAPPING'S INTERESTS

The function statement of the Positional Astronomy Section, drafted at the time of its transfer in 1971 from Mount Stromlo Observatory of the Australian National University, implies the maintenance of a precise and uniform time scale for its UT1 observations, to an accuracy and precision of 50 microseconds. For accuracy, one can not rely on VLF since it can only give time interval and is lost if either the receiver or the clock stops. In the absence of other reliable absolute time comparisons, the local time scale must remain continuous between flying clock visits. Since these may be in excess of 300 days apart, the frequency stability of the clock must be better than

2×10^{-12}, or have a drift rate rather less than 0.2 microseconds/day.

Recently, the Division has become involved with lunar laser ranging (Luck et al, 1973a, b; Bender et al, 1973). The maximum rate of change of range between the telescope and retro-reflector is about 0.6 km/sec., hence to achieve the maximum benefit of ranging at the 100 picosecond (3 cm) level, knowledge of absolute time is required to 10 microseconds to make all timing errors ignorable. Thus the stability requirement over a 300 day period is better than 5 parts in 10^{13}.

Figure 1 illustrates the frequency stability of clock DNM590 as determined from the UTC analysis. It is typical of clocks available to UTC (AUS). The variations are due to the number and distribution of the observations within the smoothing period which typically is of the order of 60 days. Long term stabilities for good clocks, such as DNM590, are better; however they are not consistently better than 5×10^{-13}. Moreover many clocks are either adjusted or fail before good statistics can be accumulated for periods in excess of 300 days. Thus in order to achieve the required accuracies for lunar laser ranging, it is necessary to run an ensemble of at least three standards all performing with stabilities better than parts in 10^{12}.

With the likely advent of combined Doppler and laser satellite tracking for geodetic purposes (Morgan 1974), the importance of precise time is further increased.

The Division maintains, of course, its own local time scale UTC (DNM) using rubidium standard DNM255 as master clock, rephased weekly after analysis of the UTC (DNM) ensemble, see Section 11. It is hoped that the NTS-1 (Timation III) satellite time transfer system can be incorporated into the system as a contributor of appropriate weight and as a condition on the remainder of the ensemble, depending on the application in hand.

4. UTC (AUS)

Let c_i, $i = 1 \ldots n$ denote the i-th clock in the ensemble.
Then UTC (AUS) is defined, after Guinot (Guinot et al, 1971), as

$$\text{UTC (AUS)} = (A + \sum_{i=1}^{n} c_i)/n \qquad (1)$$

where A is an initial constant chosen so that, on 8 February 1973, on which date the NML clocks and DNM590 were compared directly against a USNO flying clock, UTC (AUS) = UTC (USNO MC).

Explicitly, each clock is assigned unit weight. If its performance deteriorates, it is dropped from the ensemble, thereby implicitly assigning it zero weight. More sophisticated weighting schemes are not used because only TV or intra-laboratory comparisons are employed, and because the ensemble is not sufficiently large to assign weights with proper objectivity. However, with the ensemble expected to stabilise in the near future after its spate of discontinuities, and with the introduction of Timation observations as a regular factor, weighting schemes which consider the stability of the received pulse, the precision of the observations and the performance of the clock can be investigated.

The implementation of the algorithm that calculates UTC (AUS) is simple, since it is unweighted and since only individual clocks have ever been considered and not laboratory time scales as the BIH did once. Moreover, if one component clock missed a reading on any day, UTC (AUS) was not calculated on that day. Usually a missed reading is the result of TV transmission anomalies such as non-synchronised sporting telecasts, industrial trouble, or equipment failure in the receiving laboratory. Sometimes the cause of omission was late reading of the synchronising pulse which must be read at exactly $13^h\ 01^m\ 00^s \pm 0.02$ as the transmissions are not time controlled, see Section 8. This philosophy has resulted in some gaps in readings of periods as large as two weeks, particularly around the Christmas-New Year period. This is considered preferable to trying to patch up readings, as the only alternative interpolator is VLF which is notoriously ill-received here. It is possible to alleviate the problem by smoothing with appropriate intervals.

Before developing the reduction algorithm, it is to be stressed that UTC (AUS) is an independent time scale in the sense that, once its zero point has been set, it is the mean of its own clocks only; no overseas time scale affects it directly. For example, on addition of a new ensemble member, the constant A of the fundamental equation is adjusted to maintain continuity of UTC (AUS) itself. Moreover, no attempt is made at such times to maintain continuity in the first time derivative, rate, since it is considered scientifically realistic for the time scale to be the current mean of a number of actual clocks - remembering the past performance of clocks long since dead is certainly less realistic. However, notwithstanding our desire for independence, the estimated relationship to UTC (USNO MC) is calculated, separately from the algorithm, published, and used in certain analyses such as that given in Figure 1. The techniques used are given in the following development.

From the fundamental equation (1), UTC (AUS)-TV is calculated from

$$\text{UTC (AUS)-TV} = \left[\sum_{i=1}^{n} a_i + \sum_{i=1}^{n} ((c_i - \text{TV}) - t_i) \right] / n \qquad (2)$$

where $$\sum_{i=1}^{n} a_i = A, \qquad (3)$$

c_i - TV = a reading at 1301,

t_i = TV travel time relative to NML determined by DNM590 portable clock visits.

Then $$\text{UTC (AUS)} - c_j = (\text{UTC (AUS)-TV}) - ((c_j - \text{TV}) - t_j) \qquad (4)$$

where c_j may be either a constituent of the ensemble defining UTC (AUS) as in equation (1), or any other participant. The results of equations (2) and (4) are tabulated for each day on which all n current constituents have satisfactory readings, and published for interested Australians at nominally monthly intervals. Least squares straight line fits against MJD to each UTC (AUS) - c_j are also published. Table IV is an example of the published computations.

When a new clock c_{n+1} is added to the ensemble it is sufficient for continuity that A be re-evaluated (Guinot et al, 1971), resulting in a revised A^1:

$$A^1 = A + (\text{UTC (AUS)} - c_{n+1}) \qquad (5)$$

where (UTC (AUS) - c_{n+1}), is the actual value from equation (4) obtained using the previous ensemble on day T_1, the day on which c_{n+1} is added. Similarly, if clock c_k is removed on day T_1,

$$A^1 = A - (\text{UTC (AUS)} - c_k)$$

In practice, each run for publication is made with an unchanged ensemble, and the value of each UTC (AUS) - c_i on the last day of the previous run is used as a_i. This makes it very simple to control A adjustments when altering the ensemble.

The criteria on which changes occur are:

(a) A clock fails;

(b) A clock's performance against the ensemble deteriorates, as judged by its rate or standard error;

(c) A clock whose rate has been constant to within 0.02 microseconds/day over a period of, usually, two months or more, and which is in a properly controlled environment, will always be considered for admission.

Table V shows which clocks formed the ensemble between 09 February 1973 and 31 July 1975.

5. DATA FILTERING

Once all the data has been collected for a run, by telex and mail, it is checked in the office for obvious bad readings and known transmission anomalies (it is known, for example, that a jump of 10.8 microseconds occurs in the Canberra region when a change occurs in the linkage between the studio and transmitter). A preliminary run is then made for further editing, checking small errors (a reading is rejected if its UTC (AUS) - c_i residual exceeds 2 microseconds), and determining if any constituent is performing badly. A further iteration prepares the results for publication.

6. ANALYSIS

To obtain a clearer view of the long term behaviour of UTC (AUS) and its constituent clocks, a series of recomputations has been made, using only clocks of superior performance over hundreds of days as constituents. A typical set of results is presented in Figure 2. The large fluctuations are due entirely to computer plotter crossovers. Points worth noting are:

(a) The small number of clocks judged suitable for the ensemble, and the curves and jumps in the others;

(b) The number of clock failures in the period;

(c) Frequent correlated jumps in geographical areas, indicating local TV anomalies;

(d) The apparent instability of DNM590 and DNM205 after February 1975 when they were moved from Mount Stromlo to Orroral Valley is attributed to Fresnel effects due to an intermediate ridge in the line of sight path as well as to atmospheric effects. These problems are currently receiving attention.

(e) The fine performances of DNM590, despite its use as a portable clock, and of GWESF396 after its C-field adjustment in September 1973.

(f) Several apparently gradual changes in the ATC clocks, which occurred during sparse data periods, were only recently detected as real, and are evidently due to accumulative component changes in the television transmission network.

(g) The relatively small changes in (UTC (AUS) - UTC (USNO MC)) at ensemble changes.

Subsequent analysis has tidied up this picture and resolved many of the anomalies.

7. RELATIONSHIP TO UTC (USNO MC)

We use this time scale as reference, since it is directly accessible by flying clocks and Timation, and it is known to be stable.

The fundamental adopted relationship is

$$\text{UTC (USNO MC)} - \text{DNM590} = -34.70 - 0.08686\ (\text{MJD} - 42023.0) \quad (6)$$

based on Timation II experiments for rate, and these and the flying clock visit of 7 December 1973 for the constant term. This relationship was transferred directly to the ensemble of Section 6 by means of:

$$\text{UTC (USNO MC)} - \text{UTC (AUS)} = (\text{UTC (USNO MC)} - \text{DNM590}) - (\text{UTC (AUS)} - \text{DNM590}) \quad (7)$$

and is shown on Figure 2. As a check, back extrapolation to the flying clock visit of February 1973 reveals errors of rather less than one microsecond.

The UTC (AUS) reduction program contains a section in which equation (7) is updated conveniently from the fundamental period (July 73 to January 74), since the latest estimate of UTC (USNO MC) - c_i is always maintained in the input deck. The only assumption made in the update is that the ensemble clocks perform linearly, and this is checked by UTC (AUS) before the final ensemble for a run is chosen. This update makes it possible to estimate the performance of each clock against a nearly uniform reference without needing a great number of historical records. The performances can be gauged from Figure 2.

8. TELEVISION NETWORK

The transmissions originate at the Gore Hill, Sydney, studios of the Australian Broadcasting Commission, and are networked as shown in Figure 3.

Until the introduction of colour TV on 1 March 1975, the frequencies were crystal controlled with a rate of, commonly,

10 microseconds/second. Since the repetition rate is 50 Hz, the system accuracy was limited to 0.2 microseconds at best. Since 1 March 1975 rubidium standards control the frequency, hence errors are entirely due to propagation anomalies and receiving station malfunctions. There is no agreement with the ABC on controlling the precise time of transmission.

The pulse received in common is the first vertical synchronisation pulse in the vertical block (Miller, 1970). It is displayed in Figure 4. The pulse selector used in each laboratory is a simple pulse discriminator originally designed by E. Sandbach of ATC and now improved by C. Cochran of DNM.

As mentioned previously, the travel times are known to change without notice due to equipment and atmospheric changes. The latter changes affect the short term stability of the readings while the former changes affect the long term stability and are in general more easily detectable as major system changes. Table VI lists the determined travel times on the date of clock comparisons as well as 5 day mean values about the clock trip which average out the short term fluctuations. The 5 day mean values have proved their usefulness in improving our ability to predict values of UTC (USNO MC) from UTC (AUS). This is evidenced in Table III.

9. VLF

The quality of VLF reception at National Mapping was improved in 1973 following detailed discussions with Dr. Winkler. The receiver is now manually slewed each day to compensate for cycle slips which, in certain seasons, occur daily. This technique maintains all recording apparatus in a constant position, thereby minimising receiver and recorder non-linear performance. It yields acceptable results during periods of minimal transmitter misbehaviour. An example of the internal precision possible under favourable conditions is given in Table VII which reports on the status of clocks whose only connection to UTC (AUS) and UTC (USNO MC) is through these signals.

An investigation into the reliability of reception of signals from the US Naval Communications Station at North West Cape (NWC), Western Australia, was undertaken, and as a consequence weekly readings are exchanged with the University of Queensland to check on transmitter jumps before our readings are communicated to USNO. These checks can verify jumps as small as 0.2 microseconds and, along with similar checks on NLK, provide our only method of monitoring the Queensland clock. By forcing clock continuity over receiver outage periods, this monitoring agrees with DNM590 calibrations to 5 microseconds via NWC and 3 micro-

seconds via NLK, while similar monitoring of USNO via NLK agreed with USNO flying clock calibrations to within 3 microseconds between 7 December 1973 and 16 July 1975. Considerable care had to be exercised to achieve these accuracies, however, and with the likelihood of regular satellite time rather than frequency transfers, our interest in VLF will remain observational rather than operational.

10. EQUIPMENT PERFORMANCE

While beam tube failure is undoubtedly of major importance, it has been our experience that the expected life of standard tubes is in excess of three years and that repairs by the local Hewlett Packard facility are well within specifications. However, there is an incomplete knowledge and understanding at many of the local laboratories of the fine adjustments necessary to run these instruments in an optimal manner.

At the Division of National Mapping, we were forced to move our ensemble of clocks and VLF equipment in February of this year from a well proven site, Mount Stromlo, to our new site at Orroral. All clocks were carried to Orroral on vehicle power for about 90 minutes. They were then placed in their new positions and C-fielded. Unfortunately, DNM153 did not travel well and, for a considerable time, attempts to adjust it in its new location were not successful.

This difficulty of adjustment has been experienced at a number of Australian laboratories, many of which have previously accepted lower levels of performance due to operational pressures to provide time and frequency at the levels specified by the manufacturers of the equipment or to an inadequate array of available equipment with which to detect and correct such misalignments. The experiences gained by us with DNM153 have allowed us to assist in the delicate task of fine tuning a standard.

As a preparation for the move to Orroral, we developed an analysis method almost identical to the triad method of Allan (Gray and Allan, 1974). Using this method we determined the performance of the standards before moving and upon installation at Orroral. Since we have a local scale UTC (DNM), see Section 11, we were able to compute the fractional frequency stability of each clock relative to the mean via the well-known Allen variance formula.

$$\sigma^2(t) = \frac{1}{2n} \sum_{i=1}^{n} (\Delta y_i)^2 = \frac{1}{2n} \sum_{i=1}^{n} (y_{i+1} - y_i)^2 \qquad (8)$$

The application of this equation assumes that an absolute standard is available.

When two clocks are intercompared, the above becomes

$$\sigma_{ab}^2(t) = \sigma_a^2(t) + \sigma_b^2(t) - \frac{1}{n}\sum_{i=1}^{n}(\Delta y_a)(\Delta y_b) \qquad (9)$$

where the final term is a correlation term which in the limit approaches zero as n approaches infinity.
Using equation (8) at Mount Stromlo before the move and equation (9) at Orroral upon installation, we were able to detect the anomalous behaviour of DNM153. To restore DNM153 to its original state, we made a full map of the resonance curve as a function of C-field setting. This showed a number of peaks with one particular peak very much more pronounced than the others. This peak was also very narrow. Attempts to set up directly on the maximum always resulted in under or over shoot as was indicated by solving the following equation set

$$\begin{aligned} \sigma_{ab}^2 &= \sigma_a^2 + \sigma_b^2 \\ \sigma_{ac}^2 &= \sigma_a^2 + \sigma_c^2 \\ \sigma_{bc}^2 &= \sigma_b^2 + \sigma_c^2 \end{aligned} \qquad (10)$$

for σ_a^2, σ_b^2 and σ_c^2 using sample periods up to 30 hours.

We resolved the problem by obtaining an approximate setting of the C-field using the Zeeman frequency method as outlined in Hewlett Packard's equipment manual. This ensured that we were on the correct resonance peak. We then used our previously obtained C-field map to compute the final fine adjustment necessary to operate the instrument at this peak.

The operation of DNM153 in this position resulted in dramatic improvement in its stability. Figure 5 shows the fractional frequency stability of each standard before and after the move and, in the case of DNM153, during the period of adjustment.

These techniques were put to good use by the Division in a recent calibration trip to Parkes where PRKS 143 was experiencing amplifier instability problems.

11. UTC (DNM)

To evaluate the performance of our own clocks on a more regular basis and to free ourselves from our lack of knowledge of the TV delay time, a local time scale, UTC (DNM), was implemented in 1974. This is composed of the three caesium standards DNM590, DNM203 and DNM153 and is constructed from phase recordings at a scale of

20 nanoseconds per centimeter, read hourly. UTC (DNM) has an arbitrary but convenient zero which needs to be related to another reference scale. Generally this is not done as the scale is broken every time an ensemble member, usually DNM590, is unavailable for any period such as during a clock trip. Equation (1) reduces to the following simple form for an ensemble of three with a mean of zero:

$$\text{UTC (DNM)} - c_i = \frac{1}{3} \sum_{j=1}^{3} (c_j - c_i) \qquad (11)$$

Initially, the results were plotted and abnormal behaviour or impending failure detected by visual inspection. Currently a mini-computer, an HP21-MX, is being programmed to perform the data acquisition and reduction and to display this information in the form of residual plots and fractional frequency curves.

With the implementation of this more versatile data acquisition/analysis system and with the advent of Timation III data, the limitation placed on UTC (DNM) due to ensemble breaks and unknown offsets will disappear.

12. THE FUTURE

It can be expected that the precision, regularity and accuracy of the time scale UTC (AUS) will continue to improve as problems surrounding the number of ensemble constituents, mode of comparison and accuracy of setting are resolved. At the same time, daily connections of this scale with those produced by other organisations such as USNO and the BIH will become a reality leading to a more truly universal time scale as well as a fully coordinated UTC (AUS) at an unprecedented level of accuracy.

13. ACKNOWLEDGMENTS

The authors wish to thank Dr. G. Winkler and Mr. R. Easton for their support, assistance and encouragement in this work and Mr. R. Trainer and Mr. V. Thomas of ATC and Mr. R. Archer of NML for their help and cooperation.

14. REFERENCES

Australian Government Authorization, 1971. Authorization under Weights and Measures (National Standards) Act 1960-1964, Bill 60 of 64 from Commonwealth Scientific and Industrial Research Organization to Postmaster General's Department and the Division of National Mapping. July 1971.

Australian Government Legislation 1960. Weights and Measures (National Standards) Act 1960. Act number 64 of 1960 in Australian Government Statutes. Government Printer, Canberra, Australia.

Australian Government Legislation 1964. Weights and Measures (National Standards) Act 1960-1964. Subsection 2 of Section 8. Act number 6 of 1964 in Australian Government Statutes. Government Printer, Canberra, Australia.

Bender, P. L., Currie, D. G., Dicke, R. H., Eckhardt, D. H., Faller, J. E., Kaula, W. M., Mulholland, J. D., Plotkin, H. H., Poultney, S. K., Silverberg, E. C., Wilkinson, D. T., Williams, J. G., and Alley, C. O. The Lunar Laser Ranging Experiment. Science, v. 182, April 1973, pp. 229.

Easton, R. L., Morgan, P. and Smith, H. M. A Summary of Recent Satellite Time Transfers from U. S. Naval Observatory to the Royal Greenwich Observatory and to Australia. IEEE Transactions on Instrumentation and Measurement, Vol. IM-23 (4), December 1974, pp. 525-526.

Easton, R. L., Smith, H. M., and Morgan, P. Submicrosecond Time Transfer Between the United States, United Kingdom, and Australia via Satellite. Proceedings of the Fifth Annual NASA and Department of Defense Precise Time and Time Interval Planning Meeting, December 1973. NASA Publication X 814-74-225, pp. 163-182. NASA, Goddard Space Flight Center, Greenbelt, Maryland.

Gray, J. E., and Allan, D. W. A Method for Estimating the Frequency Stability of an Individual Oscillator. Proceedings of 28th Annual Symposium on Frequency Control, 1974, pp. 243-246.

Guinot, B., Feissel, M., and Granveaud, M. Annual Report for 1970, Bureau International de l'Heure. Paris, 1971.

Higa, W. H. Time Synchronization via Lunar Radar. Proceedings of the IEEE, v. 60 (5), May 1972, pp. 552-557.

Luck, J. Mck., Miller, M. J. and Morgan, P. J. National Mapping's Astrogeodetic Complex. Proceedings of Astronomical Society of Australia, v. 2 (4), 1973, pp. 203-206.

Luck, J. Mck., Miller, M. J. and Morgan, P. J. The National Mapping Lunar Laser Program. Proceedings of a Symposium on Earth's Gravitational Field and Secular Variations in Position, Sydney, Nov. 1973, pp. 413-432.

Luck, J. Mck., and Morgan, P. Statistical Analysis of Time Transfer Data from Timation II. Proceedings of Sixth Annual Precise Time and Time Interval Planning Meeting, December 1974. NASA Publication X-814-75-117, pp. 513-530. Greenbelt, Md., Goddard Space Flight Center.

McCulloch, P. M., Komesaroff, M. M., Ables, J. G., Hamilton, P. A. and Rankin, J. M. Improved Parameters for 15 Southern Pulsars. Astrophysical Letters, v. 14, 1973, pp. 169-170.

Miller, M. J. Synchronization of Distant Clocks by Television Pulse Comparisons. Proceedings of the Astronomical Society of Australia, v. 1 (7), April 1970, p. 352.

Morgan, P. A Simulation Study for Sub-Meter Geodesy in the Pacific Basin. Paper presented to Symposium in honour of Dr. G. Woollard, Hawaii, December 1974. Proceedings in press under sponsorship of American Geophysical Union.

Potts, E. E., and Wieder, B. Precise Time and Frequency Dissemination via the LORAN-C System. Proceedings of the IEEE, v. 60 (5), May 1972, pp. 530-539.

Swanson, E. R., and Kugel, C. P. VLF Timing: Conventional and Modern Techniques including Omega. Proceedings of the IEEE, v. 60 (5), May 1972, pp. 540-551.

TABLE I

AUSTRALIAN TIME AND FREQUENCY LABORATORIES

LABORATORY	MNEMONIC	LOCATION	FREQUENCY STANDARDS	COMPARISON MODE
Division of National Mapping	DNM (formerly MSO)	Orroral Valley, ACT	CS205	TV
			CS590	TV, TC
			CS153	TV
			Rb255	Interpolator, TC
Orroral Valley STDN	ORR	Orroral Valley, ACT	CS163	Weekly TC
			Rb003	Interpolator, TC
Honeysuckle Creek	HSK	Honeysuckle Ck, ACT	Rb	Irregular TC
Tidbinbilla DSIF 42	TID	Tidbinbilla, ACT	CS188	Irregular TC
Australian Telecommunication Commission	ATC (formerly APO)	Melbourne, Victoria	CS288	TV
			CS902	TV
			Rb	Interpolator, TC
Hewlett Packard (Australia) Pty Ltd	HP	Melbourne, Victoria	CS052	TV
Defence Standards Laboratories	DSL	Melbourne, Victoria	CS241	Irregular TC
Australian National Radio Astronomy Organisation	PRKS	Parkes, NSW	CS143	TV

TABLE I (cont.)

LABORATORY	MNEMONIC	LOCATION	FREQUENCY STANDARDS	COMPARISON MODE
National Measurements Laboratories	NML (formerly NSL)	Sydney, NSW	CS201 CS338	TV TV
Guided Weapons Electronic Support Facility	GWESF	St. Mary's, NSW	CS396	TV
Sydney Observatory	SYDOBS	Sydney, NSW	RB	Irregular TC
University of Queensland	BNE	Bribie Is., Qld	CS331	VLF and Irregular TC
Weapons Research Establishment	WRE	Salisbury, SA	3 Xtal	Irregular TC
Weapons Research Establishment	WMRA	Woomera, SA	CS494 CS531	Irregular TC SATCOM and Irregular TC
TRANET	TRAN	Salisbury, SA	RB519	VLF and Irregular TC
South Australian Post Office	SAPO	Adelaide, SA	3 Xtal	Irregular TC
Perth Observatory	PERTH	Bickley, WA	RB	VLF and Irregular TC
North West Cape	NWC	Exmouth, WA	CS222 CS220	VLF and Irregular TC VLF and Irregular TC
JDSRF	JDSRF	Alice Springs, N.T.	CS103 CS... CS...	VLF and Irregular TC VLF and Irregular TC VLF and Irregular TC

TABLE II

MEASUREMENTS BY PORTABLE CAESIUM STANDARD DNM590
DURING CALIBRATION TRIPS OF JULY 1975

CLOCK	DATE(UT) DAY.HRMI	OBSERVED DNM590-CLOCK	OBSERVED TV TRAVEL TIME	ESTIMATED (USNO MC)-CLOCK
		UNIT: MICROSECONDS		
ATC 902	189.0548	74.88	3295.44	-8.86
ATC 288	189.0548	75.21	3295.44	-7.46
PC1117/IC-2	189.0548	85.45	-	-
HP 052	189.0745	93.5	3246.69	9.75
WMRA494	190.0030	83.9	-	0.12
WMRA531 (SATCOM TERMINAL)	190.0500	91.4	-	7.61
PC1117/IC-2	191.0030	85.5	-	-
JDSRF 103	192.0200	59.7	-	-
SAPOXA	192.0615	60.6	-	-23.3
SAPOXB	192.0615	-89.7	-	-173.6
SAPOXC	192.0615	127.7	-	43.8
WRE XA	192.0730	85.5	-	1.61
TRAN 519	192.0815	86.0	-	2.11
PORTABLE CLOCK DNM590 RETURNED TO ORRORAL AT THIS POINT				
ORR 163	196.1300	59.0	-	-25.09
BNE 331	197.0505	-15.4	-	99.53
GWESF396	198.0150	63.38	104.33	-20.79
SYDOBS	198.0510	2144.2	-	2060.03
NML 201	198.0550	87.05	0.0	2.88
NML 338	198.0550	102.13	0.0	17.96
PC1117/IC-2	198.0550	85.821	-	-
PORTABLE CLOCK DNM590 RETURNED TO ORRORAL AT THIS POINT				
PRKS 143	219.0709	-549.6	1049.15	-634.79
PORTABLE CLOCK DNM590 FINISHED JULY CALIBRATIONS AT THIS POINT				

NOTE: PC1117/IC-2 IS THE USNO PORTABLE CLOCK

TABLE III

ACCURACY OF UTC PREDICTIONS

CLOCK	DATE	MJD	UTC (USNO MC) - CLOCK (MICROSECONDS)				
			MEASURED	PREDICTED	Δ	REVISED PREDICTION	Δ
NML 201	75 JULY 03	42596.98	4.45	10.05	5.60	12.14	7.55
NML 338	75 JULY 03	42596.98	20.51				
DNM 590	75 JULY 07	42600.27	-83.69	-82.98	0.71	-76.03	7.65
DNM 205	75 JULY 07	42600.27	- 1.50	- 0.31	1.19		
DNM 153	75 JULY 07	42600.27	3.43	3.95	0.56		
ATC 902	75 JULY 08	42601.24	- 8.91	- 5.49	3.42	1.54	7.12
HP 052	75 JULY 08	42601.31	9.75	11.45	1.70	17.90	7.19
GWESF 396	75 JULY 17	42610.06	-20.79	-13.18	7.61	-11.49	8.76
PRKS 143	75 AUG 07	42631.30	-634.79	-655.44	20.65	-643.57	-8.78

NOTE: THE REVISED PREDICTIONS ARE DUE TO THE USE OF IMPROVED MEAN TRAVEL TIMES AS A RESULT OF THE JULY 1975 CALIBRATION TRIP, SEE SECTION 8

TABLE IV

A SEGMENT OF UTC(AUS) ANALYSIS

PART 3 UTC(AUS)-CLOCK FOR CLOCKS IN REGION OF MELBOURNE

DATE		MJD	HP 052	WT	ATC 288	WT
			UNITS ONE MICROSECOND			
74MAR	1	42107	-29.01	1	18.29	1
74MAR	2	42108	********	0	********	0
74MAR	3	42109	********	0	********	0
74MAR	4	42110	-28.86	1	18.14	1
74MAR	5	42111	-29.15	1	18.35	1
74MAR	6	42112	-30.70	1	16.50	1
74MAR	7	42113	-30.71	1	16.29	1
74MAR	8	42114	-31.31	1	15.89	1
74MAR	9	42115	********	0	********	0
74MAR	10	42116	********	0	********	0
74MAR	11	42117	********	0	********	0
74MAR	12	42118	-29.16	1	17.44	1
74MAR	13	42119	-31.21	1	15.99	1
74MAR	14	42120	-29.58	1	17.52	1
74MAR	15	42121	-29.51	1	17.29	1
74MAR	16	42122	********	0	********	0
74MAR	17	42123	********	0	********	0
74MAR	18	42124	********	0	********	0
74MAR	19	42125	-29.81	1	16.89	1
74MAR	20	42126	-30.31	1	16.49	1
74MAR	21	42127	-29.81	1	16.69	1
74MAR	22	42128	********	0	********	0
74MAR	23	42129	********	0	********	0
74MAR	24	42130	********	0	********	0
74MAR	25	42131	********	0	********	0
74MAR	26	42132	-29.93	1	15.97	1
74MAR	27	42133	-30.36	1	15.44	1
74MAR	28	42134	-29.18	1	16.52	1
74MAR	29	42135	********	0	********	0

SMOOTHING COEFFICIENTS FOR EACH UTC(AUS)-CLOCK = A+B(T-TO)
WHERE DATA IS SMOOTHED FROM T1 TO T2

A	-15.65	57.45
B	-.0355	-.1014
TO	41721.	41721.
T1	74FEB 1	74FEB 1
T2	74MAR 29	74MAR 29
STANDARD ERROR	.69	.69

TABLE V

CLOCKS FORMING THE REGULAR UTC(AUS) ENSEMBLE

PERIOD	ENSEMBLE
09 Feb 73-29 June 73	DNM 205, ATC 288, NML 201, DNM 590, NML 338
29 June 73-19 Oct 73	DNM 205, DNM 590, DNM 153, NML 338, ATC 288, HP 052
19 Oct 73-31 Dec 73	DNM 205, DNM 590, NML 338, HP 052, GWESF 396
27 Dec 73-26 Apr 74	DNM 205, DNM 590, NML 338, ATC 288, HP 052, GWESF 396
26 Apr 74-31 Aug 74	GWESF 396, DNM 590, NML 338, ATC 288, HP 052
29 Aug 74-15 Nov 74	GWESF 396, DNM 590, ATC 288, HP 052, NML 201
15 Nov 74-31 Jan 75	GWESF 396, DNM 590, ATC 288, HP 052, NML 201, DNM 205
28 Jan 75-23 May 75	GWESF 396, ATC 902, HP 052, NML 201, NML 338
22 May 75-31 July 75	GWESF 396, ATC 902, HP 052, NML 201

TABLE VI

MEASURED AND COMPUTED TV TRAVEL TIMES (MICROSECONDS)

CLOCK	DATE	MEASURED DELAY TIME	Δ	COMPUTED 5 DAY MEANS	Δ
ATC 288	73 FEB 12	3289.62		3289.62	
			0.51		0.45
ATC 288	73 JUNE 11	3290.13		3290.07	
			-0.15		2.21
ATC 288	74 APR 30	3289.98		3292.28	
			4.52		2.99
ATC 902	75 MAR 13	3294.50		3295.27	
			2.17		0.17
ATC 902	75 JULY 08	3296.67		3295.44	
HP 052	73 FEB 12	3269.40		3269.40	
			0.86		2.24
HP 052	73 JUNE 12	3270.26		3271.64	
			-30.02		-30.30
HP 052	74 APR 29	3240.28		3241.34	
			4.96		4.48
HP 052	75 MAR 13	3245.24		3245.82	
			2.22		0.87
HP 052	75 JULY 08	3247.46		3246.69	
DNM 205	73 FEB 08	989.78		989.78	
			-0.41		-0.73
DNM 205	73 JUNE 19	989.37		989.05	
			-1.99		0.59
DNM 205	74 MAY 06	987.38		989.64	
			113.21		111.58
DNM 205	75 MAR 20	1100.59		1101.22	
			2.39		1.98
DNM 205	75 JULY 17	1102.98		1103.20	
PRKS143	72 DEC 06	1049.20		1049.20	
			0.55		-0.05
PRKS143	73 JUNE 20	1049.75		1049.15	
			-1.99		0.43
PRKS143	74 MAY 15	1047.76		1049.58	
			-1.12		-1.47
PRKS143	75 MAR 26	1046.64		1048.11	
			2.51		1.04
PRKS143	75 AUG 07	1049.15		1049.15	
GWESF396	73 FEB 07	105.28		105.28	
			--		-0.07
GWESF396	73 JUNE 19	105.28		105.21	
			-1.09		-0.05
GWESF396	74 MAY 06	104.19		104.71	
			0.39		-0.13
GWESF396	75 MAR 20	104.58		104.58	
			-1.17		-0.25
GWESF396	75 JULY 17	103.41		104.33	

TABLE VII

THE VLF SEGMENT OF UTC(AUS) ANALYSIS

PART 5 UTC(AUS)-CLOCK FOR CLOCKS IN REGION OF VLF RECEPTION

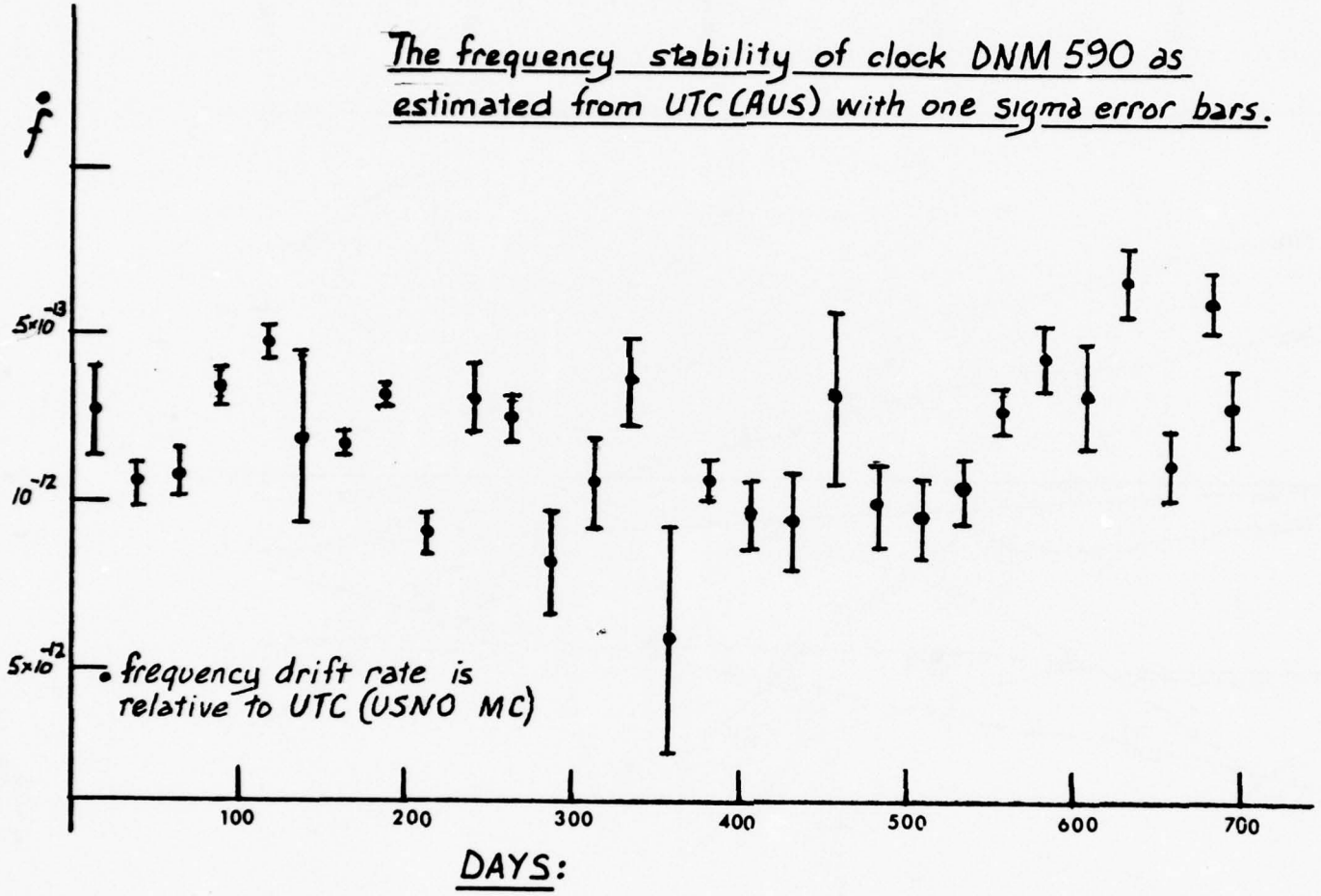
DATE	MJD	USNO MC	WT	BN 331-NLK	WT	BN 331-NWC	WT
		UNIT ONE MICROSECOND					
74MAR 1	42107	-4.45	1	-24.45	1	-22.95	1
74MAR 2	42108	********	0	********	0	********	0
74MAR 3	42109	********	0	********	0	********	0
74MAR 4	42110	-6.50	1	-24.30	1	-22.60	1
74MAR 5	42111	-5.59	1	-24.59	1	-23.19	1
74MAR 6	42112	-4.14	1	-22.94	1	-23.24	1
74MAR 7	42113	-4.55	1	-23.95	1	-23.05	1
74MAR 8	42114	-3.65	1	-22.45	1	-21.75	1
74MAR 9	42115	********	0	********	0	********	0
74MAR 10	42116	********	0	********	0	********	0
74MAR 11	42117	********	0	********	0	********	0
74MAR 12	42118	-6.10	1	-25.50	1	-22.70	1
74MAR 13	42119	-4.45	1	-23.65	1	-24.55	1
74MAR 14	42120	1.58	1	-23.82	1	-24.52	1
74MAR 15	42121	2.55	1	-16.45	1	-25.85	1
74MAR 16	42122	********	0	********	0	********	0
74MAR 17	42123	********	0	********	0	********	0
74MAR 18	42124	********	0	********	0	********	0
74MAR 19	42125	-6.45	1	-26.45	1	-24.55	1
74MAR 20	42126	-0.25	1	-22.25	1	-25.85	1
74MAR 21	42127	-2.65	1	-25.05	1	-26.55	1
74MAR 22	42128	********	0	********	0	********	0
74MAR 23	42129	********	0	********	0	********	0
74MAR 24	42130	********	0	********	0	********	0
74MAR 25	42131	********	0	********	0	********	0
74MAR 26	42132	-3.07	1	-26.07	1	-25.97	1
74MAR 27	42133	-2.80	1	-25.80	1	-26.00	1
74MAR 28	42134	-3.62	1	-26.62	1	-27.72	1
74MAR 29	42135	********	0	********	0	********	0

SMOOTHING COEFFICIENTS FOR EACH UTC(AUS)-CLOCK = A+B(T-TO)
WHERE DATA IS SMOOTHED FROM T1 TO T2

A	-137.75	-107.29	24.14
B	.3328	.2053	-.1220
TO	41721.	41721.	41721.
T1	74FEB 1	74FEB 1	74FEB 1
T2	74MAR 29	74MAR 29	74MAR 29
STANDARD ERROR	4.28	3.66	.89

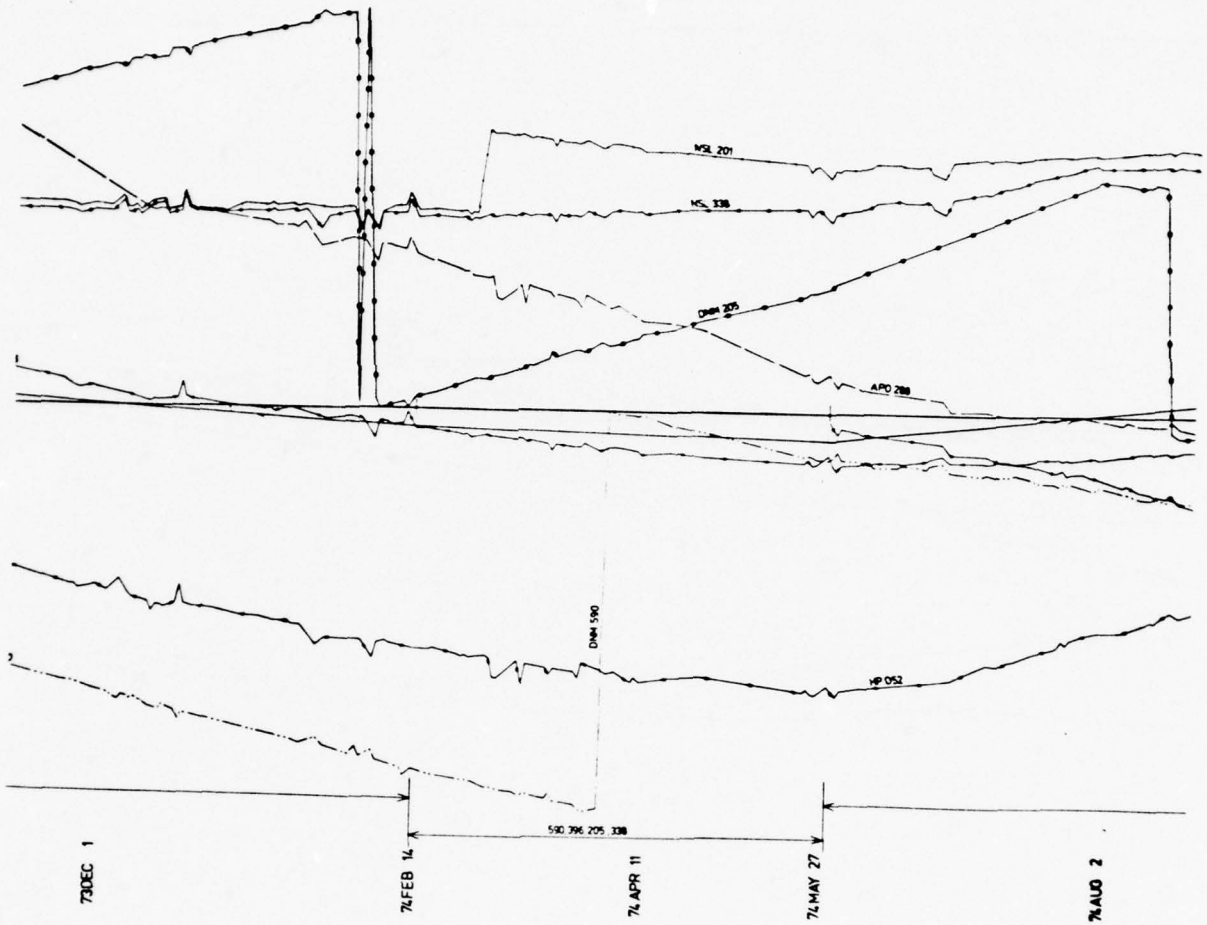
FIGURE 1

The frequency stability of clock DNM 590 as estimated from UTC(AUS) with one sigma error bars.



73FEB 0
73APR 2
73JUN 1
73AUG 1
73OCT 3
73DEC 1
UTC(AUSI)

UTC (AUS) – CLOCK
73 FEB 08 TO 75 MAY 23



UTC (NBS)
NSL 208
NSL 201
LORAN
WWV 25
APC 802
OMEGA 208
OMEGA 580
OMEGA 208
APC 208
OMEGA 208
75 APR 1
75 JAN 28
74 DEC 2
74 OCT 3
74 AUG 2

FIGURE 3.

TELEVISION NETWORKS

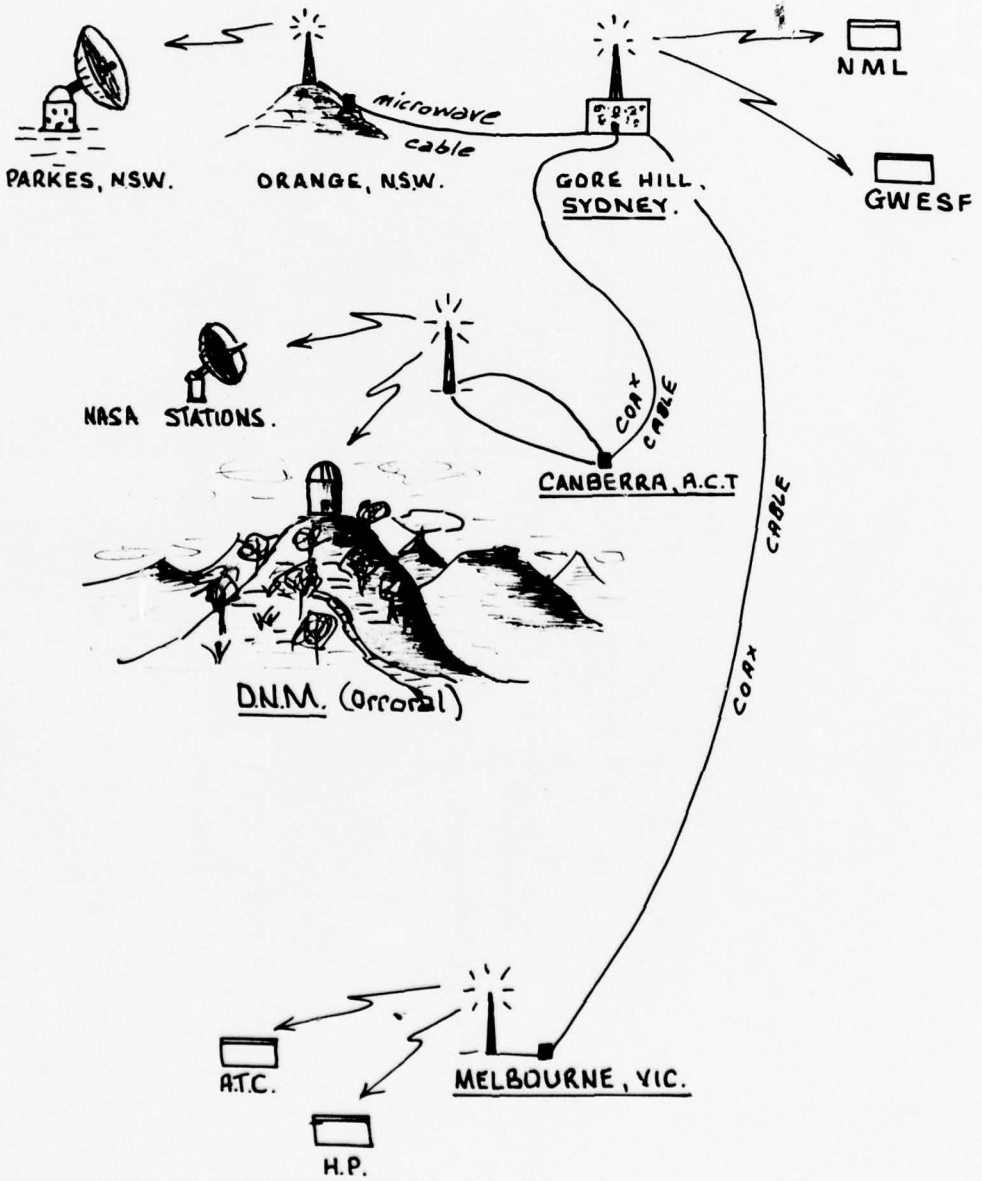


FIGURE 4

SCHEMATIC OF TV VIDEO SIGNAL AND VERTICAL SYNC PULSE BLOCK

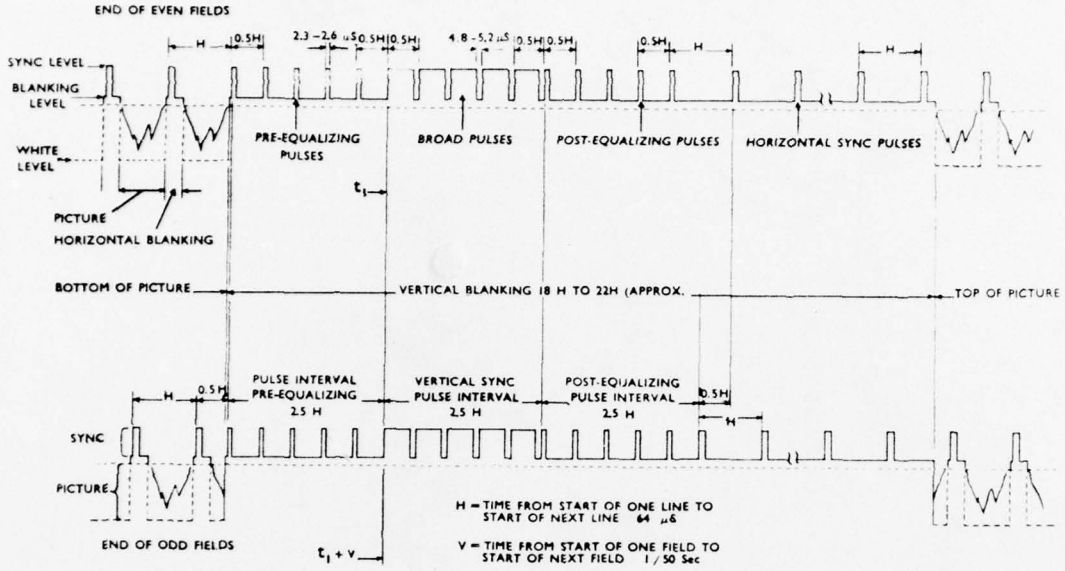
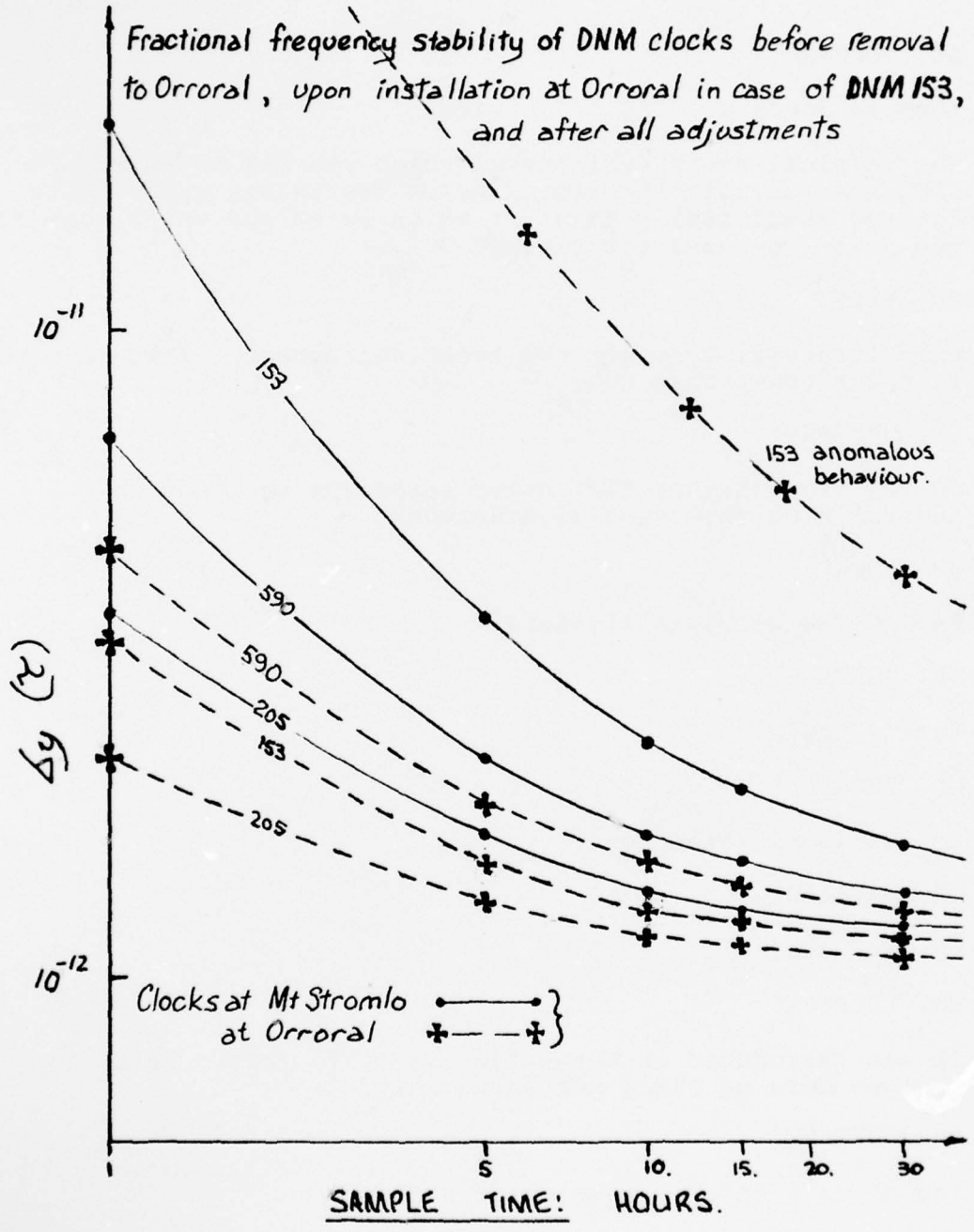


FIGURE 5


Fractional frequency stability of DNM clocks before removal to Orroral, upon installation at Orroral in case of DNM 153, and after all adjustments
153 anomalous behaviour.
153
590
590
205
153
205
10^{-11}
10^{-12}
$\Delta y(\tau)$
Clocks at Mt Stromlo
at Orroral
1
5
10.
15.
20.
30
SAMPLE TIME: HOURS.

QUESTION AND ANSWER PERIOD

DR. SHEPARD:

Leonard Shepard, ILC Industries.

The vertical re-trace interval which you had up there was NTSC and you said the timing pulse was in the upper left. Can you specifically identify which pulse and which edge of the pulse you used for timing?

MR. LUCK:

Unfortunately, I am not our technical person. I would have to think about that one.

DR. SHEPARD:

Do you know whether NTSC color standards are used in Australia on the television network?

MR. LUCK:

Is NTSC The American standard?

DR. SHEPARD:

Yes.

MR. LUCK:

No, it is the other one.

DR. SHEPARD:

PAL? I see.

MR. LUCK:

It was introduced on March the 1st, this year. Prior to that we were on black and white only.

DR. SHEPARD:

You do have color transmission now?

MR. LUCK:

Yes.

DR. SHEPARD:

How is the subcarrier stabilized?

MR. LUCK:

By rubidium standards.

DR. SHEPARD:

Do you know, with or without offset?

MR. LUCK:

It seems to be without offset.

MR. JOHNSON:

Johnson, Naval Observatory.

Do you avail yourself of the link back to the observatory that is available to you through the Womera satellite terminal?

MR. LUCK:

Yes, we are aware of it. We have visited the place with our portable standard and at the moment, our only comparison is by portable standards. We are going to investigate that further in the near future.

PTTI TECHNOLOGY IN SOUTH AFRICA AND SPECIFIC PROBLEMS GERMANE TO THIS GEOGRAPHIC AREA

J. Hers, National Physical Research Laboratory
Pretoria, South Africa

ABSTRACT

A brief historical survey of the development of time and frequency services in South Africa is followed by an account of some of the techniques presently employed at the NPRL to control the signals from radio station ZUO. Short descriptions are given of several devices which have been developed for local time dissemination, including one which transmits coded hour, minute and second data as part of the time signals themselves, a simple solar-to-sidereal time converter, and the ZUO morse code generator.

HISTORICAL SURVEY

Time in South Africa has traditionally been the responsibility of the astronomical observatories: in Cape Town the Royal Observatory (est. 1820) and in Johannesburg the Transvaal Observatory (est. 1903). The Royal Observatory distributed time from an early date by the daily firing of a naval gun, intended mainly for the benefit of shipping in Table Bay.

In Johannesburg the first hourly time signals from the observatory were sent in 1908 by landline to the Central Telegraph Office, from where they were distributed throughout the province. After the union of the four provinces in 1910 three Riefler clocks were installed at what had now become known as the Union Observatory, and the distribution network was extended to Durban, where - if all went well - a time ball was dropped at noon by a remote signal from Johannesburg.

In Cape Town time was measured astronomically as part of the meridian program, but Johannesburg had at first only a small 65 mm refractor, received on loan for a latitude observation program. The resulting time signals could seldom be relied on to better than about 0.5 second, and they might be worse after a period of cloudy nights. As early as 1923 it was found that much better results could be obtained by using the long wave radio time signals from Bordeaux and Rugby, and the astronomical observations were

PRECEDING PAGE BLANK-NOT FILMED

discontinued, to be replaced by the more accurate - if second-hand - radio time. In later years the possible installation of a Photographic Zenith Telescope has been discussed on numerous occasions, but until today there has been no basic change in this approach.

Precise time in its modern form may be said to have started in 1948, when the first quartz crystal clock was built at the Union Observatory. Although consisting mainly of discarded war surplus components, it immediately improved timekeeping accuracy by a factor of at least 100, and rendered all other clocks obsolete.

In 1949, at the request of surveyors and geophysicists who needed accurate time in the field, continuous radio time signal transmissions were started from a small portable transmitter, soon increased in size to 100 watt. The call sign of the new station - ZUO - where "UO" represented Union Observatory, has remained unchanged till the present day. ZUO is still the only time and standard frequency station on the continent of Africa, and in a very large part of the southern hemisphere.

In 1972 the time department was detached from the observatory in Johannesburg, and moved to Pretoria to become part of the Precise Physical Measurements Division of the National Physical Research Laboratory.

In 1974 it was formally laid down that, in terms of the Measuring Units and National Measuring Standards Act of 1973, the South African standard of time should be the cesium clock maintained for this purpose at the NPRL.

TIME AND FREQUENCY STANDARDS

In 1953 a set of six quartz oscillators using GT crystals, with associated frequency dividers, was obtained from the British Post Office, followed two years later by one Essen ring crystal. The ring crystal still remains in use today, but most of the others have long since stopped functioning, apparently due to failure of the solder connections.

A cesium beam standard was installed in 1966, and this has, with minor interruptions, controlled the South African time service until the present day. During this period the beam tube had to be changed on two occasions, after 26 and 61 months respectively. The cesium standard was from the beginning adjusted to give an AT output. For time signals the offset in use before 1972 was achieved by a special phase shifter, while the ZUO carrier frequency was

broadcast without offset.

A second South African cesium clock (not counting temporary installations for specific projects) was acquired by the S.A. Bureau of Standards at the beginning of 1975. The two clocks, which are located some 10 km apart, are now being regularly intercompared. All the same, one cannot feel altogether secure with a national time service which relies on two basic standards only - one of them at a distance.

Apparatus for generating the ZUO and other time pulses has always been designed and constructed locally, and we have by now gone through all the various stages, from vacuum tubes through cold cathode tubes and transistors to integrated circuits. The most recent unit combines all the following functions - very nearly the complete time service - in a single enclosure:

- Frequency dividers: 1 MHz to 1 pulse per day
- Provision for resetting and adjusting all stages
- Digital time display: both UT and SAST
- DUT1 code, with preset switching (*)
- Leap second preset switching (*)
- Morse code: ZUO and time, every 5 or 15 minutes
- Coded pulse output for controlling slave clocks in building
- Various other time pulses, e.g. "6 pips" every hour for broadcast stations.

(*) Preset on previous day, to obviate need for manual switching at 2 a.m.

TIME COMPARISON

The great distance between South Africa and the major centers of research which determine AT and UT - mostly in the northern hemisphere - leads to special problems in time coordination, and make the regular intercomparison of time signals, by every practical method, essential.

Between 1945 and 1960 the local clocks were checked daily with reference to the HF signals from WWV and WWVH. To keep the time signals in step with WWV without adjusting the oscillators, a motor-driven continuous phase shifter was constructed in 1955, which could modify the oscillator frequency from -20 to $+20 \times 10^{-9}$ in steps of 1×10^{-9}.

When in December 1960 the ZUO time signals were coordinated with those of other stations, the phase shifter was improved by the addition of an electronic drive, to give it a range

of from -99 to $+99 \times 10^{-10}$, in steps of 1×10^{-10}. (A new adjustable phase shifter built recently provides for adjustment between -999 and +999 microseconds per day, in steps of 1 microsecond per day.)

VLF Comparisons

The next step was to build two VLF receivers, permanently tuned to GBR and NBA. Phase measurements were made with the aid of a CRO, and manual adjustment. Used in conjunction with the phase shifter, these receivers now made it possible to keep the ZUO time signals within 1 millisecond of UTC, and to keep the mean ZUO frequency within about 5 parts in 10^{10} at all times.

Continuous VLF phase recordings are at present made by means of two commercial receivers, normally tuned to GBR and NAA, the two stations which in this region have proved to be the most reliable. By making use of the corrections published by the USNO it is usually possible to reconcile the various measurements to within a few microseconds.

Except for occasional disturbances due to lightning, this system has proved to be most reliable over long periods. It has sometimes been suspected that the results might be affected by seasonal variations in propagation time, but until now there has been no completely uninterrupted period sufficiently long to enable one to draw a definite conclusion.

Travelling Clocks

Absolute time differences have since 1966 been based almost wholly on the travelling cesium clocks which have been sent from time to time from the USA by the USNO and other organisations. Because such comparisons have often been motivated by the needs of particular projects, they have often taken place at rather irregular intervals, and with the recent closure of the local STADAN station there is some concern as to the future. It is highly desirable that these comparisons should continue, but it is also appreciated that one cannot expect other organisations to bear the full cost indefinitely. Future travelling clock comparisons will therefore probably have to be arranged by ourselves.

The emphasis will probably be strongly in favour of light and simple portable clocks, which should, if at all possible, have to travel by air unattended. Even if this meant that some stability might have to be sacrificed, this might

well be compensated for by faster return times and more frequent journeys.

Loran C

This has for some years been used by the STADAN station. As the distance to the nearest station (Lampedusa) is too large to make use of ground waves, accuracy is of the order of ±5 microseconds. The system therefore provides a valuable check on local time standards, and would give immediate rough synchronization after a complete interruption, but it cannot compete with travelling clocks for precision.

Satellites

More or less the same applies to the TRANSIT satellite comparisons made at the French Tracking Station, which can at present be relied on to within about 50 microseconds.

Local Comparisons

A portable rubidium clock has for the last year been used to make regular monthly time comparisons with the few organisations in the neighbourhood of Pretoria who need microsecond accuracy, viz. the French Tracking Station, the S.A. Bureau of Standards, and (until October 1975) the STADAN station at Hartebeeshoek. These comparisons have proved to be of great mutual benefit, and, if the demand warranted it, they could well be extended to other parts of the country.

The new television network at present being established offers good possibilities for time intercomparison, not only for local use, but perhaps over the whole country. At present, however, it is still too early to give results.

TIME DISTRIBUTION

ZUO Radio Signals

The ZUO signals in their present form date from the middle 1950's when, shortly before the start of the IGY, it was realised that the distribution of time in southern Africa was far from satisfactory. As it was impractical to emit radio signals at high power direct from the observatory, near the centre of Johannesburg, the South African Post Office took responsibility for time broadcasts from its new station at Olifantsfontein, about half-way between Johannesburg and Pretoria. Clocks and other time equipment remained

at the observatory, while the time signals, together with a 100 kHz standard frequency, were transmitted to Olifantsfontein by a 100 MHz radio link. At the receiver the standard frequency and time signals were separated, the former being multiplied to 5 MHz to provide the carrier frequency of the HF transmitter, which was then modulated by the latter.

New equipment installed around 1970 uses a frequency of 141 instead of 100 MHz, and the original 100 MHz transmitter was modified to transmit time signals only, as a useful service to the general public. When in 1972 the clocks were moved to their new location in Pretoria, the same equipment was used to transmit the signals to Olifantsfontein - almost the same distance as before, but now in the opposite direction. At the same time the 10 MHz transmission from Johannesburg was discontinued, and replaced by one on 2.5 MHz, which gives far more consistent results at night over the greater part of the country.

The question is asked from time to time whether such an indirect transmission system does not lead to a loss in accuracy, and the answer is, of course, that to a small extent it does. The delay between clock and 5 MHz transmitter output was measured to be about 270 microseconds, and radio propagation time accounts for about 100 of these. There are bound to be fluctuations, but users of HF signals will in any case have to contend with very much larger changes in the travel time of the HF signals themselves.

Present users of time in South Africa, and probably elsewhere, can be conveniently classified in three groups:

(A) Those who demand an accuracy in the microsecond region and beyond;
(B) Those who need millisecond accuracy, e.g. surveyors, geophysicists, astronomers;
(C) The rest, usually satisfied with an accuracy of 1 second or more.

Groups (B) and (C) are both adequately served by the ZUO transmissions, and it is only group (A) which requires special attention. It is as yet a very small group, confined to those who maintain clocks of accuracy comparable to that of the cesium clock, e.g. for satellite tracking. In the immediate neighbourhood of Pretoria these users have sometimes been able to use the 141 MHz transmissions direct, but on the whole a portable clock comparison has been more satisfactory.

Other time distribution systems

Two systems intended primarily to serve group (C) are the broadcast hour signals, and the "Speaking Clock" service provided by the telephone department. Before 1972 both signals were controlled by the observatory clocks. This came to an end when the clocks were moved to Pretoria, and since then both the S.A. Broadcasting Corporation and the Post Office have generated their own time signals, with varying degrees of success. Neither signal can at present be relied on to supply precise time.

What follows are brief descriptions of three items of apparatus developed by the author for time service use.

CODED TIME PULSE UNIT

The use of coded hour and minute data in conjunction with time signals is fairly common (as, for instance, in the case of transmissions from WWV and DCF77) but no cases are known of the time pulses themselves being used to transmit hour, minute and second data. The unit to be described, which uses this method, was developed for time distribution by line within the laboratory. It provides a digital hour, minute and second display, together with audible second and minute pulses, without any distracting audible code.

A BCD time code requires 7 bits each for minutes and seconds, and 6 bits for the hours : a total of 20. The second signals are therefore made to consist of 20 pulses, at a rate of 2000 Hz, i.e. a total length of 10 milliseconds per second. Each pulse is either short, representing "0", or long, representing "1".

The coded pulse generator is shown in the simplified schematic diagram of Fig. 1. A 20-stage parallel-in serial-out shift register is preset every second by a preset enable signal from the controlling clock. Also obtained from the clock are the sequences of 2000 Hz pulses: 20 at every second and 1000 at every minute. The output pulses are produced by two monostable multivibrators, which produce pulses of duration 50 and 250 microseconds respectively. Every input pulse produces a 50 μs. output pulse, but a 250 μs. pulse is produced only when the shift register output is "1". The output is therefore a sequence of pulses which are short or long depending on the state of the shift register output.

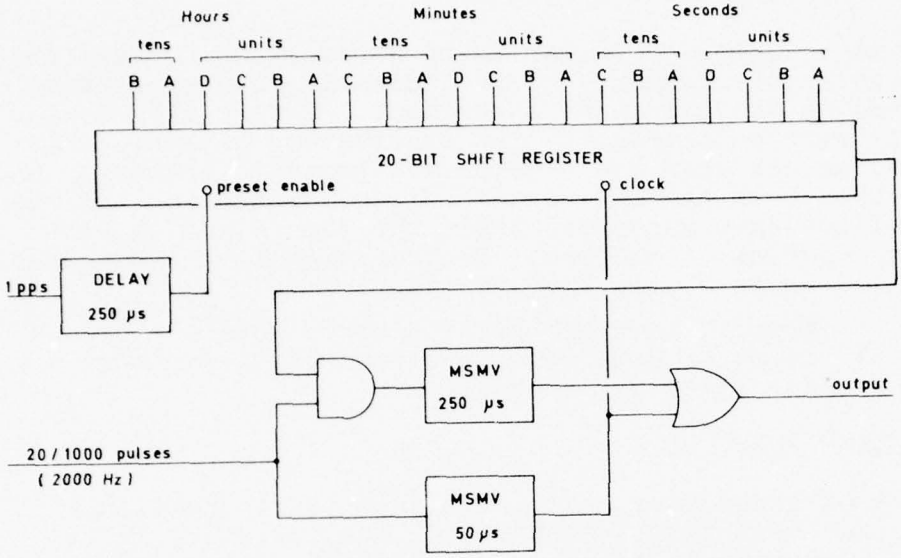


Fig. 1-Coded time pulse encoder
(master clock unit)

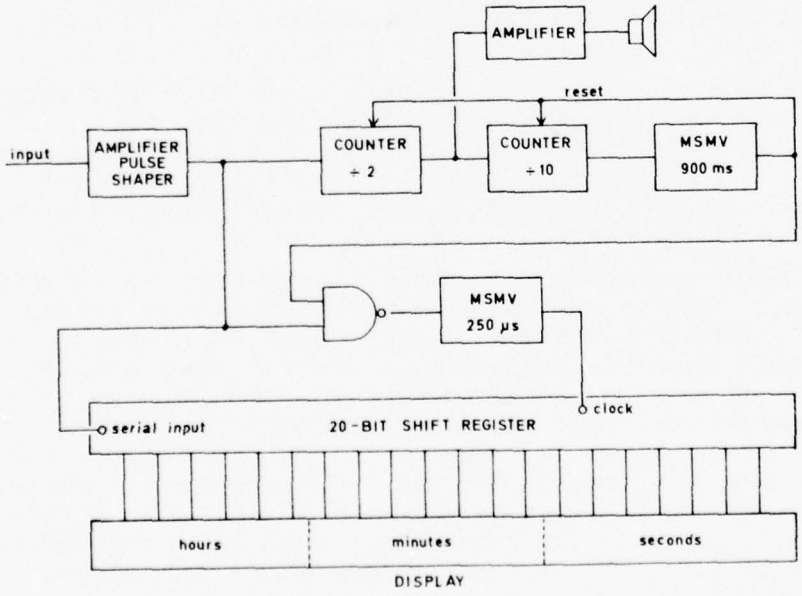


Fig. 2-Coded time pulse decoder
(remote unit)

Figure 2 shows the decoding and display unit, which uses a serial-in parallel-out shift register. Two counter stages dividing by 2 and 10 respectively trigger a monostable multivibrator after the 20th pulse, which resets and disables the counters for a period of just under a second, and prevents any further pulses reaching the 'clock' input of the shift register. When a minute signal occurs, therefore, only the first 20 pulses will be registered.

The loudspeaker is fed from the output of the first counter (divide by 2) so that the audible second signal consists of ten identical 1000 Hz pulses, irrespective of whether the incoming pulses are short or long.

SOLAR-TO-SIDEREAL TIME CONVERTER

Solar-to-sidereal time converters have a very long history. Dondi's astronomical clock of 1360 was probably the first instrument which used mechanical gears to indicate solar and sidereal time simultaneously. The ratio used was the simple one of 366/365, but since Dondi's time numerous other ratios of ever increasing complexity have been proposed, many of them ingenious rather than practical.

It is understandable that the first electronic converters tended to be designed on similar principles, with frequency dividers and multipliers now taking the place of mechanical gears. One of the first units of this kind, which had an accuracy of 1×10^{-12}, was built by the author as long ago as 1949 (Hers, J., Nature, vol. 164, 841).

Digital circuitry has now suggested a much simpler approach, based on the same principle as the adjustment of the calendar by the introduction of leap years. A first correction is made by adding an extra pulse to the clock input after every count of, say, A pulses, where A is the nearest appropriate count obtained within the clock itself, or a count closely related to it. If this correction proves to be too much (or too little) a second correction is made by deleting (or inserting) a pulse after count P (or count B), and the process may be continued indefinitely until the required accuracy is reached. Normally each additional stage will increase the accuracy by a factor of about 100.

Figure 3 shows two possible arrangements. In the upper diagram the pulses from the various divider stages of the clock are fed back to the input of the clock itself. The output therefore consists of sidereal time pulses only.

In the lower diagram the correcting pulses for the sidereal output are obtained from a parallel solar time divider, so

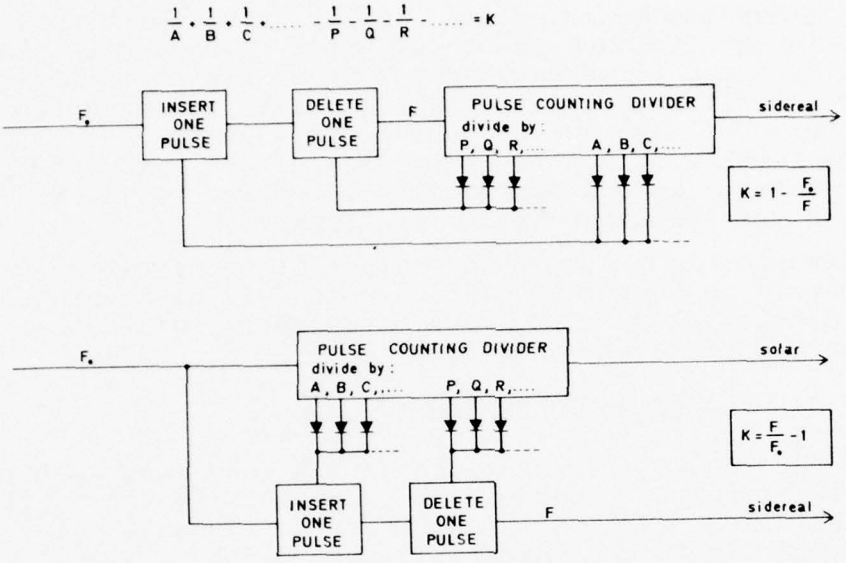


Fig. 3-Solar-to-sidereal time converter
Principle of operation

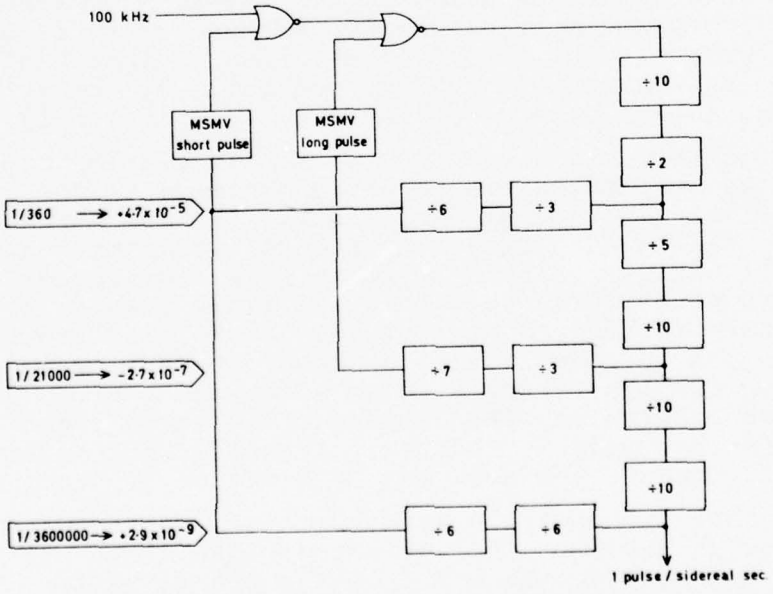


Fig. 4-Solar-to-sidereal time converter
Example of a practical design

that both solar and sidereal time pulses are obtained. (Sidereal time divider not shown.)

A practical circuit is shown in Fig. 4. Here the input consists of a 100 kHz square wave, which triggers the first counter on the high-to-low transitions. After every count of 360 a monostable multivibrator applies a pulse, which is short in relation to the input pulses, to the first NOR gate, thus inserting one extra pulse, and increasing the total count by 1.

After every count of 21 000, a second multivibrator feeds a long pulse - approximately $1\frac{3}{4}$ times the duration of one cycle of the input frequency - to the second NOR gate, which suppresses the next pulse, and decreases the total count by 1. After a count of 3 600 000, a pulse is once again inserted.

The average rate of the output pulses is:

4.7×10^{-5} high after the first correction,
2.7×10^{-7} low after the second correction,
2.9×10^{-9} high after the third correction,

and the error may be made as small as desired by adding further stages.

ZUO MORSE CODE GENERATOR

In a bilingual country such as South Africa time announcements would have to be made in both official languages, and it was therefore decided at an early stage that the ZUO transmissions should use morse code rather than voice announcements. The original code generator used mechanical contacts to produce, every 15 minutes, the announcement:

ZUO ZUO ZUO (followed by hours and minutes)

and this was kept in operation for nearly 20 years, although it was never as reliable as it should have been.

In 1973, therefore, a new all-solid-state unit was developed, which not only was capable of giving time announcements every 5 instead of every 15 minutes, but which proved to be simpler and more versatile than any similar device of which descriptions could be found.

It is based on the principle that in the morse code the digits 0 to 9 are represented by a group of 5 dots and/or dashes, arranged in a regular progressive sequence, as shown in Fig. 5. If, therefore, a 10-stage shift register is made to generate a continuous sequence of 5 dots followed by 5 dashes, any digit may be obtained by entering the ring

at the appropriate point, and stopping after the fifth stage.

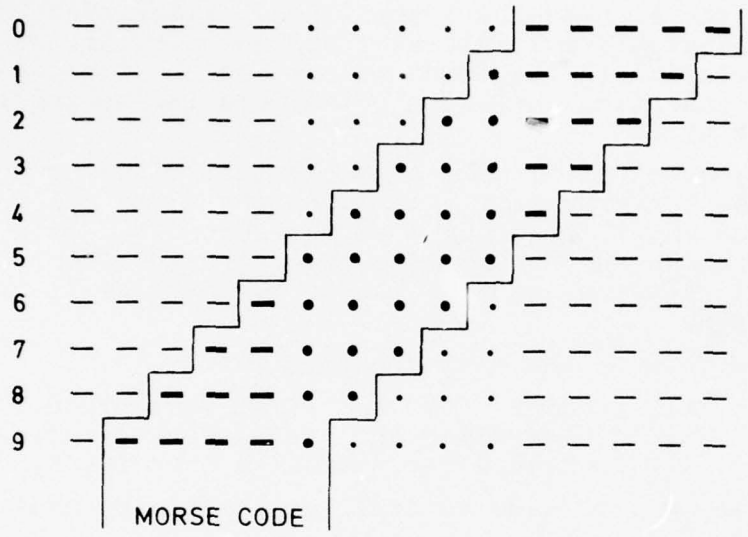


Fig. 5-Morse code characters for digits

If, instead of counting 5 consecutive symbols, one counts 4, 3, 2 or 1, the same system may be used to obtain 17 out of the 26 letters of the alphabet, as shown in the large rectangle of Fig. 6. The remaining 9 letters may be formed by combining two simpler characters, e.g. Q can be formed by M followed by A. In the case of ZUO this was fortunately not necessary.

The simplified block diagram of Fig. 6 can best be explained by starting at the end of the chain, with the SYMBOL GENERATOR. This is a 4-stage shift register which produces an output of either a dash followed by a space, or a dot followed by a space, depending on whether the sequence is started at A or at C. This shift register is clocked at a constant rate of about 10 Hz, designated in the diagram as "clock 1". (In the case of ZUO it is 8.33 Hz.)

A sequence of 'preset' pulses, to produce the sequence of dots and dashes which correspond to the required morse code characters, is derived from the CHARACTER GENERATOR, i.e. the 10-stage shift register already mentioned. Five stages

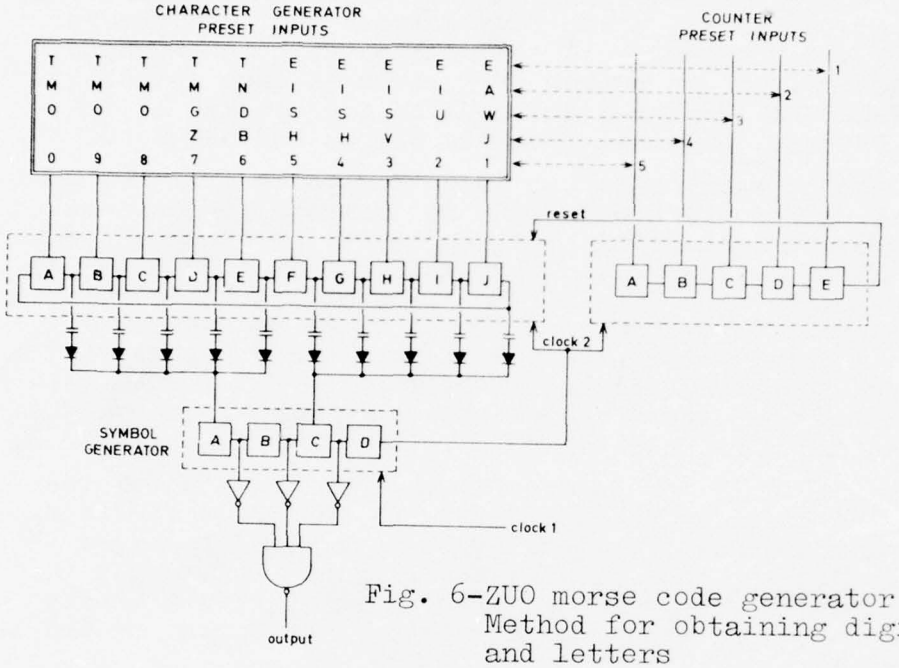


Fig. 6-ZUO morse code generator
Method for obtaining digits and letters

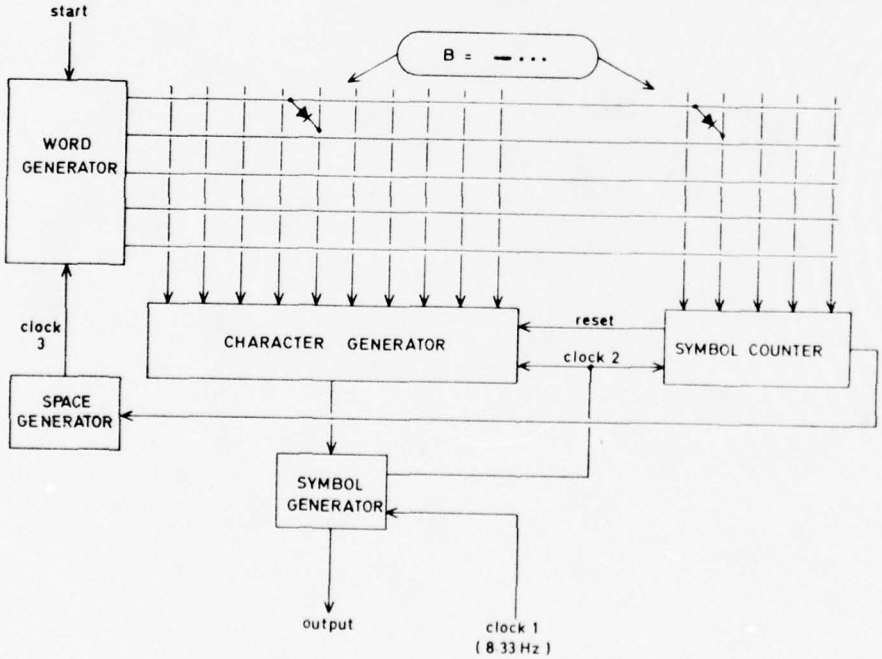


Fig. 7-ZUO morse code generator
Simplified block diagram

of this trigger the 'dash preset' input of the SYMBOL GENERATOR (A), while the other five trigger the 'dot preset' input (C). It operates in conjunction with the COUNTER, which determines the number of symbols in each character. Both CHARACTER GENERATOR and COUNTER are clocked at the "clock 2" rate, obtained from the SYMBOL GENERATOR output.

At the end of each character an output pulse from the COUNTER enables the SPACE GENERATOR to insert an additional space between characters, and feed a "clock 3" pulse to the WORD GENERATOR (Fig. 7). This again consists of a series of shift registers containing as many stages as there are characters to be transmitted. Each stage is connected, through a diode matrix, to one of the preset inputs of the CHARACTER GENERATOR and to one of the COUNTER inputs. As an example, the diagram shows the connections necessary to generate the morse code symbols representing the letter B.

The complete unit for generating the ZUO code, which includes the decoding necessary for the various 5 minute time announcements, consists of 34 type 74 IC packages, mounted on three 100x160 mm boards. Since it was put into service nearly two years ago there has not been a single instance of malfunctioning, a notable improvement on the previous unit.

QUESTION AND ANSWER PERIOD

DR. KLEPCZYNSKI:

The paper is a historical survey of South African time system. I am sure the paper has reflected these problems and pitfalls correctly.

MR. SMITH:

Smith, Royal Greenwich Observatory.

I would like to ask a question and Dr. Klepczynski needn't worry, it is not going to embarrass him in any way, I am sure. It concerns the original abstract which was given of Jan Hers' paper concerning the BCD code for giving the time signals.

Now, a similar suggestion has been put forward by Dr. Becker. He has proposed that time signals should carry a BCD coding giving the difference between the signals in UTC and the UT-1. It does appear that the navigators for whom the DUT-1 code was originally suggested are not, in fact, making use of it. It seems to have a very limited application indeed.

Nevertheless, there must be many people who would like to know the difference on a current basis between UTC and UT-1. It may, therefore, well be a better proposition to use a BCD coding rather than the very simple system which was intended for oral use by the navigator. I wondered whether at this meeting it might be possible to get any expression of opinion; first of all as to whether the DUT-1 code is proving of any practical value whatever in the form in which it was recommended by CCIR; whether there is any need for current information on the difference between the signals in UT-1; and whether CCIR should give consideration to whether this can best be given on the signals in a BCD coding.

This is a very urgent problem because the CCIR will be meeting early in the new year and one of the tasks of study group 7 will be to consider any possible modifications of the present system. Thank you.

DR. KLEPCZYNSKI:

Does anybody in the audience care to make a comment on Mr. Smith's proposal?

First of all, has anybody here in the audience utilized the DUT-1 audible code? Do we have users of that in the audience right now? Seriously, if in any way you use this code, please say so right now because this could have serious repercussions.

DR. BEEHLER:

Beehler, National Bureau of Standards.

I am not really a user, of course, of the DUT-1, a supplier rather. But, I might mention that the National Bureau of Standards recently conducted a major survey of its users and the conclusions from that, at least one conclusion, was that while there is a small group of people who said yes, the DUT-1 code is important to us, it is a very small group, at least as indicated by this survey, and there are some numbers that I could give. I don't have them on top of my head, but if someone is interested, I can get those numbers.

But, it was by far the least-used service of eight on the WWV and WWVH format. So, our conclusion is that it is, indeed, a very small group that we seem to be serving with the present technique.

DR. KLEPCZYNSKI:

I have a question. Of those who responded, who did use the audible signal. Could they in turn use a coded signal?

DR. BEEHLER:

The distribution of the users that said it was important to them seemed to show no particular trend. That is, they weren't navigators in particular, as you might expect. It was just almost down in the noise for all of the 14 user categories that we looked at, the weighting of these user categories were almost constant in their use of DUT-1. There was no peak for navigators or any other particular group. I think the group that included seismologists was actually the largest.

DR. KLEPCZYNSKI:

That is interesting. I think you recall a study made by Japanese navigators -- they do use DUT-1 code for navigation.

DR. WINKLER:

I would like to comment on that also. I think, number one, that no users can be expected to be representative here. Number two, the navigators, evidently in the large majority, do not use the DUT-1 code because for regular celestial navigation it is not important. It is below or at the level of other inaccuracies. The accuracy of a sextant sight is 1 minute of arc which would translate into several seconds of time, so a fraction of a second of time is really not their concern unless they want to be perfectionists, and there are only about 5 percent perfectionists in any profession.

Another point is another group of users, the geodesists, which would require the DUT-1 correction, are not aware of it. They don't even know about it. This surfaced during the last meeting in Grenoble of the International Union for Geodesy and Geophysics, at which discussion revealed the fact that there is a considerable need for education of these people. They are not even aware of it.

That leads me to a reply to Dr. Smith's comments. I would take the position that whether there is any use or not, it should not be changed within the next five years because the learning period seems to be on the order of between five to 10 years and if you make a change every two, three or four years you will always lose all of these users. Whatever you do, I think we must have the courage and the perserverance to hold on to a system which, fortunately, we have been able to agree upon internationally. It is a sensible system. It may not be the best one. In fact, I don't think it is the best one of all possible systems, but to change it again, after only three or four years, I think would be sheer madness and I am strictly against that, whether it is used or not.

RECENT CHANGES AND FUTURE TRENDS IN NBS TIME AND FREQUENCY DISSEMINATION SERVICES

R. E. Beehler, D. W. Hanson, and D. D. Davis
(National Bureau of Standards), Boulder, Colorado

ABSTRACT

During the past two years a number of improvements have been made in the NBS Time and Frequency (T/F) Dissemination Services. These range from making the WWVB 60 kHz broadcasts available on a continuous basis to implementing a new nationwide frequency calibration service using television techniques. NBS now provides regularly published calibrations of both the East Coast and the West Coast commercial TV network subcarrier frequencies for use as a transfer standard. With these data a user anywhere with access to a TV network signal can easily and inexpensively determine his oscillator's frequency. An accuracy of a few parts in 10^{11} relative to the NBS Frequency Standard is obtainable with only 15 minutes measuring time. Several versions of NBS-developed user equipment are described, covering a broad range of required user involvement, cost, and complexity.

During the first half of 1975 the NBS conducted an extensive survey of WWV/WWVH users to obtain their views relating to possible reductions in the present broadcast services. A summary of the results of this survey, based on about 12,000 responses, is included along with a discussion of possible actions to be taken by NBS to reduce operating costs of these services. Future trends in NBS T/F dissemination services are discussed with special emphasis on the objectives and major milestones of the NBS program to disseminate T/F information via satellite. The NBS program to provide an eventual full WWV-type service via satellite on the internationally allocated 400.1 MHz frequency is outlined, including its present status. Current efforts are centered on providing experimental time code transmissions from one of NOAA's GOES geostationary satellites and on developing detailed requirements for the later permanent service.

PRECEDING PAGE BLANK-NOT FILMED

INTRODUCTION

Since 1923 the National Bureau of Standards (NBS) has distributed highly accurate time and frequency (T/F) reference signals via radio broadcasts. Throughout the years many improvements have been incorporated into these broadcasts to provide greater coverage, easier-to-use information, more reliable reception, more useful formats, and higher accuracy. Some of the major milestones along the way are included in reference [1], which is a general description of the present NBS time and frequency dissemination services.

For many years the high-frequency (HF) time and frequency signals broadcasted from NBS station WWV (and since 1948 from WWVH in the Pacific area) were generally adequate to meet the needs of most users. The inherent reception accuracy limitations of about 1×10^{-7} in frequency and 1 ms in time, imposed mainly by variations in the propagation medium, caused significant problems in relatively few application areas. More recently, however, as the state-of-the-art in T/F technology advanced rapidly and as more and more applications came to depend in important ways on T/F technology, it became apparent that improved T/F dissemination methods were needed. The NBS responded in the 1960's by inaugurating low-frequency (LF) broadcasts from WWVB on 60 kHz and very-low-frequency (VLF) broadcasts from WWVL on 20 kHz. These broadcasts provided widespread T/F reference signals that were much less affected by the propagation medium. Under favorable reception conditions, where measurement averaging times could be extended to many hours or days, the LF and VLF signals permitted frequency comparisons to 1×10^{-11} or even better and time (phase) comparisons at the microsecond levels.

During the same period NBS began to explore other methods for distributing T/F information that might potentially offer better accuracy, reliability, coverage, and convenience than the radio broadcast services. Eventually, three dissemination techniques which seemed to offer the most promise were selected and funded for further development into new NBS T/F dissemination services. In all three cases the basic T/F information was to be "piggybacked" onto existing widespread information-distribution systems, consisting of the nationwide television network facilities, certain satellites of opportunity, and the Omega Navigation System broadcasts.

The following sections of this paper describe the progress to date and the relevant future plans for implementing and improving these new NBS services. In addition, conclusions and potential implications from the recent survey of 12,000 WWV/WWVH users are summarized.

WWV/WWVH SURVEY CONCLUSIONS

During the first half of 1975 NBS conducted an extensive survey, by questionnaire, of WWV and WWVH users. The survey was motivated by a desire on the part of NBS to explore various means for reducing the broadcast services' operating costs with as little adverse effect on the users as possible. While the survey was designed to identify those transmission frequencies or features of the format that might be discontinued with some net cost and/or energy savings, it was also recognized that the responses could provide other valuable information about the broadcast services and those who use them.

A single-page questionnaire was designed, which allowed the user to indicate his use and estimate the importance of each of the WWV/WWVH frequencies and the different forms of information contained within the broadcast format. Information was also requested on the user's geographical location, reception conditions, classification, and particular application. Space was provided for additional miscellaneous comments.

The questionnaires were distributed as widely as possible by a variety of means. About 1,500 copies were sent to those on NBS Time and Frequency Division mailing lists, and another 13,000 went to lists compiled by several yachting/boating organizations and the National Weather Service. The availability of the questionnaire was announced in voice several times per hour on both WWV and WWVH. A number of magazines and other publications, with combined circulation of several hundred thousand, printed editorials or brief publicity items about the survey. Finally, at least 10 periodicals, with a combined circulation of about 250,000, published the questionnaire itself. At the end of the survey period a total of 12,050 completed responses had been received. Twenty-three per cent of these responders purported to "officially" represent more than their own individual use of the services.

Figure 1 shows the geographical distribution of the responses. Every continent is represented in the totals. Figure 2 indicates how the users classified themselves within the 14

possible categories given on the questionnaire. In retrospect, it is now clear that three major categories were overlooked and hence tend to be lumped into the "other" group. These three are private citizen, watchmaker/jeweler, and amateur radio operator. It should be noted that in many cases users checked more than one classification category, resulting in the totals in figure 2 being greater than the number of individual questionnaires returned.

Figure 3 shows the relative use of WWV, WWVH, and the telephone time-of-day service from WWV available via the regular commercial number (303) 499-7111. The 0-3 numerical rating in each case is a weighted average of all responses where the weights 0, 1, 2, and 3 have been assigned to the four choices given on the questionnaire for "Frequency of use"--i.e., "Never," "Rarely," "Sometimes," and "Frequently," respectively. While WWV is obviously the most-used service, it is interesting to note that the least-used service, the telephone time-of-day service, receives more than one million calls per year.

Figure 4 summarizes the data on how often the various WWV/WWVH broadcast frequencies are used, again using the same 0-3 scale discussed above. Clearly, most users depend on the 5, 10, and 15 MHz transmissions. These results are not really surprising, of course, since (1) the radiated power is highest on these frequencies, (2) many commercial receivers are designed to receive 5, 10, and 15 MHz only, and (3) the present phase of the sunspot cycle tends to adversely affect the propagation characteristics of the higher frequencies of 20 and 25 MHz.

Figure 5 displays the rating (on the 0-3 scale) for each of the 14 user categories and for each of the 8 services provided by WWV and WWVH. Also shown on the matrix are the overall ratings and the sizes of each of the user categories. The 0-3 numerical ratings within the matrix represent the concensus response for a given population (i.e., a specific user group) with respect to one of the 8 WWV/WWVH services. The specific number is a weighted average of the individual responses to the question: "To what extent do you use the following information (followed by a list of the 8 services)?", where the numbers 0, 1, 2, and 3 refer to "Never," "Rarely," "Sometimes," and "Frequently," respectively, as before. The overall ratings given in the "Services" column provide a composite score for each service based on the responses of all users, irrespective of their particular user category. The most obvious features of the matrix are that

the voice time-of-day announcements are uniformly the most used aspect of the WWV/WWVH broadcasts, and the DUT1 values are uniformly the least used.

The questionnaire also invited the participants to make any miscellaneous comments about the WWV/WWVH services. More than 5,000 of the responders took advantage of this opportunity. A few of the more frequently recurring suggestions include:

a) Do not reduce radiated power--reception is already marginal
b) Add NBS time signals to VHF weather broadcasts
c) Reinstate time signals in Morse Code
d) Add weather information for the continental U. S.
e) Add one or more low-power repeater stations on the U. S. East Coast
f) Provide more detailed weather, geoalert, and radio propagation information and do it more often than once per hour
g) Reduce costs by eliminating some frequencies (2.5, 20, and 25 MHz were mentioned most often)
h) Make the WWV-by-phone number a toll-free service from anywhere in the U. S.

For a representative selection of verbatim comments taken from the returned questionnaires, as well as for more detailed results from the survey in general, see reference [2].

POSSIBLE CHANGES IN NBS BROADCAST SERVICES

As of this date (November, 1975) final decisions have not yet been made on possible reductions in WWV/WWVH services. The survey did reveal, however, that the present services are heavily used and strongly supported--especially, the primary frequencies of 5, 10, and 15 MHz. As a result, it is clear that there will be no reductions in service on at least those frequencies. If any service reductions do become necessary, the data in figure 4 suggest that minimal impact on users would result if reductions are confined to one or more of the 2.5, 20, or 25 MHz transmissions.

One cost-reduction plan under active consideration would couple the elimination of some of the lesser-used transmission frequencies with the implementation of partially automated operation at WWV and WWVH. The transmitters freed by the reductions in service would become dedicated backups for the primary 5, 10, and 15 MHz transmissions, with highly automated switchover systems to provide high reliability with unmanned operation. By thus reducing labor costs, substantial savings

may be realizable which could then be used in the continued development of new improved T/F dissemination services, such as a satellite-based operation.

NEW/EXPANDED NBS T/F DISSEMINATION SERVICES USING TELEVISION

Time Comparisons Using Line-10 Method

The time comparison technique known in the U. S. as the line-10 method was first used successfully in Czechoslovakia during the mid-1960's [3]. The technique basically consists of using a particular horizontal synchronization pulse in the normal television picture format (tenth line of the vertical interval, odd field) as a passive transfer standard for comparing two clocks within common view of the television transmission [4]. The method may be used either locally, where the two clocks can be compared with the TV pulse from a single TV station, or over widespread geographical areas, where the same network broadcast can be received simultaneously at both sites. In the local mode clock comparisons to 100 ns or better are possible (if the differential path delay is known sufficiently well), while comparisons to a few microseconds are usually possible using network transmissions to link widely separated clocks.

For several years both NBS and the U. S. Naval Observatory, as a service to users interested in making time comparisons with the NBS and USNO master clocks, have published regularly their calibrations of the three commercial TV networks' line-10 pulses at selected specified times each day [5,6]. A user wishing NBS traceability, for example, need only compare his local measurement of the received line-10 pulse with the similar measurement for that network published by NBS. Even if the appropriate path delay is not known for the local measurement, repeated comparisions--e.g., on a daily basis, can show easily whether the local clock is gaining or losing time relative to the UTC(NBS) time scale, assuming the unknown path delay remains constant. Possible changes in the network path delay can usually be detected by comparing results from measurements on two or three networks, since delay changes are usually uncorrelated.

One limitation in the past on use of the line-10 method has been the lack of NBS traceability for users in the western U. S. (Pacific Time Zone). The problem existed because: (1) the TV network signals available to West Coast users are originated in Los Angeles independently of the New York-originated transmissions; and (2) only the East Coast networks

can be received and thus calibrated by NBS in Boulder, Colorado.

Since August 1975, this limitation has been removed through a cooperative measurement program between NBS and the Hewlett-Packard Co. in Santa Clara, California. Daily measurements of the major West Coast networks' line-10 pulses are made at Hewlett-Packard Co. and then referred to the UTC(NBS) time scale by using the known relationship between the local time scale maintained in Santa Clara and UTC(NBS). The uncertainty in the West Coast-NBS link is about 1 μs. The publication [5] of both the West Coast and East Coast line-10 data referred to UTC(NBS) thus makes the technique useful on a nationwide basis. Commercial equipment to use this service is now available from several sources for several hundred dollars.

Frequency Comparisons Using 3.58 MHz Color Subcarrier

Use of the network television subcarriers as frequency transfer standards was first proposed by NBS more than four years ago [7]. Advantages include a high-resolution, stable signal originated from rubidium frequency standards at the three commercial television network operating centers in New York and Los Angeles. The frequency offsets of the network rubidium standards are measured daily and published in the NBS Time and Frequency Services Bulletin. Triple redundancy (3 networks) assures the user of a reliable signal traceable to NBS with uncertainty of less than $\pm 3 \times 10^{-11}$ for 15-minute averaging times. This represents almost four orders of magnitude improvement over HF calibration, using WWV or CHU. WWVB on 60 kHz can usually provide a calibration uncertainty of $\pm 3 \times 10^{-11}$, but only with many hours of averaging time.

The general concept of the new NBS frequency calibration service via television is illustrated in figure 6. The user, located anywhere within the U. S. where he can receive a network-originated program from one of the three commercial networks, simply makes a frequency comparison of his local oscillator with the network color subcarrier frequency available from a slightly modified color TV set. A comparison of this measurement result with the published frequency offset for that same network as calibrated by NBS provides the NBS-traceable calibration of the local oscillator. NBS has also devoted considerable effort to encouraging the commercial development of several forms of user equipment based on this technique.

As in the line-10 case discussed previously, NBS calibration of the TV network signals on a nationwide basis is complicated by the fact that East Coast and West Coast originated network signals, and hence the color subcarrier frequencies involved, are generated independently. The situation is illustrated in figure 7. The East Coast network signals are received in Boulder and calibrated directly. The West Coast-originated signals are measured via an NBS automated measurement system located in Los Angeles. The comparisons are made with respect to the ABC East Coast signal which is transmitted into the Los Angeles area for internal network use, thus providing a link between measurements made in Los Angeles and Boulder. This extension of the frequency calibration service via television to users in the Pacific Time Zone has been operational since April 1975, when NBS began regularly publishing the frequency offsets for the West Coast networks in its Time and Frequency Services Bulletin.

NBS has developed four versions of user equipment for measurement of the frequency offset between the 3.58 MHz network subcarrier and the oscillator to be calibrated. All methods depend on measurement of the period of the "beat note" between the network subcarrier and the oscillator being calibrated. Typically, this beat note period is approximately 9.3 seconds for the nominal -3000×10^{-11} offset of the network subcarriers.

The simplest version, known as the color bar comparator [8], connects easily to the antenna terminals of any color TV set and generates a colored bar on the screen. The colored bar cycles through a changing color sequence at a rate which depends on the frequency offset between the oscillator to be calibrated and the TV network subcarrier frequency. The measurement is made by manually timing with a stopwatch the period of the changing color cycle and performing a simple calculation with the result. Accuracies of 1×10^{-9} to 1×10^{-10} are possible. Commercial versions are available for about $100 plus the cost of the TV receiver.

The second version of NBS-developed user equipment requires a slight modification to the TV receiver but provides a square wave output of the beat note [8]. The period of the beat note may then be measured on any digital counter. A phase cursor output is provided for coarse frequency adjustment. A commercial version of this type is also available which displays the period measurement on an LED display and provides accuracies of about 1×10^{-10}.

A more accurate and easy-to-use beat note calibrator is called the "NBS System 358 Frequency Measurement Computer" [8]. This unit, shown in figure 8, provides a multiple digital readout of the frequency offset between the oscillator being calibrated and the network subcarrier. Operation is completely automatic, with multiple cues for easy user interpretation.

This display is presented on the screen of the 5-inch color televison receiver that also is used to supply the 3.58 MHz signal that is phase-locked to the network color burst.

The network rubidium standards are offset a nominal -3000 x 10^{-11} with respect to the NBS Frequency Standard. When a phase comparison is made with a locally generated 3.58 MHz signal with zero offset, the result is a full cycle of phase difference, or a "beat note" with a period of about 9.3 seconds. The offset computer measures the period of each beat note cycle and digitally computes the corresponding offset for that beat note period.

The left column of 4-digit numbers displayed is the offset readout for the ten most recent beat note periods, about 93 seconds of data at the nominal -3000 x 10^{-11} offset. Each of the 4-digit numbers in the right column is the average of ten readings in the left column. An average of the right column would therefore represent about 900 seconds, or 15 minutes of data.

The phase cursor provides an analog indicator of the phase difference between the local oscillator being calibrated and the 3.58 MHz television signals. The phase cursor has a "sawtooth" response that provides advance/retard phase sensing. If the oscillator being calibrated is "on frequency," the phase cursor will move slowly from left to right and rapidly retrace right to left with a period of about 9 seconds. Frequency response of the phase cursor allows the viewing of beat notes greater than 2 kHz. The system can therefore view offsets approaching 1 x 10^{-3} while allowing the user to calibrate his oscillator with an uncertainty of a few parts in 10^{11}.

Use of the measurement computer requires practically no training. The only operator adjustments required are tuning the companion television receiver to the correct channel and pushing a "reset" button that resets the display to all zeros. With a few minutes of instruction, a technician

should be capable of calibrating a stable crystal oscillator to within a few parts in 10^{11} in about 15 minutes. Commercial versions of this type of equipment are available for $2000-$3000.

Microprocessor Offset Computer (MOC)

A microprocessor version of the offset computer has recently been developed by NBS. A block diagram of the "MOC" system is shown in figure 9.

The "MOC" system was primarily developed to provide the TV network color subcarrier offset calibration published in the monthly Time and Frequency Services Bulletin. The microprocessor can store, and read out on command, four weeks (28 days) of data for each of the three networks plus a fourth comparison channel.

Figure 10 shows a one-week sample of microprocessor data for each network. In this case the "MOC" system was interrogated early on November 17, at which time only two or three 15-minute averages of each network's frequency offset had been accumulated for that day. The system then provides the daily averages for each network and the number of measurements acquired. A weighted average is also performed and printed out, using all valid 15-minute samples from the preceding seven-day period.

Although we have a very limited amount of experience with the "MOC", it appears that the standard deviation for weekly averages (30 hours of data/week) is less than 2×10^{-12}. This performance would improve in locations where more "live" network programming is available.

The microprocessor receives data from four independent "beat note" time interval counters. For network programming, and with a nominal offset of -3000×10^{-11}, the period measurement will be ~9.3 seconds. (The four-digit counters utilize a 500 Hz time base and the actual BCD four-digit count is nominally 4650. The microprocessor normalizes the offset readings by dividing them into 13968250.)

Since the microprocessor operates 24 hours per day, it receives much more local station 3.58 MHz than live network. A three-step screening process is used to reject this "bad" non-network data. Each of the four data channels has a 16-digit

"screening" word that can be entered through the keyboard interface. The format of the screening work is shown below:

300864 040 012 003 0

A B C D E

where group A = expected offset in parts in 10^{13};
group B = single period (1P) window in parts in 10^{11};
group C = 10 period (10P) window in parts in 10^{11};
group D = 100 period (100P) window in parts in 10^{11}; and
group E = 0 for ABC network, 1 for CBS, 2 for NBS, and 3 for the standard.

Each 10-second (1P) measurement is subtracted from the expected offset, and the absolute difference (without regard to sign) is compared to the 1P window. If the difference is less than the window, the 1P data are saved. After accumulating ten 1P values the screening process is repeated. All 10P data that pass are saved to form a 100P (15-minute) average. If the 100P data pass the screen, they are added to the daily total of 100P readings.

The expected offset of the screening word is changed weekly so that it is usually within 3×10^{-12} of the measured weekly average. The 3×10^{-11} 100P window represents at least 4σ for these data. The selection of the 1, 10, and 100P windows is a compromise between rejecting outliers and "skewing" the output data if the expected offset is in error.

The microprocessor, four comparators, four 4-digit counters and TTY interface are on a single 7" x 15" card. In one version, the microprocessor and power supply are in one 3 1/2" rack mount case, and the TV tuners are in a second 3 1/2" rack mount case. A second version will have the complete "MOC" in a single 7 1/2" x 16" rack mount.

FUTURE TRENDS: SATELLITE T/F DISSEMINATION

NBS has been studying the feasibility of introducing a new time and frequency service using geostationary satellites. This service would operate on the frequency of 400.1 MHz, a primary service allocation for space-to-earth broadcasts of time and frequency information.

Studies at NBS have indicated a growing need to improve the quality of our time and frequency broadcasts. They are deficient for many applications in terms of signal reception reliability, accuracy, and their ability to be processed by the user's equipment automatically.

Past experimental efforts by NBS with geostationary satellites--i.e., ATS-1, ATS-3, ATS-6, LES 6, TACSAT, and SMS-2, have verified the obvious superiority of satellite broadcasts to provide orders of magnitude improvement over our HF services via WWV/WWVH [9]. There are positive indications, also, that a satellite T/F service can save on operation expenses while still allowing for user equipment cost comparable to that required for WWV and WWVH.

The 400.1 MHz allocation is international in scope and is a primary service allocation. It confines the T/F emissions to within ± 25 kHz of the center frequency and also provides ± 25 kHz guard bands. Our studies and experiments indicate that this allocation can support a 1 μs time system with voice, ticks, tones, and an effective time code. User equipment can range from a low-cost receiver and antenna (a single quarter wave dipole) to a sophisticated system which automatically corrects itself for propagation delay and eliminates nearly all the interfacing so prevalent to terrestrial systems in existence today.

The service will not come into existence before the early 1980's, but definite plans are underway. Just recently NASA has agreed to begin a systems design and feasibility study, which should be completed by the end of FY 77.

As an interim step on the way to providing the permanent, complete T/F dissemination service on 400.1 MHz, NBS is currently transmitting an experimental time code on 468.825 MHz via NOAA's Synchronous Meterological Satellite/ Geostationary Operational Environmental Satellite (SMS/GOES) series.

The time code is used by NOAA in their data-collection program, where SMS/GOES meterological satellites collect data from remote observing platforms such as buoys, automatic weather stations, ships, aircraft, and balloons. Many of these platforms will use the time code to date the data as they are collected or to time order their data transmissions to the satellites. NBS designed and implemented the time code for these satellites. To ensure a proper interface of the time code with the data-collection platforms (DCP's), which both transmit

and receive to and from the satellites, NBS designed digital clocks using random logic and the simplest and lowest cost microprocessor available at the time. The microprocessor approach to the digital clock design was taken because it offered the lowest cost and provided the flexibility to include or delete functions through software changes rather than through hardware redesign.

As of November 1975, only one satellite at 115° West Longitude transmits the time code. Very soon a second satellite will also transmit the time code. Long-range plans for these NOAA satellites call for the positioning of one satellite at approximately 135° West Longitude, another at 75° West Longitude, and a third to be an in-orbit spare. The approximate coverage for the time code from two active satellites is shown in figure 11. The coverage area outlined by the heavier line for each satellite applies for an elevation angle of 7°, while the larger area outlined by the lighter line is valid for 3° elevation angle. As these satellites deteriorate with age, replacement satellites will be launched. This planned configuration of satellites is expected to be in effect by early 1976.

The time information, a digital time code, is multiplexed into the interrogation format relayed by the SMS/GOES satellites. The format consists of a 15-bit, maximum-length sequence (MLS) for message synchronization, immediately followed by 31 bits comprising a (31, 21) binary BCH code. Four additional bits, beginning on each half second, precede each MLS sequence and comprise a BCD word of the time code.

Figure 12 is the interrogation message format: four time code bits followed by 15 bits of the message synchronization word and 31 bits of the address word. The pattern is repeated every 0.5 second at a 100 bits-per-second rate. The first bit of every time code character defines the UTC half-second mark. Figure 12 also shows the time code format; four bits are extracted from the interrogation frame every half second for 30 seconds. The first 40 bits is the time code synchronization message consisting of 10 BCD character A's beginning on the UTC minute mark and 10 BCD 5's beginning at the UTC half-minute mark. Following the code synchronization message are 10 BCD characters of the time code, followed by 13 BCD characters representing the satellite's current position in geocentric longitude and latitude and the departure in its radial distance form a reference orbit.

Time Code Distribution

The interrogation message is sent to the SMS/GOES spacecraft at S-Band and retransmitted to the earth through a global antenna at 468.825 MHz. The message phase modulates the carrier $\pm 60^{\circ}$ after being Manchester encoded. The interrogation message is received by data-collection platform radio sets (DCPRS), which provide the communication interface with rain and river gauges, ships, buoys, seismograph stations, tide gauges, and tsunami detectors. The DCPRS derives a bit rate clock from the received interrogation message which is used to decode the interrogation message.

When a DCPRS is addressed its stored data is transmitted to the satellite for relay to the Wallops Island Command and Data Acquisition Station (CDA). In some cases, such as the monitoring of seismic activities, it is desirable to label the data with the date of occurrence. Attempts to use internal clocks set by infrequent clock carries or by reception of HF or LF radio signals are expensive, labor intensive, and subject to an unacceptable failure rate. The time-of-year code in the interrogation format eliminates these disadvantages and provides the SMS/GOES Data Collection System (DCS) user with a cheap, reliable, and simple system for data labeling or any other time-ordered function required at remote sites or in difficult environments.

Figure 13 illustrates the time-code distribution. Derived from atomic clocks located at the CDA in Wallops Island, Virginia, the time code is combined with the current satellite position, multiplexed with the interrogation address and sync word and transmitted to the satellites at S-Band. The satellites transpond the signals back to earth at 468.825 MHz, where they are received by the DCPRS's.

Time Code Generation

NBS has installed, at the CDA at Wallops Island, Virginia, equipment to generate the time code and maintain Coordinated Universal Time (UTC) to within a few microseconds of the master clock at NBS in Boulder, Colorado. Figure 14 is a block diagram of the equipment. There are two atomic frequency standards, each driving a clock and format generator, making two independent systems. Each system provides the time code and satellite position to two DCS equipment racks for multiplexing into the interrogation channels of two SMS/GOES satellites. All components of each system are backed with rechargeable batteries with sufficient capacity to

operate four hours without primary power. Should a failure be experienced in one of the time-reference systems, the other can be switched in while it is repaired. The frequency of the atomic frequency standards can be compared to the NBS Frequency Standard in Boulder, Colorado, using the television frequency comparison technique discussed previously in this paper. This comparison is accomplished by NBS staff at routine intervals. The satellite position is computed at NBS Boulder from orbital elements issued by NASA's Goddard Space Flight Center. A table of positions, with dates, is constructed at NBS and sent to Wallops Island by telephone. An automatic answering system interfaces the telephone line with a memory bank, which stores the table, valid for one week, for the two satellites. The time code format generator addresses the memory with the data (days, hours, and minutes) and fetches the currently valid position for multiplexing into the interrogation message.

The interrogation channels on both satellites are monitored continuously in Boulder. Any failure or drift of the clocks at Wallops Island is automatically noted for appropriate action.

Time Code Reception

The time signals sent from Wallops Island to the SMS/GOES satellites are advanced by the approximate time it takes the signal to travel from Wallops Island to the satellite's subsatellite point on the equator (≈260,000μs). The signals thereby arrive on the earth nearly on time.

In the case of the SMS-2, currently at 115° West Longitude, the 260,000μs advance means that the signals arrive at the earth's surface within 8ms of being "on time." The inclination and eccentricity of the satellite's orbit introduce a small "diurnal" component to this "apparent" delay. Figure 15 shows typical "diurnal" peak-to-peak values. An actual chart recording of this diurnal as received at the NBS labs in Boulder, is shown in figure 16.

For a time signal accurate to a few tens of milliseconds, the time code as received requires no delay corrections. Time to a few milliseconds requires the correction to compensate for the earth's spherical shape. Time to better than a few milliseconds requires the consideration of the "diurnal effect," which can be compensated for with the "tools" developed at NBS. Using the current satellite position provided in the interrogation channel format i.e., the satellite's

longitude, latitude, and radius, the slide rule shown in figure 17 will calculate the delay to a 10μs precision. NBS also has programmed the delay calculation in the BASIC computer language and for programmable pocket calculators. This calculation will also be handled in an expanded version of an NBS designed microprocessor time-decoder-clock. The accuracy for the time code, using satellite-position data, has consistently been better than 100μs.

Decoder-Clock

NBS has designed a digital clock for direct connection to the DCPRS's. The digital clock is a device which achieves bit synchronization, interrogation frame synchronization, and time code frame synchronization to correctly reconstruct the received data bits into the time-of-year message and satellite position. The digital clock also contains an internal clock which is set by the satellite time code. If the satellite signal is lost for any period of time, the digital clock "flywheels" the internal time with an accuracy consistent with the quality of its internal oscillator. If an incorrect time message is received by the digital clock, (corrupted by noise or interference) the digital lock tends to ignore this incorrect time and accept only the correct time for comparison or resetting its internal clock. The initial design effort on the digital-clock used a random logic design approach and is shown in figure 17. A new design using a four bit microprocessor will soon be completed. The microprocessor design will be smaller, cheaper, and more reliable while providing flexibility to include, at the user's option, many features through simple software additions rather than difficult hardware modifications [10].

These features of the microprocessor digital-clock, as shown in figure 18, can include any or all of the following:

1. LED display of the time-of-year (TOY).
2. LED display of the satellite position.
3. LED display or BCD representation of delay corrections.
4. Standard code outputs such as IRIG-H, NASA 36, etc.
5. Automated delay corrections.
6. Interrogated outputs (TOY on demand).
7. Special rate outputs, 1 pps, 10 pps, 1/10 pps, etc.
8. AC or DC power input.

FUTURE TRENDS: OTHER METHODS

Several years ago NBS developed and evaluated a T/F dissemination technique involving the addition of an active time-of-

day code to the vertical blanking interval of normal TV network program transmissions [11]. Modified television receivers could be used to decode and display the time information on the TV set screen. As a result of successful tests of the technique, using both local and nationwide TV network facilities, the Department of Commerce submitted a petition to the FCC, requesting permanent allocation of Line 21 of the vertical interval for use with this NBS TV-Time System. To date this petition has not been acted upon by the FCC. It is therefore unclear at this time whether the technique can ever be implemented on a permanent basis.

NBS also proposed the addition of a slow time-of-day code to one or more broadcasts of the Omega Navigation System [12]. The intent was to gain worldwide coverage with very high reliability at a relatively small incremental cost. In view of recent decisions by Omega personnel to prohibit any modulation of the Omega transmissions, NBS has suspended work on this technique for the foreseeable future.

REFERENCES

[1] "National Bureau of Standards Special Publication 432," available from Time and Frequency Services Section, National Bureau of Standards, Boulder, Colorado, 80302.

[2] "National Bureau of Standards Special Publication 674," available from Time and Frequency Services Section, National Bureau of Standards, Boulder, Colorado, 80302.

[3] TOLMAN, J., PTACEK, V., SOUCEK, A., and STECHER, R., "Microsecond clock comparison by means of TV synchronizing pulses," IEEE Trans. on Instrumentation and Measurement, Vol. IM-16, pp. 247-254, Sept. 1967.

[4] DAVIS, D.D., BLAIR, B. E., and BARNABA, J. F., "Long-term continental U. S. timing system via television networks," IEEE Spectrum, Vol. 8, pp. 41-52, August 1971.

[5] "NBS Time and Frequency Services Bulletin," published monthly, available from Time and Frequency Services Section, National Bureau of Standards, Boulder, Colorado, 80302.

[6] "U. S. Naval Observatory Time Service Announcement, Series 4," published weekly.

[7] DAVIS, D. D., "Frequency Standard hides in every color TV set," Electronics, pp. 96-98, May 10, 1971.

[8] DAVIS, D. D., "Calibrating crystal oscillators with TV color-reference signals," Electronics, pp. 107-112, March 20, 1975.

[9] HANSON, D. W. and HAMILTON, W. F., "Satellite broadcasting of WWV signals," IEEE Trans. on Aerospace and Electronic Systems, Vol. AES-10, No. 5, pp. 562-573, Sept. 1974.

[10] "National Bureau of Standards Technical Note," to be published.

[11] DAVIS, D. D., JESPERSEN, J. L., and KAMAS, G., "The use of television signals for time and frequency dissemination," Proc. IEEE, Vol. 58, No. 6, pp. 931-933, June 1970.

[12] HOWE, D. A., "Nationwide precise time and frequency distribution utilizing an active code within network television broadcasts," Proc. 26th Annual Symposium on Frequency Control (U. S. Army Electronics Command, Ft. Monmouth, NJ, June 6-8, 1972), pp. 292-308 (Electronic Industries Association, Washington, DC, 20006).

[13] FEY, L., "A time code for the Omega worldwide navigation system," Proc. IEEE (Lett.), Vol. 60, p. 630, May 1972.

LIST OF FIGURES

1 Geographical distribution of responses

2 Number of responses for each user category

3 Use of facilities

4 Use of the broadcast frequencies

5 Use of services for each user category

6 TV frequency calibration service

7 NBS calibration of network frequency offsets

8 NBS frequency measurement computer

9 Block diagram of microprocessor offset computer

10 One-week sample of microprocessor offset computer data

11 Approximate time code coverage from two SMS/GOES satellites

12 SMS/GOES interrogation message format

13 Illustration of SMS/GOES time code distribution

14 Block diagram of SMS/GOES time code generation equipment

15 Approximate diurnal component (peak-to-peak) of received time code from SMS-2 satellite

16 Recording of received time code showing diurnal variation at Boulder, Colorado

17 NBS-developed satellite decoder-clock and path delay slide rule

18 Features of microprocessor version of satellite decoder-clock

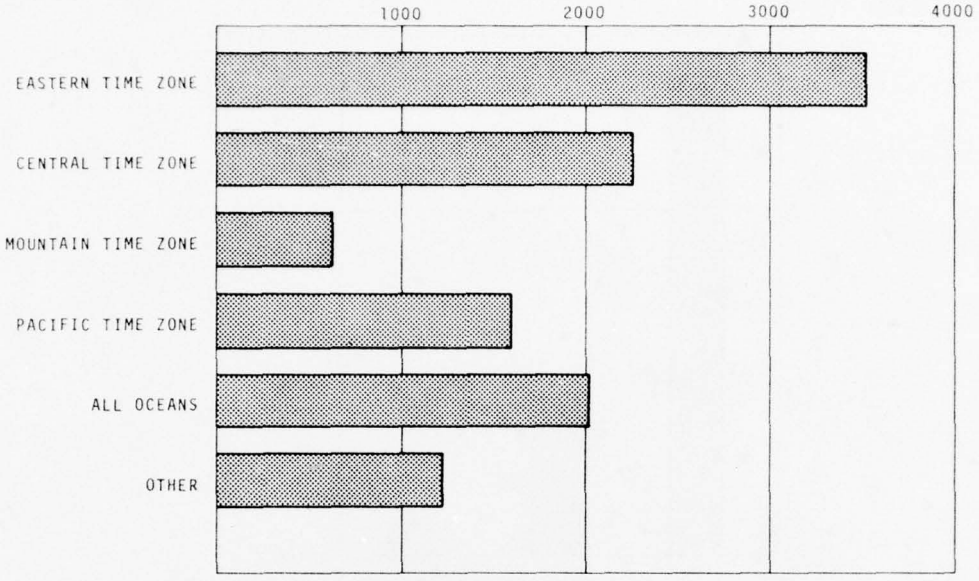


Fig. 1-Geographical distribution of responses

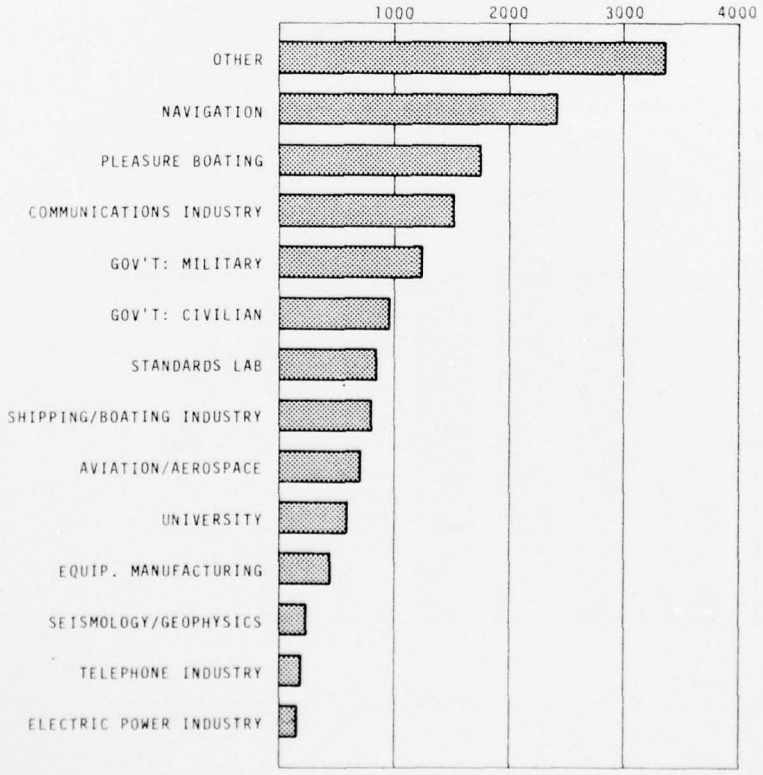


Fig. 2-Number of responses for each user category

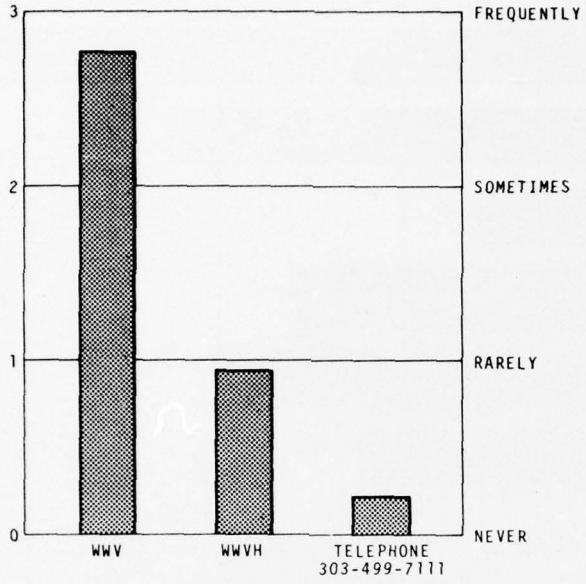


Fig. 3-Use of facilities

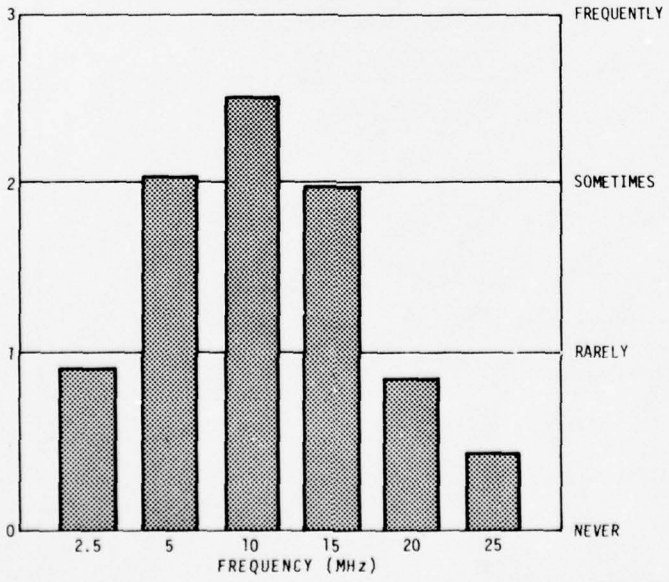
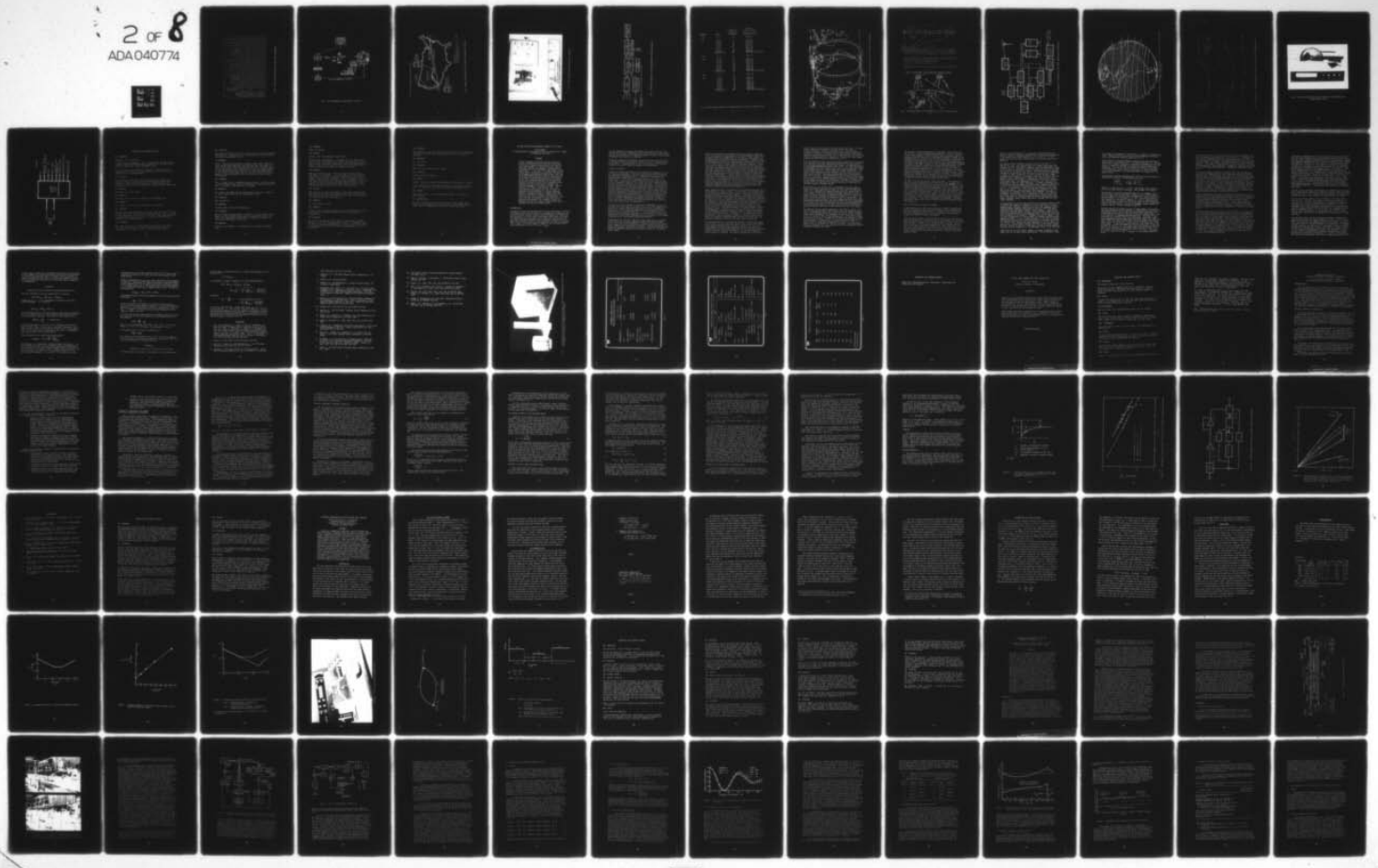


Fig. 4-Use of the broadcast frequencies

AD-A040 774 NATIONAL AERONAUTICS AND SPACE ADMINISTRATION GREENB--ETC F/G 14/2
PROCEEDINGS OF THE ANNUAL PRECISE TIME AND TIME INTERVAL (PTTI)--ETC(U)
DEC 75

UNCLASSIFIED NASA-GSFC-X-814-76-45 NL

2 OF 8
ADA040774



SERVICES (OVERALL RATING) / USER CATEGORY (NUMBER OF RESPONSES)	OTHER (3318)	NAVIGATION (2385)	COMMUNICATIONS INDUSTRY (1492)	PLEASURE BOATING (1714)	GOV'T. CIVILIAN (955)	GOV'T. MILITARY (1227)	STANDARDS LABS (817)	AVIATION/AEROSPACE (693)	UNIVERSITY (577)	SHIPPING/BOATING INDUSTRY (791)	EQUIPMENT MANUFACTURING (424)	SEISMOLOGY/GEOPHYSICS (220)	TELEPHONE INDUSTRY (174)	ELECTRIC POWER INDUSTRY (148)
Time-of-Day: Voice (2.79)	2.84	2.78	2.81	2.72	2.76	2.67	2.60	2.85	2.86	2.81	2.77	2.85	2.68	2.62
One-Second Ticks (1.97)	1.98	2.07	2.13	1.91	2.15	1.83	2.28	2.19	2.32	2.27	2.27	2.45	1.90	2.12
Standard Frequency (1.74)	1.82	1.18	2.48	1.11	1.92	1.32	2.36	1.67	1.93	1.37	2.31	1.68	2.42	2.08
Propagation Forecasts (1.40)	1.52	1.04	1.88	0.99	1.36	1.02	1.44	1.40	1.51	1.19	1.55	1.57	1.64	1.27
Weather (1.35)	1.24	1.82	1.41	1.93	1.15	0.87	1.17	1.53	1.33	1.85	1.32	1.54	1.18	1.22
Geoalerts (0.92)	1.02	0.77	1.20	0.80	0.92	0.64	0.96	0.98	1.23	0.73	1.05	1.68	1.04	0.80
Time-of-Day: BCD (0.67)	0.55	0.83	0.83	0.63	0.82	0.76	0.75	0.88	0.81	1.06	0.75	1.13	0.67	0.77
DUT1 Values (0.28)	0.25	0.25	0.41	0.21	0.34	0.29	0.47	0.38	0.47	0.24	0.42	0.45	0.31	0.38

Fig. 5-Use of services for each user category

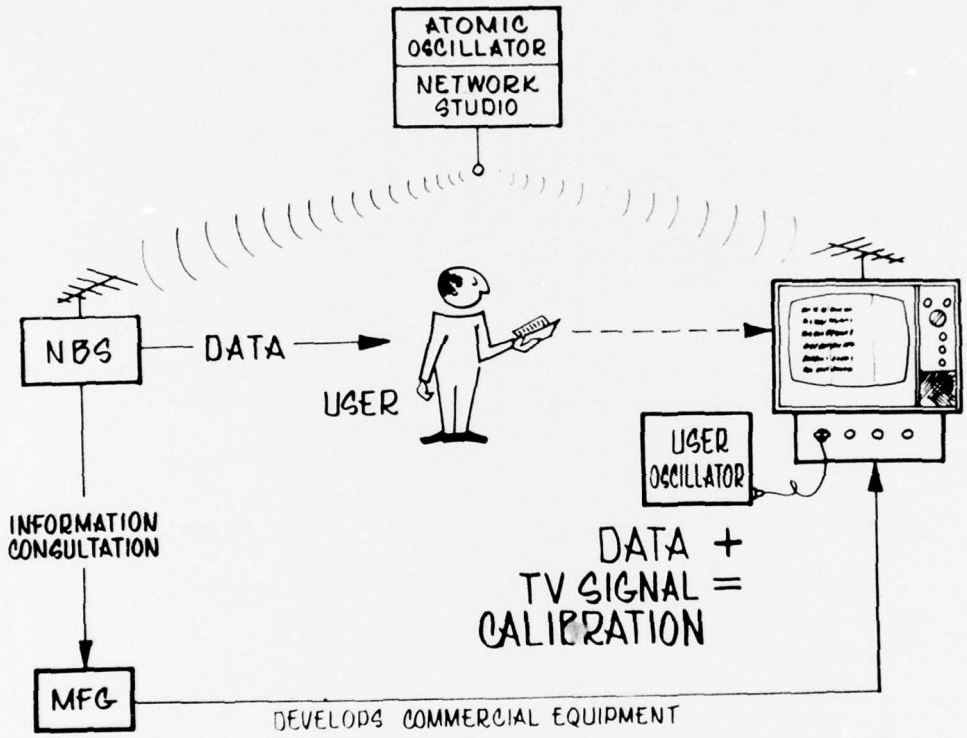


Fig. 6-TV frequency calibration service

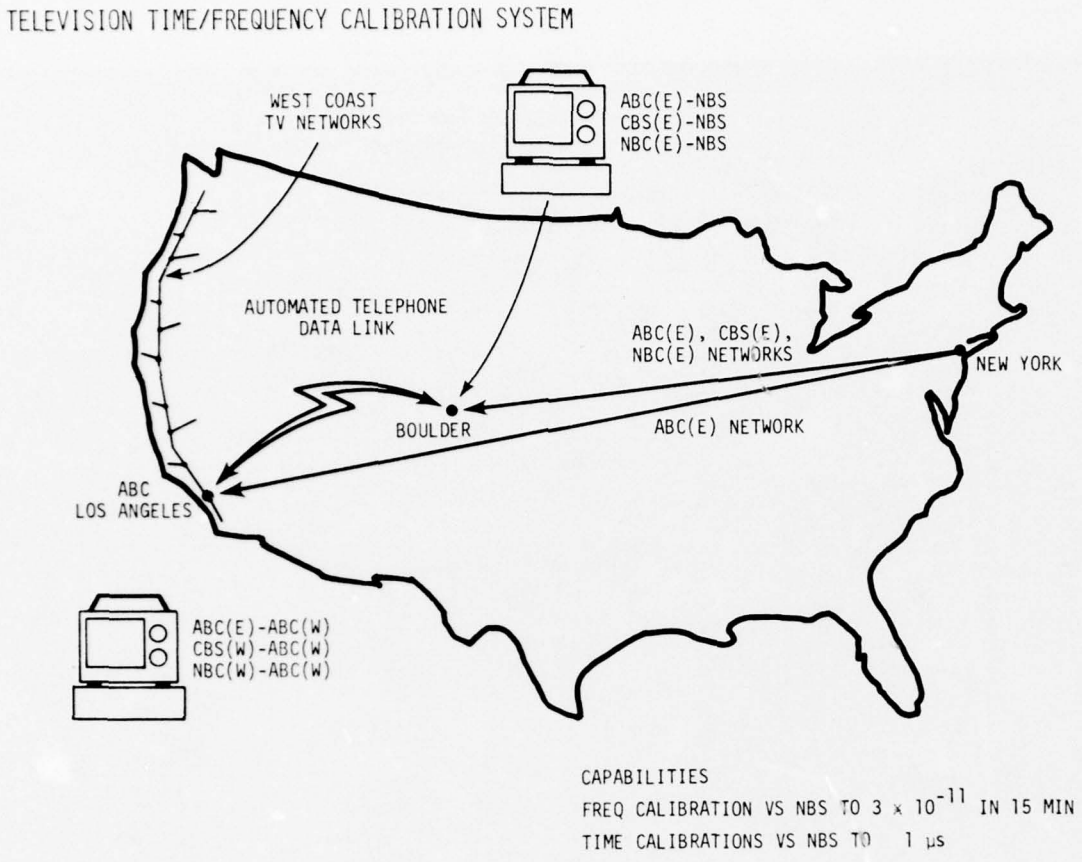


Fig. 7-NBS calibration of network frequency offsets

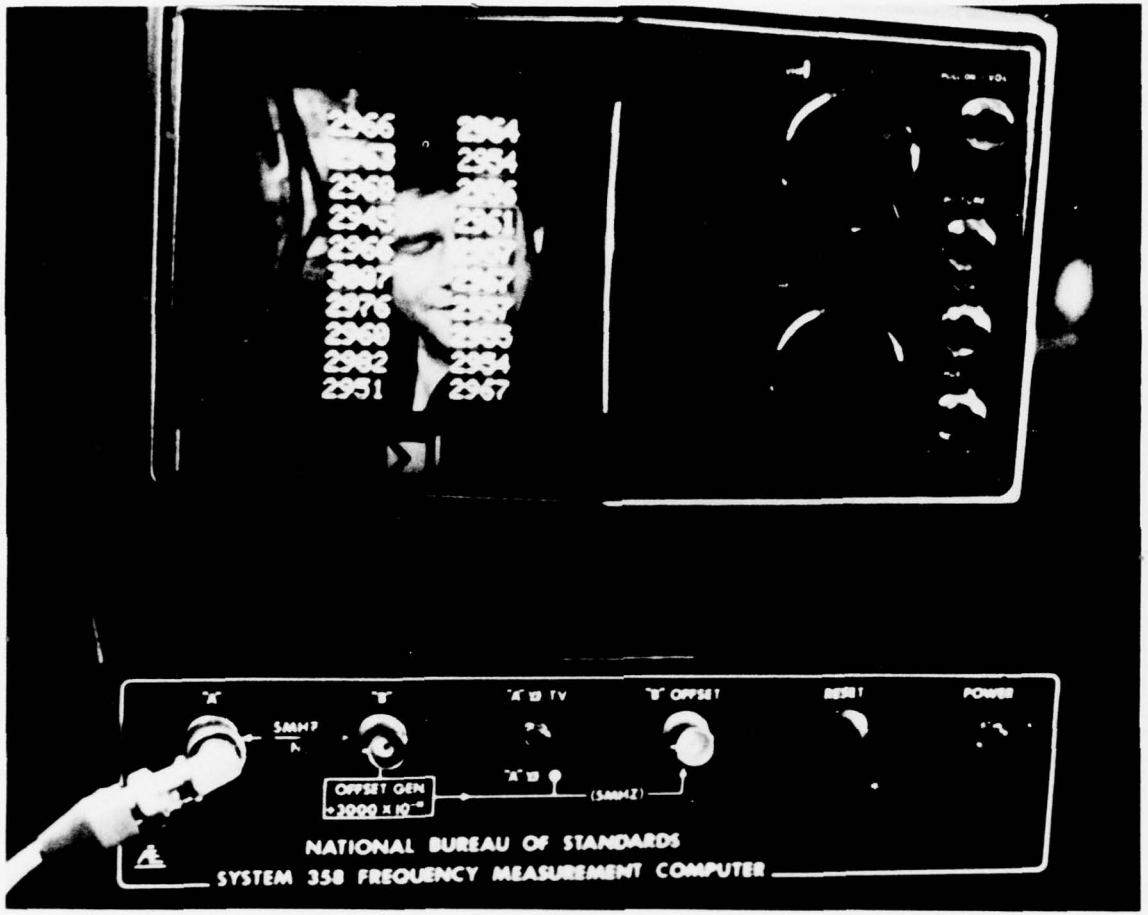


Fig. 8-NBS frequency measurement computer

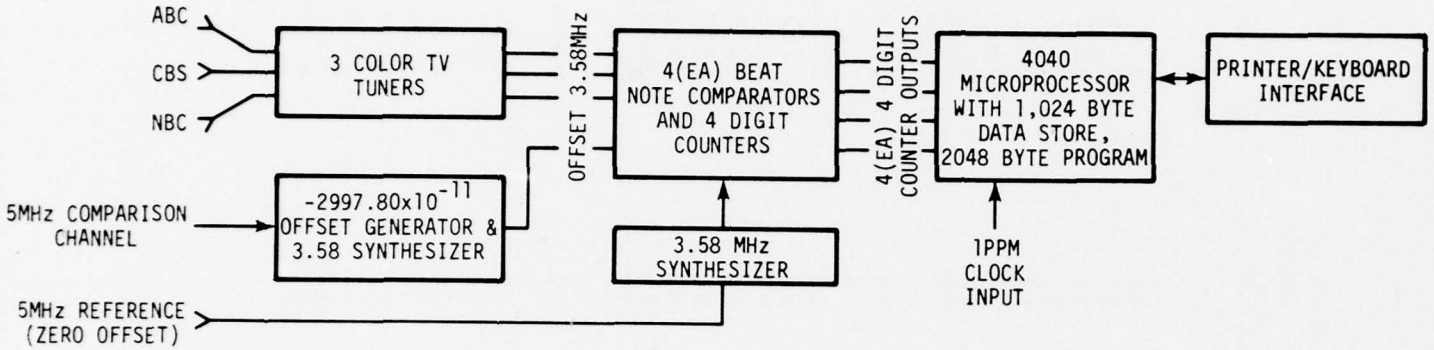


Fig. 9-Block diagram of microprocessor offset computer

NETWORK	DATE	NUMBER OF 15-MINUTE SAMPLES	AVERAGE FREQ. OFFSET PARTS IN 10^{11}	
ABC	11/17	02	3012.61	
ABC	11/16	03	3011.20	
	11/15	31	3010.97	
	11/14	17	3010.98	
	11/13	18	3010.58	
	11/12	16	3011.24	
	11/11	14	3010.49	
	11/10	20	3010.91	
	Weekly Avg.	119	3010.88	(Weighted)
CBS	11/17	03	2962.53	
CBS	11/16	07	2964.27	
	11/15	20	2962.31	
	11/14	07	2962.49	
	11/13	04	2962.59	
	11/12	04	2963.22	
	11/11	05	2962.24	
	11/10	04	2962.38	
	Weekly Avg.	51	2962.69	(Weighted)
NBC	11/17	02	3018.68	
NBC	11/16	00	0000.00	
	11/15	16	3017.77	
	11/14	14	3017.71	
	11/13	15	3018.04	
	11/12	15	3018.19	
	11/11	13	3018.01	
	11/10	14	3017.88	
	Weekly Avg.	087	3017.93	(Weighted)

Fig. 10-One-week sample of microprocessor offset computer data

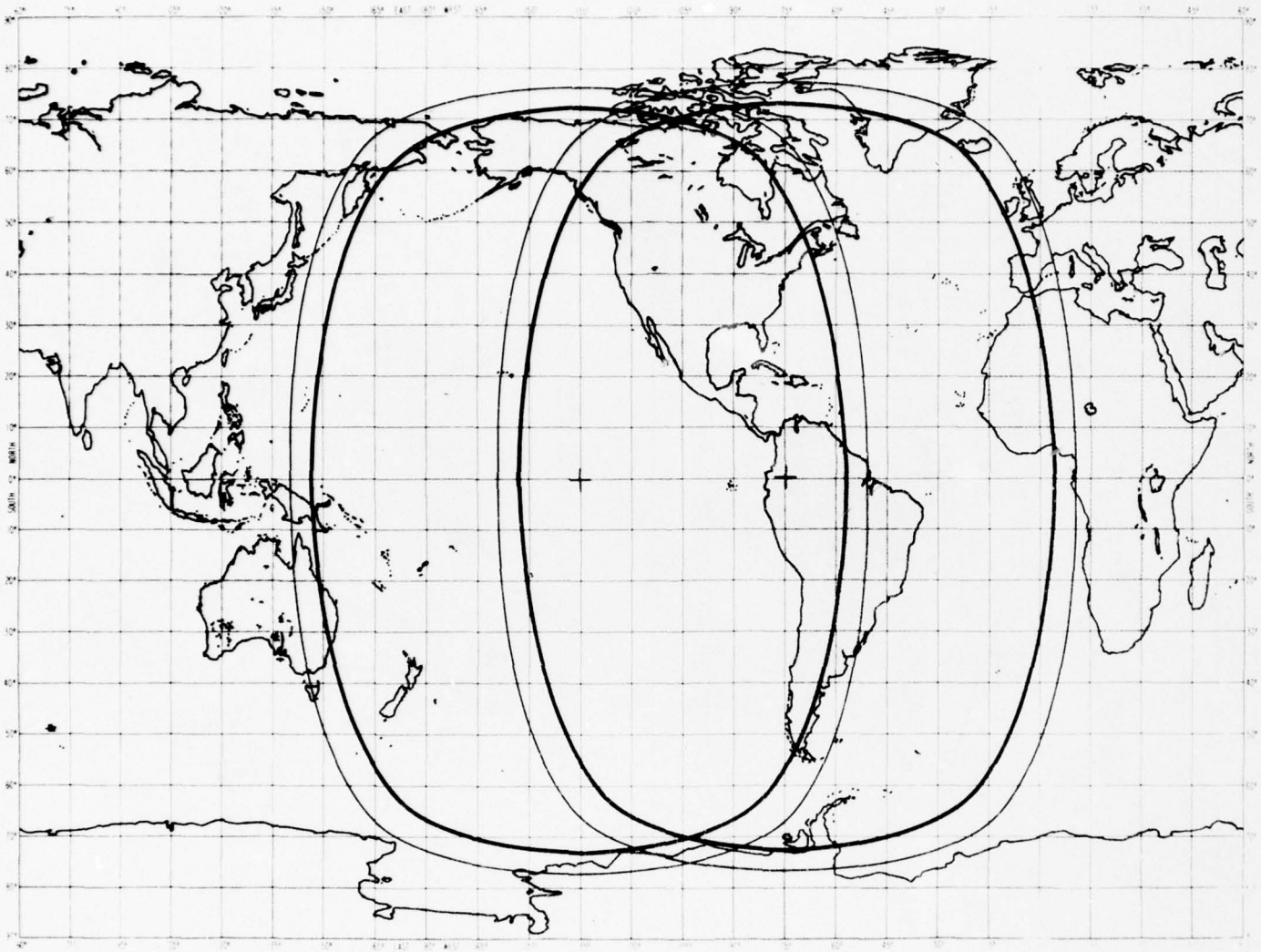


Fig. 11-Approximate time code coverage from two SMS/GOES satellites

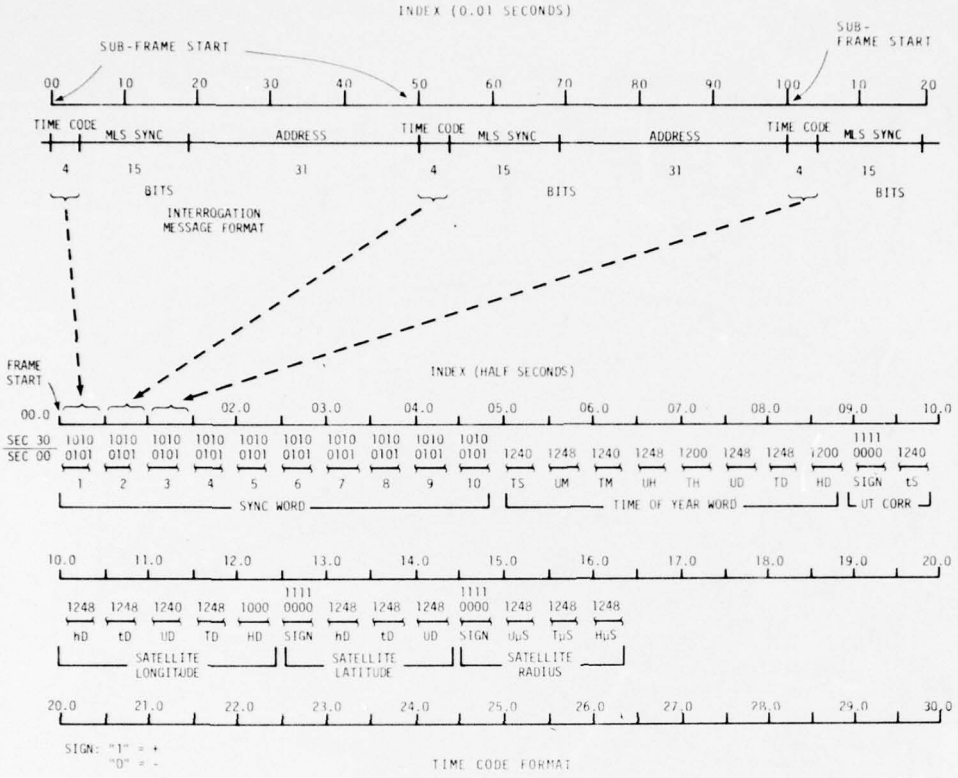


Fig. 12-SMS/GOES interrogation message format

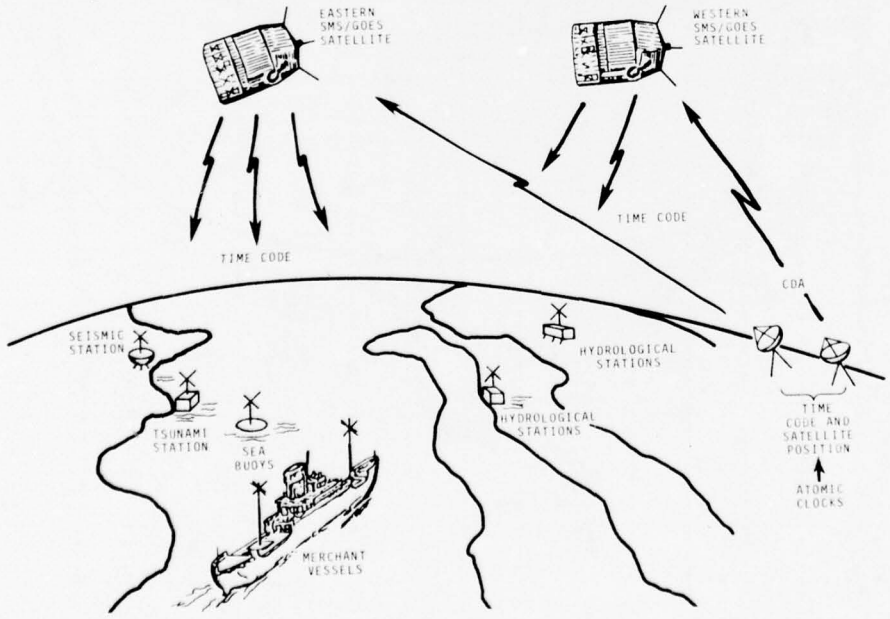


Fig. 13-Illustration of SMS/GOES time code distribution

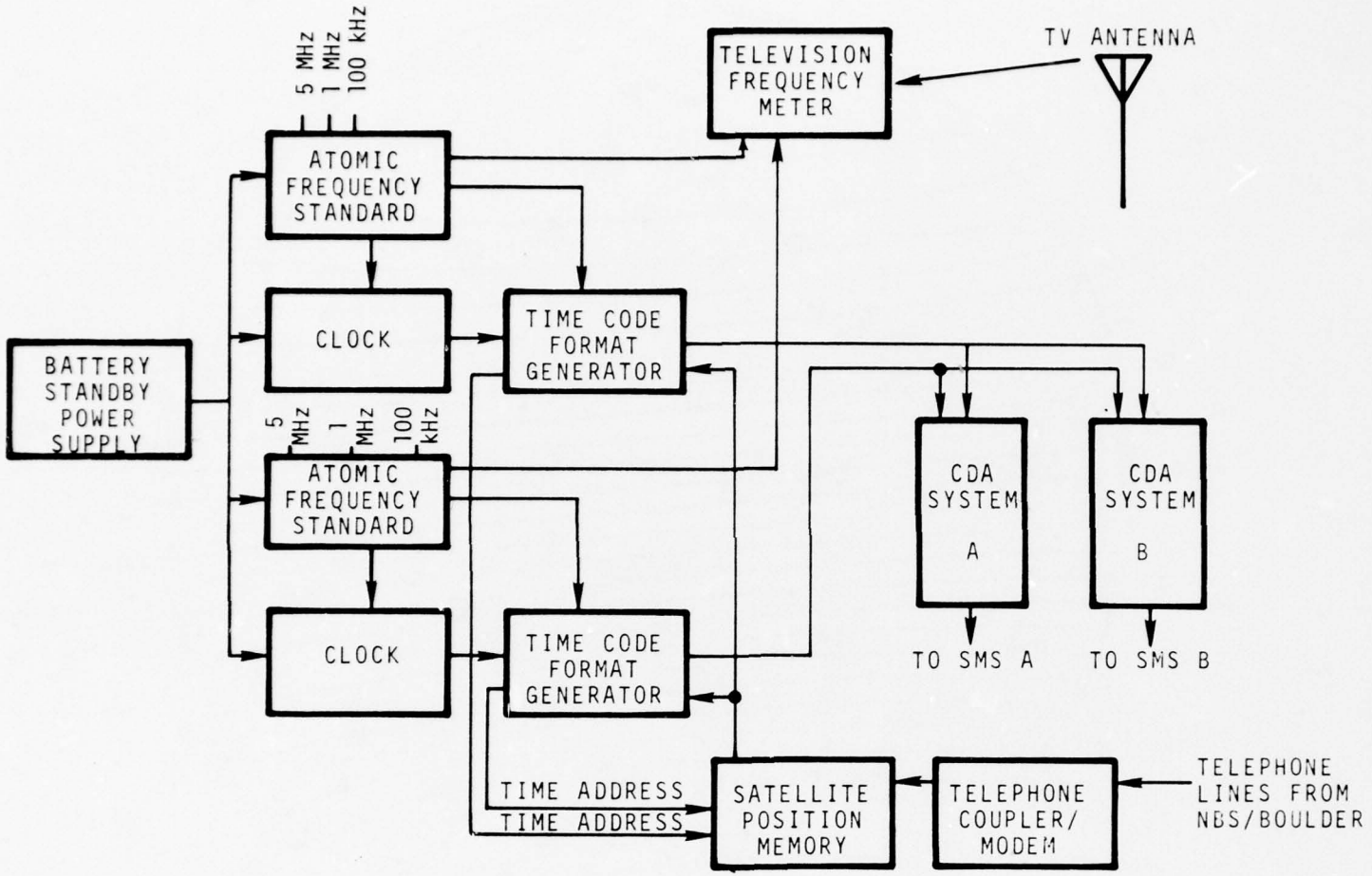


Fig. 14-Block diagram of SMS/GOES time code generation equipment



Fig. 15-Approximate diurnal component (peak-to-peak) of received time code from SMS-2 satellite

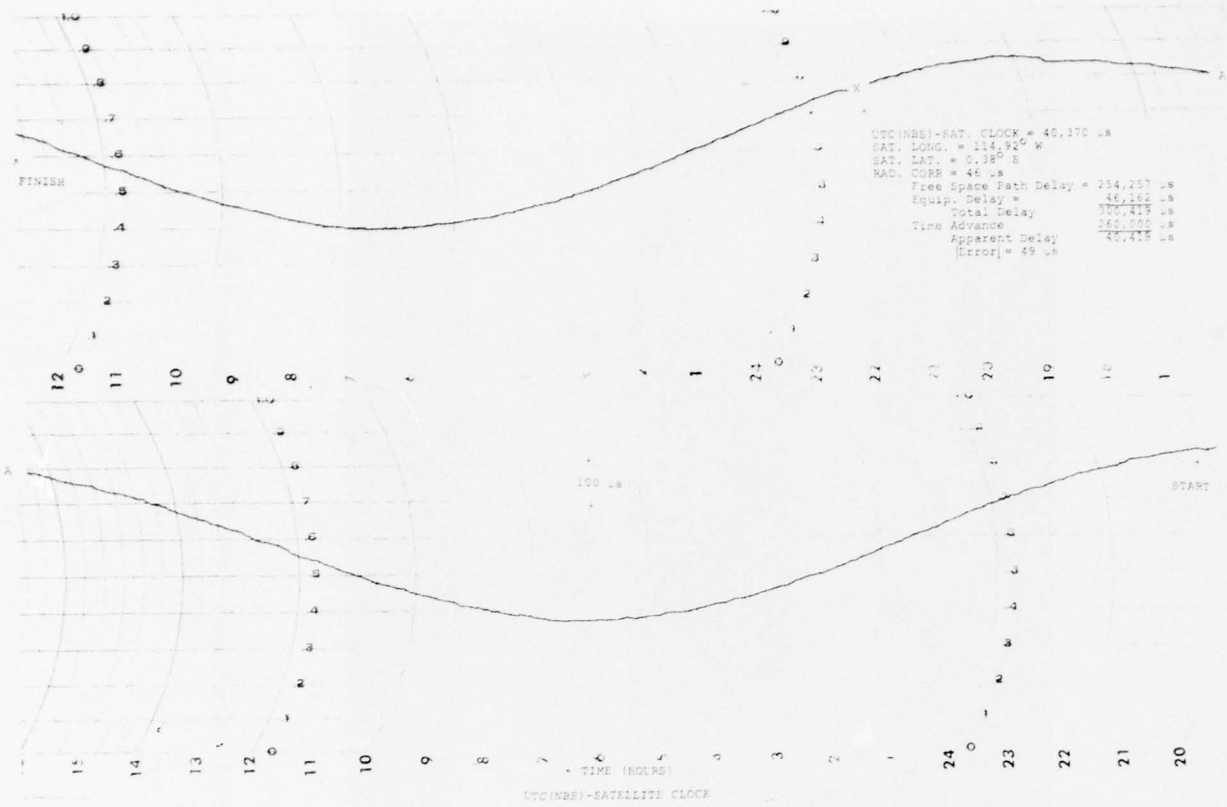


Fig. 16-Features of microprocessor version of satellite decoder-clock

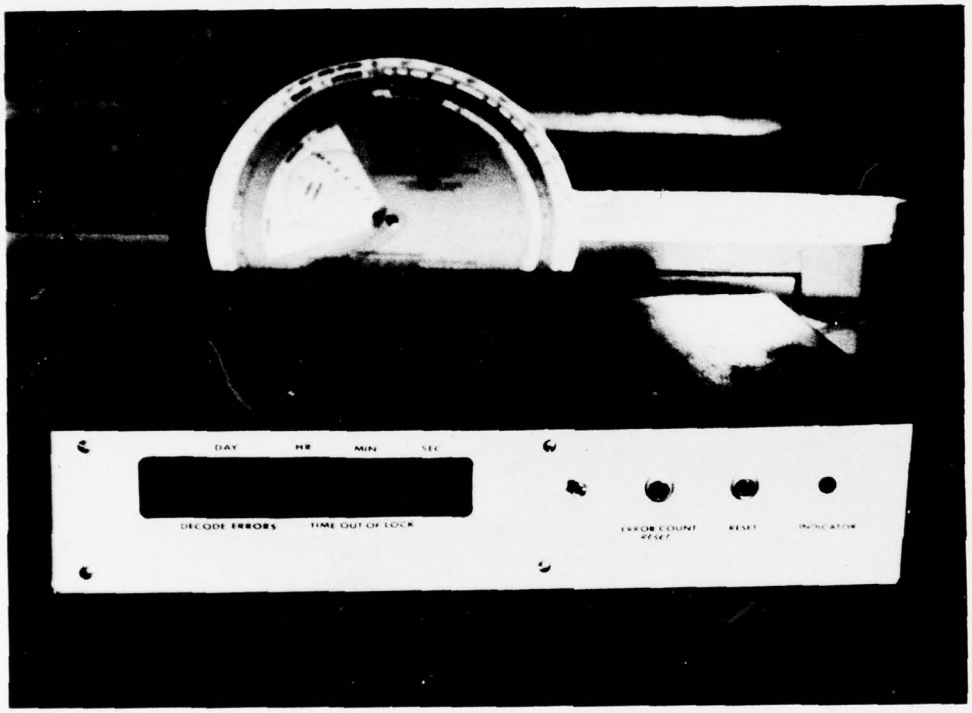


Fig. 17-NBS-developed satellite decoder-clock and path delay slide rule

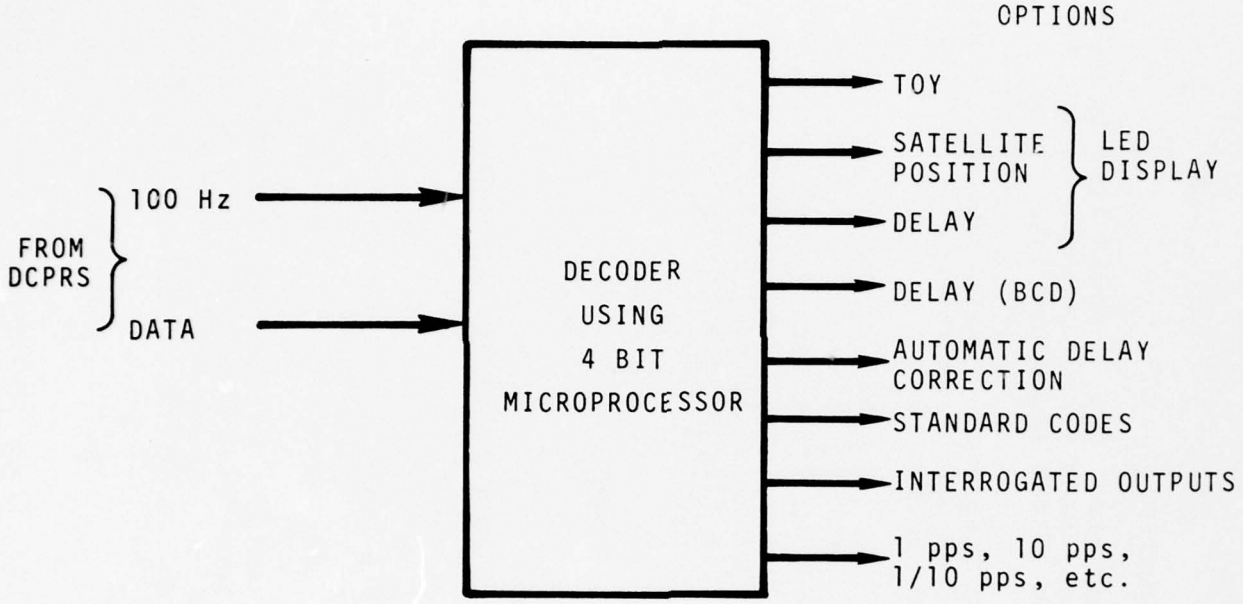


Fig. 18-Features of microprocessor version of satellite decoder-clock

QUESTION AND ANSWER PERIOD

DR. SHEPARD:

Shepard, ILC Industries.

I have several comments. One, I would like to make a suggestion that you may skew your responses if you put an in-watts on that time of day telephone line.

On the television frequency transfer, do you actually measure the frequency of the subcarrier or do you use the time difference measurements?

DR. BEEHLER:

At present, for the West Coast data we are actually using the time transfer, but we are in the process of putting another system out there which will really measure the frequency, using this microprocessor system that I mentioned.

DR. SHEPARD:

How about the East Coast?

DR. BEEHLER:

The East Coast is direct frequency measurement now.

DR. SHEPARD:

All Right. How long has this been in existence?

DR. BEEHLER:

The East Coast measurements have been done for several years. We did infer the East Coast measurements from time. I think it has been about three years. The West Coast measurements, we began publishing the offset, I believe, in the April 1975 issue of the Bulletin.

DR. SHEPARD:

But, the current East Coast data and the East Coast data for the past couple of years has been derived from the frequency rather than the day to day time difference.

DR. BEEHLER:

The East Coast data up until recently was by time difference measurement. Recently, we also switched over to the direct frequency measurement there.

DR. SHEPARD:

Okay. That was my question, because there were irregularities in the published data that would vary from week to week which would seem inconsistent with the rubidium and it was my impression that these would be due to phase changes in the program material depending on what was happening. If the World Series game was on, you get different average data by time measurement than you would by direct phase measurement.

DR. BEEHLER:

Yes, I think that is probably quite correct. In fact, that is the reason we have gone to the direct frequency measurement, it seems to be much more reliable.

DR. SHEPARD:

All right, now what is the situation on line 10, fields 1, 3, pulse edge reference at the present time?

DR. BEEHLER:

The situation?

DR. SHEPARD:

Leading edge versus trailing edge.

DR. BEEHLER:

We are using trailing edge, I believe, at the present time. There is some thought being given to making a switch at some point because the data would, indeed, be better, at least for some users if we did.

DR. SHEPARD:

There is no schedule, or nothing firm on that switchover yet?

DR. BEEHLER:

That is correct.

MR. RUEGER:

Rueger, The Johns Hopkins University

Do you have precedents for being able to phase out a service like the operation of WWV? It seems to me that some of the electronic navigation aids have been years trying to phase out the service and I don't think 20 years advance notice was enough to complete the job.

DR. BEEHLER:

That may very well be. This is kind of a theoretical argument at the moment. I think when we do get down to that stage of actually trying to implement that, we may, indeed, find similar problems. But, I think as better services come along, if they are really capable of giving the user at least as much information and doing it as cheaply or more cheaply with less effort, that it seems like we should be trying to go in that direction.

MR. RUEGER:

The criteria of the past seems to have been based on the wear-out of the users' equipment after you tell him they are going to be shut down and not the lack of the service or a different way of getting it.

DR. BEEHLER:

I am sure that is true.

DR. WINKLER:

I have, also, several questions. Do you provide or do you envision to include the DUT-1 code on the satellite broadcasts?

DR. BEEHLER:

We do not include the DUT-1 code at the moment on GOES because it is just an experimental thing. Certainly when we go to a service arrangement, if we do, the DUT-1 would be included as long as the CCIR recommendation is still effective.

DR. WINKLER:

The second, is the 100 pulse per second time code identical with the 100 pulse per second which you have on WWV subcarrier?

DR. BEEHLER:

No, it is not.

DR. WINKLER:

Where do you publish these codes?

DR. BEEHLER:

Check with Wayne Hanson.

MR. INOUYE:

Inouye, National Research Laboratory of Metrology in Japan.

I am interested in the Radio serviced area from the satellite. I could not find out if Japan is included or not.

MR. HANSON:

There are two U. S. controlled satellites. They do not cover Japan.

DR. KLEPCZYNSKI:

He said the current satellites do not cover Japan, but there is the possibility in the future, after some negotiation, that a Japanese satellite will cover the area.

OUTLOOK FOR PRECISION FREQUENCY CONTROL IN THE 1980's

ERICH HAFNER
US Army Electronics Technology and Devices Laboratories (ECOM)
Ft. Monmouth, New Jersey

ABSTRACT

Current laboratory activities that are likely to result in improved crystal oscillators and atomic or molecular frequency standards over the next ten years are examined. In the crystal area, stabilities under tactical environment - including static acceleration - in the low 10^{-10} range appear to come within reach, in one cubic inch devices; and molecular frequency standards with stabilities in the low 10^{-12} range appear feasible in 20-40 cubic inch size. The former will be made possible by a breakthrough in the static acceleration sensitivity of crystal units, now considered imminent, and by significant advances in crystal and oscillator technology; the latter by the use of saturation resonance absorption phenomena in the infrared range. Considerations are offered to demonstrate that the CO_2 resonance fluorescence cell has all major ingredients to form the heart of a novel miniature molecular frequency standard. Progress being made towards assessing the principal technological difficulties, and their resolution, are described. The paper includes a discussion of other molecular resonances with potential for frequency control application as well as a cursory review of more exotic phenomena for the more distant future.

INTRODUCTION

Tremendous strides have been made over the last two decades in the art of frequency control for application in communication, navigation and position location systems. Quartz crystal reference oscillators are now available in 15 to 30 cubic inch packages that exceed in performance those that occupied several cubic feet less than 20 years ago; and atomic frequency standards whose fundamental properties had just begun to be studied seriously in the laboratory in 1955, have matured into a range of relatively compact commercial devices whose stabilities are measured in the 10^{-12} to 10^{-15} range.

PRECEDING PAGE BLANK-NOT FILMED

Yet, the demands for improved performance have easily kept pace with the advances in device technology; and for applications in time ordered systems in particular, still higher performance in terms of size, power consumption and stability is required.

It appears appropriate, therefore, to engage in some crystal gazing in an effort to foretell the shape of things to come in frequency control in the 1980's. As appropriate for PTTI, only devices with stability potential in the 10^{-9} range and beyond will be considered.

Crystal Oscillators

Progress in crystal oscillators will be paced by the advances in crystal resonator development. The art of precision crystal manufacture by conventional techniques appears to have reached a plateau which is characterized by aging rates of 1.5×10^{-8}/mo (5×10^{-10}/day) for overtone and 5×10^{-8}/mo for fundamental mode crystal units in the 5 MHz range. Significantly better behavior can be obtained by observation of generally large lots of crystal units over extended periods of time and careful selection of the best performers. The rapidly decreasing yield of units that have to meet particularly tight specifications prevents any large scale system application of oscillators requiring specialty crystal units at this time. While aging provides a convenient and easily recognized measure of crystal quality, the manufacturing imperfections responsible for a large part of the aging behavior are also contributing dominantly to such other phenomena as lack of frequency repeatability on thermal cycling (a serious limitation in precision temperature compensated oscillators), excessive noise (poor short term stability), high resistance at very low drive levels (oscillation start up problems) etc.

The need for a major advance in crystal unit technology is clear, and the direction to be taken for establishing a high yield production capability for crystal units with more than one order of magnitude reduced aging, and corresponding improvements in related performance characteristics has been established [1]. The key elements are a) improved surface preparation techniques, b) novel means for eliminating contaminants and avoiding recontamination by continuous in-line vacuum processing and c) new resonator packaging approaches.

Implementation of the basic capability along these lines is expected by the late 1970's, providing adequate numbers of high performance crystal units for initial production of advanced high density surveillance, communication and navigation systems. Further improvements of these new processing techniques extending into the 1980's are expected, along with expanding capacities as required to meet full system production needs.

While the new processing technology will play a crucially important role in providing the large numbers of high performance crystal units required to meet the systems needs of the 1980's, recent advances in resonator theory are pointing the way to new types of resonator cuts and geometries that promise to yield characteristics superior to those of the commonly used AT or BT configurations, particularly with respect to the effects of stress fields on resonance frequency. Stress fields may be caused by the resonator mounting structure, plated-on electrodes and thermal gradients as well as by static acceleration and vibration. Relaxation of mounting and electrode stresses can contribute significantly to the aging of crystal units, and generally cause much the same problems as discussed above in relation to other manufacturing imperfections. Stresses induced by thermal gradients are implicated in the thermal transient behavior of temperature compensated oscillators, in the warmup characteristics of oven controlled oscillators and in the frequency drive level effect, which impacts on attainable short term stability. All of these, as well as the frequency excursions observed during static acceleration and vibration, have long been recognized, but have only gradually yielded to empirical efforts to achieve any significant reductions [2].

Recent theoretical work [3-5], however, has now provided the basis for a fresh approach to these problems. The functional relationship between the static (or quasistatic) stress fields involved and the high frequency vibrations of the crystal resonator, - and hence the resonance frequency - have been established. The coupling between them depends on the nonlinear elastic constants, the magnitude of which, in an anistropic body such as quartz, depends on the crystallographic orientation of the resonator. The approximate angles of cut for a resonator in which this coupling becomes very low have been identified theoretically, and early results of experiments [6] confirm the existence of a low stress effect cut in the neighborhood of the crystallographic angles defined by theory. As this cut is also, in the same sense as an AT cut, temperature compensated, which is always a primary requirement, the term temperature/stress compensated (TS) cut appears most appropriate and will be used here. Estimates [4,5] indicate that the stress sensitivity of the TS cut may be as much as (or possibly even more than [6]) two orders of magnitude lower than that of the AT cut. The potential advantages of this cut are thus clearly significant.

A significant effort will no doubt be necessary to develop the potential of the TS cut into practical crystal units. One of the problems to be resolved revolves around the fact that the TS cut is a so-called doubly rotated cut and, therefore, contains two families of piezoelectrically excited modes, where the AT cut, being singly rotated, contains only one. The two "main modes", one for each family, are closely spaced in frequency. One must be suppressed, by electronic

means at this time, to assure proper oscillator operation. The added circuit complexity introduced is a major reason why doubly rotated cuts have in the past been used only for special purpose applications [7]. Moreover, the suppression of other spurious modes that interfere with the characteristics of the desired mode is a notoriously difficult problem even for AT resonators. This may be further aggravated by the second family of modes in the TS cut.

With the attention focused now on the potential benefits to be derived, it is expected that stress compensated resonators for application in precision oven controlled reference oscillators will become available in reasonable quantities during the late 1970's. For this application, useful operation of the resonator over only a narrow temperature range is acceptable, and only a small number of standard frequencies is involved. Wide temperature range resonators of this kind, such as are required for precision temperature compensated oscillators may take until the early 80's. The development of these latter resonators, especially if arbitrary frequencies are required, is likely to be hastened by progress in the computer modeling of resonator vibrations, using finite element techniques, which eventually will make it possible to dispense with the traditionally required cut-and-try techniques for the final steps in resonator design.

While there are very obvious risks in attempting to predict what a crystal oscillator specification might be like in the mid 1980 timeframe, it is interesting to speculate about what the impact might be if a crystal resonator can indeed be developed whose sensitivity to stress fields is two orders of magnitude lower than that of an AT resonator, and whose frequency temperature characteristic is similar to that of an AT cut but with the inflection point at around 90°C. The latter aspect would provide a near zero temperature coefficient range extending over several degrees around the normal operating temperature of a crystal oven. Let us further assume that this resonator be processed by the techniques of the 1980's which eliminate contamination and mass transfer within the crystal enclosure as sources of aging.

The physical size and power consumption of the 1980's crystal oscillator is indicated by the 16 cm^3 (1 cubic inch) and 150 mW characteristics of the Tactical Miniature Crystal Oscillator, (TMXO) currently (1975) under development [8]. A photograph of this oscillator is shown in Fig. 1, next to a 200 cm^3 unit representative of the 1975 off-the-shelf state of the art. A comparison of some of the features of these two oscillators is shown in Fig. 2. A more detailed listing of the characteristics of the TMXO now projected for the late 1970's is shown in Fig. 3, together with those of the 1980's oscillator which, along with improved circuitry, contains the stress compensated crystal resonator postulated just above.

The improved warmup characteristic of the 1980's vs the 1970's version in Fig. 3 is due to the absence (reduction), in the TS resonator, of the large frequency overshoot found in the AT resonators that is caused by the stresses set up by the thermal gradients incident to the resonator warm up. Likewise, part of the improvement in short and intermediate term stability is due to the fact that minor temperature fluctuations have negligible effect on the stress compensated resonator. The aging of the 1980's resonator, with contamination and mass transfer reduced to negligible levels, will no longer be determined by the stress relaxation in the mounting structure and the electrodes, but principally by thermodynamic order - disorder phenomena in the quartz and the electrodes, which should proceed only at glacial pace. Finally, because the frequency sensitivity of the AT resonator to static acceleration and vibration is (at reasonable levels) strictly determined by the magnitude of the induced stresses, the sensitivity of the stress compensated resonators will be proportionately lower.

The TMXO is an oven controlled crystal oscillator. The potential impact of a stress compensated crystal oscillator with suitable frequency/temperature characteristics could be equally important for high stability temperature compensated oscillators (TCXO's). However, the problems of developing a stress compensated crystal unit suitable for TCXO's are almost certainly greater than for oven controlled oscillators, as already indicated above. Once they have been resolved, TCXO's with stabilities in the low 10^{-9} range, 1-2 cubic inch size, and power consumption around 50 mW would appear to become possible, perhaps by the mid 1980's. Their design would follow the principles currently being developed [9], using digital compensation techniques. The major advantage of these TCXO's would be their instant "on frequency" operation capability.

Atomic and Molecular Frequency Standards

An excellent survey of the state of the art of atomic frequency standards, including an outlook toward the probable future developments has only recently been presented [10]. The emphasis there was on high precision laboratory devices. The focus here shall be on devices suitable for tactical systems applications.

There can be no question that the devices currently on the market or under development, i.e., the Rubidium and Cesium standards and the Hydrogen maser will continue to find increasing numbers of applications well into the 1980's. There can also be no question, however, that the price, size, weight and power consumption of these devices will continue to provide a powerful incentive to the systems engineers to avoid their use wherever possible. Size, weight and power consumption alone regardless of price, prohibits their use in modern army field equipment today.

There is a need, therefore, for a very small, potentially low cost atomic or molecular frequency standard whose stability approaches that of the present day Cesium standards, *i.e.*, is in the 10^{-11} - 10^{-12} range, short and long term, under manpack and vehicular conditions of operation.

The smallest atomic frequency standard currently available [11] is a 1000 cm^3 (61 cubic inch) Rubidium gas cell standard whose power consumption is 13 W. Its nominal frequency stability (temperature range is 0^oC to 50^oC) is comparable to that projected above for the one cubic inch crystal oscillator of the 1980's. Continued innovative engineering applied to the optical unit and the use of microcircuit techniques is likely to result eventually in a unit of about 40 cubic inches, consuming in the order of 6 W of power, again for the 0^oC to 50^oC temperature range. Extending this range to the -50^oC to $+85^oC$ range would be very costly in power, as thermoelectric cooling is necessary at the upper end; - the temperature of the gas cell itself must be maintained at 75^oC for proper operation. A suitably engineered unit of this kind should be capable of maintaining a frequency stability of 1×10^{-11} in a vehicular environment; and a reduction of the aging rate to 1×10^{-11}/year is likely to have been achieved by the latter part of the 1980's. Thus, while the stability potential of the Rubidium gas cell standard would appear to be adequate, its power requirements in particular - size is marginal at best - will continue to present a serious handicap for application in highly mobile systems. The search for alternate means to derive the requisite highly stable reference signals from a very small, low power unit will continue, therefore.

An examination of available new principles for frequency control points to systems that employ, or depend on, a stabilized laser as a major element, with a molecular resonance serving as the frequency discriminator. Although frequency stabilities in the 10^{-15} range have been projected [12] for laboratory systems in this category, - they are attained with hydrogen masers already - the constraints imposed by the need for miniaturization of the standard and of linking the stabilized laser frequency to the megahertz frequency range do not appear to admit their realization in a form suitable for systems application until, perhaps, the 1990's. It is no doubt premature at this time to attempt predicting which particular system and atomic or molecular transition is likely to offer the path of least resistance to a 10^{-15} small size unit, first. The ultimate frequency standard, in the distant future, may well turn out to require no more than a pellet of active material once the intrinsic properties of the Mossbauer Effect can be harnessed.

Stabilities in the 10^{-12} range, however, do appear attainable in the 1980's for use in highly mobile applications. The system most likely

to succeed, in the opinion of this author, is based on a miniature CO_2 laser, frequency stabilized by means of the fluorescence radiation from a CO_2 saturated resonance absorption cell [13].

The principle of saturated resonance absorption has been described extensively in the literature [14]. Its major advantage is in the fact that it can eliminate the Doppler broadening which dominates the line shape of a molecular resonance as observed by normal spectroscopic techniques. As a result, the line widths of molecular transitions can be reduced by several orders of magnitude. A narrow linewidth is obviously important if the resonance should be suitable for frequency control.

The frequency stability attainable with the aid of given resonator, regardless of its nature, is approximately given by

$$\left(\frac{\Delta f}{f}\right)_\tau = \frac{1}{2Q_\ell}\left(\frac{S}{N}\right)^{-1}_\tau$$

where Q_ℓ is the line Q, $Q_\ell = \Delta\nu/\nu_o$, and $(S/N)_\tau$ is the signal to noise ratio observed with a detector time constant of τ seconds.

The narrowest line width observed [15] to date in a CO_2 resonance cell is 164 kHz, which, with a line center frequency of 3×10^{13} Hz gives a line Q of about 2×10^8 (the line Q of the atomic resonance used in a Cesium standard is in the order of 5×10^7). The factors affecting the linewidth are discussed in Appendix A. While it should be possible to achieve, in time, line Q's in the order of 10^9, optimum operation of the resonance cell in a small frequency standard occurs at somewhat lower Q_ℓ values, probably around 10^8.

The CO_2 resonance of interest occurs at 10.6μ; however, the optimum technique for detecting the resonance is, following Freed and Javan [13], the observation of a dip in the 4.3μ fluorescence signal which is emitted when the excited CO_2 molecules relax to the ground state. The 4.3μ radiation is incoherent and nondirectional. Gallagher [16] has calculated the strength of the 4.3μ fluorescence signal and finds it to be proportional to the population difference between the (10^00) and (00^01) levels at thermal equilibrium, and to the power of the 10.6μ laser signal (the difference is nearly equal to the population of the $(10^00$ level). A numerical example places the total power in the 4.3μ fluorescence line at 5.4×10^{-7} watts which considering the depth of the dip at resonance in the emitted power to be 20%, yields a usable signal, with optimum modulation, of 8×10^{-8} watts. Evaluation of the date reported by Freed [17] appears to be consistant with this value.

A listing of some of the results obtained to date in experiments with the CO_2 resonance fluorescence cell is given in Fig. 4, together with the potential frequency stability, for an integration time of τ = 1 sec, calculated on the basis of the linewidth and signal to noise data reported. Kelly, et al,[16] and Freed's[17] data pertain to a resonance cell external, Gallagher's to one internal to the laser cavity. All have used cryogenically cooled detectors. Apparently, frequency stabilities in the 10^{-12} range are attainable for integration times larger than 1 sec.

For the CO_2 frequency standard to become a small and low power unit, however, it is necessary to use room temperature detectors for the 4.3μ radiation. Unfortunately, the noise power in even the best commercially available room temperature devices is about 100 times larger than that of the InSb detector, operated at 78° K, used by Freed [17]. Accordingly, the signal to noise ratio to be expected would be in the order of 5 to 10, which is clearly inadequate for frequency standard operation. Optimization of laser power and gas pressure in the resonance cell, as shown in Appendix B, will help, but not materially affect this situation. Nevertheless, it appears clear already, that relatively high levels of the 10.6μ radiation will be required, which are most readily available inside the laser cavity.

Several approaches are possible to improve the performance of the CO_2 resonance cell for room temperature operation. The use of better detector [18] alone may already bring the signal to noise ratio up well into the 10^2 range. Among the candidates to be studied are GaAs schottky diodes[19], improved pyroelectric devices, optoacoustic devices [20] and further improvements in PbSe. Metal-metal oxide-metal diodes [21], deposited by thin film techniques to form arrays, may also be found suitable once the optimum combination of materials is identified.

The basic reason for the low signal levels involved in the CO_2 resonance is that the number of molecules taking part in the phenomenon is only a very small fraction, about 10^{-3}, of the total molecules in the cell; the lower of the two energy levels involved in the 10.6μ resonance lies above the ground state. The most effective ways to increase the signal level would appear to be, therefore, to increase the population of this state, for example, by irradiating the resonance cell with 7.4μ light, which can probably best be derived from a black body (filament) through a 7.4μ bandpass filter. An increase in the available fluorescence signal by at least two orders of magnitude appears possible, which should be adequate to reach stability levels around 1×10^{-11} for 1 second integration time, even by using currently available room temperature detectors.

The stability numbers used so far actually describe the ability to define the center frequency ν_o of the resonance, assuming implicitly that ν_o is held constant by proper control of the environment. Indeed, the resonance frequency of the CO_2 molecule is remarkably unaffected by environmental conditions [15]. Each atom in the CO_2 molecule has zero molecular spin, resulting in the absence of any hyperfine structure; and there is no permanent electric dipole moment, so that shielding against external electric and magnetic fields is not required. There are no magnets employed in its operation that could add bulk and weight to the device. The frequency shift due to variations in the gas pressure within the cell are so low that no temperature control should be required to maintain a stability of better than 1×10^{-11} over $-50^{o}C$ to $+80^{o}C$ even at cell pressures in the order of 30 mT. Power shift as opposed to power broadening, due to the 10.6μ laser light is also small; a variation of the laser power level of 10% should cause less than 1×10^{-12} frequency variation in the 100 mW range. The probable magnitude of the frequency shift due to the 7.4μ black body pumping radiation, if used, has not been assessed, but should be very small.

Overall, the CO_2 resonance fluorescence cell promises to be an exceedingly simple device, requiring a minimum on controls, with an accuracy potential in the 1×10^{-11} range. Much work remains to be done to determine how closely this potential can be approached, or exceeded.

The size of the CO_2 control cell can probably be less than 1 cubic inch (16 cm^3). The 10.6μ laser which is required to excite the resonance, and in turn is stabilized by it, through a suitable feedback network, is likely to be about 10-12 cm long [13, 16]. If the resonance cell is built internal to the laser cavity it may be reasonable to expect that the whole stabilized laser assembly can eventually be compressed into a 1 X 1.5 X 7 inch, i.e. slightly larger than 10 cubic inch package. In the more distant future, it is conceivable that the laser will be replaced by a planar source of 10.6μ radiation.

The stabilized laser does not provide an RF output as required for systems applications; the output signal is in the 3×10^{13} Hz range. While the feasibility of frequency multiplications even into the visible light range has been demonstrated [22], the equipment used thereby included, next to an assembly of large laser oscillators, a Josephson junction operating in a He cryostat. The highest frequency reached to date with room temperature, solid state devices is about 3×10^{11}, still a factor of 100 away from our goal. Yet, harmonics at orders as high as 30-40 are considered obtainable with metal-metal oxide-metal diodes at Terrahertz frequencies [23]. Progress in solid state millimeter and submillimeter wave devices research and synthesis into

the THz range is rapid, and the prospects appear good that the results of this research will permit construction of a small size multiplier to link the CO_2 stabilized laser to a quartz crystal oscillator at some time during the early 1980's. To expect the complete CO_2 laser to occupy eventually no more than 20 cubic inches does not appear to be unreasonable.

Appendix A

Linewidth of the CO_2 Saturation Resonance Absorption Cell

The total linewidth of the CO_2 resonance cell is given by

$$\Delta\nu = \Delta\nu_{hom} + \Delta\nu_{power} + \Delta\nu_{geom.}$$

whereby $\Delta\nu_{hom} = 2$ is the homogeneous linewidth of the (10^00) - (00^01) transition. It is given by

$$\Delta\nu_{hom} = \Delta\nu_{rad} + \Delta\nu_{coll}$$

The line broadening due to radiative decay of the excited state $\Delta\nu_{rad}$ is on the order of 500 Hz and thus negligible when compared to the collison broadening $\Delta\nu_{coll}$. The latter is [20], for CO_2 at 22°C,

$$\Delta\nu_{coll} = \frac{u}{\ell_{fp}} = 7.6 \text{ kHz/m Torr.}$$

If the average particle velocity $u=3.35 \times 10^4$ cm/sec, the effective mean free path is $\ell_{fp} = 4.4$ cm m Torr. Gallagher[16] obtained a linewidth of about 800 kHz with around 100 m Torr of CO_2 in the resonance cell - which in this case was internal to the laser - in apparently excellent agreement with the above values.

Power broadening can be represented by the relation

$$\Delta\nu_{power} = \Delta\nu_{hom}\sqrt{1 + \frac{KP}{\Delta\nu_{hom}}}$$

where $\Delta\nu_{hom}$ is, as shown above, essentially equal to $\Delta\nu_{coll}$. P is the incident laser power and K a parameter whose value depends on the cross sectional area of the beam and the power density distribution across that area. Gallagher's data[16], obtained with the internal cell, are consistent with a value of K in the order of unity if P is in Watts and $\Delta\nu$ in Megahertz. A value of K = 1 provides also a very

reasonable match to the data reported by Kelly et al [15], and Freed [17] respectively (see Fig. 4 of text), for cells used external to the laser cavity.

Geometric broadening $\Delta\nu_{geom}$ occurs when cancellation of the Doppler broadening is incomplete, i.e. when the incident and reflected beams in the resonance cell are not perfect plane waves, perfectly parallel to one another. Causes are a.) diffraction due to finite beam diameter a, b.) curved wave fronts due to imperfect optics and c.) tilted reflecting mirror.

$$\Delta\nu_{geom} = \Delta\nu_a + \Delta\nu_R + \Delta\nu_\varphi$$

The broadening due to finite beam diameter a, also called transit time broadening,

$$\Delta\nu_a = \frac{u}{a},$$

remains negligible when compared to collision broadening, $\Delta\nu_{coll}$, until the mean free path becomes comparable to or larger than the beam diameter; e.g., at a pressure of 4.4 m Torr, the mean free path is ℓ_{fp} = 1 cm; hence at 4.4 m Torr and with a beam diameter of 1 cm, $\Delta\nu_{coll} = \Delta\nu_a$ = 33.4 kHz.

If the optics, used for beam expansion for example, produces a curved wave surface with radius of curvature R, line broadening occurs in the amount of

$$\Delta\nu_R = \frac{\varphi}{2R}\ \frac{u}{\lambda}$$

where λ is the wavelength of the laser light. With u = 3.35 X 10^4 cm/sec, a = 1 cm, $\lambda = 10^3$; $\Delta\nu_R$ = 16.8 kHz when R = 10^3 cm.

The broadening due to a mirror misalignment is [14]

$$\Delta\nu_\varphi = \varphi\,\frac{u}{\lambda}$$

This effect has been evaluated by Kelly et al [15] who finds $\Delta\nu_\varphi$ = 35.1 kHz/milliradian, in quite good agreement with the value of 31.6 kHz/milliradian predicted by the above relation.

Appendix B

Dependence of SQ_ℓ on Cell Pressure and Laser Power

The fluorescence signal power is proportional to the incident power P

and the number of molecules per cm^3, n; hence, because $\Delta\nu_{coll}$ is proportional to n,

$$S = AP\,\Delta\nu_{coll}$$

The linewidth, as shown in Appendix A is given approximately by

$$\Delta\nu = \Delta\nu_{coll} + \Delta\nu_{power} + \Delta\nu_{geom}$$

$$= \Delta\nu_{coll}\left[\ 1+\sqrt{1+\frac{KP}{\Delta\nu_{coll}}}\ +\ \frac{\Delta\nu_{geom}}{\Delta\nu_{coll}}\right]$$

Therefore,

$$SQ_\ell = S\,\frac{\nu_o}{\Delta\nu} = \frac{P}{1+\sqrt{1+\frac{KP}{\Delta\nu_{coll}}}\ +\ \frac{\Delta\nu_{geom}}{\Delta\nu_{coll}}}$$

The optimum operating power, reached when $(K/\Delta\nu_{coll})\,P = 1$, increases with $\Delta\nu_{coll}$, i.e. the gas pressure in the cell. Once collision broadening dominates over the geometric broadening, the maximum usable gas pressure, with maximum SQ_ℓ as the criterion, will be determined by self trapping of the fluorescence radiation, or by excessive increase in pressure shift [24].

References

1. Vig, J.R., Wasshausen, H., Cook, C., Katz, M. and Hafner, E., Proc. 27th Annual Frequency Control Symposium, pp 98-112 (1973). Vig, J.R., Cook, C., Schwidtal, K., LeBus, J.W. and Hafner, E., Proc. 28th Annual Frequency Control Symposium, pp 96-108 (1974). Vig, J.R., Filler, R.L., LeBus, J.W., Proc. 29th Annual Frequency Control Symposium, pp 220-229, (1975). Vig, J.R. and Hafner, E., R&D Technical Report ECOM-4134 (1973). Hafner, E. and Blewer, R.S., Proc IEEE, 56 pp 366-368, Mar 1968.

2. Hafner, E., IEEE Trans. SU-21, pp 220-237, Oct 1974.

3. Lee, P.C.Y., Wang, Y.S. and Markenscoff, A., Proc.27th Annual Frequency Control Symposium, pp 1-10, (1973).

4. Holland, R., IEEE Trans. SU-21, pp 171-178, July 1974. Proc. 1974 Ultrasonics Symposium IEEE lot #74 CH0896-1SU, pp 593-598.

IEEE Trans SU-23, pp 72-75, Jan 1976.

5. EerNisse, E.P., Proc .29th Frequency Control Symposium, pp 1-4, (1975).

6. Kusters, J.A., to be published.

7. Hammond, D.L. and Benjaminson, A., Hewlett Packard Journal, Vol 16, pp 1-7, March 1965.

8. Greenhouse, H.M., McGill, R.L. and Clark, D.P., Proc. 27th Annual Frequency Control Symposium, pp 199-214, (1973). Greenhouse, H.M., and McGill, R.L., R&D Technical Report ECOM-0199-F, July 1975 (Final Report on ECOM Contr. DAAB07-07-73-C-0199 with the Bendix Corp.).

9. Buroker, G.E. and Frerking, M.E., Proc .27th Annual Frequency Control Symposium, pp 191-198 (1973). Mroch, A and Hykes, G, R&D Technical Report ECOM-0137-3, Sept 1975. (Report on ECOM Contr. DAAB07-73-C-0137 with the Collins Corp.)

10. Hellwig, H.W., Proc IEEE Vol 63, pp 212-229, Feb 1975.

11. Jeckart, E., Proc. 27th Annual Frequency Control Symposium, pp 387-389, (1973).

12. Barger, R.L., English, T.C. and West, J.B., Proc 29th Annual Frequency Control Symposium, pp 316-320, (1975).

13. Freed, C. and Javan, A., Appl. Phys. Lett. 17, pp 53-56, July 1970.

14. Letakhov, V.S., Fundamental and Applied Laser Physics. Proc. of the Esfahan Symposium, Feld, M.S., Javan, A and Kurnit, N.A. edit. John Wiley 1973, pp 335-367.

15. Kelly, M.J., Thomas, J.E., Monchalin, J.P., Kurnit, N.A. and Javan, A., Proc. 29th Frequency Control Symposium, pp 338-343, (1975)

16. Gallagher, J.J., Proc. 29th Annual Frequency Control Symposium, pp 344-351 (1975), R&D Technical Report ECOM-0065-F, Dec 1974 (Final Report on ECOM Contr. DAAB07-73-C-0065). Abrams, R.L., Appl. Phys. Lett. 25, pp 304-306. Sept 1974

17. Freed, C., Proc. 29th Annual Frequency Control Symposium, pp 330-337, (1975).

18. IEEE Special Issue on Infrared Technology for Remote Sensing. Proc. IEEE, Jan 75.

19. Pyee, M., Clairon, A. and Auvray, J., Electronics Letters, 10 pp 500-501, Nov 1974

20. Abrams, R.L., Appl. Phys. Lett. 25, pp 609-611, Nov 1974.

21. Small, J.G., Elchinger, G.M., Javan, A., Sanchez, A., Bachner, F. J., and Smythe, D.L., Appl. Phys. Lett. 24, pp 275 (1974).

22. Evenson, K.M. et al, Appl. Phys. Lett. 22, pp 192-195, 1973. Barger, R.L. and Hall, J.L., Appl. Phys. Lett. 22, pp 196-200, 1973.

23. Sakuma, E. and Evenson, K.M., IEEE Jour. Quantum Electronics, Vol QE-10, pp 599-603, Aug 1974.

24. Bagaev, S.N., Baklanov, E.V. and Chebotaev, V.P., Soviet Phys. JETP Lett. 16, pp 243-246, Sept 1972.

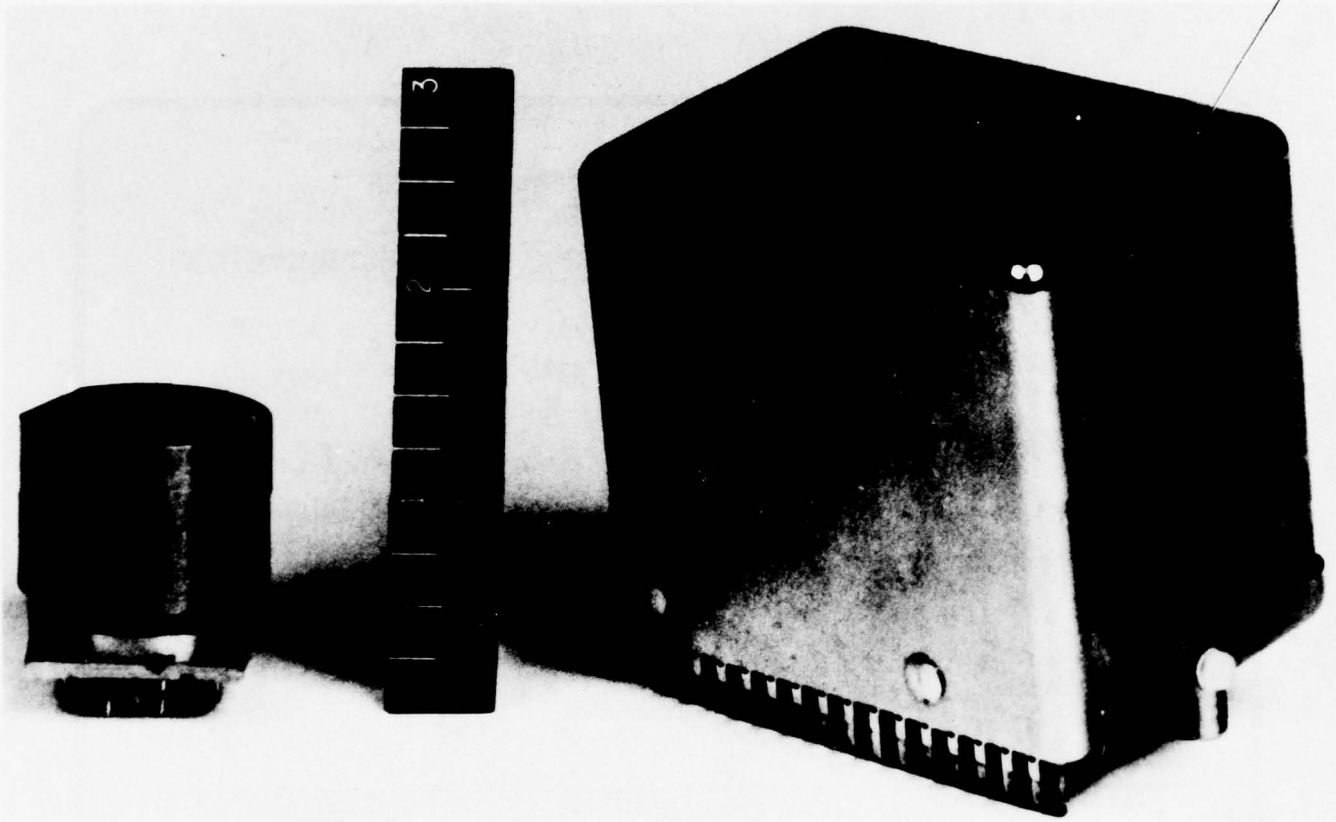


Fig. 1. Experimental oven controlled crystal oscillator (left) and representative state of the art commercial oscillator of comparable performance.



PERFORMANCE CHARACTERISTICS FOR OVEN CONTROLLED CRYSTAL OSCILLATORS

CHARACTERISTICS	STATE OF THE ART PACKAGED OSCILLATOR	TACTICAL MINIATURE OSCILLATOR (DEVELOPMENT)
SIZE	$220cm^3$	$16cm^3$
POWER CONSUMPTION		
@ 25°C	3.75 WATT	0.13 WATT
@ -45°C	8.65 WATT	0.25 WATT
STABILIZATION TIME (TO REACH 1 X 10-8 OF FINAL FREQ.)		
@ 25°C	15 MIN	2 3/4 MIN
@ -45°C	28 MIN	3 1/4 MIN
ACCELERATION COEFFICIENT	$2 \times 10^{-9}/G$ (OVERTONE)	$10 \times 10^{-9}/G$ (FUNDAMENTAL)

Fig. 2

MINIATURE OVEN CONTROLLED CRYSTAL OSCILLATOR

CHARACTERISTICS	1976	1980's
OUTPUT - FREQUENCY	5 MHz	5 MHz
VOLTAGE/LOAD	0.125V/50Ω	0.125V/50Ω
INPUT - VOLTAGE	12V ±5%	12V ±5%
POWER - OPERATING	0.25W MAX	0.20W MAX
POWER - WARMUP	10W (<1 MIN)	10W (<30 SEC)
SIZE	16 CM^3 (1 CU INCH)	16 CM^3 (1 CU INCH)
WEIGHT	75G	30G
WARMUP	3 MIN TO 1 X 10^{-8}	30 SEC TO 1 X 10^{-9}
STABILITY - AGING	1 X 10^{-8}/MONTH	1 X 10^{-10}/MONTH
SHORT TERM	5 X 10^{-11}/1 SEC	5 X 10^{-12}/1 SEC
TEMPERATURE	1 X 10^{-8}(-54°C TO + 75°C)	2 X 10^{-10}(-54°C TO +85°C)
ACCELERATION	1 X 10^{-8}/G	2 X 10^{-11}/G
VOLTAGE CONTROL - RANGE	±5 X 10^{-8}	±5 X 10^{-8}
VOLTAGE	0 - 10V	0 - 10V

Fig. 3



RESULTS OF CO_2 FLUORESCENCE CELL EXPERIMENTS

FWHM (kHz)	PRESSURE (mT)	POWER (W)	S/N	$\sigma(\tau=1)$** ($\times 10^{11}$)	REFERENCE
270	0.5	1	100	2.5	(15)
167	0.5	0.11	40	3.8	(15)
344	4.5	0.58	200	1.6	(15)
900	34	1.75	900	1.0	(17)
800	75	0.06*			(16)
1750	75	1.5*			(16)
2600	75	3.0*			(16)
3100	75	4.0*			(16)

* EXTRAPOLATED VALUES

** CALCULATED VALUES

Fig. 4

QUESTION AND ANSWER PERIOD

Paper Not Presented Orally, Therefore, There Were No Questions And Answers.

CLOCK TIME ERRORS AND TIME PREDICTION

David W. Allan
National Bureau of Standards

ABSTRACT

Based on a reasonable mathematical model which describes the time dispersion on most state-of-the-art clocks, the errors in time prediction are quantified. This model contains both random as well as non-random terms. These terms are prioritized as to the significance of their contribution to a clock's time dispersion, and this prioritization is shown to be a function of the prediction time.

Some simple methods of prediction are compared with optimum prediction and it is shown that by a judiacious choice of data processing, one can come extremely close to optimum prediction using these simple methods.

(Paper not Received)

PRECEDING PAGE BLANK-NOT FILMED

QUESTION AND ANSWER PERIOD

SGT. OSTROWSKI:

Ostrowski, Newark Air Force Station.

In the use of the chambers for these cesiums to improve their performance, has there been any definite improvements in short term stability by just putting them in a chamber?

MR. ALLAN:

I think the effects are only in the long term stability, at least as we documented it. We have not seen any material effect in the short term stability.

SGT. OSTROWSKI:

And the long term, approximately what, do you think?

MR. ALLAN:

After we were into this second environmental chamber we saw flicker levels drop at least a half an order of magnitude, maybe even an order of magnitude in some cases.

SGT. OSTROWSKI:

And the biggest effect, do you think, was temperature or vibration?

MR. ALLAN:

I think probably temperature. We also were able to measure temperature coefficients and see that it was a real effect, just due to room temperature variations.

MR. RUEGER:

For the last chart shown, could you give us a little more data on how you determined it was that good or what your reference was to make that number?

MR. ALLAN:

Okay. To go on with that, that is another hour, but let me

just see if I can give you a quick snapshot. We have seven other cesium standards, commercial standards, in our ensemble. During this period of time, for the most part, NBS was not a significant member of that ensemble. So, it is not totally true, but it is approximately true that NBS 4 and UTC NBS were almost independent.

So, what is happening here is you are seeing the time fluctuation of a weighted ensemble of 7 commercial cesiums versus NBS 4, almost. To go into more detail would take quite a bit more time. In the bottom case, we are using a recursive filter to give a best estimate or near-best estimate of the NBS source frequency for time prediction purposes. So, this is in its raw frequency. This is the filtered estimate of the frequency, filtering out the higher frequency components. I don't know whether that helps.

But, without going into quite a bit more detail, that is basically what is shown.

RADIATION EFFECTS IN CRYSTAL AND ATOMIC FREQUENCY STANDARDS*

T. M. Flanagan and R. E. Leadon
IRT Corporation, San Diego, California

INTRODUCTION

The increased use of precision frequency standards in environments where exposure to nuclear and natural radiation can be encountered has led to some detailed considerations of the effects of such radiation on the operability, stability, and accuracy of precision frequency standards. Quantifying these considerations requires combining of results from prior modeling studies on precision frequency standards (Ref. 1,2), from investigations of the effects of radiation on quartz crystals (Ref. 3-6) and from analyses on electronic systems (Ref. 7). It is the purpose of this paper to describe the results of studies to develop predictive models for precision frequency standards in radiation environments.

GENERAL EFFECTS OF RADIATION

We first consider the types of radiation and the effects on the components of a precision frequency standard. For our example, let us consider a precision frequency standard designed for satellite use. Such a standard not only must survive the radiation from the Van Allen belts but must also face the possibility of exposure to direct nuclear radiation from a nuclear detonation and the consequential enhancement of the electron belts.

The irradiating particles produced by a nuclear detonation include neutrons and gamma rays. In addition, energetic electrons are produced as secondary particles from the interaction of gamma rays with matter, and are emitted from radioactive fission products. The electrons from a nuclear detonation can become trapped in the earth's magnetic field, thus enhancing the electron flux in the Van Allen belts (Ref. 8).

The types of effects to be considered are (1) displacement effects, (2) ionization, and (3) chemical effects. Displacement effects are caused by collisions between incident nuclear particles and atoms in solids, resulting in the displacement of the struck atoms and possibly others. The

*This work was supported by the Defense Nuclear Agency under contract DNA001-75-C-0247.

PRECEDING PAGE BLANK-NOT FILMED

principal source of displacement effects is the neutrons. Ionization effects, primarily evidenced as increased conductivity, are manifestations of the mobile electrons and ions produced by the interaction of the radiation with atomic electrons. Associated with ionization is the transfer of charge by secondary irradiations in circuit elements creating electric and magnetic fields within cavities – even those with good electrical shielding – and creating space charge in insulators. These latter effects are sometimes known as internal EMP effects. Chemical effects refer to changes in molecular composition that frequently result from recombination processes following ionization.

For our consideration of a precision frequency standard for a satellite, we assert (Ref. 9):

1. Neutron fluences are such that displacement effects are of concern only in semiconductor devices and in quartz crystals which depend on a high degree of crystallinity for proper operation. Designing circuits with adequate design margin to allow for semiconductor device degradation is a developed methodology and is beyond the scope of this paper. The effects of neutrons on quartz crystals are also small compared to the effects of the ionization.

2. Chemical effects are usually of little concern because the changes in properties due to chemical radiation effects become important only for exposures which are large compared to those which result in electronic system degradation. A possible exception to this is outgassing from the walls of a vacuum chamber.

Thus, the relevant effects of radiation for a precision frequency standard are:

1. Those which result from the intense ionization resulting from a nuclear burst. The gamma-ray ionization is assumed to be sufficiently intense that the semiconductor devices are driven into saturation and that darkening of any optical components must be considered.

2. Frequency and Q shifts from exposure of the quartz crystal oscillator to gamma rays and neutrons.

3. Secondary-electron currents which may alter the magnetic fields, send large currents down coupling lines, result in outgassing from vacuum

chamber walls, and produce charge in insulators.

4. Effects of the electron belts, both natural and enhanced. We anticipate changes in Q and frequency of the quartz crystals, degradation in the characteristics of semiconductor devices, and darkening of optical components from the electron belt dose.

EFFECTS OF RADIATION ON QUARTZ PRECISION FREQUENCY STANDARDS

When a quartz oscillator is exposed to radiation, both the electronics and the quartz resonator are affected. Let us consider the resonator first. The response of quartz crystals to radiation has been fairly well documented (Ref. 3-6), and the responses of various types of quartz are reviewed in the references. In general, it has been found that sweeping (i.e., electro-diffusing at elevated temperatures along the Z axis) reduces the response of quartz to radiation. The reduction in radiation sensitivity is such that, for precision frequency applications in a radiation environment, swept synthetic Z-growth quartz is the material of choice.*

The quartz resonator in a precision frequency standard will generally be located in an oven. The materials of the oven provide sufficient shielding that the total ionization dose to the quartz resonator is generally less than 10^4 rads. The effects of the neutrons from a pulse radiation is to produce a positive frequency shift which is small compared to the negative shift induced by the ionization from the gamma rays and the electrons. Hence, we consider only ionization effects in the resonators.

Following a pulse of transient radiation, changes in frequency and Q are observed. These changes show a partial anneal toward preirradiation values for about 20 min after the cessation of radiation, after which time the changes in Q and frequency are relatively stable. Changes which anneal within 20 min or so of the cessation of radiation are called transient shifts. The steady-state shifts are not permanent, and long-term drift in the crystal parameters is observed.

*The equivalent series resistance also increases following a pulse irradiation, and the increase can be large and persistent in some natural and unswept lithium-doped synthetic material (Ref. 4). Sweeping generally reduces this problem to insignificance.

Figure 1 is an idealized illustration of the change in frequency after irradiation, showing both the transient and steady-state shifts as a function of time following a pulse of radiation. The quantity f_0 is the original preirradiation frequency, f_{ss} is the steady-state frequency taken approximately 15 to 20 min after exposure, f(t) is the instantaneous frequency at any time t, and Δf_a is the annealable portion of the frequency change. This notation is from King and Sander (Ref. 4). The annealable fraction of the frequency change following a pulse of radiation reduced to unit dose is plotted in Figure 2. The results of several investigators are presented, and there is remarkable agreement in the data even though taken over a wide range of doses and at different frequencies. The behavior of the annealable fraction is not very sensitive to the type of material and is reasonably well represented by

$$\frac{\Delta f}{f_0} = 2 \times 10^{-11} \, t^{-1/2} \, D \, , \qquad (1)$$

where t is the time in sec and D is the dose in rad(SiO_2).

The magnitude of the steady-state frequency shift is variable from crystal to crystal even for the same type of quartz, and the response shows some changes which reflect the radiation history. The initial exposure to a low dose [less than about 10^3 rad(SiO_2)] produces a frequency shift of a few parts in 10^8 which can be either positive or negative, after which the rate of frequency shift with dose drops significantly.* In the range from a few thousand rads to approximately 10^4 rads, resonators of good swept synthetic quartz can be found which will shift about 5×10^{-13} per rad(SiO_2).

As mentioned above, the steady-state frequency shift is generally measured about 20 min after exposure to a pulse of radiation. The selection of 20 min is a somewhat arbitrary choice, since the frequency continues to drift. However, the drift/sec is small compared to either the steady-state (20-min) or the transient drift discussed above. Hence, it is convenient to describe the shifts which occur after 20 min as an enhanced drift rate. The magnitude of the enhanced drift rate is not as well documented as the effects discussed above. What has been observed is that pulses of radiation

*Resonators for use in radiation environments are often exposed to doses of a few thousand rad(SiO_2) prior to installation in the oscillator. Such exposures can be used both as a screening procedure and as a conditioning procedure to achieve the lower radiation response.

in the 10^3 to 10^4 rad range result in a drift rate of about 1×10^{-9} per day or less for a few days after exposure. If no further irradiation occurs, the drift rate returns to its preirradiation value (on the order of a few parts per 10^{11} per day within a few days.

PASSIVE FREQUENCY STANDARD MODELING

Let us now turn our attention to passive frequency standards. By passive frequency standard we mean a device in which a high-quality quartz oscillator provides the output. The drift of the quartz oscillator is corrected by a feedback loop which references the quartz frequency to an atomic resonance. The cesium beam standard and the rubidium vapor standard are the most common of this type and will be used as examples in this paper. There are many ways of implementing the concept of a quartz oscillator locked to an atomic resonance device through a control loop, but a common modeling methodology obtains for systems with a first-order control loop. Due to the complexity of the systems, it is not practical to have one complete model which can be applied in all situations in a radiation environment. It is more convenient and informative to utilize several simple models, each of which is useful and adequate for a particular situation but which must be used with judgment because of its limitations.

We first distinguish between catastrophic effects which cause effective failure of the standard and effects which leave the standard operating but with degraded performance. For the purposes of this paper, catastrophic effects are those which result in a cessation of function of some critical element of the system (for example, a semiconductor device burnout). Design solutions to such problems are not unique to a frequency standard but are part of the library of tricks of the radiation effects circuit engineer, and will largely be ignored in this paper. What we wish to do is model the principal radiation effects in precision frequency standards.

Referring to Figure 3, we assume a first-order loop in which the atomic resonance device is presented as a blackbox that puts out a linear error voltage equal to $K_B \Delta f/f_0$ plus some noise. This voltage is amplified (A) and coupled to the input of an integrator. The integrator can take many forms but basically has an output which stores the integral of the error voltage over time. The output voltage of the integrator corrects the oscillator which provides the primary output.

The output of the oscillator is the nominal frequency f_1 plus a correction proportional to V_0 plus some phase noise. The frequency f_1 is multiplied by a constant M which gives a frequency close to the atomic resonance frequency. Since the atomic resonance frequency is usually not an integral multiple of the basic oscillator frequency, a separate synthesizer is used to make up the difference. This synthesizer is locked to the basic oscillator; we have represented a digital technique for doing that lock. The integral multiple of the oscillator frequency is added to the synthesizer frequency to give the input frequency to the atomic resonance device.

The overall loop gain of the system, as described by Figure 3, can be written as

$$K_L = \frac{1}{\tau_L} = \frac{K_0 K_B}{RC} \ , \qquad (2)$$

where K_0 relates the error signal to the frequency difference as seen by the Cs tube and K_B relates the frequency error into the Cs tube to the error voltage at the input of the integrator. As Eq. 2 indicates, the loop time constant τ_L involves, but is not equal to, the integrator time constant RC.

For modeling non-catastrophic radiation effects, errors are categorized as (1) steady offset errors, (2) random errors, and (3) transient errors. A catalog of errors which must be considered under each of these categories can be derived by considering those factors which affect stability and accuracy. A certain subset of those factors is perturbed by radiation and must be modeled as one of the types of errors above.

For small perturbations, the equation of motion for the system (closed loop) can be approximated as

$$\frac{d(\Delta f/f_0)}{dt} = -K_L(\Delta f/f_0) + F(t) \ , \qquad (3)$$

where F(t) is some exterior frequency perturbation such as an open-loop oscillator drift rate, and K_L is as in Eq. 2. A steady offset implies

$$\frac{d(\Delta f/f_0)}{dt} = 0 \ ,$$

and by substituting the appropriate open-loop F(t), the steady-state offset can be calculated.

Random errors are modeled as noise generators and the model is similar to that developed by Cutler and Searle (Ref. 1). Dominant noise sources in passive frequency standards are the quartz oscillator phase noise and the noise in the atomic resonance cell.

For the transient errors which result from a nuclear burst, the nonlinear effect of saturation of the electronics is combined with Eq. 3, which is applied when the system returns to linear operation. Let us now apply these models to the dominant environments.

DOSE-RATE EFFECTS FROM ELECTRON BELTS

Consider first which error terms are significant in the presence of the electron flux in the enhanced radiation belts. The flux in the enhanced belts is relatively low (3 x 10^8 to 10^9 e/cm^2-sec), so that the semiconductor device operation is not perturbed by photocurrents. Thus, we can neglect disturbances in most electronic circuits. However, the low-rate background will induce some noise in the detector in the resonance device (electron multiplier in a Cs beam tube or the optical detector in the Rb gas cell). We treat this noise from the electron belts as a white noise which influences the Allan variance through

$$\sigma_{\dot{\phi}} = \sigma_0 \frac{(S/N)_0}{(S/N)_{\dot{\phi}}} \tag{4}$$

where the σ's designate the Allan variance, S/N is the signal-to-noise ratio from the resonance device, and the subscripts indicate a zero or a $\dot{\phi}$ electron flux, respectively. The magnitude of this effect is system-dependent. The existence of this noise source has been verified in a simulation experiment performed at NRL, and at 3 x 10^8 e/cm^2-sec, an approximate increase of 20% in the $\sigma(2,\tau)$ curve was observed for a Frequency and Time Systems, Inc., Cs beam tube. The effect should be less for a Rb system optical detector, but the effect is so dependent on the amount and type of materials surrounding the detector that the experiments should be performed for each device considered.

EFFECTS OF DOSE FROM ELECTRON BELTS

The ionization dose due to the enhanced electron belts to electronic devices behind 0.040-inch Aℓ boxes accumulates at about 10^5 rad/day. An ionization dose of this magnitude causes surface charge buildup in semiconductor devices. The

manifestations in terminal characteristics are gain degradation in transistors, changes in reference voltage elements, and increased offsets in operational amplifiers. For most circuits, the design and parts selection methods are not unique to the precision frequency standards, but certain aspects are of special importance.

The changes in voltage reference elements which determine the resonator magnetic field require critical consideration, as do offsets in linear integrated circuits in voltage regulators. Changes in the C-field current are particularly troublesome. For changes in C-field current, $\Delta f/f_0 \simeq 3.5 \times 10^{-10}\ \Delta I/I$ for Cs, and $\Delta f/f_0 \simeq 2.5 \times 10^{-9}\ \Delta I/I$ for Rb. Thus, to hold the frequency to 2×10^{-13}, the C-field current must not change by more than 0.06% for Cs and 0.008% for Rb. This places a severe hardening requirement on the power supplies.

Offsets in the integrator operational amplifier produce large frequency offsets which increase with radiation. The condition for null in the control loop of Figure 3 is zero current in the integrator capacitor. Thus, the loop will compensate by a frequency error for offset currents and offset voltages in the integrator operational amplifier. The total error voltage at the integrator output from offsets is

$$V_e = I_{OS}\ R + V_{OS}\ . \tag{5}$$

A frequency error at the Cs tube will result which produces an error signal at the integrator inputs to cancel V_e. The loop again will then be null. Since the error voltage at the output of the Cs tube is

$$V_e = K_B\ \Delta f/f_0\ , \tag{6}$$

the condition for null is

$$K_B\ \Delta f/f_0 = I_{OS}\ R + V_{OS} \tag{7}$$

or

$$\Delta f/f_0 = \frac{1}{K_B}\ (I_{OS}\ R + V_{OS}) \tag{8}$$

The I_{OS} and V_{OS} are functions of dose. To obtain frequency error, empirical functions for I_{OS} and V_{OS} as a function of dose must be substituted into Eq. 8. As a numerical example, assume RC = 1 sec, $K_0 = 10^{-12}$, $\tau_L = 10$ sec, and $K_B = 10^{11}$. Generally, the radiation-induced V_{OS} dominates and $\Delta f/f = 10^{-13}\ V_{OS}$ (mV). Operational amplifiers are available which do not change V_{OS} significantly at 10^5 rads and which change

by 3 to 5 mV at 10^6 rads. Thus, a $\Delta f/f_0$ of 3 to 5 x 10^{-14}/day is achievable by careful parts selection. Lower offsets can be achieved with modest shielding.

The quartz oscillator experiences an increased drift rate due to the accumulated dose from the electron belts. To use another example, if the oven materials are equivalent to 0.5 cm (1.35 g/cm^2) Al, the average 1-day dose from the enhanced belts is about 10^4 rads. For a good swept synthetic resonator, the frequency of the quartz will drift about 5 x 10^{-9}/day or 6 x 10^{-14}/sec. Since the change is small in a time τ_L, we can treat this as a drift term and compute the frequency error from Eq. 3:

$$\Delta f/f_0 = \tau_L F(t) = 6 \times 10^{-14} \tau_L . \qquad (9)$$

For $\tau_L = 10$ sec, the frequency error is about 6 x 10^{-13} at the end of one day.

The glasses in a Rb gas cell will experience some darkening as a result of the accumulated dose. This will reduce the light intensity at the cell and at the detector. Qualitatively, the light intensity has two effects on the operation of the gas cell standard. A decrease in the light intensity decreases the signal-to-noise ratio, and a change in the light intensity induces a frequency shift. The magnitude of the light intensity shift is dependent on the buffer gas pressure, magnetic field, and optical pumping conditions. Figure 4 shows the light intensity shifts obtained by three different groups of investigators. The buffer gas pressure and pumping conditions are indicated on the figure. These experiments provide some bounds for the light intensity shifts, which range from 2 to 10 x 10^{-11}/% change in intensity. Data taken at room temperature on borosilicate glasses would seem to indicate that the radiation-induced absorption coefficients near 7800 Å are about 2 x 10^{-3} cm/rad. Based on this estimate, we would expect frequency shifts in the vicinity of several parts in 10^{12} for 10^3 rads. However, this data is taken at room temperature rather than at the Rb cell operating temperature. The shifts expected from this data are undoubtedly too large.

EFFECT OF A PULSE FROM A NUCLEAR BURST

The list of factors which affect the accuracy and stability of a frequency standard is a long one, but fortunately most error sources do not change significantly with radiation. The important effects of a nuclear burst are those listed

briefly in Section 2. In this section we discuss each in as quantitative a way as possible.

The effects of a nuclear burst on the open-loop quartz oscillator have been discussed above. When the quartz oscillator is coupled to an atomic resonance device in a control loop, the open-loop frequency errors will ultimately be nulled to insignificance. Phase errors, which are proportional to $(\Delta f/f_0)_{SS}\ \tau_L$, will result for steady offsets in quartz. As long as the control loop remains linear, the effects of the annealable portion of the open-loop frequency shift will integrate to zero phase error in a few time constants. Since the electronics saturate as a result of the ionization and since the transient frequency shift resulting from ionization may also saturate the loop electronics, the loop is not expected to be linear through the nuclear burst. Thus, the phase correction is not perfect, and the amount of error must be calculated for each system and environment.

The increased drift rate following a pulse of nuclear radiation will result in a closed-loop frequency error of less than $2.3 \times 10^{-14}\ \tau_L$. This frequency error will persist for a few days after the burst.

The optics in the Rb cell will darken with the pulse, and some of the darkening will anneal in periods extending over several seconds. At present, we know of no data on the magnitude or persistence of the effect.

Saturation of the electronics causes significant perturbation of the error loop. Saturation of the linear ICs implies that the output of the error amplifier (A) and of the integrator will assume the power supply voltages and both ICs may assume the same polarity. The input to the integrator will remain saturated for a recovery time (on the order of 10^{-5} sec), but the voltage at the output of the integrator will persist at the power supply voltage until removed by a corrective error signal. Depending on the system, this could be a catastrophic effect since the full-scale output of the integrator may shift the oscillator more than a resonant line width of the atomic device. Locking on the wrong resonant peak or simply not having enough signal to allow recovery of the integrator in a reasonable time could result. Clearly, a non-volatile integrator is required for a pulsed nuclear environment.

Usually the synthesizer is phased-locked to the main oscillator. Saturation of the electronics will cause some relative phase error to appear in the synthesizer loop,

which will be corrected by a synthesizer frequency shift. This shift will produce a transient frequency error which will be nulled out when the synthesizer loop regains lock.

In the Rb cell, since the frequency of the resonant transition is temperature-dependent, a pulse of nuclear radiation, which will cause a rise in temperature of the gas cell, will produce a frequency error. For typical conditions, the frequency temperature dependences are linear and in the range of 5 to 7 x 10^{-10}/°C. For a dose of D rads, the temperature rise in the material is given by

$$\Delta t = \frac{2.4 \times 10^{-6}}{C} D ,$$

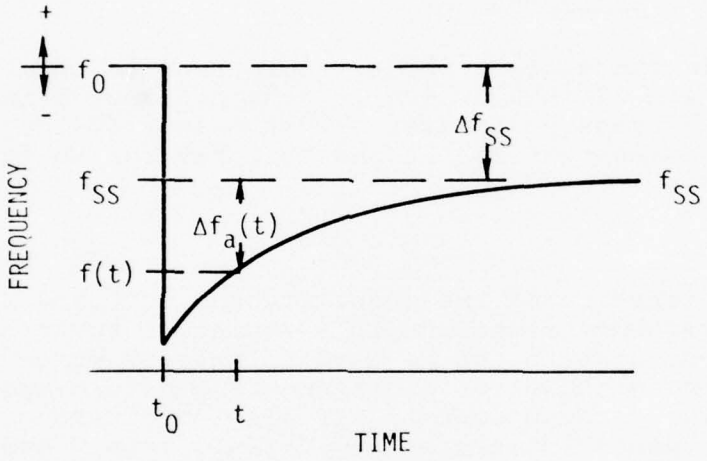
where C is the specific heat. This results in a $\Delta f/f_0$ of the order of 2 x 10^{-15} D, which is a significant effect for a dose of 10^3 rads or greater. This effect of the temperature rise will disappear as the gas cell returns to its normal temperature.

SUMMARY

Consideration of the stability and accuracy of passive atomic frequency standards in a radiation environment have led to models which can be used to predict error budgets. Some terms in the error budget must be determined experimentally. The error budget in a radiation environment indicates that a hardened integrator and C-field supply are critical items. When the electronics are hardened, the radiation-induced shifts in the quartz oscillator will dominate the error budget.

ACKNOWLEDGMENTS

The authors would like to express their appreciation to individuals whose information and counsel were invaluable in the performance of this work: Captain Richard Stead, DNA; Les Palkuti, C. A. Bartholomew, and Robert Moore, NRL; V. A. J. van Lint, consultant; Robert Kern, Frequency and Time Systems; Martin Bloch, Frequency Electronics; J. Barnes, David Allan, and Helmut Hellwig, NBS.



f_0 = ORIGINAL, PREIRRADIATION FREQUENCY

f_{SS} = STEADY-STATE FREQUENCY (∿15 MIN AFTER EXPOSURE)

$f(t)$ = INSTANTANEOUS FREQUENCY AT ANY TIME t

Δf_a = ANNEALABLE PORTION OF FREQUENCY CHANGE

RT-12885

Figure 1. Typical behavior of frequency versus time for quartz resonators following an x-ray exposure pulse (Ref. 4)

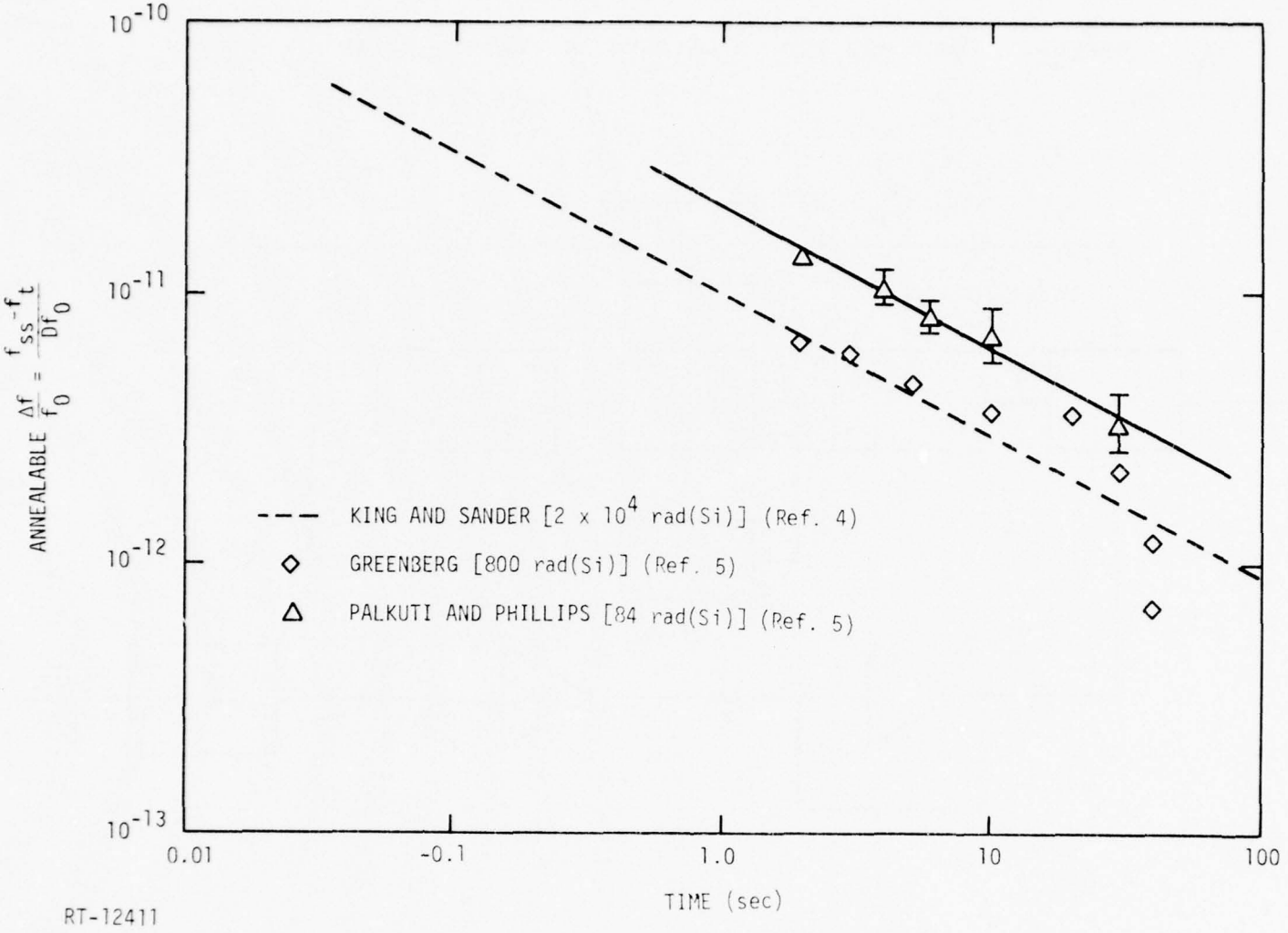


Figure 2. Annealable frequency shift versus time for swept synthetic resonators

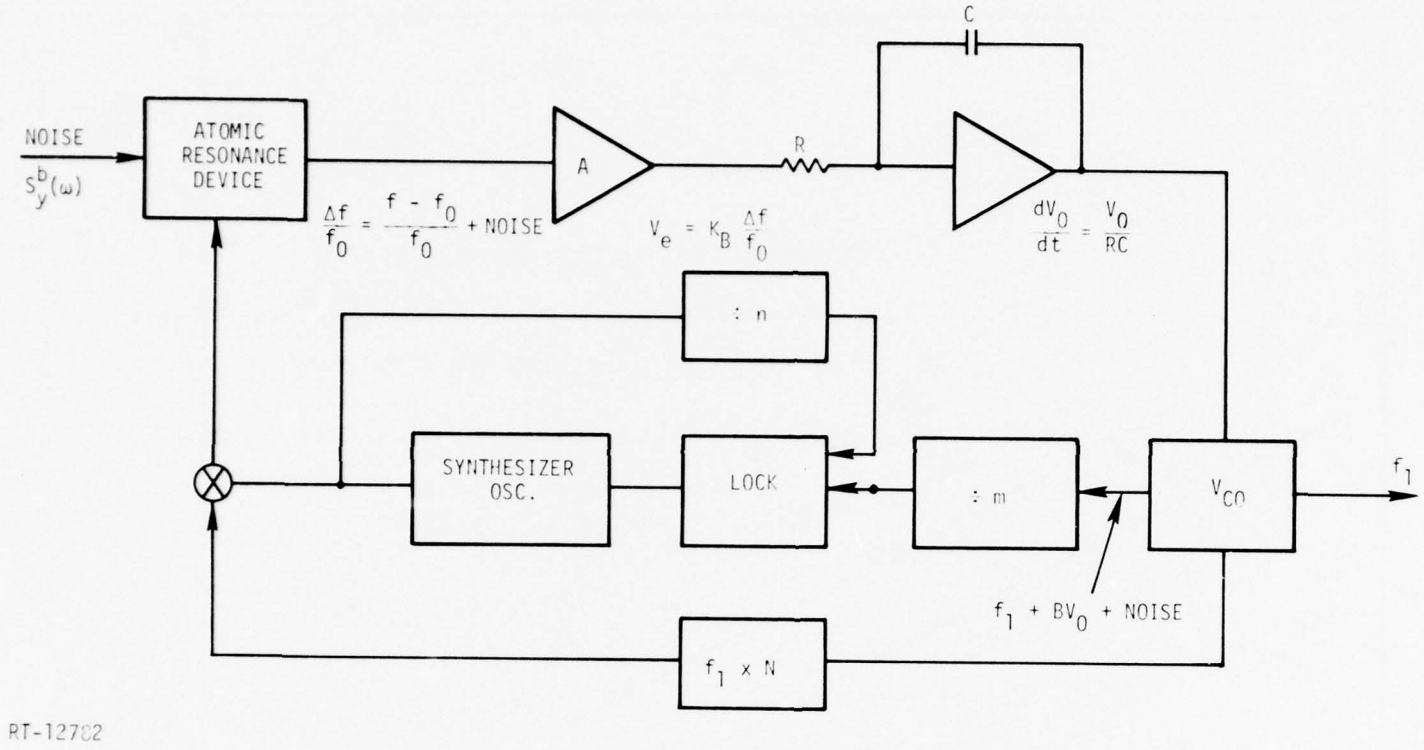


Figure 3. Block diagram of passive atomic frequency standard

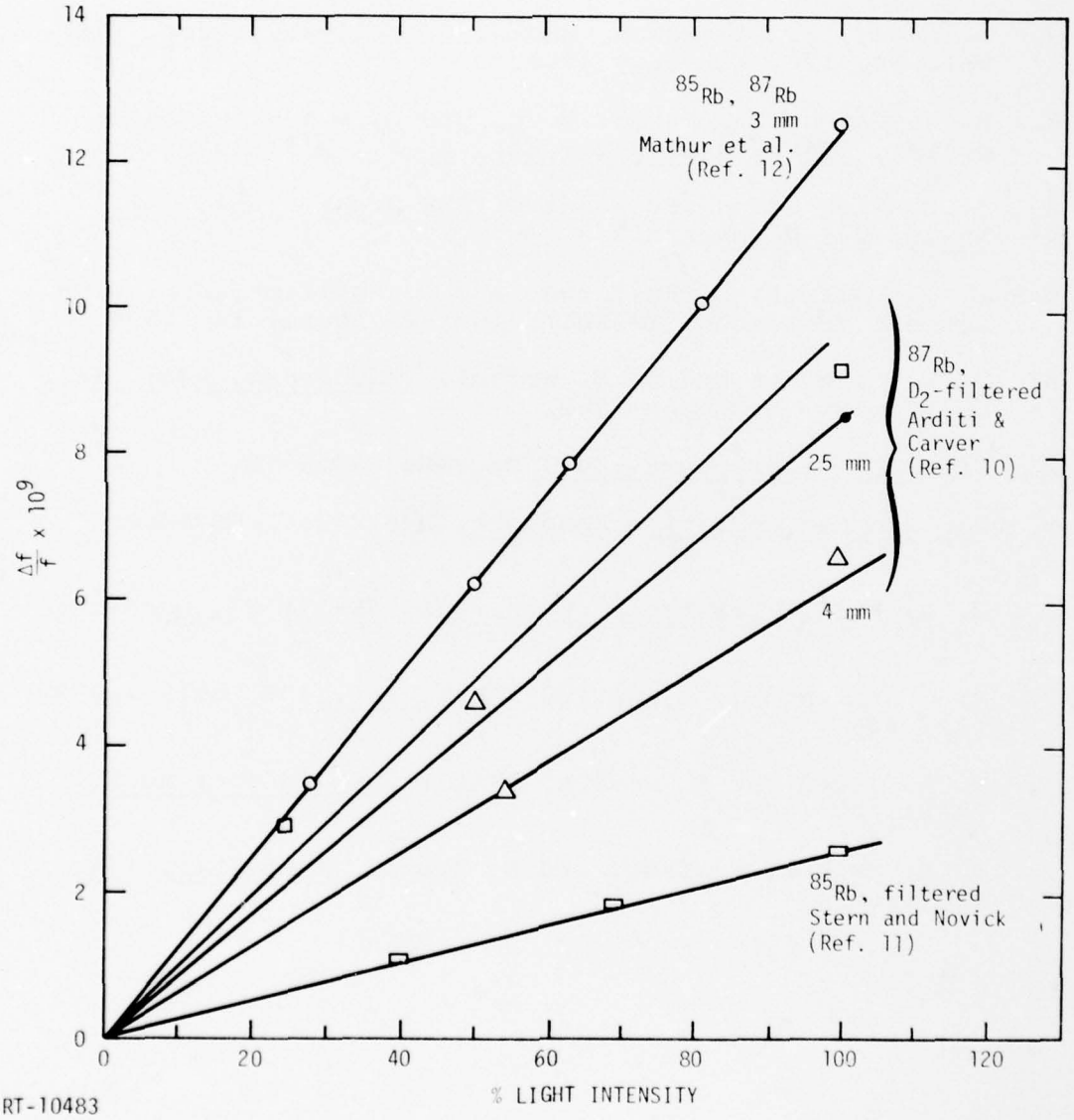


Figure 4. Light shifts in Rb (0,0) h_{fs} resonance measured in ^{87}Rb by ^{85}Rb (Mathur et al.), D_2-filtered ^{87}Rb exciting ^{87}Rb (Arditi and Carver), and filtered ^{85}Rb exciting ^{85}Rb (Stern and Novick)

REFERENCES

1. L. S. Cutler and C. T. Searle, Proc. IEEE, Vol. 54, 136, February 1966.

2. R. Lacey, A. Helgesson, and J. H. Holloway, Proc. IEEE, Vol. 54, 170, February 1966.

3. B. R. Capone, A. Kahan, R. N. Brown, and J. R. Buckmelter, IEEE Trans. Nucl. Sci. NS-17, 217 (1970).

4. J. C. King and H. H. Sander, IEEE Trans. Nucl. Sci. NS-19, 23, December 1973.

5. L. J. Palkuti, D. Phillips, and R. Phillips, U.S. Government Memorandum (USNRL)5210-187, August 14, 1974.

6. T. M. Flanagan and T. F. Wrobel, IEEE Trans. Nucl. Sci. NS-16, 130, December 1969.

7. Cf. IEEE Trans. Nucl. Sci. December 1965-75.

8. The Trapped Radiation Handbook, DNA 25244, December 1971.

9. R. A. Poll, IEEE Trans. Nucl. Sci. NS-17, 83, December 1970.

10. M. Arditi and J. R. Carver, Phys. Rev. 109, 1012 (1958), 112, 449.

11. W. A. Stern and R. Novick, IEEE Trans. Inst. & Meas. IM-21, 99 (1972).

12. B. S. Mathur, H. Tang, and W. Happer, Phys. Rev. 171, 11 (1968).

QUESTION AND ANSWER PERIOD

DR. WINKLER:

Can you give us any estimate of the difficulties of protecting Hydrogen Masers in such inclement conditions, remembering that the coefficient for the magnetic sensitivity is about 42 times larger than it is for cesium? On the other hand, you operate at about 50 times smaller magnetic fields so you regain that, but still you have to control the magnetic field of 1 milligauss to about .01 percent of its value, so what is going to be the effect of that radiation on the shield and on the current supply?

MR. FLANAGAN:

Let me take the last one first, namely, the effect on the shield. We have done some current injection tests on magnetic shield materials and have -- first of all, our intuitive feeling was that for very short pulses, which these electron currents are, there is not enough time to switch the domains. That was just a rough feeling we had. We did some experiments on some Frequency and Time System shields and that seemed to have been borne out. We did not measure with the kind of precision that you were talking about, nor at the kind of magnetic field levels because, of course, the levels are rather high for cesium.

I would say that one of the first things that I would look at would be to compute the induced currents and then do some good current injection testing to find out whether or not we had seen anything. It has been a concern of mine since the area or the volume of the magnetic shield in the maser is so much larger.

With respect to the second point, the controlling of the magnetic field current supply, as I said, by careful design, by part selection and by shielding, if you can design a supply which will survive five years of normal component aging without degrading, then we can design one that will do the same thing in the space environment. There are other areas of concern, namely outgassing from chambers and degradation of walls that one starts to get concerned about and I don't have enough empirical information right now to be able to say anything about that.

MR. RUEGER:

One of the most serious problems about these radiation hardening of time sources is to keep continuity of the signal output. Have you some solution to give the necessary flywheels so that there is no interruption in the quality of the pickup on phase of the output timing signals?

MR. FLANAGAN:

I think it has been borne out a little bit by computer analysis and somehwat by tests and it has to do with using the final output circuitry as a flywheel. You just have to design your system in such a way that the final output circuitry has a large enough Q with the semiconductor saturated so that it will continue to flywheel until they recover.

If the Q of the system is sufficiently high, then it will continue to flywheel even in the absence of driving or amplifying component.

DR. VESSOT:

With regard to magnetic field conditions in the hydrogen maser, what Dr. Winkler says is correct. I have just done a thumbnail calculation. It turns out that running at a half a millioersted which is the way we run the maser for our space experiment, the effect is a part in 10^{12} times delta I over I, which compares quite favorably with 3.5 in 10^{10} and 2.5 in 10^{9} for cesium and rubidium. This comes about by the fact that the field is running substantially lower as was pointed out earlier.

The other thing, though, that seems to me almost intuitive is the phase lock loop is far less likely to be perturbed in terms of long term frequency than a frequency lock, notably that it does not have the long term integration that characterizes so many of the frequency loops that we know are used on cesium instruments and rubidium instruments. So, I think there may be an advantage there, although, it is probably a pretty slender one in the fact that the dose rates that are being mentioned here are rather catastrophic.

A PORTABLE RUBIDIUM CLOCK FOR PRECISION TIME TRANSPORT

Helmut Hellwig and A. E. Wainwright
National Bureau of Standards
Frequency & Time Standards Section
Boulder, Colorado 80302

ABSTRACT

Based on a commercially available rubidium standard the National Bureau of Standards (NBS) developed a portable rubidium clock. Technical modifications which reduce the sensitivity against temperature, magnetic environment, and barometric changes allow stabilities in the 10^{-12} range under typical clock transport conditions. Under laboratory conditions the clock shows a best stability of 3 parts in 10^{14} . Clock packages based on sealed lead-acid batteries featuring a total weight of 21 kg and 18 hours battery operation were tested; an improved clock package was realized using silver-zinc batteries with 11 kg weight and 28 hours battery operation. Reports of several clock trips to the U.S. Naval Observatory and of one clock trip each to the Bureau International de l'Heure in Paris and to the Hewlett-Packard Company in Santa Clara, California are reported. Time transport precisions of .02 μs have been obtained. Special aspects of the clock modifications and the operating characteristics are discussed, as well as an optimal use of the data of a clock round-trip.

INTRODUCTION

For time comparisons with precisions of better than a few μs between distant locations, cesium clocks are used exclusively at present. The use of these devices is not without constraints due to their size as well as their relatively high power demands. For example, with reasonable and portable battery power supplies cesium clocks must be powered from outlets on the airplane on any transcontinental or intercontinental trip and the purchase of a separate seat is necessary. As a result, cesium clocks not only pose cost and logistics problems, but also affect the reliability of time comparisons. Commercial cesium clocks are under development which promise reduction of the above problems; nevertheless,it appeared prudent to explore the possibilities of small commercially available rubidium standards which offer the potential of very small clock packages. Even mailable clocks appear feasible.

THE BASIC RUBIDIUM STANDARD

Small rubidium standards are now commercially available. A unit was selected featuring about 1 ℓ volume (approximately 10 x 10 x 10 cm) and a weight of about 1 kg. The basic stability of the clock was measured and the results are depicted in fig. 1. The frequency stability of the clock can be described by* $\sigma_y(\tau) = 6 \times 10^{-12}\tau^{-1/2}$, a flicker floor of 3×10^{-13}, and a long term stability of about 3×10^{-12} at τ = 1 day. For time transport with a precision of 0.1 μs the frequency stability requirement can be stated as $\sigma_y(\tau=T) < 10^{-7}\ T^{-1}$, where T is the interval in seconds between the time comparison at two remote locations (trip time). From this equation and fig. 1 it is clear that the rubidium clock is basically capable of providing time comparisons to better than 0.1 μs for trip times out to many hours. It is therefore obvious that environmental effects are of primary concern. For long clock trips possible frequency drifts could be significant. Clock trips take typically less than 18 hours. Environmentally induced frequency changes should therefore be individually in the 10^{-12} range, or they should be calculable.

On a trip the clock encounters three major environmental changes: a) magnetic field; b) temperature; c) barometric pressure. The performance of the particular NBS unit was tested against these changes. For atomic frequency standards, frequency changes due to repositioning are principally magnetic field effects. The performance of the unit under test was: a) position (magnetic field): 1.2×10^{-10} worst case in the earth magnetic field; i.e., strongly dependent on the particular position or orientation. b)temperature: about 7×10^{-12} per °C in the range of 26-40 °C baseplate temperature; c)barometric pressure, parts in 10^9 from atmospheric pressure to vacuum. It was suspected that the barometric effect was related to temperature, in particular, temperature gradient effects, and that the barometric sensitivity would be much less around atmospheric pressure.

* $\sigma_y(\tau)$ is the square root of the two sample variance of fractional frequency fluctuations. τ is the sample time measured in seconds.

We therefore decided to reduce only the magnetic field and temperature sensitivity and trust that the barometric sensitivity around atmospheric pressure would pose no major problems.

In view of the need to provide the clock with a portable battery power pack the sensitivity of the frequency against supply voltage changes was of interest. Figure 2 shows this sensitivity which can be described by about 5×10^{-12} per volt. Therefore, only a relatively conventional voltage regulation was necessary if batteries with a flat discharge voltage characteristic were to be used, such as lead-acid or silver-zinc. Strongly varying voltages under discharge, such as featured by alkaline batteries, would cause non-trivial problems.

THE IMPROVED CLOCK

The existing outer magnetic shield of the unit was partially reworked. The shield was repositioned to allow at least seven millimeter distance everywhere to the inner shield, especially at the critical location of the photo detector. Also, adequate overlaps between the joining portions of the shield were introduced. A third magnetic shield was added and the space between the second and third shield was filled with foam. This latter measure highly reduces convective cooling of the unit and forces the mounting (baseplate) to act as the only significant heat sink. This reduces temperature gradients within the unit which would depend on the state of air circulation around the unit and affect frequency stability and frequency accuracy. The baseplate configuration, i.e., the layers of magnetic shields and the baseplate itself, were joined using heat conductive paint. The only openings in the outer magnetic shield are those for the wires of the necessary supply and control voltages and a small hole to provide access to the tuning capacitor of the crystal oscillator. To "harden" the unit against acceleration and vibration, all critical wires and components were glued to the circuit board, also, the adjustment potentiometer for the magnetic field current was replaced by a fixed resistor providing an offset from the nominal frequency of several parts in 10^{11}

I BAROMETRIC SENSITIVITY

BOULDER ⟶ SEA LEVEL
(~0.8 atm) (~1.0 atm)

(a) ORIGINAL UNIT $+ 1.5 \times 10^{-11}$

(b) SEALED UNIT $< + 2 \times 10^{-12}$

II MAGNETIC FIELD SENSITIVITY
(ORIENTATION IN EARTH'S FIELD)

(a) ORIGINAL UNIT 1.2×10^{-10} WORST CASE

(b) SHIELDED UNIT 3×10^{-12} WORST CASE

TABLE 1

TEMPERATURE COMPENSATION
VIA C-FIELD CURRENT ADDITION
(TEST-RANGE: 26°C TO 40°C AT BASEPLATE)

R(Ω)	1.5K	613	580	562
$\Delta\nu/\nu$ (10^{-12}) PER C	+7.2	+1.7	-0.14	-0.8

TABLE 2

The magnetic field sensitivity under the worst possible orientation in the earth's magnetic field was reduced by the measures described above to 3×10^{-12} total frequency change as shown in Table 1. The commercial rubidium standard features temperature compensation using current addition into the internal magnetic field current supply. This additional current is controlled by a temperature sensor, i.e., the atomic frequency is changed magnetically to compensate for temperature induced frequency shifts. In a series of temperature tests from 26 °C to 40 °C at the baseplate an optimum adjustment for the controlling resistor was experimentally found. The unit was mounted on a heavy plate which was temperature stabilized using a commercial temperature controller. These tests were carried out with the complete unit featuring the new third magnetic shield as described above with wires leading out of the unit to allow quick substitution of the resistor. Table 2 gives the result for four different resistors. 1.5 k was the original value supplied by the manufacturer. We can see that the temperature sensitivity could be reduced by a factor of about 50 by choosing a resistor of 580 Ω.

Finally the unit was barometrically sealed using epoxy glue to close the small gaps in the outer magnetic shield. Thus, the outer magnetic shield serves as a pressure container. Though this action highly reduces the effects of barometric pressure changes (except for residual flexing of the walls of the magnetic shield under pressure changes), it introduces a pressure problem via temperature fluctuation inside of the sealed case. The pressure will change by the same percentage by which (absolute) temperature changes occur. Nevertheless, an advantage can be gained since barometric pressure changes of the order of 10% are encountered during typical transport conditions whereas temperature changes, i.e., temperature induced pressure changes, of the order of one percent are encountered. Especially in a laboratory environment improvements were expected to be significant since the temperature is stable to a fraction of a percent whereas barometric pressure changes due to weather related effects can be very significant and be up to many percent.

Figure 3 demonstrates this dramatically. Curve A in fig. 3 depicts the performance of the unit with all modifications installed except for the barometric sealing. We see that the flicker level has substantially dropped, and that the long-term stability (now 1×10^{-13} for $\tau = 1$ day) has improved as compared to fig. 1. A reliable measurement of the drift performance of the unit could be done. The drift was typically 1×10^{-13}/day, or less during a period of many months.* The barometric sealing lowered the flicker floor to about 3×10^{-14}, which we believe is the best stability ever measured with a rubidium standard. Table 1 shows the reduction in barometric sensitivity for a change from 0.8 atm to 1.0 atm corresponding to going from Boulder Colorado to sea level. The original unit, with all improvements except for barometric sealing, showed a change of 1.5×10^{-11}. The sealed unit showed an effect of less than 2×10^{-12}.

The improved rubidium frequency standard is mounted with its baseplate inside an aluminum carrying case, thus securing adequate cooling. The output of the standard is normally 10 MHz. A divider provides externally available 5 MHz and 1 pulse/s outputs. Both outputs are buffered and can handle 50 Ω loads with a 1 volt rms signal for 5 MHz, and for the pulse a 5 volt peak with 10 ns rise time. A battery power pack was installed inside the case with a diode disconnect circuit. A regulated power supply, switchable for 115 and 230 V, supplies the standard and the divider circuit if the unit is plugged into the power line. Thus, no precaution is necessary in connecting or disconnecting from power line service. Both battery and line power supply feed their voltages to the standard via a 24.3 V regulator.

---

* During several days following a clock trip, the actual performance is somewhat worse than the performance depicted in fig. 3.

The first battery pack used was a sealed lead-acid type which gave the total unit a weight of 21 kg and 18 hours battery life. The weight of this unit caused difficulties in handling as carry-on luggage on airplanes. Therefore, the lead-acid batteries were replaced by silver-zinc batteries, giving the unit a total weight of 11 kg and 28 hours battery life. This battery pack feeds about 31 V into the regulator during most of the discharge with a somewhat higher voltage during the first half hour and a rapid voltage drop at the end of the charge life.

Initially, the silver-zinc batteries were charged from a built-in power supply. Unfortunately, this solution did not stand up to actual service and we had to go to external charging. The principal reason for this is the peculiar charge and discharge characteristic of silver-zinc batteries and a change of this characteristic with time due to a mismatch between battery type and charge current.* The principal feature of the power supply is that it must disconnect totally any charge current from the batteries when the batteries are fully charged because a trickle charge would lead to destruction of the silver-zinc batteries. It also has a total cut-off feature which disconnects the batteries from the standard if the battery voltage drops below a preset level. This stops the clock, but protects the batteries which would otherwise be destroyed. We plan to replace the present battery set by a "low current" style which will allow us to use the built-in automatic charging supply.

Figure 4 shows a photo of the complete unit. A meter is provided in the unit with six switchable positions which allow the reading of the regulator input voltage, the regulator output voltage, the battery voltage, the battery charge-discharge current, the crystal oscillator servo voltage in the standard, and the light intensity monitor voltage in the standard. Also, a lock indication is provided.

---

* The silver-zinc batteries will be gradually destroyed if charged by a too low current. Our type of battery was a "high current" design (unknown to us) and demanded > 1.5 A charge current, whereas our power supply furnished about 0.3 A.

OPTIMUM USE OF CLOCK TRIP DATA

A definition of clock transport conditions and terms is given in fig. 5. Clock transport occurs from A to B and, if possible, back to A. The time elapsed on the trip from A to B is T_{AB} and correspondingly the time from B to A is T_{BA}. The actual time spent by the clock at location B is T_B. The change in the time reading of the clock at location B with respect to the clock at B is Δt_{BB}. The so-called "closure" is Δt_{AA}, i.e., the difference of the clock reading when it returns to location A with respect to the clock at A.

The most simple assessment of a clock trip would make use only of Δt_{AA}. An assessment of the error or uncertainty of the clock comparison is then the difference between the measurement value of Δt_{AA} and the value for Δt_{AA} as predicted from the rate of the clock at A before leaving. In a round-trip, however, more data are usually available and can be used to arrive at a better estimate of the time differences of the clocks at A and B. Figure 6 illustrates this. Plotted are the fractional frequency offsets y of the portable clock as a function of real time at the various locations and during the trip. The clock has an average rate y'_A at location A before it leaves. If B is also a time-keeping laboratory with high-performance standards, i.e., clock A and clock B are at about the same rate, then a precise reading of the portable clock frequency at B can be made leading to the value y_B ($y_B = \Delta t_{BB}/T_B$). Upon return to A the clock will show the frequency y''_A which usually is not significantly different from the original rate y'_A. The average frequency for the combined trip time T_{AB} and T_{BA} can then be calculated from the following equation

$$y_B^A = \frac{\Delta t_{AA} - \Delta t_{BB}}{T_{AB} + T_{BA}} .$$

This equation is, of course, only accurate to the degree of validity of the measurement of Δt_{BB} or y_B. In other words we have to assume that the frequency or rate of the clocks at location B is not much different than those at A. This requirement is not too stringent because the requirement on our knowledge of the clocks at B in fractional frequency is the same as our requirement on the frequency of the portable clock during the trip time. Since 10^{-12} corresponds to 0.1μs in about 1 day trip time, a knowledge of the frequency of the clocks at B to 1×10^{-12} is totally adequate for most clock trip purposes. In fact, for precision time laboratories this is a near trivial requirement because typically the rate is known to much better than 1×10^{-12}.

y_B^A can then be used to predict the time reading of laboratory A at the time of arrival of the portable clock at B and the reading of laboratory B at the time of arrival of the clock back in laboratory A. The time difference between laboratory A and B for the first leg of the clock trip is $(t_A-t_B)_{AB}$, and it is $(t_A-t_B)_{BA}$ for the second leg of the clock trip. A change in clock behavior and/or in the two trip conditions would cause an error term. Obviously the error term can be estimated from the difference Δt_B^A, of the time readings between laboratories A and B obtained from the two legs of the clock trip. The following equation gives an estimate of the error of Δt_B^A.

$$\delta\Delta t_B^A \simeq |(t_A-t_B)_{AB} - (t_A-t_B)_{BA}| + \text{const.}$$

Of course the first term in the equation will tend to be non-zero if there is a rate difference between clocks A and B. If the rate difference is significant, it should be accounted for before the error assessment. In this equation we added a constant since the difference in the time differences could be small fortuitously. Thus the constant includes an estimate of the fundamental stability performance of the clock (excluding trip induced frequency changes), as well as an estimate of the uncertainty in the rates of clocks at A and B if the two legs of the clock trip are far apart in time. If only one leg of the clock trip is

successful an improved estimate of $(t_A-t_B)_{AB}$ or $(t_A-t_B)_{BA}$ and the associated error $\delta\Delta t_B^A$ can still be made using the clock rates y_B at B and y_A' and/or y_A'' at A.

CONCLUSIONS

A list of clock trips carried out during 1975 is given in Table 3. Four clock trips were done to the U. S. Naval Observatory in Washington, DC; two of which were complete round-trips. One trip was carried out to the Bureau International de l'Heure (BIH). This was only a one-way trip since the return trip was not usable because of problems due to shorting batteries. Finally, a trip to the Hewlett-Packard Company was carried out. This trip was a round-trip; however, the data from the return trip were not used due to a servo system problem in the rubidium standard itself. The first trip to the USNO in May 1975 featured the clock package with lead-acid batteries. All other clock trips were made with the silver-zinc battery. The table gives the approximate trip time in hours and the measured time difference between the time scale of the laboratories and UTC(NBS). Finally, the last column gives the estimated uncertainty of the time comparison.

The use of all available data from measurements at laboratories A and B allows a reduction in the uncertainty of the time measurement. The clock package is small enough that it could be shipped by priority air freight. On trips within the US and to Europe we never did encounter any serious difficulties with the clock being handled as carry-on luggage; not even the airport security posed any significant problems. Modifications of the battery package are obvious. For shorter trips of up to several hours, lead-acid batteries may still be the correct choice because of their comparative cheapness and reliability. If weight counts and short clock trips are only envisioned, then a small silver-zinc battery may be used with advantage reducing the weight by an additional several kg. A larger battery is possible for up to forty hours of battery operation increasing the weight of the portable clock to not more than 15 kg.

ACKNOWLEDGMENTS

The authors wish to acknowledge the help extended to them by the staffs of the cooperating laboratories: BIH, USNO, Hewlett-Packard and NBS. In particular, we wish to acknowledge the help in data taking and analysis extended to G. M. R. Winkler of USNO, and D. Allan of NBS. Also, the international clock transport would not have been possible without the cooperation by P. Giacomo of the BIPM, J. J. Gagnepain of the University of Besancon and F. Addor of Ebauches, S. A.

CLOCKTRIPS

DESTINATION	DATE (RANGE)	T_{AB} (h)	T_{BA} (h)	$(UTC)_i-(UTC)_{NBS}$ (μs)	$\delta\Delta t^A_B$ (μs)
USNO	26 MAY 75	6	-	-7.6	0.2
USNO	16/17 JULY 75	8	7	-8.10	0.03
USNO	30/31 JULY 75	7	6	-8.41	0.02
USNO	26/27 SEPT 75	6	-	-8.23	0.03
BIH(OP)	27/28 SEPT 75	18	-	-6.10	0.1
HP	9/21 NOV 75	5	(5)	-2.96	0.05

USNO = US NAVAL OBSERVATORY

BIH(OP) = BUREAU INTERNATIONAL de l'HEURE(PARIS OBSERVATORY)

HP = HEWLETT PACKARD COMPANY

TABLE 3

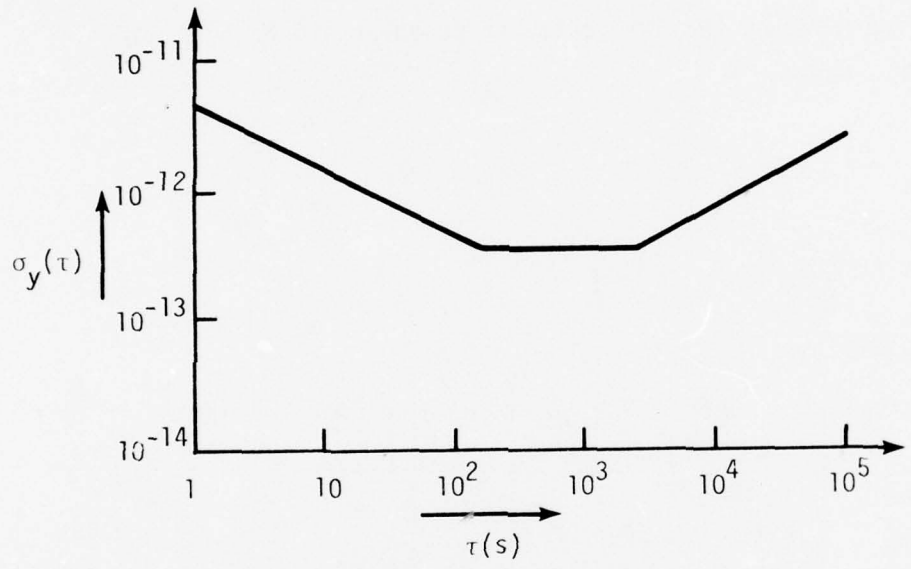


FIGURE 1. Time-Domain Stability of a Commercial Rubidium Standard.

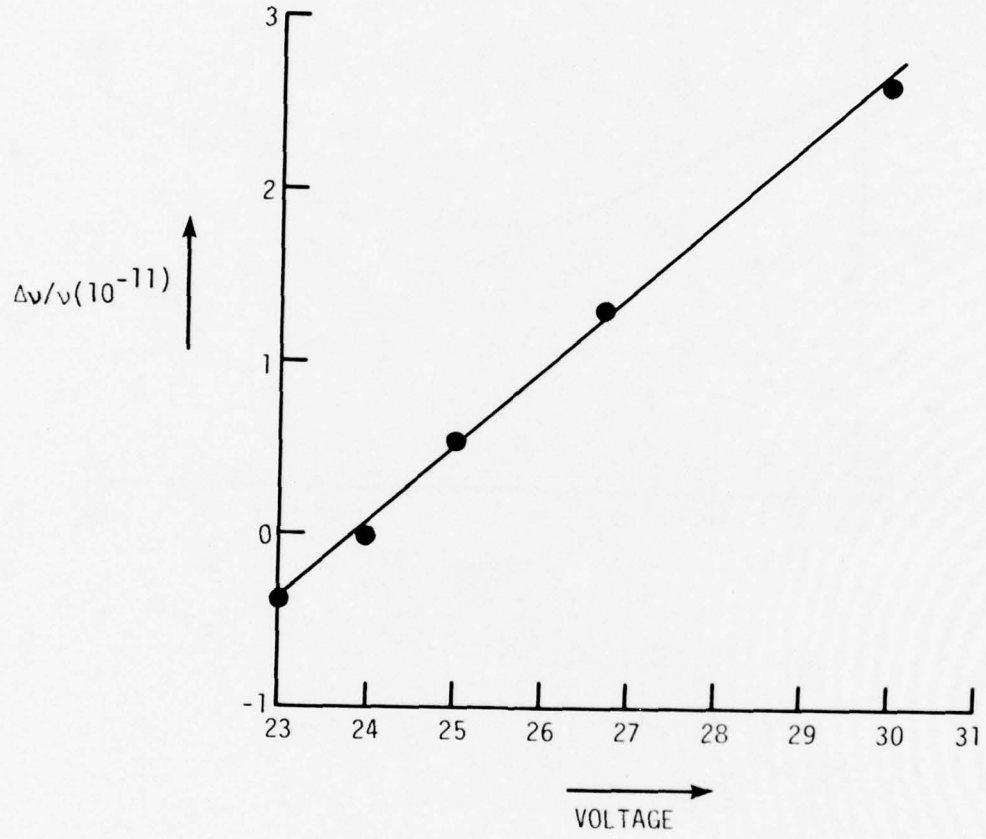


FIGURE 2. Frequency Change as a Function of Supply Voltage for the Commercial Rubidium Standard.

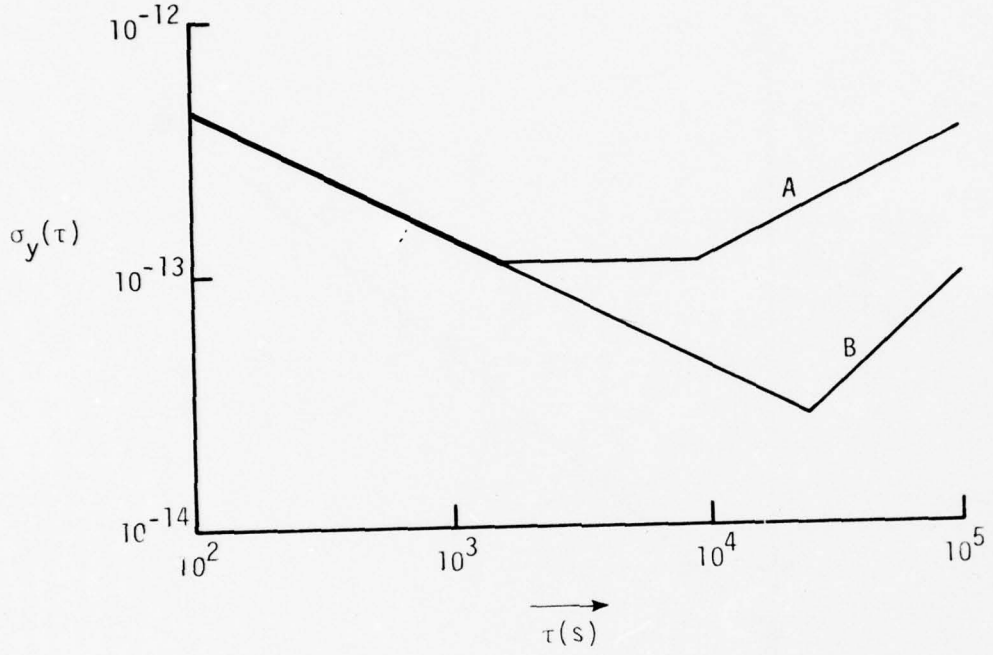


FIGURE 3. Time-Domain Frequency Stability of the Improved Unit.

curve A Improved magnetic shielding and temperature compensation.

curve B Improved magnetic shielding, temperature compensation and barometric sealing.

A frequency drift of approximately 1×10^{-13} per day is removed from the data.

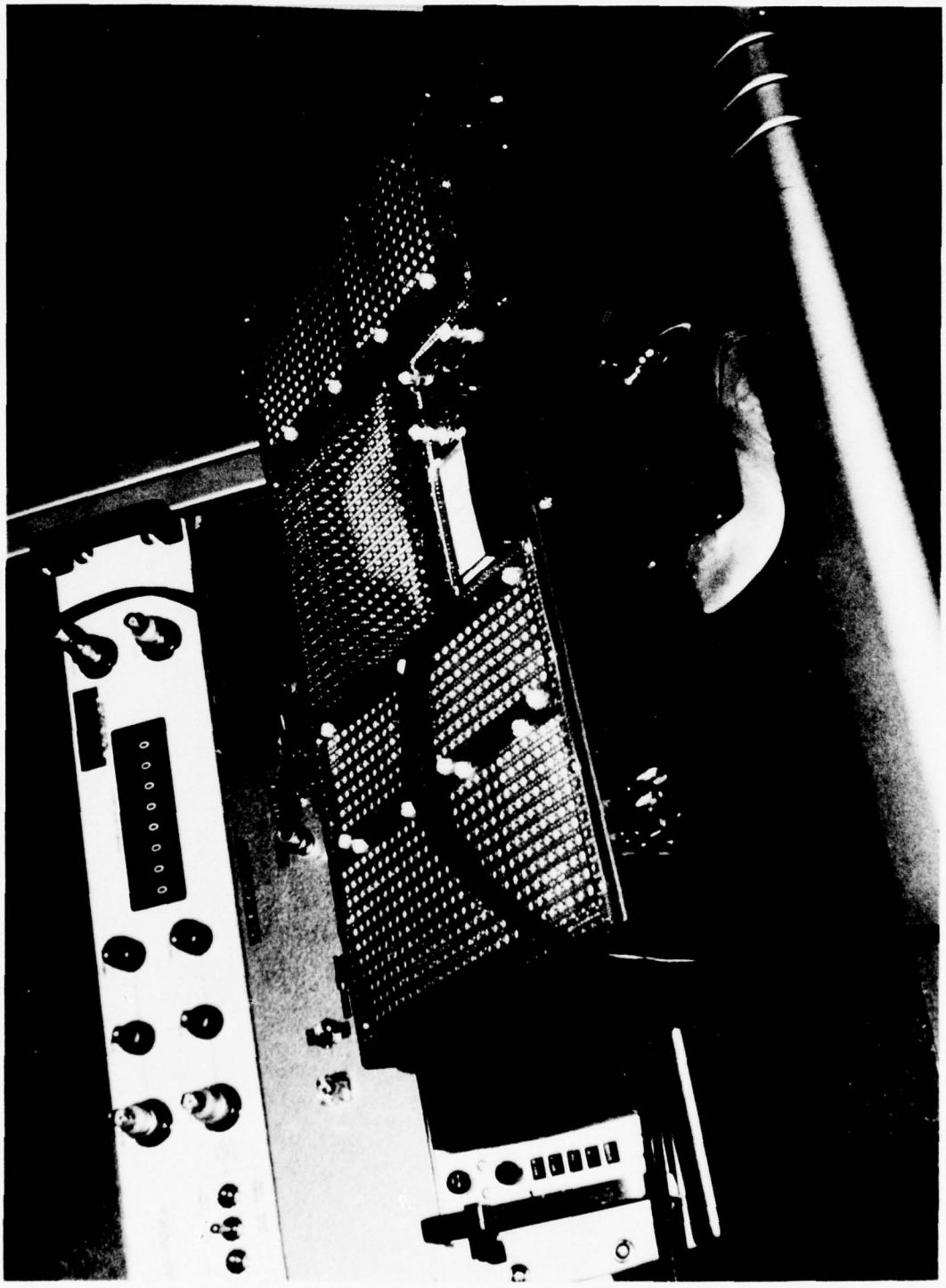


FIGURE 4. Photo of the portable rubidium clock.

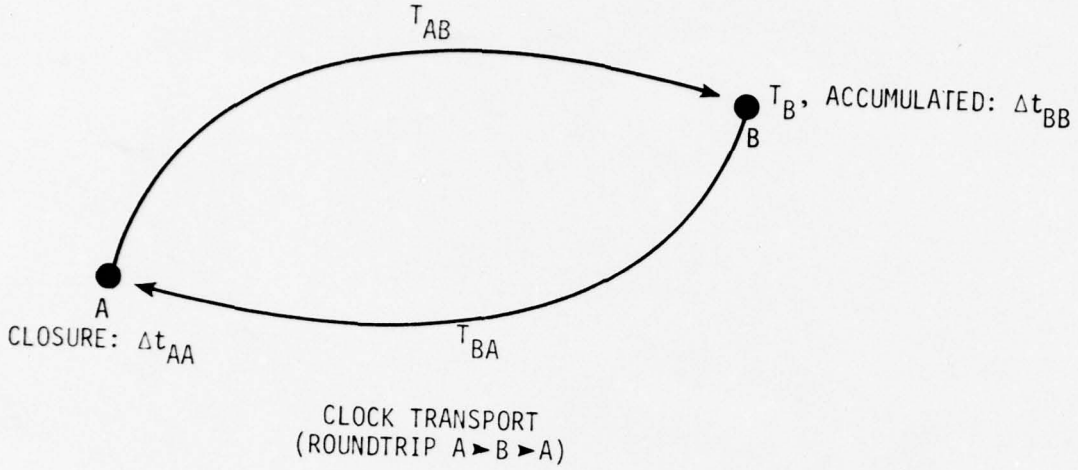
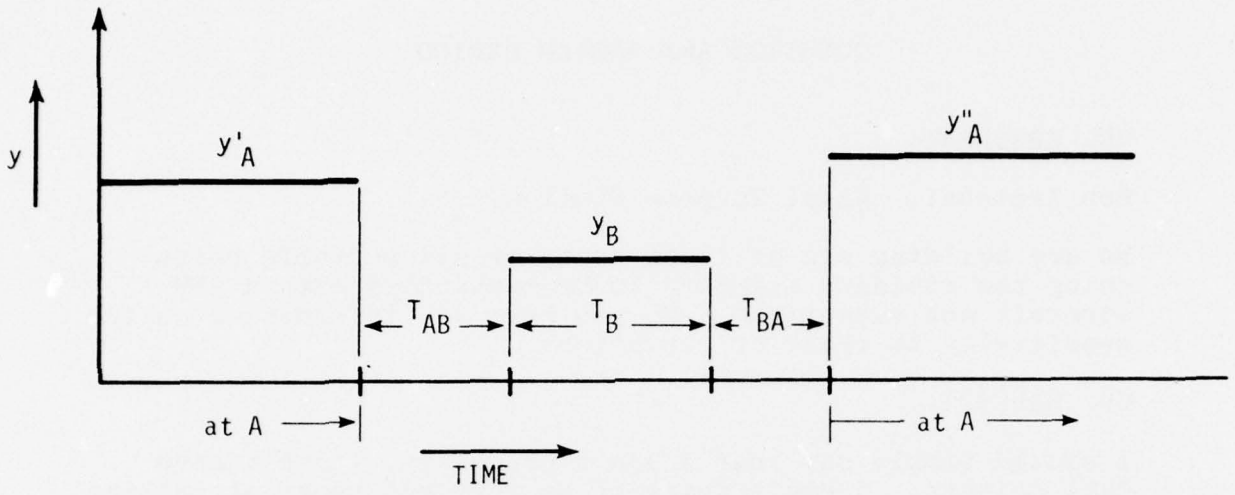


FIGURE 5. Principle of a Round-Trip Clock Transport from Laboratory A to B and Back to A.



$$y_B^A = \frac{\Delta t_{AA} - \Delta t_{BB}}{T_{AB} + T_{BA}}$$

$$\text{ERROR} \quad \delta\Delta t_B^A \approx \left| (t_A - t_B)_{AB} - (t_A - t_B)_{BA} \right| + \text{CONST}$$

FIGURE 6. Best Use of Data from a Clock Round-Trip.

y = fractional frequency.

T = trip times.

Δt_{AA} = accumulated time reading of the portable clock from leaving A and upon returning to A.

Δt_{BB} = accumulated time reading of the portable clock between arrival and departure at B.

$\delta\Delta t_B^A$ = time error for a clock trip A to B or B to A.

QUESTION AND ANSWER PERIOD

MR. KRUTENAT:

Bob Krutenat, Naval Torpedo Station.

We are building six of these units or six portable units using the rubidium standard to be manhandled aboard ASW aircraft and submarines. Do you have any information on the sensitivity to shock or vibration?

DR. HELLWIG:

I should simply say that I don't presently, I don't have data on that. I don't think it is very bad short of falling out of lock and survival problems. But, there are people in the audience who could answer that, I think. Would anyone like to answer this question?

MR. BADURA HEINZ:

Mr. Heinz, Efratom.

We are actually the manufacturer of a small clock which was supplied over to a Naval torpedo station and we actually have not been asked to supply sufficient data on shock and vibration, but we have run, of course, several tests with approved laboratories to the same specifications normally, cesium is specified. We passed all these tests. In addition, of course, we had been doing some research in connection with GPS programs and the unit is such it will survive prysically any requirement which is specified herein, so it is just a matter, actually, of let us say shock mounting properly, that you can use the unit for your requirements, which are not that severe.

This is both valid for vibration requirements and for shock requirements.

MR. LUCK:

Luck, National Mapping.

I wholeheartedly endorse Mr. Wainwright's closing remarks. Would it be possible to have some preliminary estimate of the cost of producing such a machine commercially?

DR. HELLWIG:

As estimated, you are talking basically on the clock, acquisition of parts on the order of $5,000.00. If you build yourself the power supply, case, and so on, the materials cost -- it depends on what battery, batteries are the biggest thing. The silver zinc battery pack in this clock has a value of about -- I shouldn't say that, otherwise somebody steals it because the main value is silver -- is about $1,200.00. That is easy to sell. A rubidium clock is not as easy to sell.

So, you are talking, maybe, if you build it yourself, a total of, at most, $7,000.00. If somebody wants to make a profit there is time for testing, for optimizing the temperature feedback and things like that, my guess is that I think a commercial unit of that sort should cost still less than $10K.

MR. BLOCK:

Mr. Martin Block, Frequency Electronics.

Helmut, we have had terrible experiences in unattended clock transport by commercial aircraft and I think before you attempt it, you might investigate that there are two phenomena that the airlines don't tell you. One is that the pressure in the chamber sometimes goes to 50,000 feet and the temperature typically is at 0° Centigrade and sometimes goes as low as -40 and in 20 attempts of unattended between here and L. A. we have three successful shipments of a clock that the batteries survived without going to zero because all of the batteries' capacity at -40 go to about 2 percent of the normal capacity. So, I would really check this thoroughly before starting it.

DR. HELLWIG:

You stated one of the reasons why we haven't tried it yet, because I wanted to bring it here. Let me say, if I say by priority air freight, we are envisioning transport of the clock in the cabin in the cockpit by carrying on by the crew. Airlines are willing, at some premium, to do that -- some airlines. This is the way to go, especially if you tell the pilot, you know, it is nice and he might improve his own time readings and navigate better.

DR. VESSOT:

We ran into a hill of flak when we decided to send an atomic hydrogen maser to Spain in a commercial air carrier which I was to board. We solved the problem by calling it a clock. But, there are other problems we didn't solve. We wanted to ship it while it was operating and they didn't want batteries on board and I have a feeling that the carriers are likely to get uptight if they understand that there are a few Joules. I don't know how many Joules of energy in a battery that is being left unattended that could be considered dangerous cargo if a short should occur.

This is one of the political problems I think we all have to solve. In fact, it is no more dangerous than some other things that I know are being shipped. I think there is room for some work here.

DR. HELLWIG:

I think you point out a very severe problem and I just think what we have to have is some sort of an accident with one of those clocks to wipe out our ability to compare time because the problem you are stating is not unique to that thing. It is unique to all clocks, traditional cesium, or whatever you do. We have run into, so far, only the problem of not having the freedom to use mercury batteries which would have an even better weight to power ratio, though not rechargeable.

So far, we didn't run into opposition with the thing which has a red light on and which obviously carried batteries. Dr. Winkler, do you have any comment on this?

DR. WINKLER:

My only comment is that one cannot take anything for granted. One cannot take for granted that the battery supply will work. As you can see, this is just underlining what we said this morning. I think that NBS ought to open up a section on power supplies in order to bypass this limitation in precision.

It is and remains our most difficult bottleneck, provision of primary power, and you are quite right in pointing out that we may endanger our capability to make any clock trip's and I would caution everybody here to do his utmost in preventing such an accident. I take a dim view of sending clocks unattended.

DR. HELLWIG:

There is one way out. I just found out there is an increasing, apparently, increasing market for specialized small package air freight businesses who would handle your clock like a passenger on small aircraft which just carry freight, quick delivery within 24 hours, of packages and I intend to explore that before we get it into passenger aircraft cockpits.

DR. WINKLER:

The point is that we do not have the instructions in case of an emergency. If you send a technician who is trained in handling such a thing, at least he has some idea what to do. To open up the short as quickly as possible. If it is a steward or stewardess, he would be completely helpless. If they had a fire on board, that would be the end of our business.

DR. HELLWIG: That is right. I think that is a warning we should all take to heart.

PERFORMANCE AND OPERATION OF THE NRC PRIMARY CESIUM CLOCK, CsV

A.G. Mungall, H. Daams, D. Morris, and C.C. Costain
National Research Council, Ottawa, Canada

ABSTRACT

Since May 1, 1975, the NRC primary cesium beam frequency standard, CsV, has operated as a primary clock, generating directly a new time scale, PT(NRC CsV). Steps in the development of CsV from a frequency standard to a clock, and new error evaluations using the two NRC autotuned atomic hydrogen masers as stable frequency references are outlined. Details of both mechanical and electronic construction leading to successful clock operation are also discussed. The design of a new 12.632 MHz frequency synthesizer and modulator with very low spurious sidebands is outlined. Methods of partial reevaluation of systematic errors and frequency offsets during clock operation, a procedure necessary in order to maintain primary standard accuracy, are described. The accuracy of PT(NRC CsV) is estimated to be about ± 9 ns per day if all systematic errors are additive, and about ± 5 ns per day if they act independently in a random manner. The frequency stability of PT(NRC CsV) is about 1 to 2 x 10^{-14} for periods greater than 4 hours, the short term stability being determined by the low cesium beam resonance amplitude of 1.6 to 2.0 pA normally employed for clock operation. Replenishment of the two cesium ovens is expected to be necessary at intervals of several years.

INTRODUCTION

In 1967 the internationally accepted unit of time, the SI second, was redefined as the duration of 9 192 631 770 periods of the radiation corresponding to the transition between the two hyperfine levels of the ground state of the cesium 133 atom. This definition was chosen as that most likely to provide the best basis for a unit which could be realized independently and without recourse to other standards. However, its implementation has produced two basically different types of devices, the primary long beam laboratory cesium frequency standard and the primary short beam commercially produced cesium clock. The former is devised so as to reproduce physically the unit of time to a very high degree of accuracy, but only for short periods of a few hours

PRECEDING PAGE BLANK-NOT FILMED

or days. The latter also reproduces the unit of time, but to a lesser degree of accuracy, and in addition, accumulates these units over an indefinite period up to several years to produce a time scale.

Historically, laboratory frequency standards were the first to be developed and were used to calibrate the frequency or rate of one or more clocks used to generate an atomic time scale. Initially such clocks consisted of free-running quartz crystal oscillators whose output was frequency-divided so as to yield the required hours, minutes, and seconds of the time scale. Later developments resulted in the replacement of these free-running oscillators with ones controlled by an atomic resonance, but the principle of operation remained the same. In general, frequency standards operate only for short periods either because they are not designed to function continuously or because their systematic errors are time-dependent and prolonged operation reduces rather than enhances the accuracy of a calibration.

Primary clocks have undergone intensive commercial development[1-3] during the past 10 years. Attention has centered on small, light-weight, portable instruments with accuracies of several parts in 10^{12} and stabilities over periods of weeks or months sometimes attaining and occasionally exceeding a part in 10^{13}. In national laboratories such instruments have usually been used in groups of at least four, and the primary aim has been to average their individual time scales, often with complicated weighting procedures, so as to obtain a mean scale exhibiting greater uniformity or rate stability than that provided by any member of the group. Such a mean scale can, if desired, be steered by means of periodic calibrations, widely separated in time, by a primary laboratory frequency standard so as to produce not only a more uniform but also a more accurate time scale than that realizable with any of the individual clocks. The period required for each calibration depends primarily on the stability of the clocks in the group, but may also be affected by the long term stability of the primary standard if its systematic errors are time dependent. In general however, the accuracy of the time scale so produced can only approach but never equal that of the primary standard, unless the mean rate of the ensemble is so uniform and the primary standard so stable that successive calibrations result in a statistical improvement in the accuracy. In practice, such improvement is unlikely. It is thus apparent that the application of such techniques constitutes a compromise resulting from the combination of unstable secondary clocks capable of extended periods of operation and very accurate primary laboratory frequency standards capable of continuous and accurate operation only over short periods.

The method of time-keeping used at NRC[4,5] until very recently followed this compromise procedure, with CsIII, a long beam laboratory frequency standard developed in 1963, providing twice-weekly cali-

brations of several Hewlett-Packard clocks, each of which produced alternate physical realizations of UTC(NRC) and AT(NRC). Because only two or three such clocks were usually in operation at any one time, the best was chosen as the basis of the scales actually used.

As mentioned in an earlier publication[5], it was decided about six years ago to try to combine the high accuracy of a long beam primary cesium frequency standard with the continuous operating characteristics of clocks so as to produce a single high-accuracy clock. The design had to be such that not only was continuous operation possible over extended periods, but also that the systematic frequency shifts be small, constant, and re-evaluable during clock operation, with only brief inoperative periods resulting from equipment failure or certain of the re-evaluation procedures. Such a clock has now been in operation at NRC since May 1, 1975, and its performance to date indicates that these design considerations have been met.

The results to be described in this paper show that it now appears possible to produce a highly uniform, accurate, and reliable time scale based on a single long-beam primary cesium clock and only a few stable auxiliary secondary clocks necessary to maintain continuity during evaluation periods. These results indicate that the time scale, PT(NRC CsV)*, generated by the new NRC primary clock, CsV, exhibits a uniformity of the order of ± 100 ns over an initial six-month period of operation. Comparisons with the International Atomic Time Scale, TAI, also show that the rate of PT(NRC CsV) has remained within 1.4×10^{-13} of previous short term measurements made during 1973 and 1974, which were in close agreement with those made with respect to the primary cesium standards at the National Bureau of Standards of the USA and the Physikalisch-Technische Bundesanstalt of West Germany.

In addition to these improvements and simplifications in time-keeping at NRC, continuous operation of CsV has also greatly simplified routine calibrations of commercial frequency and time standards.

EXPERIMENTAL

1. Physical and Electronic Design

Since the general physical characteristics of CsV and its performance as a frequency standard have already been described in a

---

*The terminology PT is used instead of AT since it represents a scale of proper time with no corrections being applied for altitude above sea level.

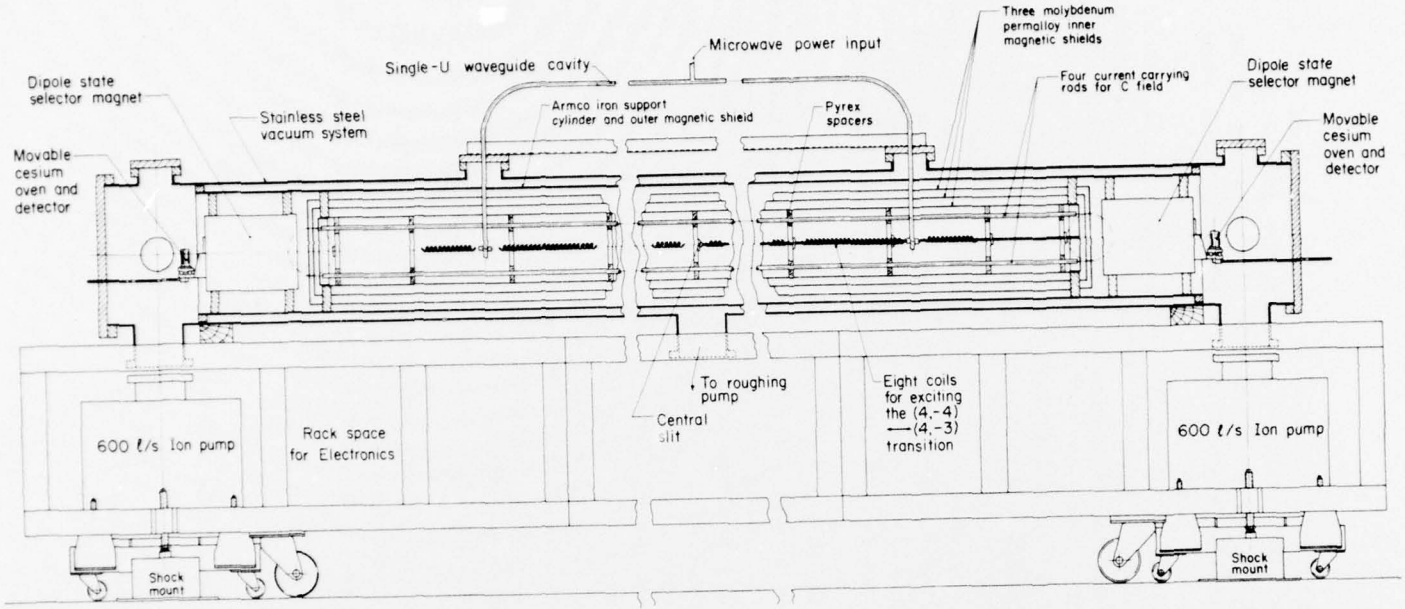


Figure 1. The NRC cesium beam primary clock, CsV.

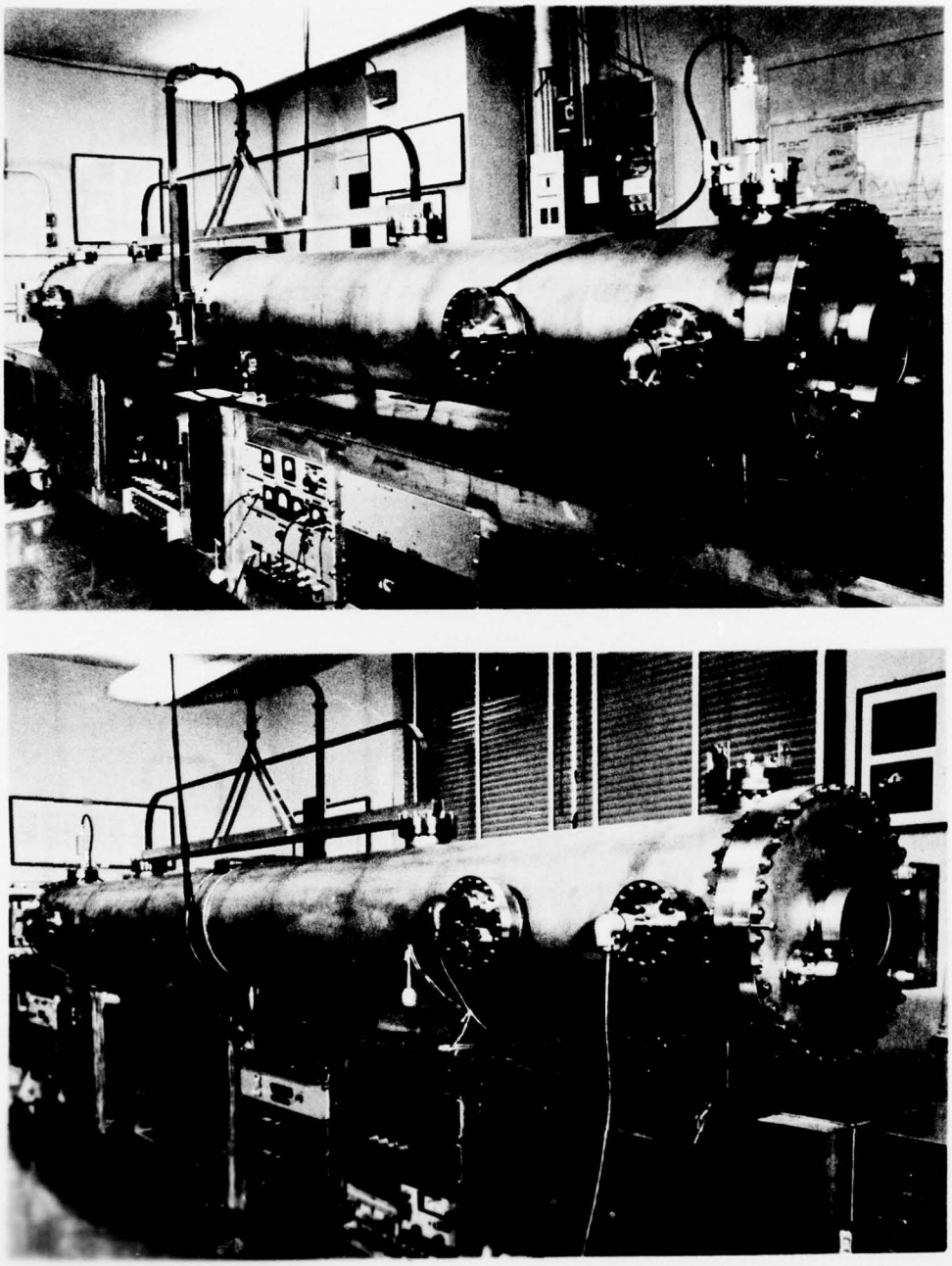


Figure 2. Photographs of CsV showing the beam tube and all electronics required for clock operation. Battery supplies are shown in the background of the lower photograph.

previous paper[7], and no major modifications to the device have been made, other than modifications to the electronics systems, only a brief outline will be given here.

A section drawing of CsV is shown in figure 1, and two photographs of it with all the modified electronics required for clock operation are shown in figure 2. In essence, CsV consists of a conventional transverse C field device with a bi-directional ribbon-type cesium beam. The dipole state selector magnets are placed outside the atomic transition region which consists of a central space magnetically shielded by three concentric molybdenum permalloy cylinders. This space contains a four-rod current-carrying structure providing a C field uniform within ± 0.06%. A series of optically ground pyrex glass spacers provides accurate alignment of the rods and also support for a series of coils used to excite the (4,-4) ↔ (4,-3) transitions required for C field measurement. The shields and state selector magnets are mounted inside an Armco iron cylinder which also provides additional magnetic shielding. The 2.1 m long microwave cavity is external to the shields and vacuum system and enters through slots in the four cylinders. The cesium beam is produced by either of a pair of transversely movable ovens, one at each end of the vacuum tube, and is detected by one of a pair of simple hot wire 80% platinum, 20% iridium detectors mounted adjacent to each oven. Each oven and detector pair is mounted on a movable carriage attached to the outer end of each state selector magnet. A low hot wire temperature of less than 800°C is used to minimize incidental heating of the adjacent oven and to provide a detector noise level of about 3×10^{-16}A in a 1 Hz bandwidth. For clock operation and a frequency stability of a few parts in 10^{14} over a 1 h averaging time, a beam current of 1.5 to 2.0 pA is required, and for frequency standard operation and systematic error evaluation, beam currents up to 20 pA provide correspondingly better stabilities. For the lower beam current required for clock operation, the 4 g cesium charge in each oven should provide an operating life of several years. The vacuum system is pumped continuously by two 600 ℓ/s ion pumps which provide a typical operating pressure of 2 to 4×10^{-9} Torr. All electronic systems, including one ion pump supply but excepting the second which is operated from 220 vac, are supplied by a pair of 28 v batteries and are mounted in the table below the vacuum tank. Total power consumption is about 200 w or 7.3 A at 28 v. The two batteries are float-charged by 0.01% voltage regulated power supplies operated from a 115 vac line emergency protected by two diesel generators.

The previous publication on CsV gives details of the general performance as regards the microwave and low frequency spectra, and these will not be repeated here. However, extensive modifications have been made to the microwave excitation system, particularly as regards the 5 MHz crystal oscillator, and multiplier and synthesizer

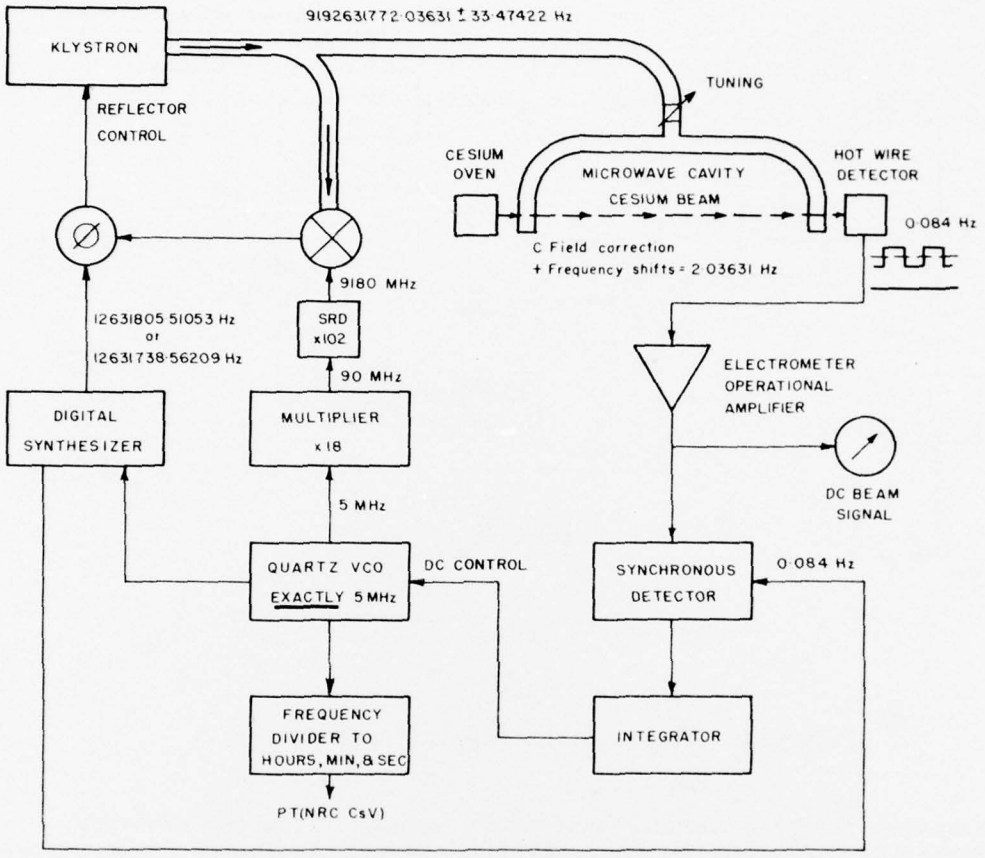


Figure 3. Complete electronics system for microwave excitation of the cesium resonance and servo control of the 5 MHz oscillator.

systems. The modified electronics systems are shown in figures 3 and 4. As a result of the improved design of the oscillator, distribution amplifier, solid state 5-90 MHz multiplier, and 12.6 MHz synthesizer and klystron phase lock system, the power dependent frequency shifts which had precluded clock operation earlier were essentially eliminated. These shifts apparently arose from time-dependent spectral impurities in the microwave excitation signal which were produced or enhanced by each of the units mentioned above. A klystron was used in preference to a Gunn diode as the microwave oscillator since the latter appeared to contribute to the spectral impurities mentioned. With the new microwave excitation system, the power dependence of the resonance

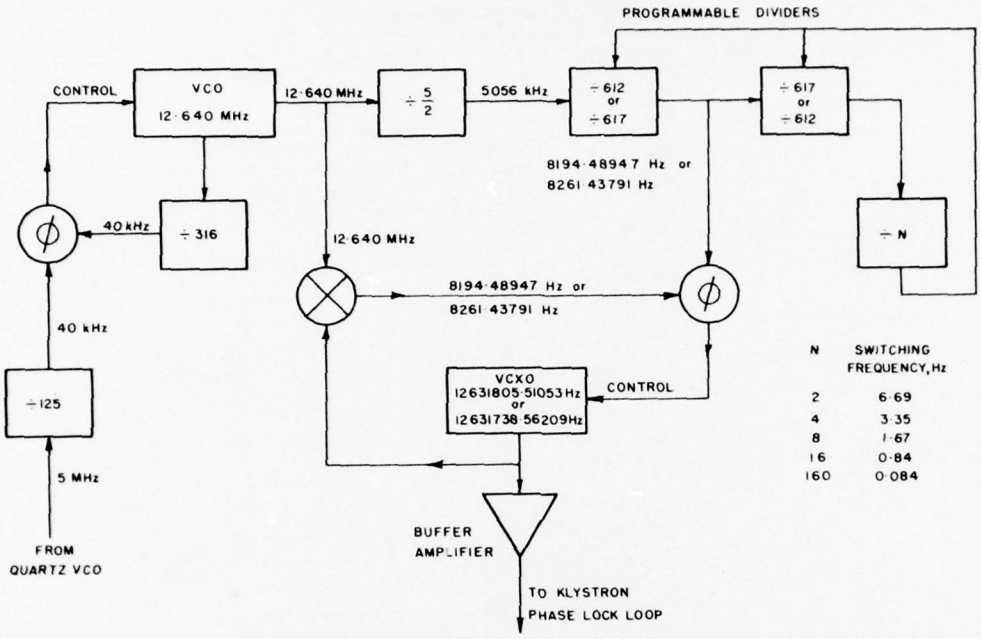


Figure 4. The 12.6 MHz digital synthesizer.

frequency is approximately that to be expected from the combined effects of the second order Doppler shift and the cavity phase difference.

One of the most important circuit modifications concerned the 12.6 MHz synthesizer, the earlier model of which had been found to give rise to troublesome sidebands at the cesium resonance frequency. A new synthesizer of fundamentally different design was constructed. With this design no sidebands occur within 8 kHz of the central frequency, and the levels of those which do occur are below 85 dB with respect to carrier. Figure 4 indicates the principle of operation. From an input frequency of exactly 5 MHz two phase-locked output frequencies of 12 631 805.510 53 and 12 631 738.562 09 Hz are selected alternately at switching frequencies of about 6.69, 3.35, 1.67, 0.84, or 0.084 Hz. The lowest frequency is normally employed for clock operation, since, as will be mentioned later, it gives rise to a negligible systematic frequency shift. Mixing of these two 12.6 MHz frequencies with the 9180 MHz signal produced by frequency multiplication from the same 5 MHz signal then provides alternately two beam excitation microwave

frequencies of 9 192 631 738.562 09 and 9 192 631 805.510 53 Hz. These two frequencies, which have a mean of 9 192 631 772.036 31 Hz are separated by about 66.9 Hz, which is slightly greater than the CsV resonance line width of about 60 Hz. Since the cesium resonant frequency is defined as exactly 9 192 631 770 Hz, the synthesized frequency is thus exactly 2.036 31 Hz or 2 215.15 parts in 10^{13} above this defined value. The sum of all the systematic frequency shifts in the CsV resonant frequency is then adjusted by altering the C field so as to be approximately equal to this offset of 2 215.15 x 10^{-13}. This is accomplished through discrete current steps in the C field supply, each step corresponding to a frequency shift of about 3.5 x 10^{-14}. Consequently, the frequency of CsV can be set with a precision of about $\pm$ 2 x 10^{-14}.

A choice of frequencies was provided for the switching rate between the two synthesized frequencies so as to enable tests to be made for possible dependence of the CsV frequency on this parameter. For frequencies of 1.67 and 3.35 Hz systematic frequency shifts of -5 and -25 x 10^{-14} from the value for 0.084 Hz were observed. No significant change occurred between switching frequencies of 0.084 and 0.84 Hz. For normal clock operation a switching rate of 0.084 Hz was chosen so as to avoid any significant systematic error and also to permit low temperature operation of the hot wire detector and consequent low detector noise level.

It will also be noted from consideration of the method used to obtain the switching frequencies that the times of frequency switching coincide with the zero crossing of the two switched frequencies, thereby obviating possible problems arising from phase discontinuities in the microwave exciting signal.

In addition to the method of synthesizing the 12.6 MHz signals outlined above, which is that normally used for clock operation, an alternate system was also devised. The latter employed a commercial synthesizer of completely different design and hence different sideband structure. Consequently, it was possible, by comparing the clock frequencies produced by the two different systems, to determine whether these sidebands caused significant resonant frequency shifts. The alternate synthesizer was one which could be binary-code remotely programmed by a specially constructed auxiliary unit so as to switch between frequencies of 631 772.036 $\pm$ 30 Hz at switching rates of 0.1 and 1.0 Hz. Summation of these frequencies with exactly 12 MHz derived from the master 5 MHz oscillator then provided the 12.6 MHz signal required for the klystron phase lock loop. Measurement of the CsV output frequency for operation with either synthesizer system indicated that no significant frequency difference existed. Since it was known that the sideband levels for the synthesizer normally used were very much lower than those for the alternate system, frequency shifts arising from any such sidebands were considered to be negligible.

2. Measurement of Systematic Frequency Shifts

A. General

As mentioned in the previous section, the C field correction is adjusted so that the sum of it, the frequency offset arising from the method of frequency synthesis, and all the known calculable or measurable systematic shifts are approximately zero, within the limits of precision of setting of the C field current source. In this way, the clock frequency is adjusted to within 2×10^{-14} of the nominal value.

In CsV the known systematic frequency offsets are those arising from the C field, δf_H, the cavity phase difference, δf_c, the Millman effect, δf_m, and the second order Doppler effect, δf_d. In general each of these is dependent on both the beam direction and the C field direction, and these two parameters can be denoted by the subscripts AB, BA, N, and R, the first pair referring to beam direction, and the second pair to normal or reversed C field direction. A normal C field direction is one for which the magnetic field is in the same direction throughout both state selectors and the C field region.

Measurements of the changes in the CsV frequency are made with respect to the stable reference frequency provided at 1420 MHz by one of the two auto-tuned NRC hydrogen masers. If the cesium and hydrogen normalized frequencies are defined by f_{CsV} and f_M, and a constant K is used to account for the setting of the synthesizer in the 5 to 1420 MHz maser frequency synthesizer chain required to provide a suitably slow beat between the cesium and hydrogen frequencies, the following relationships may be shown to exist between them and the systematic frequency shifts. In these expressions, δf_m and δf_c are arbitrarily chosen as those for the AB and N subscripts, and the sign of each changes with either beam or C field reversal. The beat frequency, normalized with respect to 1420 MHz, is a measure of the difference $f_{CsV} - f_M$.

$$\Sigma\delta f_{iAB,N} = + \delta f_m + \delta f_c + \delta f_{HAB,N} + \delta f_{dAB} = f_{CsVAB,N} - f_M + K \qquad (1)$$

$$\Sigma\delta f_{iBA,N} = - \delta f_m - \delta f_c + \delta f_{HBA,N} + \delta f_{dBA} = f_{CsVBA,N} - f_M + K \qquad (2)$$

$$\Sigma\delta f_{iAB,R} = - \delta f_m + \delta f_c + \delta f_{HAB,R} + \delta f_{dAB} = f_{CsVAB,R} - f_M + K \qquad (3)$$

$$\Sigma\delta f_{iBA,R} = + \delta f_m - \delta f_c + \delta f_{HBA,R} + \delta f_{dBA} = f_{CsVBA,R} - f_M + K \qquad (4)$$

Methods of determining each of these quantities will now be outlined.

B. C field Correction

As mentioned in the earlier paper describing CsV, the C field correction δf_H is determined from the mean square value of the $(4,-4) \leftrightarrow (4,-3)$ transition frequencies measured by means of the 6 axially oriented low frequency exciting coils which are located between the two microwave interaction regions. As in the previous analysis the value of δf_H was given by the expressions

$$\delta f_H = \Delta f_H / 9\ 192\ 631\ 770$$

and

$$\Delta f_H = 427.18 \left[\Sigma (f_o/349746)^2\right] /6$$

where f_o is the resonant frequency measured for each of the coils, and the two constants are those which were experimentally verified in the previous evaluation. In practice, however, because of the ± 0.06% C field uniformity the simpler expression

$$\Delta f_H = 427.18 \left[\frac{\Sigma f_o/6}{349746}\right]^2$$

provides the same result within 2×10^{-16} with reference to the cesium resonance frequency. Because of uncertainties in the experimental determination of the two constants, which have not been improved since the previous evaluation, the uncertainty in the values of δf_H is of the order of $\pm 4 \times 10^{-14}$ with reference to the cesium resonance frequency.

C. Second Order Doppler Effect

The second order Doppler effect, which gives rise to the frequency offset δf_d, is determined from the shape of the Ramsey resonance by means of a curve-fitting technique described in a previous publication[8]. This technique is based on the assumption that a truncated Maxwellian velocity distribution can be used to approximate the actual distribution of atomic velocities which exists in the detected beam. Small alterations in the beam optics subsequent to the first evaluation of CsV and prior to inception of clock operation resulted in velocity distributions which were essentially the same for both beam directions. Figure 5 shows the Ramsey resonances for the two beam directions, measured for an exciting power level 3 dB below that for maximum transition probability. The closest fit between experimental and calculated resonances occurs for $p_{min} = 1.0$ and $p_{max} = 1.8$, the parameters p_{min} and p_{max} representing the ratios of the low and high beam velocity cutoffs with respect to the most probable atomic velocity in the cesium oven. For these values δf_d is -4.1×10^{-13}, and the estimated uncertainty resulting from errors in curve-fitting is about 2×10^{-14}.

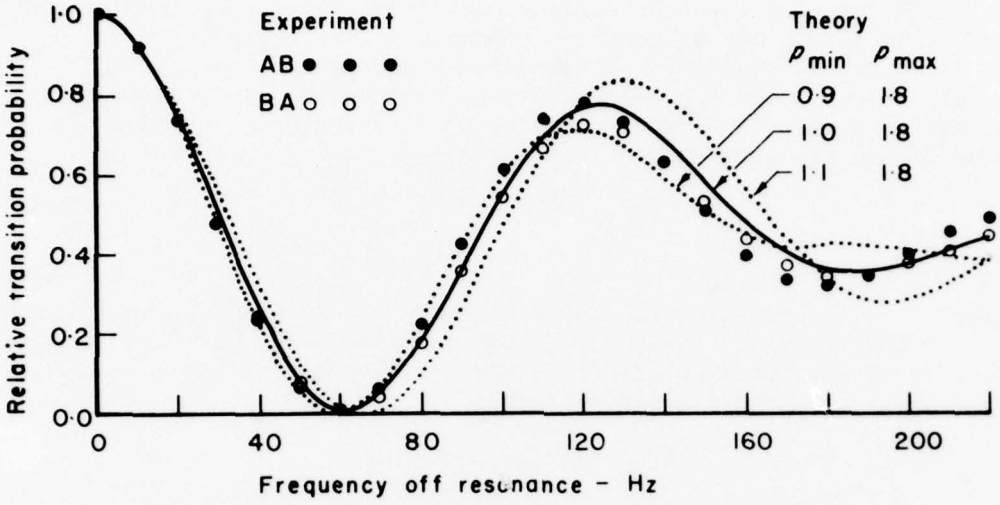


Figure 5. Measured and calculated Ramsey resonances for both beam directions.

D. Cavity Phase Difference and Millman Effect

The systematic errors resulting from a cavity phase difference and from a change in angle between the C field and the microwave exciting field along the beam direction, represented by δf_c and δf_m respectively, can be determined by C field and beam reversal. The quantity δf_m, which represents the Millman effect[10] as applied to σ transitions, cannot be isolated from δf_c by means of beam reversal alone, since both δf_m and δf_c change sign with reversal of the beam direction. However, C field reversal does not affect the sign of δf_c, and consequently the two frequency shifts can be separated, as is apparent from inspection of equations 1 to 4. In practice, also, since both δf_c and δf_m as well as δf_d are dependent on the beam velocity distribution [9,10], and hence the microwave excitation level, these frequency shifts must be determined as a function of the exciting power level. The dependence of δf_m on power level is, however, of much lesser importance[10]. With regard to δf_c and δf_d, since the sign of the former reverses with beam direction, for a given C field direction the power shifts tend to cancel for one beam direction and add for the other.

The values of δf_m, δf_c, and the combined power dependence of

δf_m, δf_c, and δf_d were measured both immediately prior to inception of clock operation on May 1, 1975, and again after about 4.5 months of continuous operation, in mid-September. In the April series of measurements the beam direction was reversed a total of 4 times, and the C field 12 times. In the September series, the C field was again reversed 12 times, but the beam direction only once, so as to minimize time scale errors during the period that the clock was inoperative. No significant differences were found between the two sets of measurements, the value of δf_m being 2.0×10^{-13} for both cases, and value of δf_c being -3.1×10^{-13} for the first and -3.4×10^{-13} for the second.

It is difficult to estimate the total uncertainty for δf_c and δf_m, and also δf_d and their combined power dependence, since they all act simultaneously. In addition, it is not known how accurately the power dependence predicted by the theory[8,9,10] based on the assumption of a truncated Maxwellian velocity distribution portrays the actual physical conditions. As indicated in the previous paper describing CsV as a frequency standard[7], a total frequency decrease of about 3 or 4 parts in 10^{14} is predicted as the power level drops to zero from the usual operating level 3 dB below that for maximum transition probability. For the A to B beam direction, the measured shift was about 5×10^{-14} and for the B to A direction about 3×10^{-14}, as determined from both the most recent measurements made in September and those made earlier in April, 1975. The uncertainty of these measurements was affected to some degree by barometric-pressure induced frequency shifts of several parts in 10^{14} in the frequency of the reference hydrogen maser[13]. However, a combined uncertainty in the determination of δf_c and δf_m of about $\pm 2 \times 10^{-14}$ appears not unreasonable on the basis of these measurements.

An important factor influencing the accuracy of determination of δf_c is the time elapsed between clock operation for one beam direction and in the reverse direction. At the time of the most recent beam reversal in September, it was found that the long, 4.5 month period of clock operation in the A to B direction had resulted in poisoning of the hot wire detector which was adjacent to the A oven. A period of about 26 h was required to restore normal operation of the A detector hot wire, the temperature of which was maintained near to 1200°C for about 7 h in order to evaporate from the wire the deposited cesium. It is hoped that in future it will be possible to avoid such long inoperative periods by at least partial prior cleaning of the detector wire to be used after beam reversal. However, despite the 26 hour period during which CsV was inoperative because of poisoning of the hot wire, comparisons with the best NRC secondary clock, HP 911, show that a time scale error exceeding 5 ns is unlikely.

One of the problems inherent in the experimental determination of δf_m by C field reversal concerns changes in the magnetic charac-

teristics of the magnetic shields arising from reversal of their direction of magnetization. As might be expected, following each C field reversal the value of δf_H did not repeat exactly, even though the current through the C field rods remained constant. A gradual decrease of several parts in 10^{15} in δf_H occurred, as shown in table I, for the most recent series of measurements.

Table I - Change in C field correction, parts in 10^{13}, with successive C field reversals, for both beam directions.

Beam Direction A-B			Beam Direction B-A		
Run No.	$\delta f_{HAB,N}$	$\delta f_{HAB,R}$	Run No.	$\delta f_{HBA,N}$	$\delta f_{HBA,R}$
1	2220.43		1	2218.31	
2		2216.51	2		2208.11
3	2220.42		3	2218.27	
4		2216.64	4		2208.07
5	2220.39		5	2218.21	
6		2216.58	6		2207.99
7	2220.39		7	2218.24	

E. Time Dependent Variation of the C Field

One of the most important factors limiting the accuracy of a primary cesium clock is the long term stability of the C field, since the C field frequency offset, δf_H, can be remeasured only at relatively widely spaced intervals. Earlier experiments with CsIII had shown that occasional frequency variations up to several parts in 10^{13} could occur as a result of C field changes which were not due to changes in the current flowing in the C field rods. Presumably, alterations in the magnetization of the magnetic shields were responsible for such changes. In CsIII only one mu-metal shield was used, although, as in CsV, an Armco iron support cylinder did provide some additional shielding. In the design of CsV much more complete magnetic shielding is provided, with three concentric molybdenum permalloy cylindrical magnetic shields enclosing the C field region, as shown in figure 1.

The long term C field stability of CsV, shown in figure 6, is much superior to that of CsIII, but some variation, which is probably not due solely to a gradual drift of the current in the C field rods, does occur. Only partial correlation between this current, measured by means of a standard resistance in the C field current circuit and a differential voltmeter, and the C field correction was observed. The

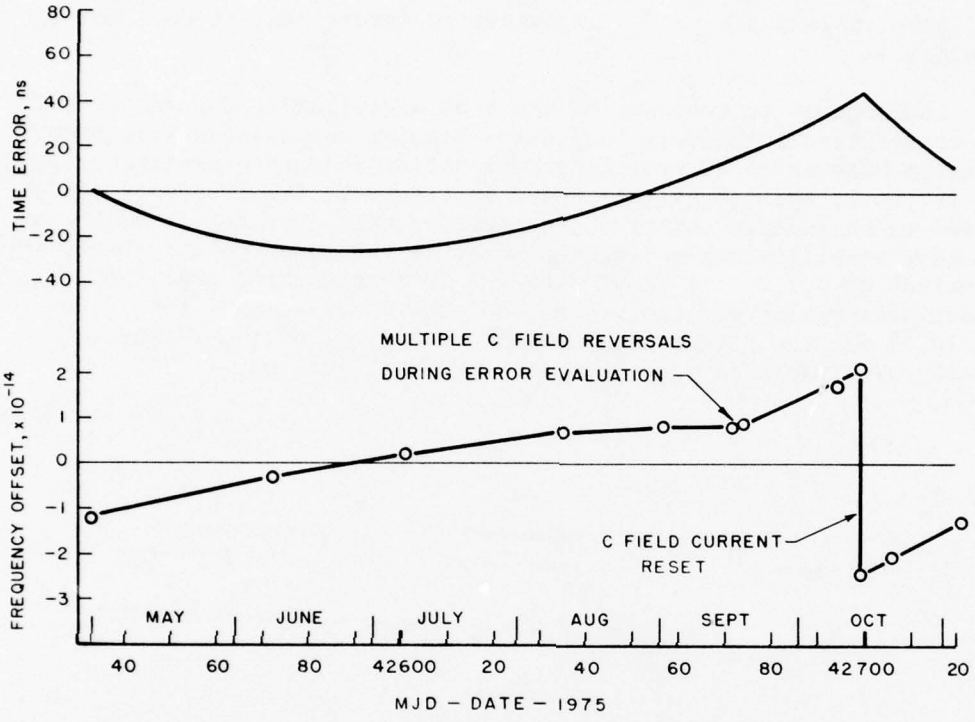


Figure 6. Time dependence of the C field correction, δf_H, during the period May-October, 1975, and resultant time scale error.

change in slope of the graph of figure 6 at the time of the most recent re-evaluation, which included multiple C field reversals, indicates that changes in magnetization of the shields are probably responsible for a considerable portion of the C field variation, which averaged about 5×10^{-15} per month. Also shown in figure 6 is the time dependence of the time scale error, which attained a maximum value of about 45 ns on October 14, 1975. Resetting of the C field current on that date resulted in a steady diminution of this error.

F. Frequency Dependence on Beam Intensity

It is essential that the frequency of a primary clock not be dependent on the beam current intensity since systematic errors are normally determined at high beam currents with concomitant improved short term frequency stability and clock operation depends on prolonged operation at low beam currents. Although such a dependence would not

actually be anticipated, it is important to ensure that it does not in fact exist.

Subsequent to reversal of the beam direction in September, 1975, three consecutive relatively long CsV - H maser comparisons were made for cesium beam currents providing peak-valley resonance amplitudes of about 1.7, 4.2, and 1.7 pA. As shown in figure 7, the frequency of CsV appeared to be independent of the changes in beam current, although the short term stability was noticeably worse at the lower beam current, with values of $\sigma(2,2h)$ of about 2 to 4 x 10^{-14} occurring over the first and last measurement periods, each about 20h in duration. The value of 1.3 x 10^{-14} for the higher beam current is typical of the relative stability obtainable during systematic error evaluation.

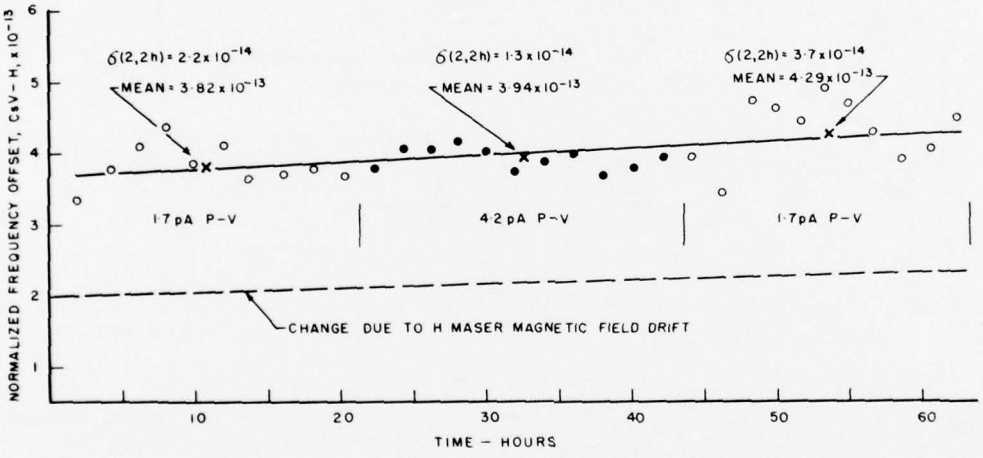


Figure 7. Dependence of the frequency of CsV on beam current.

Also shown in this figure is a dashed line indicating a 3 x 10^{-14} frequency drift arising from changes in the magnetic field of the maser. This drift is based on two measurements of the magnetic field immediately prior to and following the 70 hour total measurement period. The mean frequency offsets for each of the three runs indicate a somewhat larger drift of about 5 x 10^{-14}. The difference between these two drifts of 2 x 10^{-14} could have been in part the result of barometric pressure effects on the maser or simply a statistical fluctuation of the measurements.

G. Summary of Systematic Frequency Shifts

In the following table summarizing the uncertainties in the systematic frequency shifts characteristic of CsV, it is assumed that any variation of the frequency with beam current intensity is negligible, implying that the frequency is the same for either clock operation or operation as a frequency standard.

In addition, any frequency uncertainty arising from pulling of the resonance by cavity mistuning is considered to be the same as in the previous evaluation, or 2×10^{-15}.

Table II - Summary of the uncertainties of the known frequency shifts characteristic of CsV

Frequency Shift	Uncertainty, e_i Parts in 10^{14}
Second order Doppler effect, uncertainty in curve fitting	2
Combined uncertainty in values of δf_m and δf_c and power dependence of δf_m, δf_c, and δf_d	2
Combined uncertainty in value of δf_H arising from (a) constants used in its calculation (b) measurement of the mean square value of the $(4,-4) \leftrightarrow (4,-3)$ transition frequencies	4
Servo system frequency offset based on measured shift with modulation frequency	2
Frequency pulling for estimated maximum cavity detuning of 5 MHz	0.2

Total uncertainty for:

(a) random individual uncertainties, $(\Sigma e_i^2)^{1/2} = 5.3 \times 10^{-14}$ or 4.6 ns/day

(b) additive individual uncertainties, $\Sigma e_i = 10.2 \times 10^{-14}$ or 8.8 ns/day.

It also must be stressed that this table summarizes only the uncertainties of the known systematic errors, and no attempt has been made to predict or compensate for errors which may appear as further experience with CsV is gained during future operation. In this regard, it could be mentioned that the Millman effect, discussed in this paper,

did not appear to be significant at the time of the first evaluation of CsV in 1973, but did in the two evaluations carried out during 1975. Improved measurement techniques were probably responsible for the appearance of this effect, although possible changes in the standard itself cannot be ruled out entirely. It is, however, important to note that although in the 1973 evaluation the Millman effect was not isolated from the cavity phase difference frequency shift, the combined effects were compensated for by beam reversal. It would, indeed, be surprising if future work at NRC and other laboratories were not to uncover other new and unsuspected sources of systematic frequency shifts, especially as measurement techniques improve. If such shifts appear they will be reported and the rate of PT(NRC CsV) will be adjusted accordingly.

3. Time Comparisons with Secondary Clocks and Other Time Scales

A. General

Although internal estimates of accuracy and stability such as those outlined above are essential in the evaluation of the performance of a primary standard such as CsV, they are of little value unless they are corroborated by comparisons with other clocks or frequency standards either within or outside the laboratory. Such comparisons leading in general to support for the accuracy and stability estimates given for CsV have been made with the NRC hydrogen masers, the three best NRC secondary cesium clocks, the present NRC primary cesium frequency standard, CsIII, the International Atomic Time Scale, TAI, and the UTC time scales of the National Bureau of Standards and the US Naval Observatory. Details of these comparisons are given below.

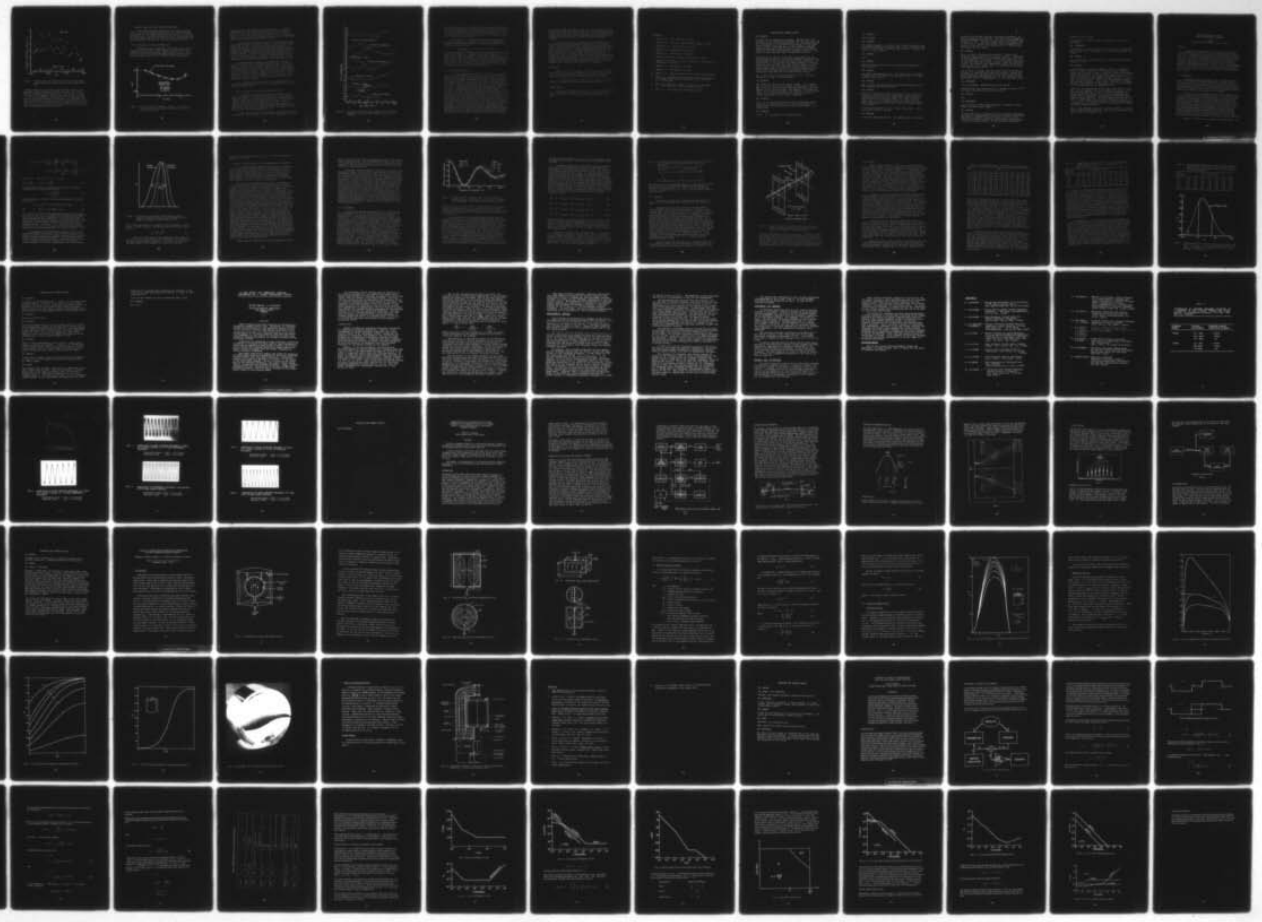
B. Frequency Comparisons with CsIII

During the period May-October, 1975, a total of 36 6h comparisons were made between the frequencies of CsIII and CsV, as shown in figure 8. The estimated uncertainties of each of the comparisons is about 2×10^{-13}, and the value of $\sigma(2,T,\tau)$ for T, the time between measurements, of about 4 days, and τ, the time for an individual measurement, of about 6 h, is 1.6×10^{-13}. The comparisons indicate that the mean frequency of CsIII is 10.7×10^{-13} above that of CsV. The value found in 1973 for a much shorter period of several days[7] was 10.5×10^{-13}. An unpublished value measured in mid-1974 and given at the July 1974 meeting of the Consultative Committee for the Definition of the Second was 11.0×10^{-13}. The latter was based on 15 6-hour measurements. The close agreement shown in these three comparisons is, however, probably fortuitous, since it is apparent from figure 8 that

AD-A040 774 NATIONAL AERONAUTICS AND SPACE ADMINISTRATION GREENB--ETC F/G 14/2
PROCEEDINGS OF THE ANNUAL PRECISE TIME AND TIME INTERVAL (PTTI)--ETC(U)
DEC 75

UNCLASSIFIED NASA-GSFC-X-814-76-45 NL

3 OF 8
ADA040774



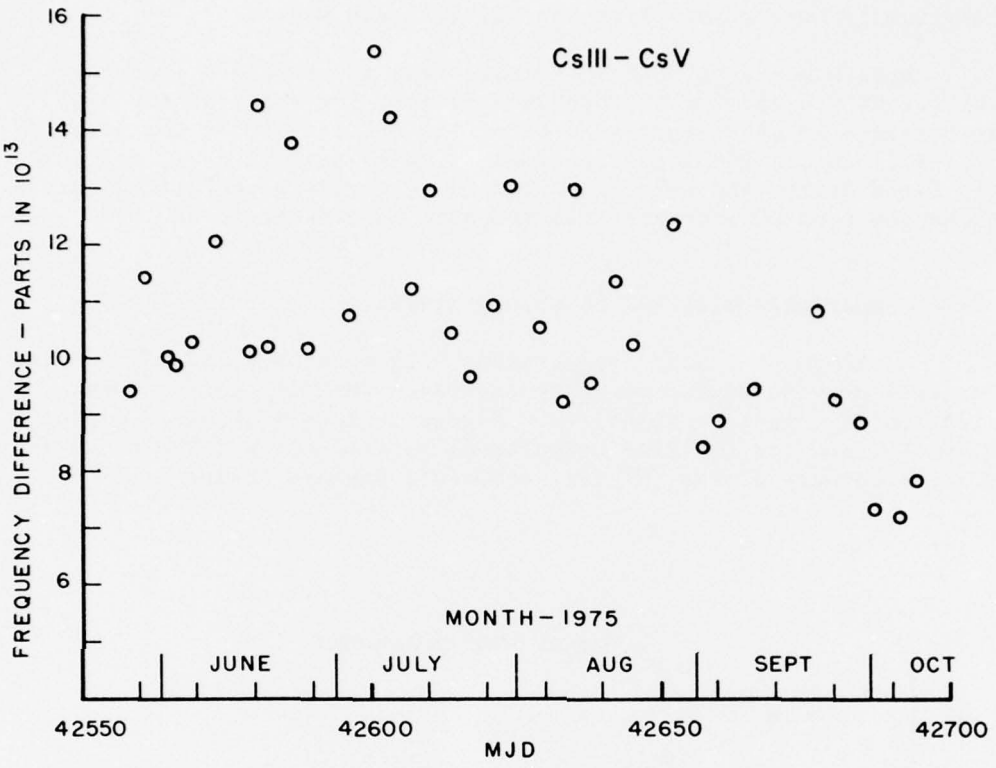


Figure 8. Frequency difference between CsIII and CsV measured over 6-hour calibration periods during the interval May-October 1975.

a gradual change of several parts in 10^{13} probably occurred in the frequency of CsIII during the period May to October, 1975, and, in addition, comparisons between the NRC time scales based on CsIII and TAI indicate that frequency variations over several months of about 2×10^{-13} are not uncommon. Such variations in CsIII may arise from changes in the spectral purity of the microwave exciting signal. However, within the lower accuracy and precision attainable with CsIII, of about 10^{-12} and 2×10^{-13} respectively, there appears to be no conflict between the internal estimates of accuracy and stability given for CsV and those determined with respect to CsIII.

C. Frequency Comparisons With the NRC Hydrogen Masers

Data already presented indicate that the relative frequency stability of CsV and the NRC hydrogen masers, for sufficiently high beam currents in CsV, appears to be of the order of 10^{-14} for periods of several hours. For longer periods of up to several days, maser magnetic field drifts and effects on the maser cavity of barometric pressure changes tend to increase this value to several parts in 10^{14}.

D. Time Comparisons with NRC Secondary Clocks

Although time scale comparisons with secondary clocks do not in general provide useful accuracy estimates they do provide some indication of long term stability. Figure 9 shows a $\sigma(2,\tau)$ - τ plot for 48, 80, and 112 day time comparisons between CsV and the best of the NRC secondary clocks, HP 911, a Hewlett-Packard cesium clock

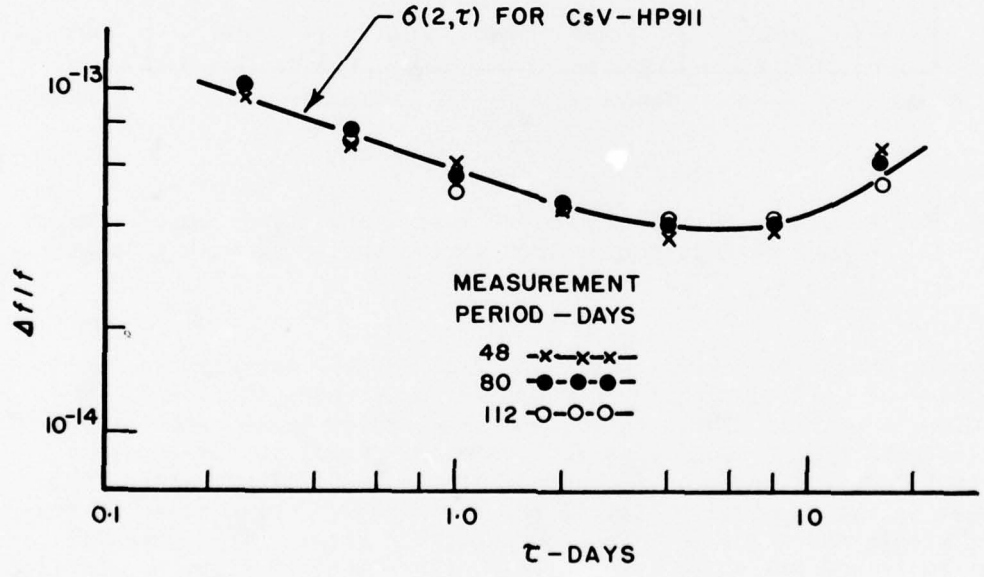


Figure 9. Relative fractional frequency stability, $\sigma(2,\tau)$ for CsV and HP 911 for three concurrent measurement periods of 48, 80, and 112 days.

equipped with the high performance cesium beam tube. It is apparent from comparison of the values of $\sigma(2,\tau)$ for these three concurrent periods of 48, 80, and 112 days, for $\tau<16$ days, that the statistics describe an effectively stationary noise process, since no significant changes occur for the different total measurement periods. The minimum value of $\sigma(2,\tau)$ is about 4×10^{-14} for $\tau = 6$ days.

Essentially the same data is shown in a different form in one of the graphs of figure 10, which indicates the time difference between PT(NRC CsV), the time scale based on CsV, and that provided by HP 911. Despite the apparent stationarity of the data for $\tau< 16$ days, it is evident that a change in slope of this graph occurs about the beginning of August, and that the new slope is maintained thereafter with no observable change. The absence of any significant change in slope in the vicinity of September 18 - 19, when a re-evaluation of CsV including beam reversal was carried out, indicates that any change in the frequency of CsV at that time is unlikely to have exceeded 2×10^{-14}.

Two other graphs in figure 10 show comparisons of PT(NRC CsV) and the time scales derived from the HP clocks 122 and 267, both of which are equipped with the standard cesium beam tubes. Some correlation between the 267 and 911 plots is apparent in this figure, and if it were not for the other plots, to be described later, which indicate no such correlation, it might be inferred that the frequency of CsV had altered some time during July or August by almost 1×10^{-13}. Such an alteration is, however, extremely unlikely, as outlined below. The third plot, showing CsV versus 122 indicates no correlation with the CsV-911 or the CsV-267 graphs.

It is evident that the results of these comparisons between CsV and the NRC secondary clocks are not in conflict with the internal stability estimate for CsV.

E. Time Scale Comparisons With Other National Laboratories

In comparing the time scale PT(NRC CsV) with those of other national laboratories an additional problem arises in any estimate of either the accuracy or stability, since the means of comparison may introduce significant errors[5], especially in the case of methods involving the transmission and reception of radio signals. However, if comparisons made with respect to the time scales maintained by two different laboratories are carried out using two quite different propagation paths, uncertainties arising from changes in propagation delay may be at least partially compensated for.

Comparisons of PT(NRC CsV) with UTC(NBS) and UTC(USNO) are shown in figure 10. These indicate, in the absence of propagation anomalies

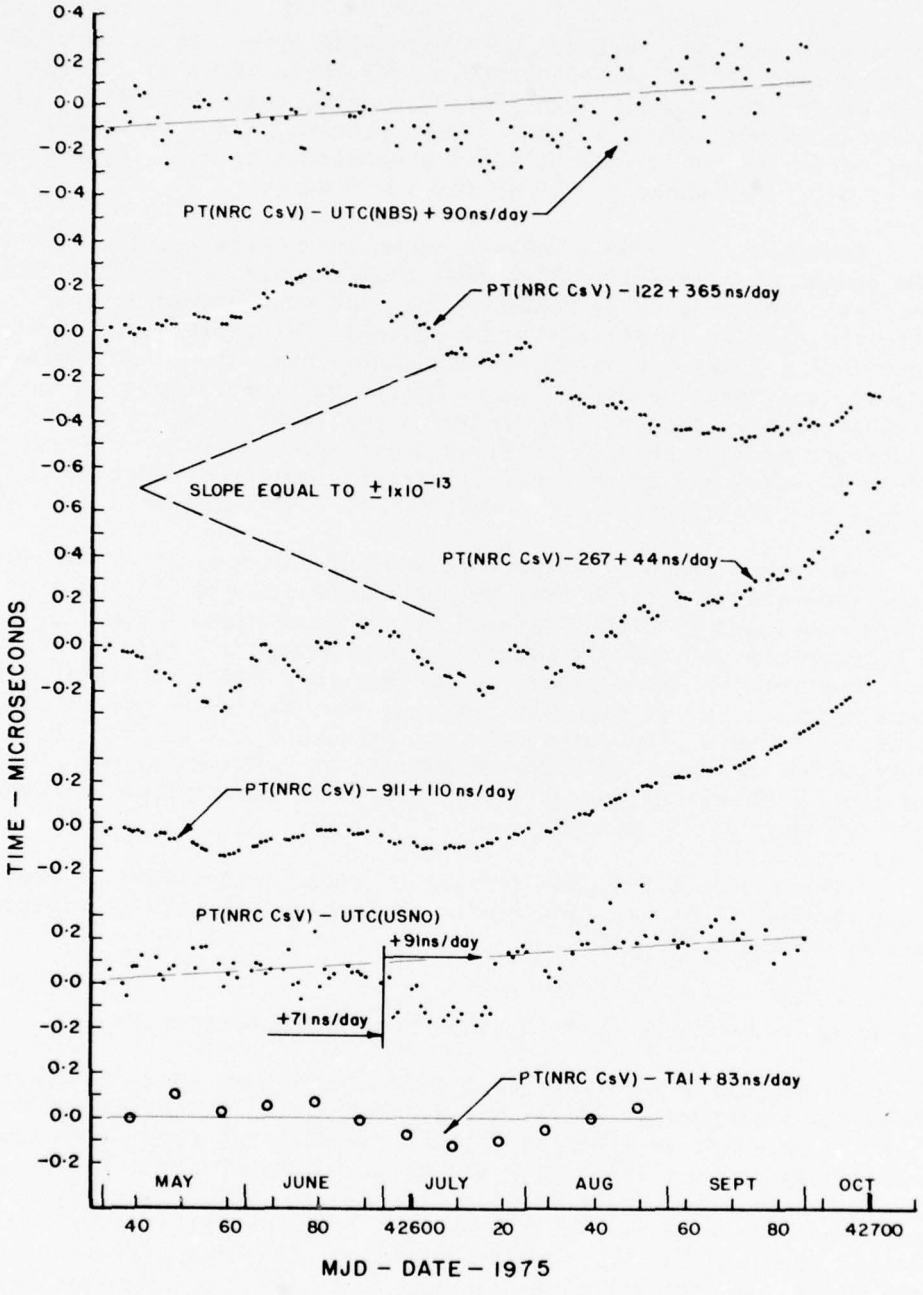


Figure 10. Time scale comparisons between PT(NRC CsV) and UTC(NBS), UTC(USNO), TAI, and the NRC secondary clocks 122, 267 and 911.

in the Loran C signal used as the basis of the comparisons, that the uniformity of PT(NRC CsV) is probably appreciably better than 1×10^{-13} over any one month period, and is likely to be a few parts in 10^{14} over the entire 6-month period. In connection with the USNO plot, it will be noted that the rate change of 20 ns/day made to UTC(USNO) on July 1, 1975, has been taken into account.

The PT(NRC CsV) - UTC(NBS) plot also provides a comparison of the absolute values of the frequencies of CsV and the NBS primary frequency standards NBS-4 and NBS-6. According to the NBS time and frequency bulletins for 1975,

$$f_{UTC(NBS)} = f_{Cs} \ (1 + (6.9 \pm 1.2) \times 10^{-13})$$

The frequency offset of UTC(NBS) from PT(NRC CsV) derived from the mean slope of the PT(NRC CsV) - UTC(NBS) plot is about 89 ns/day or 10.3×10^{-13}. There is, therefore, a difference of about 3.4×10^{-13} between the NRC and NBS estimates of the cesium resonant frequency and hence the SI second. This difference is greater than the sum of the error limits for the primary standards of the two laboratories, which is less than 2×10^{-13}. Possible implications of this rather large discrepancy will be discussed in the next section.

F. Time Comparisons With TAI

The relationship between PT(NRC CsV) and TAI is also shown in figure 10. Point scatter for this plot is less than for any of the others and this appears to imply better uniformity. This plot also provides the only long term estimate of the rate of TAI based directly on a primary laboratory cesium clock. According to this comparison the frequency of TAI is above the nominal value by about 83 ns/day, or 9.6×10^{-13}, implying that the TAI second is of too short a duration by this factor. In the 1973 evaluation of CsV the comparable value was 10×10^{-13}. Measurements made by the PTB indicated a value of 12×10^{-13} in mid-1973 and a decrease prior to this of about 1×10^{-13} per year[11]. if such a decrease continued during the period 1973 - 1975, the PTB value would be in the vicinity of 10×10^{-13} by mid-1975, and hence in close agreement with the NRC CsV value. It may also be mentioned that since the frequency of CsIII has been very close to that of TAI during the period 1973 - 1975, the mid-1974 value mentioned earlier for the ratio of the CsIII and CsV frequencies of 11.0×10^{-13} also applies to the rate of TAI at that time. The frequency offset for TAI quoted in the 1974 BIH report, and based on NBS, PTB, and NRC measurements, was 1×10^{-12}, which is also in good agreement with the present NRC CsV value. Indeed, the NBS mid-1974 value for the rate of TAI was[12] 10×10^{-13}. However, the mid-1975 NBS value for TAI, which can be derived from the plots of figure 10 and the rate of UTC(NBS)

with respect to NBS-4 and NBS-6, is only 6.2×10^{-13}, implying that the rate of TAI must have decreased by 3.8×10^{-13} over the one year period from mid-1974 to mid-1975. This discrepancy of 3.4×10^{-13} between NBS and NRC estimates of the rate of TAI can only indicate the presence of unrecognized systematic errors in either the NRC or NBS primary standards.

In connection with the contribution to TAI of PT(NRC CsV) it is interesting to note that the weight attributed to the NRC secondary clock 267, which, from figure 10, is noticeably less stable than CsV, is 100. This constitutes the maximum weight attributable to any of the clocks contributing to TAI. Since the uniformity of PT(NRC CsV) is quite comparable with that of UTC(NBS) or UTC(USNO), or even TAI, the question then arises as to what weight should be attributed to a primary clock such as CsV which is clearly similar in both accuracy and stability to quite large groups of other less accurate or stable clocks. As additional such primary clocks, similar to CsV, become available, a modified weighting procedure for TAI may become necessary if the best uniformity and accuracy for this scale are to be attained.

CONCLUSIONS

Operation of CsV as a primary clock during an initial 6-month test period has shown that the intended goal of a highly accurate and stable atomic time scale based primarily on a single, continuously operating laboratory-type cesium beam standard has been achieved.

It is expected that as of January 1, 1976, the NRC time scales UTC(NRC) and AT(NRC) will both be derived directly from CsV.

ACKNOWLEDGEMENTS

The authors are indebted to H. Lam, J. Lauriault, and W. Ekholm who were responsible for much of the electronic and mechanical construction of CsV and also for many of the time and frequency comparisons.

REFERENCES

1. Hellwig, H.W.: Proc. IEEE 63, 212 (1975).

2. Ramsey, N.F.: IEEE Trans. Instr. and Meas. IM-21, 90 (1972).

3. McCoubrey, A.O.: Proc. IEEE 54, 116 (1966).

4. Mungall, A.G.: Metrologia 10, 105 (1974).

5. Mungall, A.G.: Metrologia 7, 146 (1971).

6. Bureau International de l'Heure Annual Report for 1974.

7. Mungall, A.G., Bailey, R., Daams, H., Morris, D., and Costain, C.C.: Metrologia 9, 113 (1973).

8. Mungall, A.G.: Metrologia 7, 49 (1971).

9. Mungall, A.G.: Metrologia 8, 28 (1972).

10. Mungall, A.G.: Paper presented at the 1975 PTTI Planning Meeting.

11. Becker, G.: Conference on Precision Electromagnetic Measurements 1974 (CPEM74) IEEE Conference Publication No. 113, IEEE Cat. No. 74, CH0770-81M.

12. Glaze, D.J., Hellwig, H., Allan, D.W., Jarvis, S., Wainwright, A.E.: IEEE Trans. Instr. and Meas. IM-23, 489 (1974).

13. Morris, D.: To be published in Metrologia 12 (1976).

QUESTION AND ANSWER PERIOD

DR. HELLWIG:

I would like to comment on accuracy. We have been very cautious in quoting accuracy numbers over the past year and in a certain way I am surprised that you are reducing your accuracy number into the 10^{-14} region where, at the same time, we have a drifting apart of the primary standard values as you have correctly stated, and I should add to that that PTB, the third primary standard activity in the world, is drifting also away, in many parts in 10^{13}.

Our approach at NBS is to be very, very careful in not overstating accuracy at the present moment because we have encountered effects we have not previously considered. In other words, if one states an accuracy budget it contains elements which you know and some elements where you might have only an idea that they might cause trouble or not cause trouble and to restrict an accuracy budget only on the effects you know can have consequences of 10 sigma deviations from internally stated accuracy values.

So, I don't believe our own one part in 10^{13}, which we quoted a year ago, totally anymore.

DR. WINKLER:

The answer is that you both may be wrong. Or, I should say, at least one of you is wrong, whichever you prefer. But, I do have two questions that are related to that and number one is, when you make your magnetic field measurements, do you make them while the standard is still operating in its microwave resonance, or what do you do to insure continuity of your clock operation?

DR. COSTAIN:

Well, it is monitored normally with the hydrogen masers operating or when we make the C-field measurements or against 911 and we feel that we lose no more than 1 to 2 nanoseconds.

DR. WINKLER:

I see. So, you don't do it simultaneously?

DR. COSTAIN:

That's Right.

DR. WINKLER:

The second question, on one of your slides you said it was the difference NRC-3 minus NRC-5 and it gave something like 13 parts, an average, there was some scatter, 13 parts in 10^{13}. Is that correct?

DR. COSTAIN:

Yes.

DR. WINKLER:

The difference between your two primary standards was 13 parts in 10^{13}?

DR. COSTAIN:

Individual measurements, yes. The advertised, published, claimed value for cesium-3 was 15 parts in 10^{13}. It has proved to be correct.

DR. WINKLER:

But, I don't understand how the difference between these two standards can be that large.

DR. COSTAIN:

There is a large difference in the noise level, the efficiency in the detector, the efficiency of the magnetic shielding and in claiming, making the claim of accuracy that we have at the present time it is, and I have to admit this, it is our known errors and based on experimental measurements against the error of hydrogen, among other things.

If there are unknown errors, we don't know them. I am sorry that is all I can say.

DR. WINKLER:

I have not explained myself. My question was, the slide

stated the difference between two primary standards, not their frequency and stability. The difference between two primary standards and that was the order of between 10 and 16 parts in 10^{13}. In other words, how do you explain that in the face of claims that accuracy has a standard deviation of 1 part in 10^{13} or 4 parts in 10^{14}? How can the difference be that large?

DR. COSTAIN:

Well, in their evaluation of cesium-3, I believe its claimed accuracy initially was 1 part in 10^{11}. Eventually, with some improvement in the magnetic shielding, 15 parts in 10^{13} and this is 10 parts. It is well within our claim. It had been much more stable, in fact, than the frequency offset. We think it has changed only about 2 parts in 10^{13} over the past five years. But, its accuracy is certainly less than 10 parts in 10^{13}.

All of these, I think, and the lessons that we learned in cesium-3, I think we have taken into account, and we can be wrong in our evaluation of the cesium-5, but they have been essentially the figures we give, the results of the past three years of measurements. So, we will have to see.

DR. REINHARDT:

Victor Reinhardt, Goddard Space Flight Center.

You mentioned that an accuracy of a couple of parts in 10^{14} was due to an uncertainty in the G factor?

DR. COSTAIN:

Yes.

DR. REINHARDT:

Did you convert from Zeeman frequency to magnetic field units and then convert again?

DR. COSTAIN:

We have done both in measuring the low frequency resonance, the delta f displacement of the high frequency transitions and with the present current that we can put on the C-field, the present values, the experimental determination is about the same accuracy as the previously published

values of the G factor.

We think we can improve that measurement by an order of magnitude.

DR. REINHARDT:

My question is, did you take into account the cancellation that occurs in the equations if you use direct Zeeman frequency.

MR. COSTAIN:

Yes. That comes out essentially to the same limitation, 4 parts in 10^{14}.

DR. HELLWIG:

I would like to comment on unknown errors, two subparts. Part A is what you said, we don't know them. Though I claim that you have a hunch at getting a numerical value on those and the hunch is if you compare devices of different design, accuracy claims without the unknown errors, or sort of discounting the unknown errors, and that is exactly what I tried to state. That is the disagreement between the primary standards of the world. They are of different design. They disagree by many parts in 10^{13} now, so that is a good estimate of the unknown errors.

Part B of the unknown errors are the errors where we don't know how to measure them, but we know they exist. Just to quote one and that is what I call the distributive cavity phase shift which is a trajectory-dependent frequency shift, especially, in beam tubes featuring large beams of high intensity. Our best theoretical estimate at that for beam tubes of your and our design is about 1 to 1.5 in 10^{13}. This best estimate is based on optimistic assumptions about conductivity of the cavity walls, symetry of cavity design and so on.

We put this unknown error into our error budget. I would like to add we don't know yet, really, how to measure that but we have to account for it.

THE MILLMAN EFFECT IN CESIUM BEAM ATOMIC FREQUENCY STANDARDS

A.G. Mungall
National Research Council, Ottawa, Canada

ABSTRACT

A systematic frequency shift which reverses sign with either C field or beam reversal and which can be interpreted as the consequence of the Millman effect has been found in the new NRC cesium beam clock, CsV. A method of calculating the resonance asymmetry resulting from this effect and the dependence on the velocity distribution and exciting microwave power level of the frequency shift caused by it is described. Application of this theory to CsV leads to reasonable agreement with experimental results. Possible origins for the Millman effect in cesium beam standards are discussed, and it is concluded that the most likely source is a very small variation in the direction of the C field over normal beam trajectories within the microwave interaction regions.

I. INTRODUCTION

Cesium beam frequency standards, first developed in the mid-1950's, have undergone continuous improvement in accuracy[1] from an initial value of the order of 10^{-9} to current values approaching 10^{-13}. One of the results of such improvements in performance is that certain systematic errors which were at one time of minor consequence have now become of such importance that they can constitute the primary factors limiting the stability or the accuracy of the standard.

During the 20-year development period of these standards, the limiting instabilities and inaccuracies were to a large extent related to factors such as magnetic field inhomogeneities, crystal oscillator instability, indeterminate cavity phase differences, unknown atomic beam velocity distributions, and spectral impurities in the microwave excitation signal. Within the past five years, several methods have been described which provide estimates of the actual velocity distributions existing in practical cesium standards, and these have led to much improved understanding and measurement of the power dependent frequency shifts arising from the cavity phase difference and the second order Doppler effect. Advances in crystal oscillator design have also led to the essential elimination of the more or less unpredictable power-dependent frequency shifts due to spectral impurities.

However, as in other areas of high precision measurements, the

PRECEDING PAGE BLANK-NOT FILMED

consecutive removal of each limiting source of systematic error has tended to expose more clearly further underlying sources, and recent work on CsV at NRC has proven no exception to this rule. A previous paper[2] on CsV outlined a number of sources of error, and at that time (1973) the limiting factor was spectral impurities in the exciting microwave signal which caused unpredictable time-dependent frequency shifts which varied with the power level. Extensive redesign and reconstruction of the electronics systems led to the final apparent elimination of these difficulties, and also to the measurement of another important frequency shift. This shift, which reverses sign with C field or beam reversal, can be interpreted as the consequence of the Millman effect, whose presence in CsV had not been previously detected. Resolution of this problem was accomplished during April, 1975, and since May 1, 1975, CsV has operated satisfactorily as a clock.

This paper will discuss the experimental determination of the Millman effect in CsV, propose a possible explanation for its origin in this standard, and also outline a general method of calculating its dependence on transition excitation level, beam velocity distribution, and servo-system modulation offset frequency.

II. THEORY

A. Theory of the Millman Effect

As outlined by Ramsey[3], and first described by Millman[4], the Millman effect is an alteration in the frequency experienced by an atom in an oscillating exciting field resulting from a change in direction of that field relative to a d.c. orienting magnetic field during its passage through the excitation region. It is in effect a spatially-induced frequency increment to the impressed oscillating field. Although this effect was originally considered to act only when the oscillating and orienting fields are perpendicular (π transitions). Hahn[7] has shown that a similar effect also occurs when they are parallel (σ transitions) if a spatial rotation of the orienting field occurs along the direction of the beam. Since cesium beam atomic frequency standards are based on the σ transition, $(F = 4, m_F = 0) \leftrightarrow (F = 3, m_F = 0)$, this effect is of importance in such standards. As pointed out by Hahn, it is dependent on the directions of both the orienting field and the beam. It is thus experimentally separable from the cavity phase difference frequency shift since the latter is dependent only on the beam direction and not on the direction of the orienting field.

The magnitude of the Millman effect, expressed as an incremental angular frequency $\delta\omega_m$, is related to the change in angle between

the directing and oscillating fields, γ, during the passage of an atom travelling at a velocity v through an interaction region of length ℓ by

$$\delta\omega_m = \frac{\gamma v}{\ell} \qquad (1)$$

B. Calculation of the Frequency Shift Averaged Over a Distribution of Atomic Velocities.

The dependence of $\delta\omega_m$ on v indicates that in the general case for which a range of atomic velocities occurs the Millman effect not only causes a frequency shift but also gives rise to a resonance asymmetry, with consequent dependence of the measured transition frequency on exciting power level, velocity distribution, and servo-system modulation frequency offset. The form of its dependence can be expected to be quite different from either that arising from the second order Doppler effect, which varies as $v^2/2c^2$, or that for the cavity phase difference, which causes only a phase change between the two oscillating fields. Since in practical cesium standards the atomic beam includes atoms having a range of velocities comprising an appreciable fraction of the Maxwellian distribution, some method of integrating equation 1 over such a fraction is essential in the explanation of the measured frequency shifts.

A method first employed at NRC for calculating the frequency shift arising from the second order Doppler effect[5] and later for that due to a cavity phase difference[6], can also be employed in the present case. It involves the assumption that the distribution function of the velocities of the atoms contributing to the resonance can be satisfactorily approximated by a truncated Maxwellian distribution, with lower and upper velocity cut-offs determined by the physical constants of the standard in question. In accordance with the terminology used previously, an atomic velocity v_i is related to the most probable velocity in the cesium oven, α, by

$$p_i = v_i/\alpha \qquad (2)$$

and the maximum and minimum velocities by

$$p_{max} = v_{max}/\alpha \quad \text{and} \quad p_{min} = v_{min}/\alpha \qquad (3)$$

The transition probability P_i for a velocity defined by p_i is then calculated from Ramsey's general expression[3], with ω replaced by $\omega-\delta\omega_m$. In such a substitution, the value of γ, effectively a phase increment in each of the two oscillating fields, may be considered to a first approximation as $\frac{1}{2}\cdot(L/\ell)\cdot\ell\delta\omega_m/v$, by analogy with Ramsey's result that if $\Delta\omega$ is the difference between the resonant frequency in the oscillatory and drift regions, the observed resonance is shifted by only $(\ell/L)\cdot\Delta\omega$.

$$P_i = 4 \sin^2\theta \sin^2 \frac{a\ell}{2p_i\alpha} \cos\left[\frac{(\omega_o - \omega + \delta\omega_m)L}{2p_i\alpha} \cos \frac{a\ell}{2p_i\alpha}\right.$$

$$\left. - \cos\theta \sin \frac{(\omega_o - \omega + \delta\omega_m)}{2p_i\alpha} \sin \frac{a\ell}{2p_i\alpha}\right]^2 \qquad (4)$$

where $\sin\theta = -2b/a$, $\cos\theta = (\omega_o - \omega + \delta\omega_m)/a$,

and $$a = \left[(\omega_o - \omega + \delta\omega_m)^2 + (2b)^2\right]^{\frac{1}{2}} \qquad (5)$$

A weighted total transition probability P_t, defined by the upper and lower velocity limits, is then given by

$$P_t = \frac{\Sigma_i P_i w_i}{\Sigma_i w_i} \qquad (6)$$

where the weights w_i are given by the truncated Maxwellian velocity distribution

$$w_i = p_i^3 \exp(1 - p_i^2) \text{ for } p_{min} \leq p_i \leq p_{max} \qquad (7)$$

and $$w_i = 0 \text{ for } p_i < p_{min} \text{ and } p_i > p_{max} \qquad (8)$$

The value of α is known from the operating temperature of the cesium oven, and the value of b is determined from an approximate knowledge of the velocity limits and the dependence of the calculated and experimental maximum transition probabilities on exciting power level. The exact values of p_{min} and p_{max}, and hence the velocity distribution, are determined by curve fitting of calculated and experimental Ramsey resonance patterns. In practice, it is evident that sharp velocity cutoffs do not in fact occur, but their equivalent values can be estimated by this curve-fitting procedure to a precision of about $\pm$ 0.05 α.

The magnitude of the Millman effect frequency shift is then calculated by computer simulation of the response to the square wave frequency modulation applied to the atomic resonance by the clock servo system. Because of the resonance asymmetry the shift must be calculated for a range of frequency offsets. A transition probability P_{t1} is first calculated for an input frequency offset Δf_1 below the resonant frequency, and then the corresponding value Δf_2 for an equal

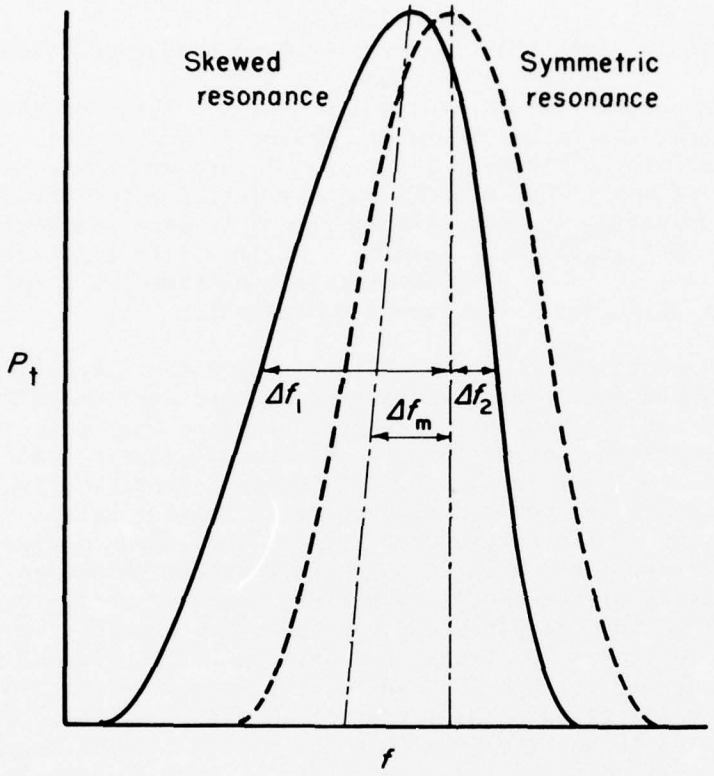


Figure 1. Calculation of the Millman effect frequency shift by computer simulation of servo-system interrogation of an asymmetric, frequency shifted resonance curve.

total transition probability P_{t2} above the resonant frequency is determined. As shown in figure 1, the Millman frequency shift Δf_m is then given by

$$\Delta f_m = \frac{\Delta f_2 - \Delta f_1}{2} \tag{9}$$

Inherent in this method is the assumption that the values of P_{t1} and P_{t2} are not affected by the rate of frequency switching between the upper and lower offset frequencies. In practice, no significant measurable change in the frequency of CsV occurs for switching

frequencies in the range 0.08 Hz to 1.0 Hz. The normal switching frequency used is 0.08 Hz.

C. Origin of the Millman Effect in Cesium Beam Frequency Standards

It is apparent from the foregoing analysis that for parameters typical of present long beam laboratory cesium standards such as CsV, e.g., a beam velocity of about 3×10^4 cm s^{-1}, and drift and interaction lengths of about 200 cm and 1 cm, a relative rotation of the angle between orienting and oscillating fields in each interaction region of only 10^{-4} radian will lead to a Millman effect frequency shift of about 4×10^{-13} or 0.004 Hz. This constitutes a surprisingly large frequency shift for a very small perturbation.

The origin of such a perturbation is open to some question, since present mechanical construction techniques do not provide precisions of this order. However, it should be noted that γ is actually a change in orientation rather than an absolute alignment error. Several possible explanations can be considered. Historically, the Millman effect was first noticed when current-carrying hairpins, curved upward at each end of the interaction region, were used to provide a vertical oscillating field perpendicular to the beam direction. The change in direction of the oscillating field magnetic vector over the curved sections of the hairpin was found to be the source of the effect. It is possible to propose a similar explanation in the present case, since an atom passing through the ends of the waveguide resonant cavity traverses regions of fringing electromagnetic fields which in general are not parallel with the fields within the cavity. These regions are, however, very short, and the field intensity in them is very low. In CsV, sections of K-band waveguide 2.5 cm in length cover the beam entrance and exit slots in the cavity, and effectively prevent radiation of microwave energy from the cavity. In these sections, the magnetic field vector is rotated through 90° compared with that in the cavity, and the attenuation of the microwave signal is such that the amplitude drops to about 1/3 in a distance of 5 mm. In addition, the efficiency of mode conversion from one waveguide to the other, and the radiation efficiency of the slot are both extremely low. The atomic transition probability for fields in these K-band sections would therefore be expected to be very small. If it is assumed, however, that a 90° angular change in the oscillating field does occur over a distance of 5 mm at both entrance and exit to the cavity, then the corresponding Millman effect is about 5 kHz. It is conceivable that a few atoms do in fact undergo such transitions, but it is apparent that such an explanation for the observed Millman effect, described later in this paper as about 0.002 Hz, cannot be valid.

Another possible explanation concerns misalignment of the wave-

guide in such a way that the oscillating magnetic field is not parallel with the orienting field. Such misalignment could produce the π transitions mentioned in the earlier paper[2], but not a Millman effect which depends on a relative spatial rotation between oscillating and orienting fields in the beam direction.

A much more likely but unproven explanation can be based on the following reasoning. First, because of the beam optics design of CsV, which employs lateral deflection of a ribbon cross-section atomic beam by state selector magnets and passage of this beam through a central slit located on the oven-detector axis, the atomic trajectories through the waveguide interaction regions do not remain parallel with the longitudinal axis. Second, the orienting C field, produced by a four-rod current carrying structure enclosed by an open-ended cylindrical magnetic shield pierced by slots to permit entry of the waveguide cavity, is subject to small changes in direction with distance from the axis. The combination of these two physical circumstances leads to a slow relative rotation of the orienting C field with respect to the oscillating field experienced by the atom in its passage through the cavity. Furthermore, the level of microwave excitation within the cavity is usually one which approximates that for maximum transition probability. Consequently, both the necessary criteria for a Millman effect of the required order of magnitude are present. The experimental and semiquantitative aspects of such an explanation will be examined in detail in the following section.

III. EXPERIMENTAL

In the first preliminary evaluation of CsV, a search was made for the Millman effect, but none was found within the uncertainty of the measurements. This uncertainty was dictated by two factors: instabilities in the hydrogen masers used as reference standards, and instabilities in CsV arising most probably from time-dependent changes in the spectral purity of the exciting microwave signal. Subsequent to these preliminary tests, automatic tuning devices were built for the hydrogen masers, and extensive alterations were made to the electronics systems of CsV. In addition, a small change in the alignment of CsV was made when both cesium ovens were refilled at the end of 1974, in preparation for long-term operation of the device as a primary clock. As a consequence of this change of alignment, the Ramsey resonance patterns for the two beam directions are now approximately the same, as indicated in figure 2. If the second explanation proposed earlier is in fact valid, such a change in alignment would be expected to change the Millman effect, and in the experiments to be described later, a Millman effect was found. The more precise determination of this effect was facilitated by the significant improvements in frequency stability produced both in the masers and CsV. The relative stability

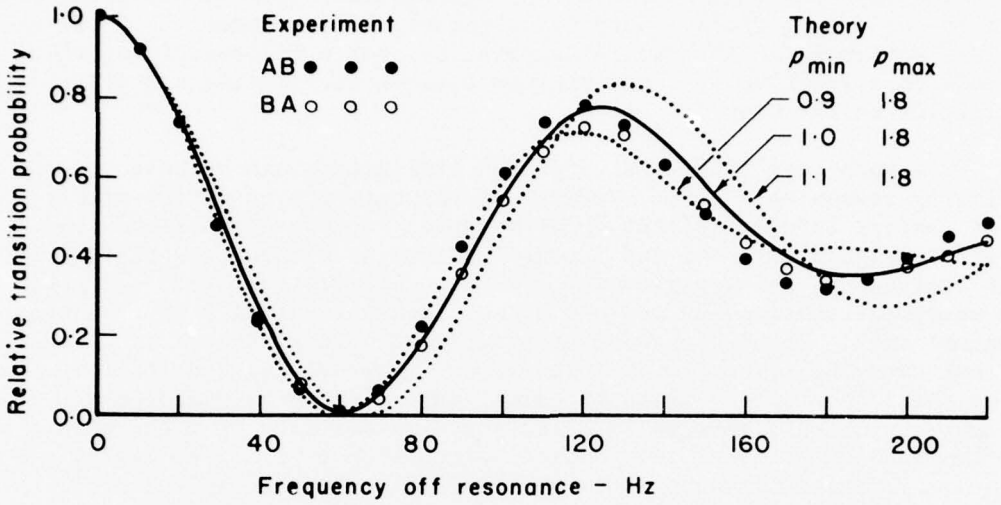


Figure 2. Normalized Ramsey resonance curves calculated from the theory for p_{max} = 1.8 and p_{min} = 0.9, 1.0, and 1.1 compared with experimental results for beam directions AB and BA.

of the two masers was about 2×10^{-14} over periods of several hundred seconds to several days, and it was therefore possible to attain measurement uncertainties for systematic errors in CsV of between 1 and 2×10^{-14} for measurement periods in excess of about 30 minutes and up to several days.

As mentioned earlier, the Millman effect frequency shift is separable from that due to a cavity phase difference, since the latter depends only on beam direction whereas the former depends on both beam and C field direction. In order to measure the Millman effect frequency shift, measurements were made of the frequency of CsV relative to one of the hydrogen masers at several different power levels for both directions of the beam and the C field. A total of 4 beam and 12 C field reversals was made during April, 1975, and one beam reversal and 12 C field reversals during September, 1975. Some maser frequency drift, corroborated by simultaneous maser-maser frequency comparisons, occurred, and this was taken into account in the calculations of the frequency shifts. In addition, a small and decreasing drop in the C field correction, corresponding to several parts in 10^{15} in the cesium frequency, was observed following each C field reversal. At the conclusion of the measurements the C field correction, calculated from

the mean of six low frequency, (4, -4) ↔ (4, -3) resonances, showed no change within two parts in 10^{15} on reversion to the normal C field direction.

Although measurement of the cavity phase difference frequency shift and the second order Doppler shift are not necessary in the determination of the Millman effect frequency shift, since the latter can be measured solely by C field reversal, beam reversal can cause alterations in both the other shifts. It is therefore useful in discussing the various inter-relationships between these quantities to describe them algebraically as follows. If the fractional frequency values of the shifts arising from the Millman effect, the cavity phase difference, the C field, and the second order Doppler effect are given by δf_m, δf_c, δf_h, and δf_d, the beam directions by subscripts AB and BA, the C field directions by N and R, referring to normal and reversed, then the difference between the normalized frequency of CsV, f_{CsV} and that of the maser reference, f_M, is given as follows, with the various K values accounting for maser drift and the numerical constants associated with the electronic frequency multiplication and synthesis techniques employed:

$$\delta f_m + \delta f_c + \delta f_{h\ AB,N} + \delta f_d = f_{CsV\ AB,N} - f_M + K_1 \tag{10a}$$

$$-\delta f_m - \delta f_c + \delta f_{h\ BA,N} + \delta f_d = f_{CsV\ BA,N} - f_M + K_2 \tag{10b}$$

$$-\delta f_m + \delta f_c + \delta f_{h\ AB,R} + \delta f_d = f_{CsV\ AB,R} - f_M + K_3 \tag{10c}$$

$$\delta f_m - \delta f_c + \delta f_{h\ BA,R} + \delta f_d = f_{CsV\ BA,R} + f_M + K_4 \tag{10d}$$

In these equations, δf_c and δf_m are arbitrarily chosen as those referring to the AB beam direction and normal, N, C field direction. In addition, since the Ramsey resonance patterns for the two beam directions are so nearly identical, both δf_c and δf_m are assumed only to change sign with beam reversal, and δf_d is assumed to be the same for both beam directions.

Reference to equations 10a - 10d shows that it is indeed possible to determine δf_m simply by C field reversal alone, the beam direction being maintained constant. In the April, 1975, re-evaluation of systematic errors, measurements were made corresponding to the equation pairs 10a and 10c, and 10b and 10d, for two different power levels, one corresponding to that for maximum transition probability, P_O, and the other at P_O - 3 dB. The results are shown in Table I.

Table I. The Millman effect frequency shift expressed in parts in 10^{13} for two different exciting power levels and both beam directions.

Power Level	Beam Direction	
	AB	BA
P_o	2.1	1.9
P_o - 3 dB	1.9	2.1

Within the precision of measurement, which is of the order of 1×10^{-14}, no significant power dependence nor dependence on beam direction is apparent, and the mean value is 2.0×10^{-13}. For the September re-evaluation, carried out only at P_o - 3 dB, the mean frequency shift was also 2.0×10^{-13}.

IV. DISCUSSION

The observed Millman effect frequency shift must now be explained in terms of imperfections in the mechanical construction of CsV.

The magnitude of this effect indicates that the required relative angular rotation between orienting and oscillating fields is extremely small, of the order of a few tens of microradians. Such a rotation could conceivably be produced in the vicinity of the waveguide interaction regions by a number of factors, all dependent on the C field generated by the four current-carrying rods, and hence all dependent on the direction of current flow through these rods. Such factors could constitute perturbations arising from the open ends of the cylindrical magnetic shields, those from the current carrying leads feeding the four-rod structure, those due to the slots cut through the shields to permit entry of the waveguide cavity, and also variations in permeability of the shields along the longitudinal seams or at the spot welds. All these factors would in general give rise to a three dimensional curvature of the C field which would be similar at both the waveguide interaction regions. It is known also that the C field, averaged over 30-cm lengths between the two excitation regions and measured by means of the (4, -4) $\leftrightarrow$ (4, -3) resonances, exhibits variations of about $\pm$ 0.06%.

However, despite the existence of these unknown but quite possibly significant sources of C field curvature, it is of interest to estimate the degree of curvature to be expected in the magnetic field

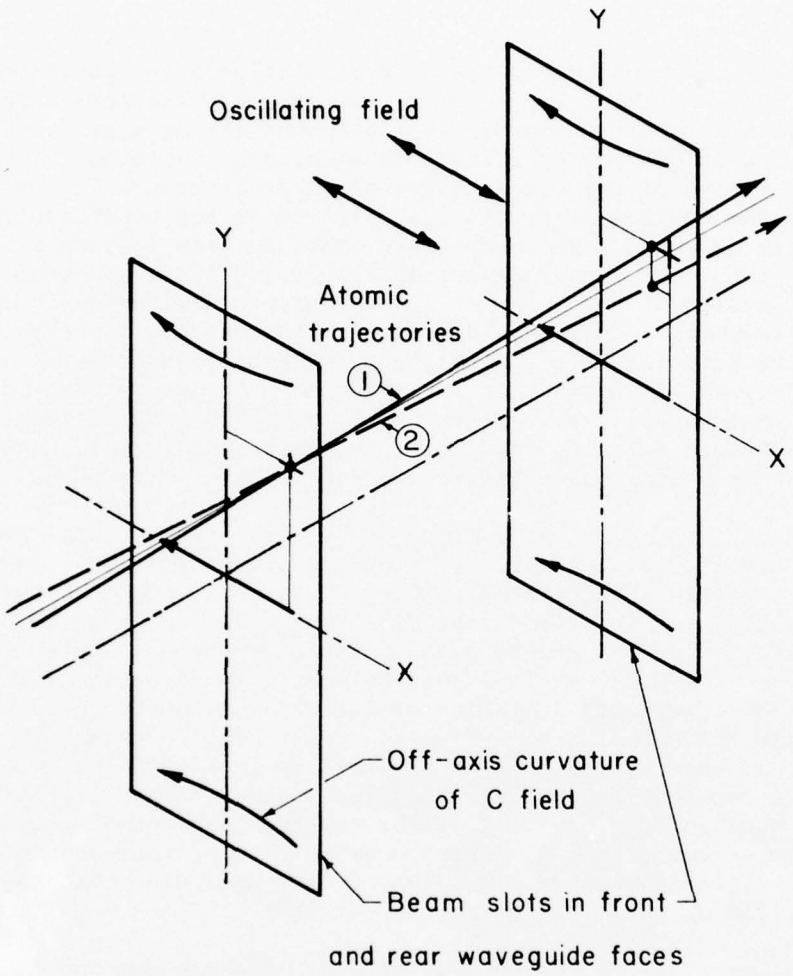


Figure 3. Atomic trajectories through the microwave interaction region for which the angle between orienting and oscillating fields undergoes a continuous change.

produced by the four-rod structure used in CsV. It should be borne in mind, though, that this could be outweighed by that resulting from the uncalculable sources mentioned above, and consequently, little more than an order of magnitude calculation is truly significant. With this proviso, this source of curvature will now be examined in detail. The requirement is that a gradual change in the angle between oscillating and orienting fields occur as the atom progresses through each inter-

action region.

Figure 3 shows two possible atomic trajectories which could result in such a change. One case characterizes trajectories for which the atom maintains its y coordinate throughout its passage from oven to detector, and only the x coordinate changes, e.g., an atom which leaves the upper section of the oven collimator, passes through the upper section of the central slit, and is collected on the upper section of the hot wire detector. The other case characterizes trajectories for which both the x and y coordinates change, e.g., an atom which leaves the upper section of the oven collimator and drops linearly in its passage through the central slit and is collected on a lower portion of the hot wire detector. In general, both types of trajectories occur, and in addition, all trajectories will be more or less parabolic, depending on the atomic velocities, as a result of gravitational acceleration. The general case is, therefore, quite complicated, and consequently only a semi-quantitative analysis will be attempted.

In CsV, the C field is produced by a four-rod current-carrying structure symmetrically located within three concentric molybdenum permalloy magnetic shields of diameters 20.3, 25.4, and 30.5 cm. The x and y spacings of these rods are 8.045 and 13.969 cm respectively, with the x coordinate indicating the C field direction. These spacings were chosen by computer analysis of the near-axis magnetic field with the criterion of minimal deviation of the total magnetic field at any point within the normal beam deflection cross section from that existing on axis. The calculations were initially performed for free-space location of the four current carrying rods, and a later check with allowance made for the presence of the innermost magnetic shield, but not for the effect either of finite permeability of this shield nor for the effect of the waveguide slots through it, indicated that the magnetic field uniformity was improved by it.

Calculations were also made of the angle between the total magnetic field and the x-axis, for free-space location of the four rods, and these results are shown in Table II. Examination of this table shows that this angle varies from zero on the x and y axes to a maximum of about 9 microradians over a cross section limited by $0<|x|<2$ mm, $0<|y|<5$ mm which corresponds approximately to the area of the slot cut into the waveguide cavity to allow passage of the cesium beam. Because of the wide variation of this angle, as indicated in the table, and the actual atomic beam, any explanation based on this table can only be qualitative.

Since each cavity is about 1 cm wide in the beam direction, and is located about 106 cm from the central slit, atoms traversing the cavity must undergo a change in their x coordinate of about 1% during their passage from one waveguide face to the other. Because of the

Table II. Angle between total C field and x-axis, microradians

y-mm	x-mm										
	0.0	0.2	0.4	0.6	0.8	1.0	1.2	1.4	1.6	1.8	2.0
0.0	0.00	0.00	0.00	0.00	0.00	0.00	0.00	0.00	0.00	0.00	0.00
0.5	0.00	0.11	0.22	0.34	0.47	0.60	0.74	0.90	1.08	1.27	1.48
1.0	0.00	0.21	0.42	0.64	0.88	1.13	1.40	1.71	2.04	2.41	2.82
1.5	0.00	0.28	0.56	0.86	1.17	1.52	1.89	2.31	2.78	3.30	3.88
2.0	0.00	0.30	0.61	0.94	1.30	1.69	2.13	2.62	3.18	3.81	4.52
2.5	0.00	0.27	0.55	0.86	1.20	1.58	2.02	2.53	3.12	3.80	4.59
3.0	0.00	0.17	0.35	0.56	0.81	1.12	1.49	1.95	2.50	3.16	3.95
3.5	0.00	-0.02	-0.02	0.01	0.08	0.23	0.45	0.76	1.19	1.75	2.45
4.0	0.00	-0.31	-0.60	-0.85	-1.04	-1.17	-1.20	-1.12	-0.91	-0.56	-0.04
4.5	0.00	-0.71	-1.40	-2.04	-2.63	-3.13	-3.53	-3.81	-3.93	-3.90	-3.68
5.0	0.00	-1.24	-2.46	-3.63	-4.73	-5.74	-6.64	-7.40	-7.99	-8.40	-8.60

presence of 1 mm diameter stop wires at the innermost ends of both state selector magnets, the inverse variation with velocity of the deflection of the atoms from the axis, and the ribbon cross-section of the beam, most of the atoms will be in the region defined by 1.0 mm $<|x|<2.0$ mm and $|y|<3.5$ mm. Except for atoms near the x axis, it is apparent that changes of only a few hundredths of a microradian occur for atoms following most of the possible trajectories, including those for which the y coordinate changes as well. For example, an atom which enters the excitation region at x = 1.600 mm, y = 2.000 mm, and leaves at x = 1.584 mm, y = 2.000 mm, experiences a change in angle between oscillating and orienting fields of about 0.05 microradian. For atoms closer to the y axis, the change is smaller, and for those farther away from the y axis, it is greater. However, it is clear that in the case of the four rods located in free space, the angular changes to be expected for typical atomic trajectories are about 3 orders of magnitude too small to explain the observed Millman frequency shift.

As mentioned earlier, however, the presence of the magnetic shields, and particularly the field leakage through both the waveguide slots and the open ends of the shields, can be expected to alter to some degree the magnetic field produced by the four rods. In addition, the experimental observation that the C field varies by ± 0.06% from one 30 cm length to another between the interaction regions indicates most probably that there are significant variations in the effective permeability of the innermost shield. Apparently, all these perturbations combine to produce inhomogeneities and curvature of the C field at the cavity beam slots such as to give rise to the Millman effect measured.

Table III. Millman effect frequency shift, mHz, for lower and upper velocity limits of 1.0α and 1.8α, characteristic of normal operation of CsV.

Exciting Power, α/ℓ	Frequency Offset, Hz									
	5	10	15	20	25	30	35	40	45	50
0.2	1.92	1.88	1.91	1.92	1.96	1.92	1.96	1.98	2.02	2.08
0.4	1.75	1.77	1.77	1.77	1.79	1.79	1.82	1.85	1.90	1.99
0.6	1.78	1.82	1.75	1.82	1.80	1.82	1.83	1.87	1.91	2.01
0.8	1.75	1.81	1.78	1.82	1.80	1.82	1.86	1.89	1.94	2.03
1.0	1.81	1.94	1.84	1.87	1.88	1.89	1.90	1.93	1.98	2.05
1.2	1.92	1.88	1.91	1.92	1.96	1.92	1.96	1.98	2.02	2.08

Despite this somewhat unsatisfactory explanation of the origin of this effect, it is of interest to calculate from the theory presented earlier a mean value of γ required to account for the measured Millman effect frequency shift of 2.0×10^{-13}, or about 0.0018 Hz in the cesium transition frequency. The physical significance of such a mean value of γ is, however, open to question. Table III shows results of calculations based on this theory for a value of γ of 45.3 microradians, which was chosen so as to provide agreement with experimental observations for the normal operating point of CsV, characterized by a servo frequency offset of about 35 Hz and a value of α/ℓ of 0.8. This table shows that only a small power dependence should be expected, the Millman effect frequency shift changing by less than 0.0001 Hz between values of α/ℓ of 0.8 and 1.0, which correspond to power levels of P_o - 3 dB and P_o. A similar power dependence was in fact measured, indicating that the concept of a mean value of γ may actually have physical significance.

This apparent lack of dependence on either exciting power level or offset frequency for CsV in its normal mode of operation should not, however, be construed as indicating that in a more general case with a wider velocity distribution no such dependence exists. Table IV shows values of the Millman effect frequency shift calculated for the same physical constants characteristic of CsV, but with a wider velocity distribution having upper and lower velocity limits of 2.4 and 0.4 α. Such a distribution could be obtained in CsV by use of state selector magnets having smaller magnetic field gradients and by eliminating the stop wires. The entries in this table vary by a factor greater than 2. Consequently, the use of wide velocity distributions and somewhat less uniform C fields could, in standards such as CsV, lead to very significant power and frequency offset dependence of the Millman effect frequency shift. These two velocity distributions are shown in figure 4.

PRECEDING PAGE BLANK-NOT FILMED

Table IV. Millman effect frequency shift, mHz, for lower and upper velocity limits of 0.4α and 2.4α, which could result from operation of CsV without stop wires and with weaker state selector magnets.

Exciting Power, α/ℓ	Frequency Offset, Hz						
	5	10	15	20	25	30	35
0.2	1.04	1.09	1.15	1.27	1.50	2.03	3.89
0.4	1.11	1.18	1.24	1.34	1.50	1.79	2.34
0.6	1.41	1.37	1.38	1.46	1.56	1.66	1.90
0.8	1.52	1.56	1.54	1.66	1.66	1.75	1.85
1.0	1.57	1.61	1.65	1.76	1.87	1.96	2.04
1.2	1.64	1.66	1.74	1.82	1.99	2.06	2.22

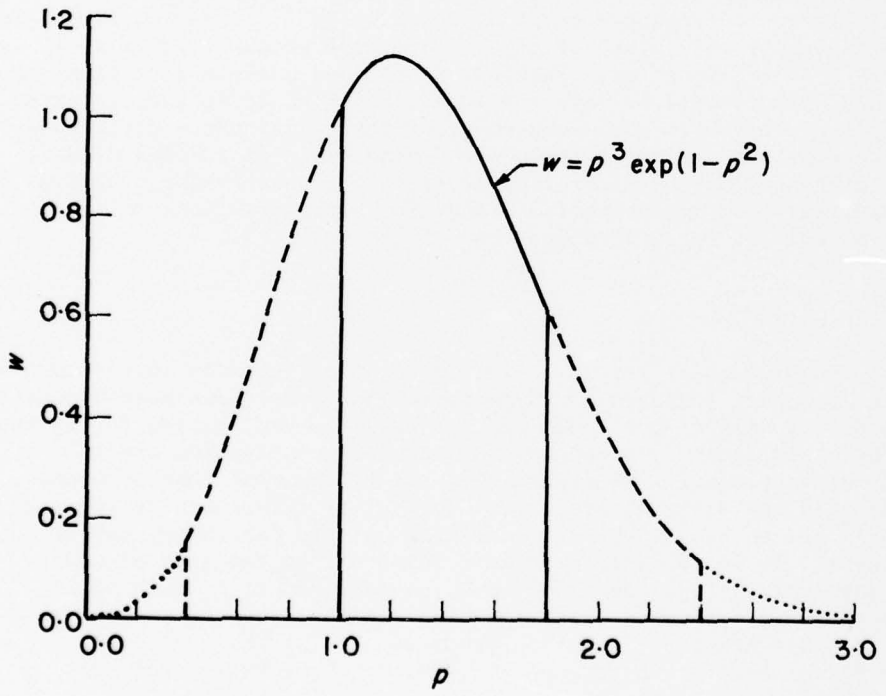


Figure 4. Truncated Maxwellian velocity distributions of atoms in the beam, $w = p^3 \exp(1 - p^2)$, for normal operation of CsV with $p_{min} = 1.0$ and $p_{max} = 1.8$, and for wider velocity limits with $p_{min} = 0.4$ and $p_{max} = 2.4$.

For commercial cesium standards with wide velocity distributions, greater resonance line widths, and probably greater C field non-uniformities, it is likely that the Millman effect could cause significantly large systematic errors. These could also be time-dependent as the result of changes in the magnetization of the magnetic shields.

It was pointed out earlier that reversal of the C field constituted the only means of separating the Millman and cavity phase difference frequency shifts. Reference to equations 10a - d shows that it is possible for these two effects to partially cancel each other, depending on the C field and beam directions employed. If only the beam direction is reversed in the evaluation of systematic errors, with the consequence that δf_m and δf_c are not resolved independently, then it is evident that quite an erroneous estimate of the cavity phase difference frequency shift and its power dependence could be made. Errors in such an estimate would be expected to increase with increasing resonance line width, and hence to be of particular importance in standards, with short interaction lengths. Even for long beam standards, a cavity phase difference frequency shift approaching 10^{-12} is not unreasonable. For example, if the values of δf_c and δf_m were actually 1.0×10^{-12} and 0.9×10^{-12}, then for a particular beam and C field direction, the combined effect would be only 1×10^{-13}, which would lead to an order of magnitude error in the measurement of the cavity phase difference, with concomitant errors in the power dependence. It is thus evident that in the evaluation of systematic errors in cesium beam standards it is essential that measurements be made for both directions of the C field as well as for both directions of the beam.

V. CONCLUSIONS

The Millman effect as a limiting systematic error in cesium beam atomic frequency standards, and specifically in CsV, has been discussed and means of measuring it outlined. A possible explanation for it has been proposed, and calculations based on this explanation are in reasonable agreement with experiment. It is apparent that an understanding of the Millman effect is important if accuracies of the order of 10^{-13} are to be attained in long-beam primary laboratory cesium standards. It is probably even more important in the case of short-beam commercial standards which would be expected to be much more susceptible to frequency shifts arising from this effect. It is in fact possible that the frequency jumps and drifts which have been observed in these standards may be related to the Millman effect.

ACKNOWLEDGEMENTS

The author is indebted to C.C. Costain, D. Morris, and H. Daams for many helpful comments and useful discussions.

REFERENCES

1. Hellwig, H.W.: Proc. IEEE 63, 212 (1975.

2. Mungall, A.G., Bailey, R., Daams, H., Morris, D., Costain, C.C.: Metrologia 9, 113 (1973).

3. Ramsey, N.F.: Molecular Beams, 128, 139, 155, Oxford University Press (1956).

4. Millman, S.: Phys. Rev. 55, 628 (1939).

5. Mungall, A.G.: Metrologia 7, 49 (1971).

6. Mungall, A.G.: Metrologia 8, 28 (1972).

7. Hahn, S.L.: Bulletin de l'Academie Polonaise des Sciences 23, 249 (1975).

QUESTION AND ANSWER PERIOD

DR. HELLWIG:

A comment on the Millman effect. First, I do not doubt that the measurement, of course, is as precise as Dr. Costain reported. We have sort of looked into the Millman effect at NBS and came to the conclusion without going into much theoretical detail now, that it cannot be the Millman effect which explains your measurements because the Millman effect--

DR. COSTAIN:

Would you repeat that?

DR. HELLWIG:

That the Millman effect is not the right vehicle to explain your measurements because the Millman effect should not be of any significant magnitude for magnetic field independent transitions delta MF = 0 transitions. The basic physical reason for that is that the orientation of the dipole moment of the flying atoms is random with regard to being perpendicular to the orienting magnetic field.

DR. COSTAIN:

There is some disagreement on this factor, I know, and I think we continue to disagree. I think it is the Millman effect we are seeing. One of our difficulties is that our correspondence has been rather limited in the past eight weeks. We have not yet had an opinion from Dr. Hahn.

DR. HELLWIG:

I know that Dr. Hahn's paper is the theoretical foundation to that, so I have to add to that that we disagree with Dr. Hahn's paper.

MR. ALLAN:

One comment that may affect many users of commercial cesium that I would like to make. We have found and, of course, HP now has in the high performance tube, the ability to degauss the unit. When you do change the C field in a standard there is a residual which takes time to accommodate domain changes in the surrounding shielding and this some-

times can be a problem when measuring the reversal of the C field, it seems that would be an entry, at least in long term stability.

I don't know whether you have encountered that or not.

DR. COSTAIN:

Yes, it is.

A NEW METHOD FOR GENERATING OVERTONE FREQUENCIES IN A QUARTZ OSCILLATING CIRCUIT

Harish Bahadur & R.Parshad

National Physical Laboratory
New Delhi-110012
(INDIA)

ABSTRACT

Quartz crystals have been operated in overtones for obtaining standard frequencies. Excitation in overtones enables the inductance of the equivalent series circuit of the crystal to be made high enough (inductance value increasing as the cube of the overtone number) for obtaining a high degree of frequency stability and, also, the resistive impedance of the crystal at resonance becomes high enough in overtone excitation for proper operation in the oscillator circuit.

Along with the advantage of high stability, excitation of quartz in overtones can have another great advantage of being able to generate a high enough frequency at the out set to reduce the frequency multiplier chain linking the quartz crystal frequency with the atomic frequency in atomic frequency standards.

This paper describes a simple and effective technique for generating overtone frequencies of almost any required overtone number with ease and reliability. The method consists in coupling a parallel L-C circuit to the quartz in the oscillator network. As L-C is tuned in the proximity of the overtone frequency, the quartz crystal takes control to generate the overtone frequency. Thus, overtone frequencies in the neighbourhood of 60 and 100 MHz using different crystals could be easily obtained in the first single stage of a multiplier chain.

PRECEDING PAGE BLANK-NOT FILMED

An interesting effect noticed was the splitting of an overtone frequency in two values, the higher value being obtained when the resonance frequency of the L-C was varied from the higher to the lower values. The lower overtone frequency was obtained when the variation of the L-C resonant frequency was in the opposite direction. The frequency splitting probably arises as a result of the coupling of the two resonators, the L-C and the quartz. This explanation is supported by the fact that the splitting between the overtone doublet decreased as the coupling between the L-C and the quartz was decreased. Starting with any of the overtone doublet in each case only the lower frequency is obtained after the interruption of voltage supply and, hence, for repeatibility, is the one to be used in practical application in the frequency multiplier chain.

INTRODUCTION

Quartz crystals are essential electronic components for generating standard frequencies. Earlier to the development of atomic frequency standards, the quartz crystal itself in an oscillator circuit served as the standard of frequency, the ageing of the crystal being allowed for by resetting the crystal frequency through astronomical observations. Presently, the quartz crystals serve as slave oscillators in atomic frequency standards. In both the cases it is essential that the frequency stability of the quartz crystal be the highest.

Warner (1-3) at Bell Telephone Laboratories has developed design of quartz crystals for obtaining very high Q ($\approx 5 \times 10^6$). The improvement obtained in the Q's is an order of magnitude higher than that obtained earlier. At about the same time appreciable progress has been made to reduce the ageing rate of the crystals. Thus, the frequency stability of the quartz crystals has been pushed up from 1×10^{-8} to 1×10^{-10}. Due to this fact, the quartz crystals not only become better slave oscillators for the atomic frequency standards but also tend to compete with the atomic standards for independent working over a long period of time.

Due to the availability of high Q crystals, the question arises in what mode (fundamental or the overtone) should the crystal be excited? Due to the very high Q's, the series resistance of the quartz crystal equivalent circuit becomes so low that it becomes difficult to efficiently match the crystal to the rest of the circuit for its efficient operation. Warner has shown that for the best utilization of the high Q crystals it should be operated in higher overtones. This is because the equivalent resistance of the quartz crystal in the overtone operation will increase fast with the overtone number because the equivalent inductance of the series circuit increases as the cube of the overtone number and the $Q = \omega L/R$ itself will remain almost unchanged, both for the fundamental and the overtone frequencies. The operation in the overtone gives an additional stability of operation due to increase of inductance. It can be shown that

$$\frac{\Delta f}{f} = \frac{\Delta Xe}{2\omega L} = \frac{\Delta Xe}{S_I}$$

where Xe is the effective reactance, L is the equivalent series inductance of the quartz crystal and S_I is the stability index of the crystal.

The operation of the quartz crystal in overtones not only helps to obtain a stable frequency in the way indicated above but also can be effective in reducing the frequency multiplier chain between the slave quartz crystal oscillator and the atomic frequency. For this purpose the higher the overtone number the greater would, of course, be the multiplier chain compression, contributing to increased portability of the standard, reduction of cost and simplicity of the electronic circuitry involved.

For excitation of the quartz crystals in overtones, different workers have employed different techniques(4-14). The basic consideration in these techniques is to suppress, by use of filters or otherwise, the fundamental and provide enoughgain to theoscillator circuit at one of the overtone frequencies for oscillations to take place at this frequency. It may be mentioned that much earlier to the development of high Q crystals Mason and Fair (15) had given a technique for overtone excitation in an oscillator circuit. However, the method was complex and hardly any use seems to have been made of it in subsequent frequency standard work.

This paper presents a general, practical and relatively easy method of exciting the quartz crystal in the oscillator circuit to almost any overtone number desired, limited, of course, by the frequency capability of the rest of the circuit. The technique for production of overtones simply consists of coupling an L-C network to the quartz crystal and bringing the resonant frequency of the L-C network in the neighborhood of the desired overtone frequency. At this stage the quartz crystal takes control, resulting in the generation of the overtone frequency.

EXPERIMENTAL DETAILS

Fig.1 depicts a representative example of the use of the technique for producing overtones, the oscillator circuit used being of the Colpitts fashion. In order to prevent d.c. shorting of the bias on the crystal a blocking capacitor (C_3) is used as shown in fig.1. Change of this capacitor also enables variation of the coupling between the LC and the quartz crystal.

In order to show the working of the circuit of fig. 1 for overtone generation the capacitance of the L-C circuit was varied continuously from higher C values to lower and vice-versa so that the overtone frequency of the quartz crystal lay in the range of resonant frequencies of the LC circuit. Starting from higher or lower limits of C, a region was obtained when the frequency became insensitive to further variation of capacitance, this frequency being the desired overtone frequency.

As expected, the frequency stability in this region was the maximum, showing that the quartz crystal had taken control of the frequency generated. It was found that as the capacitance was varied from either side, the onset and termination of the overtone generation in the regions I & II of stable frequencies (fig.2&3) were indicated by the production of a momentary shift of the C.R.O. waveforms appearing at the output of the oscillating circuit. This shift in the waveform can be used to monitor visually when the frequency control by the quartz crystal is taking place. As expected, no such shift was observed when the quartz crystal was replaced by its equivalent electrode capacitance. Figures 4 and 5 illustrate the voltage waveforms of the third and fifth overtones generated by a quartz crystal of fundamental resonance frequency of 1.87MHz

by use of circuit of fig. 1. The amplitude of the overtones was found to be comparable to that of the fundamental.

An interesting fact noticed from the figures 2 & 3 is, what may be called, frequency splitting of each of the third and fifth overtones in two values and the production of a hysteresis-type curve located in the region of the production of the overtone frequencies. It was found that only the lower overtone frequency was stable against interruption of voltage supply and will be, of course, the one to be used in practical applications. The splitting of the overtone frequencies was found to be a direct function of the coupling of the L-C circuit with the quartz crystal. Table (I) depicts these results. In this table the coupling capacity between the L-C circuit and the quartz crystal is progressively changed from one set of values to the others for obtaining the corresponding interval between the overtone-frequency doublet.

The method of obtaining overtone frequencies described in the paper was tried in different kinds of quartz crystal oscillating circuits apart from that described in fig. 1. In all cases, the overtone frequencies were easily obtained. In one circuit using the quartz crystal of 20MHz fundamental frequency overtone frequencies of nominal values 60 & 100 MHz were obtained. Fig.6,7 and 8 depict the fundamental third and fifth overtone frequencies (20,60 & 100 MHz) of a quartz crystal.

In order to illustrate the effective control of the quartz crystal for producing the overtone frequencies the following observations were obtained for a particular circuit, using a quartz crystal of 20 MHz as fundamental frequency.

The resonant L-C frequency was changed between two limits in two different sets (I & II) of observations, the values in set I lying below the overtone frequency and those in set II lying above the overtone frequency. Table II depicts the results. It can be seen from the table that even for a big enough interval between the two frequency limits in each set the overtone frequency is obtainable, its frequency hardly changing between the two limits of set I, though there is a greater corresponding change for limits of set II. The extent of control the quartz crystal can have, seems to depend also on the type of oscillating circuit used.

The significant difference in the overtone frequencies corresponding to use of set I and II is the frequency splitting already described in fig.2 for use of the 1.87 MHz crystals.

DISCUSSION OF RESULTS

It has been shown that use of a L-C circuit directly coupled to the quartz crystal is effective in generating overtone frequencies. In principle any overtone number can be generated consistent with the frequency capability of the oscillator circuit. For example, in circuit of fig.1 the thirteenth overtone frequency of the 1.87 MHz crystal was obtained, no attempt being made to obtain still higher overtones. The usefulness of the coupled L-C network is shown by the fact that as soon as, during the production of overtone frequencies, the L-C is mechanically decoupled only the fundamental frequency gets generated.

The overtone frequency splitting is probably due to well known coupling of two tuned circuits of the same individual resonance frequencies (16-17). The doublet will tend to vanish as the coupling is decreased, as actually found.

It may be expected that by use of active solid state devices of the oscillator circuit of high enough frequency capability, generation of overtone frequencies of the order of 500 MHz should be feasible, in the first stage of a frequency multiplier chain for an atomic frequency standard. For this purpose, it would of course be desirable to have the fundamental frequency of the crystal as high as possible.

SUMMARY AND CONCLUSION

The paper presents a new method of generating overtone frequencies of quartz crystals. A parallel, tunable L-C circuit is coupled to the quartz crystal in an oscillator circuit. On tuning the L-C for its resonant frequency to lie in the neighbourhood of an overtone frequency, the quartz crystal takes control for generating the pure overtone frequency of amplitude comparable to that obtained for the fundamental oscillations.

Each overtone frequency exhibits a splitting in two, the higher frequency being obtained when the L-C resonance frequency approaches the overtone frequency from the higher values. The reverse is the case when the overtone frequency is approached from the lower values. The lower overtone split frequency is stable against the interruption of the voltage supply and, therefore, is the one to be used for practical applications.

The method for obtaining overtone frequencies makes it easily possible to excite high Q crystals in the higher overtones for which the quartz crystals would have impedance levels better matched to the oscillating circuit and also have higher stability index. In this way standard frequencies can be generated efficiently using high Q crystals. Also, exciting a crystal of preferably high fundamental frequency in an high enough overtone the frequency multiplier chain linking the quartz crystal frequency with the atomic frequency in an atomic frequency standard can be appreciably compressed, this fact leading to better portability, lower cost and simplification of electronics involved. As an example, an overtone frequency of 100 MHz was easily obtained for the first stage of a frequency multiplier.

ACKNOWLEDGEMENT

One of the authors (Harish Bahadur) thanks the Department of Atomic Energy, Govt. Of India for the award of research fellowship.

REFERENCES

1. A.W.WARNER - "Design and Performance of Ultra-Precise 2.5 Mc Quartz Crystal Units" Bell System Tech.Jour. 39, p.1193,(1960)

2. A.W.WARNER - "Ultra Precise Quartz Crystal Frequency Standard" IRE Trans. Instrumentation, I-7, p. 185, (1958).

3. A.W.WARNER - "High Frequency Crystal Units for Primary Frequency Standards", Proc. I.R.E. 40, p. 1030, (1952).

4. T.C.ANDERSON, F.G.MERRIL - "Crystal Controlled Primary Frequency Standards - Latest Advances for Long Term Stability" I.R.E. Trans. Instrumentation I-9, p.136, Sept.'(1960)

5. R.A.SYKES - "Modes of Motion in Quartz Crystals" cited in QUARTZ CRYSTALS FOR ELECTRICAL CIRCUITS (ed. R.A.Heising), D.Van Nostrand, New York; also Bell Syst. Tech. Jour. 23, No.1, Jan.'(1944).

6. R.A.SYKES - "High Frequency Plated Quartz Crystal Units" Proc. I.R.E., 36, p.4 (1948).

7. J.J.VORMER - "Quartz Filter Crystals with Low Inductance" Proc.I.R.E., 36, p.802, (1948).

8. J.J.VORMER - "Crystal-Plates Without Overtones" Proc. I.R.E., 39, p.1086 (1951).

9. W.P.MASON - "Electromechanical Transducers and Wave Filters" D.Van Nostrand Inc., p.1941, (1948).

10. W.P.MASON - " Electrical Wave Filters Employing Quartz Crystals as Elements" Bell.Syst. Tech.Jour. 13, p.405, July (1934).

11. W.P.MASON - "Method for Exciting a Single Harmonic of a Longitudinally Vibrating Bar" paper contributed to "PHYSICS OF SOLID STATE, Commemoration Volume to Prof. S.Bhagwantam (ed. S.Balakrishna, M.Krishnamurthi & B.R.Rao), Academic Press, London & New York p.381, (1969).

12. W.L.SMITH - "Miniature Transistorized Crystal Controlled Precision Oscillators" I.R.E. Trans. Instrumentation, I-9, P.141, (1960).

13. E.P.FELCH & J.O. ISRAEL- "A Simple Circuit for Frequency Standard Employing Overtone Crystals" Proc. I.R.E., 43, p.596, (1955).

14. O.O.LAYDEN, - W.L.SMITH, A.E.ANDERSON, M.B.BLOCK, D.E.NEWELL & P.C.SULZER "Crystal - Controlled Oscillators" IEEE Trans. Instru. & Meas. IM-21, No. 3, p. 277, Aug'(1972).

15. W.P.MASON & I.E.FAIR - "A New Direct Crystal Controlled Oscillator for Generating Ultra-Short Wave Frequencies" Proc. I.R.E. 30, p.464, Oct'(1942).

16. F.E.TERMAN - "Electronic and Radio Engineering" Mc Graw Hill Electrical and Electronic Engineering Series, Mc Graw Hill, New York, (1955).

17. SAMUEL SEELY- "Electronic Circuits" Rinehart and Winston Series in Electrical Engineering, Electronics and Systems, Rinehard and Winston, New Yor, (1968).

TABLE (I)

ILLUSTRATION OF OVERTONE FREQUENCY SPLITTING AS A FUNCTION OF THE COUPLING BETWEEN THE QUARTZ CRYSTAL (of fundamental frequency = 1.87 MHz) AND THE L-C CIRCUIT.

OVERTONE NUMBER	COUPLING CAPACITANCE	OVERTONE DOUBLET SEPARATION IN HERTZ
THIRD	0.1 μfd	213413
	220 μμfd	79468
	110 μμfd	127
FIFTH	0.1 μfd	413216
	220 μμfd	12624
	110 μμfd	152

TABLE (II)

ILLUSTRATION OF EFFECTIVE CONTROL OF QUARTZ AT OVERTONE FREQUENCY WITH THE CORRESPONDING L-C FREQUENCY VARIATIONS IN THE REGION OF PRODUCTION OF OVERTONES.

SET NO.	L-C FREQUENCY VARIATIONS	QUARTZ OVERTONE FREQUENCY FOR THE RANGE OF L-C FREQUENCY VARIATION
I	49.8128 MHz	60.001124 MHz
	56.7538 MHz	60.001125 MHz
II	62.3241 MHz	60.003794 MHz
	67.4629 MHz	60.009162 MHz

BEST AVAILABLE COPY

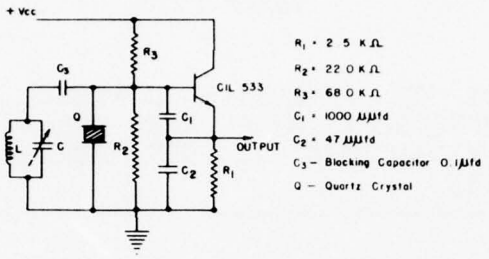


Fig 1 CIRCUIT DIAGRAM OF A CRYSTAL CONTROLLED OSCILLATOR SHOWING THE USE OF A PARRALLEL TUNED L-C CIRCUIT ACROSS THE QUARTZ CRYSTAL FOR THE GENERATION OF OVERTONE FREQUENCIES

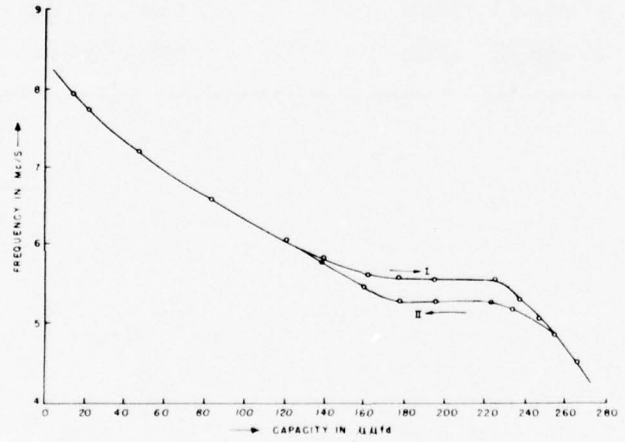


Fig 2 FREQUENCY VARIATION WITH DIRECTIONAL CHANGE OF CAPACITANCE FROM LOWER VALUES TO HIGHER AND BACK, FOR EXCITATION OF QUARTZ IN THIRD OVERTONE

BEST AVAILABLE COPY

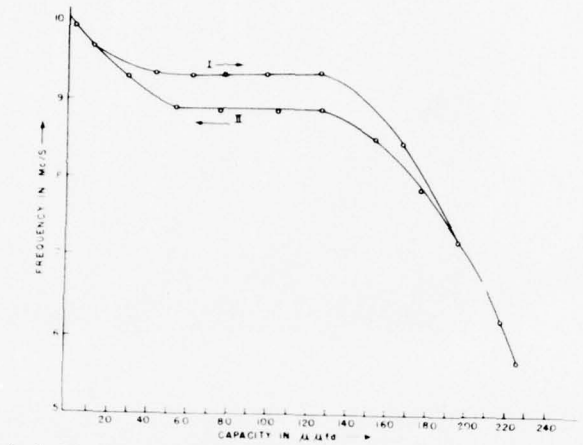


Fig. 3 FREQUENCY VARIATION WITH DIRECTIONAL CHANGE OF CAPACITANCE FROM LOWER VALUES TO HIGHER AND BACK, FOR EXCITATION OF QUARTZ IN FIFTH OVERTONE

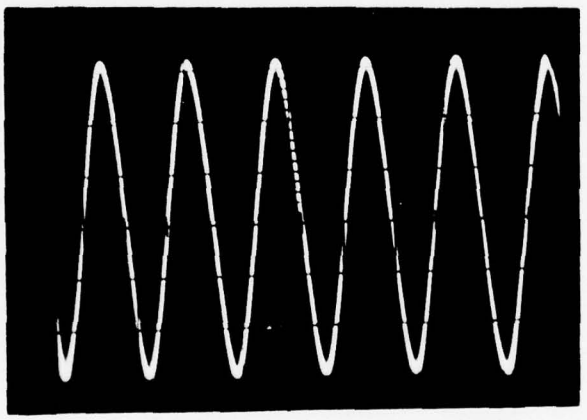


FIG.4 GENERATION OF THIRD OVERTONE FREQUENCY (5.6 MHz) OF A QUARTZ CRYSTAL OF 1.87 MHz FUNDAMENTAL FREQUENCY.

Horizontal Scale 1 div. = 0.1 μ sec.
Vertical Scale 1 div. = 2.0 volts

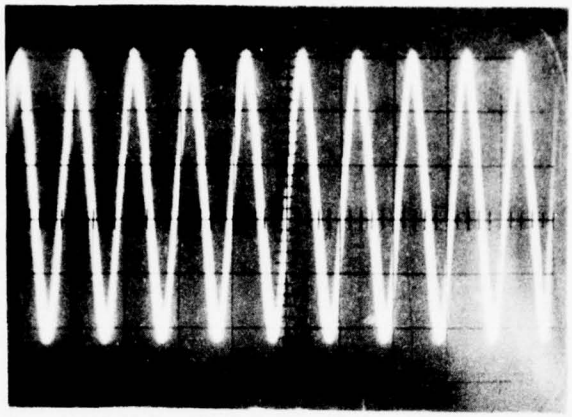


FIG. 5 GENERATION OF FIFTH OVERTONE FREQUENCY (9.3MHz) OF A QUARTZ CRYSTAL OF 1.87 MHz FUNDAMENTAL FREQUENCY.

Horizontal Scale 1 div. = 0.1 μ sec.
Vertical Scale 1 div. = 2.0 volts

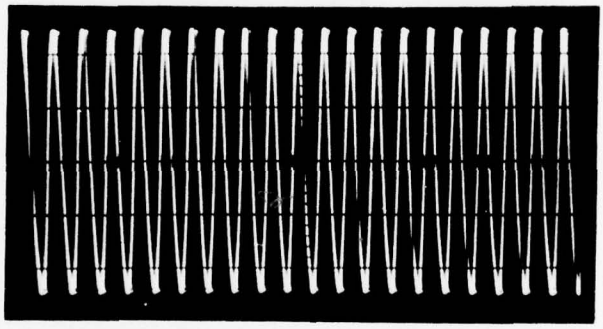


FIG. 6 GENERATION OF FUNDAMENTAL FREQUENCY OSCILLATIONS OF A 20 MHz QUARTZ CRYSTAL.

Horizontal Scale 1 div. = 0.1 μ sec.
Vertical Scale 1 div. = 2.0 volts

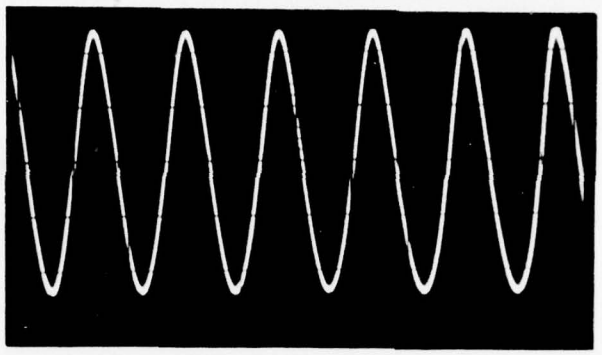


FIG.7 GENERATION OF THIRD OVERTONE FREQUENCY (60 MHz) OF A QUARTZ CRYSTAL OF 20 MHz FUNDAMENTAL FREQUENCY.

Horizontal Scale 1 div. = 1.0 μ sec.
Vertical Scale 1 div. = 2.0 volts

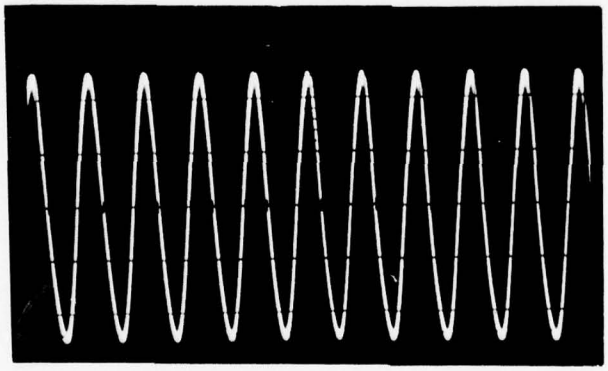


FIG.8 GENERATION OF FIFTH OVERTONE FREQUENCY (100 MHz) OF A 20 MHz QUARTZ CRYSTAL.

Horizontal Scale 1 div. = 1.0 μ sec.
Vertical Scale 1 div. = 2.0 volts

QUESTION AND ANSWER PERIOD

NO DISCUSSION

DEMONSTRATION OF THE FREQUENCY OFFSET ERRORS INTRODUCED BY AN INCORRECT SETTING OF THE ZEEMAN/ MAGNETIC FIELD ADJUSTMENT ON THE CESIUM BEAM FREQUENCY STANDARD

Donald C. Kaufmann
NASA Goddard Space Flight Center

ABSTRACT

The fine frequency setting of a cesium beam frequency standard is accomplished by adjusting the C field control with the appropriate Zeeman frequency applied to the harmonic generator.

A novice operator in the field, even when using the correct Zeeman frequency input, may mistakenly set the C field to any one of seven major Beam I peaks (fingers) represented by the Ramsey curve. This can result in frequency offset errors of as much as 2.5 parts in ten to the tenth.

The effects of misadjustment will be demonstrated and suggestions discussed on how to avoid the subtle traps associated with C field adjustments.

INTRODUCTION

The Hewlett Packard Model 5061A Cesium Beam Frequency Standard is a self calibrating device requiring no other reference frequency to insure its frequency accuracy to within 1×10^{-11} of all other Cesium Beam Frequency Standards. Although this statement is literally correct, it is critically dependent on the magnetic C Field setting. The magnetic C Field is adjusted to the correct central Beam I peak (within one of seven families of Ramsey Curves) with the appropriate Zeeman Frequency applied to the harmonic generator. However, the initial turn on procedure covering this adjustment is inadequately covered in the technical literature. It is further complicated by the fact that selection of undesired cesium atom energy level transitions can result in beam current (Beam I) outputs from the cesium tube of slightly greater than or near equal to the Beam I developed during the desired transition. The incorrect setting of the magnetic C Field can result in frequency error offsets of as little as one part in ten to the eleventh when the incorrect sub-central peak is selected or as much as two and one half parts in ten to the tenth when the incorrect

central peak is chosen. The new Hewlett Packard Cesium Standards (1974 on) with the higher resolution C Field Control will allow an offset which is limited to the adjacent sub-central peak of the desired transition. It should be noted that in every case of erroneously setting the C Field, the Cesium Standard indicates normal operation; continuous operation lamp on, alarm lamp off, and all front panel meter readings of the operating parameters within the normal range.

The purpose of this paper is to describe the means of demonstrating this effect and suggesting the means for avoiding the pitfalls associated with setting of the magnetic C Field. However, before discussing the demonstration it is desirable to review the theory of operation of the standard on a block diagram level, the cesium beam tube details, the hyperfine energy level diagrams of Cs atom 133, and the initial turn on procedure.

OPERATION OF THE CESIUM BEAM FREQUENCY STANDARD

Figure 1 is a simplified block diagram of the HP 5061A Cesium Beam Frequency Standard. The voltage controlled Quartz Oscillator (A10 provides a 5 MHz sinewave to a X 18 multiplier (A3). The multiplier outputs a phase modulated 90 MHz signal to the Harmonic Generator (A4). The 5 MHz from the Quartz Oscillator is inputted to the Synthesizer via a buffer in the Multiplier and both Multiplier and Synthesizer outputs are applied to the Harmonic Generator. Here the phase (Ø) modulated 90 MHz is multiplied by 102 times and added to the Synthesizer output resulting in a Ø modulated 9192.63----MHz being applied to the microwave cavity surrounding the Cesium Beam Tube (A12) interaction region. The Beam Tube acting as a high Q bandpass filter provides discriminator action and outputs the fundamental (137 Hz) and its 2nd harmonic (274 Hz). When the frequency of the injected signal is in agreement with the hyperfine energy level transition of the Cesium Atom the beam tube output is primarily 274 Hz. The 137 hertz output is an error signal proportional in amplitude and direction to the difference in frequency between the injected signal and the Cs atom transition frequency. Both the fundamental and the 2nd harmonic frequencies are amplified in the AC Amplifier (A7). The fundamental is then fed to a synchronous Phase Detector (A8), the output of which is applied to an operational amplifier (A9) where the Ø error signal is converted to a DC voltage used to control the Quartz Oscillator (A10) thru VCO action. Thus the frequency stability and accuracy of cesium atom 133 hyperfine energy level transition is transferred to the Quartz Oscillator via the Ø locked loop and outputted to the users in the signal format of 5 MHz, 1 MHz, and 100 KHz.

In addition to the phase locked loop, there are four other circuits. Buffer Amplifier (A13) outputs the 5 MHz 1 volt RMS sinewave. The Frequency Divider (A6) takes the 5 MHz input and divides down to 1 MHz and 100 KHz and provides these signals via buffers at 1 volt RMS. Cesium Oven Controller (A11) provides the heat source for cesium atom effusion within the Beam Tube. Finally, the Logic Module (A14) detects fundamental, 2nd harmonic, error signal limits and synthesizer failures.

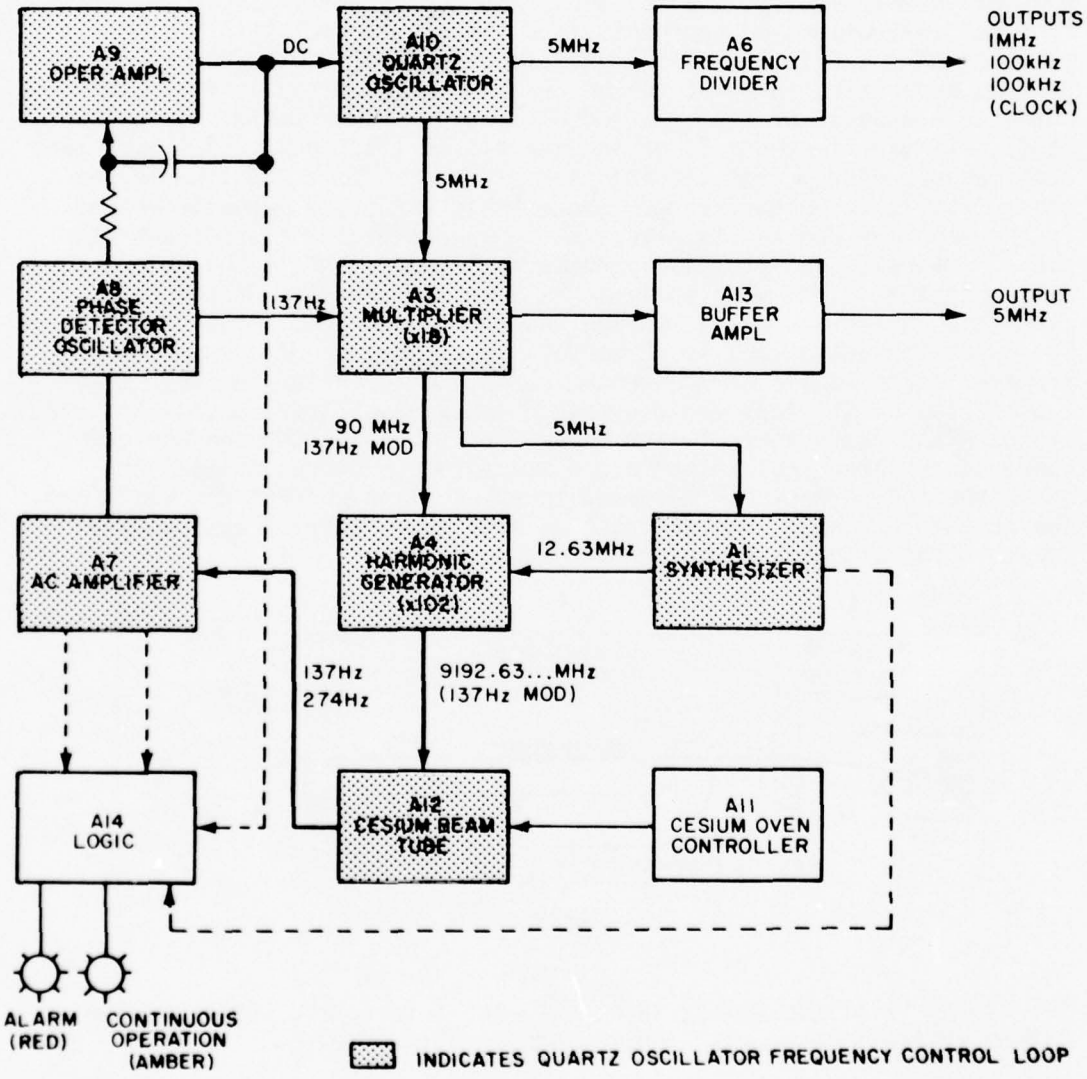


Fig. 1

CESIUM BEAM TUBE OPERATION

The schematic representation of the Cesium Beam Tube in Fig. 2 delineates the internal components and the cesium beam trajectory. Cesium atoms effuse from the oven source and are formed into a ribbon-like beam by a collimator. The beam passes through inhomogenous magnetic field of the first state selector magnet, the "A" magnet. The force experienced by a particular atom depends upon its effective magnetic moment hence upon its energy state, and also upon the gradient of the field; thus, atoms are selectively deflected into the interaction cavity. Two fields are present in this cavity, the "C" field and the microwave field resulting from multiplication and synthesis from the quartz oscillator. The presence of the C field, a steady-state, low level field, causes the desired separation to exist in the cesium atom's energy levels. The magnetic component of the injected microwave field interacts with the atoms. If the frequency is at the transition frequency, 9192+ MHz, then atoms absorb energy from the injected microwave field and flop to the other transition energy state. Since their effective magnetic moment is thereby reversed in its direction, a second state selector magnet, the "B" magnet, can selectively deflect flopped atoms to the detector. This detector, a hot wire ionizer, is a heated tantalum ribbon upon which the cesium atoms are ionized and then evaporated. The cesium ions pass through a mass spectrometer. The function of the mass spectrometer is to remove common contaminants such as potassium that might cause noise bursts that could overload the AC Amplifier in the frequency standard and cause loss of lock. The ions that pass through the mass spectrometer are accelerated into a multistage electron multiplier, where the ion current is converted to an electron current and amplified. The output current of the electron multiplier is carried by a coaxial cable to the signal processing electronics.

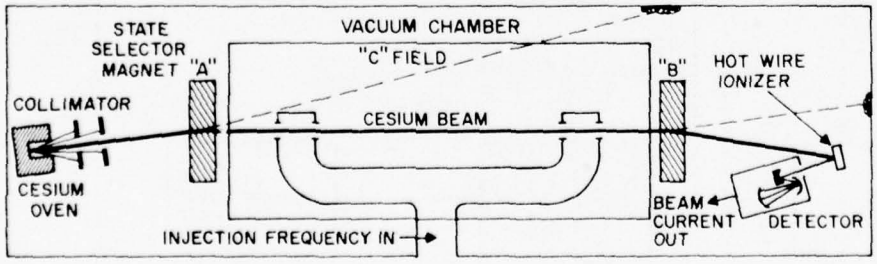


Fig. 2

The cavity is of the Ramsey type, with two interaction regions. The entire system is evacuated and is magnetically shielded.

BEAM TUBE DISCRIMINATOR ACTION

The cesium beam tube, in a simplified sense, is a passive device of extremely high Q that acts like a bandpass filter which by means of discriminator action provides an error signal to correct the phase of a quartz oscillator. Fig. 3 depicts the discriminator action. When the injected microwave signal is matched to the cesium atom transition frequency only the second harmonic component of the phase modulated signal appears in the beam current output. When the injected signal lies above or below the desired value, both the fundamental and the 2nd harmonic are outputted from the beam tube, with the fundamental (error signal) containing both phase and magnitude information used to control the quartz oscillator.

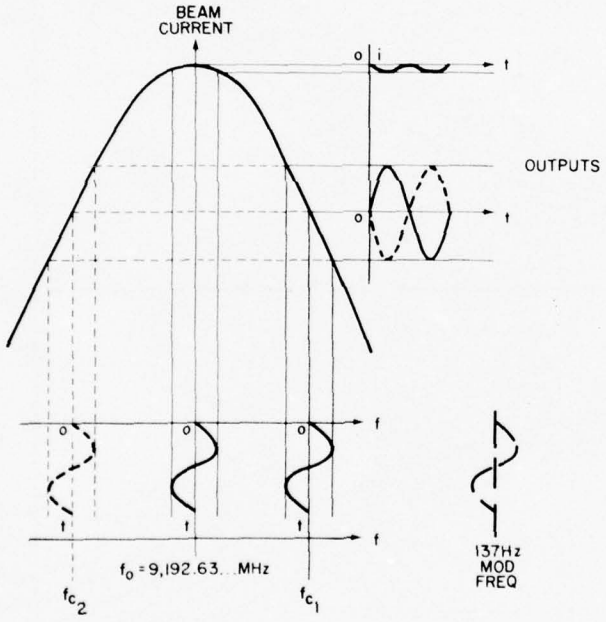


Fig. 3

ENERGY LEVELS

At zero magnetic field there are only two energy levels in which a neutral cesium atom can exist. However, upon application of a small

magnetic field (C Field) these two levels are split into 16 hyperfine levels, the higher energy (F=4) group into nine and the lower energy (F=3) group into seven. Figure 4 plots the hyperfine energy level subsets versus magnetic C Field strength. The dotted vertical line is representative of the typical C field setting of 60 milligauss. This value was chosen so that the field - independent transition; F=3, M_f=0 to F=4, M_f=0, is utilized.

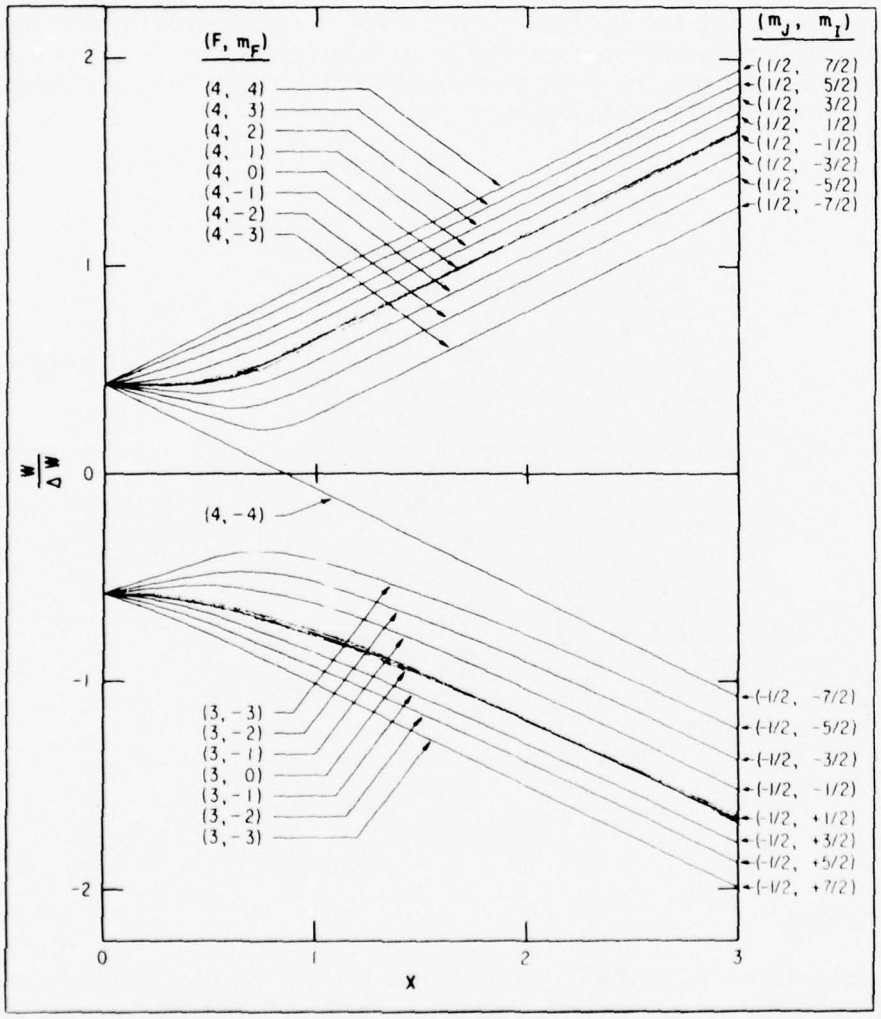


Fig. 4

C FIELD SETTING

The setting of the magnetic C Field is accomplished by applying the appropriate Zeeman frequency (42. 82 KHz for setting the Al Rate) to the harmonic generator which in turn excites the microwave cavity in the Cesium Standard. Figure 5 shows the beam tube output (Beam I) as a function of the microwave frequency. The center pedestal, labeled 0. 0) represents the desired energy level transition. Each transition contains a family of curves (Ramsey Fingers) consisting of a central peak and symmetrical sub-central peaks. Illustrated above the 0, 0 transition (i.e., F=4, Mf=0 and F=3, Mf=0) is a family of Ramsey Curves (fingers). With a fixed Zeeman frequency input the families of Ramsey curves depicted in Fig. 5 can be obtained by ranging through the Cesium Standard's "C Field" control.

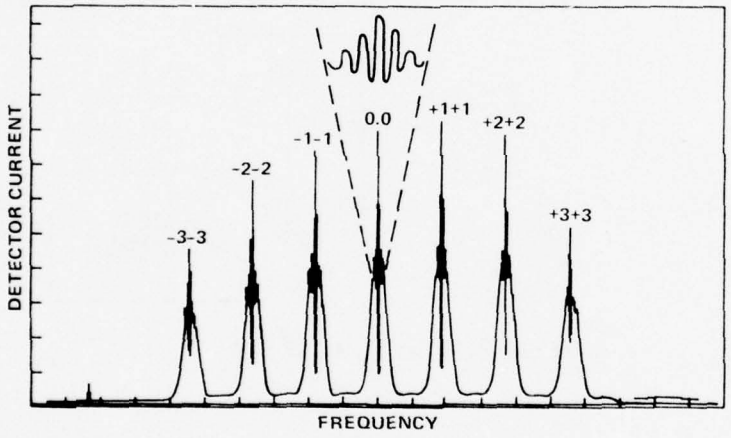
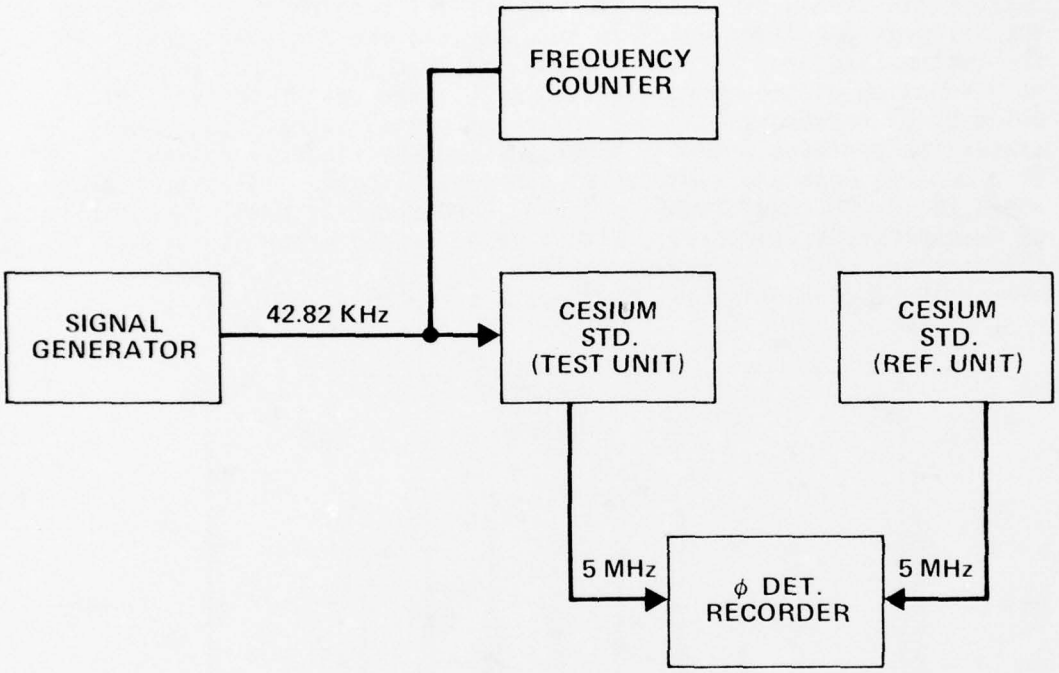


Fig. 5

ZEEMAN/C FIELD TEST SET

Fig. 6 is a block diagram of the test set used to demonstrate the effects of misadjusting the magnetic C Field. It consists of two cesiums, a test unit and a reference unit, from which the 5 MHz outputs are phase compared. The reference units's C Field has been correctly set and its output frequency verified to be within one part in ten to the twelfth of the Naval Observatory's master clock. The signal generator provides the Zeeman input, in this

case 42.82 KHz, for developing the A1 rate in the unit under test. The frequency counter substantiates the correctness of the Zeeman Frequency.



ZEEMAN/C FIELD TEST SET

Figure 6

THE DEMONSTRATION

On the Cesium Standard under test, set the mod switch to "OFF" and the mode switch to "OPEN". With the test set mentioned above and with the signal generator adjusted to the A1 Zeeman rate of 1 volt RMS amplitude and interfaced to the "ZEEMAN IN" jack of the cesium under test, slowly rotate the ten turn "C Field" control while monitoring "Beam I". Start with the "C Field" potentiometer maximum clockwise and rotate the control slowly through its entire range. Record all Beam I peaks and their associated "C Field" control settings. Select the maximum "Beam I" "C Field" control setting and switch to "MOD ON" and to "MODE OPERATE". The alarm lamp should

go out and upon depressing the "LOGIC RESET" button the "CONTINUOUS" operation lamp should come on. NOTE: Selection of any Beam I peak, central or sub-central, of any Ramsey family of curves, will result in the "CONTINUOUS" operation lamp on, indicating normal operation.

ANALYSIS OF THE RESULTS

Figure 7 is a tabulation of the families of Ramsey fingers detected for two Hewlett-Packard Model 5061A Cesium Standards. The "Beam I" their associated "C Field" values, the energy level transitions, the frequency offsets of the sub-central to the central peaks, and the maximum frequency difference (between the central peaks of the the most widely displaced Ramsey families) are listed. By virtue of the tabulation the following facts become evident: There is excellent symmetry in both amplitude and frequency offset of the sub-central peaks; the difference in amplitude between the central and the adjacent sub-central peaks is small and suggest care in setting the "C Field" to avoid aligning to a sub-central peak; a real possibility

			BEAM I – C FIELD		
	ZEEMAN TRANSITION	Δf	HI SIDE	CENTER PK.	LO SIDE
SERIAL NO. 218	3,0 → 4,0	8×10^{-12}	40	50	40
			7.22	7.06	6.88
	3,1 → 4,1	3×10^{-12}	19	20	19
			4.72	4.66	4.60
	3,2 → 4,2	4×10^{-12}	35	42	35
			3.56	3.48	3.38
	3,3 → 4,3	3×10^{-12}	32	36	32.5
			2.34	2.28	2.22
SERIAL NO. 166	3,0 → 4,0	9×10^{-12}	47	50	47
			7.36	7.18	7.00
	3,1 → 4,1	4.5×10^{-12}	45	47.5	45.5
			3.53	3.44	3.37
	3,2 → 4,2	3×10^{-12}	42	44	42.5
			2.26	2.20	2.15

MAX. Δf BETWEEN CENTER PEAKS

SER. NO. 218 = 2.39×10^{-10}

SER. NO. 166 = 2.49×10^{-10}

FIGURE 7

of setting to an incorrect central peak because of the high Beam I values attainable, thus resulting in significant frequency offset error; and finally the correct frequency setting is defined by the two to one greater frequency offset between the sub-central peak and the central peak of the desired transition versus the ΔF of the undesired transitions. This latter fact provides verification of when you have selected the correct central peak and may be used when no other means of verification, such as portable clock, Loran-C or VLF phase comparisons are available. It is well to note, that by design, all Hewlett Packard Model 5061A Cesium Frequency Standards (Pre 1974), correct "C Field" settings always fall within 6.50 and 7.55 on the "C Field" control dial.

Figure 8 shows approximately 8 hours of phase (Ø) comparisons between the test unit serial number 166 and the reference unit for three different magnetic "C Field" settings. The first hour of the Ø plot is representative of the worst case, where the C Field is set to the central peak resulting in the greatest frequency offset, followed by 4 hours of Ø comparing with the C Field set to the adjacent sub-central peak of the desired transition and finally 3 hours of the 5 MHz data with the "C Field" set to the central peak of the desired transition.

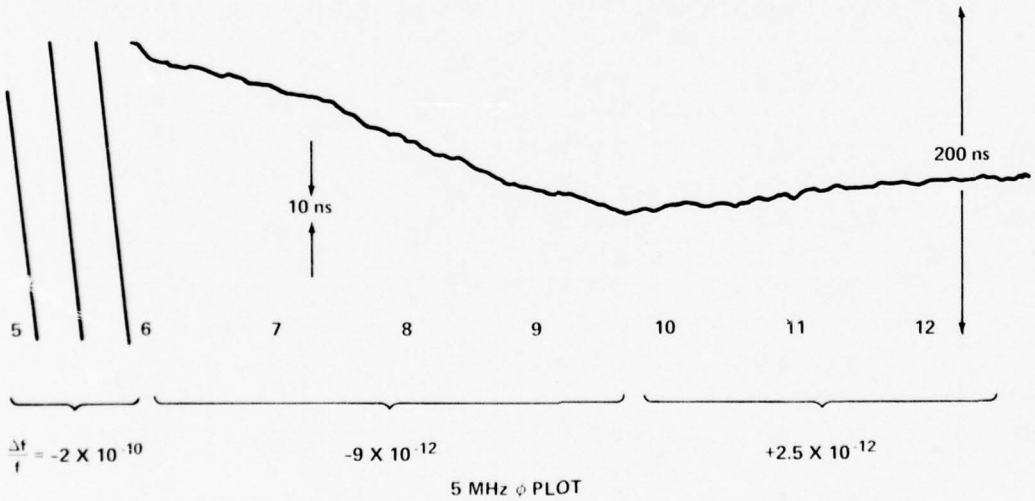


Fig. 8

In conclusion it should be emphasized that since 1974 the Hewlett Packard Model 5061A Cesium Standard, high performanc (004) version as well as the standard version, have a higher resolution "C Field" control with a much reduced range, only 2.5 X 10^{-11}, and therefore the magnetic "C Field" in these units can only be misadjusted to an adjacent sub-central peak of the correct energy level transition resulting in a maximum frequency offset error of 1 X 10^{-11}.

QUESTION AND ANSWER PERIOD

DR. REDER:

(Comments not recorded due to remote microphone intermittent operation) - Regarding problems of locking on.

MR. BEATY:

Jim Beaty, FAA NAPEC.

Perhaps I could share the benefit of some experience that we had in Atlantic City. As noted, the central peak or the proper peak, of the Ramsey tube is symmetrical for the types of accuracies we are talking about in commercial clocks, while the peaks below or above are slightly asymmetrical. In fact, this is the basis for the logic that HP uses in detecting the false peak. However, an added check would be if one is setting the C field and then one has a synthesizer, preferably, but even very carefully with a stable oscillator and a counter, one can set up your 42.82 Zeeman frequency and then center that very carefully and then if one changes the Zeeman frequency by a plus or minus of 100 cycles, then the decrease in beam I ought to be the same, if you are on the symmetrical curve.

It is not the same when you are on one of the other peaks and you have to readjust. We have used this very successfully. In fact, it is a good way to make sure that you are right on top of the proper curve, in fact, because that is rather insensitive. The panel meter is rather insensitive to very, very small differences in beam I and if you don't have an auxilliary meter there, you can just punch up on your synthesizer, for instance, 42.92, 42.72, and your beam I should decrease the same amount if you are right on the center.

A STUDY OF HYDROGEN MASER RESONATORS AND STORAGE BULBS FOR USE IN GROUND AND SATELLITE MASERS *

Edward M. Mattison, Robert F. C. Vessot, and Martin W. Levine

Smithsonian Astrophysical Observatory
Cambridge, Mass. 02138

I Introduction

Experiments using hydrogen masers in rocket probes and earth-orbiting satellites have motivated the design of small, light-weight, rugged masers. Masers now in laboratory use typically weigh 275 kg (600 lb) and occupy 0.6 m^3 (20 ft^3) or more. Smaller masers, weighing 41 kg (89 lb), have been built for a rocket-borne gravitational red-shift experiment.[1] These may be the forerunners of still smaller space masers that will utilize new technology and novel cavity designs.

Traditional masers use a cylindrical TE_{011}-mode resonant cavity in which is mounted a spherical or ellipsoidal fused-quartz bulb (Fig. 1). The bulb confines the hydrogen atoms to a region in which the longitudinal component of the oscillating magnetic field is uniform in phase and direction. Its interior surface is coated with Teflon to reduce interactions between the hydrogen atoms and the bulb wall. A typical TE_{011} maser cavity, resonant at the hydrogen hyperfine frequency f_{hfs} = 1420.405 MHz, is approximately 28 cm (11 inches) in diameter and 25.4 cm (10 inches) long. The cavity dimensions determine the minimum size, and hence weight, of the surrounding vacuum tank and magnetic shields. In order to make masers smaller, lighter, and more rugged, it is desirable to reduce the size of the cavity and to eliminate the separate quartz bulb. These changes would have several added benefits. The smaller size would decrease the power required

PRECEDING PAGE BLANK-NOT FILMED

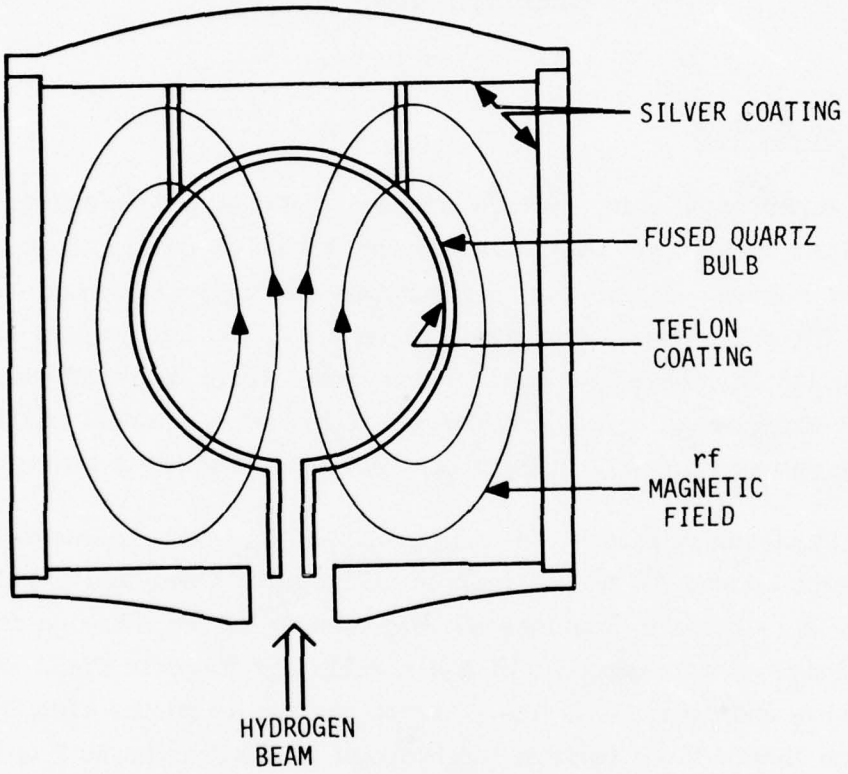


Fig. 1 Conventional TE_{011}-Mode Maser Cavity

by the temperature control circuits, improve thermal control of the cavity by reducing temperature gradients, and permit the use of optimally shaped magnetic shields in a smaller space. Eliminating the bulb would increase the cavity Q and decrease the maser's sensitivity to temperature changes by removing dielectric material from within the resonator.

We have proposed[2,3] two general designs for small bulbless maser cavities, and have constructed examples for tests. The first design employs a cylindrical TE_{011} or spherical TE_{101} cavity with thick dielectric walls (Fig. 2). The walls, which are coated on the outside with silver to form the electromagnetic resonator and on the inside with Teflon to form the atom-confining boundary, load the cavity, making it smaller than an unloaded cavity resonant at the same frequency. At the same time they form a bulb that is integral with the cavity, creating a rugged, monolithic structure.

The second proposed type of small maser cavity (Fig. 3) uses an unloaded resonator supporting either the rectangular TE_{101} or the cylindrical TE_{111} mode. A thin septum divides the cavity into two regions of oppositely directed oscillating magnetic field, and splits the entering hydrogen beam so that half of the atoms go into each region. The interior surfaces of the cavity are coated with Teflon, and the septum is made of sheet Teflon or of thin Teflon-coated material.

Not all cavity-bulb structures can support self-oscillation. The power radiated by the incoming hydrogen atoms must exceed the losses in the cavity. This places a lower limit on the cavity Q, and also on the strength of the oscillating magnetic field stimulating the atoms. In the next section we describe a new oscillation criterion that takes into account the field distribution in the cavity, the geometry of the atom-confining region, and the conductivity of the

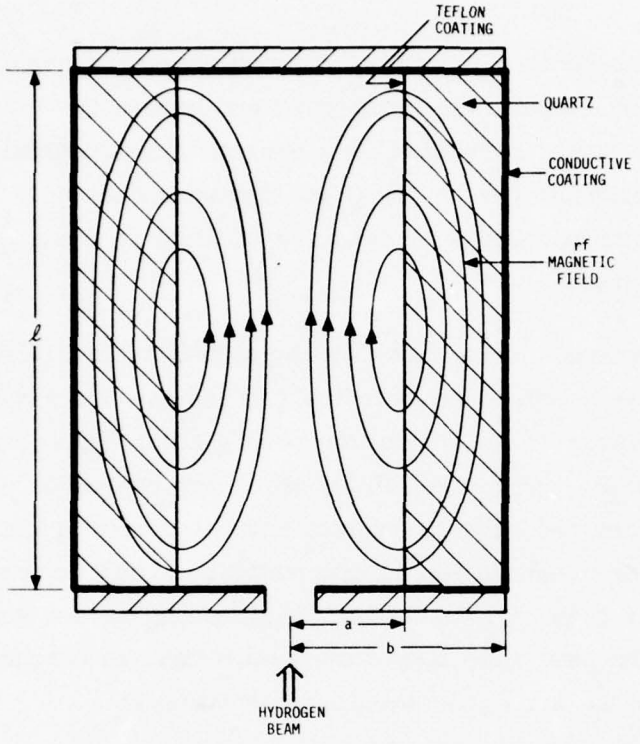


Fig. 2a Cylindrical TE_{011} Dielectric-Loaded Maser Cavity

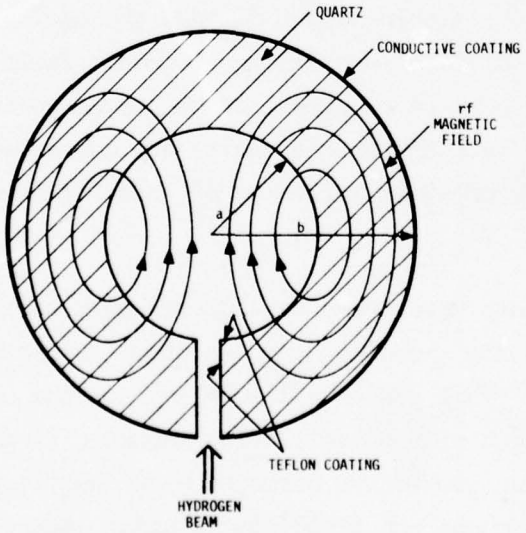


Fig. 2b Spherical TE_{101} Dielectric-Loaded Maser Cavity

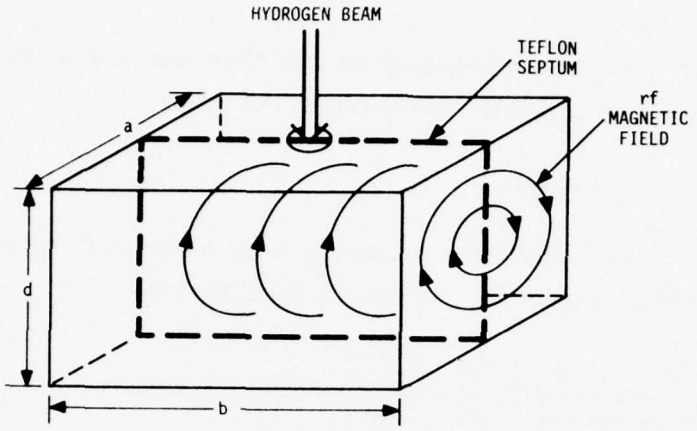


Fig. 3a Rectangular TE_{101} Septum Maser Cavity

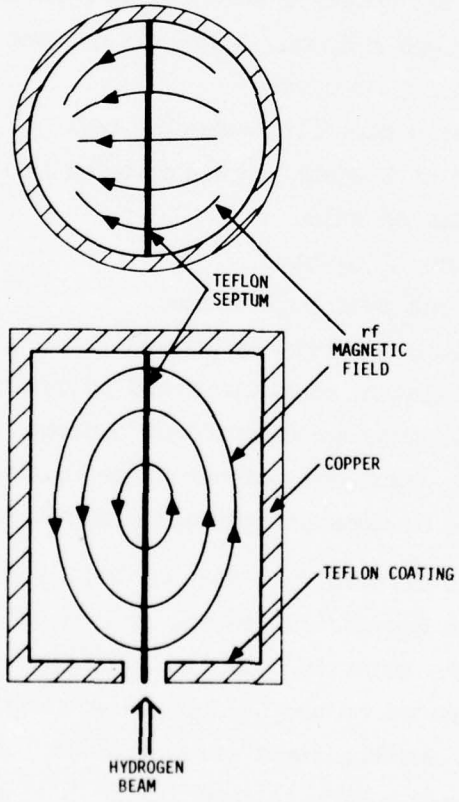


Fig. 3b Cylindrical TE_{111} Septum Maser Cavity

cavity walls. In succeeding sections we use this measure to evaluate the feasibility of the proposed small maser cavities.

II Maser Oscillation Criterion

It has been shown[4] that the following inequality must be satisfied if a single-bulb maser is to sustain oscillation:

$$q \equiv \left[\frac{\sigma \bar{v}_r \hbar}{8\pi\mu_o^2}\right] \cdot \frac{\gamma_t}{\gamma_\ell} \cdot \frac{I_{tot}}{I} \cdot \frac{V_c}{V_b} \cdot \frac{\langle H^2\rangle_c}{\langle H_z^2\rangle_b} \cdot \frac{1}{Q} \leq 0.172 \qquad (1)$$

Here

μ_o = Bohr magneton

$\bar{v}_r$ = average relative velocity of hydrogen atoms in bulb

σ = hydrogen-hydrogen spin-flip crossection

Q = loaded Q of cavity

I_{tot} = total H atom flux entering bulb

I = flux of H atoms entering bulb in $F = 1$, $M_F = 0$ state

V_b = volume of bulb

V_c = volume of cavity

$\langle\ \rangle_b$ = average over bulb volume

$\langle\ \rangle_c$ = average over cavity volume

H_z, H^2 = oscillating magnetic field in cavity

γ_t = total density-independent hydrogen relaxation rate (excludes spin-exchange relaxation)

γ_ℓ = rate of loss of hydrogen atoms from bulb

The notation of Eq. 1 differs from that of Ref. 4 to emphasize that γ_ℓ does not equal the geometrical escape rate γ_b of atoms from the bulb. Implicit in the quantity q is the hydrogen atom density in the bulb, which is determined by the balance between the rate at which H-atoms enter the bulb and the total rate at which they are lost. The loss mechanisms include escape through the bulb's aperture, recombination on the bulb's wall to form hydrogen molecules, and adsorption on

or chemical combination with the wall. Escape and recombination are the dominant loss mechanisms contributing to γ_ℓ, and it has been shown experimentally[5] that to a good approximation

$$\gamma_t / \gamma_\ell = 1 \tag{2}$$

The quantities in square brackets in Eq. 1 depend upon properties of the hydrogen atom; for a cavity temperature of 50 C, their values[4] give

$$\frac{\sigma \bar{v}_r \hbar}{8\pi \mu_o^2} = 510 \tag{3}$$

The type of state selector used in present hydrogen masers focuses into the cavity equal numbers of atoms in the states F = 1, m_F = 1 and F = 1, m_F = 0, making

$$I_{tot}/I = 2 \tag{4}$$

Combining Eqs. 2, 3, and 4 with Eq. 1 gives the following criterion[6] for maser oscillation:

$$S \equiv Q\eta' \geq 5.9 \times 10^3 \tag{5}$$

where

$$\eta' \equiv \frac{V_b}{V_c} \frac{\langle H_z \rangle_b^2}{\langle H^2 \rangle_c} \tag{6}$$

η' is called the bulb filling factor. The oscillation criterion for a septum cavity is the same as Eq. 5, but the filling factor is defined by

$$\eta' = \frac{2V_b}{V_c} \frac{\langle H_z \rangle_b^2}{\langle H^2 \rangle_c} \tag{6b}$$

where V_b is the volume of a single bulb region (equal to half of the cavity volume) and $< >_b$ is an average over one bulb region. We emphasize that it is the quantity S, and not the cavity Q or the filling factor alone, that determines the ability of a given cavity and bulb to support maser oscillation.

Because the amount of power coupled from the cavity is not known a priori, we define

$$S_o = Q_o \eta' \tag{7}$$

where Q_o is the unloaded cavity Q. S_o and S are related by

$$S = \frac{S_o}{1 + \beta} \tag{8}$$

where β is the cavity's external coupling factor.

III Dielectric-loaded Cavities

Cylindrical Cavity

A cylindrical loaded cavity, which resembles conventional maser cavities and which would be simple to fabricate and tune, is shown in Fig. 2. Graphs of S_o as a function of cavity dimentions are shown in Fig. 4. The graphs indicate that for a dielectric loss tangent $\delta = 6 \times 10^{-5}$ the threshold condition on S cannot be satisfied by any cylindrical cavity of practical shape. We have calculated the maximum permissible loss tangent for a quartz cylindrical cavity with $\ell/b = 2.4$, $a/b = 0.5$ ($a = 3.95$ cm, $b = 7.00$ cm, and $\ell = 18.95$ cm), assuming the most favorable conditions found in practice: $\beta = 0.1$, and actual Q equal to 70% of the theoretically calculated Q. With an

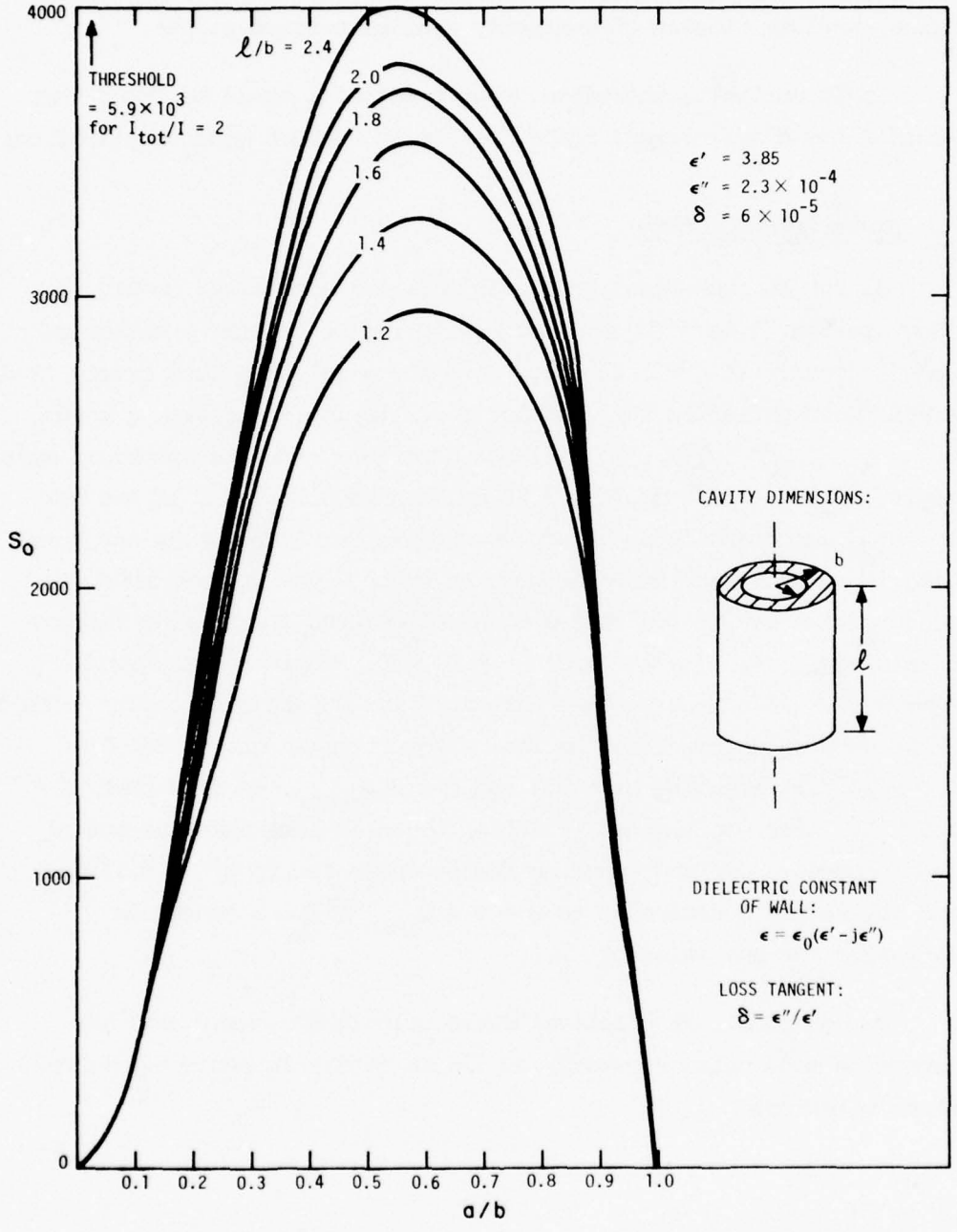


Fig. 4 S_o for Cylindrical Dielectric-Loaded Maser Cavity

ideal silver coating, the cavity would require $\delta \leq 1.2 \times 10^{-5}$, well below the loss tangent of currently available fused silica.[6,7]

It is unlikely, therefore, that a material could be found that would allow a cylindrical loaded cavity to support maser oscillation.

Spherical Cavity

S_o for the spherical TE_{101} dielectric-loaded maser cavity is shown in Fig. 5 as a function of cavity radius for three values of loss tangent. If $\delta = 3.25 \times 10^{-5}$, S_o for a silver-coated cavity 19 cm in diameter satisfies the oscillation criterion. However, a maser with $\beta > 0$ and $Q < Q_{theor}$ will not oscillate. Such a spherical maser cavity, with a = 6.4 cm, b = 9.83 cm, has been built.[2] It has not operated successfully as an active oscillator, although it has been used in a maser with external gain to enhance the Q.[9] We have measured the cavity's unloaded Q and calculated its filling factor, obtaining $Q_o = 17.2 \times 10^3$ and $\eta' = 0.3450$. These values give $S_o = 5.92 \times 10^3$, barely above threshold for an isolated cavity. (From these data we deduce that the loss tangent of the quartz is $\delta = 3.1 \times 10^{-5}$.) Assuming $\beta = 0.1$ and $Q = 0.7\, Q_{theor}$, we find that $\delta \leq 1.0 \times 10^{-5}$ for oscillation, a factor of three less than the actual loss tangent. (If the coupling factor increases to $\beta = 0.15$ and and the cavity Q decreases to $Q = 0.6\, Q_{theor}$, Eq. 5 cannot be satisfied for any value of δ.)

We conclude that practical dielectric-loaded maser cavities cannot be made using currently available materials and conventional state selectors.

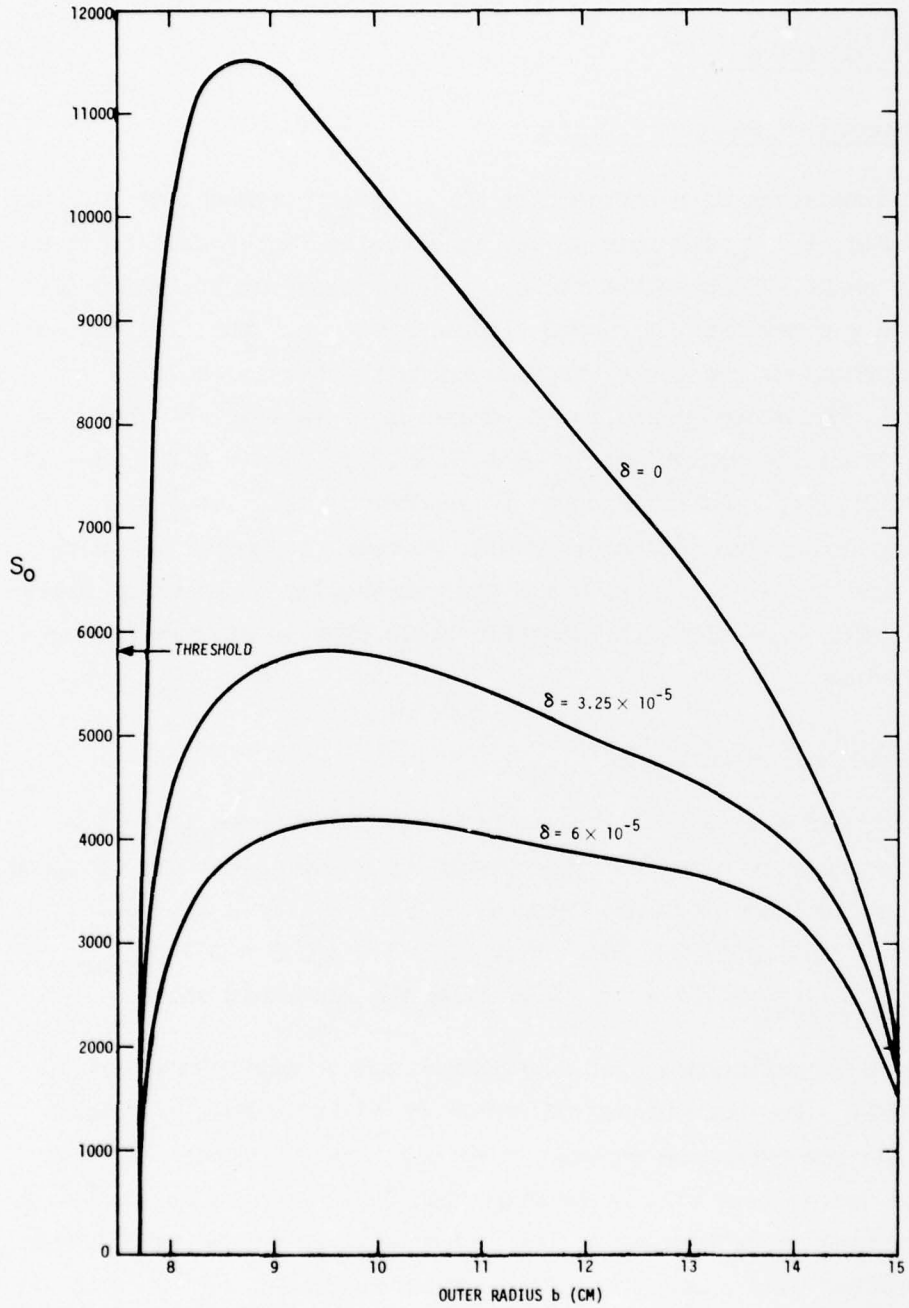


Fig. 5 S_o for Spherical Dielectric-Loaded Maser Cavity

IV Septum Cavities

Rectangular Septum Cavity

The dimensions of a rectangular TE_{101} cavity resonant at f_{hfs} are shown in Fig. 6. S_o for this cavity is given in Fig. 7 as a function of cavity shape. Because the fields in this resonator are independent of the y coordinate, Q_o and S_o increase with b. The filling factor η' improves as the cavity is made thinner (that is, as a/d decreases), but as shown in Fig. 6, d increases rapidly as a becomes smaller. A cavity approximately 19 x 19 x 13 cm (d/a = 0.7, b/d = 1) has $S_o = 13 \times 10^3$, and is expected to support oscillation. Its relatively large size (23 cm diagonal), however, is comparable with that of traditional cavities, while its rectangular shape makes difficult the production of a d.c. magnetic field that is uniform throughout its volume.

Cylindrical Septum Cavity

S_o for the cylindrical TE_{111} septum cavity is shown in Fig. 8. A convenient cavity size from the standpoint of efficient use of space and mimimum surafce-to-volume ratio is $\ell/D \sim 1$. S_o for a cavity with $\ell/D = 1.25$ is 13.2×10^3. With $\beta = 0.2$ and $Q = 0.7\ Q_{theor}$, this gives $S_{actual} = 7.7 \times 10^3$, 23% above the threshold value.

Fig. 9 is a photograph of a prototype septum cavity now being completed. For convenience of construction it is made of copper rather than low-expansion ceramic or glass. The rf output loop and the diode tuning loop will be covered with Teflon-coated quartz hoods, and the entire inner surface of the cavity will be coated with Teflon. The two halves will clamp the Teflon septum in place.

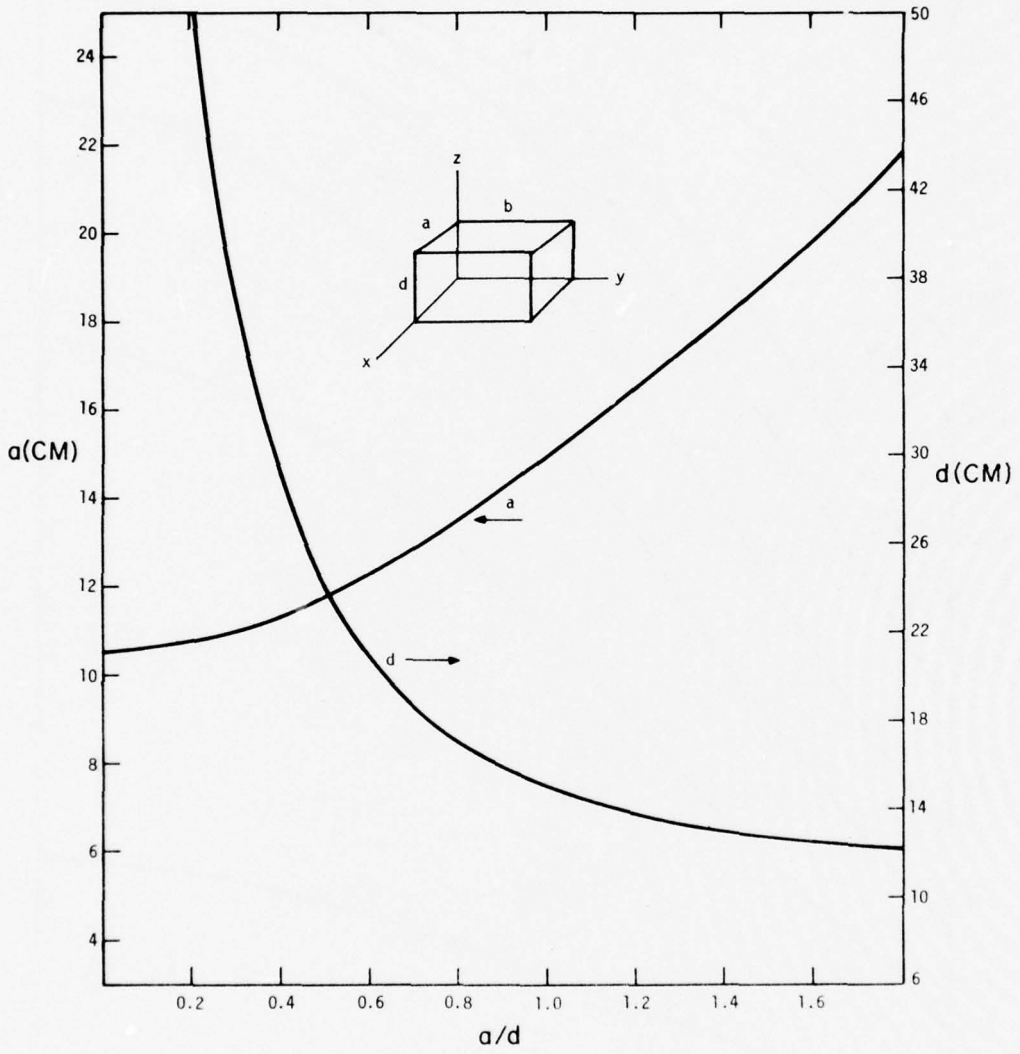


Fig. 6 Dimensions of TE_{101} Rectangular Septum Maser Cavity

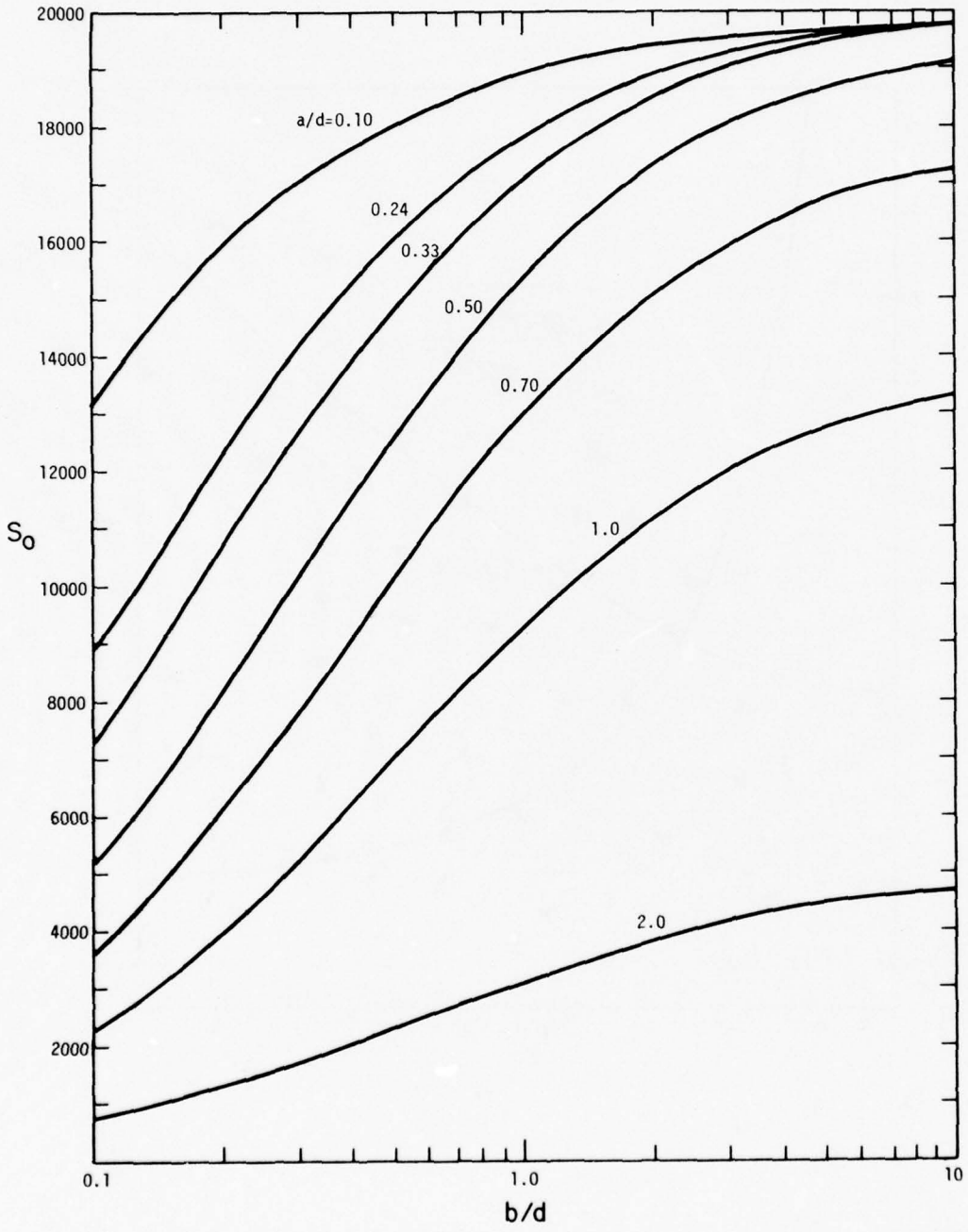


Fig. 7 S_o for TE101 Rectangular Septum Maser Cavity

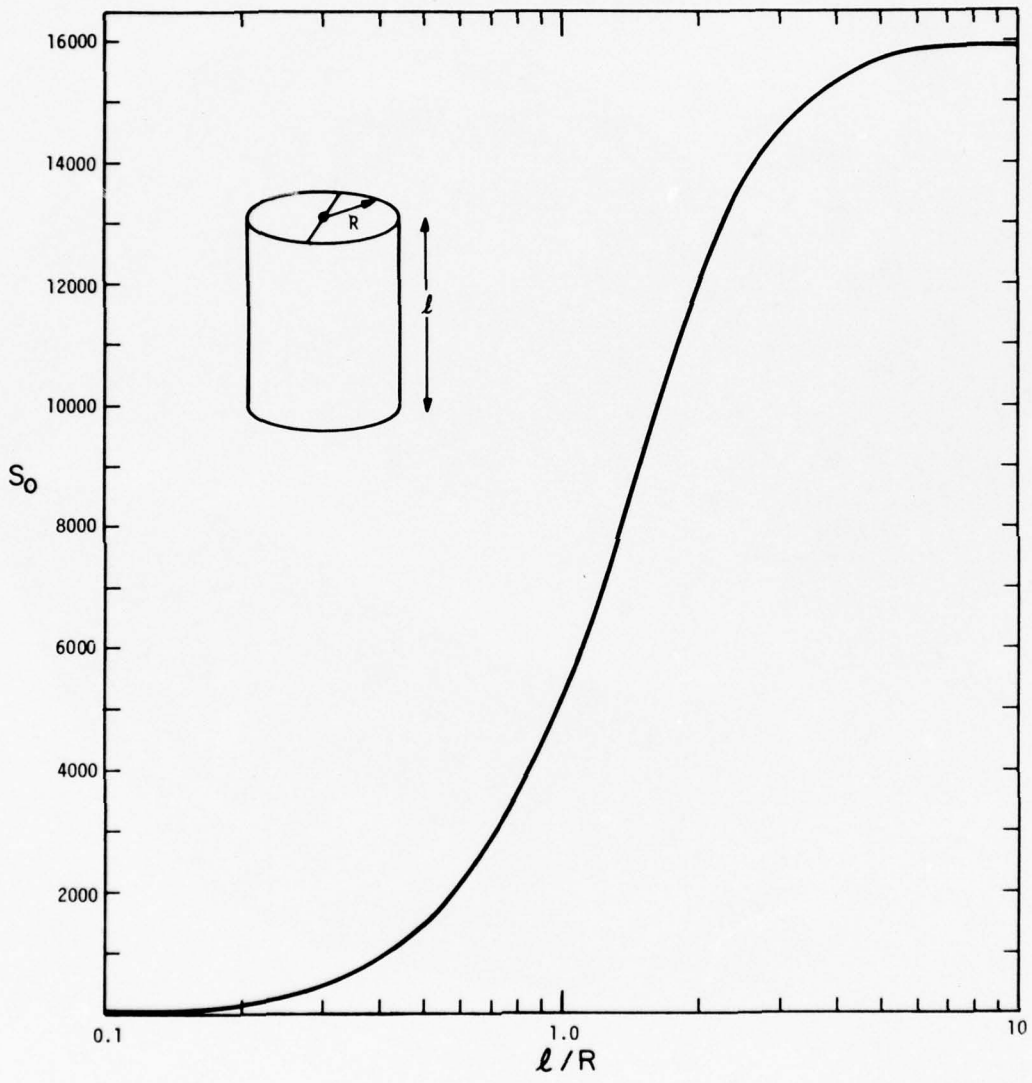


Fig. 8 S_o for TE_{111} Cylindrical Septum Maser Cavity

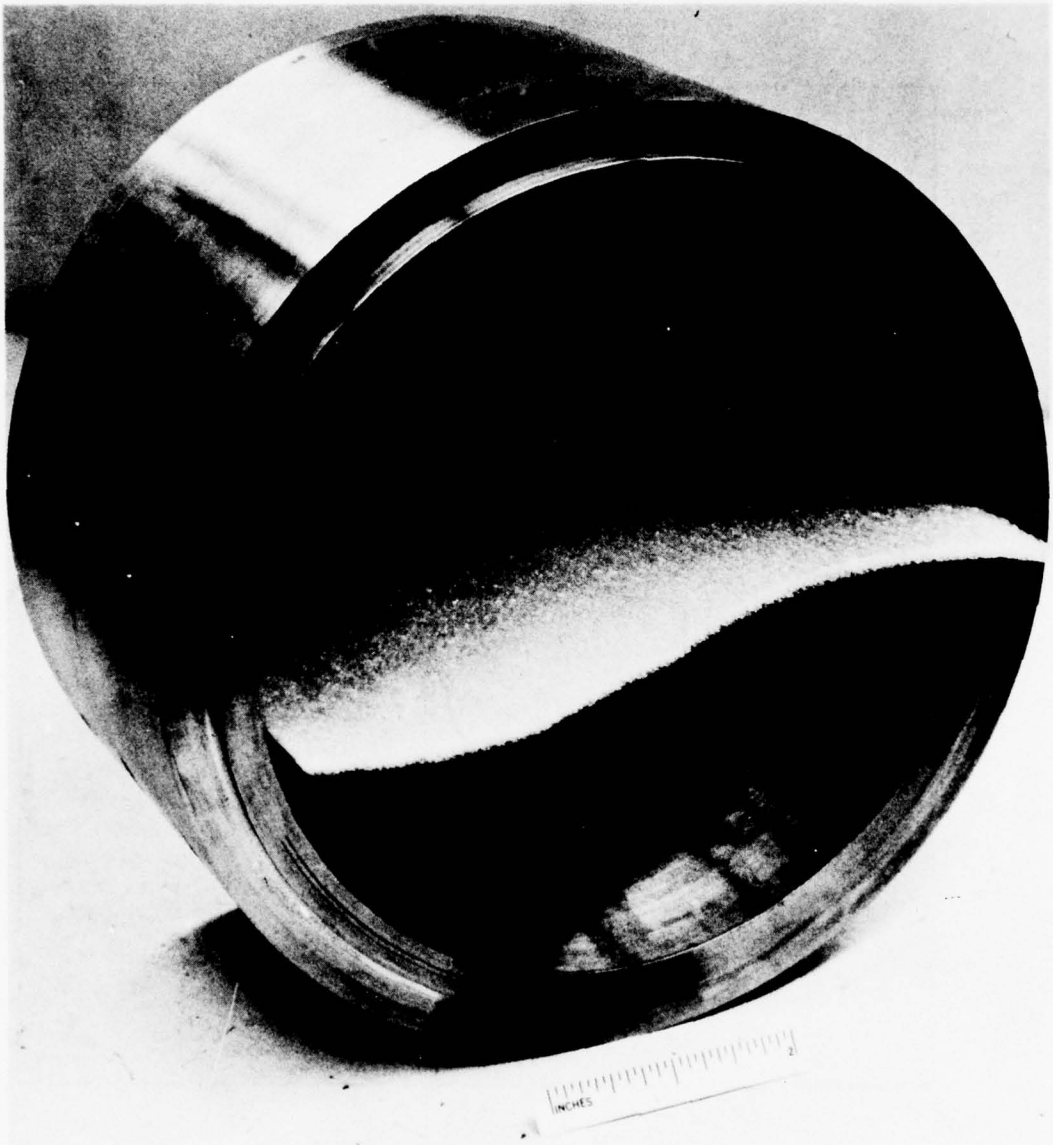


Fig. 9 Test Model of Cylindrical Septum Maser Cavity

V Maser for Space Applications

A conceptual design of a space maser is shown in Fig. 10. It is based on a cylindrical TE_{111} septum resonator, and uses cylindrical magnetic shields with rounded endcaps. We have measured the shielding factor $S_m = \frac{\Delta H \text{ ext}}{\Delta H \text{ int}}$ of such a shield, made of .036 cm (.014 inches) molypermalloy and found that S_m axial = 114, 37% greater than the axial shielding factor of a flat-ended shield of similar dimensions. The hydrogen source is a canister of lithium-aluminum hydride ($LiAlH_4$) whose output is regulated and purified by a heated palladium-silver diaphragm. Spent hydrogen is removed by three sorption pumps, while any residual gases are trapped by a small ion pump. Photodetectors monitor the light emitted by hydrogen atoms and molecules in the r.f. source discharge, permitting remote measurement of conditions in the discharge. (Many of these techniques have been developed for existing probe-rocket masers.) Power consumption is estimated at less than 25 watts. The maser is 58 cm (23 inches) long and 32 cm (12.5 inches) in diameter, with an estimated weight of 23 kg (50 lb).

Acknowledgement

We have recently learned from V. Reinhardt of independent work on a septum cavity by H. Peters and associates at Goddard Space Flight Center.

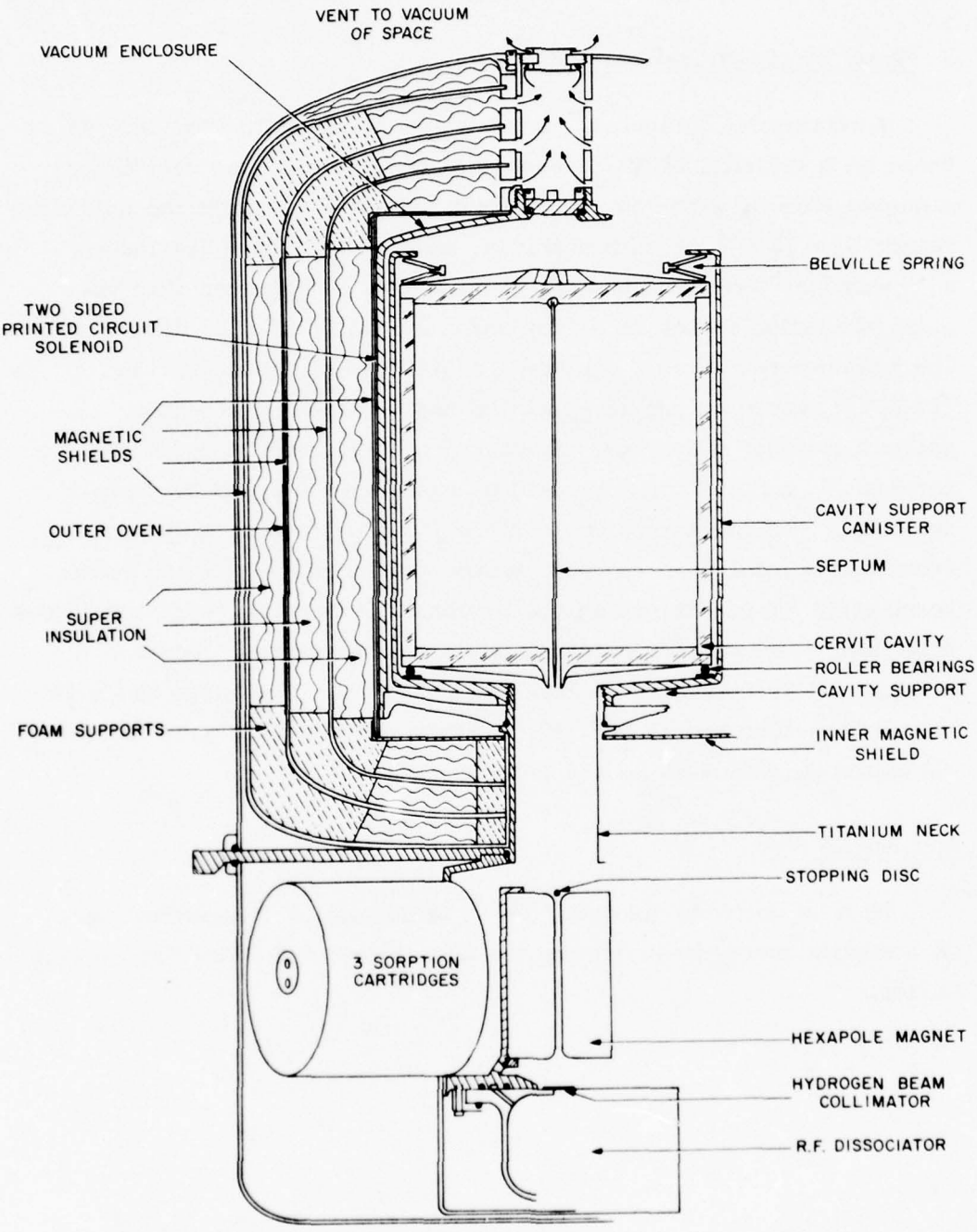


Fig. 10 Conceptual Design of Maser for Space Applications, Using TE_{111} Cylindrical Septum Cavity

References

* Work supported by U.S. Naval Research Laboratory, Contract N00014-71-A0110-0003.

1. Vessot, R.F.C., "Lectures on Frequency Stability and Clocks and on the Gravitational Redshift Experiment", in Experimental Gravitation, Proceedings of the International School of Physics "Enrico Fermi", B. Bertotti, ed. Academic Press, New York, 1974.

2. Repair of Government-Furnished Spherical Fused Quartz Hydrogen-Maser Cavity, Smithsonian Astrophysical Observatory, Cambridge, Mass., February 1971. U.S. Army Contract DAAB 07-70-C-A108.

3. Mattison, E. M., and R. F. C. Vessot, Evaluation of Dielectric-Loaded Maser Cavities, Smithsonian Astrophysical Observatory, Cambridge, Mass., April 1975. U.S. Navy Contract N00014-71-A-0110-0003.

4. Kleppner, D., H. C. Berg, S. B. Crampton, N. F. Ramsey, R. F. C. Vessot, H. E. Peters, and J. Vanier, "Hydrogen Maser Principles and Techniques", Phys. Rev. 138, 972 (1965).

5. Vanier, J., and R. F. C. Vessot, "Relaxation in the Level F = 1 of the Ground State of Hydrogen: Application to the Hydrogen Maser", IEEE J. Quant. Elect. QE-2, 391 (1966)

6. Vanier, J., and R. F. C. Vessot, Hydrogen Maser Research, Varian Associates, Beverley, Mass., February 1967. NASA Contract NAS8-2604 (Task K).

7. Adam, R. J., Thermal American Fused Quartz Company, Montville, N. J. Private communication.

8. Cogan, R. M., General Electric Company, Newton Upper Falls, Mass. Private communication.

9. Hellwig, H., R. McKnight, and E. Pannaci, in Conference Internationale de Chronometrie, Paris, August 1969.

QUESTION AND ANSWER PERIOD

DR. REDER:

Dr. Reder, Fort Monmouth.

Wouldn't the septum introduce vibration sensitivity?

DR. MATTlSON:

I don't believe it should. It would vibrate to a small extent, but it wouldn't change the frequency of the cavity to any great extent.

DR. REDER:

I must say the progress in this field is tremendous. Two years ago we talked about a walk-in maser.

MR. WARD:

Sam Ward, Jet Propulsion Lab.

What function do those roller bearings have?

DR. MATTISON:

Oh, that is also a means of isolating the cavity from any motion of the base support. In other words, the base can flex and those rollers take up any motion without causing flexure of the cavity base plate itself which would change the frequency of the cavity.

FREQUENCY STABILITY REQUIREMENTS FOR TWO WAY RANGE RATE TRACKING

Victor Reinhardt
NASA/Goddard Space Flight Center, Greenbelt, Maryland

ABSTRACT

Accuracy limitations to two way range rate doppler tracking due to master (reference) oscillator frequency instabilities are discussed. Theory is developed to treat both the effects of random and non-random oscillator instabilities. The non-random instabilities treated are drift, environmental effects, and coherent phase modulation. The effects of random instabilities on range rate accuracy are shown to be describable in terms of $\sigma_y(2, T, \tau)$. For the typical noise processes encountered in precision oscillators, range rate error is related to the more familiar $\sigma_y(\tau)$ and $\mathcal{L}(f)$. Three examples are discussed to show how to determine range rate error from given $\sigma_y(\tau)$ or $\mathcal{L}(f)$ curves, and approximations are developed to simplify the treatment of complex systems. An error analysis of range determined from range rate data is also given.

INTRODUCTION

Two way range rate doppler tracking (TWDT) is a means of measuring range rate by observing the doppler shift in a radio signal coherently transponded from a satellite. Recently proposed applications of TWDT to Earth and ocean physics have range rate accuracy requirements of 0.003 to 0.005 cm/sec.[1, 2] These stringent accuracy requirements impose constraints on TWDT systems which make careful analysis and minimization of system errors imperative. One source of error in TWDT systems is the instability of the master oscillator (reference oscillator). Others have analyzed the effects of this error source,[3, 4, 5] but have either not treated the problem in sufficient detail, made some errors in their analysis, or not treated the problem directly as it applies to TWDT systems for satellites. This paper will attempt to correct these defects. The paper will not discuss individual TWDT systems, but will take a generalized approach. Existing systems and requirements, however, will be kept in mind to ensure the utility of the paper's results.

PRECEDING PAGE BLANK-NOT FILMED

STATISTICS OF RANGE RATE ERROR

A generalized schematic of a TWDT system is shown in Figure 1. In a TWDT system, a reference frequency, f_0, provided by the master oscillator is transmitted to the satellite and transponded back to the receiver. The doppler shifted frequency, $f_0 + f_D$, is then mixed with f_0 to produce f_D. After passing through a band pass filter, f_D is measured in a frequency or period counter. In actual systems, f_D is biased by an arbitrary frequency[4] so that the doppler signal can be averaged over any time, T. The master oscillator also supplies the time base for the counter. The accuracy requirements for this are not stringent, and will not be treated here.

The counter used to measure f_D can fit into four possible categories.[4] The first two categories deal with the way individual measurements are taken. The

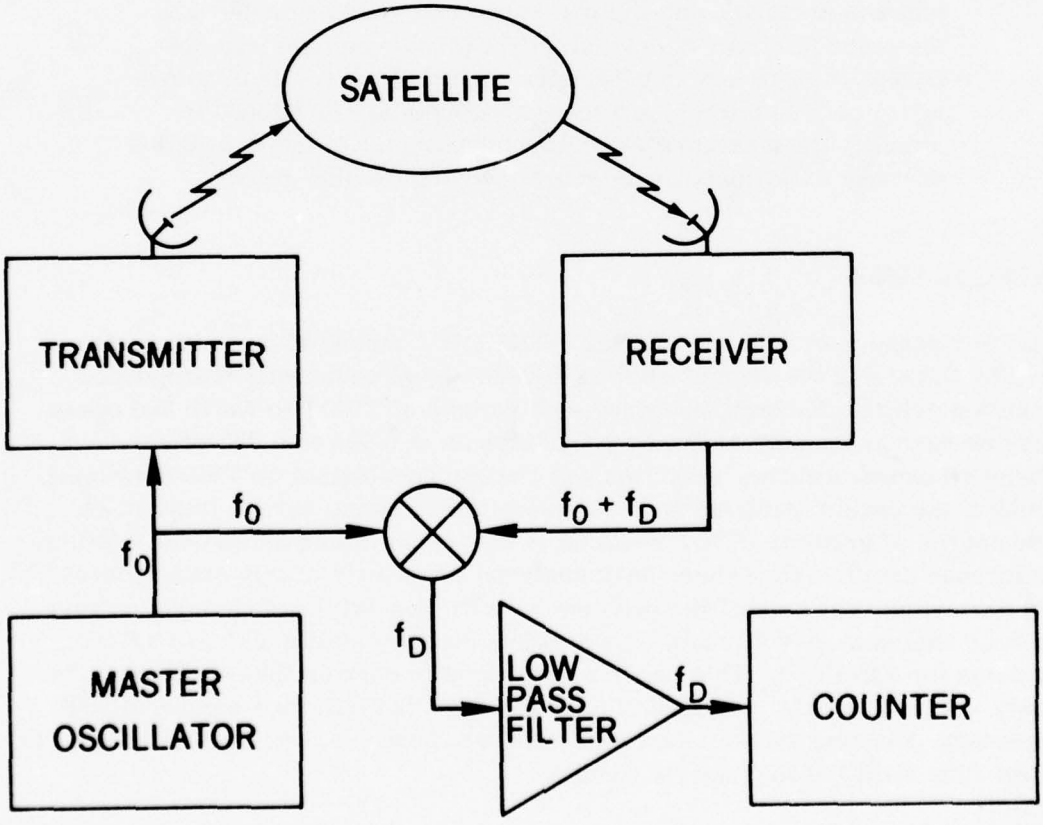


Fig. 1—Two way doppler tracking

counter can measure the total number of periods of f_D for a fixed elapsed time, T, or it can measure the total elapsed time for a fixed number of periods. In this paper, we shall consider T given; the results can be related to the fixed period case through an estimate of the behavior of f_D. The other two categories deal with the way in which successive measurements are treated. The counter is considered destructive or non-destructive depending on whether it is cleared or not cleared after each measurement. In the destructive case, the counter acts as a conventional period or frequency counter. In the non-destructive case, the counter acts as a real time clock. The effects of destructive versus non-destructive data taking will be discussed later.

Nominally, when f_0 is subtracted from $f_0 + f_D$, all that remains is f_D. The tracking signal, however, takes a finite time, τ, to propagate from the transmitter to the receiver. If the frequency of the master oscillator shifts, in time τ, by δf_0, the counter will measure $f_D + \delta f_0$ as the doppler shift. Since there is no way to distinguish between f_D and δf_0 in the counter, δf_0 will introduce a range rate error.

No matter how frequencies are coherently changed as signals propagate through the TWDT system, the doppler shift will be given by[6]:

$$\frac{f_D}{f_0} = \frac{2v}{c} \tag{1}$$

where v is the satellite's range rate and where c is the velocity of light. Using (1), it can be shown that the range rate error from master oscillator instability for averaging time, T, is given by:

$$\delta v(t, T, \tau) = \frac{c}{2T}\left[\int_{t+\tau}^{t+T+\tau} y(t')\,dt' - \int_{t}^{t+T} y(t')\,dt'\right] \tag{2}$$

y(t) is the normalized master oscillator frequency change:

$$y(t) = \frac{f_0(t) - f_0}{f_0}$$

and f_0 is the nominal oscillator frequency. For $\tau < T$, this can be rewritten as (see Figure 2):

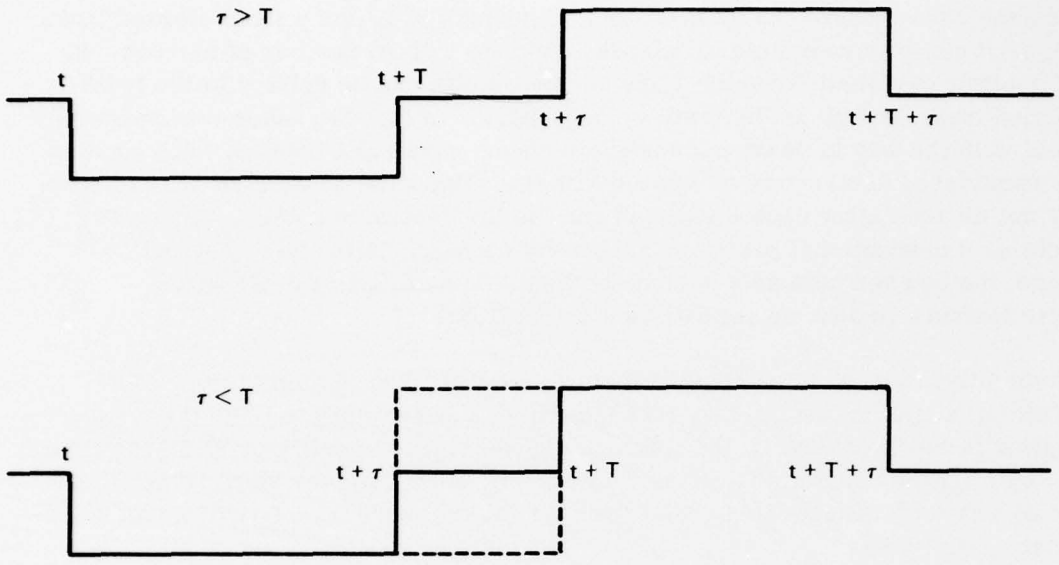


Fig. 2—Response functions for range rate error

$(\tau < T)$

$$\delta v(t, T, \tau) = \frac{c}{2T}\left[\int_{t+T}^{t+\tau+T} y(t')\,dt' - \int_{t}^{t+\tau} y(t')\,dt'\right] \tag{3}$$

If the master oscillator instabilities are random, range rate errors can be described in terms of the variance of $\delta v(t, T, \tau)$:

$$\sigma_v^2(T, \tau) = \left\langle \left(\delta v(t, T, \tau)\right)^2 \right\rangle.$$

<A> denotes the average of A over time, t. Using equation 3, for $\tau < T$, the variance becomes:

$(\tau < T)$

$$\sigma_v^2 = \frac{c^2}{2}\left(\frac{\tau}{T}\right)^2 \sigma_y^2(2, T, \tau) \tag{4}$$

where $\sigma_y^2(2, t_1, t_2)$ is the two sample Allan variance of y(t) for averaging time t_2 and dead time $t_1 - t_2$ given by[7,8]:

$$\sigma_y^2(2, t_1, t_2) = \frac{1}{2} \left\langle \left(\int_t^{t+t_2} y(t')\, dt' - \int_{t+t_1}^{t+t_1+t_2} y(t')\, dt' \right)^2 \right\rangle$$

For $\tau \geq T$, the variance is:

$$(\tau \geq T)$$

$$\sigma_v^2 = \frac{c^2}{2}\, \sigma_y^2(2, \tau, T) \tag{5}$$

Notice that in the case of (5), the definitions of τ and T are reversed from those of references 7 and 8.

In general, $\sigma_y^2(2, T, \tau)$ is not a statistic which is given in oscillator specifications. In the time domain, generally, $\sigma_y^2(\tau) \equiv \sigma_y^2(2, \tau, \tau)$ is what is specified. One can relate these two statistics by[7,8]:

$$\sigma_y^2(2, T, \tau) = B_2(r, \mu)\, \sigma_y^2(\tau) \tag{6}$$

where $r = T/\tau$, and where μ characterizes the noise process involved.

Another typical way in which an oscillator is specified is by $\mathcal{L}(f)$, the power density in one phase modulation side band divided by the total oscillator power.[8] $\mathcal{L}(f)$ can be related to $\sigma_y^2(2, T, \tau)$ by[8]:

$$\sigma_y^2(2, T, \tau) = \frac{4}{(\pi f_0 \tau)^2} \int_0^\infty df\, \mathcal{L}(f) \left| h_\rho(f) \right|^2 H(f) \tag{7}$$

where $h_\rho(f - f_D)$ is the frequency response function of the post mixer filter of Figure 1, and where:

$$H(f) = \sin^2(\pi f \tau)\, \sin^2(\pi f T)$$

TYPICAL OSCILLATOR INSTABILITIES

Master oscillator frequency instabilities can be divided into two classes, random and non-random effects. We shall first consider two non-random effects, frequency drift and coherent phase modulation.

An oscillator's frequency drift is defined by:

$$y(t) = Dt$$

Using this and equations 2 and 3, one can show that for both $\tau < T$ and $\tau \geq T$:

$$\delta v = \frac{c D}{2} \tau \tag{8}$$

If we use $\delta v = 0.001$ cm/sec as a target error and $\tau = 0.3$ sec as a typical worst case delay, we obtain for D a maximum allowable value of:

$$D = 1.92 \times 10^{-8} / \text{day}$$

Clearly this is easily met with most good crystal oscillators.

Equation 8 can also be used to determine environmental constraints if the frequency change per unit environmental change is known. If, for example, an oscillator changes its fractional frequency by 1×10^{-12} per °C, and $\delta v \leq 0.001$ cm/sec is required, one can write:

$$D = 1 \times 10^{-12} / {}^{\circ}\text{C} \times K \left({}^{\circ}\text{C} / \text{sec} \right)$$

Using equation 8, we obtain:

$$K \leq 0.22 \ {}^{\circ}\text{C} / \text{sec}$$

How coherent phase modulation of the master oscillator effects a TWDT system depends not only on the modulation amplitude and frequency, but also on the precise phase relationships between the modulation and the data taking process.

We can, however, obtain approximate results by ignoring phase, and describing the modulation by:

$$\mathcal{S}_M(f) = \frac{1}{2} P_M \delta(f - f_M)$$

where f_M is the modulation frequency, and where $1/2\ P_M$ is the fractional power in one modulation sideband. Using this in (7), we obtain:

$$\sigma_y^2(2, T, \tau) = \frac{2 P_M}{(\pi f_0 \tau)^2} |h_\ell(f_M)|^2 H(f_M)$$

Since $H(f) \leq 1$, we obtain the inequality:

$$\sigma_y^2(2, T, \tau) \leq \frac{2 P_M}{(\pi f_0 \tau)^2} |h_\ell(f_M)|^2$$

Substituting this in (4) and (5), gives:

$(\tau < T)$

$$\sigma_v^2 \leq \frac{c^2}{(\pi f_0 T)^2} |h_\ell(f_M)|^2 P_M \tag{9}$$

and:

$(\tau \geq T)$

$$\sigma_v^2 \leq \frac{c^2}{(\pi f_0 \tau)^2} |h_\ell(f_M)|^2 P_M \tag{10}$$

As an example, let $\sigma_v = 0.001$ cm/sec, $\tau = 0.3$ sec, $T = 5$ sec, and $f_0 = 5$ M Hz. We obtain:

$$|h_\ell(f_M)|^2 P_M \simeq -112 \text{ db}$$

as the estimated upper limit of filtered phase modulation that can be tolerated.

Random processes typically encountered in precision oscillators can be described as weighted and filtered sums of power spectral densities of y(t) given by[7,8]:

$$S_y(f) = \frac{h_\alpha}{f^\alpha}$$

with:

$$\alpha = 2, 1, 0, -1, -2$$

$S_y(f)$ can be related to $\mathcal{L}(f)$ by[8]:

$$\mathcal{L}(f) = \frac{1}{2}\left(\frac{f_0}{f}\right)^2 S_y(f) \qquad (10)$$

Using (10), (4), (5), and previously derived equations relating $\sigma_y^2(\tau)$ and $\sigma_y^2(2, T, \tau)$ for each noise process,[9] one can relate $\mathcal{L}(f)$, $\sigma_y(\tau)$ and $\sigma_v^2(T, \tau)$. Chart 1 gives these relationships. The chart assumes that the post-mixer band pass filter is infinitely sharp with a pass band of $f_D - f_h$ to $f_D + f_h$, that $2\pi f_h \tau >> 1$, and that $2\pi f_h T >> 1$. For completeness, drift is included even though it is not a random process. To simplify formulae in the chart, the following are used:

$$r = \frac{T}{\tau}$$

$$x = \int y\,dt = \frac{\text{phase}}{2\pi f_0}$$

$$\delta_{r,1} = \begin{cases} 1 \text{ for } r = 1 \\ 0 \text{ for } r \neq 0 \end{cases}$$

Chart 1—Range Rate Error for Various Noise Processes

Process	$\mathcal{L}(f)$	$\sigma_y^2(\tau)$	$r = \frac{T}{\tau}$ $\delta_{r,1} = \begin{cases} 1 & r = 1 \\ 0 & r \neq 1 \end{cases}$ $\sigma_v^2(T, \tau)$
White x $Sy = h_2 f^2$	$\frac{h_2 f_0^2}{2}$	$\frac{3 h_2 f_h}{(2\pi\tau)^2}$	$\frac{h_2 f_h c^2 \left(1 + \frac{1}{2}\delta_{r,1}\right)}{(2\pi T)^2}$
Flicker x $Sy = h_1 f$	$\frac{h_1 f_0^2}{2f}$	$\frac{h_1}{(2\pi\tau)^2}\left[\frac{9}{2} - \ln 2 + \ln(2\pi f_h \tau)\right]$	$\frac{h_1 c^2}{(2\pi T)^2}\left[\frac{3}{2} + \ln(2\pi f_h \tau)\right]$ $r \gg 1$ $\frac{h_1 c^2}{(2\pi T)^2}\left[\frac{3}{2} + \ln(2\pi f_h T)\right]$ $r \ll 1$
White y $Sy = h_0$	$\frac{h_0 f_0^2}{2f^2}$	$\frac{h_0}{2\tau}$	$\frac{h_0 c^2 \tau}{4T^2}$ $r > 1$ $\frac{h_0 c^2}{4T}$ $r \leq 1$
Flicker y $Sy = \frac{h_{-1}}{f}$	$\frac{h_{-1} f_0^2}{2f^3}$	$h_{-1} 2 \ln 2$	$r \geq 1$: $\frac{h_{-1} c^2 \tau^2}{4T^2}\left[(r+1)^2 \ln(r+1) + (r-1)^2 \ln\lvert r-1\rvert - 2r^2 \ln r\right]$ $r < 1$: $\frac{h_{-1} c^2}{4}\left[\left(1 + \frac{1}{r}\right)^2 \ln\left(1 + \frac{1}{r}\right) + \left(1 - \frac{1}{r}\right)^2 \ln\left\lvert 1 - \frac{1}{r}\right\rvert + \frac{2}{r^2} \ln r\right]$
Random walk y $Sy = \frac{h_{-2}}{f^2}$	$\frac{h_{-2} f_0^2}{2f^4}$	$\frac{1}{6} h_{-2} (2\pi)^2 \tau$	$\frac{h_{-2}(\pi c)^2 \tau^3}{6T}\left[3r - 1\right]$ $r \geq 1$ $\frac{h_{-2}(\pi c)^2 T}{6}\left[\frac{3}{r} - 1\right]$ $r < 1$
Drift	———	$\frac{D^2 \tau^2}{2}$	$\left(\frac{c D \tau}{2}\right)^2$

Notice that for all processes but random walk y and drift, when $\tau < T$, σ_v^2 is proportional to T^{-2}. By statistically averaging N successively taken counter readings, one improves the variance of the average by N^{-1} or T^{-1}. This means that as long as random walk y or drift processes are not involved, smaller errors are obtained by going to longer averaging times or taking non-destructive data rather than by statistically averaging data. Even when taking non-destructive data, to obtain the smallest σ_v^2 for a given T, one should only use data every T seconds apart, and not least squares fit the data from smaller time intervals.

Notice also that for white x noise, σ_v^2 is proportional to f_h. This allows one to reduce the white noise contribution to σ_v^2 by reducing f_h. Flicker x also depends on f_h, but in such a slowly varying manner that it can essentially be considered fixed.

APPLICATION TO TYPICAL REFERENCE OSCILLATORS

In this section, $\sigma_v(T, \tau)$ shall be derived for three reference oscillators, an Oscilloquartz crystal oscillator, a Hewlett-Packard cesium standard, and a NASA hydrogen maser, to demonstrate techniques for using the theory of the previous sections. The results for the two commercial oscillators used are based on manufacturers specifications. Their use is for the purpose of example only, and does not constitute an endorsement of these products or a confirmation of their specifications.

The first oscillator we will consider is the Oscilloquartz B-5400 crystal oscillator.[10] Its $\mathcal{L}(f)$ spectrum is given in Figure 3 and its $\sigma_y(\tau)$ curve is given in Figure 4. Deriving σ_v for this device is very simple; since its instabilities are just the sum of simple processes (white y, flicker x, flicker y, drift), σ_v^2 is just the sum of the results taken from Chart 1 for each process. Figure 5 shows $\sigma_v(T, \tau)$ for $\tau = 0.3$ s.

The second oscillator to be considered is the Hewlett-Packard 5061A High Performance Cesium Beam Standard.[11] $\mathcal{L}(f)$ for this device is shown in Figure 6. Notice that, in this case, we don't have just the sum of simple processes. Equation 7 could be used to generate σ_v^2 from $\mathcal{L}(f)$, but this tedious method can be avoided; we can quickly obtain an approximate curve for $\sigma_v(T, \tau)$ by using the limiting properties of $H(f)$ in relation to $\mathcal{L}(f)$.

For our approximation, we shall rely on the fact that $\mathcal{L}(f)$ can be broken in two general categories: a short term $\mathcal{L}_s(f)$ which changes slowly with f, and a long term $\mathcal{L}_\ell(f)$ which blows up as f goes to zero and makes a negligible contribution for large f. Using this, we can write:

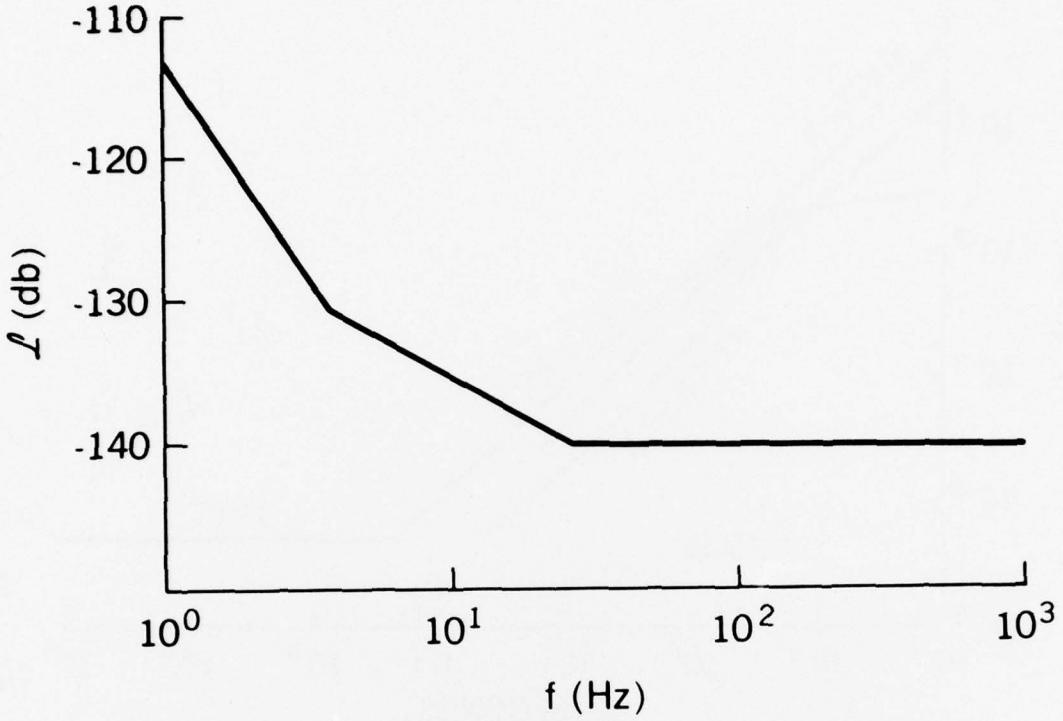


Fig. 3—ℒ(f) for Oscilloquartz B-5400

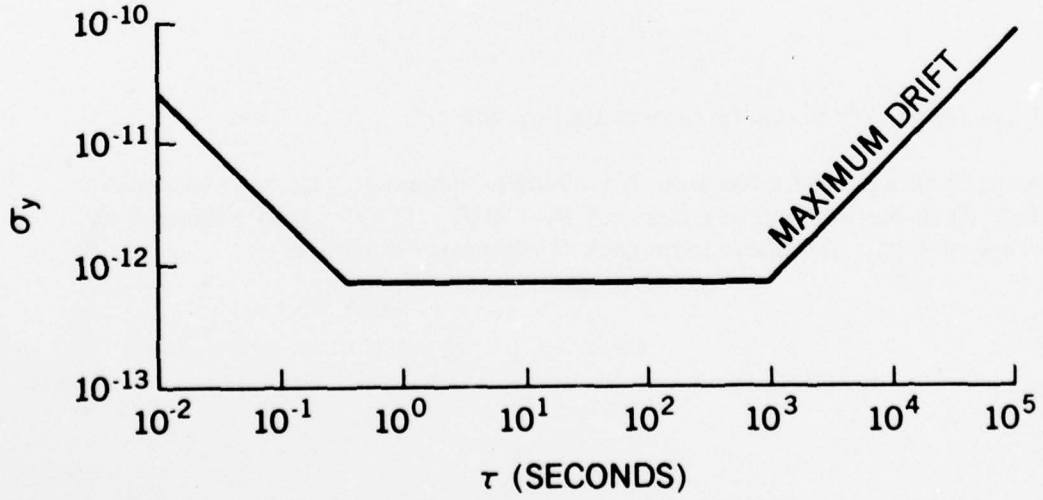


Fig. 4—$\sigma_y(\tau)$ for Oscilloquartz B-5400

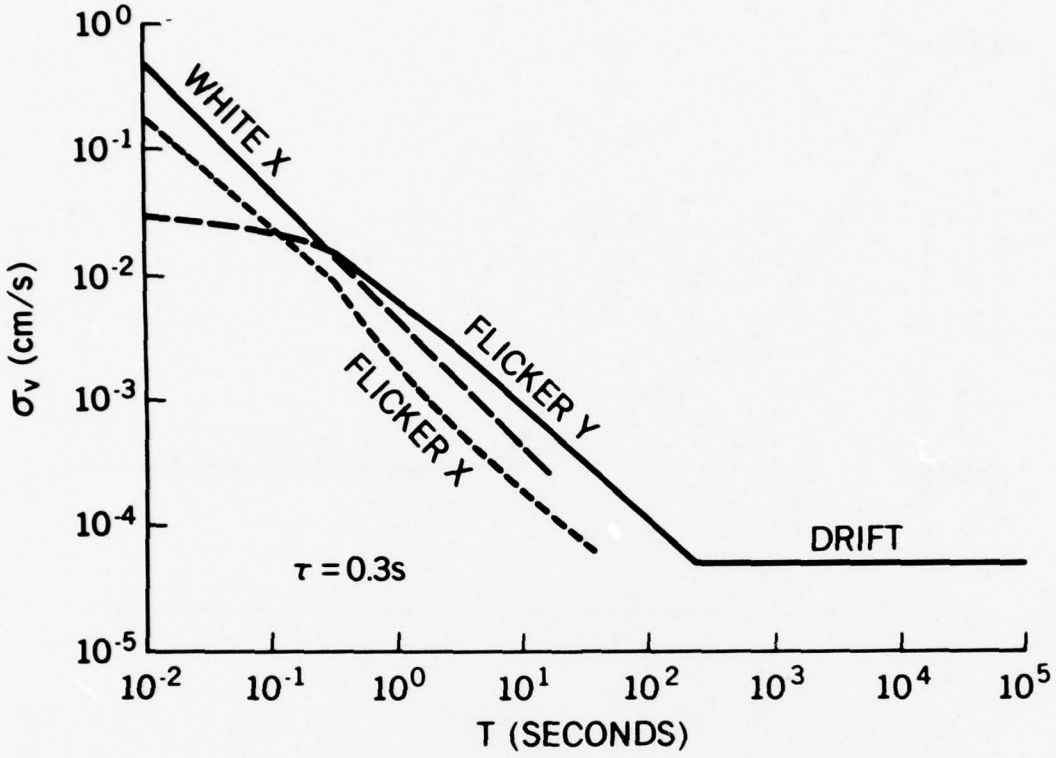


Fig. 5—σ_v (T, 0.3 s) for Oscilloquartz B-5400

$$\sigma_y^2(2, T, \tau) \simeq \sigma_{ys}^2 + \sigma_{y\ell}^2$$

and use (4) and (5) to obtain approximations for σ_v^2.

Since H(f) is a periodic function, for a slowly changing $\mathcal{L}_s(f)$, we can replace H(f) $\mathcal{L}_s(f)$ in the integral of equation 7 by $< H(f) > \mathcal{L}_s(f)$. $< H(f) >$ denotes the average of H(f). The short term part of equation 7 becomes:

$$\sigma_{ys}^2(2, T, \tau) = \frac{1 + \frac{1}{2}\delta_{r,1}}{(\pi f_0 \tau)^2} \int_0^\infty |h_\ell(f)|^2 \mathcal{L}(f)\, df \qquad (11)$$

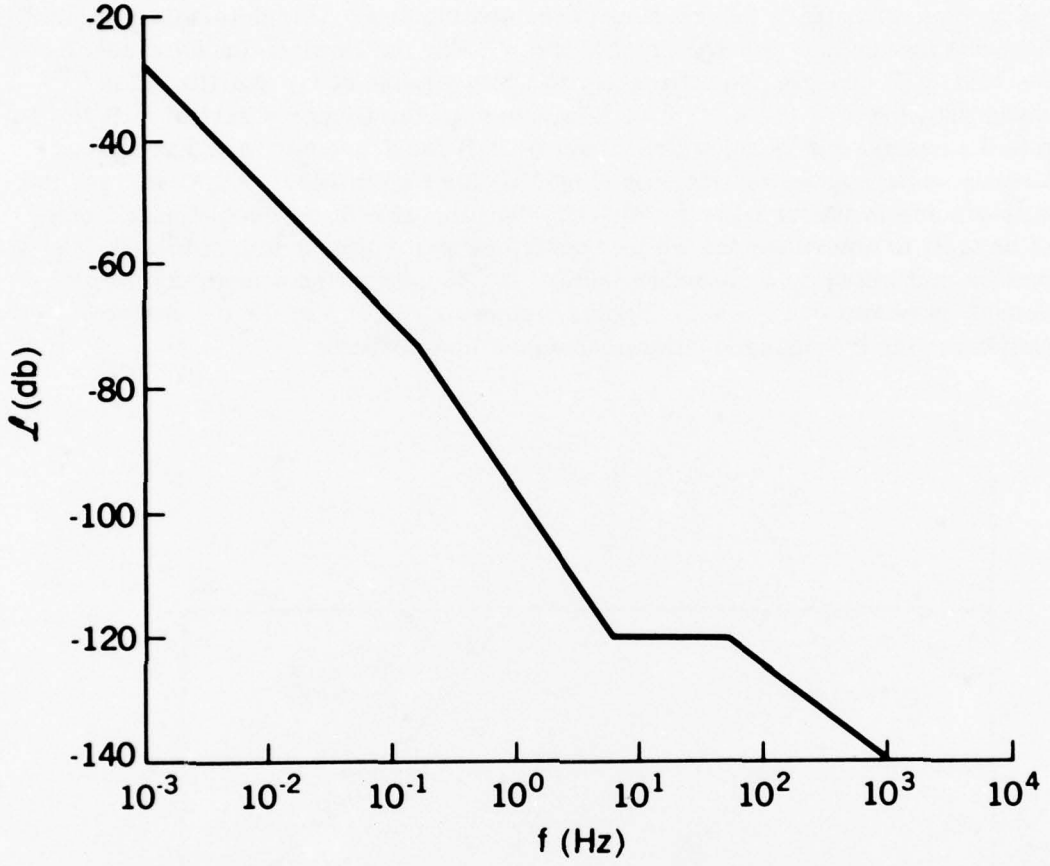


Fig. 6—$\mathfrak{L}(f)$ for Hewlett-Packard High Performance Cesium Standard

The long term part of $\sigma_y^2(2, T, \tau)$ is determined by $H(f)\ \mathfrak{L}_\ell(f)$ in a region near $f = 0$. For long term noise processes, $\sigma_y^2(2, T, \tau)$ is determined by $H(f)\ \mathfrak{L}_\ell(f)$ in the regions of f given in the following chart ($\tau < T$):

noise process	region of contribution
white y	$\frac{1}{2T} \lesssim f \lesssim \frac{1}{2\tau}$
flicker y	$f \simeq \frac{1}{2T}$
random walk y	$f \lesssim \frac{1}{2T}$

For a complex $\mathcal{L}_\ell$ (f), which noise process contributes $\sigma_{y\ell}^2$ is determined by the chart and the appropriate values of T and τ. For the Hewlett-Packard cesium standard, $\mathcal{L}$ (f) changes from flicker y to white y noise at f = 0.1 Hz. This means that, for τ = 0.3 s, $\sigma_{y\ell}^2$ is determined by the flicker y part of $\mathcal{L}$(f) for T up to 5 seconds, and by the white y part of $\mathcal{L}$(f) for T greater than 5 seconds. Because white y noise is determined by $\mathcal{L}$(f) for f up to $1/2\tau$ = 1.67 Hz, and the white y noise is truncated at f = 0.1 Hz, the full value of σ_v^2 from Chart 1 cannot be used to determine the white y contribution for the cesium standard, but must be multiplied by a reduction factor, ρ. An approximate method for calculating ρ is shown in Figure 7. Figure 8 shows σ_v(T, 0.3 s) for the cesium standard using the approximation techniques just derived.

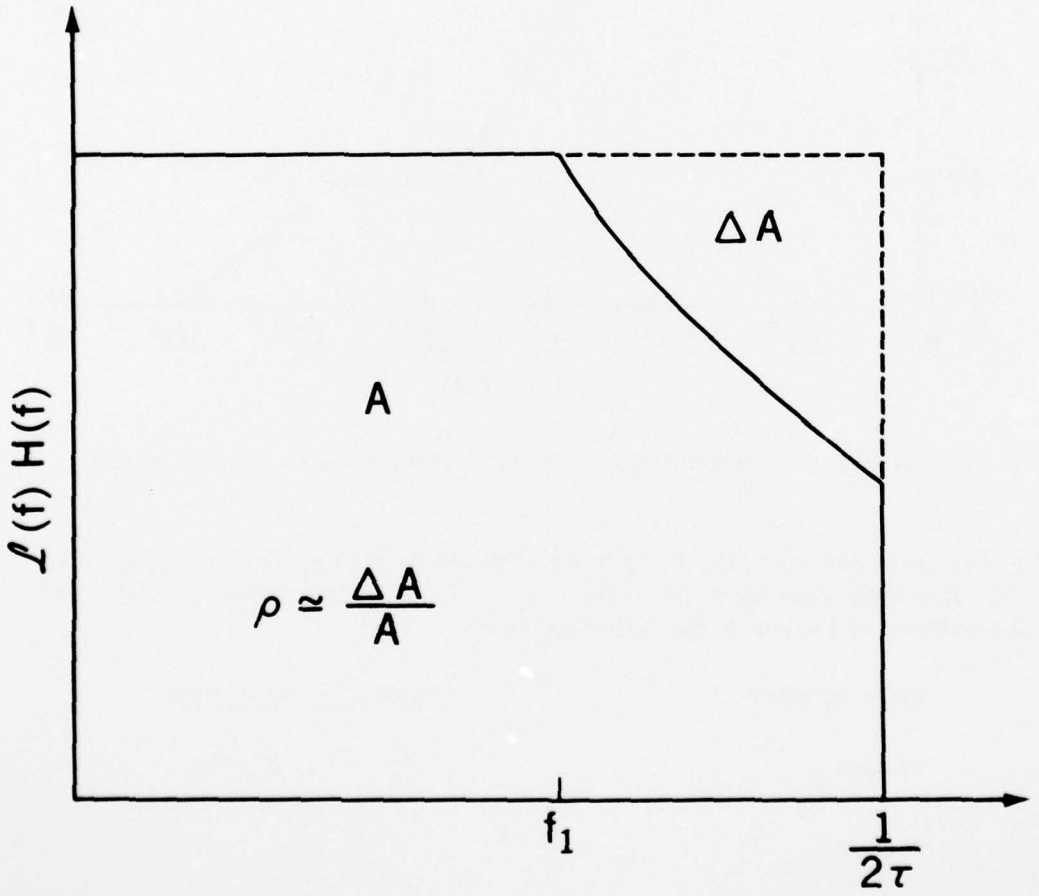


Fig. 7— Approximate calculation of ρ

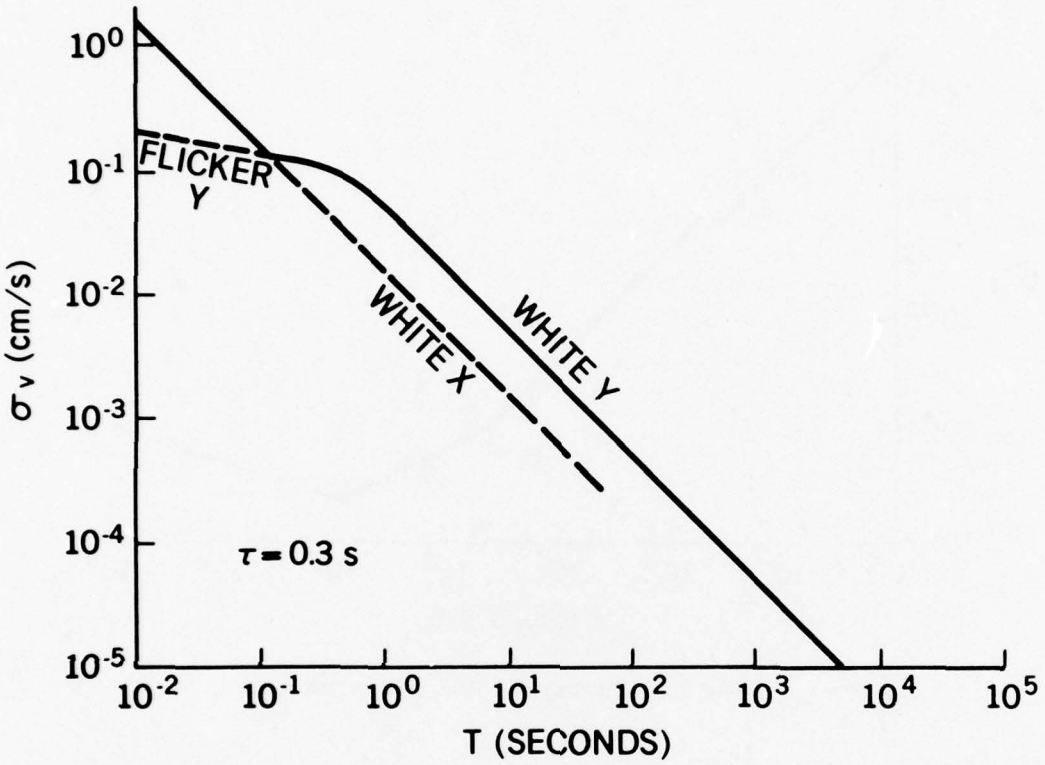


Fig. 8—σ_v(T, 0.3 s) for Hewlett-Packard High Performance Cesium Standard

The last device we will consider is NASA's latest generation hydrogen maser. The $\sigma_y(\tau)$ curve is shown in Figure 9. The device uses an Oscilloquartz B-5400 as a local oscillator which it phase locks to the maser with a 1 Hz loop. Using this fact and Figure 9, by indirectly using (11), we can calculate the white x noise contribution to σ_v^2 with a 1 KHz band width as the sum of the oscilloquartz contribution with a 1 KHz bandwidth and the maser's contribution with a 1 Hz bandwidth. In this case, the other noise processes make a negligible contribution. σ_v(T, 0.3 sec) is shown in Figure 10. Even though σ_v is determined by white x noise, σ_v cannot be appreciably reduced by reducing f_h; σ_v is determined principally by the maser white x noise in the 1 Hz loop bandwidth.

RANGE FROM RANGE RATE

Integrating f_D yields the integral of range rate: range. Since the averaging process involves integration, not dividing the information stored in the counter

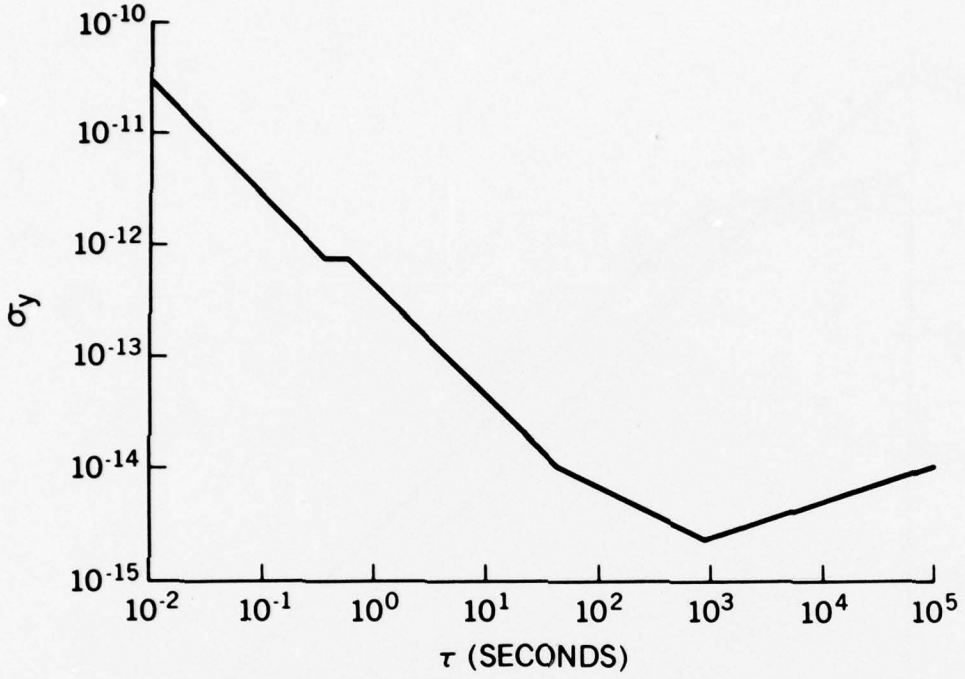


Fig. 9—$\sigma_y(\tau)$ for non-autotuned NASA hydrogen maser

register by T turns range rate data into range data. This means that the error in taking range data produced by the master oscillator is just:

$$\delta s(t, T, \tau) = T \delta v(t, T, \tau)$$

Similarly, this also means for random processes:

$$\sigma_s^2(T, \tau) = T^2 \sigma_v^2(T, \tau).$$

For the three sample oscillators, Figure 11 shows $\sigma_s(T, 0.3\ s)$. Notice again that taking non-destructive data instead of destructive data will yield better results in all cases but that of the crystal oscillator for T greater than 400 seconds.

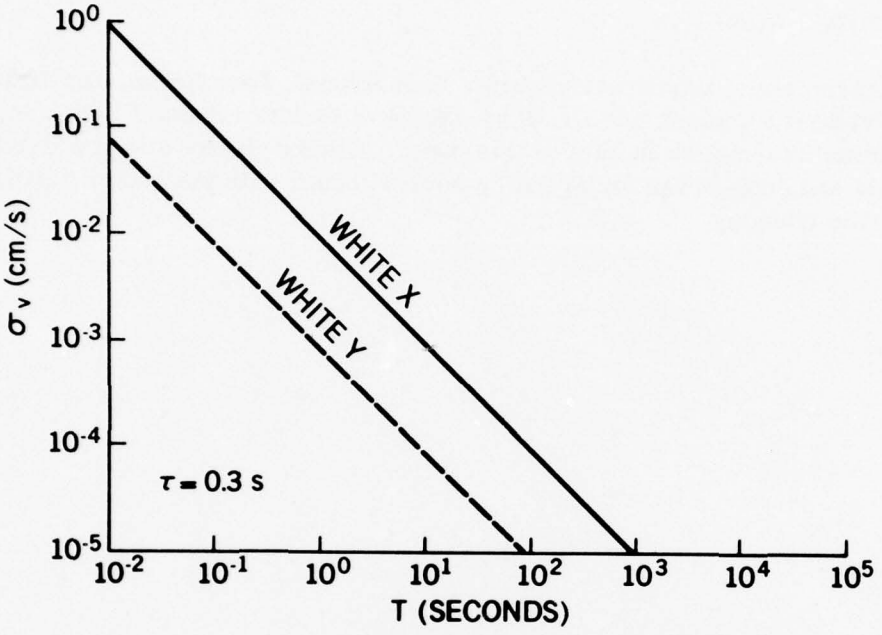


Fig. 10—σ_v(T, 0.3 s) for NASA hydrogen maser

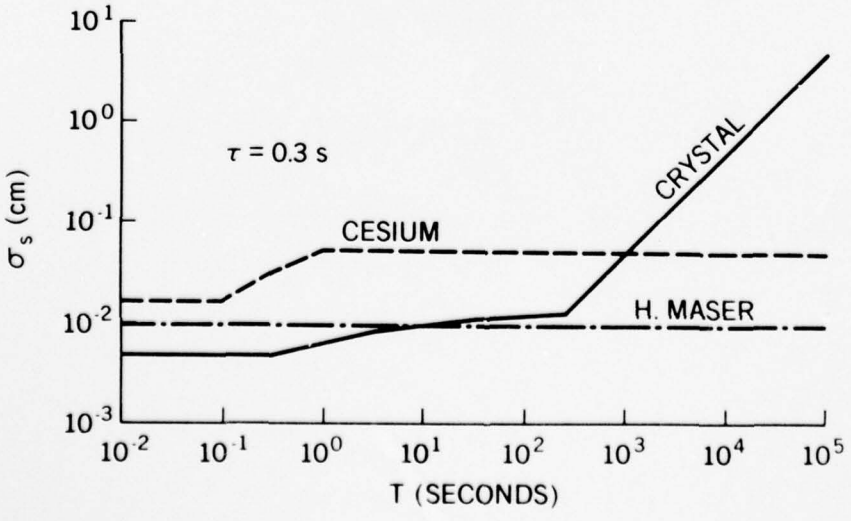


Fig. 11—σ_s(T, 0.3 s) for three master oscillators

ACKNOWLEDGMENTS

The author would like to acknowledge Paul Schmid, John Bryan, Jim Bradford, Dr. Friedrick Vonbun, and Dr. John Marini of Goddard Space Flight Center for providing information helpful to this paper. Special thanks are in order to Paul Schmid and John Bryan for spending several hours with the author discussing rate rate tracking.

AD-A040 774 NATIONAL AERONAUTICS AND SPACE ADMINISTRATION GREENB--ETC F/G 14/2
PROCEEDINGS OF THE ANNUAL PRECISE TIME AND TIME INTERVAL (PTTI)--ETC(U)
DEC 75

UNCLASSIFIED NASA-GSFC-X-814-76-45 NL

4 OF 8
ADA040774



REFERENCES

1. NASA Internal Report, "Earth and Ocean Physics Applications Program" V. II, (September, 1972).

2. Massachusetts Institute of Technology, "The Terrestrial Environment: Solid-Earth and Ocean Physics," NASA Contractor Report CR-1579, NTIS N70-26126-132 (April, 1970).

3. R. S. Raven, "Requirements on Master Oscillators for Coherent Radar," Proc. IEEE 54 p. 237 (1966).

4. C. A. Filippi, "Radio Tracking System Study for the GEOPAUSE Spacecraft," Magnavox Co. Report ASAO-PR20044-1 (November, 1973).

5. F. O. Von Bun, "Time and Frequency Requirements for the Earth and Ocean Physics Applications Program," Proceedings of the 6th NASA/DOD PTTI Conference (1974).

6. B. Kruger, "The Doppler Equation in Range and Range Rate Measurement," NASA Document X-507-65-385 (October, 1965).

7. J. A. Barnes, et al., "Characterization of Frequency Stability," IEEE Trans. IM-20, p. 105 (1971).

8. B. E. Blair, ed., Time and Frequency: Theory and Fundamentals, NBS Monograph 140, CODEN: NBSMA6, U.S. Superintendent of Documents, Catalogue # C13.44:140, Ch. 8 (1974).

9. Both references 7 and 8 contain the relationships between $\sigma_y^2(\tau)$ and $\sigma_y^2(2, T, \tau)$. However, reference 7 has some errors which have been corrected in reference 8, so only reference 8 has been used to calculate the values given in Table 1.

10. Oscilloquartz S. A. CH-2002 Neuchatel 2, Suisse.

11. Hewlett-Packard Co. 1501 Page Mill Road, Palo Alto, California 94304.

QUESTION AND ANSWER PERIOD

MR. ALLAN:

One might suppose that the 60 hertz side bands will always plague us. One approach that we are going to take, haven't yet, is using for instruments that are displaced a long ways is optical fibers to connect the RF signals.

DR. REINHARDT:

Yes, I think that is a very good idea. I think that we are investigating that at NASA also, as a means for transmitting signals for longer distances.

HIGH PRECISION TIME TRANSFERS IN THE FIELD

W. J. Klepczynski
U.S. Naval Observatory

ABSTRACT

During May-July 1975, the Naval Observatory aided the Applied Physics Laboratory of the Johns Hopkins University in a program (under contract to the U. S. Air Force and Defense Advanced Research Projects Agency) to improve the accuracy and precision of the Loran-C navigation system. One phase of this program consisted in accurately measuring the path delay undergone by a Loran-C signal between ten pairs of points. Each pair of points consisted of a fixed site located on the grounds of the Naval Observatory and one of ten remote sites located within a radius of 800 miles of the Naval Observatory and also along a ray path to one of the following three East Coast Loran-C transmitters - Carolina Beach, Nantucket and Dana.

The Naval Observatory's function in the program was to perform time transfers between the fixed site and each of the ten remote sites when data were recorded at a remote site.

Eleven time transfers were performed during the time period. The average length of a portable clock trip was about eight hours. Analysis indicated that the probable error of any one time transfer was ± 27 ns for the remote sites and ± 11 ns for the fixed site. Thus, the two clocks could be synchronized with a probable error of ± 29 ns.

INTRODUCTION

During May-July, 1975, the Applied Physics Laboratory (APL) conducted a number of field measurements in conjunction with an experiment attempting to improve the navigation capability of the Loran-C system. One aspect of the field measurements was to accurately measure the path delay undergone by a Loran-C signal as it passed between two points.

The experiment involved two sets of identical precision measuring equipment. One set was located at the U. S. Naval Observatory (USNO). The other set was located in a mobile van and moved sequentially to ten different sites located on ray paths from Loran-C transmitters through USNO. The sites were within an 800 mile radius of the USNO. Precise geodetic coordinates for the ten sites were determined by the DMA Topographic Center using TRANSIT.

The USNO's function in the program was to perform time transfers (synchronize the clocks) between the fixed site (USNO) and each of the ten remote sites when data were being recorded at a remote site. Knowing the distance between each site and the propagation time as measured by the instant of reception of the same pulse at the fixed and remote sites, one could measure the difference between the predicted and the observed travel time of the signal.

In this paper, a simple and straightforward method of evaluating the precision of measurement of a clock difference is presented. The use of a more sophisticated method was obviated by the performance of the portable clock during the trips as will be discussed later.

It is believed that the results presented here reflect the precision with which time transfers in the field can presently be performed with state-of-the-art equipment, with little or no special care and/or preparation.

OPERATIONAL PROCEDURE

Three HP 5061 Cesium Beam Frequency Standards, all with option 004 (High Performance Cesium Beam Tube), were used for the experiment. They were designated as follows:

a. PC - Cesium Clock 787 used as the portable clock;
b. FIX - Cesium Clock 871 located at the fixed site on the grounds of USNO;
c. VAN - Cesium Clock 862 located in the mobile van.

In order to minimize the handling of PC during the field trips, it was decided to charter a small single engine plane (Piper Cherokee) out of Dulles International Airport for transport of the PC. The advantages of adopting such a procedure were:

1. Excessive handling of the PC at the air terminals at both ends of the trip was eliminated. One only

had to drive the car transporting the PC from USNO up to the plane and transfer the clock to the plane.

2. The transport of the PC through or close by airport surveillance devices was eliminated.
3. The possibility of having to transport the clock on commercial propellor driven aircraft on which there was no access to electrical power was avoided. The aircraft used in the experiment was wired to run the PC from its battery.
4. Flexibility in time of departure was gained, thus minimizing the duration of the trip.
5. Airports could be selected as close as possible to the remote site, thus minimizing the transportation of the clock from airport to remote site.

Eleven portable clock trips were made, the first site being visited twice. Table I lists the places and duration of the trips.

On each clock trip, the following procedures were performed. The PC was compared to the USNO Master Clock (MC) using a tick to tick measurement with an HP 5345A Electronic Counter. Next, the fixed site clock was compared against the PC, since it was located in a building which did not have access to the USNO MC. Because of the short duration between the comparison of PC with USNO MC and the comparison of PC with FIX, the fixed site clock could immediately be related to USNO MC. The PC was then transported to the remote site, and a comparison with VAN was made. After returning from the trip, the fixed site clock was again compared to the PC. Finally, the PC was compared to the USNO MC.

It should be pointed out that at the outset of each trip, the PC was not adjusted to agree with the USNO MC either in frequency or epoch. It, as well as all clocks in the experiment, was left free-running.

PROBABLE ERRORS OF TIME TRANSFERS

If one had no figure of merit other than the precision with which the measurements could be made, one could easily develope an erroneous picture of the precision with which one could say that the clock at the fixed site could be synchronized with the clock in the van.

One figure of merit which could be used to evaluate a

clock's performance after a field trip is the closure value, i.e., the difference between the comparison of the portable clock with the reference clock at the beginning and end of the trip. However, this value, in itself, has no real significance unless we know or assume that the portable clock had a rate identical to the reference clock at the start of the trip. What would be of greater statistical interest is the difference between the observed closure and that which we would expect based on our past knowledge of the performance of the clocks involved.

Any difference between the observed and predicted closure means that during the trip either a change in frequency or a jump in clock time occurred in one or both of the clocks concerned. When this event occurred or to which clock, we do not know. Therefore, the value for the difference between the two involved clocks interpolated to some instant between the beginning and end of the trip could be in error by the full amount of this difference depending on the kind of event and when it occurred. (In fact, the error could even be larger!)

During the course of the clock trips, it became evident that the clock selected for the PC had troubles with its divider circuitry. Testing in the laboratory showed that sudden accelerations could cause a jump of one nanosecond in time. This meant that throughout the duration of the clock trip, we could expect the accumulation of these random jumps in time to be significant. Phase comparison tracings of the PC with that of the USNO MC immediately before and after the trips indicated that no significant rate changes occurred during most trips. This indicated that most of the difference between the observed and predicted closure was entirely due to the random jumps in time caused by handling of the clock during the trip. Nevertheless, the difference between the observed and predicted closures is the only statistical information we have. It is the only information we can use to assess the precision of our ability to synchronize two clocks.

Table II summarizes the data for the difference between USNO MC and the fixed site clock. The first column gives the Modified Julian Date (MJD) on which the clock trip started. The second column gives the values of the observed closures for each of the trips. The next column lists the predicted closures based on a linear extrapolation of the rate difference between the USNO MC and FIX. The interval of time on which the extrapolated rate difference was based

varied as a function of the duration between trips. The last column contains the difference between the observed and predicted closures.

Assuming that these differences reflect our errors in determining (USNO MC - FIX), we can compute the probable error of a single determination. This turns out to be ± 11 ns. The probable error of a single determination is determined from

$$\varepsilon = 0.6745 \sqrt{\frac{\Sigma r_i^2}{n}}$$

where ε is the probable error of a single determination, r_i is the difference between the observed and predicted closure of the ith measurement, and n is the number of determinations. It will be assumed that this is the precision with which we can determine an interpolated value for the (USNO MC - FIX).

The precision with which we can compute the difference between the remote clock and USNO MC will reflect the precision with which we can interpolate the difference (USNO MC - PC) because it is through the portable clock that we relate the remote clock (VAN) to USNO MC.

An analysis indentical to the one given earlier can be done again to obtain the precision with which one can determine an interpolated value of (USNO MC - PC). Table III lists for the various trips the differences between the observed and predicted closures for (USNO MC - PC). It should be noted that the (O-P)s exhibit a systematic trend which can be explained by the accumulation of the aforementioned jumps in the portable clock divider circuitry. Again, assuming these differences to be the errors in our determinations, we compute the probable error of a single determination to be ± 27 ns. It will be assumed that this is the precision with which we can determine the interpolated value for (USNO MC - PC).

The value (PC - VAN) is an observed value having associated with it the precision with which we can make our readings (± 2 ns). Therefore, the precision with which we can determine (USNO MC - VAN) is simply the square root of the sum of the squares of the respective probable errors, i.e., ± 27 ns.

DISCUSSION

The analysis seems to have been complicated by the fact that it was decided to reference all measures to the USNO MC. The remote and fixed site clocks could have been related through the portable clock alone. The introduction of the USNO MC had the advantage of referring the fixed site clock to a reference clock which was in a rigidly controlled environment and therefore, hopefully, less susceptable to changes in frequency or jumps in clock time. As a result, it was hoped that the differences between the observed and predicted closures would be minimized because the values would be reflecting changes in only one of the two clocks. If the analysis had been performed without referring the measures to the USNO MC, but only by referring all measures to the portable clock, the probable error associated with differences between the fixed and remote site clocks would have been ± 38 ns, a degradation of 30% of the results cited earlier.

Plots of the differences (USNO MC - VAN) and (USNO MC - FIX) indicated no unusual behavior and indicate reasonable confidence in the results.

It should be noted that no corrections for relativity, special or general, were applied. The duration of trips and the speeds and altitudes at which the plane flew did not warrant them.

ACKNOWLEDGEMENTS

The efforts of a large number of persons went into the successful completion of this experiment. I would like to thank Don Percival for his comments and suggestions on this paper; Jean Lavanceau for his suggestion to use the small plane for the clock trips; Ken Putkovich for his many suggestions, help, and cooperation and who was ultimately responsible for the successful completion of the experiment; and Carl Lukac for his help in performing the field trips. The cooperation of SAID, Inc. from whom the plane was chartered is to be specially noted. In addition, my thanks go to the members of the APL team who made participation in this experiment an enjoyable event. Support of the USAF Electronics System Division for the clock trips is gratefully appreciated.

Date	MJD	Length	Place
(1975)			
29 May	42 561	7^h 57^m	Toms River, NJ
30 May	42 562	7 26	Toms River, NJ
5 Jun	42 568	6 34	Georgetown, DE
10 Jun	42 573	8 05	Marietta, OH
12 Jun	42 575	12 56	Danville, IN
17 Jun	42 580	8 14	Bluefield, WV
19 Jun	42 582	5 39	Grottos, VA
24 Jun	42 587	6 26	Emporia, VA
26 Jun	42 589	11 09	Wilmington, NC
30 Jun	42 593	9 29	Dexter, NY
2 Jul	42 595	7 18	Towanda, PA

Table I - History of Clock Trips

MJD	Observed Closure	Predicted Closure	Difference (O-P) Closure
42 561	-6ns	11ns	-17ns
42 562	2	7	- 5
42 568	8	12	- 4
42 573	-6	5	-11
42 575	7	3	4
42 580	-6	23	-29
42 582	-1	21	-22
42 587	7	22	-15
42 589	18	40	-22
42 593	-1	7	- 8
42 595	7	17	-10

Probable Error of Single Determination = ±11ns

Table II - Data for (USNO MC - FIX)

MJD	Difference (O-P) Closure
42 561	83ns
42 562	38
42 568	22
42 573	- 3
42 575	44
42 580	37
42 582	-53
42 587	- 4
42 589	33
42 593	19
42 595	34

Probable Error of Single Determination = ±29ns

Table III - Data for (USNO MC - PC)

QUESTION AND ANSWER PERIOD

DR. WINKLER:

It is obvious that the more sophisticated you are in your data reduction, the poorer the results become and I have a wondering about that. It seems to be just another part of Murphy's law, that any corrections which you can think of, when applied make your results worse.

MR. ALLEN:

Perhaps you could tell me what prediction routine you use to predict the closure?

DR. KLEPCZYNSKI:

Just simple linear extrapolation of the rate. Looking at their prior rates, the samplings we had of the clocks, just extend that rate forward right before the clock trip started.

MR. ALLAN:

How long?

DR. KLEPCZYNSKI:

Usually there was about at least one day's worth of data or two days. The clock trips, when we started going, were occurring about every other day. When the clock was at the observatory, we could measure two or three points during the day, to base our extrapolation on.

The plots were not changing frequency that often.

MR. ALLAN:

Okay, so if I understand right, the prediction time, then, was based on about a previous 24-hour period?

DR. KLEPCZYNSKI:

That is correct.

MR. ALLAN:

That is quite a bit of error because you are still basically in the white noise region of the clock if, you know, if the

clock doesn't have any abnormal perturbations otherwise. It may, in portable clock usage, but one could do quite a bit better than that, I think.

I have a question on the first slide which showed degradation as you applied your corrections.

It is the master clock where you have the predicted versus closure time and the addition of the two to give the total error. You can obviously see what may be an apparent bias.

DR. KLEPCZYNSKI:

Yes, there is.

MR. ALLAN:

And one wonders if, perhaps, that is due to a systematic in the prediction.

DR. KLEPCZYNSKI:

I would think so. But, I think as a reasonable number, the probable error then even becomes more real, that this is really what we would expect the results to show.

MR. ALLAN:

You are very conservative.

DR. KLEPCZYNSKI:

That is what I am trying to do, right?

DR. VESSOT:

I think the prediction algorithms are fine if you can use them, but I really believe that the portable clock under the conditions of its existence, while it is traveling around, is probably beyond any statistical rescue. If you are going to make such a statistic you have got to take the clock and look at the drift that it encounters under fairly controlled transportation conditions. I don't believe that the statistics one obtains in the lab can apply to the behavior of the clock while it is being environmentally gyrated in a small plane and moved about in the earth's magnetic field. I don't think that statistics are

going to help there.

DR. WINKLER:

I would like to make a comment to that. I think you are beyond statistics in one specific sense and that is that I am firmly convinced, and I think you may hear about that later this afternoon, that for such clock trips the main effect is the change in the temperature that is producing a systematic bias because all of these clock trips were executed during the same part of the year, in summer. The clock, when moved outside the laboratory, was always exposed to a higher temperature, and it did not have time to settle down. I believe a substantial part of these biases are due to temperature phase shifts in the output circuits.

Of course, the data has not been collected, for these short trips, has not been sufficient to warrant, I think, anything more sophisticated. What has been done almost simultaneously, however, and this explains why we didn't have particularly high performing clocks available for that purpose. I think better results could be had if you tested these clocks carefully for temperature behavior and account for that.

I think more interesting results can be gotten if you sent clock sets onto a trip where some of these are as perfectly protected against environmental changes and others are not. Then you can evaluate what really happens. That is part of the experiment which will be reported on, I hope, by Carroll Alley this afternoon, and the effect is profound on their portable clock if it is not protected.

FREQUENCY CONVERTER FROM 3.58 MHz to 5.0 MHz FOR FREQUENCY COMPARISON BY MEANS OF TV COLOR SUB-CARRIER

Tadao Inouye (National Research Laboratory of Metrology)
and Chikao Takeuchi (Fujitsu Limited)

ABSTRACT

For frequency comparison by TV color sub-carrier, a frequency converter has been joined newly in the comparison system. This is a phase locked oscillator, in which a voltage controled crystal oscillator locks its output frequency, 5.0 MHz, to the 3.58 MHz sub-carrier. The measurement scheme realizes comparisons between two round frequency signals, and results of the comparisons between the sub-carrier and a cesium frequency standard show the resolution of 1 ns and the frequency stability within 2×10^{-12} at averaging time of 20 minutes. Phase jumps occured by station breaks have no influence on the frequency comparison, because the measurements can effect its purpose during one live program of broadcasts.

INTRODUCTION

In Japan, an experiment of frequency comparison of cesium clocks by TV color sub-carrier which is used as a reference frequency was made also between Radio Research Laboratories and International Latitude Observatory of Mizu-

PRECEDING PAGE BLANK-NOT FILMED

sawa in 1972[1].

In the previous[1)2)3)], freqency comparisons have been made between a local frequency standard and color sub-carrier, frequency of the local standard was synthesized into 3.58 MHz so far. But, it is convenient to convert frequency of sub-carrier to 5.0 MHz which is fed to one input of a linear comparater, because of a round frequency and utilizing plain comparaters. Of course, another input of the comparater is a round frequency from the local standard. It seems that this converter is usefull especially for calibrating some frequency sources by color sub-carrier derived from a rubidium controled oscillator of a TV studio. This paper describes the theory of operation of the converter and the result of frequency stability measurement on a prototype one. Commercial type of this frequency converter which is named Phase Lock Oscillator has been sold by Fujitsu Limited.

THEORY OF OPERATION

Figure 1 shows schema of the converter. Output frequency of a voltage controlled crystal oscillator, 5.0 MHz, is divided by eighty eight. The divided signals, about 51.818 kHz, are shaped to pulses with 0.1 μs width, which are supplied to a gate. In time of the pulse width, the gate samples amplitude of sinusoidal signal of the color sub-carrier which comes from a color TV receiver. Pulse heights of the sampled pulses are averaged by passing through a lowpass filter and becomes DC voltage in proportion to the pulse heights. The DC voltage continues to vary, until the rela-

tion between the output frequency of VCXO and frequency of the color sub-carrier reaches to the ratio of 88 to 63. When the circuit is not inphase, wave form being observed actually at the gate output, voltage is already averaged and changed in steps increasingly or decreasingly each one period of 51.818 kHz, due to a capacitor added to the input of the amplifier.

Lock range is about $\pm$ 2 x 10^{-7} in fractional frequency, and synchronizing characteristic of frequencies at input and output is shown in Fig. 2 for manifesting linearity of the characteristics in the half of lock range.

FREQUENCY STABILITY FOR RECEIVING TV SIGNALS

Figure 3 is a representative strip chart record comparing the output frequency of the converter with the NRLMś frequency standard. The phase difference can be resolve to 1 ns on the chart. Block diagram of the phase comparison system is shown in upper part of Fig. 4. Under part of Fig. 4 shows the measuring system for short term stability. Fractional frequency stability of the output of the converter in terms of Allan variance is given typically in Fig. 5. The squares in Fig. 5 show the stability data calculated by reading of the linear traces such as Fig. 3. Also plotted in Fig. 5 as the circles are the data of the short term stability obtained by a computing counter. This stability is not worse than the previous experiments[1)3)]

These values are given by next formulas. With M values of f_i, which is output frequency of the mixer, about 40 kHz,

the displayed value of the computing counter, σ, is:

$$\sigma = \frac{1}{f} \left[\frac{1}{2(M-1)} \sum_{i=1}^{M-1} (f_{i+1} - f_i)^2 \right]^{\frac{1}{2}}$$

It being dispersed by the frequency multiplier, frequency stability, $\sigma_y(\tau)$, is:

$$\sigma_y(\tau) = \frac{f}{K\ n\ F_o} \sum_{m=1}^{K} (\sigma)_m$$

at K times measurements, where n is multiple factor of frequency multiplier,and F_o output frequency of the converter. In this measurement n equals 10.

It is estimated that the stability at averaging time larger than 100 seconds is limited mainly by receiving broadcasts signal and uncertainty of drawing a straight line on the linear trace, and short term stability by instability of VCXO mainly.

These broadcasts received in the above measurements were General program of NHK which is a public television networks in Japan.

FREQUENCY OF THE MAJOR TV NETWORKS IN JAPAN AND NOTE FOR CALIBRATIONS

Frequency resettability of the broadcast has been measured during about one week, average and distribution of frequencies are shown in Fig. 6 and Table 1. These data were calculated from the strip chart records, in which continuous traces were used except any phase jumps by station breaks and other sources of distortion.

Table 1 indicates that it is enough for a continuous trace made by the comparison during 10 minutes to get the precision to one part in 10^{11} (three sigma).

The broadcasting stations are not responsible for deviation of the signals being so accurate. It seems by monitoring frequency of color sub-carrier, that frequency of rubidium controled oscillators used by the major TV networks have been adjusted to keep its deviation in one part in 10^{10}, a local frquency source can be calibrated by the comparison to within 1×10^{-10} in Japan. On the calibration for the local frequency sources except atomic standards, it is necessary to observe with a notice that frequencies of two major networks, NHK and NET which is a big one of broadcasting companies in Tokyo, are close to each other within one part in 10^{10}. [4)]

Since frequency deviations of color sub-carrier are measured a week by RRL also, and these values of NHK and NET are given within one part in 10^{12} by the bulletin published with RRL and the journal of the institute of electronics and communication engineering of Japan, it is serviceable for the users wanting more accurate calibrations.

CONCLUSION

It is convenient for the calibration that this converter generates a round frequency by converting color sub-carrier. On the frequency comparison with the converter, these chart records indicate that it is possible to resolve the phase difference between the converted 5.0 MHz from the sub-carrier and the local frequency sources to 1 ns. It is estimated

that stability of frequency comparison between the sub-carrier and the cesium standard of NRLM, in terms of Allan variance, was 2×10^{-12} at averaging time of 20 minutes.

Mutual frequency comparison between two remote cesium clocks by using the converter within the comparison system each can be expected a good result, it is scheduled to make by NRLM at Tokyo and Osaka in Japan.

Acknowledgment: The authers would express their acnowledgment to Dr. S. Takata and Mr. Y. Koga, National Research Laboratory of Metrology, for providing with facilities. They also wish to thank Mr. Y. Nakadan, Mr. J. Yoda and Mr. M. Nara of National Research Laboratory of Metrology for preparing the illustrations of this paper.

REFERENCES

1) Saburi,Y., Yasuda,Y., Kobayashi,S. and Sato,T. "Precision comparison of time and frequency by means of TV signals" (in Japanese) Rev. of RRL, Vol.18, 433-444, Nov. 1972.
2) Davis,D.D. "Frequency standard hides in every color TV set" Electronics, Vol.44, No.10, 96-98, May 10 1971.
3) Allan,D.W., Blair,B.E., Daivis,D.D. and Machlan,E.H. "Precision and accuracy of remote synchronization via network television broadcasts, Loran-C and portable clocks" Metrologia, Vol.8, April 1972.
4) Kobayashi,S. "Standard frequency and time emission and its utilization" (in Japanese) Butsuri, Vol.30, 741-747, Oct. 1975.

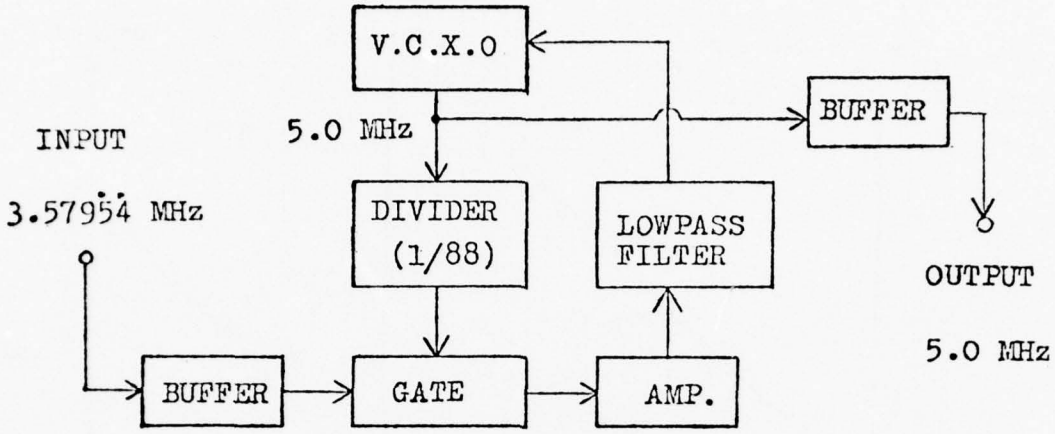


Fig.1 Scheme of freuency converter from 3.58 MHz to 5.0 MHz

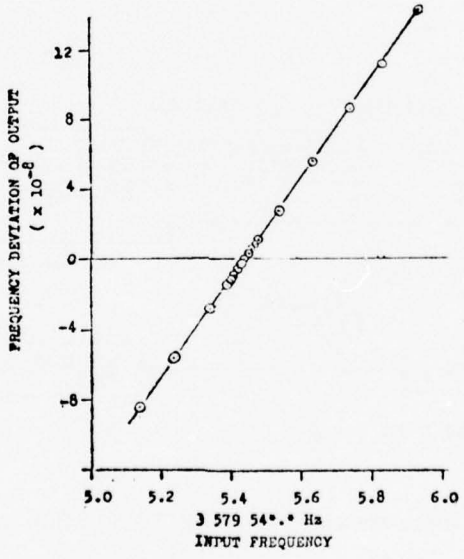


Fig. 2 Synchronizing characteristic between I/O frequencies of the converter.

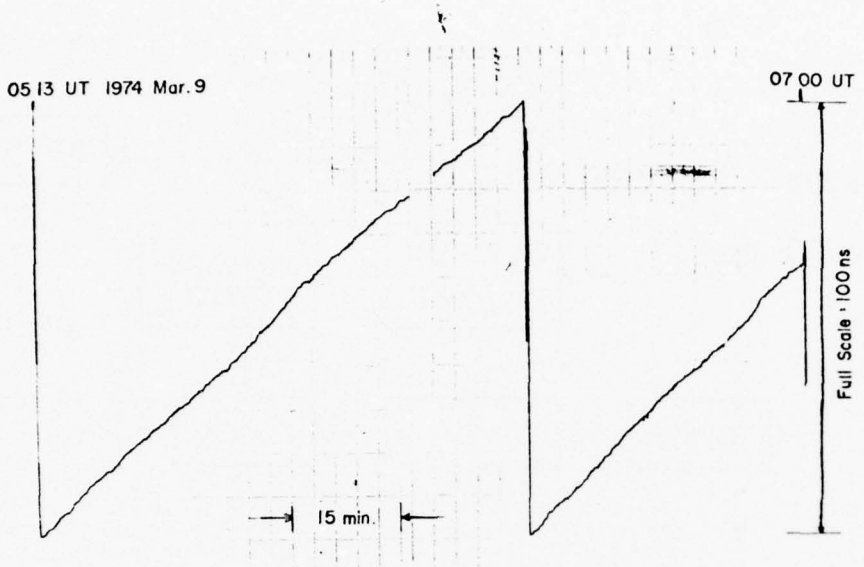


Fig.3 An example of the strip chart record of the phase comparison

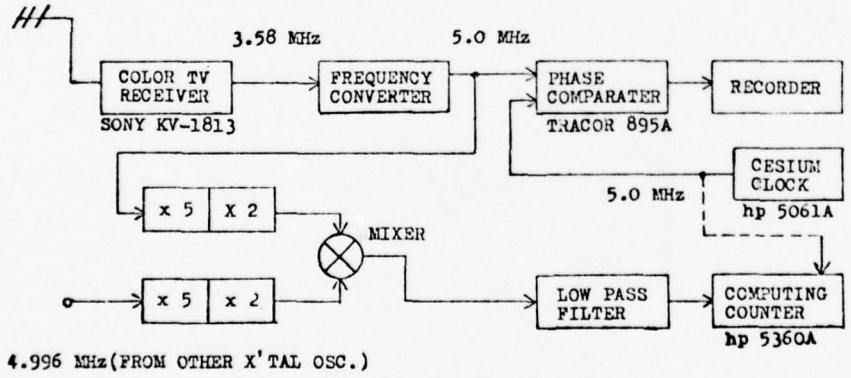


Fig. 4 Measurement system for phase comparison and frequency stability.

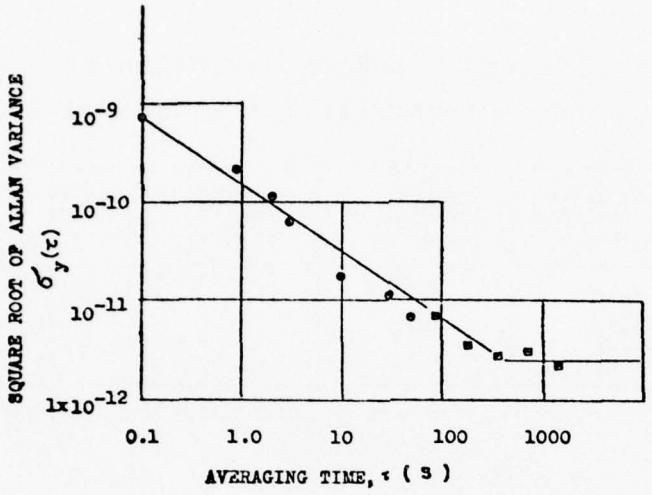


Fig.5 Relative fractional frequency stability for a color TV sub-carrier

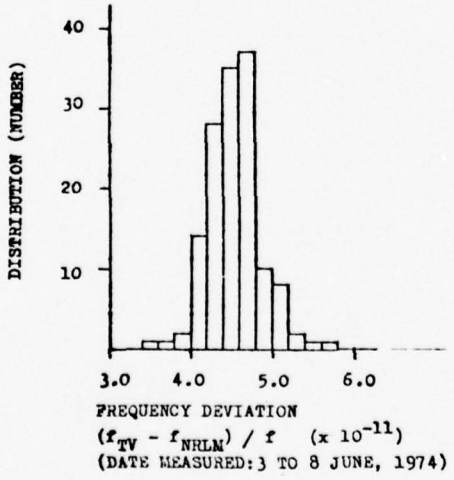


Fig. 6 Distribution of measured frequency on a color sub-carrier.
(NHK General program)

Table.1 Mean value and standard deviation of frequency of a color sub-carrier (NHK General program)

MEAN VALUE OF FREQ. DEVIATION (x 10^{-11})	STANDARD DEVIATION (x 10^{-11})	AVERAGING TIME (MIN.)	SUM OF DATA NUMBER
4.5_3	0.3_3	10	140
4.5_2	0.2_0	20	52
4.4_8	0.1_5	30	18

(MEASUREMENT PERIOD:3 TO 8 JUNE, 1974)

APPENDIX

CLOCK COMPARISONS BY TV, SELECTED TOPICS PERTAINING TO JAPAN

Precise time comparisons by TV synchronizing pulses have been performed in many countries. In Japan, succeeding to an experiment of time comparison by TV pulses made first by the Radio Research Laboratories (RRL) in 1970[1], time comparison experiments by TV pulses among atomic clocks in various institutions have been carried on[2)3)]. The line 10 timing method has been used in the comparison. Some improvements of receiving equipments have been made in order to obtain higher stability and accuracy, and these improvements have brought good results on the comparison in practice[4)-7)].

At present, clock comparison by TV signals has been made on a routine basis among five institutions, RRL, the National Research Laboratory of Metrology (NRLM), the International Latitude Observatory of Mizusawa (ILOM), the Tokyo Astronomical Observatory (TAO), and the Kanozan Geodetic Observatory (KGO). Fig. 1 shows locations of these institutions. Distances from a common transmitting antenna are less than 50 km, except ILOM which is situated about 400 km north of Tokyo.

Items of the improvements adopted in the present comparisons are

(a) to stabilize the frequency of the local oscillator in TV tuner,
(b) to fix the setting of the automatic gain control (AGC) in IF amplifier.

Fig. 2 shows a result of comparison between cesium clocks at NRLM and RRL, which is given by frequency dispersion in μs/day obtained from 5 day differences in time comparison data. During the period A in the figure, the measurements at NRLM were made by adjusting the fine tuning control of a TV tuner, monitoring the level of color burst signal. While, during another period B, a quartz crystal local oscillator was used in the TV tuner and the trigger level of the pulse selector for line 10 pulses was fixed. Frequency stability in terms of Allan variance of the result is ahown in Fig. 3. The value during the period B attained to 1×10^{-13} at averaging time of 10 days, including the instability of the two clocks concerned[4)7)].

An experiment has been made by NRLM to measure variation in relative time delay between two improved equipments of the same type. The variation could be reduced to 10 ns (one sigma) for a single equipment, as compared with that of 20 to 30 ns (one sigma) given in the case of commercial TV receivers[4)].

In the comparison of cesium clocks via TV pulses made between TAO and KGO, to keep the starting voltage of AGC and to observe the frequency of the local oscillator in TV tuner were taken into consideration in particular. The standard deviation of 40 ns from a linear trend was obtained from

the data during a month in 1974[5)7)].

When the frequency of the local oscillator is changed by adjustment of fine tuning control or any other cause, the change in the phase and amplitude of a detected signal must be raised according to the band-pass characteristics of the IF amplifier. When the starting voltage of AGC in the TV receiver varies, the output voltage from the IF amplifier, hence the delay time in the receiver, is changed by the same reason as mentioned above. Fig. 4 shows the variation in delay time against the frequency of local oscillator in a commercial TV receiver, for three levels of the starting voltage of the AGC as parameter. Abscissa in the figure is given by the frequency in the IF amplfier instead[5)].

In the comparison through microwave links via two different routes made between RRL and ILOM, it was found that the accuracy of ± 2 μs was obtained except abrupt changes in the microwave networks[3)].

The leading edge of line 10 pulses is measured as usual in the time comparison. It may be recommended to use the trailing edge of the TV pulse for higher stability, as the slope of the trailing edge is much steeper than that of the leading edge at their sliced points. The trailing edge may be less sensitive to the change in the video signal amplifier and to the noise. A result of comparison between the measurements on the trailing edge and the leading edge, made at RRL, is shown in Fig. 5, where the abscissa gives the amplitude of the synchronizing pulse in the video signal

and the ordinate the relative delay time. The variation in the former case is less than half of the latter. It may be said from this result that the variations in the delay time would be further reduced[7].

The time of transmission of TV synchronizing pulses and the frequency deviation of color subcarrier on the NHK and the NET signals have been published by RRL since April 1975. Interests to the use of TV synchronizer are growing in Japan, but the user market for them is still limited. Any gadget for time comparison by TV synchronizing pulses has not yet been commercially producted in Japan.

The authors are much indebted to Prof. S. Iijima and Dr. N. Matsunami of TAO, Dr. Y. Saburi of RRL, Mr. Y. Koga of NRLM, and their staff for the compilation of this report.

REFERENCES

1) Saburi, Y., Yasuda, Y., Kobayashi, S. and Sato, T., "Precision comparison of time and frequency by means of TV signals" (in Japanese), Rev. of RRL, Vol. 18, 433-444, Nov. 1972.

2) Horiai, K., Hara, T. and Aihara, M., "Time comparison by network television broadcasts" (in Japanese), Proc. of ILOM, No. 13, March 1973.

3) CCIR Document 7/26-E, Oct. 1973.

4) Inouye, T. and Nara, M., "The stability of time comparison by TV signal of common emission" (in Japanese), Trans. Society of Instrument and Control Engineers, Japan, Vol. 11,

No. 3, June 1975.
5) Fujiwara, K., Kato, T., Hokugo, S. and Miyazaki, K., "Precise clock comparison by mens of TV signals" (in Japanese), Univ. of Tokyo, Tokyo Astron. Obs. Report, Vol. 17, No. 2, March 1975.
6) National Report of Japan presented to URSI (Lima), page 4 Aug. 1975.
7) CCIR Document of Study Group 7, 1976 Interim Meeting, submitted from Japan.

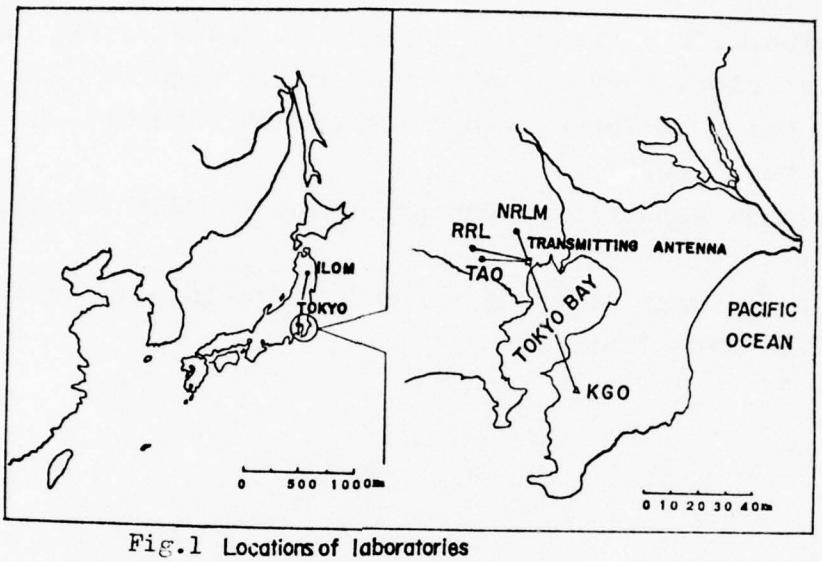


Fig.1 Locations of laboratories

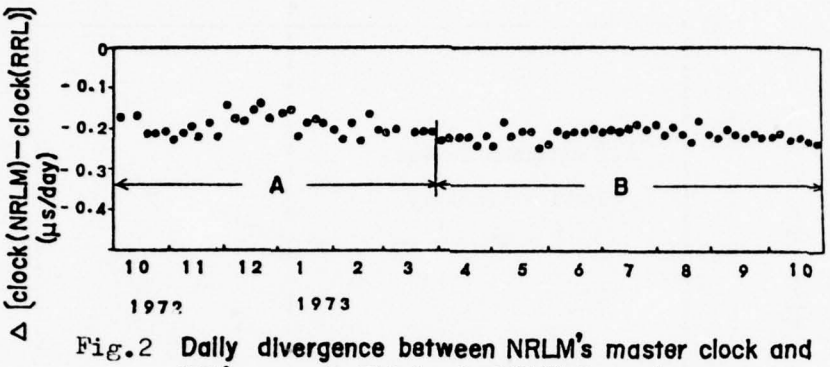


Fig.2 Daily divergence between NRLM's master clock and RRL's one via TV signal of NHK General program

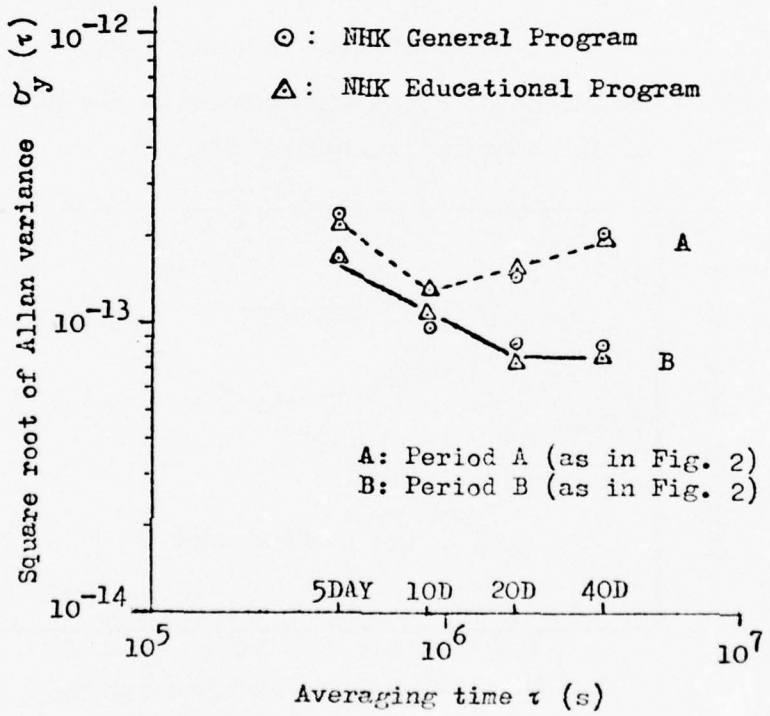


Fig.3 Mutual frequency stability of cesium clocks at NRLM and RRL as compared via TV pulses.

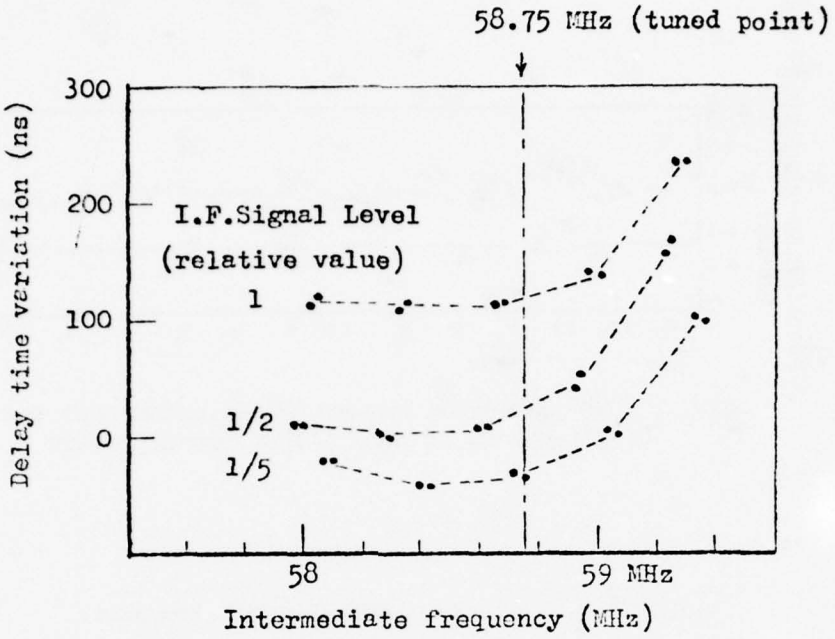


Fig.4 Variation of delay time caused by the adjustment of the starting voltage of AGC.

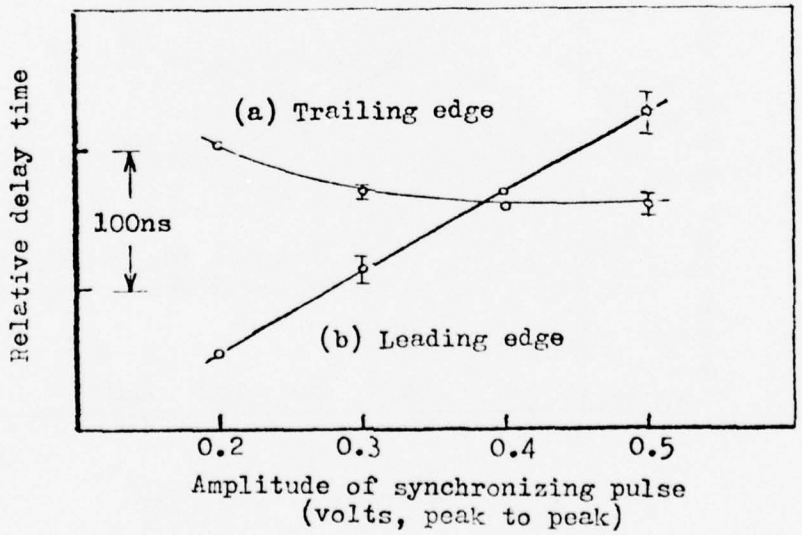


Fig.5 Relative delays and scatters (one sigma) of separated synchronizing pulse vs. amplitude of the synchronizing pulse in video signals.

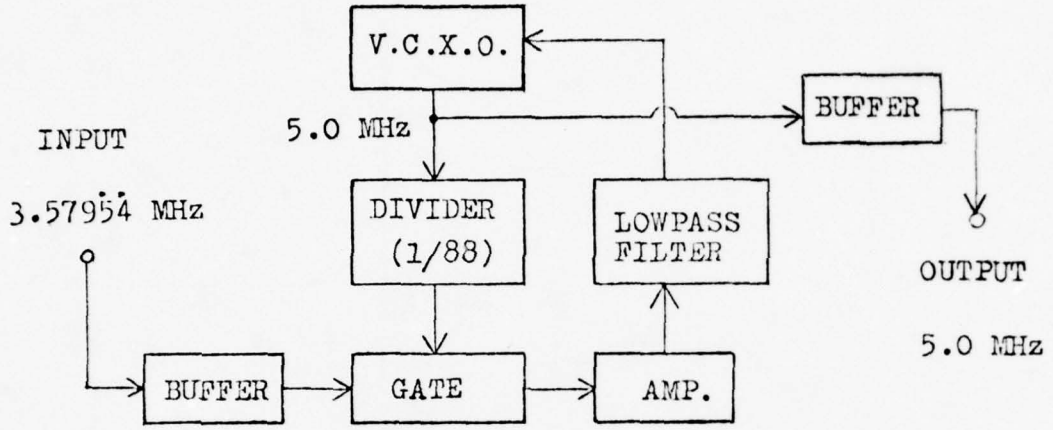


Fig.1 Scheme of freuency converter from 3.58 MHz to 5.0 MHz

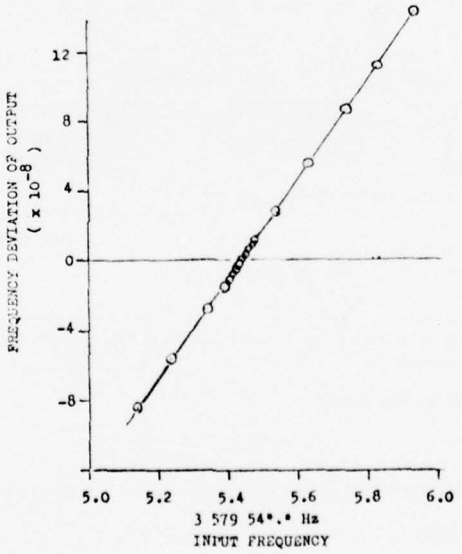


Fig. 2 Synchronizing characteristic between I/O frequencies of the converter.

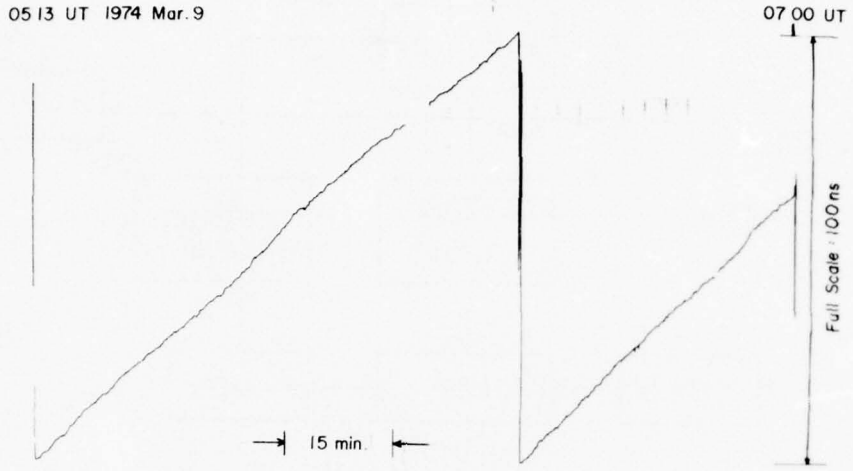


Fig. 3 An example of the strip chart record of the phase comparison

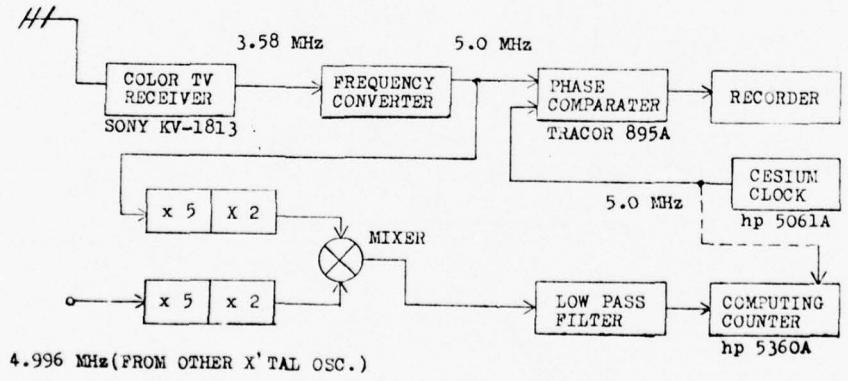


Fig. 4 Measurement system for phase comparison and frequency stability.

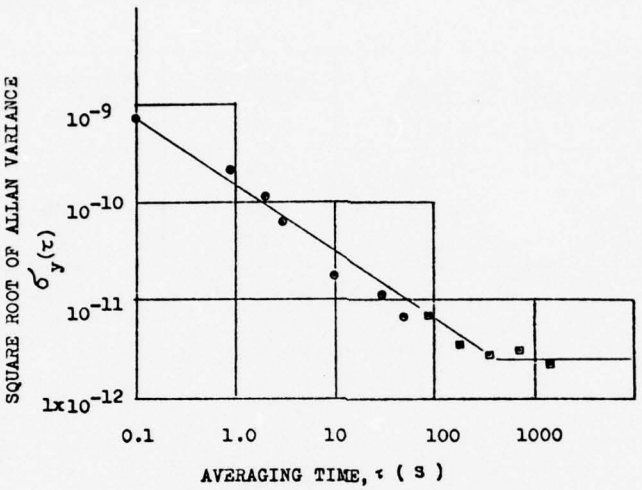


Fig.5 **Relative fractional frequency stability for a color TV sub-carrier**

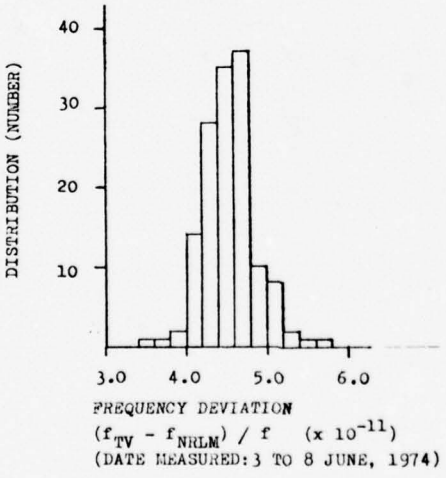


Fig. 6 Distribution of measured frequency on a color sub-carrier.
(NHK General program)

Table.1 Mean value and standard deviation of frequency of a color sub-carrier (NHK General program)

MEAN VALUE OF FREQ. DEVIATION (x 10^{-11})	STANDARD DEVIATION (x 10^{-11})	AVERAGING TIME (MIN.)	SUM OF DATA NUMBER
4.5_3	0.3_3	10	140
4.5_2	0.2_0	20	52
4.4_8	0.1_5	30	18

(MEASUREMENT PERIOD:3 TO 8 JUNE, 1974)

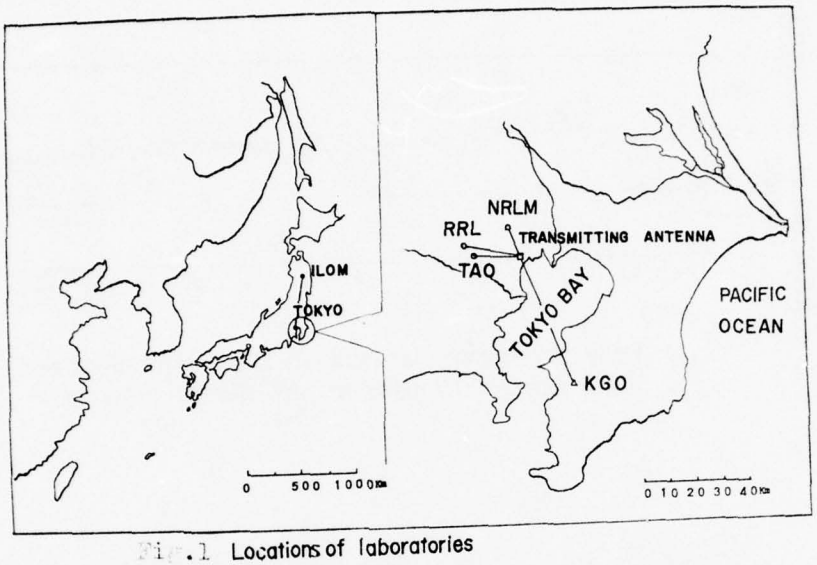


Fig.1 Locations of laboratories

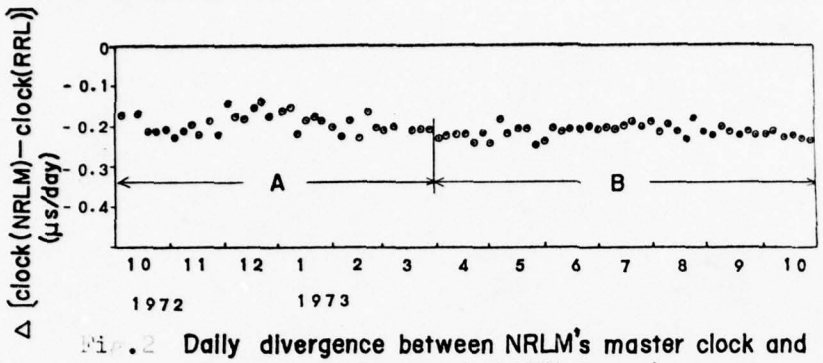


Fig.2 Daily divergence between NRLM's master clock and RRL's one via TV signal of NHK General program

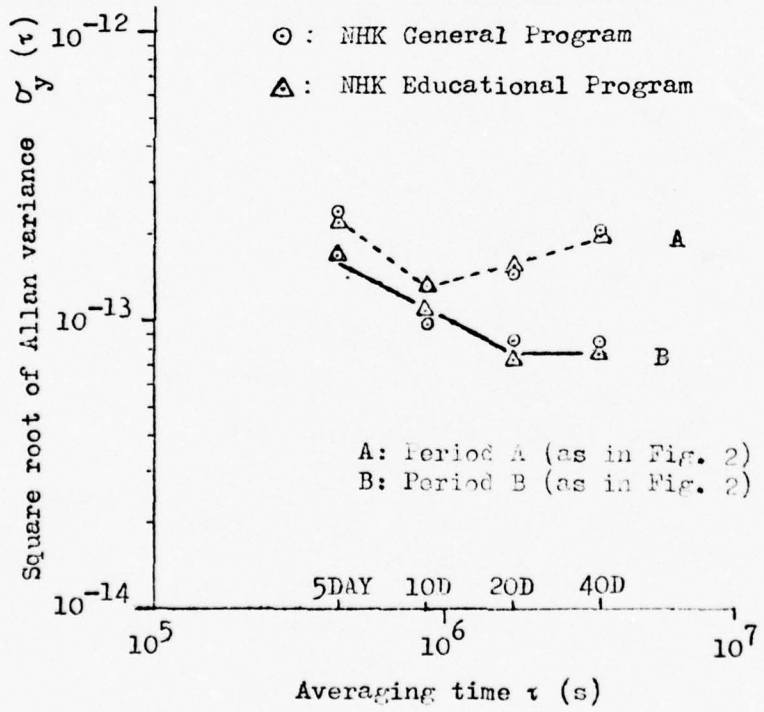


Fig.3 Mutual frequency stability of cesium clocks at NRLM and RRL as compared via TV pulses.

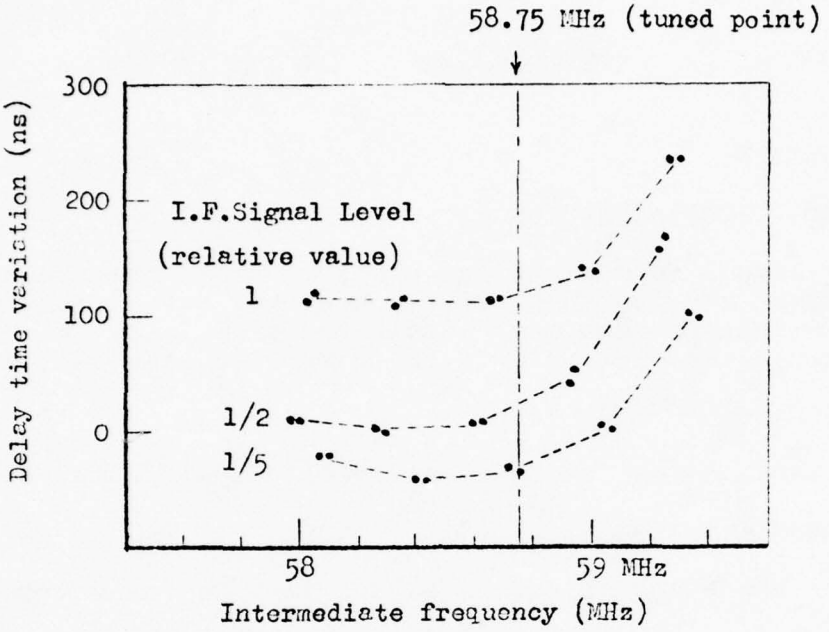


Fig.4 Variation of delay time caused by the adjustment of the starting voltage of AGC.

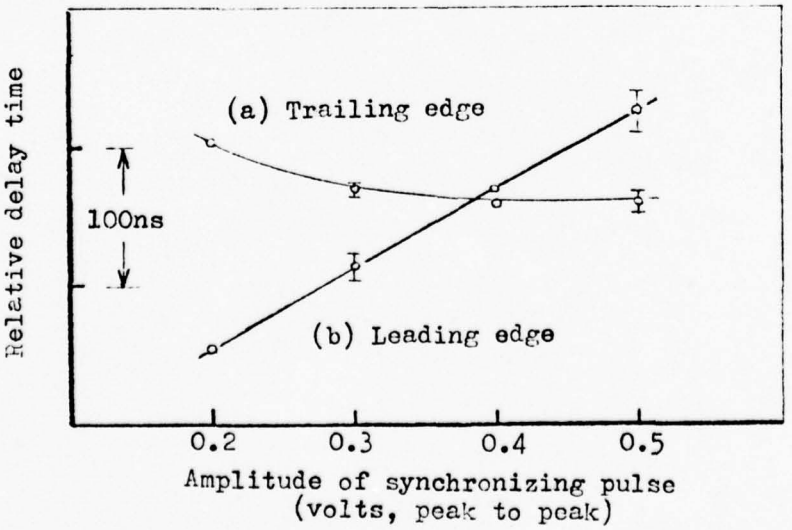


Fig.5 Relative delays and scatters (one sigma) of separated synchronizing pulse vs. amplitude of the synchronizing pulse in video signals.

QUESTION AND ANSWER PERIOD

DR. SHEPARD:

Shepard, ILC Industries.

We may have a communications problem here. The synchronizing pulses and the subcarrier, were they taken from the synchronization separator within the television or were they separated outside from the composite video signal?

DR. INOUYE:

At present, we use another receiver, two different receivers.

DR. SHEPARD:

One for the synchronization pulses and one for the subcarrier?

DR. INOUYE:

Yes.

HIGH PRECISION TIME TRANSFER METHODS

Kenneth Putkovich
U. S. Naval Observatory

ABSTRACT

This paper specifically addresses the problems encountered in making high precision (0.1 microsecond or less) time interval measurements as applied to precise time transfers. Included is a brief overview of what measurements are necessary, what uncertainties can be expected in the measurement, how the measurement can be applied to time transfer techniques in use today (portable clocks, SATCOM, TV, Loran-C), the pitfalls that can be encountered, the errors which result from being a victim of pitfalls, and an indication of the type of hardware available for measurements of this type. It is demonstrated that cumulative uncertainties can be reduced to less than 100 nanoseconds in even the more complex, long distance measurement situations if proper attention is paid to measurement techniques.

INTRODUCTION

The purpose of this paper is to present an investigation and analysis of the measurement errors encountered in making Precise Time and Time Interval (PTTI) measurements. With the advent of frequency standards having stabilities in parts in 10^{-12} to 10^{-14} and digital clocks with pulse jitter in the tens of picoseconds, measurement errors which previously could be ignored as second order have now become important. Since the majority of time transfers or synchronizations are realized by means of time interval measurements between two clocks, the investigation is limited to such measurements.

Errors can be classified as either residual or systematic. Residual errors are by definition those which remain after all known systematic errors have been eliminated and are therefore the limiting factors in regard to the accuracy which can be associated with the quantity measured. They are subject to reduction only by improving the measured system. Systematic errors on the other hand, are associated with the measuring system or techniques and are those which can be avoided, corrected or reduced. The major emphasis of

the investigation was further limited to systematic errors. Systematic errors can be divided into three catagories:

1. Gross errors - These are mistakes or blunders attributable to the investigator and include misreading instruments, improper adjustment, using the wrong instrument, recording the wrong number, reading the wrong quantity, etc.

2. Instrument errors - These are inherent problems in the measuring system itself such as calibration, time base error, synchronous averaging, etc.

3. Measurement errors - These are caused by physical effects on the measured quantity such as distortion of the signal, improper impedance matching, transmission problems, etc.

Suggestions for reducing the category 1 errors and analyzing the category 2 and 3 errors are presented. A simple model of a general time interval measurement system is developed. A simple mathematical formula which can be used to combine estimates of error for relative system evaluations is presented. Examples of commonly used PTTI systems and equipment are examined and discussed.

GENERALIZED MEASURING SYSTEM

Figure 1 presents a diagram of a general PTTI system. Every PPTI system can be broken down into these segments for analsis. In the general case, the two clocks produce coherent output signals at repetition rates which have periodic times of coincidence. In the simplest case they are 1 pulse per second.

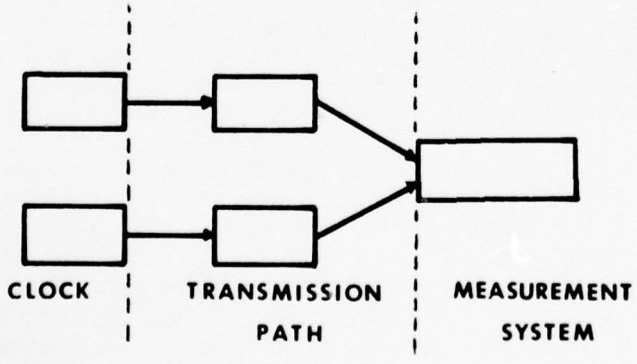


FIG. 1 GENERALIZED SYSTEM

These signals pass through transmission medium and set into motion a measurement process which results in a measurement of the relative position of two events in the time domain.

To establish a basis for comparison of various systems, a simple means of determining a relative value of uncertainty is necessary. If we examine Figure 1 and assign an uncertainty X_{ij} to each system component in the start and stop channel and X_k to the common measuring equipment (as shown in Figure 2) the entire system relative uncertainty can be expressed as

$$\sigma = \sqrt{\Sigma X_{ij}^2 + X_k^2}$$

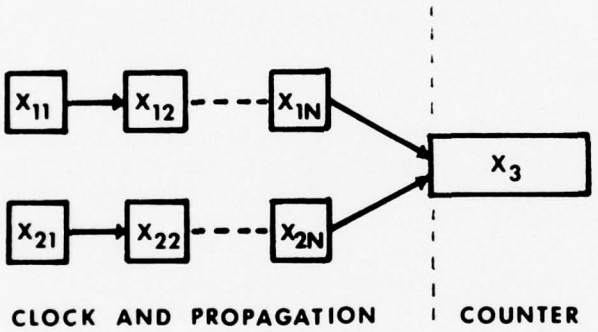


FIG. 2 GENERALIZED UNCERTAINTIES

It can be shown [1] that if we combine two or more measurements, using a clock as a transfer standard to determine the relative position in time of two other clocks, the total relative uncertainty can be expressed as

$$\sigma = \sqrt{\sigma_1^2 + \sigma_2^2 + \ldots + \sigma_n^2}$$

Before applying this to some typical measurement situations, we should examine briefly the components of the generalized measuring system.

Clocks

For the purposes of this paper, we shall define a clock as a device generating a one pulse per second (IPPS) signal. Although the purpose of this clock is to maintain a precise time scale over long periods of time, the clock characteristic of concern in this paper is how the clock behaves over the short interval of time necessary to make time interval measurements. The behavior of a number of clocks is presented in Appendix A, Table 2. In summary, this shows that the best clocks available have an uncertainty (jitter) of ± 0.05 nanoseconds, while older clocks may have up to ± 2 microseconds of jitter. This uncertainty falls into the residual category since it is inherent to the clock system and subject to reduction only by improving the clock system. In most cases, one has little control over the circumstances which determine the residual uncertainties of the clocks being measured and the estimates of uncertainty due to clock performance must be accepted and dealt with accordingly.

Transmission Path

When the signal leaves the clock, degeneration immediately sets in. All classes of systematic uncertainties begin to accumulate along with the residuals. In the simplest case, the transmission path is a short piece of coaxial cable; in its most complex form, the path may include long cable runs, microwave links, radio transmitters, satellites, and receivers. Here the possibility of a gross uncertainty appears and the possibility of other systematic errors increases in proportion to the complexity of the path. Uncertainties introduced by short coaxial lines are usually insignificant. They become significant when they exceed a few meters in length and the delay caused by their introduction is neglected. Uncertainties introduced by complex transmission paths can amount to hundreds of nanoseconds in fixed propagation path configurations and microseconds in variable path configurations. In all cases, the total uncertainty is the accumulation of uncertainties in each segment of the propagation or transmission path. The majority of the measurement uncertainties develop in this area and it is also a likely location for gross uncertainties to appear. Table 3 of Appendix A gives estimates of systematic uncertainties due to transmission path for typical transmission media. Many of these uncertainties can be reduced and propagation delays determined with detailed investigation into the transmission processes involved, but initial or one time measurements are subject to these errors and the uncertainties must be accounted for in any systems measurement.

Measuring Instrument

The point is finally reached where the clock pulse is to be measured. It may be the same pulse virtually undistorted, it may be the same pulse distorted or it may be a new pulse reconstituted from the transmitted information. The problem becomes one of making a well defined, repeatable measurement with a minimum of measurement and instrument errors and no gross errors. The measurement error is reduced by attention to proper termination of the transmission line to prevent reflections and distortion due to discontinuties and impedance mismatch. Instrument error is reduced by optimizing measurement conditions and giving attention to the details of operation and idiosyncrasies of the instrument being used. Gross errors are eliminated only by experience and careful attention to each measurement situation.

In general, uncertainties in the measuring system fall into four areas: the ± 1 count error, the internal trigger error, time base error, and error due to minimum measurable intervals. Since these subjects are covered in detail quite well elsewhere [2, 3] only the basic general concepts and their contribution to the uncertainty will be discussed.

The ± 1 count error is inherent in all digital systems relying on direct counting of the output cycles of a time base gated by the measured signals. Thus a counter with a 10 mHz time base can have an error of ± 0.1 μsec.

Trigger error is due to both the internal noise developed in the start and stop channels and the precision attainable in repeated setting of the trigger level controls. Internal trigger error is generally insignificant, but that due to the settability of the level controls can be quite large and contribute significant amounts to the measurement uncertainty.

Time base errors are generally insignificant since the internal oscillators of high quality counters are stable in the range from 1×10^{-7} to 1×10^{-9}, measurement times are general less than one second, and a highly stable external time base is usually available.

Error due to the smallest measurable time interval becomes a problem when the instrument has a very high resolution, but cannot distinguish between closely spaced input pulses. For example, if an instrument has a resolution of .01 microsecond, but cannot make a reliable measurement when input

pulses are spaced closer than 0.1 microsecond, the error can be as large as the measured value when measuring short intervals. This generally is not a problem in newer counters utilizing highspeed digital logic and improved counting techniques.

PTTI MEASUREMENT TECHNIQUES

Every effort must be made to reduce the likelihood of gross errors in PTTI measurements. Operator errors are much more likely if measurements are made by personnel with minimal training and understanding of what is being measured and what the measurement process actually is. Fatigue after long, involved itinararies and the attendant lack of attention to necessary details in procedures also contribute to gross errors when measurements are made in the field. For this reason, standard measurement and reporting procedures must be established and followed. Personnel must understand the measurement if gross errors are to be minimized.

All measurements in any series of measurements should be made using the same equipment, particularly the time interval counter. For example, if for any reason a long cable must be used to measure a clock at a remote site, then the same cable should be used in making all the other measurements. Prior to making a measurement, the following must be accomplished:

1. The measurement criteria must be defined. At what polarity, level and slope is the measurement to be taken? What is the proper termination impedance?

2. The measured quantity should be examined and compared to prior data, if available, to ascertain that the measurement criteria and the measured quantity are consistent. A record (photo or sketch) of the measured pulse should be made and annotated with pertinent data such as amplitude, width, rise time, etc. Any distortion should be noted and a determination made of how this might affect the measurement.

The time interval counter is then prepared for the measurement:

1. The best available source of frequency is selected for a time base.

2. The counter is tested or calibrated using internal

and/or external signals to test for proper operation and counting.

3. Input levels, slopes and slope polarities are set.

4. Input lines are checked for proper termination.

Once this has been done, the measurement can be made in the following manner:

The two clocks are connected to the time interval counter such that the smaller of the two possible numbers is displayed. The result is recorded as

Start Clock - Stop Clock = Reading.

This procedure has several advantages. The result is always the smaller of two possible answers, it is recorded as a positive number, it has less digits to record, the start-stop convention is logical and easily remembered, arithmetic is involved and the shorter interval results in reduced time base error. Having taken these steps to reduced gross uncertainties, we can proceed with the analysis of other systematic errors.

TYPICAL SYSTEMS

Using the analysis and measurement techniques so far presented we can look at several typical measurement situations encountered in PTTI.

Portable Clocks

The most straightforward and often encountered high precision time transfer is that involving portable clock operations. A portable clock is measured against a reference, taken to a remote clock against which another measurement is made, and returned to the reference clock for a final measurement to close the loop (closure). A straight line fit is assumed between the initial and final measurements so that any difference between the two is apportioned linearly over the time elapsed between the two measurements. The validity of this technique may be open to question; however, one is free to assign his own estimate of this closure error using any criteria desired. Since for the purposes of this paper this uncertainty is residual, we need only examine the sources of systematic uncertainties. Assuming we are synchronizing (measuring) a portable, high performance cesium clock to the USNO Master Clock, using

short coaxial cables and a high resolution time interval counter driven from the portable clock, an estimate of the contribution of each component in the system can be determined from the tables in the appendix.

X_{11} - HP 5061A CS OPT 004 = 5×10^{-12} = .005 nsec

X_{12} - TSI Nanoclock = 0.05 nsec

X_{13} - Coax Cable = 0

X_{21} - HP 5061A CS OPT 004 = 5×10^{-12} = 0.005 nsec

X_{22} - HP 5061A Clock = 1.0 nsec

X_{23} - Coax Cable = 0

X_3 - HP 5345L Counter

Time Base = .005 nsec

Trigger Error = .02 nsec

Count Error = 2 nsec

(In each case X represents the uncertainty contributed by each segment of the measuring system in Figures 1 and 2.)

$$\sigma_1 = \sqrt{\Sigma X_{ij}^2 + \Sigma X_k^2} = 2.2 \times 10^{-9} \text{ sec.}$$

If we now perform a typical portable clock operation (See Figure 3.)

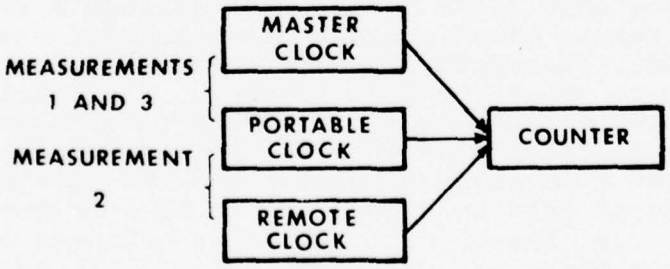


FIG. 3 PORTABLE CLOCK TIME TRANSFER

using the portable clock as a transfer standard and measuring another clock having the same specifications as the portable clock, we determine that the second measurement uncertainty is

$$\sigma_2 = 2.5 \times 10^{-9} \text{ sec.}$$

Returning and making a measurement against the Master Clock (assuming zero closure), we find a third uncertainty of

$$\sigma_3 = 2.2 \times 10^{-9} \text{ sec.}$$

Combining these using

$$\sigma = \sqrt{\sigma_1^2 + \sigma_2^2 + \sigma_3^2}$$

we find a total uncertainty for a portable clock (pc) measurement of

$$\sigma_{pc} = 4 \times 10^{-9} \text{ sec.}$$

For a 1965 vintage system (HP 5060 cesium with 115 BR clocks and a 5245L counter) we find

$$\sigma_{pc} = 2.5 \times 10^{-6} \text{ sec.}$$

Loran-C

High precision time transfers utilizing Loran-C (Figure 4) can be examined by considering the simple case, for example, of determing the difference between the USNO Master Clock and another clock within groundwave range of the East Coast Chain Master Station at Cape Fear, North Carolina. This case is analogous to a two measurement portable clock situation with the addition of uncertainties in the transmission path, X_{23}, which includes the transmitter, antennas, receivers, and complex oversea and overland propagation paths.

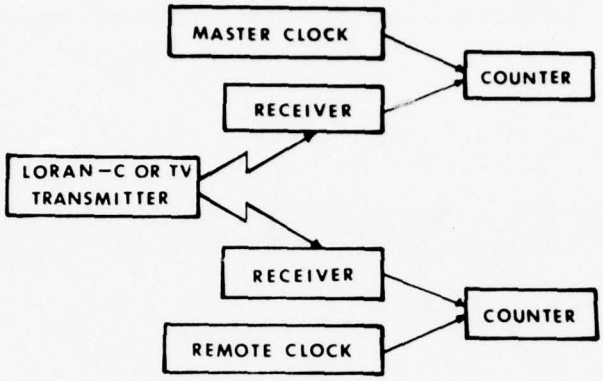


FIG. 4 LORAN-C OR TV TIME TRANSFER

An analysis of uncertainties, including estimates of those of interest has been published by Pakos [4]. This combined with uncertainties from Appendix A for loran receivers yields an estimate for X_{23} of

$$X_{23} = \sqrt{X_{pa}^2 + X_{pe}^2 + X_{1c}^2 + X_r^2}$$

where

X_{pa} = propagation anomaly = 0.2 μsec

X_{pe} = propagation path prediction = 0.1 μsec

X_{1c} = transmitted signal uncertainty = 0.02 μsec

X_r = receiving system delay uncertainty = 0.01 μsec

$$X_{23} = 0.23 \times 10^{-6} \text{ sec.}$$

Substituting this value in the previous calculation and assuming the same instrumentation at both sites yields

$$\sigma_1 = \sigma_2 = .23 \times 10^{-6} \text{ sec}$$

and

$$\sigma_{1c} = \sqrt{\sigma_1^2 + \sigma_2^2} = .33 \times 10^{-6} \text{ sec.}$$

The largest contributor to the total uncertainty is that associated with the transmission path. It should be emphasized that this is the uncertainty associated with a single measurement using conservative values for propagation uncertainties. In most cases these can be reduced an order of magnitude by portable clock synchronization to verify projected propagation delays, by observing the behavior of the received signal over a period of time and by tuning the system to reduced the effect of propagation anomalies. If X_{pa} and X_{pe} are reduced by a factor of ten then

$$X_{23} = 0.03 \times 10^{-6} \text{ sec}$$

$$\sigma_1 = \sigma_2 = 30 \times 10^{-9} \text{ sec}$$

$$\sigma_{1c} = 42 \times 10^{-9} \text{ sec.}$$

Television

The concept of high precision time transfers employing TV is exactly analogous to Loran-C. The loran clock is replaced by a TV clock in Figure 4. If we consider a simple case involving, for example, the USNO and WTTG Channel 5 in Washington, we can determine the measurement uncertainties very easily. The transmission path uncertainties are

$$X_{pa} = 0.005 \ \mu\text{sec}$$

$$X_{pe} = 0.05 \ \mu\text{sec}$$

$$X_{tv} = 0.02 \ \mu\text{sec}$$

$$X_r = 0.01 \ \mu\text{sec}$$

$$X_{23} = .055 \times 10^{-6} \text{ sec}$$

$$\sigma_1 = \sigma_2 = .055 \times 10^{-6} \text{ sec}$$

and

$$\sigma_{tv} = \sqrt{\sigma_1^2 + \sigma_2^2} = 80 \times 10^{-9} \text{ sec.}$$

Satellite

Time transfers between two SATCOM satellite terminals are somewhat different in comparison to the measurement techniques previously covered. Since this mode of making high precision transfers involves a simultaneous two way transmission of the time data at high frequencies through a synchronous satellite, the uncertainties due to propagation anomalies and path predictions are reduced. The nature of the transmitted information and the high data rates possible require that the transmitters and receivers be highly stable. The readout of the time transfer data has a ± 1 count error at present, which amounts to 0.1 microsecond. This limits the system to an uncertainty of

$$\sigma = 0.14 \times 10^{-6} \text{ sec.}$$

Improvement in this case is dependent on improvement of the measuring equipment. Increasing the resolution to 0.01 microsecond in future systems should result in the uncertainty being reduced to less than

$$\sigma s = 20 \times 10^{-9} \text{ sec.}$$

Composite System

If we examine a typical operational system, we should be able to arrive at a meaningful estimate of uncertainty in the the measurement chain. For example, The Naval Observatory has a Precise Time Reference Station in Hawaii which monitors Loran-C and determines the difference between the Master Clock and the Central Pacific Loran-C Chain (4990). What uncertainty exists in this value that can be attributed to the measurement systems? The total system consists of the following links and transfer methods:

USNO to SATCOM (Brandywine, MD) - Portable Clock

SATCOM (Brandywine) to SATCOM (Hawaii) - Satellite

SATCOM (Hawaii) to Reference Station - TV

Reference Station to Loran-C Transmitter - Loran-C.

Combining the values previously determined for these links (as they presently exist) we find, under ideal conditions,

$$\sigma_{NO-4990} = \sqrt{\sigma_{pc}^2 + \sigma_s^2 + \sigma_{tv}^2 + \sigma_{lc}^2}$$

$$= 2 \times 10^{-7} \text{ sec.}$$

CONCLUSION

This paper has presented a discussion of high precision time transfer techniques and the uncertainties one can expect in making relative measurements between clocks using these techniques. It must be emphasized that these results are what can be expected from a competent investigator using state-of-the-art equipment under relatively good operating conditions. Generally, total uncertainties are greater due to operation under less than ideal circumstances and the existence of residual errors not amenable to easy analysis and reduction.

ACKNOWLEDGMENT

The author wishes to thank Ms. Dorothy M. Outlaw and Ms. Sarah F. Pleasants for their speedy and efficient efforts in preparing the manuscript and Mr. Paul Wheeler and Mr. William Dabney for their help in preparing the demonstration which accompanied the presentation of the paper.

REFERENCES

[1] Ernst, Frank, "Electrical Measurement Analysis", McGraw-Hill, New York, NY, 1959, ch. 7.

[2] Hewlett-Packard Company, Time Interval Averaging, Application Note 162-1.

[3] Hewlett-Packard Company, Application Note 52-3.

[4] Pakos, Paul E., "Use of the Loran-C System for Time and Frequency Dissemination", Frequency Technology, Vol 7, pp. 13-18, 1969.

APPENDIX A

The data in this appendix are typical of what can be expected from the classes of equipment specified. When available, the information was taken from the instruction manuals for the equipment named. When this was not available, an estimate based on the author's past experience was used. Uncertainties are given in units of seconds for a measurement interval of less than one second.

Table 1. Oscillators

Type	Example	Uncertainty
Cesium-High Performance	HP 5061A-004	5×10^{-12}
Cesium-Older	HP 5060	1×10^{-11}
Rubidium	Tracor 204B	1×10^{-11}
Crystal	URQ-10	1×10^{-10}

Table 2. Clocks

Type	Example	Uncertainty
Lab Type-Digital	TSI 915 (Nanoclock)	0.05×10^{-9}
Portable-New	HP-5061A-001	1×10^{-9}
Lab Type-Transistor	Tracor 401A	0.1×10^{-6}
Portable-Old	HP-115BR	2×10^{-6}

Table 3. Transmission Systems

Type	Example	Uncertainty
Coaxial Cable-Short	RG 58/U-3 Feet	0
" " -Long	" " " 100 Feet	0.1×10^{-9}
LF Carrier (Groundwave)	Loran-C	0.2×10^{-6}
VLF Carrier (Line of Sight)	Television	0.05×10^{-9}
Microwave (Line of Sight)	SATCOM	0.05×10^{-9}

Table 4. Time Interval Counters

Type	Example	Uncertainty
Computing	HP 5360	1×10^{-9}
Nanosecond	Eldorado 796	1×10^{-9}
"	HP 5345	2×10^{-9}
Ten Nanosecond	Eldorado 784	2×10^{-8}
"	HP 5326	0.2×10^{-6}
Microsecond	HP 5245L	0.1×10^{-6}

Table 5. Receivers

Type	Example	Uncertainty
Loran-C Timing	Austron 2000C	0.05×10^{-9}
Television Line 10	Beta 214	0.03×10^{-9}
Microwave	SATCOM	0.1×10^{-9}

QUESTION AND ANSWER PERIOD

SGT. OSTROWSKI:

Sgt. Ostrowski, Newark Air Force Station.

Ken, in your remarks to get to the microsecond and the nanosecond, I understand it is unavoidable, but we forgot the hour-minute and second and if the clocks are not within a half-second of one another, the microsecond is unrelatable.

MR. PUTKOVICH:

True.

I have had that happen to me a number of times.

MR. LUCK:

John Luck, National Mapping.

When you returned from your round the world clock trips, what interpolation technique do you actually use when you publish your final results and what time period do you use to get your interpolations?

MR. PUTKOVICH:

We use strictly a straight line interpolation unless we have some indication that we have had a phase jump and can pin it down quite well. It is usually just a straight line interpolation from the beginning of the trip to the end of the trip and aportion the difference over the trip, in a straight line interpolation between the two points, beginning of the trip and the end of the trip.

MR. LUCK:

In other words, you don't use the history, say for 20 days before you set out and for 20 days after you return?

MR. PUTKOVICH:

We try to take the clocks out, the portable clocks particularly, we try and have them set with essentially a zero offset to the master clock. This helps.

MR. BABITCH:

Dan Babitch, Hewlett Packard.

Early in the talk you gave an unwitting, but very vivid demonstration of one other error source when you subtracted 7 from 14 microseconds and got 8.

MR. PUTKOVICH:

That ruined my whole amazing demonstration, by the way. I didn't know what to do when that happened.

MR. NeSMITH:

Bill NeSmith, Hawaii Stadn.

I notice you had a problem on the 5 microsecond due to the antenna reversal. We had a similar situation in Hawaii. We received two antennas about two years apart. The first antenna, we had the same type of problem you have. We contacted the manufacturer and found out the arrow was painted on backwards.

MR. PUTKOVICH.

That is what the error usually is. You take them at face value as having been checked out and they are not.

DR. WINKLER:

Maybe one should suggest here, as a standard routine, if you exchange LORAN equipment, to test it against your previous setup. If you have a new receiver, leave everything else the same, just change the antenna lead into the new receiver, and establish a differential delay and use your old propagation constants as a reference. One can go very far in doing that, by using arbitrarily the first receiver as a set of reference because there you have the longest history with portable clock calibrations.

This must be done routinely. If you insert a multifilter, for instance, or a multi-coupler, it will add delays on the order of a microsecond or so and you determine that in the field. If you change the tuning of the slot filter it will change the delay of the multi-filter and you determine the effect compared to your previous setting. With just one receiver one can determine all these relative changes and

provide continuity in recordings and measurements.

LCDR. POTTS:

Potts, Coast Guard.

Actually, there is a superior method, I think, Ken, to the 5-microsound ambiguity and that is to use a whip antenna.

MR. FULLERTON:

Les Fullerton, U. S. Coast Guard.

Do you utilize a tick-to-phase measurement before and after making clock trips?

Mr. Putkovich:

Yes, we do. The tick-to-phase was an outgrowth of using 115 BR plots in the early days of vertical clock measurements when we had quite a bit of possibility of having a change in the tick-to-phase measurement, when what you wanted to do was ascertain that the clock was still in step with the oscillator.

We still do it, but I don't know whether it is necessary. It is just a carryover from early times. I like to use it because it gives you a little bit of additional information on the trip in the event that you do have some sort of a failure. There is a slight possibility that you are going to have a jump in your divider chain driving the clock, something like that. So, it is a little bit of extra data.

INTERNATIONAL TIME TRANSFER BETWEEN USNO AND RGO VIA NTS-1 SATELLITE

H.M. Smith, N.P.J. O'Hora, (Royal Greenwich Observatory)
R. Easton, J. Buisson, T. McCaskill, (Naval Research Laboratory)

ABSTRACT

Time transfer data was taken at NRL and RGO during July-August 1975. The NRL station was reference to USNO via portable clock and Loran-C. The data indicates continuous sub-microsecond clock synchronisation during the experiment.

INTRODUCTION

The only operational system at present generally available for continuous precise time comparisons between clocks in different locations is provided by the chains of Loran-C navigational emissions which now furnish the link between participating agencies and the Bureau International de l'Heure for the formation of TAI, the international scale of atomic time. A serious disadvantage is that good clocks at establishments outside the present Loran-C coverage area are automatically excluded. It is also obviously desirable that fully independent checks should be made to confirm the synchronisation of the various chains. Such checks can be made periodically by the physical transport of clocks between the various locations but such procedures are expensive and cannot be operated continuously.

In 1963 Study Group VII of the International Radio Consultative Committee referred to the advantages, which might be expected to accrue from the use of time signal emissions from artificial earth satellites, and urged studies of the technical factors involved. (1). In 1970 R L Easton of the U S Naval Research Laboratory reported on the use for time synchronisation of the Timation satellites employed in navigational experiments. (2). Following successful experiments between sites in the U S A, the low-altitude satellite Timation II was used for a brief period for time comparisons between the U S Naval Observatory and the Royal Greenwich Observatory. The frequency difference between RGO and USNO was observed to be less than 5×10^{-12}. The standard deviation of the individual time measures was $\pm$ 0.3 microsecond. After servicing at NRL the receiver was sent to Australia where in more extended tests the standard deviation was reduced to approximately $\pm$ 0.1 microsecond. (3).

Timation III

The NRL Timation project was merged in 1973 with the U S Air Force 621B project to form a combined Department of Defense (DOD) programme called the NAVSTAR Global Positioning System (GPS) and the NRL Timation III satellite was redesignated GPS Navigational Technology Satellite 1 (NTS-1). Our interest here is restricted to the potentialities of the system in a world-wide precise time synchronisation facility. The satellite moves in a nearly circular orbit with a radius 3.13 times the equatorial radius of the Earth and with an orbital inclination of 125°. The period of revolution is 469 minutes. The satellite motion is monitored by Doppler measures at 5 stations and the orbit calculated at the U S Naval Weapons Laboratory (NWL). Predicted positions are made available at reception points through a data link to a central computer. NTS-1 incorporates rubidium gas cell standards, a quartz oscillator, and a retroreflector panel to permit direct measure of range.

Two programmes of particular relevance in timekeeping have been planned. One is to make direct comparisons between the USNO and RGO both via Loran-C and via NTS-1 and to check these by occasional travelling clock trips. In this way it is hoped to determine if there are any significant seasonal variations and to estimate the accuracy of the two systems in practice. Another experiment involves the intercomparison of standards in USA, Australia, New Zealand, Hawaii, Japan and the UK. The present report is an interim discussion of the results obtained in the first month of the USA/UK comparisons.

Clock Comparisons

Time differences between the satellite clock and the clock at the ground station are made by a sequence of phase measures made at ten related frequencies. (4). The comparison frequencies are emitted each minute between seconds 55 and 60. It is normally possible to commence a series of measures shortly after the satellite appears above the horizon, and to continue measures throughout the pass until the satellite disappears below the horizon. All transmission frequencies are of the order of 330 MHz and, in order to derive the lower frequencies necessary for the phase comparisons covering the range 10^{-3} to 10^{-9} second, an additional frequency in the same wave band is transmitted. This is known as the satellite reference frequency and it is transmitted over the whole five seconds in which the ten side tones are radiated.

Data Acquisition

The ground station equipment consists essentially of a radio receiver together with circuits for deriving from the station clock a range of comparison frequencies matching those of the satellite and a comparator for effecting the phase comparisons. All incoming signals from the

satellite are affected by Doppler shifts. These effects are eliminated using a method of differencing in which a receiver generated oscillation is firstly phase locked to the incoming satellite reference frequency and then differenced from the incoming side tones. The difference frequencies obtained in this way reproduce at the station the phase of the satellite oscillator and consequently the dial reading of the satellite clock at the epoch of emission of the signal. These frequencies are then phase compared with the equivalent range of frequencies derived from the station clock. The reduction of measured phase differences to give directly the time difference between the satellite clock at the epoch of emission and the station clock at the epoch of reception is made by an on-line mini-computer linked to the phase comparator. The computer provides a visual display of the measure for each minute and also files the value on magnetic tape for subsequent analysis. From the orbital elements and the station coordinates in the same reference frame it is possible to predict instantaneous values of the satellite range. Pre-computed range values for each minute of the pass, expressed as propagation times of the radio signals over the calculated ranges, are available to the observer for each observation. By comparing these tabulated range values (T) with the measured or observed values (O) that are being obtained the observer can make an on-the-spot assessment of the quality of the reception and measurement.

Reduction of Observations

The measured difference between the clocks is composed of the true difference (i.e.,difference in the clock dial readings) at the epoch of measurement and the travel time of the satellite signal. The travel time comprises both the propagation time and the equipment lags that can be measured in the laboratory. By correcting for the travel time the true difference between the clocks can be calculated. The propagation times (T values) supplied for use during an observation are computed up to several months in advance and consequently may only be of first order accuracy by the date of observation. More accurate T values, deduced from the Doppler tracking of the satellite about the date of observation, are used in the subsequent reductions. Neglecting errors of measurement and the equipment lags and assuming that the T value represents the correct propagation time, then the T-O value for any minute represents the time difference between the clocks at that instant. Furthermore, if the relative rate of the two clocks is zero the T-O values obtained for each minute of the pass should all be equal.

In tracking the satellite over a pass, clock comparisons are normally obtained for each minute in which the satellite altitude is greater than 5°. As a result both the length and the sector of the atmosphere

traversed by the radio signals are continuously changing so that atmospheric inhomogeneities affect both signal velocity and wave refraction in a variable manner. In passes where high altitudes are attained the shorter atmospheric path gives more consistent results. Also, independent of the altitude attained, the best measures are obtained around the time of closest approach (TCA) of the satellite when both the range and the rate of change of range are minimum. Where the T values do not truly represent the orbital behaviour of the satellite, the source of the errors in T can be deduced from the nature of the variations in T-O around TCA when conditions approaching "steady state" exist in the experiment.

Figure 1 shows the measures obtained (O), the T values and data for various stages in the reduction of pass number 1144 in which the NTS-1 clock was compared with clocks at RGO and at NRL. The results for the two stations are quite independent but each set exhibits the salient features of the data obtained in a pass.

Figure 1 shows:

(a) T and O values for the minutes at which meaningful measures were obtained at the two stations

(b) T-O differences, plotted with a scale 500 times that of (a)

(c) T-O corrected by a linear term which has zero value at TCA.

As explained above, an essential condition for obtaining equal T-O values throughout a pass is that the relative rate of the two clocks being compared is zero. However, the satellite clock differs by about 49.2×10^{-10} from nominal while the departures of the caesium beam atomic clocks used in the two stations are only of the order 5×10^{-13}. The relatively very large rate of the satellite clock is reflected in the two sets of T-O values which, to first order, change by 0.3 usec min^{-1}. Because of its unique features the TCA is the fiducial reference time for which the adopted pass result is quoted and rate corrections are consequently applied to the results obtained at all other times throughout the pass to reduce all results to the epoch of TCA.

The rate is not required with great precision at this stage but, as may be seen in (b) and (c) of Figure 1, the adopted value has furnished corrections that have removed about 95% of the drift in T-O. Furthermore, although the final result is quoted for the epoch corresponding to TCA, it is clear that virtually all of the measures at both stations are within 1 μsec of the values at TCA. For passes in which spurious measures are received at TCA, a T-O value for this epoch can be deduced from adjacent measures.

TABLE 1

Inter-Observatory Clock Comparisons via TIMATION III

Date 1975 July	RGO Data TCA h m	RGO Data T-O μs	NRL Data TCA h m	NRL Data T-O μs	NTS1 Data Rate μs/min	NTS1 Data Correction μs	NRL minus RGO
2.5	12 13	+5977.10	12 44	+2955.75	-.2969	- 9.20	+3012.15
3.5	11 43	+5559.45	12 13	+2538.40	-.2961	- 8.88	+3012.17
4.5	11 12	+5142.30	11 47	+2119.90	-.2957	-10.35	+3012.05
7.4	09 39	+3891.30	10 23	+ 866.35	-.2959	-13.02	+3011.93
8.4	09 10	+3474.05	09 55	+ 448.76	-.2948	-13.27	+3012.02
9.4	08 41	+4228.60	09 27	+1203.04	-.2953	-13.58	+3011.98
11.4	07 41	+3398.13	08 31	+ 371.24	-.2946	-14.73	+3012.16
15.5	12 35	+1612.35	13 00	-1407.19	-.2950	- 7.37	+3012.17
16.5	12 04	+1196.59	12 31	-1823.80	-.2958	- 7.99	+3012.40
17.5	11 31	+ 781.29	12 02	-2240.25	-.2957	- 9.17	+3012.37
21.4	09 30	- 885.30	10 09	-3909.13	-.2956	-11.53	+3012.30
22.4	09 00	-1302.04	09 41	- 326.50	-.2963	-12.15	- 987.69
23.4	08 31	-1719.95	09 13	- 744.72	-.2969	-12.47	- 987.70
24.1	01 24	-2019.74	02 21	-1049.03	-.2974	-16.95	- 987.66
25.1	00 55	-3790.87	01 52	+ 179.67	-.2960	-16.87	-3987.41

TABLE 2

Clock Comparisons by TIMATION III and LORAN-C (microseconds)

Date 1975 July	NRL minus RGO	Difference in Receiver Lags	NRL minus RGO	UTC minus NRL	UTC minus RGO (TIMATION)	UTC minus RGO (LORAN-C)	Method Differences
2.5	12.15	-8.90	3.25	-19.18	-15.93	-16.4	+0.5
3.5	12.17	-8.90	3.27	-19.27	-16.00	-16.3	+0.3
4.5	12.05	-8.90	3.15	-19.33	-16.18	-16.3	+0.1
7.4	11.93	-8.90	3.03	-19.52	-16.49	-16.8	+0.3
8.4	12.02	-8.90	3.12	-19.58	-16.46	-16.6	+0.1
9.4	11.98	-8.90	3.08	-19.65	-16.57	-16.7	+0.1
11.4	12.16	-8.90	3.26	-19.77	-16.51	-16.6	+0.1
15.5	12.17	-8.90	3.27	-20.00	-16.73	-16.7	0.0
16.5	12.40	-8.90	3.50	-20.06	-16.56	-16.9	+0.3
17.5	12.37	-8.90	3.47	-20.12	-16.65	-16.7	+0.1
21.4	12.30	-8.90	3.40	-20.34	-16.94	-17.3	+0.4
22.4	12.31	-8.90	3.41	-20.40	-16.99	-17.4	+0.4
23.4	12.30	-8.90	3.40	-20.46	-17.06	-17.6	+0.5
24.1	12.34	-8.90	3.44	-20.50	-17.06	-17.5	+0.4
25.1	12.59	-8.90	3.69	-20.56	-16.87	-17.6	+0.7

Comparisons of RGO and NRL Clocks

It is evident that independent comparisons of clocks at two stations with the satellite clock can be used to determine differences between the clocks at the two ground stations. Similar equipment was used at RGO and at NRL, that at RGO being loaned by NRL for the duration of the experiment. In order to minimise effects of the large rate of the NTS-1 clock the results discussed here are based only on passes during which simultaneous measures were made at both stations.

At satellite rising or setting, the great circle distance of the sub-satellite point from an observing station is 72° so the circle with this radius and centred on the station may be taken as the effective horizon of the satellite. The surface area common to two such circles with their centres separated by 57° (the Herstmonceux-Washington great circle distance) thus represents the common effective horizon of NRL and RGO. Due to the configuration of the stations and the satellite orbit, in a common pass TCA at the RGO generally occurs half to one hour before TCA at NRL. An ideal pass in which zenith transit of the two stations occurs is impossible and indeed high altitude passes that are equally high at the two stations are exceedingly rare. Figure 2 shows the subsatellite tracks of the common passes discussed in this paper and also the two points on each track that mark the TCA for each station. The 3-digit numbers in the figure denote the date of the pass (1975 day number).

Figure 2 also shows the area surrounding each station within which the satellite altitude exceeds 60°. Of the 15 passes discussed, TCA at NRL for 14 were within this area while in the RGO high altitude area TCA occurred only 5 times. No doubt as the period of the experiment is extended this inequality will diminish. Also, although the reception equipment in use at the RGO functioned satisfactorily, there are grounds for believing that it is marginally inferior to the equipment in use at NRL. The differences in altitude and equipment may explain why the reception efficiency at the RGO, i.e. the ratio of measures secured to the number that might have been obtained, was about 75% of that achieved at NRL. There is, however, no significant difference in the overall accuracy of the two stations over the period discussed.

Results

The measures made at the two stations and the deduced differences between the stations' clocks are summarised in Table 1. The tabulated T-O values represent clock differences, in the sense satellite minus station clock, at TCA for both stations. A correction for the rate of NTS-1 is applied to the RGO measures to reduce them to the epoch of TCA for NRL. Because differences in TCAs for the two stations are of the order 50 minutes, the rate of NTS-1 is required with an accuracy

of better than 0.002 μsecs min^{-1} (equivalent to 3×10^{-11}) to achieve 0.1 μsec precision in the station differences which are tabulated in the final column. The true station difference only amounts to a few microseconds; the values given in the table are much larger due to the presence in the data of integer milliseconds that are included in the software for convenience in data handling.

Loran-C receivers at the RGO furnish a daily measure of the departure of the station clock from the UTC system of the US Naval Observatory and even more refined comparisons with this system are carried out at NRL. The quality of the RGO-NRL link via TIMATION may be assessed by comparing it with that achieved through Loran-C on the same dates. The comparisons are set out in Table 2 in which the first data column is the final column of Table 1, with integer milliseconds removed. It should perhaps be stressed that in the table the time system designated RGO is that of the station clock (CsJ) used in the satellite comparisons and not the UTC system of the RGO which is based on all the observatory clocks. As mentioned above, the UTC system employed here is that of the USNO. The comparisons indicate that; (i) there is a systematic difference of 0.3 μsec between the two methods and (ii) the methods are of the same order of accuracy. Assuming, as the data suggest, that UTC-RGO changes linearly over the period, the departures of the two sets about a line with slope 0.05 μsec day^{-1} have been calculated. The dispersion is shown in Figure 3 in which it may be seen that in the small sample available the TIMATION results are more consistent, with a standard deviation of $\pm$ 0.13 μsec as against $\pm$ 0.17 for Loran-C.

The results may be seen as a success for the time transfer experiment with TIMATION because the accuracy is already of the same order as Loran-C and the coverage is virtually world wide. The comparison accuracy at a single station is of the order $\pm$ 0.01 μsec; the disproportionate loss in accuracy in inter-station comparisons may be attributed to the critical dependence upon precise evaluation of the rate - and also upon the stability of the rate - of the NTS-1 clock. This limitation would hardly exist if the satellite was furnished with an atomic clock.

The continuation of the comparisons of the Timation and Loran-C links between the USA and UK should thus prove of great value and it is perhaps permissible to express appreciation of the willing co-operation of NRL and the USNO. It is already evident that, as the system is extended and used by ground stations world wide, the degree of timing precision that can now be achieved fully justifies the decision to incorporate a caesium clock in NTS-2.

REFERENCES

1. Documents Xth Plenary Assembly CCIR, Volume 3, page 219 (Study Programme 249A (VII) Geneva 1963.

2. Proceedings PTTI Strategic Planning Meeting, Volume 1, page 108. 1970.

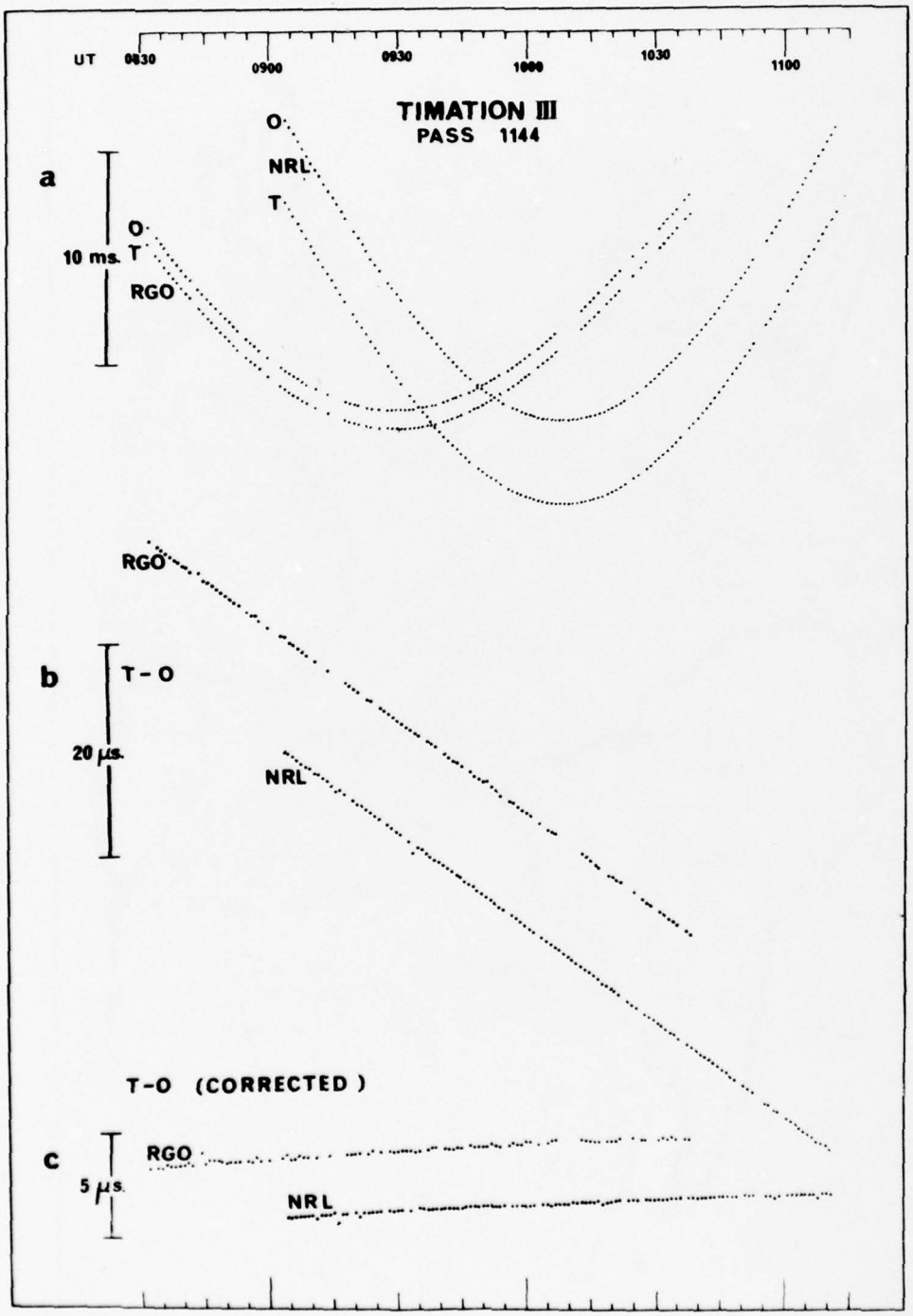
3. R L Easton, P Morgan and H M Smith
IEEE trans: Instrumentation & Measurement, p 525, Volume IM-23, No. 4. December 1974.

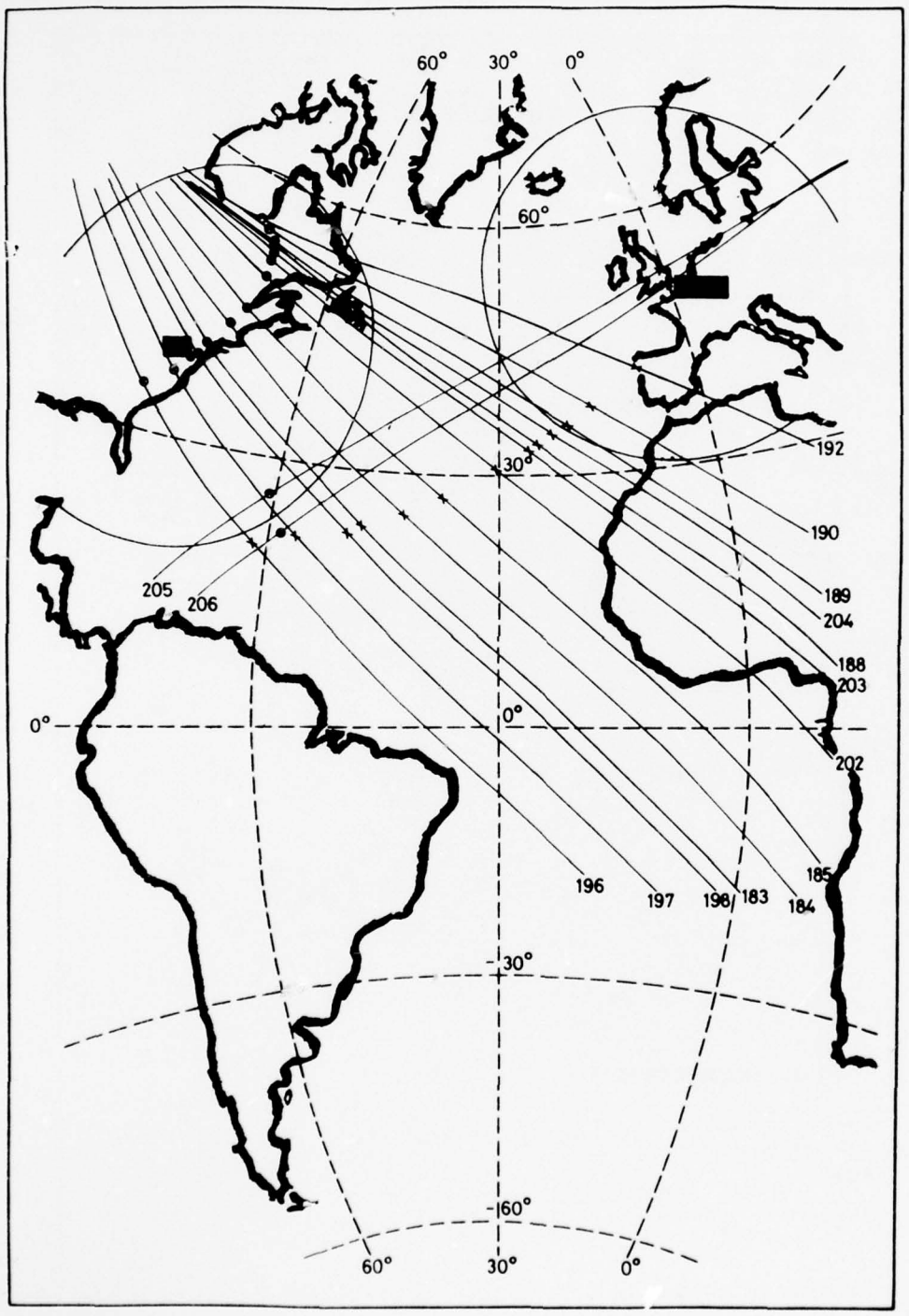
4. Proc. 2nd Cagliari International Meeting on Time Determination, Dissemination and Synchronisation, p. 87. Cagliari, 1975.
(paper by H M Smith; wrongly attributed to R L Easton)

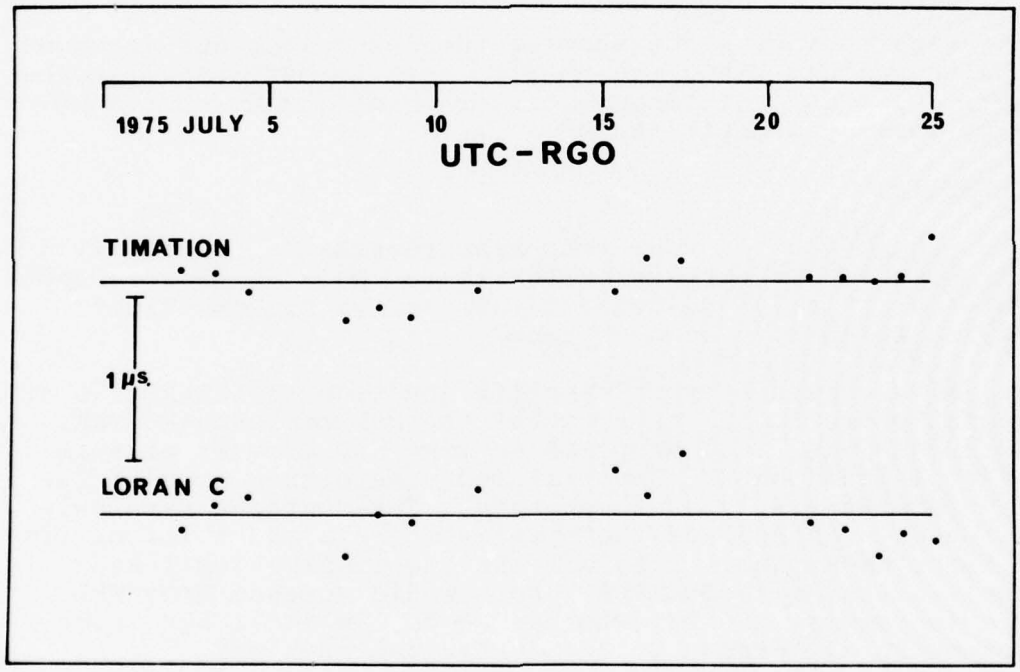
Figure 1. For explanation see opposite.

Figure 2. Subsatellite positions corresponding to TCA at NRL (o) and at RGO (x). For explanation see opposite.

Figure 3. Scatter in comparisons between RGO and UTC (USNO).


UT
0830
0900
0930
1000
1030
1100
TIMATION III
PASS 1144
a
10 ms.
O
T
RGO
O
NRL
T
RGO
b
T-O
20 μs.
NRL
T-O (CORRECTED)
c
5 μs.
RGO
NRL


60°
30°
0°
60°
192
30°
190
205
206
189
204
188
203
0°
0°
202
196
197
198
183
184
185
30°
60°
60°
30°
0°


1975 JULY 5
10
15
20
25
UTC - RGO
TIMATION
1 μs.
LORAN C

QUESTION AND ANSWER PERIOD

MR. LUCK:

John Luck, National Mapping, Australia.

I have been out of Australia since before this latest series of experiments was conducted. This is my first view of the results, and I am quite delighted and I would like to join with Mr. Smith in thanking Dr. Winkler, Roger Easton and all the others in coming to Australia in particular and the other places. I cannot express how grateful we really are.

Referring to your slide showing the Australian and Japanese results against USNO, the results seem to have two lines on them. Is this just random scatter or do you suspect something more systematic there?

MR. SMITH:

Well, thank you for your very kind remarks and certainly I join with you in expressing thanks to those who were responsible for this. I do congratulate you on the excellent results which have been obtained.

But, with regard to your specific question, I think I am at a point where I call upon one of the NRL representatives. Whether he will feel disposed to make any comment at this stage, I don't know. You will appreciate that some of the travelers have only just returned. These graphs have only just been produced and they really haven't had a lot of time to think about answers to all the questions which I know they are asking themselves. But, would someone from NRL like to comment and say whether we do, in fact, have some systematic difference in the Australian results?

MR. LYNCH:

Don Lynch, Naval Research Lab.

I was fortunate enough to go on this trip. In regard to John's question, this is true. These represent passes at different times of day and there is a combination of reasons for why there is this spread. There is a small amount due to residual ionospheric effect at different times of day. I think in this case, although, we haven't gone into the

final analysis, I think you will find that this is primarily due to the different geometry. That is, we are looking at the satellite on a different part of the orbit.

There is a preliminary analysis we have been using, predicting the position of the satellite, which is several weeks old. Now, what we intend to try to do in removing or examining this further, is to update our position of the satellite, using newer data for tracking purposes, re-evaluate the position of the satellite and see if this doesn't remove part of this error. But, I think it is primarily due to these two effects, the geometry due to the old trajectory and the ionospheric effect.

DR. HELLWIG:

You refer to the importance of the performance of the satellite clock; what kind of clock was really used on NTS-1 for these experiments?

MR. LYNCH:

The clock that was used in the satellite during the time period of these experiments was the quartz clock.

DR. HELLWIG:

I would like to ask why wasn't the rubidium used?

MR. LYNCH:

We were using the quartz during this period. We had been evaluating the behavior of the quartz and we had a little more history on it. The other thing is that we did experience, in using the rubidium clock, some unlocking of the rubidium and discontinuity and we thought, probably, during this experiment we would be better off using the quartz even though it might be less stable. But, we had limited time to perform this experiment and we wanted to use something that we thought was probably going to hold in and not unlock on us, although we had no way of knowing whether or not the rubidium would have stayed in, had we tried it.

A TWO-WAY TIME TRANSFER EXPERIMENT USING A SYNCHRONOUS SATELLITE

A. R. Chi - Goddard Space Flight Center/NASA
E. Byron - Applied Physics Laboratory/JHU

ABSTRACT

A time transfer experiment using the Applications Technology Satellite, ATS-1, was conducted in 1973-75 under joint sponsorship of the Goddard Space Flight Center (GSFC) and the Federal Aviation Administration (FAA). The experiment is designed with a capability to serve a large number of users and to achieve a time synchronization accuracy of 0.5 microseconds at 3 sigma values. A two-way satellite time transfer technique is used to eliminate the need for a priori knowledge of the propagation path delay. Thus, the technique is inherently capable of transferring precise time on a real-time basis from a master time station to a host of user or slave stations.

INTRODUCTION

The precision time transfer experiment reported upon in this paper was conducted under an interagency agreement between the Federal Aviation Administration of the Department of Transportation and the National Aeronautics and Space Administration.

The objective of the experiment was to demonstrate the feasibility of a system designed to disseminate a precision time reference from a master station clock to a remotely located clock via a synchronous satellite. The experiment was conducted in four phases: Phase one consisted of an RF terminal design and the modification of several pieces of available equipment. The second phase was comprised of the design and construction of the RF terminal as well as several RF link studies. Phase three consisted of the calibration of the system, and RF tests using one station, in which time transfer equipment and clocks were colocated. Phase four was conducted to demonstrate the feasibility of transferring time from a master station to a remote station and to provide the data necessary to evaluate the system accuracy. It is the phase four experimental results which we will be primarily concerned with in this paper.

PRECEDING PAGE BLANK-NOT FILMED

The phase four tests were conducted during the period from March 14 to April 1, 1975, and consisted of a series of measurements performed during this period of time. An rms error, between the transferred (slave) reference signal and the master system reference, not exceeding 167 nanoseconds was established as the system design goal. The purpose of the measurements, of course, was to provide the data necessary to verify the accuracy of the system. In another section of this paper we will discuss the data which were collected, as well as the methods used to analyze the data in order to ascertain if the system objectives were satisfied.

In this paper our objectives are: to briefly describe the system and how precision time is disseminated, evaluate and discuss the experimental data collected during phase four test and the results achieved disseminating time from Mojave, California to Rosman, North Carolina, and finally to discuss, as appropriate, the problems encountered.

SYSTEM DESCRIPTION

The overall system consists of essentially two radio stations linked to each other by a wideband RF channel relayed by the ATS-1 synchronous satellite. The satellite simply acts as a "bent pipe" repeater, receiving on 6.3 GHz and transmitting on 4.18 GHz. Each station contains three major subsystems: a transmitter, a receiver, and a MODEM terminal. The MODEM interfaces with the transmitter and receiver at 70 MHz.

The MODEM terminal equipment complement encompasses a spread spectrum modulator/demodulator system, time interval counters and control equipment. The clocks and clock control equipment are also included as a part of the terminal. An overall block diagram of the system (excluding the satellite) is illustrated in Figure 1.

The modulator contains a pseudorandom noise (PN) code sequence generator whose repetition rate is controlled by a voltage controlled crystal oscillator (VCXO). The PN code is biphase modulated on a 70 MHz signal which serves as the IF of the C-band carrier of the uplink signal from the ground to the satellite. The demodulator serves to recover the PN coded signal by correlating the received signal with a locally generated replica of the transmitted PN sequence.

The PN code generator used in this experiment has an eleven stage shift register. The shift register clock is a VCXO

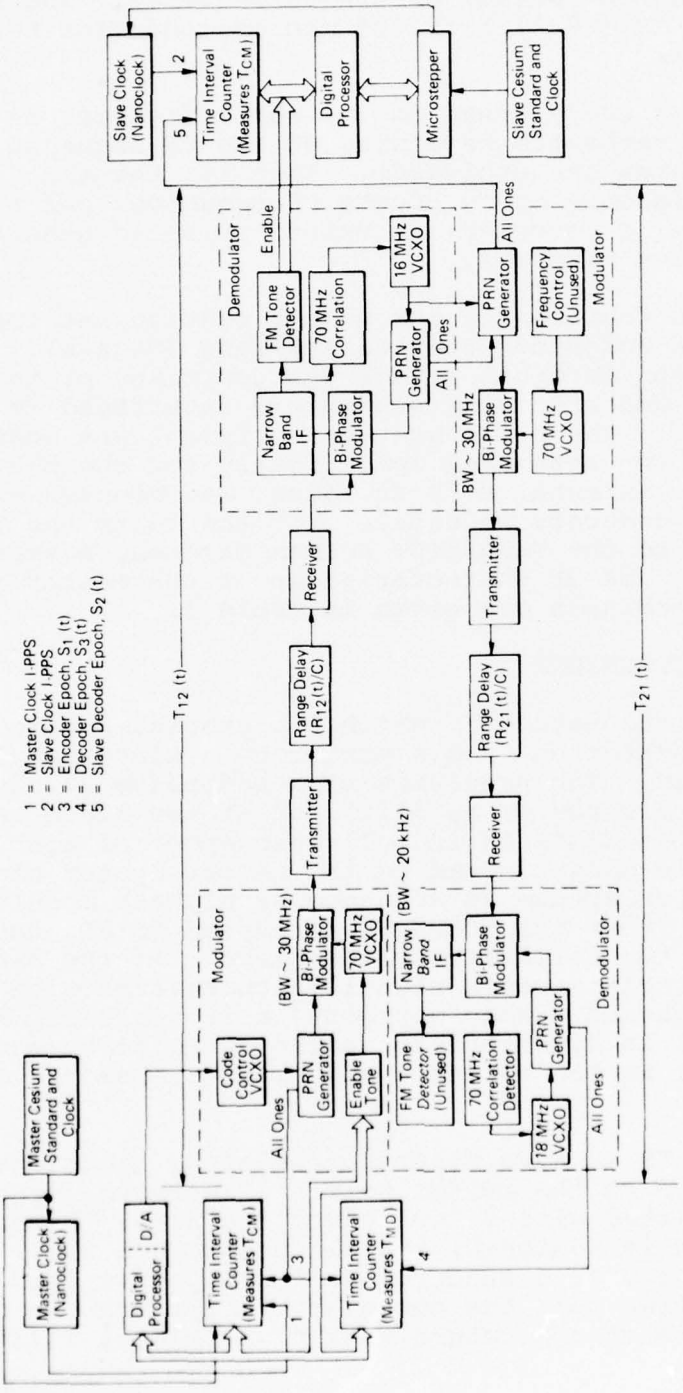


Fig. 1 Block Diagram of Precision Time Disseminating System

at 16.376 MHz. The frequency of the VCXO can be binarily divided to extend the period of the PN sequence. The period of the sequence is $(2^n-1)/f$ or 125 microseconds for n=11 and f=16.376 MHz.

When the state of every stage in the shift register is a logic "1", it marks the beginning of the PN sequence (the all 0's states are excluded). That is, the all 1's state is the reference epoch of the PN sequence, and whenever an all 1's state is detected, an output pulse is generated for time measuring purposes.

During the phase four tests, the master station was located at the NASA/STDN Goldstone Station ATS-wing (Mojave). The master station terminal system was comprised of the ATS transmitter and receiving subsystems interfaced to a MODEM terminal. The slave station equipment was housed in an RF mobile Van assembled specifically for the phase four tests. The antenna, a 10 ft. dish, was mounted external to the Van on a concrete pedestal. For the tests the Van was transferred to the NASA/STDN Rosman Station, Rosman, North Carolina. The RF characteristics of the master and slave station terminals are given in Table 1.

DESCRIPTION OF TECHNIQUE

In this section the method by which the precision time reference is transferred from a master to a slave terminal will be discussed. The precision time reference at the master will be referred to as S1(t) and at the slave as S2(t). The signal S1(t) is the all-ones epoch of a PN sequence which is phase locked to the master system clock 1-pps. The master system PN sequence is biphase modulated onto the 70 MHz IF of the MODEM, heterodyned to RF, and relayed through the satellite to the slave. At the slave terminal a similarly encoded signal is correlated with the received sequence. When correlation is achieved, a second PN signal is synchronized to the correlation epoch. The signal S2(t) is the all-ones epochs of the second PN sequence.

The slave MODEM IF is also biphase modulated, translated to RF and relayed to the master terminal where the received signal is correlated with a replica of the slave PN sequence. When correlation is achieved, the all-ones epoch S3(t) of the locally generated sequence will be synchronized to S2(t). Assuming that the correlator errors can be neglected, then for forward and return path time delays, T12(t)

TABLE 1. RF TERMINAL SYSTEM CHARACTERISTICS

OPER. MODE	CARRIER FREQ (MHz)		ANTENNA			XMT POWER (WATTS)	RCV SYSTEM	
			DIAMETER (METER)	GAINS (db)			C/N BW 20 KHz (db)	NOISE TEMP °K
	XMT	RCV		XMT	RCV			
MASTER[1]	6301.0	4178.6	12	54.6	51.0	40 — 50	15 — 19	76
SLAVE[2]	6301.0	4178.6	3	40.1	39.7	600 — 800	15 — 19	316

(1) NASA ATS TRACKING STATION TERMINAL AT MOJAVE, CALIFORNIA

(2) EXPERIMENTAL MODEL PORTABLE TERMINAL

and T21(t)*, the all-ones epoch, S2, corresponds very nearly to S1 delayed by the forward path delay, T12. Also, S3 corresponds to S2 delayed by the return path delay, T21. Once correlation between the code sequences is achieved at the master station, the time interval between S1 and the master clock 1-pps (Tmc) and the time interval between S1 and S3 (Tmd) are measured, and Tmc is compared with Tmd/2 in a feedback loop. The loop error signal, which is proportional to (Tmd-2Tmc)/2, is periodically adjusted (once per second) to minimize the loop error.

When the loop error is less than a predetermined value a command tone is frequency modulated on the master terminal 70 MHz IF, and subsequently detected at the slave terminal. The command tone signals the slave to begin measuring the error between the slave clock 1-pps signal and the locally generated precision time reference, S2(t). The time differential between the slave clock 1-pps and S2(t), say $\hat{T}_{cm}$, will be proportional to T12-Tmc+ΔT, where ΔT is the error between the master and slave clock 1-pps signals, and Tmc, of course, is the time interval by which S1(t) precedes the master clock 1-pps.

Explicit expressions relating Tmc and Tmd can be rigorously developed. It can be shown also that the time interval between S1 and S3 is approximately equal to the round trip time delay modulo To (i.e., nTo+Tmd$\approx$T12+T21). If we assume that T12=T21 and the feedback loop error signal is negligibly small, then Tmc$\approx$T12 and the time interval $\hat{T}_{cm}$ is very nearly a measure of the error between the master and slave clock 1-pps signals. The locally generated signal then, S2(t), constitutes the precision time reference available at the slave and the objectives of the system are accomplished if the difference between the clock error and the time interval $\hat{T}_{cm}$ can be kept negligibly small, i.e., when $\hat{T}_{cm}-\Delta T\rightarrow 0$. It is this difference which we will be primarily concerned with in the remainder of this paper. Before discussing this, however, we would like to point out some advantages of using PN sequences.

Some Advantages of Encoding the Reference Signal S1(t) As a PN Sequence

In the previous discussion, no justification for using PN encoded sequences was ventured. There are, of course,

---

* The forward and return path delays vary with time because the RF carrier is relayed through the satellite which moves relative to the two stations.

several very good reasons and we would like to highlight just a few. The first of these relates to the tradeoff between resolving the ambiguity problem inherent with all periodic sequences, and the desired accuracy. Among other attributes the PN sequence satisfies both of these requirements simultaneously since the ambiguity of the precision reference is equal to the period of the sequence and the phase accuracy is a small fraction of the chip period. Another, and particularly important, advantage is that several sequences can be transmitted simultaneously through the same RF channel without significantly interfering with one another. Consequently, the forward and return path delays through the satellite repeater are identical and thereby cancel. Still another advantage is that by using a variation of the time transfer technique we discussed previously, it appears practical to transfer precise time to several remote sites simultaneously (Reference 1). Finally, the possibility of coexisting with other types of communication signals over the same RF channel with negligible interference also appears feasible (Reference 2).

System Ambiguity

In the previous section it was pointed out that one of the advantages of PN sequences was the increased ambiguity periods achievable. This is important because the absolute accuracy of a time transfer depends upon the ambiguity interval of the system. In this regard, we should like to point out that the system ambiguity is one-half the sequence period, and further emphasizes the desirability of relatively long sequences. We can discuss other aspects of the ambiguity problem, but these are not germain to our present objectives and consequently we will continue with a very brief discussion of the system controllers.

SYSTEM CONTROL PROGRAMS

There are three programs associated with the system. Two of these control the operation of the system, whereas the third is used for collecting statistical data. Each of these programs is briefly summarized below.

Master System Control Program

There are essentially two routines associated with the master system controller. The first routine comprises an automatic frequency control (AFC) loop which functions to set the VCXO frequency to 16.376 MHz ±0.0001%. Once this accuracy has been achieved, the controller tests the

MODEM status word to determine if the PN sequences are "tracking". If the demodulator indicates an in-track condition, then the AFC routine is passed over to the code epoch control routine. If the demodulator is not tracking, the entire AFC mode is repeated.

Briefly, the code-epoch control routine executes the following functions:

1. Performs the necessary measurements (by controlling various measuring equipment) to calculate the phase differences between the modulator all-ones epoch and the clock 1-pps, and the demodulator all-ones epoch and the clock 1-pps.

2. Calculates the phase error signal and controls the VCXO voltage corresponding to the phase error and filter weighting function. The filter weighting function approximates a filter characteristic associated with a second order phase lock loop. This filter characteristic was chosen because a second-order phase lock loop is capable of tracking a signal whose frequency is changing linearly with time (Doppler).

3. Calculates the mean squared phase error and activates the TONE-1 frequency generator, thereby signaling the slave system control program, when the mean squared phase error is smaller than a predetermined value, and indicates this action by setting the "loop locked" flag.

Slave System Control Program

The slave system controller is considerably simpler than the master system. Briefly, the functions this routine performs are:

1. The controller examines the MODEM status word, i.e., looks for the master system TONE-1 command.

2. Measures the time difference, $T\dot{c}m$, between the received PN sequence "all ones" epoch and the slave clock 1-pps.

3. Calculates the average time error over a preselected number of samples.

4. Adds a bias correction factor to the average value calculated in 3. The value of the bias depends upon the asymmetry between the forward and return path delays.

Statistical Routine

This routine performs the functions listed in items 1 through 3 for the slave system controller. In addition to the average error, however, the routine also calculates the maximum and minimum errors as well as the variance. The results of the four calculations are subsequently formatted and printed. During operation of the statistical routine the slave clock is not corrected.

TEST DATA

The tests consisted of a series of measurements designed to provide the data necessary to determine the accuracy of the system. Essentially, two types of timing data were collected. The first type of data are comprised of measurements between the primary cesium standards and are independent of the time disseminating system. The second type of data collected are comprised of the measurements relating to the system.

Primary Clock Data

Maintaining precise time between both terminal clocks is central to the problem of corroborating the accuracy of a precision time transfer. Here we will address the problem of maintaining and coordinating precise time between the clocks at the Mojave and Van sites during the test period. Briefly, time keeping at each site was maintained with primary atomic time standards. The standards used were Hewlett-Packard type 5061A cesium standards with option 004, utilizing high performance cesium beam tubes. The relative time between each standard was compared indirectly with an HP5061A Flying Clock transported via FAA and commercial aircraft.

During the first part of the test period the Mojave standard (the master) was synchronized to the portable clock. The portable clock was subsequently flown to the Van (slave station) where the difference in time between the two clocks was monitored. Two types of data were recorded; the relative phase ($\Delta\phi$) between the two 5 MHz reference frequencies and the time differential between the Van and portable cesium 1-pps outputs (TVcs/Pcs).

Initially it was decided not to synchronize the Van cesium to the portable clock, however, this proved to be awkward because the Van clock was stopped while the Van was being moved from the GSFC to the Rosman STDN, and a large time

difference had accrued. After several days, the Van cesium clock was synchronized to the portable clock. The portable clock remained on the Van for approximately six days during which time the TVcs/Pcs and the $\Delta\phi$ data were recorded. Following this period, the portable clock was returned to Mojave and the time difference between the Mojave and portable cesium clocks (TMcs/Pcs), along with phase data, were recorded. Immediately following the tests the portable clock was again flown to the Van and TVcs/Pcs was measured for closure. No phase data was recorded. The results of these measurements are plotted in Figure 2.

In addition to the primary clocks, each terminal maintained a secondary clock system (trade name Nanoclock). Dual clocks were included with each terminal for the tests to facilitate introducing known offsets with respect to each station without disrupting each station's reference time (the 1-pps output of the cesium clocks).

For the master terminal the Nanoclock reference signal was obtained from the cesium standard's 5 MHz output. For the slave, the reference was obtained from the microstepper which is phase locked to the 1 MHz output from the cesium standard. The clock arrangement may be clearer if we refer to Figure 1.

Time Transfer Data

We will discuss now, very briefly, the procedure used during the tests to obtain the time transfer data.

At the beginning of each test period the clock offsets between the respective Nanoclock and cesium standard at each terminal were measured and recorded, along with the time of day. Following this, the RF signal levels were adjusted until the carrier-to-noise ratio measured at each terminal was essentially equal. Once the RF levels were optimized, the master and slave system controllers were loaded with the respective clock correction program, and both the master and slave MODEM systems subsequently locked up. Upon detection of a command tone from the master, the slave Nanoclock would be adjusted by an amount equal to the average measured error between the nanoclock and precision time reference transferred to the slave. The amount by which the clock was corrected and the time of day were recorded on the system printer provided for this purpose (the time of day was annotated manually). Following a clock correction, one of the Nanoclocks (usually the Van's) would again be offset and the procedure repeated.

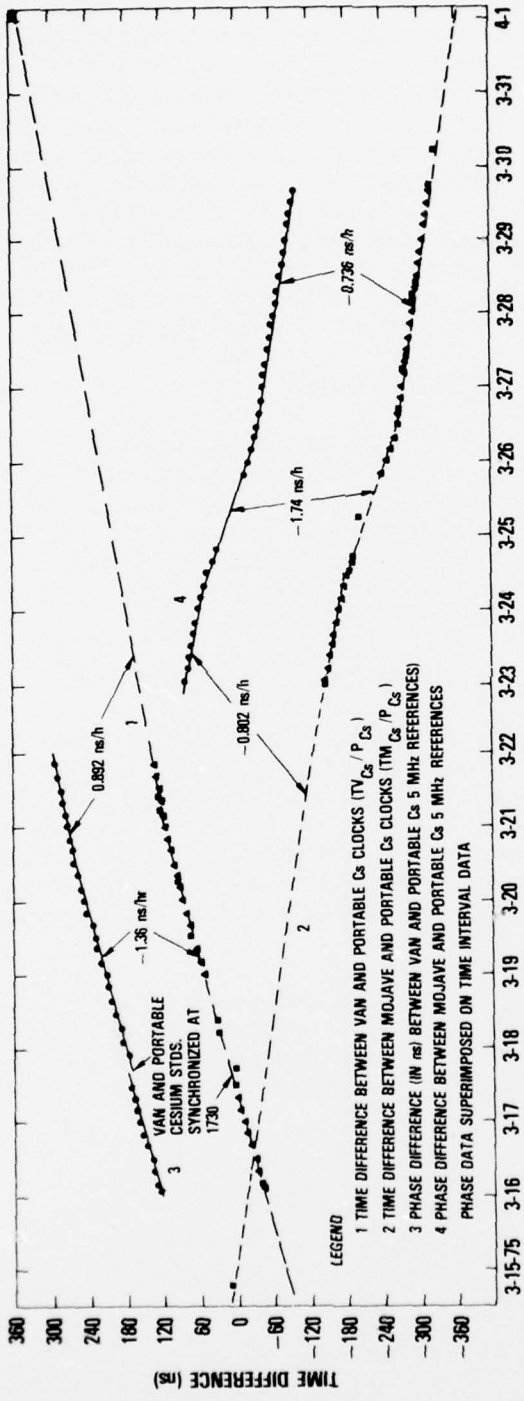


FIG. 2 **MEASURED TIME DIFFERENCES BETWEEN TERMINAL AND PORTABLE CLOCKS**

After several offsets and corrections, the slave system control program would be changed to the statistics routine and statistical data would be recorded for relatively long periods of time. In addition to the average error between the all 1's pulses and the Nanoclock, (T1's/Nv), the statistical routine printout also printed the maximum, minimum and variance of T1's/Nv over the averaging interval. If time allowed, the test period was usually terminated with a clock correction. In Figure 3, alternate data points taken from the statistical data recorded during the March 24 test period are plotted. We will discuss this figure shortly but first we would like to discuss briefly how we determine the accuracy of a time transfer.

DETERMINING THE SYSTEM ACCURACY

If the time between the two terminal clocks is known with sufficient precision, then the problem of verifying the system accuracy is fairly straightforward. Thus, if TMcs/Vcs is the "known" offset between the Mojave and Van cesium standards, and $\hat{T}$Mcs/Vcs is the offset between the Mojave and Van cesium standards estimated from the time transfer data, then the system error, say ε, is

$$\varepsilon = \text{TMcs/Vcs} - \hat{\text{TMcs/Vcs}}. \qquad (1)$$

We consider now, the factors which influence the accuracy of each of the above parameters. As will be seen, the accuracy of the predicted offset between the Mojave and Van cesium clocks, TMcs/Vcs, will depend upon the reliability of the portable clock data, whereas the accuracy of $\hat{T}$Mcs/Vcs will depend upon the capability of the system. Following the discussion of these factors, the system error is considered.

Previously we considered the procedure used for collecting the data to predict TMcs/Vcs. From the data several equations predicting TMcs/Vcs at every instant of time* were derived. These expressions are summarized in Table 2.

---

* "Time" implies master system time.

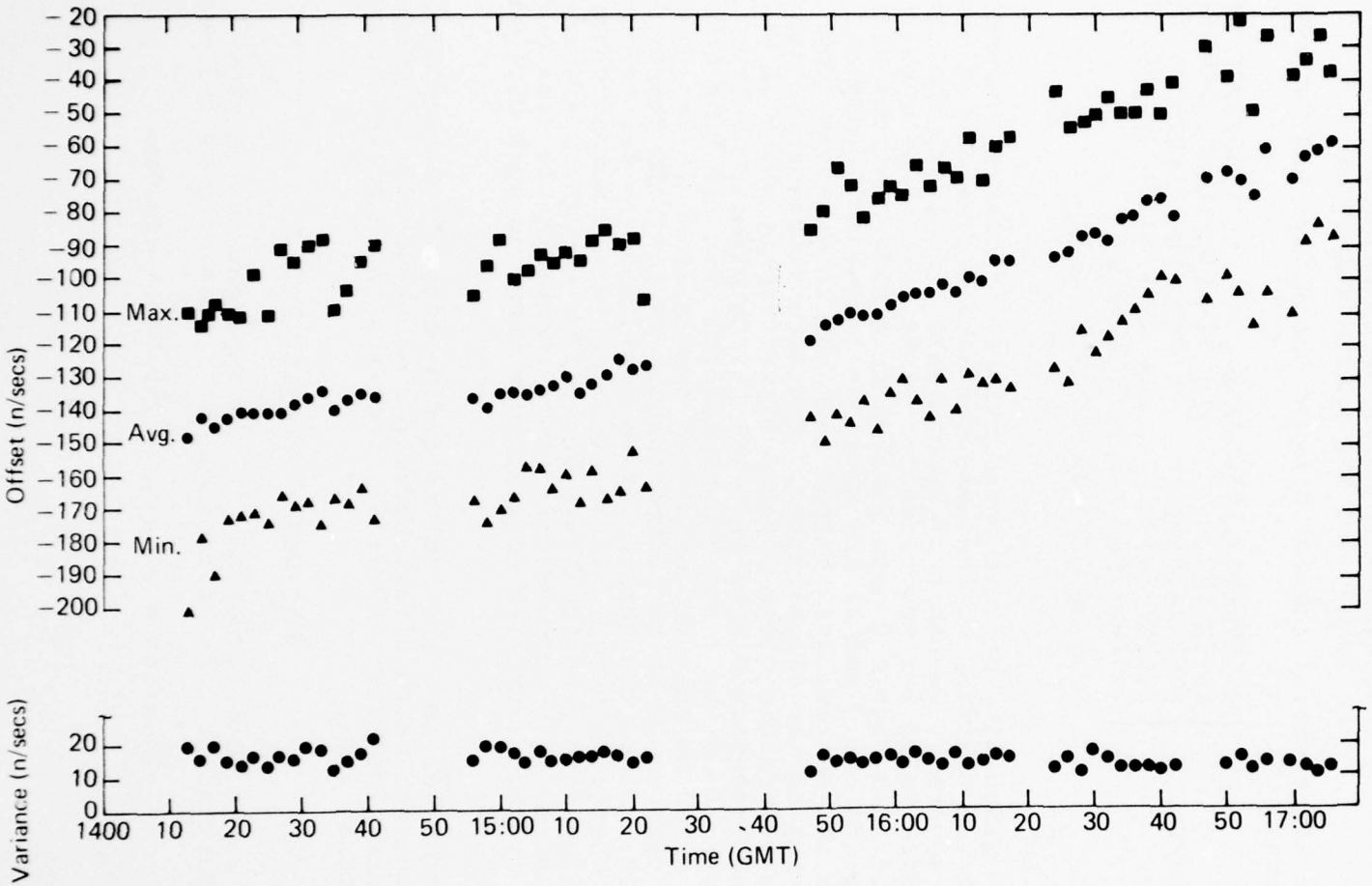


Fig. 3 Statistics Data for Mar. 24, 1975 (4 MHz PN Clock)

TABLE 2

PREDICTED TIME DIFFERENCES BETWEEN
THE MOJAVE AND VAN CESIUM STANDARDS

Time differential (nsecs) between the Mojave and Van cesium clocks

$$\text{TMcs/Vcs} = \begin{cases} 2.162\tau - 482{,}845{,}563 & ; \quad t \le 17{:}30/3/17/75 \\ 2.162\tau + 42 & ; \quad 17{:}30 < t \le 16{:}00/3/20/75 \\ 1.694\tau + 79 & ; \quad 16{:}00 < t \le 0400/3/24/75 \\ 2.632\tau - 73 & ; \quad 0400 < t \le 10{:}00/3/26/75 \\ 1.628\tau + 144 & ; \quad 10{:}00 < t \end{cases}$$

$\tau = t - 10{:}00/3/17/75$ GMT-Hours

The reliability of these predictions, of course, depend upon the validity of the measured data but we cannot prove its accuracy, we can only hypothesize. However, the data appears valid for two reasons: First, slopes of curves 1 and 2 in Figure 2 were derived primarily from the phase data (curves 3 and 4) and were not chosen to intersect with the extreme data points as might be expected from looking at the illustration. The second reason is that, if the portable clock changed significantly while it was being transferred from one site to the other, then the slopes of curves 1 and 2 extrapolated over the time intervals for which no measured data were available would be incorrect, and this would be reflected through Eq. (1), to the system error. Since the extrapolation would tend to smooth out any change, however, transport errors would not necessarily be immediately noticeable. Gradually, though, a significant change would become evident as an unexplainable bias on the system error. As we will soon show, no such bias was detected.

We consider now, the factors influencing the determination of the estimated offset between the Mojave and Van cesium clocks ($\hat{\text{TMcs/Vcs}}$). Briefly, $\hat{\text{TMcs/Vcs}}$ is comprised of two factors, i.e.,

$$\hat{\text{TMcs/Vcs}} = \tilde{\text{TMcs/Vcs}} + \Delta\hat{\text{T}}. \qquad (2)$$

The first term, $\tilde{\text{TMcs/Vcs}}$, is the apparent cesium clock offset and is determined from the system data as follows:

$$\tilde{\text{TMcs/Vcs}} = \text{T1's/Nv} + \text{TNv/Vcs} - \text{TNm/Mcs} \qquad (3)$$

where:

T1's/Nv, is the average time interval (Modulo To/2) between the all 1's epoch and the Van nanoclock. This is the quantity calculated in the slave control program.

TNv/Vcs, is the offset, in nanoseconds, between the Van nanoclock and cesium clock 1-pps signals.

TNm/Mcs, is the offset, in nanoseconds, between the Mojave nanoclock and ceisum clock 1-pps signals.

The second term in Eq. (2), $\Delta\hat{T}$, is a correction factor consisting of a fixed bias plus a variable component proportional to the doppler rates ($\dot{R}vs$ and $\dot{R}ms$) between the Mojave and Van terminals and the satellite. Thus,

$$\Delta\hat{T} = k(\dot{R}vs + \dot{R}ms) + B \ , \qquad (4)$$

where:

$k = 3.6$ nsecs/mtr/sec

$$B = \begin{cases} 210 \text{ nsecs for the 4 MHz PN Clock rate} \\ 187 \text{ nsecs for the 8 MHz PN Clock rate} \\ 176 \text{ nsecs for the 16 MHz PN Clock rate.} \end{cases}$$

The expression for $\Delta\hat{T}$ has been derived analytically and it can be shown that the bias term, B, is equal to one-half the difference between the forward and return path terminal time delays. Although B can be determined experimentally, sufficient time was not available for making the necessary measurements prior to the test; and, consequently, B was derived empirically from the test data.

Prior to the tests, the component proportional to doppler was not well understood. Indeed it was unexpected because the closed loop transfer function of the master system control algorithm is equivalent to a second order phase-lock loop and consequently, the doppler error should be negligible. Subsequent to the tests, however, we found that the error term proportional to doppler arises predominantly through a peculiarity in the system instrumentation. The system error has been analyzed in considerable detail and we can show that most of the error due to doppler arises because the time intervals Tmd and Tcm are not measured at the same instants of time. That is, the time interval, Tcm, is measured, as it should be, at precisely the one-second time marks, but the time interval, Tmd, is measured

almost one second early. If we had been aware of this peculiarity prior to the tests, then the correction factor, $\Delta\hat{T}$, would have been incorporated into the system control programs and thereby reflected into the system measurement T1's/Nv. The advantage of doing this, of course, would be to preserve the real time capability of the system. Nevertheless, the achievable precision of a time transfer is unaffected by whether or not the correction is made in real time.

In the previous paragraphs the factors involved in the determination of the system error were discussed. In Figure 3 we showed the clock offsets prior to making any corrections and the effects of doppler are clearly evident. In Figure 4, we have plotted the system error for several days. As can be seen from these figures, the average daily error is not zero, but nevertheless, is usually small. The reason the average daily error is not zero is not clear, but it is believed to be a peculiarity of the system MODEM spread spectrum correlators.

If all systematic errors can be predicted, and thereby removed, then ideally the residual error should be randomly distributed with zero mean and negligibly* small variance. In Figure 4 the average daily error ($\bar{\varepsilon}$) is indicated by the dashed lines, and it should be apparent that the variance about the average is relatively small. This is, of course, a desirable condition. To show the trend for the entire test period the average daily error, as well as the extreme errors for each test day are replotted in Figure 5. Notice that there does not appear to be any consistent bias associated with the system error, and this seems to lend credence to our earlier hypothesis regarding the portable clock measurements.

If we list $\bar{\varepsilon}$ for each test day (Table 3 below):

TABLE 3

AVERAGE DAILY ERROR FOR PTDE TIME TRANSFERS

	DATE:										
MAR.	15	18	19	20	21	24	25	26	27	28	29/30
$\bar{\varepsilon}$(n·s)	20	-2	-19	-17	-6	16	7	-13	17	8	-7

* Statistically, of course, it is not necessary that the variance be negligibly small; however, practically, this is a system requirement.

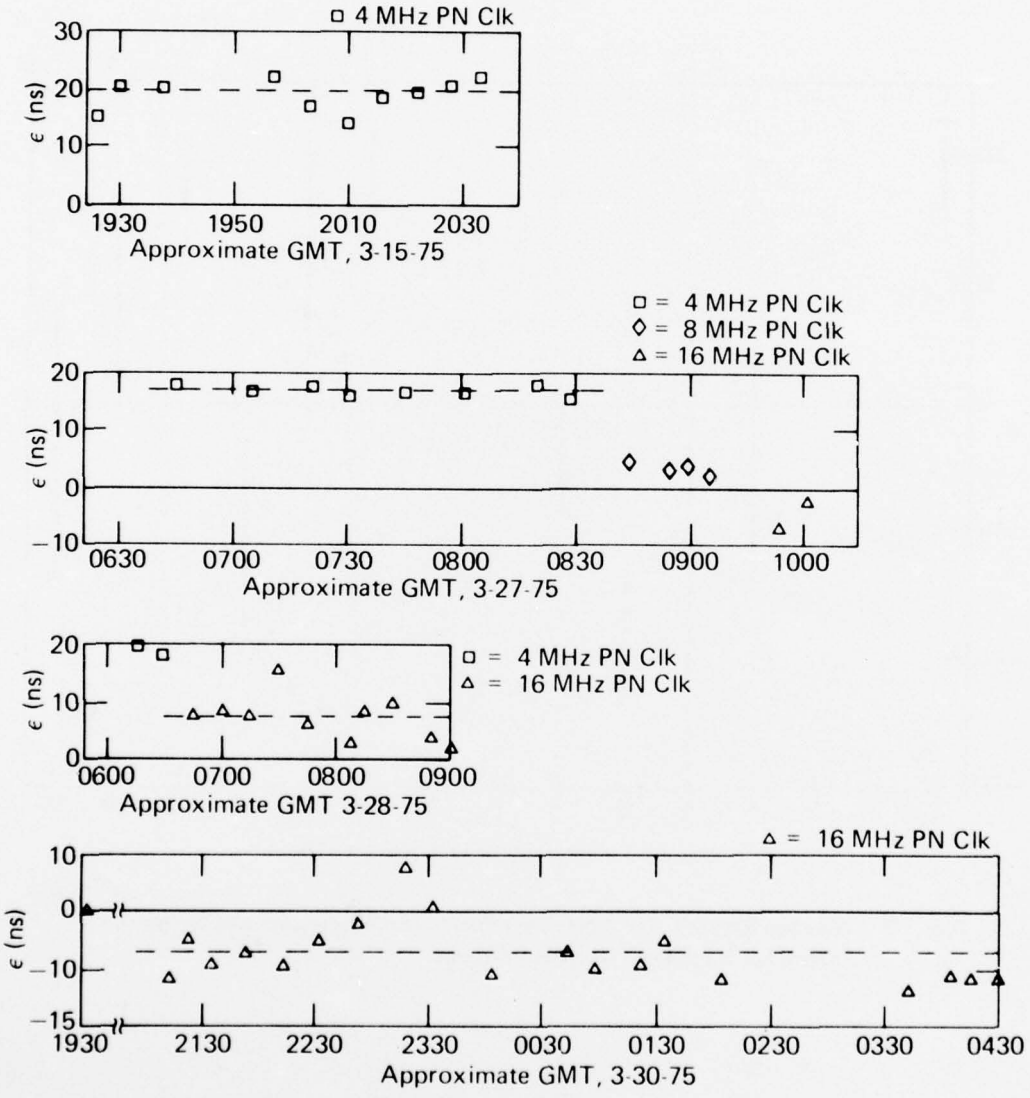


Fig. 4 PTDS Residual Error for March 15, 27, 28, 29/30

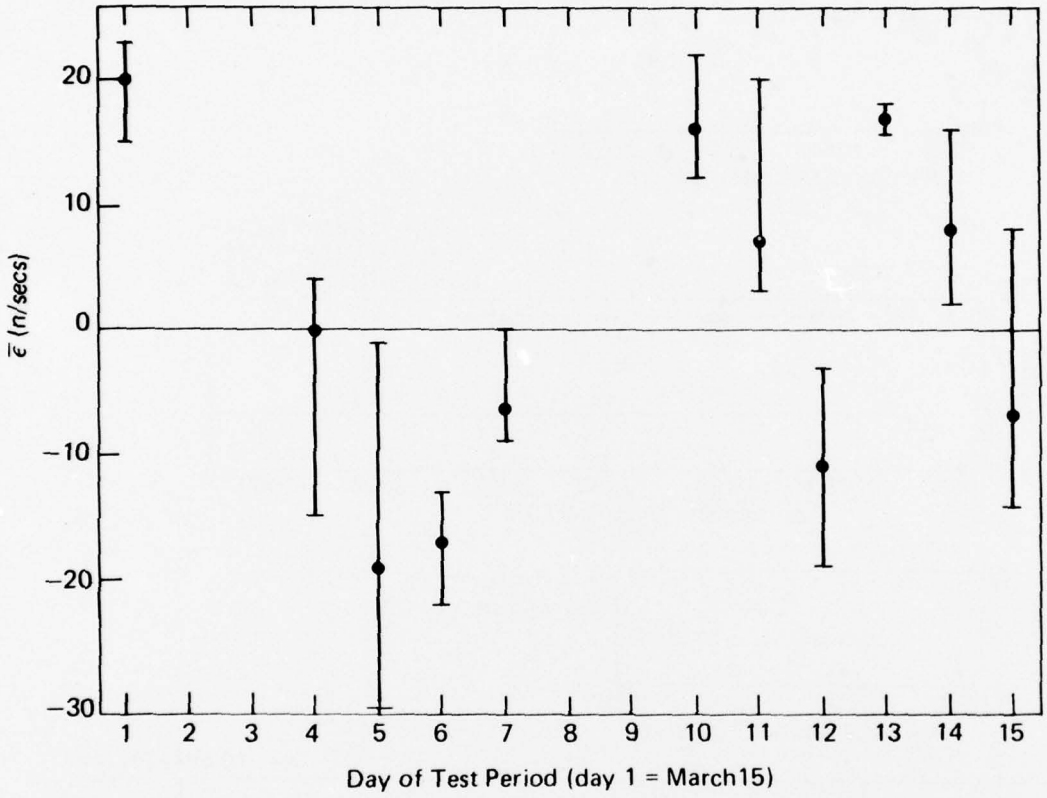


Fig. 5 Average Error, $\bar{\epsilon}$, for Each Test Day. The Maximum and Minimum Errors for Each Day Are Also Shown

then we can easily calculate the average error over the entire test period. Accordingly,

$$\langle \varepsilon \rangle = \frac{1}{N} \sum_{i=1}^{N} \bar{\varepsilon}_i \approx 0.2 \text{ nsecs},$$

and the variance of $\bar{\varepsilon}$ is

$$\sigma_{\bar{\varepsilon}} = \sqrt{\frac{1}{N} \sum_{i=1}^{N} (\bar{\varepsilon}_i - \langle \varepsilon \rangle)^2} \approx 11 \text{ nsecs}.$$

It can be seen (Table 3) that the average error, $\bar{\varepsilon}$ is less than $2\sigma_{\bar{\varepsilon}}$. Furthermore, from Figure 5 it can be seen that

$$|\bar{\varepsilon}| < 3\sigma_{\bar{\varepsilon}} \ (\approx 33 \text{ nsecs}) << 0.5 \ \mu\text{secs}.$$

and therefore, it can be reasonably concluded that the experiment objectives were achieved.

ACKNOWLEDGEMENT

The authors would like to acknowledge the many people who contributed to making the experiment a success. We would like to particularly single out Messers. J. Brannan and O. McIntyre of the FAA, Mr. G. Whitworth of the APL, Mr. L. Fleishman from Westinghouse, Messers T. Keating, P. Mitchell and W. Mazur from GSFC, Mr. J. Beatty of NAFEC, and last but certainly not least, personnel from the ATS Project Office and NASA Mojave and Rosman tracking stations, without whose contributions the experiment could not have succeeded.

REFERENCES

1. Sixth Quarterly Progress Report, "Precise Time Dissemination Experiment", GSFC Project No. 636-18-51-08, July 1974, Appendix B.

2. Mazur, W., "Spread Spectrum Random Access (SSRA) Time Transfer Modems - A System Review", GSFC Report No. X-814-74-149, May 1974.

QUESTION AND ANSWER PERIOD

NO DISCUSSION

THE STATE TIME AND FREQUENCY SERVICE IN THE USSR

V. V. Sajin, V. G. Iljin (USSR GOSSTANDART), Moscow

ABSTRACT

The paper describes the existing metrological distribution system for the USSR users working in the field of precise time and frequency measurements. The characteristic of the standard system, its location as well as the technique and means of mutual comparisons are given. The accuracies obtained by independent clock time scales and their intercomparisons are quoted in the paper. The structure and description of the USSR time signals, their frequency of emission, and their metrological characteristics are given. The problems of astronomical determination of time are considered.

INTRODUCTION

At present, standard frequency and precise time signals are used in many fields of science and technology. The necessity of providing equal and accurate separate measurements is the main feature of numerous applications. In the Soviet Union these are provided by the USSR State time and frequency service. The time service was established in 1947 principally for astronomical determination of the time and frequency of the State standards. At present, the time service is also engaged in measurement technology covering our country's requirements in the field of time and frequency measurement.

The System of Standards

The State standard producing precise time and frequency for the National time scale is the basis of the USSR State time and frequency service. In addition to the State standard, the standard system includes also secondary standards which are kept in metrological Institutes of Irkutsk, Novosibirsk, Kharkov and other cities. By their characteristics these standards only insignificantly yield to the State standard. They provide frequency, determined by the USSR State standard, with an error of the order of 1×10^{-12}.

The main function of the standard system operation is to coordinate the time scale of the State standard with the time scales of secondary and working standards. At the present time, the error of such coordination is of the order of not more than a few microseconds for the most remote standards. This value is periodically defined more precisely to the tenth parts of a microsecond with the aid of portable clock time transfers.

The System of Time Signal Emission.

LF- and HF- range stations are the basic means for standard frequency and time signal emissions in the system of the State time and frequency service.

At present, there are three LF- radio stations in the State time service. They are as follows: RBU, Moscow - 66 2/3 kHz; RTZ, Irkutsk - 50 kHz and RB-166, Irkutsk - 200 kHz. Normally, these stations transmit standard frequency and time signals all day and all night on the schedule and program determined for each year. Recently, the error of time signal emission was substantially reduced by means of facility modifications at these stations. Currently, the frequency error is of the order of 7×10^{-11}.

Short-wave radio stations (Moscow, Irkutsk, Novosibirsk, Tashkent) are primarily used for time signal emission with a medium accuracy. Fluctuations of time dissemination do not permit these stations to be used for time signal emissions with an arror of less than 10^{-9} in frequency and 300 μs in time. Nevertheless, such accuracy meets the requirements of the majority of today's users.

The systematic comparison of time scales kept by the standards in Moscow and Kharkov are carried out with the aid of a meteoric synchronization line. The long-term usage of this channel showed that the error of the time scales compared is less than 1 μs.

Great expectations exist for the accuracy of standard frequency and time signal emissions provided by the use of television channels. At the present time, signals are transmitted from the USSR State standard on the first program of All-Union TV-broadcasting. These signals are transmitted in the 6th line during the display of the clock face and other studio broadcasting. They contain information for current time and standard frequency (1 MHz). For the present, the requirements of many organizations in

Leningrad, Moscow, Kharkov, Kiev and other cities are covered by means of this system of time signal emission. Comparison of the USSR standard with the DDR standard was twice performed via TV in 1975. Processing the results of the comparisons showed that such a comparison method yields an accuracy of not worse than 1 to 2 μs.

The Astronomical Determination of Time.

The astronomical determination of time is of significant importance in the USSR State time and frequency service. The calculation of Universal time is presently performed on the results of astronomical observations of 10 USSR observatories and 9 observatories of other countries.

On the basis of these data, the Metrological Center of the time service issues monthly bulletins giving departures of Universal time scale from the Atomic time scale.

The existing structure of the State time service provides the technology to disseminate the metrological service of the National economy for time and frequency measurements. Thus, on the base of secondary standards, which are distributed over the territory of the USSR, the certification of the most accurate time and frequency measurements and their periodical calibrations are carried out.

The metrological control and calibration of high accuracy measurement equipment (frequency meters, generators, clocks) is effected by a number of State controlled laboratories which are equipped with standard measurement facilities and disposed practically in all big cities of the USSR.

QUESTION AND ANSWER PERIOD

DR. WINKLER:

Now, before we ask the questions, I would like to ask for your understanding that in view of the difficulty of communication -- English for a foreigner is a very difficult language when it is transmitted through a microphone. We will have a translator translate the question for Mr. Sazhin and then he will answer.

DR. REINHARDT:

Victor Reinhardt, NASA.

You didn't mention what type of standards do you use as primary standards and the secondary standards in your standard plot?

MR. SAZHIN:

The primary standards of the USSR is the next paper that Mr. Iljin will be delivering.

TRANSLATOR:

He said that the secondary standards are almost the same as the primary standards- but a little smaller.

SGT. OSTROWSKI:

Sergeant Ostrowski, Newark Air Force Station.

I have a question about the Loran service. Does it disseminate precise time information?

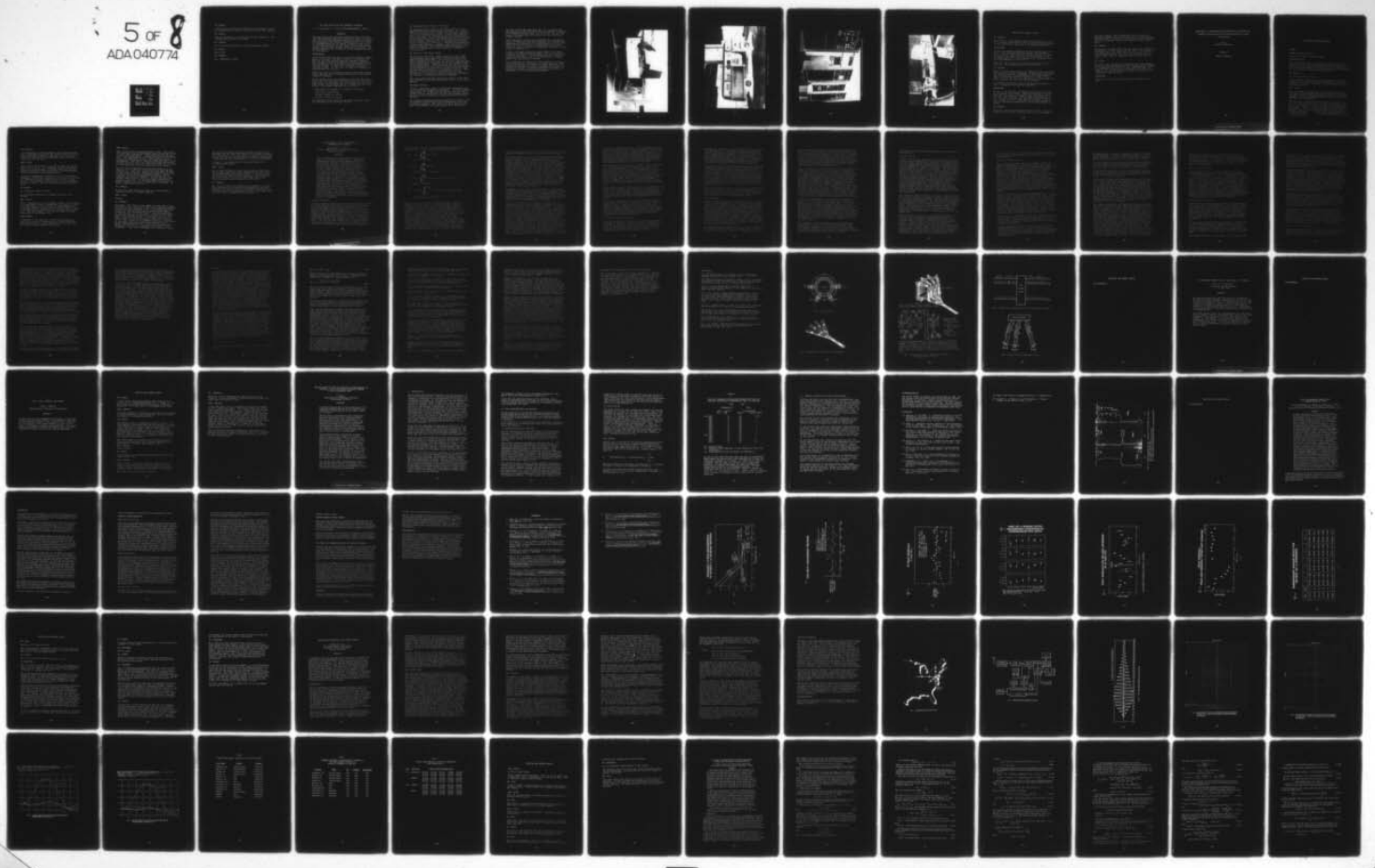
MR. SAZHIN:

Yes, in Moscow we don't receive the Loran signal. We receive its signals in Leningrad and in Nikolav and other cities on the edges of our country. We do not use it for time comparison between our standards, but we use it for comparison with standards of other countries.

AD-A040 774 NATIONAL AERONAUTICS AND SPACE ADMINISTRATION GREENB--ETC F/G 14/2
PROCEEDINGS OF THE ANNUAL PRECISE TIME AND TIME INTERVAL (PTTI)--ETC(U)
DEC 75

UNCLASSIFIED NASA-GSFC-X-814-76-45 NL

5 OF 8
ADA040774



MR. RUEGER:

I would like to know how you handle the leap second, or are you transmitting in atomic time scale for your time signals?

MR. SAZHIN:

With our broadcast, it is the same as other countries. Our coordination with BIH is the same.

DR. WINKLER:

Is it the same UTC system as the International system?

MR. SAZHIN:

Since 1972.

DR. WINKLER:

Yes. Beginning in 1972.

THE USSR STATE TIME AND FREQUENCY STANDARD

V. G. Iljin and V. V. Sajin (USSR GOSSTANDART), Moscow

ABSTRACT

The paper deals with detailed information about the State time and frequency standard of the Soviet Union, its structure, service conditions and operation of the basic systems. The metrological and technical characteristics of a group of standards producing the nominal frequency value as well as the characteristics of time scale clock systems and of internal and external standard comparisons are given. The systems providing the reliability of the standard operation are considered.

INTRODUCTION

In the Soviet Union the unity of time and frequency measurements on a scale of the whole country is achieved on the basis of the State primary time and frequency standard. The standard is kept in VNIIFTRI (All-Union Research Institute for Physics and Radio Engineering Measurements) situated near Moscow. It was first confirmed as the State standard in 1967. At that time, an error of frequency reproducibility was 1×10^{-11}.

Since that time, the standard parameters have been substantially improved and the standard structure has been almost completely changed.

At the present time, the standard not only reproduces frequency, but also provides a continuous clock on the National time scale. In connection with this capability, the standard includes four primary and two secondary apparatus complexes. The primary complexes are as follows:

- reproducibility system of a measure of frequency;
- time scale clock system;
- internal comparison system;
- external comparison system;

The regulated power system and the data processing system are considered to be secondary systems.

PRECEDING PAGE BLANK-NOT FILMED

The Reproducibility System of Frequency

The reproducibility system of frequency consists of six hydrogen and one cesium frequency standards. On a regular basis, two or three times a week, the standards' frequencies are corrected on the results of their intercomparisons and on the results of comparisons with the frequencies of atomic time scale clocks. The reproducibility of an average real frequency value is taken for the main characteristic of this system. Currently, it is expressed by a relative error of the order of 1×10^{-13}. Frequency reproducibility of the cesium standard is somewhat worse than that of the hydrogen standard. The magnitude characterizing the accuracy of the metrological cesium standard is currently $(3 \text{ to } 5) \times 10^{-13}$.

The System of Time Scale Clocks.

The system of time scale clocks consists of eight atomic hydrogen masers and eight Hewlett-Packard cesium atomic beam standards model 5061A. As a rule, from four to six atomic standards of each group are operating simultaneously. The remaining atomic standards are on cold standby or preventive maintenance. Each clock forms its own time scale. Intercomparisons of all scales are carried out automatically on the comparison program with a one hour interval. Comparisons are carried out at a resolution of 10 nsec. Processing of single results is performed in two steps: Provisionally - directly by means of comparison equipment; and finally - by universal electronic computer.

The clock system provides deviation of scales of two standard semisets of the order of not more than 1 μs for three months.

Secondary Systems.

Internal comparison system is a multiplex measurement system for time and frequency measurements. Accurate frequency measurements (F = 5 MHz) are carried out with the help of decade frequency multipliers (to 10^4) and frequency meters. The results are recorded on a perforated tape and digital printer.

The external comparison system incorporates a number of VLF, LF and VHF receiving devices and corresponding receiving - recording equipment. With the aid of these devices a 24-hour (10-12 times) time signal reception of such radio

stations as GBR, OMA, RBU, NAA, NVC, etc. is carried out. The comparison with the USSR secondary standards is effected by TV channels with an error of (1 to 3) μs. For the last years a few comparisons were carried out with the help of portable clocks.

These comparisons enabled the determination of systematic delays in radio and television channels. For instance, the comparison with the help of an Oscilloquartz clock in 1974 permitted the calibration of a comparison path on short waves and took into account a systematical departure of time scales to within 1 μs.

A system of standby energy was established for the power supply of the whole standard complex. This system consists of battery facilities, a diesel-generator and a system of automatic switching in case of an interruption of energy supply from the electrical network.

All information for operation of the standard is systematically processed on a universal electronic computer. This information includes the results of single measurements of frequency deviation of separate standards and clocks, the results of external signal receptionl and the results of measurements of the environment parameters.

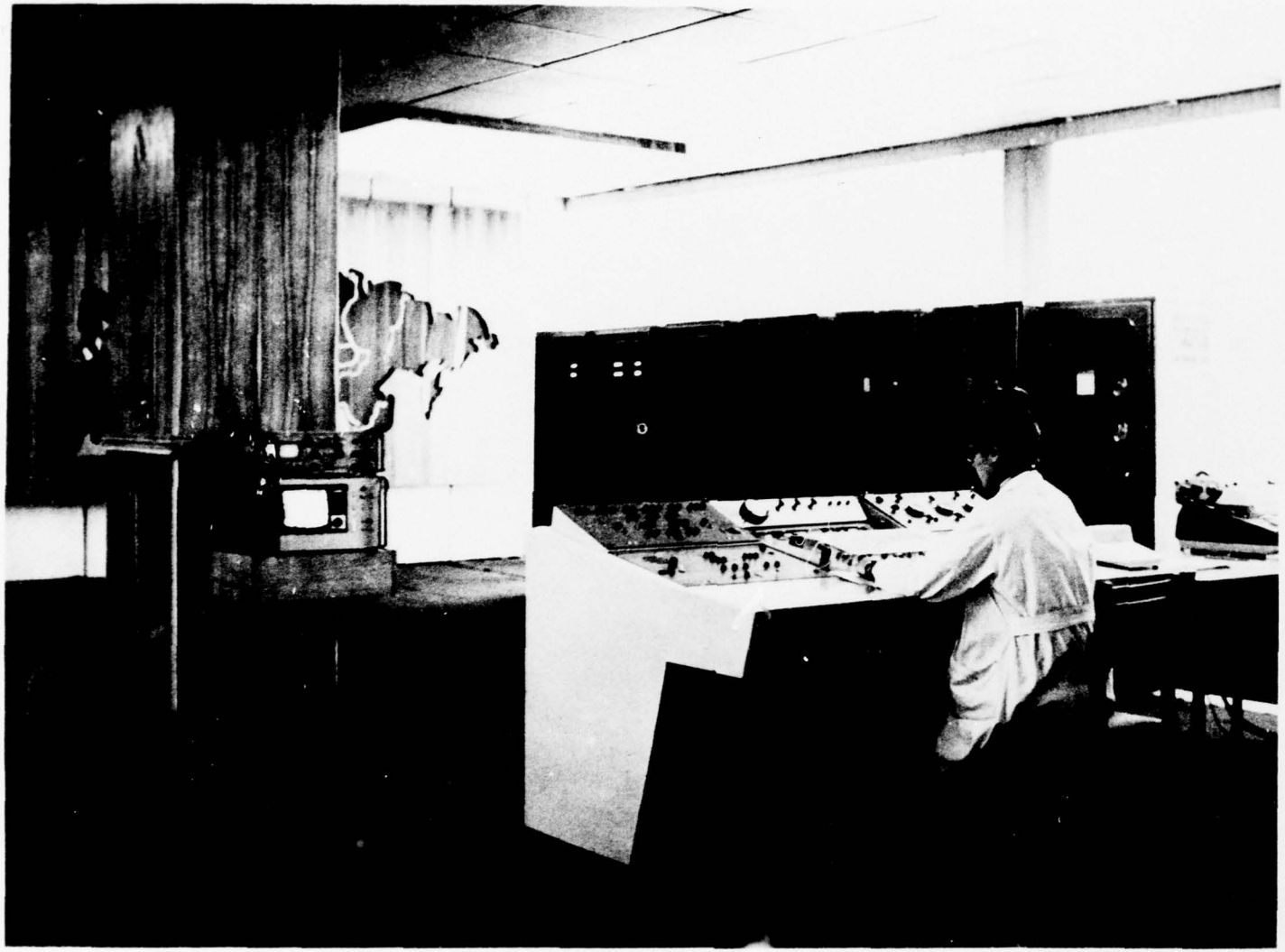


Figure 1. The main apparatus hall of the time service



Figure 2. Portable comparison standard.

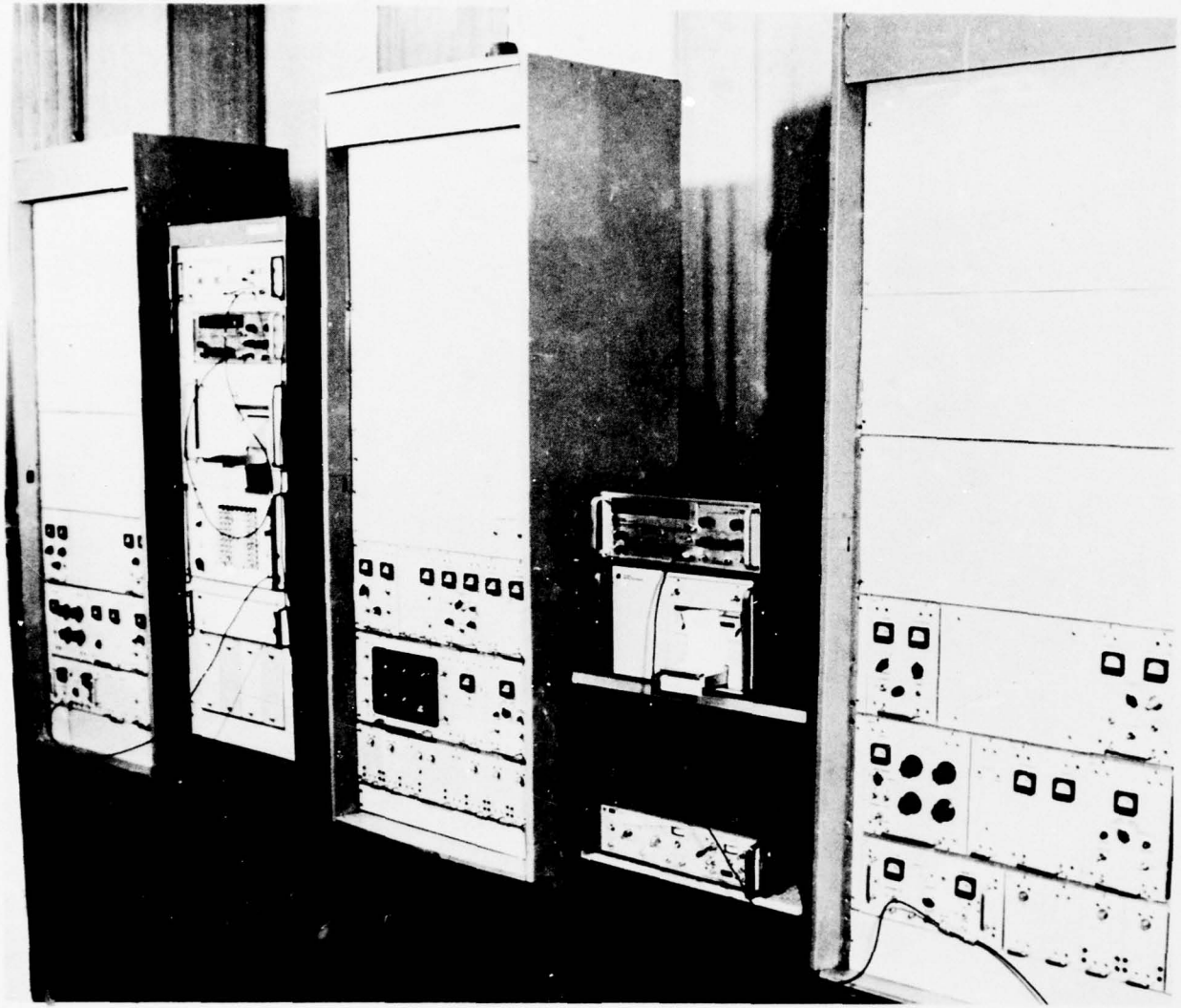


Figure 3. A set of hydrogen time-scale keepers of the USSR State standard.

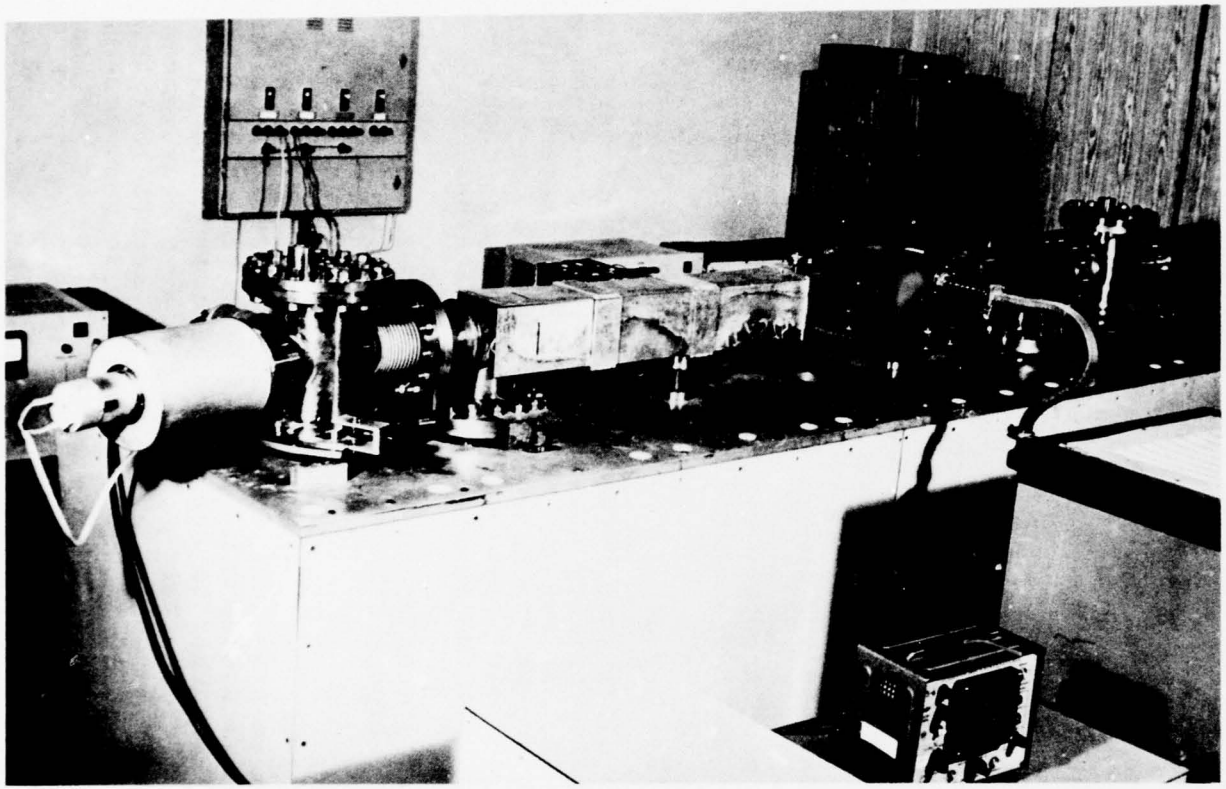


Figure 4. Cesium frequency Reper of the USSR gosstandart.

QUESTION AND ANSWER PERIOD

DR. HELLWIG:

With respect to the hydrogen and the cesium devices, first of all on the cesium device, was it designed and constructed at your laboratory? How long is it and such parameters?

TRANSLATOR:

He said the hydrogen apparatus has been working about five years. The cesium metrological system, they started a year or so ago. They have had practical results for about six months from their research. He says because of this, he cannot give you an exact reading on the accuracy of it, only approximately 3 to 5 X 10^{-13}.

They have good accuracy with the hydrogen work, 2 X 10^{-12} accuracy. The reproducibility is 1 or 2 X 10^{-13}.

DR. COSTAIN:

There is a difference between our hydrogen primary standards and our cesium primary standards. We think our cesium is by far the best, but our measurements at the moment indicate that the hydrogen frequency decreases at a rate of more than 1 part in 10^{12} per year, and this is no doubt characteristic or partly the fault of our old machines.

I would be interested to know if in subsequent years you have a comparison between your standards.

TRANSLATOR:

He says it is true that the hydrogen system is not as good as the cesium system today. They were not able to break down their accuracy to the degree they required as far as the units are concerned. They did make a measurement in the last year, a cesium unit, and the accuracy of this is 3 or 5 units in 10^{-13}. These data are in good agreement with the National Standard data, both for West Germany and Canada.

DR. WINKLER:

Could you leave the microphone with Dr. Costain, because I would like to ask him a question and that is, in regard to

your last comment, did I understand that you said the hydrogen frequency seems to decrease after all allowances have been made for wall shift and possible chemical changes in the wall coating? Would you elaborate on that statement?

DR. COSTAIN:

Essentially, the past year in an autotuned pair, and one is decreasing at a rate faster than the other. We presume it is changes due to the wall shift, but we have not in fact made the measurements. The results in rate now seem a little higher than the cumulative rate over the past five years.

MR. ALLAN:

Mr. Iljin, you indicated good agreement with the Canadian primary cesium standard and the West German primary standard. If I understand you correctly, this would mean that you would say the international second used by the BIH is too short or too high in frequency by about 1 part in 10^{12}, if I understood you correctly.

TRANSLATOR:

Correct. He says he has an accuracy now of about 1.6 X 10^{-12}.

SUBNANOSEC – LASER-PULSE TIME TRANSFER TO AN AIRCRAFT TO MEASURE THE GEN. RELATIV. ALTITUDE EFFECTS ON ATOMIC CLOCK RATES

C. Alley
University of Maryland

ABSTRACT

"Paper Not Received"

PRECEDING PAGE BLANK-NOT FILMED

QUESTION AND ANSWER PERIOD

McDADE:

McDade, General Electric.

Why do you double your light beams?

PROFFESOR ALLEY:

The photo multipliers we use have phot cathodes that are sensitive to the green, and not sensitive to the infra-red, so we get better quality efficiency that way. There is some slight improvement in the pulse width from the doubling but it is mainly a quantum efficiency reason.

MR. BABITCH:

Dan Babitch, Hewlett-Packard.

Did you happen to make any fractional frequency stability analysis of the data on that last viewgraph of the airborne standards? It looked like about 1.5 nanoseconds peak to peak for two days.

PROF. ALLEY:

Yes, we have done calculations of the Allan variance as a function of the averaging time, and unfortunately I don't have any viewgraphs prepared with that, but, on the cesium standards, we see them getting down to below 10^{-13} level in something like three hours.

The stability, I think, would be down in a few parts to 10^{14} over that period of time. We have not ever been able to run our clocks for very long periods, so that we could have a large number of several-day intervals contiguous to one another. There is always something required to be changed or moved, so we just don't have a full calculation of that performance yet, but after the experiments are concluded, we hope to have some uninterrupted time in which to log that kind of data.

MR. BABITCH:

I was wondering if the data shown on the airborne system met or exceeded or was worse than similar data for laboratory ground-based systems of the same type. In other words, how good was your environmental isolation? Did it really do a lot for you?

PROF. ALLEY:

Yes, it did a great deal for us, but it didn't do all we would like it to do. It is somewhat worse on the planes than it is on the ground. We suffer there from sort of a primary difficulty, in that the plane's own environmental control system never has worked properly.

We can get temperature excursions up to 18 to 20 degrees Fahrenheit in the plane, whereas in the trailer we can keep our temperature within a degree or better, over a long period. Our shielding is not perfect. And the gradients, of course, change. They are particularly bad in the airplane.

DR. REPASS:

Dr. Don Repass, Naval Avionics.

I was wondering what kind of changes you made to the HP-5061.

PROF. ALLEY:

Well, I mentioned two of the changes; namely, the increased oven temperature to get a larger beam flux, which of course is at the expense of the lifetime of the standards, but Dr. Winkler kindly consented to that change, and the other I mentioned was the introduction of a second order control loop. The third change is one that HP wishes to remain proprietary at the present time.

HARRY PETERS:

I wondered if you could tell us what the resolution on relativity effects of potential and velocity should have been theoretically in your experiment and from your data how close you might approach this value.

PROF. ALLEY:

Well, we are still analyzing the data, Harry. Harry and I discussed this type of measurement several years ago at one of these PTTI conferences. I am hopeful that we can get down to the approximately 1 percent accuracy on the measurement. The comparisons so far -- and we haven't fully assessed the uncertainties that the range introduces in its measurements. They have an elevation altitude uncertainly of about 100 feet, but it is their angles that are a little bit more uncertain, and that enters into the velocity.

We have tried to keep those uncertainties down to on the order of .3 of a percent, but I am not sure that has been achieved yet. Right now, roughly the measurement accuracy on each flight is about a nanosecond, which is about 2 or 3 percent in a 40 to 50 nanosecond difference, and by combining these several flights -- we have had four long flights, and we have a fifth long flight scheduled for hopefully next week -- it may be possible to get down to around 1 percent, but don't mistake what I am saying. We haven't really done that yet.

DR. WINKLER:

At any rate, your resolution seems to be good enough to discover errors in the range tracking.

PROF. ALLEY:

Perhaps.

DR. WINKLER:

Very good. But, there is one comment I would like to make, and that is that I have two sincere hopes connected with the execution of that experiment; No. 1, it undoubtedly demonstrates the ultimate which can be achieved with today's technology; this technology which is available right now, if you use every one of our assets. This includes unprecedented time transfer precision in the order of 10 to the minus 10 seconds resolution. It includes stabilities of these clocks in hostile environment, which is a few parts in 10^{14}, but I have also a second hope and that is that such an experiment executed, again as the previous one by Hafele and Keating with real clocks which have been calibrated and sent out into a distance and returned to the laboratory -- that these experiments will hopefully finally

put to rest an endless scientific dispute carried out by sometimes not very qualified people in all kinds of journals, and establish as a fact the reality of these effects which we have to take into account when we talk about nanoseconds timekeeping and time measurements in an actual environment.

I think -- I am convinced that these experiments will accomplish these goals.

PROF. ALLEY:

May I respond briefly to that? One of the justifications for the Navy supporting these measurements has been that in the planned global positioning system, if the positioning accuracies that they talk about publicly of 10 to 20 feet are to be achieved, one has to make these relativistic corrections due to the ellipticity of the orbit.

DR. WINKLER:

But, even in other time transfers, for instance, in experiments which have been carried out between here and Japan recently, that was a correction which had to be applied to the portable clock measurements in order to make them agree with the results through the ATS satellite.

APPLICATIONS OF PTTI TECHNIQUES IN COMMUNICATIONS SYSTEMS

Dr. Harris A. Stover
Defense Communications Engineering Center
Reston, Virginia

ABSTRACT

Time and time interval have always been of importance in electrical communications. Ronalds synchronized equipment for communicating between two locations in 1816 and Samuel Morse used relative time intervals for symbol identification in his first commercial electrical telegraph system in 1844. Today, time and time interval are of even greater importance, pervading nearly every area of the communications field. Also, the radio spectrum is becoming crowded, and more precise timing can be one tool for its more efficient use. As applications of digital communications increase, there is a concomitant increase in synchronous transmission, spread spectrum transmission, time division multiplexing, time division switching, and time division multiple access to communications satellites. In the future, extensive high capacity switched digital communications networks will require timing coordination among the many nodes of the network. The use of a precise standard time such as Coordinated Universal Time (UTC) for fulfilling many of the communications timing requirements expected to arise in the future should be considered.

GENERAL DISCUSSION

At first thought it might seem that the applications of PTTI in communications could simply be listed and the relationship of each application to PTTI indicated. It is not really that simple. So closely are time and time interval interwoven with electrical communications that it could almost be said that they form the very fabric of electrical communications. A brief look at journals in the field of communications engineering reveals that most mathematical expressions employed are functions of time. They occur in nearly all areas of study related to electrical communications. This is even more evident when we consider that functions of frequency are essentially functions of time because of the direct correspondence between frequency and

PRECEDING PAGE BLANK-NOT FILMED

time resulting from the Fourier and Laplace transforms and their inverses as shown in equations (1) through (4).

$$(1)\quad G(f) = \int_{-\infty}^{\infty} g(t)e^{-j2\pi ft}dt$$

Fourier Transform

$$(2)\quad g(t) = \int_{-\infty}^{\infty} G(f)e^{j2\pi ft}df$$

Inverse Fourier Transform

$$(3)\quad F(s) = \int_{o}^{\infty} f(t)e^{-st}dt;\ s = \sigma + j\omega,\ \omega = 2\pi f$$

Laplace Transform

$$(4)\quad f(t) = \frac{1}{2\pi j}\int_{\sigma-j\omega}^{\sigma+j\omega} F(s)\ e^{st}dt;\ s = \sigma + j\omega,\ \omega = 2\pi f$$

Inverse Laplace Transform

Because of the relationship established between time and frequency by these two sets of transformations, and also because of the importance of time and frequency functions to communications, it is often said that communications engineers use the dual languages of time and frequency. The question of whether a time or frequency function is a PTTI function depends upon the frequencies, time intervals, and time accuracy being used and also upon the definition of PTTI. In general, high frequencies imply high time-interval accuracy and long time intervals imply high frequency-accuracy. Many applications of time and time interval in communications are candidates for improvement through increases in precision. Since communications engineers are so consistently involved with applications of time, they usually don't perceive the extent of this involvement; and because they normally work in terms of phase relationships

rather than nanoseconds and picoseconds, they usually don't perceive the degree of time precision that they employ.

To further observe the close relationship between communications and time (frequency), consider some of the broad areas of study related to communications engineering. Circuit theory usually includes both network analysis and network synthesis. In addition to various active elements in which time functions are involved, electrical circuit theory employs three types of passive elements: resistors, capacitors, and inductors. The properties of these basic elements are usually defined by their current and voltage relationships as functions of time. For a given network (collection of elements connected or coupled together), network analysis is concerned with determining the response (voltage or current) of the network as a function of time (or frequency) for a given excitation (voltage or current) as a function of time (or frequency). Network synthesis provides the reverse procedure of defining a network to provide the desired time or frequency response based on experience from network analysis.

Fundamental to the study of electromagnetic field theory are Maxwell's equations and the related electromagnetic wave equations used to describe the space-time relationships of electric and magnetic fields to their environment. These relationships are important in studying many areas including transmission lines, resonant electromagnetic structures, antennas, and the propagation of radio waves.

There are a number of electromagnetic devices used for communications with properties that are dependent on space-time relationships of electromagnetic fields. One such device which lends itself to illustration is a ring hybrid shown in Figure 1. In a ring hybrid, the two separate signal paths between ports 1 and 4 differ in signal transit time by one half period of the signal. Signals arriving at one of these two ports over the two paths from the other port will cancel and there is no coupling between ports 1 and 4. The same relationship applies to ports 2 and 3. However, a signal originating at port 1 will arrive at port 3 with equal transit times for the two paths and add in phase while signals on the two paths from port 1 will arrive at port 2 differing by exactly one signal period and will also add in phase. Therefore, there is no coupling between ports 1 and 4 except by virture of reflections in ports 2 and 3, but there is direct coupling between port 1 and ports 2 and 3. Clearly, at microwave frequencies these time relationships must be precise (picoseconds at SHF) for the

equipment to function properly. Many electromagnetic field devices depend upon precise time relationships such as this which are relatively easy to achieve and which are of great importance in communications engineering. Also, many electronic devices used in communications depend for their operation on the interaction of electrons and electromagnetic fields. These interactions in turn depend upon the space-time characteristics of both the electrons and the electromagnetic fields with which they interact.

Modulation is a process whereby a message signal is imposed on a carrier wave by varying one or more of the carrier wave's characteristics. In continuous modulation, the amplitude, phase, frequency or any combination of them can be varied. If phase or frequency is the characteristic which is varied by the message signal, this is a time related process. In pulse modulation the parameter varied by the message signal might be the pulse amplitude (PAM) or the pulse time (PTM). Pulse time modulation (PTM) is further subdivided into pulse width (or duration) modulation, pulse position modulation and pulse frequency modulation.

These examples provide some indication of the breadth of the application of time and time interval in communications. Of course it is far from complete, as the time relationships to antennas (phased arrays in particular), transmission lines, radio wave propagation, diversity transmission techniques, and many other important areas haven't been discussed.

Although the applications of time and time interval discussed above are directly related to the general field of communications, it might be desirable to discuss some broader systems considerations and those applications of recently growing importance. Two important areas of direct concern to communications systems are the frequency spectrum occupied by the modulated signals and the broad area of scheduling of message signals, which includes the important field of synchronization.

The Radio Frequency Spectrum

The radio frequency spectrum is a natural resource which although not expended or depleted by use is limited in its availability and can be wasted by unwise or inefficient use. New applications of the radio spectrum and rapid expansion of old applications can be expected to place increasing pressures on this limited resource.

Availability of precise time and time interval can aid in the efficient use of the radio spectrum. Consider, for example, that much of the military amplitude modulation voice communications equipment used in the 225 mHz to 400 mHz frequency band in the 1950s and 1960s had 100 kHz channel spacing, although 6 kHz or 8 kHz would have been sufficient for the modulation sidebands. The remainder of the allocated channel bandwidth accommodated frequency tolerances in transmitting and receiving equipments.

The application of single-sideband suppressed-carrier voice transmissions which require only half the radio frequency spectrum required for double sideband modulation, was technically and economically delayed because of the precision required of the carrier frequency generated at the receiver relative to the carrier suppressed at the transmitter. Although single-sideband modulation techniques have been widely used for frequency division multiplexing of telephone channels, and have been extensively used by radio amateurs for nearly two decades, many users of the congested high frequency radio bands have only recently begun to use them.

From these examples alone it seems clear that more precision in time and frequency have permitted improvement in the effective utilization of the radio frequency spectrum in the recent past. Further improvement is still needed and many possibilities for this improvement exist.

Synchronization

The most rapidly expanding application of PTTI in communications is synchronization. This is largely the natural result of a very rapid expansion of digital communications. Although this expansion of digital communications can be partially attributed to communications with digital computers, it is also partly due to advantages that digital transmission can provide for other communications service such as voice transmission. Digital transmission can provide signal-to-noise advantages for signals that must be relayed (repeated) over long distances because it permits regeneration of a nearly noise-free signal at each relay point, reducing the accumulation of noise. Digital transmission is also convenient when encryption is required for military and other applications.

Although synchronous communications are probably growing at the greatest rate in history, it is not a new concept. Perhaps the first truly synchronous communications system

was that operated by Ronalds in 1816 over a distance of 8 miles (1). In this system he installed clocks which rotated paper discs so as to expose one letter of the alphabet at a time through an aperture in a cover. When the clocks at the two ends of the communications system were synchronized, the same letter was visible at the two locations simultaneously. A spark initiated by an electrical connection at one location coincident with a specific exposed letter would occur and be observed at the other location coincident with the same exposed letter.

This, of course, is a close relative of the teleprinters so widely used during the last few decades. In these teleprinters, instead of one pulse per letter (or symbol), each character is composed of a 5-bit code group preceded by a start pulse and followed by a stop pulse. Presence or absence of individual pulses in the 5-bit code group can form 32 combinations to identify 32 different symbols. Because of the start-stop mode of operation it is only necessary to maintain the required synchronism during the transmission of a single symbol. Synchronism is automatically reestablished at the beginning of the next symbol. Obviously, the start-stop mode of transmission wastes considerable transmission capacity by transmitting both start and stop pulses with each symbol. Much of this capacity could be more usefully applied if a long string of equally spaced bits were transmitted with only occasional synchronizing pulses to permit synchronization of the receiver.

In digital communications it is desirable to maximize the ratio of the peak signal to rms noise for each bit (or symbol) so as to reduce the bit error rate. One method of doing this is by using a correlation detector in which the product of the received signal and a noise-free replica of each of the possible waveforms is integrated over a waveform period. If the possible waveforms are orthogonal, the resulting integration will maximize the signal contribution in the integration corresponding to the transmitted signal, while only the noise will contribute to the others. Obviously the receiver must know when to start and stop the integration process; i.e., it must be synchronized to the received signal.

The relatively straightforward process of transmitting binary digits over a point-to-point transmission link connecting a transmitter and a synchronous receiver has been commonly applied for several years. Its application is increasing and higher bit rates are being used. However, there are several other applications of digital

transmission which provide new dimensions to the application of PTTI.

Spread Spectrum

Consider the frequent requirement for resistance to interference, either deliberate or accidental, or consider the need for covert communications where it is desired to fulfill the communication requirement while minimizing the use of the communication signal for purposes of detecting and position-fixing the source of the signal. The same type of solution can be applied to both of these problems: Spread Spectrum communications (2). In a spread spectrum transmitter, the RF carrier is subjected to a double modulation process, one by the message signal and the other by a spectrum spreading sequence. The most widely used method of spectrum spreading has been phased shift keying by a high-speed sequence, where "high speed" means much faster than the baseband data rate. The sequences used for spread spectrum transmission are called pseudo-noise sequences because they possess properties like those of random sequences but are systematic and easy to generate. Another spread spectrum technique called frequency-hopping employs frequency shift keying to a large number of possible frequencies.

When either of these techniques are used, a correlator in the receiver performs the inverse process of that performed by the spread spectrum modulator. For each phase reversal or frequency shift applied at the spread spectrum modulator, a corresponding complementary phase reversal or frequency shift is applied at the correlator when the signal arrives there. This returns the message modulated carrier to its original bandwidth while at the same time spreading the interference (the action of the correlator) in the same manner that the message modulated carrier was spread at the transmitter.

Quite obviously, timing is an essential requirement. The replica of the pseudo-noise waveform generated at the receiver must be accurately synchronized to that of the arriving signal in order to recover the message modulated carrier. A major problem is to initially bring the receiver timing to within a fraction of a pseudo-noise code element of the received signal. One method of doing this is to slew the receiver timing across the time uncertainty interval until the signal power is observed in the message demodulator. The desirability of minimizing the time uncertainty between the transmitter and the receiver is

quite obvious. This is particularly true when synchronization must be acquired during severe interference or intentional jamming.

Time Division Multiplexing

We can expect that some time in the future a switched digital communications network will connect many remote parts of the world and that such a network will employ time division multiplexing and/or time division switching. Figure 2 illustrates, in analog form, a time division multiplexer in which bits arriving on four separate channels at the left are interleaved into a single bit stream on the right. Each bit in each stream entering from the left must arrive at exactly the moment that it is needed to fill its assigned time slot in the multiplexed bit stream. Because of variations in transmission delays (transit time) and differences in clocks at different nodes, the probability of each bit arriving from another node at exactly the moment when it is needed is very small. In a practical application, provision must be made to be sure that the bits will be available at the moment they are needed.

Figure 3 illustrates a method of accommodating the variations in time of arrival of bits from other nodes. Storage buffers in each incoming data stream act as reservoirs in which the bits are temporarily stored. The nodal clock removes them from storage at exactly the right moment for them to fill their assigned time slot in the multiplexed bit stream. However, the clocks at the other nodes must be coordinated well enough with the local clock to assure that the buffers will neither overflow nor empty. Note that in a switched network the channels to be multiplexed at any specific multiplexer can originate anywhere in the network so that all nodal clocks are involved.

Many methods of providing the required coordination of the network clocks have been proposed, and some are in use (3). They include precise independent clocks, master-slave, external time reference, mutual synchronization, and time reference distribution.

In the independent clocks technique there is no timing communication between nodes. Each node has its own precise frequency clock. Since these clocks have slightly different frequencies, timing errors accumulate and it is necessary to occasionally interrupt traffic to reset the storage buffers.

The master-slave technique is perhaps the most obvious and straightforward. In this technique all nodes are slaved either directly or indirectly to a single master clock by phase locking the local clock to a received bit stream.

In the external time reference technique each node receives its time reference from a source external to the network, such as a Loran-C navigation signal, so that all nodal clocks are set to the same time within some tolerance.

In the mutual technique, each node adjusts the frequency of the local clock in such a way as to minimize the phase difference between itself and some weighted average of the phases of the received signals.

In the time reference distribution technique, all nodes are kept within a specified time tolerance of the master node (4). Nodal clocks run independently most of the time but are occasionally updated. Time reference information is transferred between all connected nodes with the effects of transmission time removed, but the time reference used at any node is that which comes over the best path to the highest ranking node. At each node, a simple set of rules is applied to information received from adjacent nodes so as to assure the selection of the best path to the highest ranking surviving node (5). The effects of signal transit time on time reference transfers over high capacity duplex digital transmission links can be removed by a simple procedure (4, 6) (see appendix).

One suggested method of providing the required clock coordination in a large digital communications network extending over a major part of the earth uses several of these basic techniques, each where it is best suited to the needs of the system, in a network referenced to Coordinated Universal Time (UTC) (6). It is illustrated in Figure 4. In this system, the highest level of the timing hierarchy comprises the satellite terminals because satellite links have superior capability for making precise time transfers over very long distances. Time reference distribution is used for the major nodes (any node connected to more than two other nodes). Minor nodes and PBXs have their nodal clocks slaved either directly or indirectly to the major nodes by phase locking them to received signals. Since the entire network is referenced to UTC, if some major node should have trouble getting a time reference via the normal time reference distribution, a Loran-C receiver or some other external UTC reference could be used temporarily. As a last resort backup, all nodes are provided with the

capability to operate in the independent clock mode, in which traffic must occasionally be interrupted to reset the buffers in order to prevent them from either overflowing or emptying. This provides a very highly redundant and dependable system in addition to a number of advantages resulting from having an accurate time available at all nodes (see appendix).

Time Division Switching

A time division switch is a device which interchanges communications time slots for the purpose of performing the switching function (7). This is illustrated in Figure 5. The time division switch has the capability of connecting an incoming channel in any time slot on any received digital transmission link to an outgoing channel in any time slot on any transmitted digital transmission link. In Figure 5, the channel α of time slot 1 of the received signal A_R appears in time slot 1 of the transmitted signal B_T while the channel β of time slot 2 in the received signal B_R appears in time slot 3 of the transmitted signal A_T. In effect, the time division switch performs both multiplexing and switching functions. In a switched digital network, the time division switch has timing requirements similar to those of time division multiplexers in a synchronous network with space division switches.

Communications Satellites

Communications satellites are becoming increasingly important in the field of communications. For various reasons, including cost, it is desirable to serve a large number of users from each communications satellite. Because of the complexity that would be required to provide separate transponders for each pair of users, it is desirable to provide a large number of accesses per satellite transponder. Although there is some overlap and hybrid systems are possible, there are four basic categories of multiple access (8).

Frequency Division Multiple Access (FDMA) is characterized by allocating an orthogonal frequency channel to each access. It is the least dependent on PTTI techniques of all multiple access techniques, but it is difficult to maintain orthogonality through the transponder for a large number of channels while efficiently using the transponder power.

Time Division Multiple Access (TDMA) allots separate time

slots to each user. With proper network timing (PTTI application), it is a truly orthogonal system (because one user at a time has exclusive use of the transponder) which is energy efficient, bandwidth efficient, readily achievable and is relatively insensitive to transponder characteristics. Although it is vulnerable to selective jamming and requires storage buffers, TDMA appears to be one of the most attractive methods of multiple access.

Spread Spectrum Multiple Access (SSMA) is a coded multiplexing technique. Although orthogonal codes could be used to achieve orthogonal channels, quasi-orthogonal codes are attractive to remove the requirement for precise network timing and control. Of course, even with quasi-orthogonal operation, each receiver must be accurately synchronized to the received code for its particular channel, and the other quasi-orthogonal users will appear as independent additive noise. For quasi-orthogonal operation SSMA requires no central network timing and has inherent antijam capability with a large number of possible addresses, but its energy efficiency and its bandwidth efficiency are poor and it requires up-link power coordination.

Pulse Address Multiple Access (PAMA) like SSMA allots separate codes to each user, but it also uses on-off amplitude modulation in addition to phase or frequency coding. Although it has inherent antijam capability and does not require network timing (only synchronization of the receiver to the code of the desired received signal), it has low multiple access efficiency in a nonjamming environment using a hard limiting transponder.

The time division multiple access technique appears to be one of the most attractive for digital transmission and is illustrated in Figure 6 where three ground terminals transmit to a single transponder in the satellite. The signal from each ground terminal is correctly timed so that it will arrive at the satellite at the correct moment to fill its time slot. Signals received at the transponder are therefore retransmitted with correct interleaving in a single signal which is received by all ground terminals.

Some Concluding Observations

Although applications of PTTI pervade the entire field of electrical communications, the most rapidly expanding application is for synchronization. This results from the rapidly expanding use of digital communications. To date,

most applications of PTTI for synchronization of digital communications have been for individual node to node digital transmission links or for individual channels transmitted over analog transmission facilities employing modems at each terminal. In both of these applications, the signal to be synchronized consists of relatively short (in numbers of bits) periodic time frames and there is no digital multiplexing of signals from different sources. It is relatively simple to phase lock the receiver to the repetitive frame code of the received signal because the total timing uncertainty can never exceed the length of a frame.

In order to preserve desirable characteristics of spread spectrum transmission, it is undesirable to use codes with a short repetition period so that codes with very long periods are used. This long frame period places no effective limit on the size of the time uncertainty so that it is desirable to limit it by other means, such as accurate clocks.

With complex switched digital networks employing time division multiplexing, not only must receivers be synchronized with the received signals, but all remotely located originators of digital channels that must be capable of being time division multiplexed with one another somewhere in the network must be adequately synchronized with one another.

With communications satellites employing time division multiple access, not only must the ground terminal receivers be synchronized with the received signals, but the arrival of the signals received at the satellite from different ground terminals must be synchronized so as to not overlap and interfere with one another.

All of these synchronization problems could either be solved or greatly alleviated if an accurate standard time, e.g. UTC, was available wherever it was needed. For some applications, such as low frequency radio communications, the availability of such an accurate standard time will permit communications to be prearranged on an accurate schedule that will reduce or eliminate the message exchange used only to establish communications. At extremely low radio frequencies, not only could the accurate time be used to predetermine the time of occurrence of a bit, but it could also be used to determine the phase of the received signal.

An application where availability of a standard time such as UTC would be very advantageous would be at all major nodes

of a large, complex, switched digital communications network consisting of many nodes covering a large geographical area and interconnected by high capacity duplex transmission links. It is interesting to observe that such a network also has the desirable combination of characteristics by which it could efficiently distribute the standard time reference, e.g. UTC, to where it is needed.

The use of such a standard time in communications applications can have the same advantages as standardization in any application. It will reduce interfacing problems, provide a common basis for measurement and permit the use of alternate sources. The use of the same time standard for all digital communications systems would make it convenient to temporarily combine independent communications operations into networks for their mutual support whenever desirable. In addition, the actual process of distributing a time reference through a highly connected digital communications network can be a useful tool for self-monitoring, and other similar advantages are conceivable. The use of the same time standard, (UTC) for all communications and navigation systems would enable them to provide backup to one another in the timing function. Because of advantages such as these, the relationship between the utility of a standard time (UTC) at all major nodes of a switched digital communications network, the unique capability of such a network to distribute the time standard to these nodes, and the likelihood that new applications for this accurate time reference will arise once it is available, should be given careful consideration.

Appendix

In the suggested integrated timing system for time division multiplexed switched digital networks (6), several basic timing techniques including external time references, time reference distribution, slaving, and independent clocks are all used in the same network, which is referenced to Coordinated Universal Time (UTC). This system employs time reference distribution (4) among the major nodes of the network to keep clocks at each node very close to the time of the master which is referenced to UTC. Minor nodes are slaved either directly or indirectly to the major nodes by phase locking their clocks to received signals. Since the network is referenced to UTC an external UTC reference can be used for a backup anywhere in the network. The independent clock mode of operation can serve as a last resort backup, but its use will require occasional interruption of traffic to reset buffers. There are three major functions related to time reference distribution among the major nodes of the network: measurement of the local clock's time error, correction of the time error in the local clock, and selection of the paths over which the time reference will be distributed from the master (ultimate reference) through the network, including selection of a new master when necessary.

Digital transmission normally uses a framing code to allow the receivers to be accurately synchronized to the received signals. These frame synchronization codes can be initiated by the nodal clock at each transmitter, their time of arrival can be measured by the nodal clock at each receiver. Neglecting noise, the measured time difference between the received synchronization code and the nodal clock at the receiver is due to two sources: the transit time of the signal, and the time difference between the two clocks. Let T_A be the time of the clock at node A, T_B be the time of the clock at node B, D_{AB} be the signal transit time from node A to node B, and D_{BA} the signal transit time from node B to node A. Then, the time difference measured at node A between the synchronization code received from node B and the local clock at node A is given by equation (1A).

$$K_A = T_A - (T_B - D_{BA}) \qquad (1A)$$

The time difference measured at node B is given by equation (2A).

$$K_B = T_B - (T_A - D_{AB}) \qquad (2A)$$

Node A transmits the measurement K_A to node B, and node B transmits the measurement K_B to node A. Subtracting K_A from K_B and dividing by 2 gives equation (3A).

$$T_B - T_A = \frac{K_B - K_A}{2} + \frac{D_{BA} - D_{AB}}{2} \qquad (3A)$$

When the transit times in the two directions are the same ($D_{BA} = D_{AB}$), they cancel, giving the time difference between the two nodal clocks with the transmission transit times removed. Normally, for high capacity transmission links, the difference in transit time in the two directions will be very small and the last term of (3A) can be neglected.

Although this discussion has assumed that the framing code is used for time comparison, under some circumstances it might be preferable to use a low-level spread spectrum signal superimposed on the transmitted data signal.

After the time difference between clocks at two adjacent nodes has been measured, it might seem natural that the node taking a time reference from the other node would immediately correct its clock for the benefit of other nodes which use its clock as a reference; but the resulting disturbance might be undesirable. It seems preferable to place a limit on the maximum rate of clock correction, such as one nanosecond per second (except during the initial setting). In order to provide an accurate reference for each node farther along a tandem string, each node transmits to its neighbors its measured but uncorrected error. When this information is combined with the measured time difference between nodal clocks, an accurate time reference is provided. This makes it possible for the correction of the nodal clocks to be relatively independent from the accurate distribution of time.

Two types of information transmitted by each major node to its neighbors have already been mentioned. By assigning a unique rank to each clock in the network and adding some additional types of information that are transmitted by each node to its neighbors, a simple set of rules can be used at each node to select its time reference from the neighboring node that will provide the best timing path to the highest ranking node in the network. Such a

systematic approach for selecting slaving paths in a master-slave network was described by Darwin and Prim (5).

It might be desirable for each node to transmit six types of data to its neighbors. These are:

T1. The time difference between the local clock and the clock at the other end of the link as observed at the local clock (This time difference includes transit time).

T2. The measured but uncorrected error in the local clock relative to its ultimate master reference.

T3. The rank of the node used as the ultimate master reference for the local clock.

T4. The merit (demerit rating) of the transmission path over which the time reference information is passed from the ultimate reference clock to the local clock.

T5. The rank of the local clock. (It is necessary to transmit this information because a node may have more than one clock with significantly different ranks.)

T6. Delay interval information. (This is information that can be used by the node to determine how long it must wait after tentatively selecting a new neighboring node as immediate reference before it may actually start using it as a reference for its own clock.)

The first two types of information are used to provide time reference information over every transmission link connecting major nodes (6). This provides a high degree of redundancy (with the resulting reliability and survivability). The rest of the information is used at each node to select a time reference from the neighboring node that will provide the best time reference path to the highest ranking node. The rules used at each node are:

Rule 1. A node initially entering the network will temporarily reference its own clock until a better selection is made.

Rule 2. Whenever the link or neighboring node used for immediate time reference fails, the node will temporarily reference its own clock until an alternate selection is made.

Rule 3. If a neighboring node being used as the immediate

reference should have a change in its ultimate reference to one of a lower rank, the local node will temporarily reference its own clock until an alternate selection (which could be the same one again) is made.

Rule 4. The third of the six types of data above, as received, provides the rank of the master time reference used by each connected node. The time reference for the local clock is taken from the connected node which uses the highest ranking clock as its ultimate master time reference. However, if the local clock outranks the others, the local clock (perhaps employing an external UTC reference if available) is used as reference. If any two links come from nodes ultimately referencing the same highest ranking clock, the criterion is inconclusive and rule 5 must be applied.

Rule 5. The fourth type of data above provides information about the merit (actually demerit) rating of the path from each connected node to the ultimate master time reference. Combining this information with the known merit (demerit) of the path from the local node to the connected node gives the overall merit (demerit) rating for paths to the master reference through each link entering the node. When the test of rule 1 is inconclusive because more than one of the immediate time references come from nodes ultimately referencing the same highest ranking clock, use this fourth type of data to select from among them the time reference that comes over the transmission path with the highest merit, i.e., the one with the best time transfer capability. If two or more of these come over paths with the same highest merit rating, this test will also be inconclusive and rule 6 must be applied.

Rule 6. The fifth type of data above provides the rank of the clock at each neighboring, i.e., directly connected, node. When the tests of rules 4 and 5 are both inconclusive, this fifth type of data is used to select from among those links with ultimate time reference coming from the same highest ranking clock, over paths with the same highest merit rating, that one which comes from the highest ranking, directly connected node. This produces an unambiguous decision.

Rule 7. If no time reference is available, the node will divert to the free-running clock mode (referencing its own accurate independent clock). When operating in this mode, data storage buffers at this and neighboring nodes will have to reset occasionally to accommodate the slight

frequency error that will exist at the local node.

When a node must revert to its own clock due to a failure, as required by rules 2 and 3, there probably will still be obsolete information in the network, i.e., some nodes will be indicating that they are referencing the node that is failed. This results because of the length of time required for the information to disseminate to all nodes that were using the failed node. The information only progresses one node farther from the failed node for each information exchange period. The sixth type of information above is used to assure that this obsolete information has had time to have been swept from a newly selected immediate (neighboring node) reference before a node is permitted to reference it.

References

(1) William R. Bennett and James R. Davey, Data Transmission, McGraw-Hill Book Company, 1965.

(2) Naval Electronics Laboratory Center, TD 271, AD-915852, "Proceedings of the 1973 Symposium on Spread Spectrum Communications, Volume I," M. L. Schiff, March 1973.

(3) J. W. Pan, "Synchronizing and Multiplexing in a Digital Communications Network," Proc. IEEE, Vol. 60, No. 5, (May 1976) pp. 594-601.

(4) H. A. Stover, "A Time Reference Distribution Concept for a Time Division Communication Network," Proceedings of Fifth Annual NASA Department of Defense Precise Time and Time Interval (PTTI) Planning Meeting, NASA, Goddard Space Flight Center, Greenbelt, Maryland (December 4-6, 1973).

(5) G. P. Darwin and R. C. Prim, U.S. Patent No. 2,986,723, "Synchronization of a System of Interconnected Units."

(6) Harris A. Stover, "Coordinated Universal Time as a Timing Basis for a Digital Communications Network," EASCON 1974 Record, Washington, DC, October 7, 8, and 9, 1974.

(7) Patric Marino, T. H. Gordon, R. J. Pilc, "A Time-Division Switch," IEEE Transactions on Communications, Vol. COM-22, No. 11, November 1974.

(8) D. T. Magill, "Multiple-Access Modulation Techniques," AIAA Communications Satellite Systems Conference," Washington, DC, May 2-4, 1966.

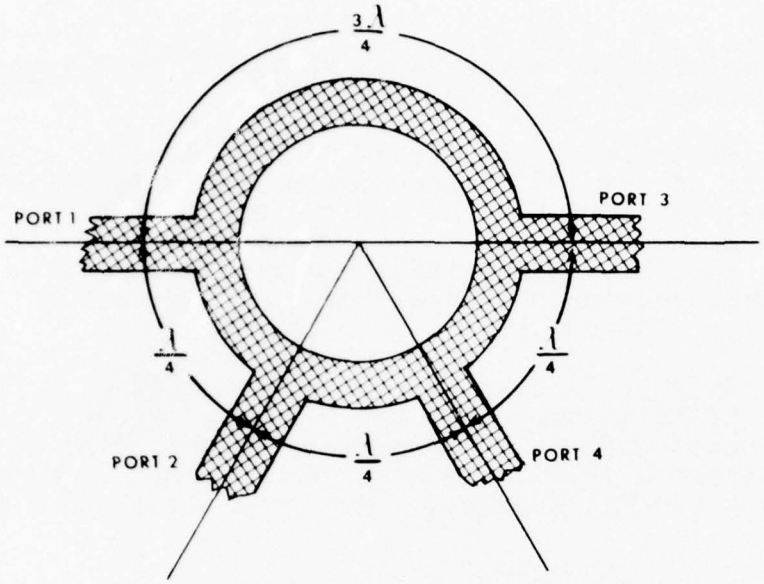


Fig. 1--Ring Hybrid

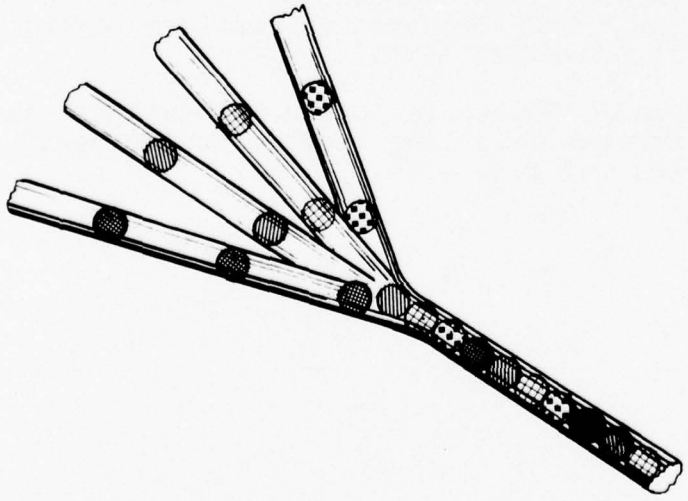


Fig. 2--Analog of Time Division Multiplexer

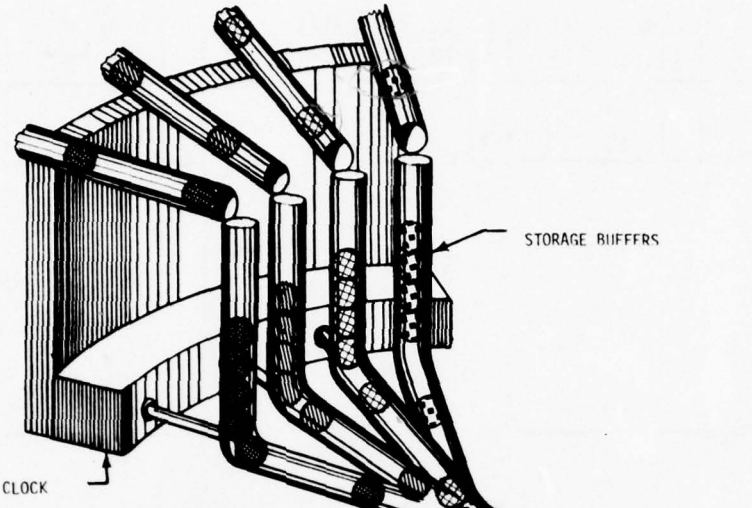
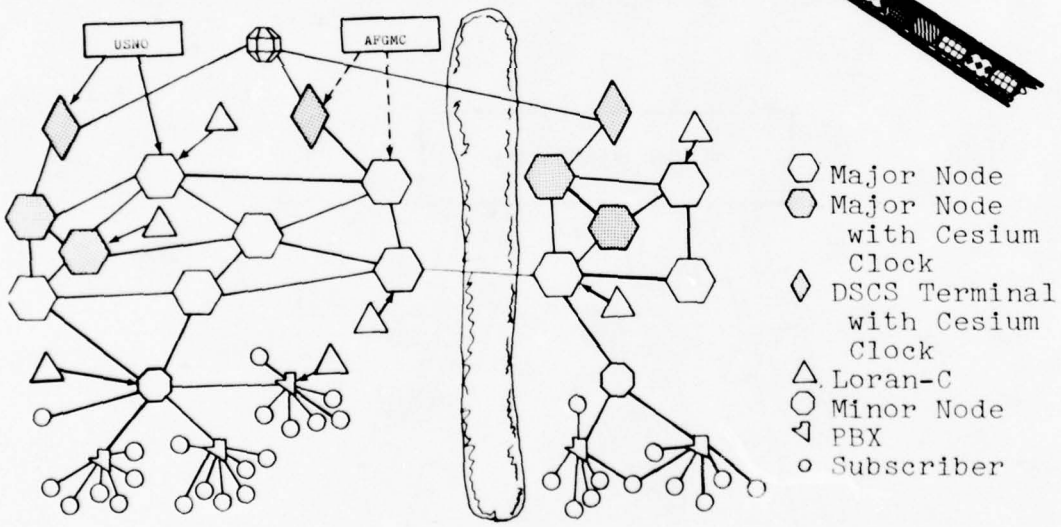


Fig. 3--Analog of Time Division Multiplexer with Elastic Storage Buffer



Active master node uses UTC reference from U.S. Naval Observatory (USNO), Air Force Guidance and Metrology Center (AFGMC), or Loran-C. Major nodes use Time Reference Distribution or option for external time reference (Loran-C). Minor nodes, PBXs, and subscribers slaved to received signals. All nodes capable of independent clock mode of operation.

Fig. 4--Suggested Timing System for Digital Communications Network

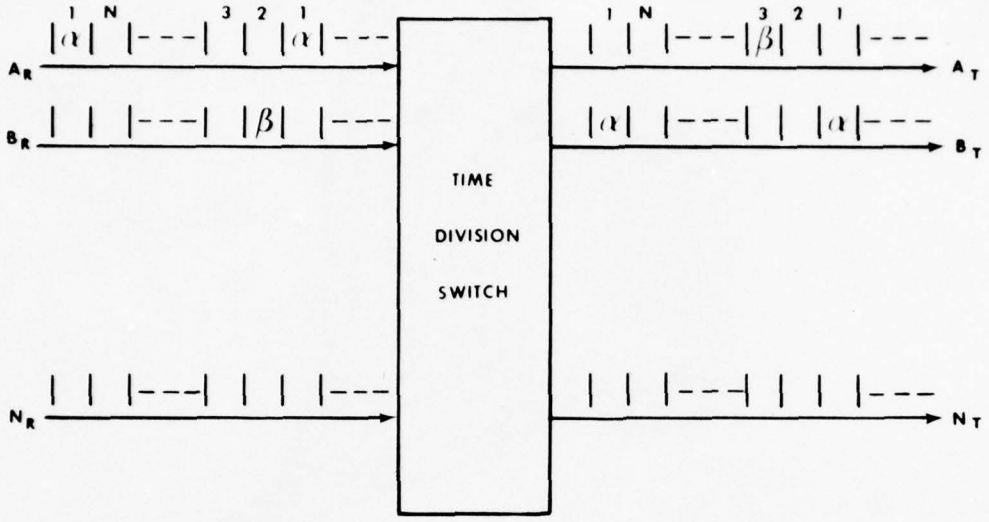


Fig. 5--Time Slot Interchange for Time Division Switching

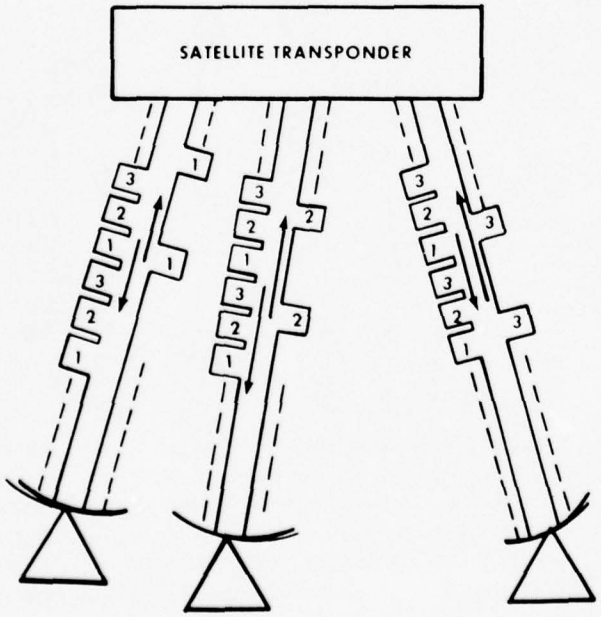


Fig. 6--Time Division Multiple Access

QUESTION AND ANSWER PERIOD

NO DISCUSSION

AN INTEGRATED COMMUNICATION, NAVIGATION, IFF SYSTEM

Major J. A. Krupinski

Electronic Systems Command
U. S. Air Force

ABSTRACT

The DOD has established the Joint Tactical Information Distribution System (JTIDS) Program Office at the Air Force Electronic Systems Division. The primary objective of the program is to develop a secure, jam-resistant, Digital Information Distribution System which will incorporate a capability of determining relative position. Additionally, it must be capable of providing identification information on friend and foe.

The JTIDS concept relies for synchronization of the terminals on simple, crystal oscillators that serve as the local standards. Bias and drift of these local clocks with respect to the "Master" system clock are derived from evaluation of the times of arrival of signals from three or more transmitting units. It is this same time of arrival that is used to determine the relative position of the local terminal.

PRECEDING PAGE BLANK-NOT FILMED

QUESTION AND ANSWER PERIOD

NO DISCUSSION

VLBI: PAST, PRESENT, AND FUTURE

Irwin I. Shapiro
Massachusetts Institute of Technology

ABSTRACT

A brief review of the fundamental principles of very-long-baseline interferometry (VLBI), with emphasis on the role of the frequency standard, will be given first, followed by a discussion of the accomplishments to date in the fields of astrometry, geodesy, and geophysics. The instrumental improvements now under development and their consequences for these sciences will then be described.

QUESTION AND ANSWER PERIOD

DR. VESSOT:

I think these astronomical papers often leave us in a little bit of a mind-boggled condition. I wonder, do you have a gee-whiz number which tells us what a milliarc second is? Is it the size of a Volkswagen on the moon?

PROF. SHAPIRO:

A milliarc second is 5 times 10 to the minus ninth radians so 1,000 kilometers is 10^8 centimeters, so it is a half a centimeter at a thousand kilometers.

DR. VESSOT:

This field, to me, is extremely exciting in that it is a very immediate indication that time is related to a lot of other things, and in future these conferences may well be called the PTTI in length or PTTI in angle measuring, because distance is going to be in -- is, right now -- philosophically not separable from time interval, and I know well that the work at the Bureau of Standards which Helwig is headed toward, is to integrate the question of time interval and distance.

Now, Irwin Shapiro has measured the distance across the solar system in terms of time, so your yardstick isn't scratches on a kilometer bar someplace, but --

PROF. SHAPIRO:

Light seconds.

DR. VESSOT:

Light seconds, or scratches on some other bar, but a different kind of bar.

PROF. SHAPIRO:

In fact, none of the work, either the VLBI work on the earth or the radar work in the solar system is at all related to the -- well, that is not quite so, but it is effectively that kilometers are relevant for our work.

The light second is the key to success.

MR. KRUTENAT:

Would you care to expand on the expansion of those two centers? I heard two numbers, twice the speed of light and three times the speed of light.

PROF. SHAPIRO:

I just did that to see if I would get a rise out of anyone, to see if anyone was awake. That did not imply any violation of general relativity. It is simply that you can take two sources and have them expand, one from the other, in their frame at, say, .95 times the speed of light, and look at them. Look at the light that arrives from one of them where you are, and look at the light that arrives from the other one where you are, but those two are arriving at the same time, and with trivial elementary algebra that you would learn in high school, you can then calculate what the apparent speed of separation is, looked at, on the plane normal to your line of sight, and you can get arbitrarily high apparent velocity.

That is why there was that sub-apparent, and there is no implied violation of general relativity, but it is certainly an implication that things are happening rapidly, and that is why I stressed that.

PRECISE TIME FOR VERY LONG BASELINE INTERFEROMETRY AT SANTIAGO, CHILE AND RELATED PROBLEMS GERMANE TO THIS GEOGRAPHIC AREA

F. Noël
Observatorio Astronómico Nacional
Universidad de Chile

ABSTRACT

A general description of the activities of the Time and Latitude Service of the National Astronomical Observatory at Cerro Calán, Santiago, is given.

Precise time is provided by Cerro Calán Time and Latitude Service for a radio-astronomy project, which using VLBI technique, has been carried out in collaboration with the University of Florida in order to determine accurate positions and sizes of Jupiter's radiosources. According to the frequency of the signal recorded at the observing sites, the required accuracy in time synchronization must be better than 10 microseconds.

Time synchronization is based on a cesium atomic clock of Cerro Calán Time Service, which is synchronized through a flying clock of NASA with UTC(USNO). It is shown in this paper that the synchronization can be kept at Santiago, better than the required accuracy, measuring the mean monthly frequency difference of the local standard with respect to USNO, by observing daily relative phase variations of VLF signal of station NBA. With the observed frequency differences, a daily estimated error in time is computed for Cerro Calán atomic clock. This computed error is in good agreement with the observed error obtained via flying clock after 15 months of operation.

The services for time dissemination through the country for scientific and public use, as well as the future plans of development including accurate clock synchronization by means of TV line 10 method are described.

PRECEDING PAGE BLANK-NOT FILMED

I. INTRODUCTION

The National Astronomical Observatory of the University of Chile was founded in 1850. Its main activities concern the research in Astrophysics, Radioastronomy and specially in Fundamental Astronomy. At the present time the Observatory is located on Cerro Calán, a small hill in the eastern suburbs of Santiago, where a Time and Latitude Service for scientific purposes is in operation. The main scope of this service is the accurate determination of UTO and latitude, which are used in investigations of the earth rotation and the variations of the local geographic coordinates. Both determinations, UTO and latitude, are based on the observations made with a Danjon Astrolabe, which is working at Cerro Calán since 1965, under an agreement signed between the European Southern Observatory and the University of Chile for a joint research project whose main goal is the improvement of the Fundamental Reference System at the southern hemisphere (1, 2, 3).

Since 1971 the astrolabe of Santiago is one of the 17 astronomical instrumentsof 12 observatories determining time and/or latitude, whose results are used regularly by the BIH for the Rapid Service which provides accurate UT1 and polar coordinates to the JET PROPULSION LABORATORY (JPL). These data are used by the JPL in spacecraft navigation (4).

Until 1973 our time reference for the astronomical observations was based on a Rohde und Schwarz quartz clocks unit of type CAA with a frequency stability of 1×10^{-10}. The phase of the master clock was compared with that of the 24 kHz standard frequency of NBA by means of a Rohde und Schwarz VLF receiver type XKE. Synchronization with UTC was made through the reception of time signals (WWV) in HF, so the uncertainty in our epoch was of the order of 2ms.

In 1973 a time service with an accuracy of ±10 microseconds with respect to UTC, was required to provide precise time for a Very Long Baseline Interferometry (VLBI) project which is being undertaken by our Radio-Astronomy group at the Radio-Observatory of Maipú, through a joint program with the University of Florida. The purpose of this project is to obtain information on the sizes of the radio-sources of the powerful decametric bursts from the planet Jupiter. Simultaneous radio observations of Jupiter at 18MHz with a narrow banwith (2.4 kHz), are being made at Maipú, about 30 Km to the SW of Santiago, at Gainesville, Florida and at Bowling Green, Western Kentucky.

The baseline is about 7100 Km for Maipú-Gainesville and about 7900 Km for Maipú-Bowling Green (5, 6).

Since the time synchronization of the observing sites should be performed using UTC(USNO) as the transfer standard, I shall describe how we are achieving at Santiago a precise time comparison with USNO:

II. PTTI AVAILABILITIES AT SANTIAGO

In the plans for a precise time service we considered our timing requirements and the PTTI availabilities for these requirements at our geographic area, i.e. accurate synchronization and reliable phase control that could be obtained at Santiago.

Since Santiago is a rather faraway area from PTTI dissemination systems, it is interesting to show how we are trying to solve our problems.

1) Synchronization with UTC(USNO)

For the synchronization with UTC (USNO) with the required accuracy, we obtained the kind cooperation of NASA which offered to us the facilities of its flying clock that comes periodically to the Spaceflight Tracking and Data Network (STDN) station of Peldehue, about 40 Km north of Santiago.

Since NASA's flying clock comes to Santiago more or less once in the year, we realized that, in order to make a regular and profitable use of these facilities a strong improvement should be made in our time keepers. This improvement was implemented by means of a cesium beam frequency standard HP 5061 A, which was got by the National Observatory with funds provided by the Scientific Research Office of the University of Chile. The cesium standard was put in operation at the end of 1973 and the first synchronization through flying clock was made in February 11, 1974 and the second one in May 13, 1975.

Time synchronization, through LORAN-C was also considered. However, if we take into account the distance from Santiago to any LORAN-C station, we must conclude that the accuracy which could be obtained through this method should be below our requirements (7). To our knowledge this is confirm at the STDN station of Peldehue, where the skywave propagated signals of the LORAN-C stationsof UPOLO and JOHNSTON ISLAND are regularly received. If we consider that Santiago is

located at a higher southern latitude than that of NASA's STDN station of Carnarvon, Australia, we might deduce, at least theoretically, that the precision in time synchronization which could be obtained at Santiago through LORAN-C, should be of the same order as that obtained at Carnarvon, that is ±75 microseconds (8).

2) Phase control

For phase control we have a Rohde und Schwarz VLF receiver mentioned in I, which is fix tuned for 24 kHz, that is the frequency of station NBA. We know that the reception of only one VLF station is unreliable for a continuous phase tracking, (9) however for the moment these are our only instrumental possibilities. At Santiago, although we have a clean reception of NBA during day propagation, there are frequently phase jumps during sunrise and sunset, which produce troublesome phase discontinuities. (Fig. 1) (10). So, if phase tracking, using NBA, is unreliable to estimate the rate of our atomic clock, it is best to compute from the phase comparisons the relative frequency difference between UTC(USNO) and our atomic standard. A numerical integration could give us the time difference USNO - National Observatory (11).

III. RESULTS

Let UTC(NAO) be the UTC of the National Astronomical Observatory and DF the relative frequency difference between USNO MC and the local atomic clock. DF is computed from the daily phase comparisons with the VLF of NBA. The time difference USNO-NAO is obtained for a certain epoch t, in days, by

$$1) \qquad (UTC(USNO\text{-}NAO))_t = (UTC(USNO\text{-}NAO))_0 + \int_{t_0}^{t} DF\,dt$$

where the integration constant $(UTC(USNO\text{-}NAO))_0$ is derived by means of flying clock comparison at epoch t_0.

In Table 1 we give the results obtained applying this method between two flying clock comparisons: February 11, 1974 and May 13, 1975.

TABLE I

TIME AND FREQUENCY COMPARISONS BETWEEN USNO AND THE NATIONAL ASTRONOMICAL OBSERVATORY (NAO) AT SANTIAGO

	USNO	NAO	
	FREQUENCY(1)	TIME	
	UNIT: 1×10^{-12}	1 microsecond	
	VIA : NBA	NBA(2)	Flying Clock
1974 FEB.	+1	00	0(3)
MAR.	-1	00	-
APR.	-1	-03	-
MAY.	-1	-05	-
JUN.	0	-06	-
JUL.	-2	-09	-
AUG.	-2	-14	-
SEP.	-4	-22	-
OCT.	-1	-29	-
NOV.	-1	-30	-
DEC.	-1	-33	-
1975 JAN.	-2	-36	-
FEB.	+3	-35	-
MAR.	-2	-33	-
APR.	-1	-37	-
MAY.	+1	-37	-33

(1) Monthly means.
(2) Computed using equation. 1) and referred to the 13 of each month.
(3) Synchronization with UTC(USNO) on February 11.

It can be seen from this data that the time at the National Observatory was kept within 5 microseconds with respect to USNO after a period of 15 months. It seems to us that the frequency data for Sep. 1974 and Feb. 1975 look ratner abnormal. Perhaps these values are due to propagation anomalies or seasonal disturbances affecting the phase comparisons or may be to an abnormal behaviour of the equipment produced by environmental causes. However, we think that it is necessary to have a longer period of observations in order to disclose the real causes of the observed anomalies.

IV. PRESENT SERVICES AND FUTURE DEVELOPMENTS.

Although the agency who has the legal responsability for time determination and dissemination in Chile is the Hydrographic Institute of the Chilean Navy, two special services for time dissemination through the country are operated by the National Observatory. One is transmitted in HF, four times a day, for the network of seismological stations of the Geophysical Department of the University of Chile. The other one, for public use, provides time signals every thirty minutes through telephone lines, to the commercial radiobroadcasting stations of Santiago.

The accuracy of the time services for seismology at the sites of reception is limited by the HF propagation mode. The time signals are similar to those of WWV and with a special code, some minutes and hours are identified.

At the present time there are five atomic clocks operating in Chile: two cesium of the Hydrographic Institute of the Navy at Valparaiso, one cesium and one rubidium at the STDN station of NASA at Peldehue and a cesium at the National Observatory. All these clocks are located in a small area of the country; the longest distance between them is more or less 100 Km.

We are implementing now a project in order to link the cesium atomic clocks of the National Observatory with those of the STDN station of NASA by means of the TV line 10 method. Strong signals of TV National Channel, emitted from the same station, are received at Cerro Calán and Peldehue. In this way we expect to make a strong improvement in our time keeping which will be of significant benefit for both institutions.

For a near future it is expected to get an agreement with the Chilean Navy to compare by means of TV, the atomic clocks of the Hydrographic Institute at Valparaiso with those of Cerro Calán and Peldehue near Santiago.

The transmissions of TV National Channel are received practically through all the country. So, time comparisons along the Chilean territory, using line 10 method could be easily made in the future if the corresponding delays are previously measured.

ACKNOWLEDGEMENTS

The author wishes to express his gratefulness to NASA for the flying clock facilities given to the Chilean National Observatory at Santiago. NASA's collaboration was a significant support to our Time Service. The participation of the author in this Seventh Annual PTTI Planning Meeting was possible through a grant kindly provided by the Association of Universities for Research in Astronomy (AURA Inc.).

REFERENCES

(1) Anguita, C. and Noël, F., "Systematic Errors in the FK4 Fundamental Catalogue as Deduced from Astrolabe and Meridian Observations in the Southern Hemisphere". The Astronomical Journal, Vol. 74, Nr. 7, Sep. 1969.

(2) Noël, F., "Seasonal Effects Observed in Time Determinations at Santiago", IAU, Symposium Nr. 48, The Rotation of the Earth, Proceedings p. 139; Morioka, Japan 1971.

(3) Anguita, C. and Noël, F., "Time and Latitude Results of the Danjon Astrolabe Program at Santiago"; IAU, Colloquium Nr. 1, The Problems of the Variations of the Geographical Coordinates in the Southern Hemisphere, Proceedings p. 36, La Plata, Argentina 1968.

(4) Guinot, B. and Feissel, M., "Report on the Rapid Determinations of the Pole Path and UT1 (June 1972)", BIH, Private communication.

(5) Carr, T.D. et al., "Very Long Baseline Interferometry of Jupiter at 18 MHz", Radio Science Vol. 5, Nr. 10, Oct. 1970.

(6) May, J. and Carr, T.D., "Interferometry of Jupiter at 18 MHz", Quarterly Journal of the Florida Accademy of Sciences, 30, 1-9, 1967.

(7) Jespersen, J.L., Blair, B.E. and Getteres, L.E., "Characterization and Concepts of Time-Frequency Dissemination"; Proceedings of the IEEE, Vol. 60, Nr. 5, May 1972.

(8) Chi, A.R., "Performance of LORAN-C Chains Relative to UTC"; Proceedings of the Sixth Annual PTTI Planning Meeting. p. 263, 1974.

(9) USNO, Time Service Information Letter, 15 August 1973.

(10) Guinot, B., Feissel, M. and Grauveaud, M., Annual Report of the BIH for 1970, p. 14.

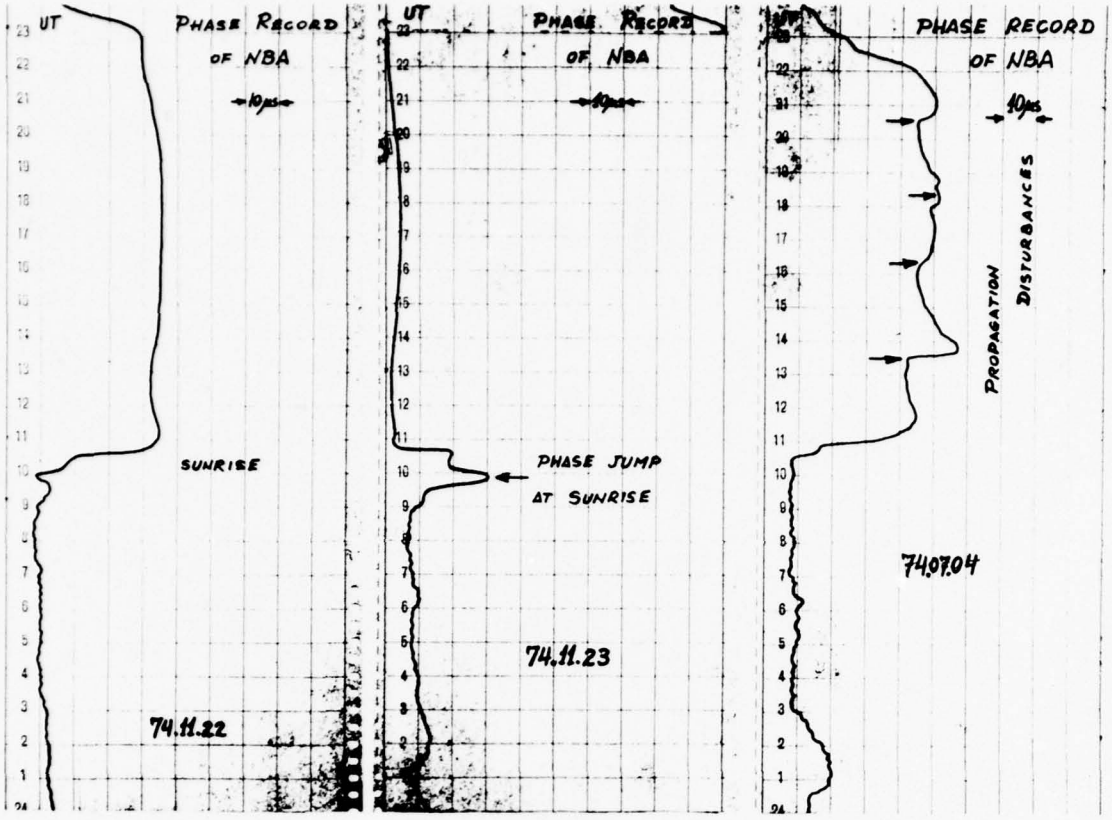


Fig. 1) Phase Records of NBA obtained at Santiago de Chile.
(a) Normal reception.
(b) Phase jump ocurred at sunrise.
(c) With strong disturbances during day propagation.

QUESTION AND ANSWER PERIOD

NO DISCUSSION

RADIO INTERFEROMETRIC GEODESY USING A RUBIDIUM FREQUENCY SYSTEM

Peter F. MacDoran, J. B. Thomas, K. M. Ong, H. F. Fliegel and D. D. Morabito, Jet Propulsion Laboratory, California Institute of Technology, Pasadena, California 91103 *

ABSTRACT

In order to be useful for geophysical applications, geodetic baseline measurement accuracy must be at the few centimeter level. For independent station radio interferometric geodetic systems the accuracy requirement of a few centimeters is most often translated into frequency system performance of $\Delta f/f = 10^{-14}$ or better. However, for specific applications such as determining three baseline vector components and two or three instrumental parameters the frequency system requirements can be made a factor of approximately 30 less stringent so that the Rubidium frequency system comes close to meeting the required performance at S-band. A simplified analysis is developed which illustrates the performance needed to achieve 3 cm baseline precision in terms of short, medium and long term fractional frequency deviation. These analytic approaches have been tested in actual independent station radio interferometry. From December 1973 to June 1974, a series of four independent station interferometry experiments were conducted on a 307 meter baseline using the 9 meter transportable ARIES (Astronomical Radio Interferometric Earth Surveying) station, and the 64-meter MARS station of the Goldstone Deep Space Communications Complex. The ARIES station was equipped with an HP 5065A Rubidium frequency system while the 64-m station used a JPL Hydrogen maser. The three-dimensional baseline precisions obtained were 10 cm or better from individual six-hour experiments, 3-cm precision for a weighted average of 23 hours of data and accuracies of 0.1 cm to 4.9 cm when compared with a geodetic survey between the stations. The Rubidium frequency system performance achieved in these experiments was $\Delta f/f = 2 \times 10^{-13}$, about a factor of two better than the Hewlett Packard specification.

* This paper presents the results of one phase of research carried out at the Jet Propulsion Laboratory, California Institute of Technology, under Contract No. NAS 7-100, sponsored by the National Aeronautics and Space Administration, Office of Applications, Earth and Ocean Dynamics Applications Program.

INTRODUCTION

A cursory look at the requirements on a frequency and time system to be considered for use in an independent station radio interferometric geodetic measurement would likely conclude only a Hydrogen maser or similar device was adequate to the task.

For example, in the fringe frequency domain the partial derivative sensitivity to baseline is 0.5×10^{-3} Hz per meter. Thus, to achieve a 3 cm sensitivity at S-band (2.3 GHz) would require $\Delta f/f = 7 \times 10^{-15}$. In the time domain, the sensitivity is that imposed by the speed of light or about 3 nanoseconds per meter, so that over the duration of a six-hour experiment the 3 cm performance requirement appears to be $\Delta T/T = 5 \times 10^{-15}$.

Although Project ARIES (Astronomical Radio Interferometric Earth Surveying) has currently progressed to operating on baselines of about 200 km, the frequency system factors are best illustrated with data from earlier 307 m system verification experiments (Ref. 6). The reasoning is that the frequency system contributions to the overall behavior of the system are better understood when factors such as transmission media, source positions and Earth orientation parameters are minimized. Also, the 307 m baseline could be conveniently surveyed in three dimensions so that system accuracy can be assessed.

When the initial planning implementation of the ARIES station began in late 1972 and early 1973, it was clear that the resources available could not include a Hydrogen maser frequency system. Thus, alternative strategies were sought to make some other less expensive frequency system useable. The commercially available rubidium and cesium devices were, of course, the prime candidates. In late 1972, an interferometry experiment was conducted on the 16 km Goldstone baseline using a JPL H-maser at the 64-m MARS station and the operational ECHO (26m) tracking station standard, HP 5065A rubidium. The result was encouraging since the Rb/H-maser combination had baseline noise of 7 to 10 cm and agreed well with the 4 cm precision (signal to noise limited) results of that baseline when run with H-masers at each station. By this time the radio source observing strategy had evolved to the point of obtaining a set of sources to accomplish a baseline solution as quickly as possible which is further discussed in the requirements section of this paper.

The rubidium performance discussed here is pessimistic since a great many elements are involved in actually obtaining delay residuals from which fractional frequency deviations are deduced. Also, the Hydrogen maser used at the 64-m station is assumed to have contributed no significant noise in these measurements.

For those interested in the specifics of the geodetic surveying by

radio interferometry, the reader will find the References useful.

FREQUENCY SYSTEM REQUIREMENTS

Short Term (1 to 10^2 Sec)

First there is the requirement that fringes be obtained and this forms short term requirements. The detailed mechanization of this processing is discussed elsewhere (Ref. 9 to 12) and we will merely state that the stability needed at each station is that neither local oscillator shall gain or lose a tenth of an RF cycle of the received frequency over whatever averaging time is required in the cross-correlation signal processing. For strong quasar sources, the coherent averaging time may be as small as 1 second while weak sources may require coherent averaging times of 100 seconds or more. At S-band the performance requirements then become $\Delta f/f = 5 \times 10^{-11}$ for strong sources and $\Delta f/f = 5 \times 10^{-13}$ or better for weak sources. At X-band (8.4 GHz) the requirements range from 1.4×10^{-11} to 1.4×10^{-13}. There is little that can be done here to relax these requirements except to redesign the telecommunications parameters to achieve larger signal to noise ratios to stay away from the weak signal case. Basically, a Rubidium system can be relied upon at S-band but would become marginal at X-band for satisfying these short term interferometry needs, see Figure 1 and 2.

Medium Term (10^3 Sec)

Over a period of several hours the two interferometry stations observe the extragalactic radio sources on a cycle of about six minutes on the source and ten minutes to move the antennas to the next source governed entirely by the slewing rate of the large antenna. Typically the sources are about 90 degrees apart on the sky. So that about 10^3 second elapses between individual source observations. Within a given six hour experiment, 24 observations are made of six or more sources. Assuming that we are solving for six parameters (three baseline and three instrumental) the solution set is a factor of 4 over-determined. If the desired baseline precision is 3 cm then the individual source observations need a precision of 6 cm since the over-determined nature of the solution will help by a factor of two assuming geometrically well distributed sources. The 6 cm implies 0.2 nsec over periods of 10^3 seconds or a $\Delta f/f = 2 \times 10^{-13}$. These performance levels have been seen with the HP 5065A in the actual experiments. Such performance is a factor of two better than the Hewlett Packard specified performance, see Figures 1 and 3.

Long Term (10^4 to 10^5 Sec)

Initially, there is the assumption that the phase noise introduced into the system be uncorrelated with the delay observable partial derivative

sensitivity to the individual baseline components. This assumption is not always satisfied causing baseline solution degradations of a factor of 2 to 4, see Table 1 and Figures 4 and 5.

Using the 24 observations accumulated over six hours, a simultaneous solution must be accomplished for the three baseline vector components and either two or three instrumental parameters (clock and frequency synchronization plus a possible time dependent frequency term). It is possible to accomplish this simultaneous six parameter estimation because the instrumental parameters do not depend upon the directions in which the two antennas are pointed. Meanwhile, the delay of the incoming quasar wavefront, of course, depends upon the DOT product of the baseline vector and the vector direction to the radio source (i.e. the directions in which the antennas are pointed). One must be careful to examine the instrumentation to assure that such an assumption of electrical phase stability is in fact correct within required limits. For example, if differential phase shifts were occurring in cables as the antenna moved to different positions then the clock offset term would take on the appearance of being related to one or more baseline components. Actual measurements of such differential phase shifts have been performed for both the ARIES and MARS stations and have been found to be at about the 1 cm baseline vector equivalent level and are not thought to be of sufficient magnitude to warrant direct calibration at this time.

The ability to estimate clock and frequency offset terms affecting the entire data set is a strong self-calibration feature. It is only those frequency system instabilities that remain after the offset removals which forms the concern as to what will actually disturb the baseline vector estimation. In effect what is done is to find time spans during the experiment when the frequency system behavior is easily parameterized. Specifically that the delay be describable by a constant delay offset, a constant time rate of change of delay and possibly a quadratic delay term to account for frequency drift. Figure 3 is an example of an experiment with a six parameter estimation (three baseline, constant offset, constant rate and frequency drift). If situations are encountered where the system does not exhibit such easily parameterized behavior, then the solution set is segmented into regions where it does apply. The limit to such segmenting obviously occurs when an insufficient number of sources have been observed with a wide geometric sky spread. Figure 5 illustrates the breaking of a solution set to analytically describe long term performance. Thus, over periods of hours the frequency system needs to behave in a smooth continuous manner so that the medium term performance of $\Delta f/f = 2 \times 10^{-13}$ can be exploited to yield 3 cm baseline results. Abrupt changes in offset and slope, as seen in Figure 6, can be tolerated provided that there are stable intervals in which to obtain five or six parameter solutions. While the change in slope may appear large in Figure 6, it actually amounts to 5×10^{-13}, exactly the specified performance for the HP 5065A for

averaging times of hours.

COMBINED FREQUENCY SYSTEM APPROACH

There exists the possibility of further system stabilization of the long term by using a cesium beam resonator in combination with the rubidium. In this way the rubidium would govern the short and medium term performance and the cesium the long term. Thus, the overall baseline solution would be stronger since fewer instrumental terms would have to be estimated.

There is the desire to make observations at X-band to minimize charged particle delay effects of the transmission medium but the rubidium is marginal for that short term application. Again, a combined frequency system of crystal and rubidium is useful as already shown in Reference 1.

THE INTERPLAY OF FREQUENCY STABILITY AND CHOICE OF ANTENNAS

As seen in the actual rubidium data, (Figures 5 and 6) the system tends to behave well over time intervals of 30-90 minutes and even out to 10 hours (see Figure 3) but occasionally makes an abrupt change in phase offset and rate which forces the interferometer baseline solution to be restarted to estimate new instrumental parameters. If an insufficient set of sources have been observed during the well-behaved interval, the baseline vector solution will tend to absorb the frequency system excursion as being similar in character to the baseline components.

The use of the 64-m MARS station brings with it a factor of 2.8 better signal-to-noise ratio than a 26-m station but also requires longer move times between sources. The 64-m station needs between 6 and 30 minutes to go between sources depending upon the cable wraps. A 26-m station can move at a faster slewing rate so that only 2 to 3 minutes are needed to cover a 90 degree move. Thus, one can choose an option to observe sets of five or six sources in one-half hour and obtain stand-alone data sets (possessing sufficient data to solve for baseline and instrumental parameters) during probable periods of well-behaved Rubidium performance. These half-hour data sets would then be combined together over the 8 to 24 hour data acquisition interval to yield an overall baseline precision of 4 to 6 cm.

Thus, the apparent paradox that using a smaller diameter antenna can improve the baseline measurement accuracy.

CONCLUSION

A cursory estimation of frequency system requirements to accomplish independent station radio interferometry baseline measurements might

conclude that only a Hydrogen maser could perform the job.

However, such an estimation needs to take into account the ability of the radio interferometer to be somewhat self-calibrating. It has been shown, analytically and experimentally with 307 m baseline data, that the frequency system requirements are actually $\Delta f/f = 2 \times 10^{-13}$ to achieve 3 cm baseline accuracy at S-band. This amounts to being a factor of 30 to 40 less severe than the cursory estimate and makes the Rubidium (HP 5065A) system a very useful device for geodesy by radio interferometry.

ACKNOWLEDGMENTS

The authors wish to acknowledge the contributions of many JPL colleagues, particularly J. L. Fanselow, A. E. Niell, R. A. Preston, G. M. Resch, D. W. Trask and J. G. Williams for valuable discussions; K. F. Fox for data reduction; P. D. Batelaan, J. A. Carpenter, M. G. Newsted, S. R. Paine and R. J. Wallace for assistance with ARIES station implementation; B. B. Johnson, L. J. Skjerve and D. J. Spitzmesser for special digital instrumentation and experiment conduct; W. R. Bollinger and M and Q Pacific for geodetic surveying at Goldstone. We are also indebted to the National Radio Astronomy Observatory for their hospitality regarding the Mark II Data Processor with thanks to B. G. Clark and B. Rayhrer. We also thank the Satellite Communications Agency, U. S. Army, Fort Monmouth, N. J. for the transfer of the surplus transportable 9-m station to NASA/JPL; the NASA Office of Tracking and Data Acquisition for cooperation in scheduling ARIES experiments and the personnel of the MARS Deep Space Station for experiment conduct.

REFERENCES

1. Cohen, M. H., Introduction to very-long baseline interferometry, Proc. IEEE, 61, 1192, 1973.

2. Counselman III, C. C., Very-long baseline interferometry techniques applied to problems of geodesy, geophysics, planetary science, astronomy, and general relativity, Proc. IEEE, 61, 1225, 1973.

3. Fanselow, J. L., P. F. MacDoran, J. B. Thomas, J. G. Williams, C. J. Finnie, T. Soto, L. Skjerve, and D. J. Spitzmesser, The goldstone interferometer for earth physics, in The Deep Space Network Progress Report, Technical Report 32-1526, Vol. V, p. 45, Jet Propulsion Laboratory, Pasadena, California, 1971.

4. Hinteregger, H. F., I. I. Shapiro, D. S. Robertson, C. A. Knight, R. A. Ergos, A. R. Whitney, A. E. E. Rogers, J. M. Moran, T. A. Clark, and B. F. Burke, Precise geodesy via radio interferometry, Science, 178, 396, 1972.

5. MacDoran, P. F., Radio Interferometry for International Study of the Earthquake Mechanism, Acta Astro., Vol. 1, pp. 1427-1444, Pergamon Press, 1974.

6. Ong, K. M., P. F. MacDoran, J. B. Thomas, H. F. Fliegel, L. J. Skjerve, D. J. Spitzmesser, P. D. Batelaan, S. R. Paine, M. G. Newsted, "A Demonstration of Radio Interferometric Surveying Using DSS14 and the Project ARIES Transportable Antenna", JPL Deep Space Network Progress Report 42-26, February 1975. (A revised version of this paper has been submitted for publication in the Journal of Geophysical Research).

7. Shapiro, I. I., and C. A. Knight, Geophysical Applications of long-baseline radio interferometry, in Earthquake Displacement Fields and the Rotation of the Earth, edited by L. Mansinha, D. E. Smylie, and A. E. Beck, p. 284, Springer-Verlag, New York, New York, 1970.

8. Shapiro, I. I., D. S. Robertson, C. A. Knight, C. C. Counselman, A. E. E. Rogers, H. F. Hinteregger, S. Lippincott, A. R. Whitney, T. A. Clark, A. E. Niell, and D. J. Spitzmesser, Transcontinental baselines and the rotation of the earth measured by radio interferometry, Science, 186, 920, 1974.

9. Thomas, J. B., An analysis of long baseline radio interferometry, in The Deep Space Network Progress Report, Technical Report 32-1526, Vol. VII, p. 37, Jet Propulsion Laboratory, Pasadena, California, 1972a.

10. Thomas, J. B., An analysis of long baseline radio interferometry, part II, in The Deep Space Network Progress Report, Technical Report 32-1526, Vol. VIII, p. 29, Jet Propulsion Laboratory, Pasadena, California, 1972b.

11. Thomas, J. B., An analysis of long baseline radio interferometry, part III, in The Deep Space Network Progress Report, Technical Report 32-1526, Vol. XVI, p. 47, Jet Propulsion Laboratory, Pasadena, California, 1972b.

12. Thomas, J. B., J. L. Fanselow, P. F. MacDoran, D. J. Spitzmesser, and L. Skjerve, Radio interferometry measurements of a 16 km baseline with 4-cm precision, in The Deep Space Network Progress Report, Technical Report 32-1526, Vol. XIX, p. 1, Jet Propulsion Laboratory, Pasadena, California, 1974.

13. Williams, J. G., Very long baseline interferometry and its sensitivity to geophysical and astronomical effects, in The Deep Space Network, Space Programs Summary 37-62, Vol. II, p. 49, Jet Propulsion Laboratory, Pasadena, California, 1970.

FREQUENCY SYSTEM REQUIREMENTS TO ACHIEVE 3 cm BASELINE PRECISION

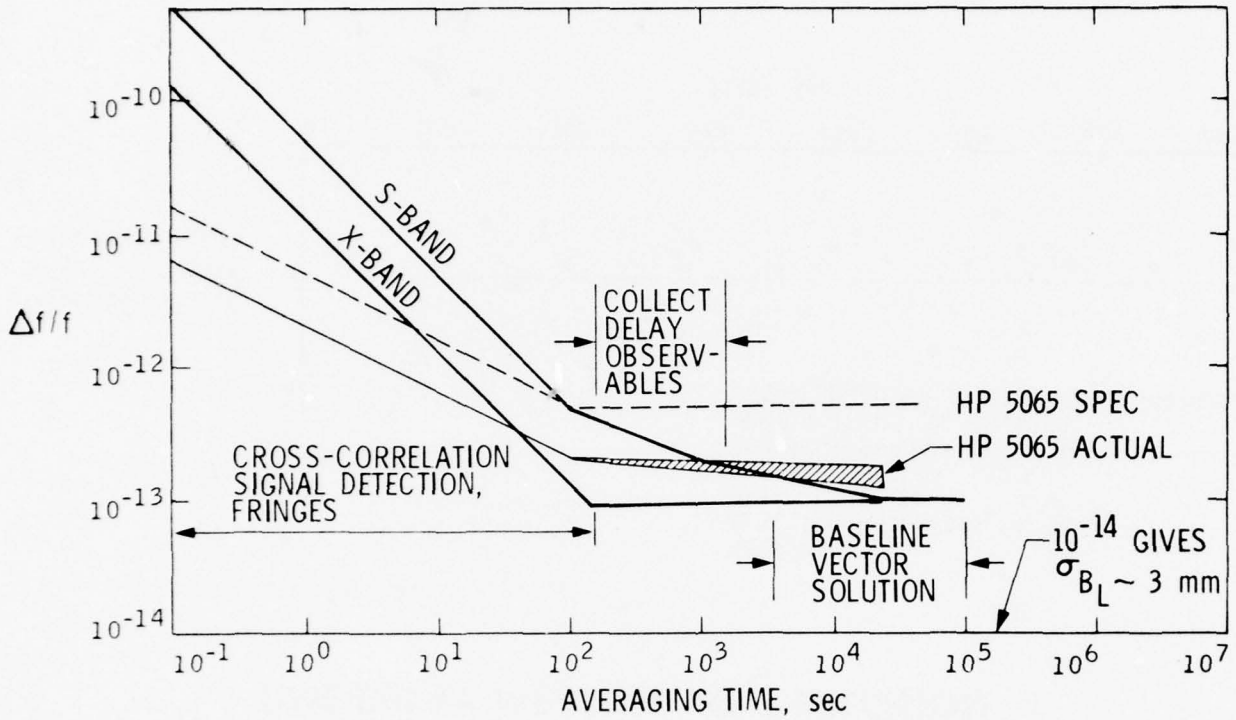


Figure 1

♈ TIME DELAY MEASUREMENT PRECISION

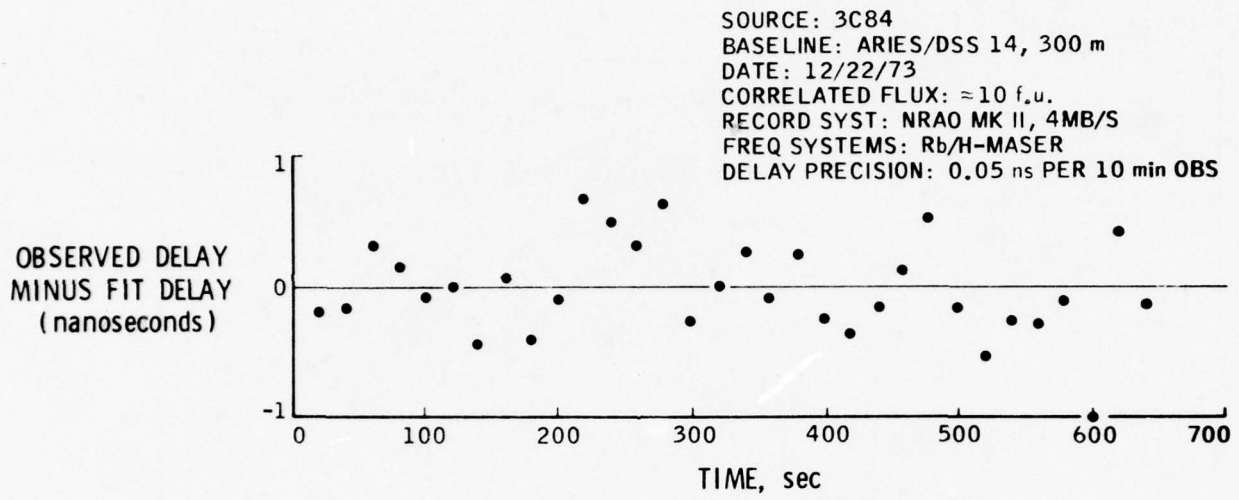


Figure 2

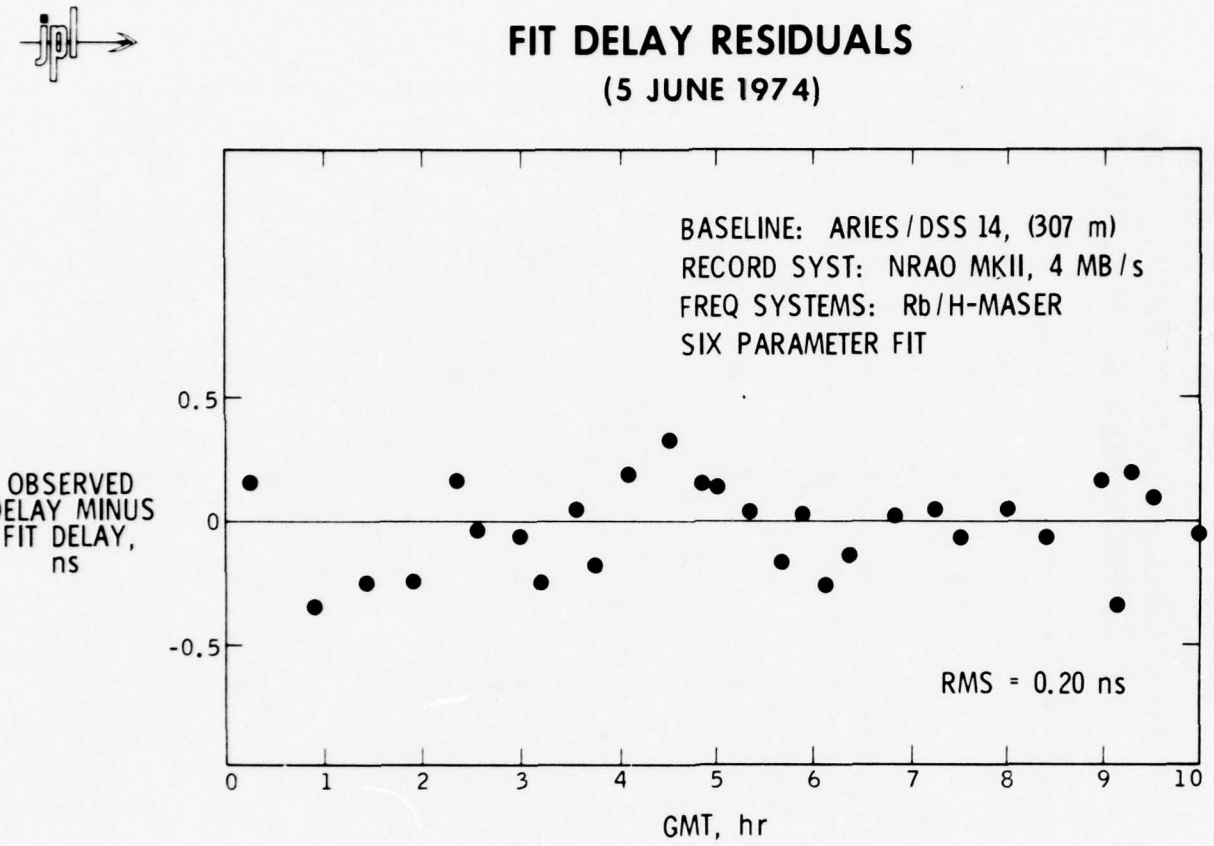

FIT DELAY RESIDUALS
(5 JUNE 1974)
BASELINE: ARIES / DSS 14, (307 m)
RECORD SYST: NRAO MKII, 4 MB / s
FREQ SYSTEMS: Rb / H-MASER
SIX PARAMETER FIT
RMS = 0.20 ns
OBSERVED DELAY MINUS FIT DELAY, ns
0.5
0
-0.5
0
1
2
3
4
5
6
7
8
9
10
GMT, hr

Figure 3

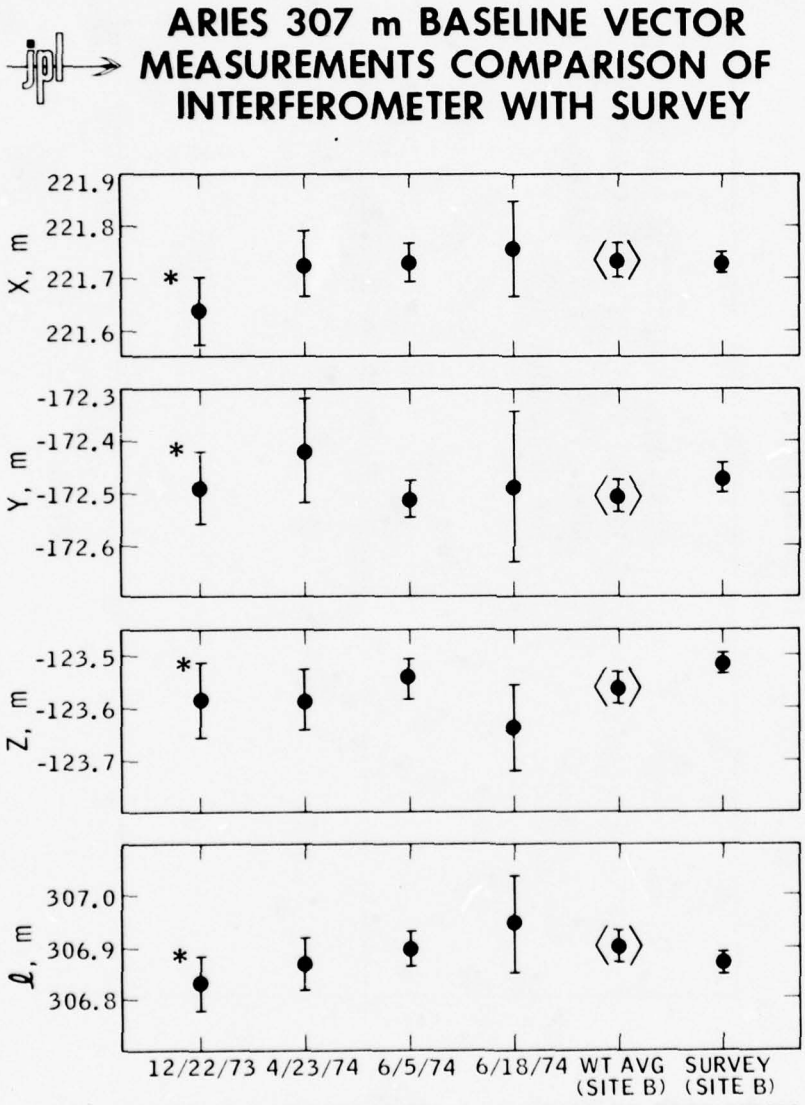

ARIES 307 m BASELINE VECTOR MEASUREMENTS COMPARISON OF INTERFEROMETER WITH SURVEY
221.9
221.8
221.7
221.6
X, m
-172.3
-172.4
-172.5
-172.6
Y, m
-123.5
-123.6
-123.7
Z, m
307.0
306.9
306.8
ℓ, m
12/22/73
4/23/74
6/5/74
6/18/74
WT AVG (SITE B)
SURVEY (SITE B)
*DEC '73 ARIES POSITION (SITE A) ADJUSTED TO POST FEB'74 POSITION (SITE B) BY ΔX = -16 cm, ΔY = -36 cm, ΔZ = -25 cm, Δℓ = 19 cm

Figure 4

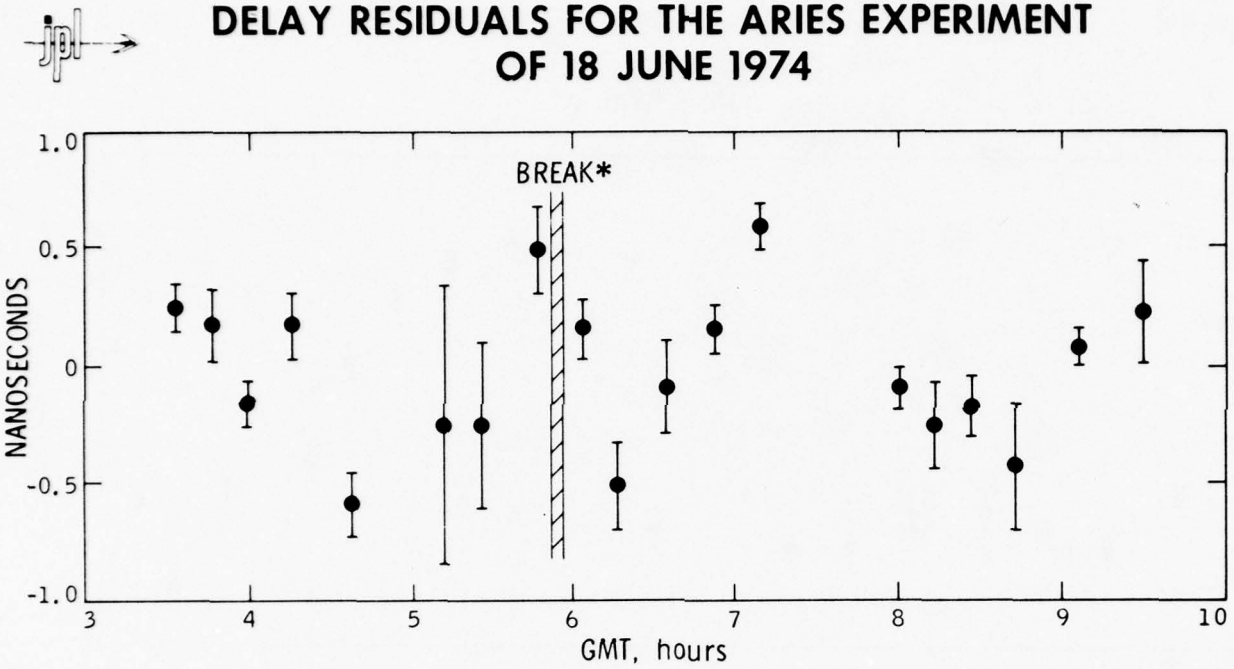

DELAY RESIDUALS FOR THE ARIES EXPERIMENT
OF 18 JUNE 1974
BREAK*
NANOSECONDS
1.0
0.5
0
-0.5
-1.0
3
4
5
6
7
8
9
10
GMT, hours
*INSTRUMENTAL PARAMETERS SEPARATELY ESTIMATED

Figure 5

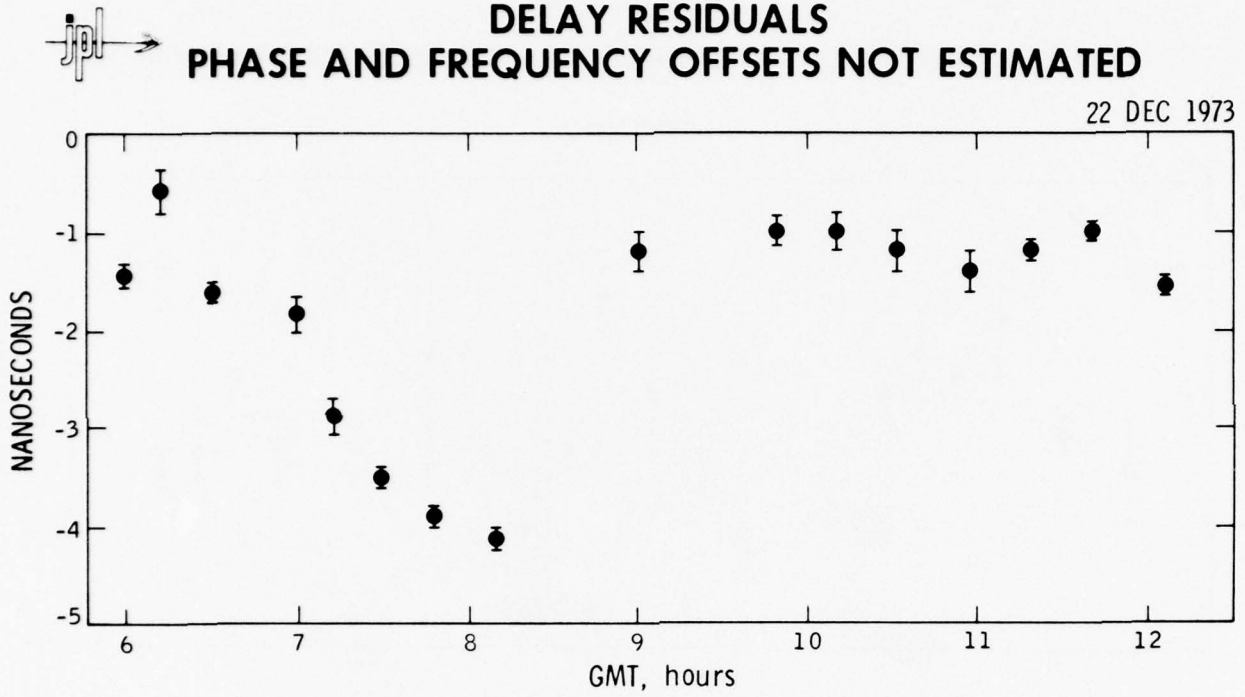

DELAY RESIDUALS
PHASE AND FREQUENCY OFFSETS NOT ESTIMATED
22 DEC 1973
NANOSECONDS
0
-1
-2
-3
-4
-5
6
7
8
9
10
11
12
GMT, hours

Figure 6

INTERFEROMETRY BASELINE RESULTS FOR THE ARIES 307 m EXPERIMENTS

DATE	SITE	X, m	Y, m	Z, m	ℓ, m
12/22/73	A	221.795 ± 0.066	-172.126 ± 0.075	-123.332 ± 0.075	306.645 ± 0.050
4/23/74	B	221.728 ± 0.06	-172.423 ± 0.10	-123.584 ± 0.06	306.866 ± 0.05
6/05/74	B	221.732 ± 0.039	-172.516 ± 0.032	-123.538 ± 0.038	306.902 ± 0.034
6/18/74	B	221.763 ± 0.091	-172.488 ± 0.145	-123.639 ± 0.084	306.948 ± 0.086
WT AVG	B	221.734 ± 0.031	-172.507 ± 0.030	-123.562 ± 0.030	306.896 ± 0.027
SURVEY	B	221.733 ± 0.02	-172.471 ± 0.03	-123.513 ± 0.02	306.867 ± 0.02

Table 1

QUESTION AND ANSWER PERIOD

MR. WARD.

Sam Ward, Jet Propulsion Lab.

Have there been any observable results as to the basic purpose of the thing, the relative drift of the east and the west side of the San Andreas Fault?

DR. VESSOT:

That is not the real purpose for this, is it?

DR. MELBOURNE:

Yes, for those of us who live out there in Earthquakeville, that is a real concern. What we see could be explained by other factors. There is no clear signal. Let me give a little bit of insight into this.

One of the mechanisms that appears to be going on in the geophysics area is something called dilatantcy, which says something about the rock failure mechanism prior to the quake, and that says that the ground underneath of the rocks down 5 kilometers or so, begin opening up little cracks and the ground swells up.

Now, the Soviet version of the observed phenomena regarding seismic velocities from which dilatantcy was deduced, claim that the uplift is going to be at the several meter level and is going to happen over hundreds of kilometers. The seismological lab at Cal Tech says yes, it could be like 1 or 2 meters, but they don't believe that the 10 meter approximations the Soviets make are realistic, but we are talking about pretty big, definite signals as a possibility. It depends upon the porosity of rocks, where the dilatantcy is occurring, but possible uplifted geometric signals are maybe at the meter level, with lower limits down around 10 centimeters. Now, if something is going on there at the 10 centimeter level, we probably have difficulty seeing it right now.

If it is a signal, a geometric deformation that is occurring at the 1 meter level, I think that we would definitely see this.

DR. VESSOT:

I should think you would probably see it as plate motion in a matter of a few years.

DR. MELBOURNE:

That is right.

DR. VESSOT:

These are motions of tectonic plates that describe the geological surface of the earth, and they have been very well proven to be moving.

DR. MELBOURNE:

Yes, it seems an incontrovertible fact that there is some kind of a horizontal deformation going on. It is only a debate about the magnitude. One line of reasoning would hold that the rate could be as much as 6 centimeters per year. Well, you can see that even with the current accuracy that we have of 10 centimeters, within a period of a decade or less, we are going to be able to see those kinds of deformations.

Now, we see, by the way, many ways of improving the system. I have talked about just the time and frequency aspects, but certainly with regard to transmission media, calibrations, and the telecommunication parameters and so on, one can see ways of making this system accurate to about 1 centimeter, given about 30 hours of data at a given location, so once you get down to those kinds of levels, then you are going to be able to resolve differences; whether deformation rates in the horizontal are 2 or 3 or 6 centimeters.

DR. VESSOT:

I would like to ask a question of how many oil companies have been beating a path to your door for doing surveys, notably in regions of our world that are not accessible. I can think of no more miserable task than surveying my way up into Alaska or the Yukon Territory, a job that certainly would take a great many years, and the accuracy, I think, would depend an awful lot on just plain luck. Whereas here you are with a helicopter, presumably you could drop

this gadget, and within several days or weeks, you may end up with numbers on the order of centimeters.

DR. MELBOURNE:

Well, there has been expressed some interest from the Trans-Alaska Pipeline people, as well as from local utilities wanting to build nuclear power plants; not so much that this is going to be an integral part, but this is new technology. We are up against a real bind in a lot of areas. Some of them are environmental -- well, particularly in environmental impact, and I think they are legitimately trying to wrestle with those problems and deal with them properly, and they are looking to these new kinds of technologies.

DR. VESSOT:

I just want to make one other comment. It is astonishing to me to look at the prospect of using random noise from these celestial objects as a means for time synchronization. It means that we are going back to astronomy or astrology to get our time. We mustn't forget that for, I think, probably thousands of years, that time has been an astronomical behavior. It has been inexorably linked in our heritage that time is the motion of heavenly bodies. We now have gone to atoms, and I am just wondering whether or not we are not going to go looking out to space again for time.

It might take awhile, so I think a few of us clock makers may be safe for a while.

PATH DELAY CORRECTIONS FOR LORAN SIGNALS

Ronald G. Roll
The Johns Hopkins University
Applied Physics Laboratory
Laurel, Maryland

ABSTRACT

In November 1973, an experiment was initiated to explore the possibility that measurements of the Loran pulse location relative to the phase of the carrier could be used to infer path delay corrections. The Applied Physics Laboratory was joined in this effort by the U.S. Naval Observatory and the Defense Mapping Agency. Measurement of the transit time of the Loran-C wave between a site at the U.S. Naval Observatory and 10 field sites were made in the summer of 1975. The instrumentation and the results of the test are described along with statistical estimates of the precision of measurement and of the quality of the data. The precise nature of the transmitted signal and the precision of time recovery is inferred from the data. Status of the development of a path delay correction is also described.

INTRODUCTION

APL is conducting a research program including a field test for the U.S. Air Force and the Defense Advanced Research Projects Agency to determine the validity of one facet of the theory of ground wave propagation at 100 kHz. The theory indicates that if proper account is taken of group and phase velocities in the propagation of pulses of the Loran-C radio navigation service, then geodetic position could be computed by using the vacuum speed of light and the times of arrival of the pulse and the carrier. Specifically, the goal is to determine if an analytic function can be developed for operational use which relates secondary phase factor to envelope to cycle difference (ECD) so that geodetic position can be computed accurately and in real time.

The field test was conducted in the eastern United States using the East Coast Loran-C chain and required two identical sets of precision equipment, one in a mobile test van and the other at a fixed site at the U.S. Naval Observatory

(NAVOBSY). The van occupied 10 field sites during the course of the test. See Fig. 1. The positions of all sites were precisely surveyed by the Defense Mapping Agency Topographic Center (DMATC) using the Navy Navigation Satellite System and are located on ray paths from Loran-C stations through NAVOBSY. The collected data include very accurate measurements of the Loran-C ground wave phase and pulse envelope times of arrival at the 10 fixed sites and simultaneously at NAVOBSY.

APL was assisted in this test by NAVOBSY and DMATC. In addition to the satellite survey, DMATC computed all required geodetic distances. NAVOBSY executed time transfers on each test day using low noise cesium beam clocks. The APL development effort includes measurement system definition, assembly and checkout of equipment, acquisition and analysis of field test data, and a final report documenting the test and incorporating pertinent test results. Currently, APL is performing analysis of field test data.

TEST DESCRIPTION

The test instrumentation is shown functionally in Fig. 2. Two identical systems were designed and assembled, one for the van and one for the NAVOBSY site. Referring to Fig. 2, the Loran-C signal is inputted to a fixed gain tuned receiver via a wide-band variable attenuator. The purpose of the wide-band attenuator is to standardize the Loran-C pulse amplitude as seen by the tuned receiver without distorting the signal waveform or causing a phase shift which varies with signal strength. At least 3 dB of attenuation always remains in the attenuator to minimize mismatch effects between the antenna and the input to the tuned receiver. The output of the tuned receiver is adjusted by the wide-band attenuator to give a Loran-C pulse amplitude of 0.5 volt at the positive peak of the fifth cycle (i.e., with positive phase code). The receiver output connects to an analog-to-digital converter, which digitizes wave samples at sample points on the Loran-C pulse. Sample triggers open a sample and hold circuit at the input of the analog-to-digital converter, and the converter then digitizes the analong voltage at the output of the sample and hold circuit to 13 bits pulse a sign bit. Data sampling was done as shown in Fig. 3. Only the first pulse of each group was sampled and a total of 32 voltage measurements were taken on each of these pulses. The first 16 were at 2.5 microsecond intervals, and the second 16 were at 7.5 microsecond intervals. The sample triggers are generated by sample gates. Timing of the sample gates is

derived from a group repetition interval (GRI) preset counter. The phase of the preset counter can be adjusted in plus or minus 0.1 μs time intervals by phase slewing circuitry. The phase of the GRI counter is adjusted such that the sample triggers, displayed on one channel of an oscilloscope, must nearly match the desired sample points on the Loran-C pulse which is displayed on a second channel of the oscilloscope. The precision timing for the GRI preset counter, and also for a Universal Time Coordinated (UTC) clock, is derived from a low noise Cesium beam frequency standard.

The digitized Loran-C pulse waveforms, along with a synchronous output from the UTC clock and fixed data input information stored in digiswitches, are formatted by a digital formatter and stored on computer-compatible digital magnetic tape. The tape block size, i.e., the number of eight-bit characters written in one continuous block, is 512. This number of characters allows for point values from seven Loran-C pulses, a UTC clock time, and the input information stored in the digiswitches to be stored on each tape block in a standardized format.

DATA ANALYSIS

One segment of the data consists of 32 measurements of voltage on each of 12,000 pulses. These data are obtained in 20 minutes of recording in the East Coast Loran-C chain. Simultaneous recordings consisting of three consecutive 20 minute segments were made at the NAVOBSY site and each van site, both of which are accurately located on the ray path from a transmitter. The location of all the sites along with the distance between them and the Loran-C stations are presented in Table 1. Pairs of these simultaneous recordings along with the distance between them permit analyses of propagation effects experienced by the pulse during its travel from one site to the other.

Measurements of the pulse made at individual sites were analyzed in several ways. The statistics of the raw measurements on individual pulses were computed as well as the statistics of the averages computed for 50 pulses and for 700 pulses. Statistics of edited data were also computed. By "edited" we mean that all the measurements on each pulse are rejected and the pulse is not counted if any of the measurements on the pulse are more than two standard deviations different from the mean value of that measurement based on the raw data. Of the 12,000 pulses measured in a 20 minute recording, editing threw out 1180 to 5500 pulses depending on the character of the noise.

Figures 4 and 5 are two-dimensional histrograms of two adjacent measurements on the leadingedge of the pulse 2.5 microseconds apart. The first of the two adjacent measurements, Q, is in quadrature with the carrier and the second, I, is in phase. I is plotted as the abscissa and Q as the ordinate. The histogram is generated by considering each pair of Is and Qs to be coordinates of a point in the plane and counting how many points lie in each cell of preselected size. The cell size is 0.0032 volts for Figure 4 and 0.0210 volts for Figure 5 which correspond to 0.017 and 0.365 microseconds of phase respectively. It is very clear that the data are not normally distributed. If they were, we would expect 5 data points to be outside a 16 by 16 cell square centered on Figure 5, whereas the actual number is 215. The probability that this would happen by chance for a normal distribution is less than 10^{-30}.

These histograms can be considered to be phasor diagrams which show the frequency with which the terminus of the electrical vector falls in each cell. The angle of the vector determinable therefrom with respect to the vertical is the error in phase with respect to the phase track point.

The histograms can also be considered a representation of the input to a third cycle phase tracking loop which has no loop closure. Superimposed on the figures are editing windows equivalent to $\pm$0.102 microseconds for Fig. 4 and $\pm$1.82 microseconds for Fig. 5. The effect of accepting only data that falls within the window is clearly beneficial since many data outside the window individually would cause large disturbances to the phase tracking loop.

The output of a phase tracking loop is estimated by averaging 700 contiguous edited pulses. Such a tracking loop in the East Coast Chain would have a time constant of about 9 seconds if all of the group of eight pulses were used each GRI. The standard deviation of the estimated output was computed for all first 20-minute segments of data. These results are presented in Table 2. The standard deviations of the differences between the output of such tracking loops at van and NAVOBSY are also presented in Table 2.

We also estimated the standard deviation of the measurement of propagation time between van and NAVOBSY using the averages of the 20 minute edited data segments for all sites as single samples. This standard deviation is 4.8 nanoseconds which includes the deviations due to distance, weather or residual noise.

These same 20-minute averages were used to construct an analytic model of the transmitted Loran-C pulse. Assuming that the pulse is formed by modulation of a 100 kHz carrier, the measured data can be represented over the data span by an equation of the form

$$L(t) = I(t) \sin \omega t + Q(t) \cos \omega t$$

where

$L(t)$ is the loran pulse (non-propagating)

$I(t)$ is the sine modulation

$Q(t)$ is the cosine modulation, and

ω is the 100 kHz circular frequency

The functions $I(t)$ and $Q(t)$ were chosen to be 10th degree polynomials in t, computed such that the energy in the $Q(t)$ modulation over the data span from 10 to 70 microseconds was a minimum. These polynomials represent the data with negligible error, typically the standard deviation is one millivolt about mean errors which are less than 28 microvolts. These models were normalized to the same energy at the field sites and at NAVOSBY and used to plot the $I(t)$ and $Q(t)$ functions observed at both sites. Figures 6 and 7 are samples of these plots.

Refer to Figure 6. This figure is an example of those cases in which very little change in the modulations has taken place over the path. We can say, therefore, that what we have measured as the transit time of the pulse (e.g. based on 3rd cycle zero crossing) is indeed the transit time. However, consider Figure 7. Considerable change has taken place in the $Q(t)$ modulation. In this case, it is clear that measurement of the time of arrival of the third cycle zero crossing at both van and NAVOBSY does not produce the transit time. This problem is highlighted in Table 3 which shows the time of zero crossing near 30 microseconds corresponding to the modulation of Figures 6 and 7. Note that the difference between the third cycle zero crossing at the van site at Wilmington and NAVOBSY is about 28 nanoseconds whereas between NAVOBSY and Dexter it is about 240 nanoseconds.

For those cases where the wave form has not changed, the displacement of the envelope at the van with respect to the envelope at NAVOBSY is determined by the difference between group transit time and phase transit time. For the other cases, group and phase transit times have so far refused to be identified. Analysis is continuing in the hope of resolving this problem.

CONCLUDING REMARKS

Analysis of the measurements made on the first pulse of groups of eight in the East Coast Loran-C chain indicate that, over the short term, i.e., 1 hour, these transmitted pulses are very stable. Averages of 700 contiguous pulses exhibit standard deviations between 5 and 40 nanoseconds relative to the mean of the pulses observed during one hour, provided the pulses averaged are limited to those accepted by the editing procedure. This observation applies to all the distances over which the observed pulses were transmitted, a wide variety of weather conditions, and man-made interference. The same statistics apply to the measurement of the transit time of the pulse over the distances used in the test. In a related paper presented by Dr. Klepczynski at this meeting he indicates a probable error of 29 nanoseconds in making clock transfers over the distances of the test. It should be possible therefore to coordinate time by Loran-C to well under a microsecond.

The Loran-C stations transmit both amplitude and phase modulation of the 100 kHz carrier. Over paths which did not substantially modify the phase modulation, both group and phase arrival times can be identified. When the phase modulation is substantially modified over the path, we have not yet discovered a consistent estimator for group or phase arrival times.

During the extensive analyses which have been under way since the first of last July (i.e., July 1975), nothing has been discovered which definitively rules out the eventual accomplishment of our goal, which is to relate group and phase velocities to the vacuum speed of light. We expect to achieve this goal when the propagation of the phase modulation is finally understood.

ACKNOWLEDGEMENT

The author is grateful for the contributions to this paper made by his associates Leo F. Fehlner, Thomas A. McCarty and Thomas W. Jerardi.

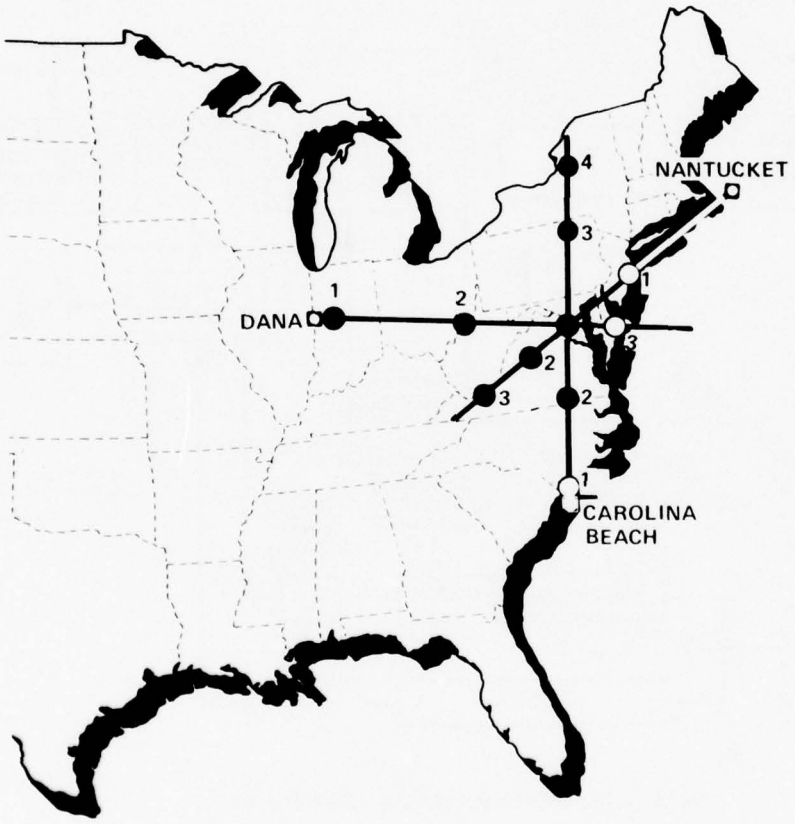


Fig. 1 LOCATIONS OF FIELD TEST SITES

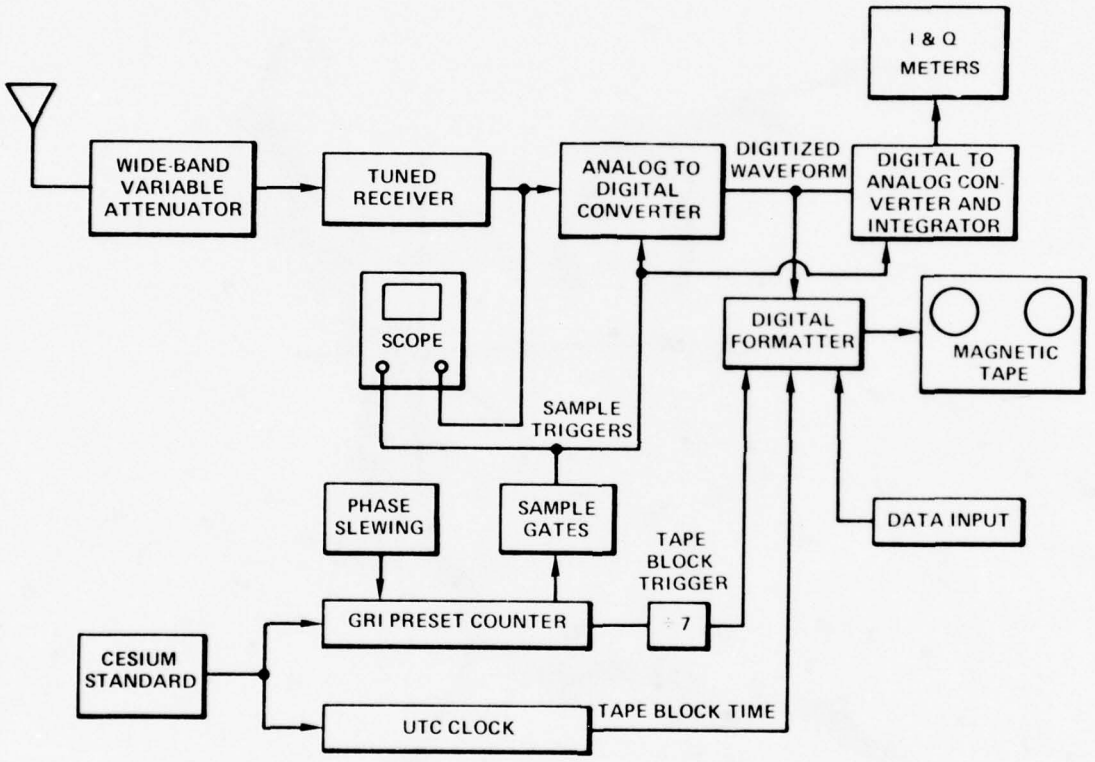


Fig. 2 GROUP/PHASE MEASUREMENT SYSTEM

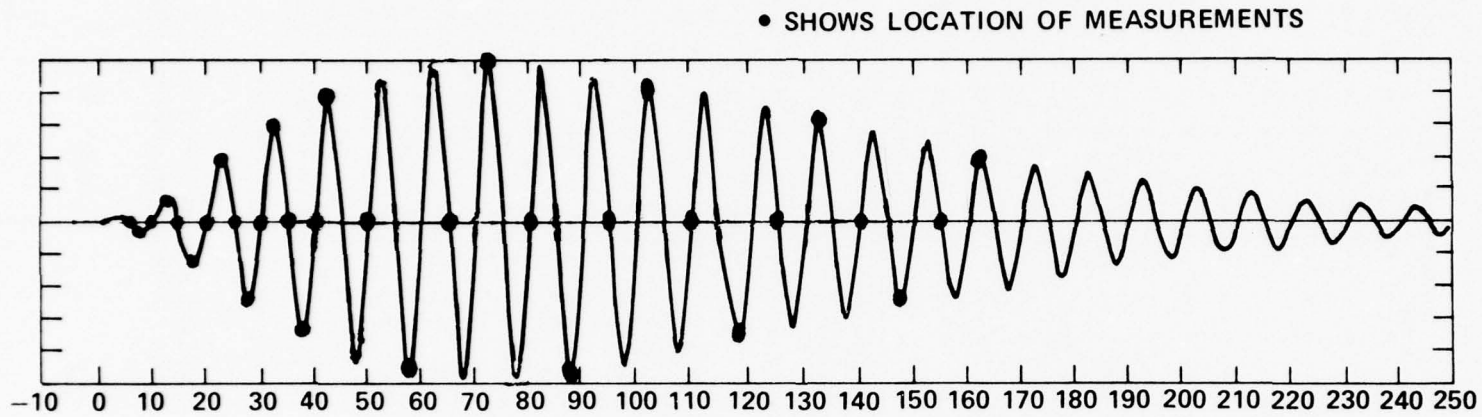


Fig. 3 VOLTAGE MEASUREMENTS ON LORAN PULSE

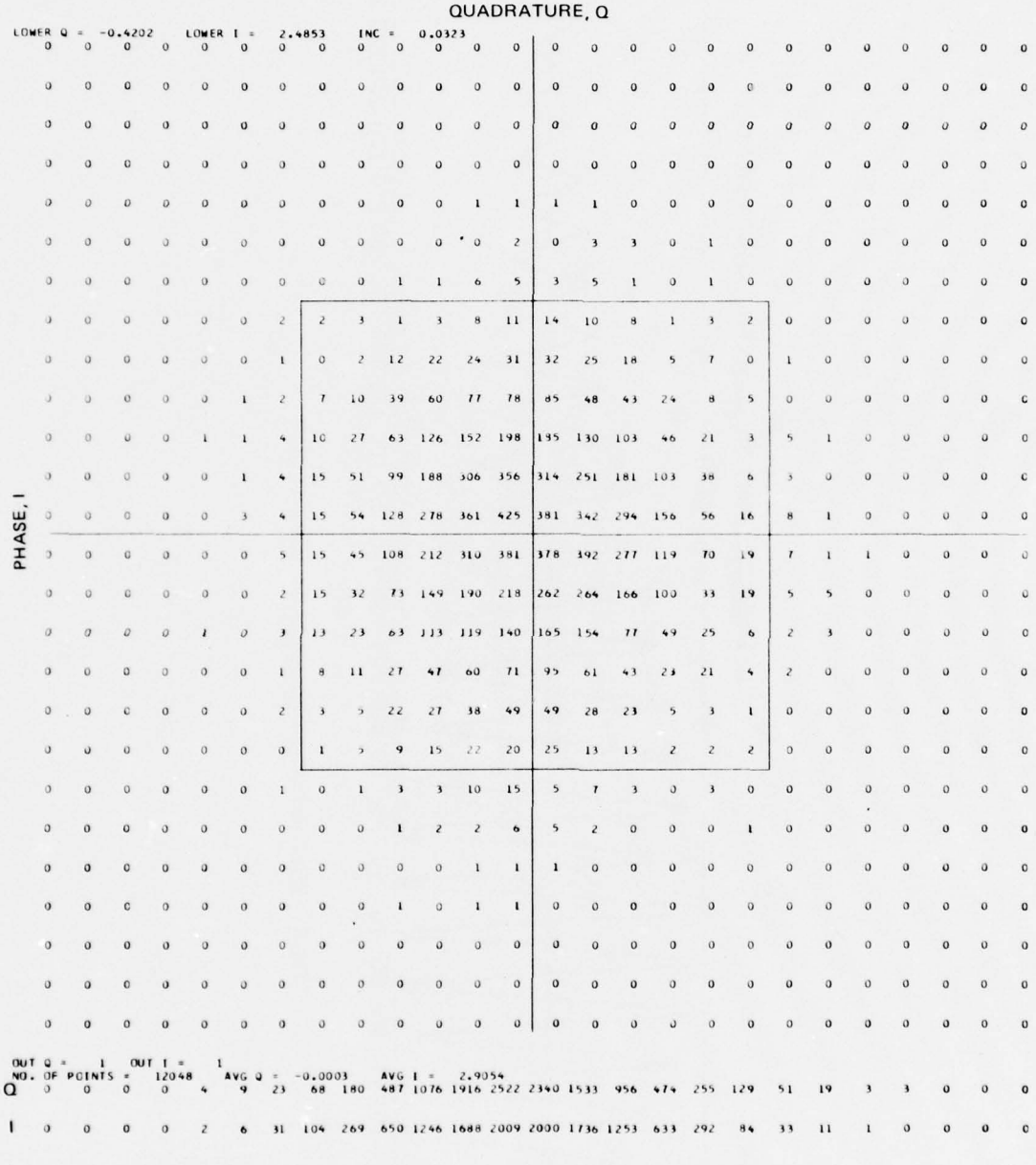


Fig. 4 HISTOGRAMS OF IN-PLACE AND QUADRATURE DATA TAKEN AT DANVILLE, IN. Q AND I (AT BOTTOM) ARE ONE-DIMENSIONAL HISTOGRAMS

BEST AVAILABLE COPY

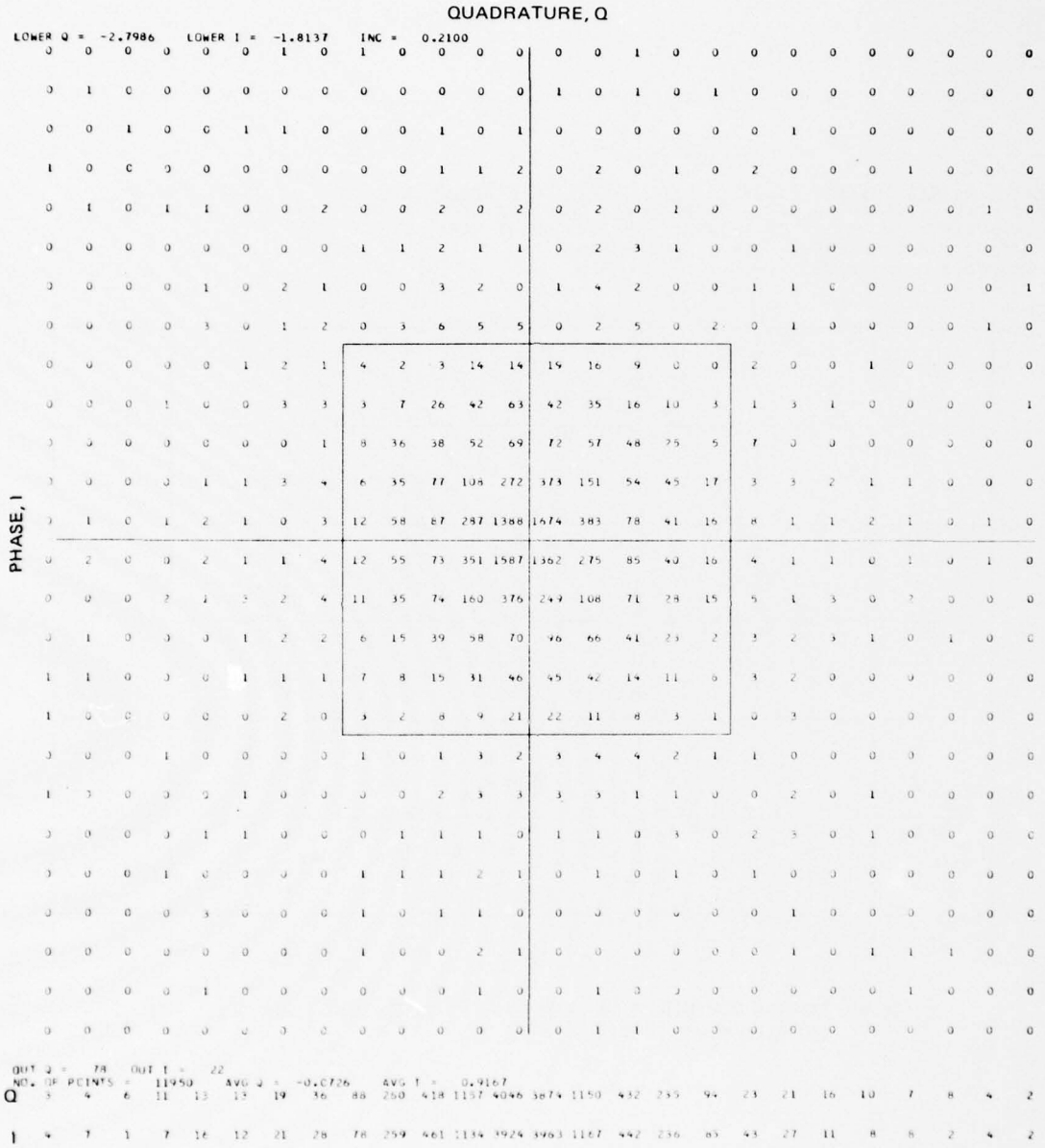


Fig. 5 HISTOGRAMS OF IN-PHASE AND QUADRATURE DATA TAKEN AT BLUEFIELD, WV. Q AND I (AT BOTTOM) ARE ONE-DIMENSIONAL HISTOGRAMS

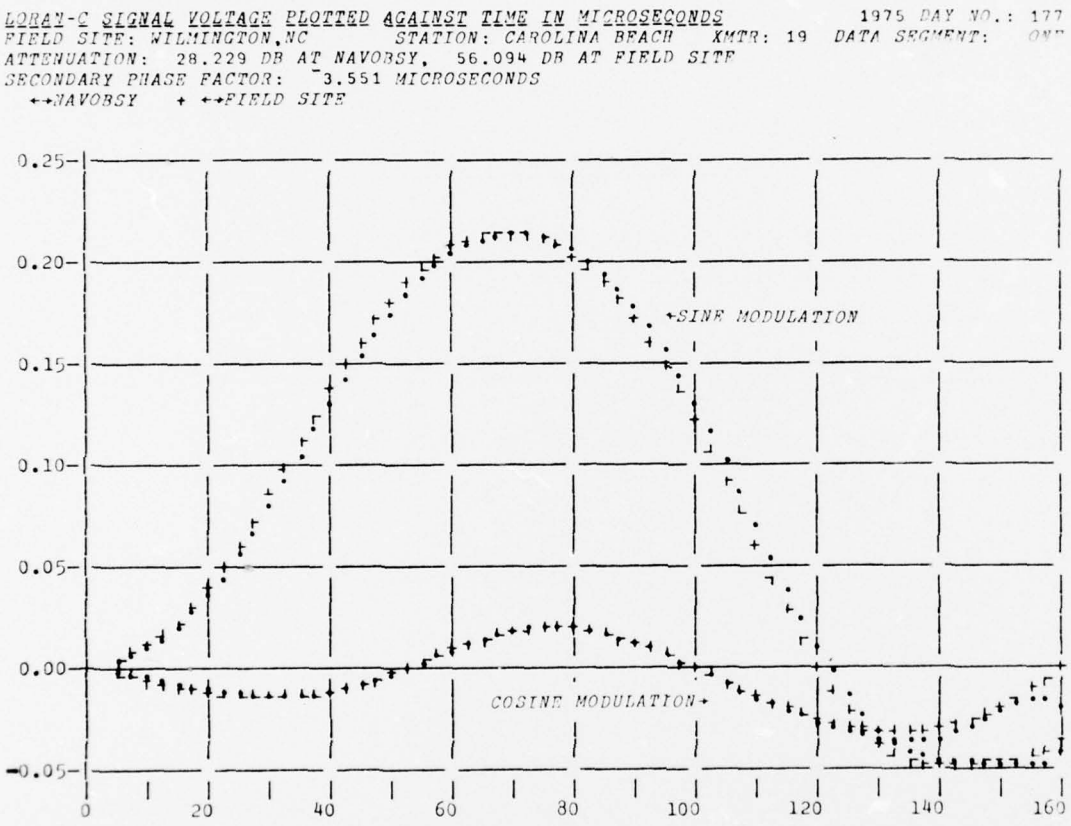


Fig. 6 LORAN-C SIGNAL VOLTAGE PLOTTED AGAINST TIME IN MICROSECONDS: 1975 DAY NO. 177

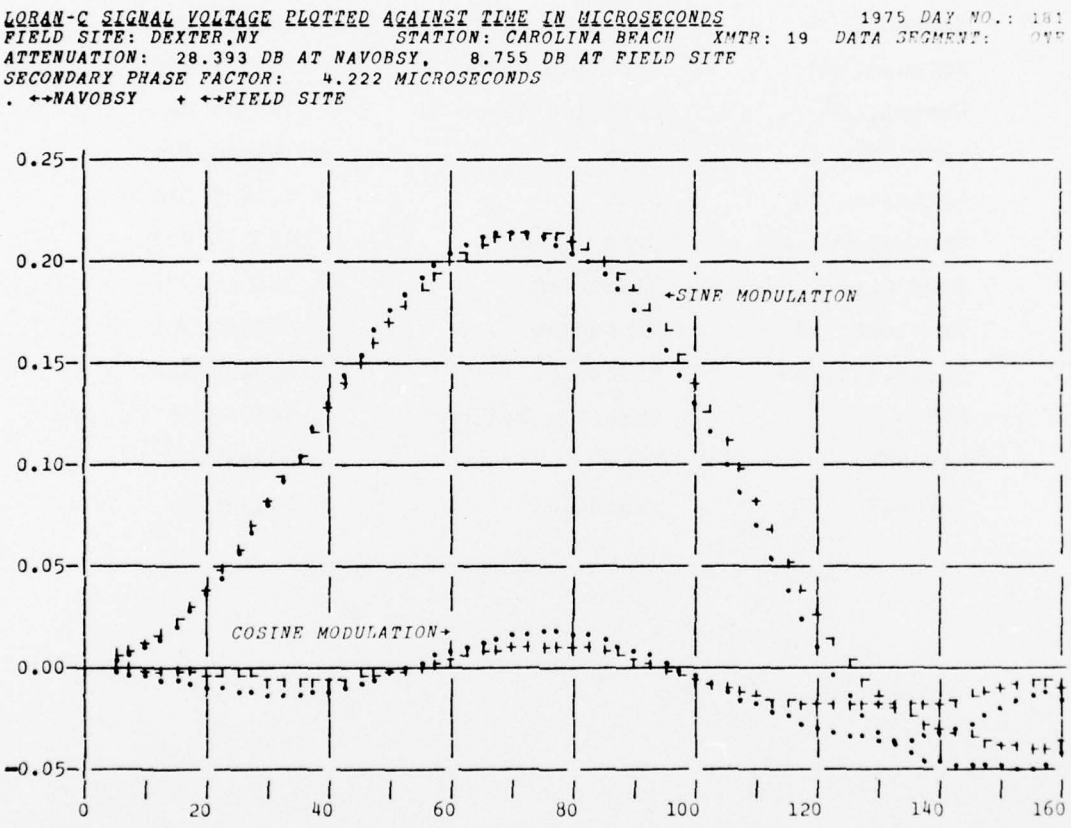


Fig. 7 LORAN-C SIGNAL VOLTAGE PLOTTED AGAINST TIME IN MICROSECONDS: 1975 DAY NO. 181

Table 1

DISTANCE FROM LORAN-C STATIONS TO TEST SITES IN METERS

Test Sites	Station	Distance
Wilmington, NC	Carolina Beach	23572.074
Emporia, VA	Carolina Beach	293343.813
Towanda, PA	Carolina Beach	867731.246
Dexter, NY	Carolina Beach	1113945.864
Danville, IN	Dana	85946.204
Marietta, OH	Dana	526905.326
Georgetown, DE	Dana	1053516.979
Toms River, NJ	Nantucket	384345.877
Grottoes, VA	Nantucket	827589.501
Bluefield, WV	Nantucket	1063424.588
NAVOBSY	Carolina Beach	544243.957
NAVOBSY	Dana	903083.427
NAVOBSY	Nantucket	657576.077

Table 2

STANDARD DEVIATIONS IN MICROSECONDS OF AVERAGES OF
700 PULSES DURING THE FIRST 20
MINUTES OF RECORDING AT EACH SITE

Van Site	XMTR	Van	NAVOBSY	Van-NAVOBSY
Wilmington, NC	Carolina Beach	.005	.010	.006
Emporia, VA	Carolina Beach	.005	.008	.005
Towanda, PA	Carolina Beach	.023	.016	.027
Dexter, NY	Carolina Beach	.008	.010	.013
Danville, IN	Dana	.005	.027	.027
Marietta, OH	Dana	.008	.026	.023
Georgetown, DE	Dana	.022	.022	.029
Toms River, NJ	Nantucket	.011	.040	.038
Grottoes, VA	Nantucket	.015	.012	.022
Bluefield, WV	Nantucket	.024	.010	.021

Table 3

TIME OF ZERO CROSSINGS IN THE PULSE TRANSMITTED
FROM CAROLINA BEACH

Day	Test Site	Time of Zero Crossing (μsec)				
177	Wilmington	20.3274	25.2266	30.1417	35.0691	40.0045
		20.3272	25.2269	30.1422	35.0697	40.0048
		20.3259	25.2260	30.1416	35.0693	40.0047
	NAVOBSY	20.3380	25.2486	30.1706	35.1021	40.0389
		20.3401	25.2493	30.1705	35.1016	40.0384
		20.3354	25.2479	30.1705	35.1020	40.0386
181	NAVOBSY	20.3299	25.2497	30.1772	35.1124	40.0526
		20.3326	25.2465	30.1756	35.1156	40.0607
		20.3224	25.2368	30.1667	35.1071	40.0527
	Dexter	19.9644	24.9466	29.9347	34.9229	39.9074
		19.9657	24.9511	29.9394	34.9260	39.9083
		19.9524	24.9419	29.9332	34.9215	39.9046

QUESTION AND ANSWER PERIOD

LCDR. POTTS:

Cy Potts, Coast Guard.

I have several brief questions. First of all, I would like to know what type of distribution you saw in the data. Did it approach a normal distribution?

MR. ROLL:

It was a normal contaminated by the sporadic interference -- impulsive stuff. It was clearly not a normal distribution as a whole.

LCDR. POTTS:

Were the synchronization adjustments made by the stations removed from the data?

MR. ROLL:

There were no synchronization adjustments made during the data runs by cooperation of the chain commander.

LCDR. POTTS:

And how did you handle interference, synchronous and near-synchronous?

MR. ROLL:

There were four notch filters which were tuned to the NSS frequencies and were nailed down. We had no other problems other than NSS.

DR. REDER:

Is it out of the question that the cosine modulation which you saw was introduced by the propagation media? Has a measurement been taken close to the transmitter site?

MR. ROLL:

One of the measurements, the one at Wilmington, North Carolina is only 25 kilometers; it is there, and it has not

substantially changed after 500 kilometers.

DR. REINHARDT:

Victor Reinhardt, Goddard Space Flight Center.

You mentioned that the scatter for short-term data taking was 30 nanoseconds. Did you take any data with respect to diurnal variations?

MR. ROLL:

Data were taken with respect to diurnal, but have not been analyzed. We have several hours reporting on a sunset, during sunset, at both ends of the path where the terminator crosses the path. We have that data, but it has not been analyzed.

EM FIELDS IN NONUNIFORM MULTILAYERED STRUCTURES STEADY STATE AND LORAN C PULSE EXCITATION

E. Bahar, Electrical Engineering Department
University of Nebraska--Lincoln, Nebraska 68588

ABSTRACT

The steady-state electromagnetic field response from nonuniform layered models of the earth's crust are used to compute the transient response due to LORAN C pulse excitations. Using a full wave approach, the electromagnetic fields are expressed completely in terms of a continuous spectrum of vertically polarized waves (the radiation term) and a discrete set of vertically polarized surface waves (the waveguide modes of the structure). Thus the scattered radiation fields and surface waves due to incident plane waves are computed. The full wave solutions satisfy the reciprocity relationships in electromagnetic theory.

These investigations are relevant to problems of navigation since it is possible to facilitate the derivation of the LORAN grid corrections due to ground effects if the propagation delays of the LORAN pulses can be related to the LORAN pulse distortions. Thus in this work analytical expressions are derived for the propagation delays due to ground effects (compared with the smooth perfectly conducting case) and the dependence of the distortions of the received signal upon the ground parameters along the propagation path is determined for different excitations.

This approach could also be used to determine the effects of a nonuniform stratified model of the ionosphere upon satellite navigation signals.

1. INTRODUCTION

A full wave solution for the steady state electromagnetic fields due to a magnetic line source over a nonuniform stratified model of the earth is the basis for the present investigation [1],[2]. The complete expansion of the electromagnetic fields consists of the radiation term (continuous spectrum of vertically polarized waves) and the surface waves (discrete set of vertically polarized waves). Since these solutions are shown to satisfy the reciprocity relationships in electromagnetic theory the scattered radiation fields and surface waves due to incident plane waves are considered in detail.

The scattered electromagnetic fields were computed earlier for $\exp(i\omega t)$ excitations for various nonuniform models of the earth's crust to determine the feasibility of using a radio wave for geophysical prospecting [3]. It is seen from the formal solution of the problem that considerable physical insight could be gained by determining the electromagnetic response to transient excitations of nonuniform stratified

structures [4]. Thus in this work the transient electromagnetic fields due to LORAN C pulse excitations over the earth's surface are evaluated using both analytic methods and Fast Fourier transform techniques.

The principal motivations for this work are twofold.

(a) To determine the distortions an electromagnetic pulse undergoes when it is scattered by a nonuniform stratified model of the earth's crust.

(b) To determine whether the propagation delays of the LORAN pulses due to ground effects can be related to the LORAN pulse distortions.

Thus analytical expressions are derived for the propagation delays due to ground effects (compared with the smooth perfectly conducting case). In addition, the dependence of the distortions of the received signals upon ground parameters along the propagation path is determined for different excitations. This approach could also be used to predict the effects of a nonuniform stratified model of the ionosphere upon satellite navigation signals.

2. FORMULATION OF THE PROBLEM

In this work the scattering of vertically polarized waves only is considered in detail. Thus, the excitations are assumed to be due to a z-directed magnetic line source $\bar{J}_m$ (see Fig. 1), where

$$\bar{J}_m = K\delta(x - x_o)\delta(y - y_o)\bar{a}_z \tag{2.1}$$

The dual problem, scattering of horizontally polarized waves, can be analyzed in a similar manner by considering excitations due to z-directed electric line sources.

The dielectric coefficient of the overburden ($o > y > -h$) is

$$\varepsilon_1 = \varepsilon_o \varepsilon_r(s) \tag{2.2a}$$

where

$$\varepsilon_r(s) = \varepsilon_R + \sigma/s = \varepsilon_R + \varepsilon_I(\omega_o/s) \tag{2.2b}$$

in which ε_R and the conductivity $\sigma = \varepsilon_I \omega_o$ are positive real numbers independent of frequency, $s = \alpha + i\omega$ is the complex frequency, ω_o is the radio wave carrier frequency in radians/sec. and ε_o is the permittivity of free space. The permeability of the overburden is assumed to be that of free space μ_o (non-magnetic material), thus the overburden intrinsic impedance is $\eta_1 = (\mu_o/\varepsilon_1)^{\frac{1}{2}}$.

It is convenient to characterize the substratum by a surface impedance

$$Z_s = \sqrt{\mu_o/\varepsilon_2} \tag{2.3}$$

where

$$|\varepsilon_2(\omega_o)/\varepsilon_1(\omega_o)| \gg 1$$

and ε_2 is the substratum dielectric coefficient.

The overburden depth is

$$h(x) = h_o + \delta x \qquad -L < x < L \tag{2.4}$$

where h_o is the average overburden depth, $\delta = \tan \Delta$ is the slope of the overburden-substratum interface.

Explicit solutions for the electromagnetic fields scattered by an overburden of nonuniform depth (2.4) have been derived for steady state ($\exp(i\omega t)$) excitations. Since the problem is two dimensional, both the incident and the scattered fields are vertically polarized.

The wave vectors for free space and the overburden are expressed as:

$$\bar{k}_{o,1} = \beta \bar{a}_x + u_{o,1} \bar{a}_y \tag{2.5a}$$

in which the longitudinal wave number β is positive real for the radiation term; $0 \leq \beta < k_o$ for the propagating waves, $\beta > k_o$ for evanescent waves, and

$$k_{o,1} = \omega\sqrt{\mu_o \varepsilon_{o,1}} \tag{2.5b}$$

Thus the transverse wave number is

$$u_{o,1} = (k_{o,1}^2 - \beta^2)^{\frac{1}{2}} \tag{2.5c}$$

The square roots in (2.5) are chosen such that $\mathrm{Im}(k_{o,1}) \leq 0$ and $\mathrm{Im}(u_{o,1}) \leq 0$ at the carrier frequency. The wave parameters $u_{o,1}$ and β are also expressed in terms of the complex cosine and sine of the angles θ_o and θ_1. Thus

$$u_{o,1} = k_{o,1} \cos \theta_{o,1} = k_{o,1} C_{o,1}, \beta = k_{o,1} \sin \theta_{o,1} = k_{o,1} S_{o,1} \tag{2.6}$$

Hence for $0 \leq \beta < k_o$, θ_o is the angle between the wave vector $\bar{k}_o$ and the y axis. The transverse wave impedance is

$$Z(u) = \beta/\omega\varepsilon = \begin{cases} \beta/\omega\varepsilon_o = Z_o, y > 0 \\ \beta/\omega\varepsilon_1 = Z_1, -h < y < 0 \end{cases} \tag{2.7}$$

For $0 > y > -h$, the basis function for the radiation term is

$$\Psi(u,y) = \{\exp[iu_1(y+h)] + R_{21}(u) \cdot \exp[-iu_1(y+h)]\}\Psi(u,-h)/T_{21}(u) \tag{2.8a}$$

where

$$\Psi(u,-h) = \exp(-iu_1 h) T_{21}(u) T_{1o}(u) / (\angle\pi\ Z_o(u))^{\frac{1}{2}} [1 - R_{o1}(u) R_1(u)] \tag{2.8b}$$

The reflection coefficients looking in the negative y direction at the air-overburden interface and the overburden-substratum interface are respectively

$$R_o(u) = (K_o - z_1)/(K_o + z_1) \tag{2.9a}$$

$$R_1(u) = R_{21}(u)\exp(-2iu_1 h) = [(K_1 - Z_s)/(K_1 + Z_s)] \cdot \exp(-2iu_1 h) \tag{2.9b}$$

in which

$$z_1(u) = K_1(Z_s + iK_1 \tan u_1 h)/(iZ_s \tan u_1 h + K_1) \tag{2.9c}$$

$$K_{o,1} = u_{o,1}/\omega\varepsilon_{o,1} \tag{2.9d}$$

and the two-medium Fresnel reflection and transmission coefficients for the air-overburden interface and the overburden-substratum interface are given by

$$R_{o1}(u) = (K_1 - K_o)/(K_1 + K_o), R_{21}(u) = (K_1 - Z_s)/(K_1 + Z_s) \tag{2.10a}$$

$$T_{1o}(u) = 1 + R_{1o}(u) = 1 - R_{o1}(u), \; T_{21}(u) = 1 + R_{21}(u) \tag{2.10b}$$

When the receiver and the source are far from the nonuniform region, ($k_o\rho >> 1$ and $k_o\rho_o >> 1$) (see Fig. 1), the forward scattered radiation field is [3],

$$H_z^f(x,y) = (2\pi/k_o\rho)^{\frac{1}{2}} \exp(-ik_o\rho) \exp(i\pi/4) P(u^f,u^i) \tag{2.11a}$$

where the radiation pattern is given by

$$P(u^f,u^i) = P_o(u^f,u^i) \sum_{p,q}^{\infty} I_{p,q}(u^f,u^i) \tag{2.11b}$$

$$P_o(u^f,u^i) = H_m^i(1-S_1^f S_1^i - z_s^2) T_{21}(u^f) T_{1o}(u^f) T_{21}(u^i) T_{1o}(u^i)/4\pi\sqrt{\varepsilon_r} \tag{2.11c}$$

$$H_m^i = - a_o/[2\pi Z_o(u^i)]^{\frac{1}{2}} \tag{2.11d}$$

and

$$a_o = \tfrac{1}{2} K \exp(i\pi/4)(\omega\varepsilon_o\beta^i/k_o\rho_o)^{\frac{1}{2}} \exp(-ik_o\rho_o) \tag{2.11e}$$

In (2.11c) the incident and scattered waves are in the directions of $\bar{k}_o^i$ and $\bar{k}_o^f$ respectively and H_m^i is the magnitude of the incident magnetic field, H_z, at the origin, excited by the magnetic line source of intensity K (2.1) (Fig. 2). The normalized surface impedance is $z_s = Z_s/\eta_1$. Furthermore

$$\sum_{p,q}^{\infty} I_{p,q}(u^f,u^i) = \frac{1}{S_1^f - S_1^i} \int_{-L}^{L} \Big\{ k_o h'(x) \exp[i(\beta^f - \beta^i)x - i(u_1^f + u_1^i)h] \tag{2.12}$$

$$\cdot \sum_{p=1}^{\infty} [R_{o1}(u^f) R_{21}(u^f) \exp(-2iu_1^f h)]^{p-1}$$

$$\cdot \sum_{q=1}^{\infty} [R_{o1}(u^i) R_{21}(u^i) \exp(-2iu_1^i h)]^{q-1} \Big\} dx$$

where

$$h'(x) = dh(x)/dx \tag{2.13}$$

The infinite geometric series expansions of the terms $1/[1-R_{o1}R_{21}\exp(-2iu_1h)]$ used in the above derivations are valid only for $|R_{o1}R_{21}\exp(-2iu_1h)| < 1$. The coefficient $I_{p,q}(u^f,u^i)$ can be integrated by parts [4]. After neglecting the term identified with the edge effect in the theory of scattering by rough surfaces [5],[6], the general expression for the coefficient $I_{p,q}(u^f,u^i)$ for $h = h_o + \delta x, (-L < x < L)$, is found to be

$$I_{p,q}(u^f,u^i) = \frac{[R_{o1}(u^f)R_{21}(u^f)]^{p-1}[R_{o1}(u^i)R_{21}(u^i)]^{q-1}}{(2p-1)C_1^f + (2q-1)C_1^i}$$
$$\cdot\exp[-i\{(2p-1)u_1^f + (2q-1)u_1^i\}h_o]2k_oL$$
$$\cdot\operatorname{sinc}[(\beta^f-\beta^i) - \{(2p-1)u_1^f + (2q-1)u_1^i\}\delta] \qquad (2.14)$$

where

$$\operatorname{sinc}(v) = \sin(v)/v \qquad (2.15)$$

The terms corresponding to $p \neq 1$ are missing from the geometrical optical solution [3].

For the special case $\delta = 0$, $h =$ constant (parallel stratified earth) the terms $1/[1 - R_{o1}R_{21}\exp(-2iu_1h)]$ are not functions of x. In this case it is not necessary to expand these factors in a geometric series to facilitate the integration. Thus, for $\delta = 0$, the radiation pattern is

$$P(u^f,u^i) = P_o(u^f,u^i)I_{11}(u^f,u^i)\cdot(1/[1-R_{o1}(u^f)R_{21}(u^f)\exp(-2iu_i^fh)])$$
$$\cdot 1/[1-R_{o1}(u^i)R_{21}(u^i)\exp(-2iu_1^ih)] \qquad (2.16)$$

Substitute (2.13) for I_{11} into (2.16) to get

$P(u^f,u^i)$

$$= \frac{P_o(u^f,u^i)\exp[-i(u_1^f+u_1^i)h_o]2k_oL\ \operatorname{sinc} L(\beta^f-\beta^i)}{(C_1^f+C_1^i)[1-R_{o1}(u^f)R_{21}(u^f)\exp(-2iu_1^fh_o)][1-R_{o1}(u^i)R_{21}(u^i)\exp(-2iu_1^i)]} \qquad (2.17)$$

For the special case $k_o = k_1$ and $S_o^i = S_o^f$ (2.17)

$$P_o(u^f,u^i) = H_m^i(C_1^{i2}-z_s^2)C_1^{i2}/\pi(C_1^i+z_s)^2 = H_m^i\ C_1^{i2}\ R_{21}^i/\pi \qquad (2.18)$$

thus

$$H_z^f(x,y) = H_m^i(i/2\pi\ k_o\rho)^{1/2}\exp(-ik_o\rho)2\ k_oLC_1^iR_1 \qquad (2.19)$$

Equation (2.19) is the expression for diffuse scattering in the specular direction.

The back scattered radiation field H_z^b at an angle θ_o^b from the y axis can be obtained from (2.11) by replacing β^f by $-\beta^b = -k_o \sin\theta_o^b$.

The modal equation for the surface wave is

$$\frac{1}{R_o} = \frac{1-R_{o1}R_1}{R_1-R_{o1}} = 0 \tag{2.20a}$$

Thus

$$R_{o1}R_1 = R_{o1}R_{21}\exp(-2iu_1h) = 1 \tag{2.20b}$$

It is convenient to express (2.20b) as

$$i\tan u_1h = \left(-\frac{u_o\varepsilon_r}{u_1} - \frac{z_s\sqrt{\varepsilon_r k_o}}{u_1}\right)\Big/\left(1+\frac{u_o\varepsilon_r}{u_1}\frac{z_s\sqrt{\varepsilon_r k_o}}{u_1}\right) \tag{2.20c}$$

The modal equation (2.20c) is solved numerically for the nth root, $u_{on}(x)$, using the Richmond process [7]. The corresponding values for β_n and u_{1n} are obtained by (2.5).

The solution for the scattered radiation field excited by an incident surface wave is greatly simplified by replacing $\beta_n(x)$ by $\bar{\beta}_n = \beta_n(o)$. The subscript $n = 0$ denotes the dominant surface wave mode.

The surface wave excited by an incident plane wave is [3].

$$H_z^f(x,y) = \exp(-i\bar{\beta}_n x)\Psi(u_n,y)\Psi(u_n,o)(2\pi/\omega\varepsilon_o)P(\bar{u},u^i) \tag{2.21}$$

in which the surface wave basis functions are

$$\Psi(u_n,y) = \Psi(u_n,o)\cdot\begin{cases}\cdot\exp(-iu_oy) & , y > 0\\ \cdot\exp[(-iu_1y)+R_{o1}\exp(iu_oy)]/(1+R_{o1}), & y < 0\end{cases} \tag{2.22a}$$

and

$$[\Psi(u_n,o)]^2 = 2iu_{on}/Z_o\left[1-\left(\frac{u_{on}}{u_{1n}}\right)^2\cdot\left\{1+\frac{Z_s(K_1^2-K_o^2)}{K_o(K_1^2+Z_s^2)} - \frac{iu_1h(K_1^2-K_o^2)}{K_1K_o}\right\}\right] \tag{2.22b}$$

The surface wave basis functions are both explicit functions of y and implicit functions of x through h(x). Thus in (2.21) $\Psi(u_n,y)$ is evaluated at the field point (x,y) and $\Psi(u_n,o)$ is evaluated at the origin. Furthermore

$$P(\bar{u},u^i) = P_o(\bar{u},u^i)\sum_{pq} I_{pq} \qquad p,q=1,2,3\ldots \tag{2.23}$$

where

$$P_o(\bar{u},u^i) = H_m^i(1-S_1^i\bar{S}_{1n}-z_s)T_{21}(u^i)T_{1o}(u^i)T_{21}(\bar{u})/4\pi\sqrt{\varepsilon_r} \tag{2.24a}$$

On neglecting the edge effect

$$I_{pq}(u^i,\bar{u}) = \frac{[R_{21}(u^i)R_{o1}(u^i)]^{p-1}[-R_{21}(\bar{u})]^{q-1}}{(2p-1)C_1^i + (2q-1)\bar{C}_{1n}}$$

$$\cdot\exp[-i\ (2p-1)u_1^i + (2q-1)\bar{u}_{1n}\ h_o]2k_oL$$

$$\cdot \operatorname{sinc}\left[L[\bar{\beta}_n-\beta^i)-\{(2p-1)u_1^i+(2q-1)\bar{u}_{1n}\}\delta]\right] \quad p,q=1,2,3... \tag{2.24b}$$

and H_m^i is given by (2.11d). Equation (2.25d) is valid for

$$|R_{o1}(u^i)R_{21}(u^i)\exp(-2iu_1^i h_o)| < 1 \text{ and } |R_{21}(\bar{u})\exp(-2i\bar{u}_1 h_o)| < 1. \tag{2.25e}$$

For the special case $\delta=0$, the closed form solution for H_z^f is

$$H_z^f(x,y) = \exp(-i\bar{\beta}_n x)\Psi(u_n,y)\Psi(u_n,o)(2\pi/\omega\varepsilon_o)P_o(u_n,u^i) \tag{2.26}$$
$$\cdot \frac{\exp[-i(u_1^i+\bar{u}_1)h_o]2k_oL \operatorname{sinc} L(\bar{\beta}_n-\beta^i)}{(C_1^i+\bar{C}_{1n})[i-R_{o1}(u^i)R_{21}(u^i)\exp(-2iu_1^i h_o)][1+R_{21}(\bar{u})\exp(-2i\bar{u}_{1n}h_o)]}$$

The WKB solutions for the surface waves excited by the magnetic line source are given by [3],

$$H_z^f(x,y) \approx -\frac{K}{2}\Psi(u_n,y_o)\Psi(u_n,y)\exp\left(-i\int_{x_o}^{x}\beta_n dx\right) \tag{2.27a}$$

in which the basis function $\Psi(u_n,y_o)$ is evaluated at the source point (x_o,y_o), (2.22).

The steady state response $H_z(\omega)$ is derived for time harmonic excitations. For arbitrary time varying excitations the instantaneous expression for the magnetic line source is

$$\bar{J}_m(\bar{r},t) = \text{Re } f_s(t)\delta(x-x_o)\delta(y-y_o)\bar{a}_z \tag{2.27b}$$

The excitation function $f_s(t)$ is taken to be complex for convenience. The Fourier transform of $f_s(t)$ is

$$F(\omega) = F[f_s(t)] = \int_{-\infty}^{\infty} f_s(t)\exp(-i\omega t)dt \tag{2.28}$$

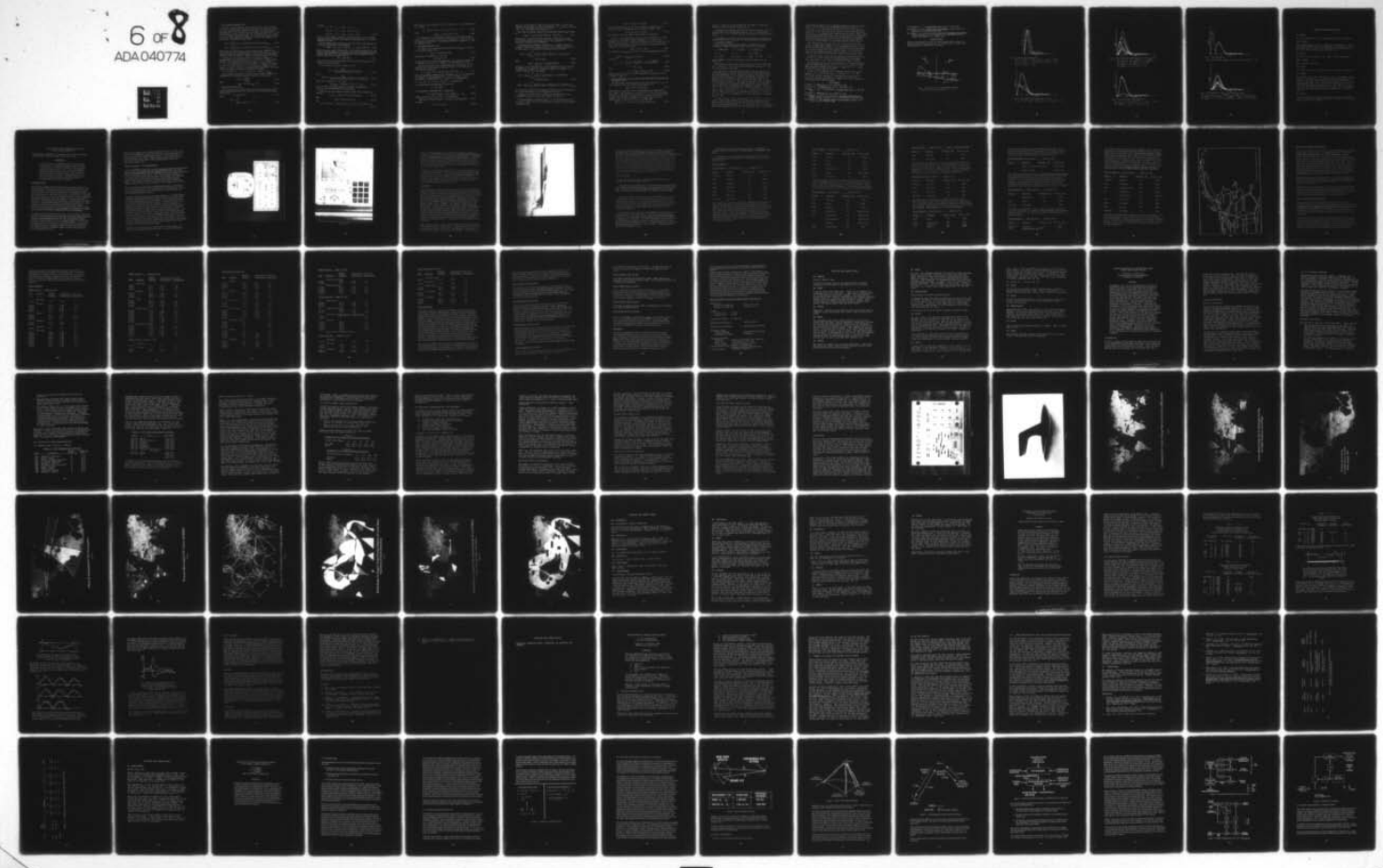
and $F(\omega) = F(-\omega)^*$ only when $f_s(t)$ is real. The asterisk denotes the complex conjugate. Thus on applying Fourier transform techniques and noting that $H_z(\omega) = H_z^*(-\omega)$, the transient response can be given by

$$h(\bar{r},t) = \text{Re } F^{-1}[H_z(\omega)\cdot F(\omega)] = \text{Re}\left(\frac{1}{2\pi}\int_{-\infty}^{\infty} H_z(\omega)F(\omega)\exp(i\omega t)d\omega\right)$$
$$\equiv \text{Re } h_s(\bar{r},t) \tag{2.29}$$

AD-A040 774 NATIONAL AERONAUTICS AND SPACE ADMINISTRATION GREENB--ETC F/G 14/2
PROCEEDINGS OF THE ANNUAL PRECISE TIME AND TIME INTERVAL (PTTI)--ETC(U)
DEC 75

UNCLASSIFIED NASA-GSFC-X-814-76-45 NL

6 OF 8
ADA040774



3. FAST FOURIER TRANSFORM (FFT)

The fast Fourier transform (FFT) algorithm [8] is used to perform the numerical integration required to evaluate either a Fourier transform or an inverse Fourier transform. The number of samples used in subroutine FFT is $N = 2^m$ where m is an integer. For this choice of N the FFT algorithm is most efficient [8]. Let the symbols k(k= 1,2...N) and n = 1,2...N denote the sample number in the time and frequency domains respectively. The summations performed to evaluate the transform and the inverse transform are respectively,

$$F(n) = \frac{1}{N} \sum_{k=1}^{N} [f_r(k) + if_i(k)] \exp[-2i\pi(n-1)(k-1)/N] \cdot t_{max} \qquad (3.1a)$$

$$f^*(k) = \frac{1}{N} \sum_{n=1}^{N} [F_r(n) + iF_i(n)]^* \exp[-2i\pi(n-1)(k-1)/N] \cdot 2f_{max} \qquad (3.1b)$$

Because the same subroutine is used to evaluate the transform F(n) (3.1a) and the inverse transform f(k) (3.1b), $f^*(k)$ (3.1b) is initially evaluated using the complex conjugate of the frequency domain samples $F^*(n)$ and f(k) is obtained by taking the complex conjugate of (3.1b).

The values of the N samples F(n) in the frequency domain are obtained from N + 1 values of $F(\alpha + i\omega)$ taken at N + 1 points equally spaced on the imaginary axis (ω) from $-\omega_{max}$ to $+\omega_{max}$. Samples n = 1,2...N/2 correspond to $F[(n-1)\Delta\omega]$ where $\Delta\omega = 2\omega_{max}/N$. The sample n = N/2 + 1 is given by $F(N/2 + 1) = [F(-i\omega_{max}) + F(i\omega_{max})]/2$. The samples n = N/2 + 2, N/2 + 3...N correspond to $F[(n-1-N)\Delta\omega]$. Similarly, in the time domain the numbering scheme is as follows:

$f(k) = f[(k-1)\Delta t]$, k = 1,...N, and $f(1) = f(N+1) = f(t_{max})$.

The increments in frequency $\Delta\omega$ and in time Δt between samples are determined by the Shannon criteria [8] which for this case is

$$N = 2^m = \frac{2 f_{max}}{1/t_{max}} \qquad (3.2a)$$

where

$$2 f_{max} = N\Delta f \text{ and } t_{max} = N\Delta t \qquad (3.2b)$$

4. EXCITATION-LORAN-C PULSE

The excitation (2.27) used in this work is the Loran-C pulse. This pulse can be represented as the real part of the sum of three damped sinusoids [9].

$$f(t) = Re[f_s(t)] \qquad (4.1a)$$

where

$$f_s(t) = \begin{cases} 0 & t < 0 \\ \sum_{j=1}^{3} A_j \exp(-\Gamma_j t) & t > 0 \end{cases} \qquad (4.1b)$$

in which

$$A_1 = i/2 \quad \Gamma_1 = c + i\omega_1 \quad \omega_1 = \omega_o$$

$$A_2 = -i/4 \quad \Gamma_2 = c + i\omega_2 \quad \omega_2 = \omega_o + 2\omega_p$$

$$A_3 = -1/4 \quad \Gamma_3 = c + i\omega_3 \quad \omega_3 = \omega_o - 2\omega_p \tag{4.1c}$$

where ω_o is the radian frequency of the carrier and ω_p is the radian frequency of the envelope (the modulation frequency) and $c > 0$ is the damping coefficient.

For the Loran-C pulse excitation (4.1) f(t) and its derivatives are continuous. Furthermore, for the values

$$c = 25000 \quad f_p = \omega_p/2\pi = 2500 \text{ Hz} \quad f_o = \omega_o/2\pi = 100 \text{ k Hz} \tag{4.1d}$$

99% of the input power is between 90 to 110 k Hz. This property of the Loran-C pulse considerably facilitates the numerical analysis since the Fourier transform $H(\omega)$ of the response h(t) can be regarded as band-limited. The Fourier transform $H(\omega)$ is

$$H(\omega) = F(\omega)\, H_z(\omega) \tag{4.2}$$

where $F(\omega)$ is the Fourier transform of $f_s(t)$ (4.1b) and $H_z(\omega)$ is the transfer function, Section 2.

For the values of A_j and Γ_j given in (4.1c)

$$F(\omega) = \frac{2i\omega_p^2}{[i(\omega+\omega_o)+c][\{i(\omega+\omega_o)+c\}^2 + 4\omega_p^2]} \tag{4.3}$$

and

$$|F(\omega)|^2 = \frac{4\omega_p^4}{[(\omega+\omega_o)^2+c^2][\{c^2+4\omega_p^2-(\omega+\omega_o)^2\}^2 + 4c^2(\omega+\omega_o)^2]} \tag{4.4a}$$

Thus $|F(\omega)|^2$ peaks at $\omega = -\omega_o$, and

$$|F(\omega)|_{max} = 1/4[\omega_p D(1 + D^2)], \; D = c/2\omega_p \tag{4.4b}$$

If D is fixed, increasing ω_p (and c) decreases the magnitude of $|F(\omega)|_{max}$ and the bandwidth of $F(\omega)$ increases.

The sum of the three damped sinusoids (4.1b) can be expressed as follows:

$$f_s(t) = i \exp(-ct) \sin^2 \omega_p t \exp(-i\omega_o t). \tag{4.5a}$$

Thus

$$|f_s(t)| = \exp(-ct)\sin^2 \omega_p t \tag{4.5b}$$

and

$$f(t) = \text{Re } f_s(t) = \exp(-ct) \sin^2 \omega_p t \sin \omega_o t = |f_s(t)| \sin \omega_o t. \tag{4.5c}$$

Thus $|f_s(t)|$ is the envelope of f(t). It peaks at $t = t_p$ and vanishes at $t = t_z$ where

$$t_p = \frac{1}{\omega_p} \tan^{-1}(1/D), \quad t_z = m\pi/\ _p, \quad m = 0, \pm 1, \pm 2... \tag{4.6a}$$

Hence,

$$|f_s(t_p)| = \exp(-ct_p)/(1 + D^2) \tag{4.6b}$$

The envelope of the input Loran C pulse $|f_s(t)|$ is shown in Fig. 2 for $f_o = 3 \times 10^2$ H_z, $f_p = f_o/30$, $f_o/40$, $f_o/50$, and $c = 5f_p$, $10f_p$, $15f_p$ to illustrate the effects of changing the modulation frequency f_p and the damping factor c.

5. SCATTERED RADIATION FIELD

The steady state scattered radiation field in db H_{db} as a function of the scatter angle θ^f is

$$H_{db} = 20 \log|H_z(x,y)/H_z^o| \tag{5.1a}$$

where $H_z(x,y)$ is given by (2.11a) and

$$H_z^o = H_z(\theta^f = \theta^i) \tag{5.1b}$$

for the case $\delta = 0$. (2.4). The plane wave at an angle of incidence θ^i is assumed to be excited by a magnetic line source $\bar{J}_m(\bar{r},t)$, (2.27).

The dips and peaks in the response H_{db} (as a function of θ^f) are primarily due to the minima and maxima of $|\text{sinc } v|$ (2.15)(except for near grazing incidences)

$$v = k_o L[S_o^f - S_o^i - \{(2p-1)C_1^f + (2q-1)C_1^i\}\sqrt{\varepsilon_r \delta}] = n\pi \tag{5.2}$$

where the principal maximum of θ^f corresponds to n = 0. The minima for $\theta^f < \theta_m^f$ and $\theta^f > \theta_m^f$ correspond to n = -1,-2,-3...and n = 1,2,3... respectively. The maxima for $\theta^f < \theta_m^f$ and $\theta^f > \theta_m^f$ correspond to $n = -\frac{1}{2}, -\frac{3}{2}, -\frac{5}{2}$ ... and $n = \frac{1}{2}, \frac{3}{2}, \frac{5}{2}$ ... respectively.

For nondissipative overburdens S_o^f is real and

$$\theta^f = \sin^{-1}(S_o^f) \tag{5.3a}$$

For dissipative overburdens S_o^f is complex and

$$\theta^f = \text{Re}[\sin^{-1}(S_o^f)] \simeq \sin^{-1} \text{Re}(S_o^f), \quad \varepsilon_I << \varepsilon_R \tag{5.3b}$$

Using (2.11d), (2.11e), and (2.7), it follows that

$$H_m^i(2\pi/k_o\rho)^{\frac{1}{2}} \exp[i(\pi/4 - k_o\rho)] = -iK \exp(-i\omega t_o)/(2\eta_o[\rho\rho_o]^{\frac{1}{2}}) \tag{5.4a}$$

in which

$$t_o = (\rho + \rho_o)/v_o \tag{5.4b}$$

and v_o is the velocity of light in free space. Thus, t_o is the time required for the signal to travel the distance $\rho + \rho_o$ (Fig. 1) in free space. For convenience set $K/(2\eta_o[\rho\rho_o]^{\frac{1}{2}}) = 1$.

The computer program evaluates the normalized response $h_{sN}(t)$ given by

$$h_{sN}(t) = h_s(t)/|f_s(t_p)|\cdot|H_z(\omega_o)| = h_s(t)/h_{os} \tag{5.5}$$

where $H_z(\omega_o)$ is the steady state response to $\exp(i\omega_o t)$ excitations (2.11a) for a specified reference case. Thus $|h_{sN}(t)|_{max} \simeq 1$ for the particular reference case considered.

For dissipative overburdens and when Z_s is a complex function of frequency the transfer function $H_z(s)$ is not an analytic function of s. In these cases it is convenient to express $h_s(t)$ as follows:

$$h_s(t) = \frac{1}{2\pi i}\int_{-i\infty}^{i\infty} \sum_{p,q} H^1_{pq}(s)\, H^2_{pq}(s) \sum_{j=1}^{3}[A_j/(s+\Gamma_j)]\exp(st)ds$$

$$= h_L(t) + h_H(t) \tag{5.6a}$$

where

$$H_z(s) = \sum_{pq} H_{pq}(s) = \sum_{pq} H^1_{pq}(s)\, H^2_{pq}(s) \tag{5.6b}$$

and $H_{pq}(s)$ is an individual term in the expression for $H_z(s)$. All the singularities of $H_{pq}(s)$ are contained in $H^1_{pq}(s)$ while $H^2_{pq}(s)$ is an analytic function of s. Furthermore

$$h_L(t) = \frac{1}{2\pi i}\sum_{j=1}^{3}\int_{-i\infty}^{i\infty} \sum_{pq} H^1_{pq}(-\Gamma_j)H^2_{pq}(s)[A_j/(s+\Gamma_j)]\exp(st)ds$$

$$= h_E(t)\exp(-i\omega_o t) \tag{5.6c}$$

$$h_H(t) = \frac{1}{2\pi i}\sum_{j=1}^{3}\int_{-i\infty}^{i\infty} \sum_{pq}[H^1_{pq}(s)-H^1_{pq}(-\Gamma_j)]H^2_{pq}(s)[A_j/(s+\Gamma_j)]\exp(st)ds \tag{5.6d}$$

In (5.6) $h_L(t)$ is due to the residues of the poles of F(s) and $h_H(t)$ is due to the contributions of the singularities of $H_z(s)$.

If $H^2_{pq}(s)$ in (5.6d) does not possess any singularities in the vicinity of the poles of F(s), (Γ_j), $|h_H(t)| << |h_L(t)|$.

For nondissipative overburdens $h_H(t) = 0$ and the envelope of h(t) is given by $|h_E(t)|$ (5.6c). For the general case $h_H(t) \neq 0$ (dissipative overburdens) and

$$h(t) = \text{Re } h_L(t) + \text{Re } h_H(t) \tag{5.7a}$$

Thus the envelope $h_T(t)$ of the total response is regarded as the envelope of $h_L(t)$ superimposed on the function Re $h_H(t)$. Hence

$$h_T(t) = \text{Re } h_H(t) \pm |h_E(t)| \tag{5.7b}$$

The envelope (5.7b) is symmetric with respect to $\text{Re}[h_H(t)]$.

In view of the singularities of $H_{pq}(s)$, the functions $h_s(t)$, $h_L(t)$ and $h_H(t)$ are evaluated by numerical methods. As a check on the numerical values, $h_L(t)$, the major contribution to the response $h_s(t)$ is also evaluated by analytical methods and $h_H(t)$ is evaluated directly using (5.6) and indirectly from

$$h_H(t) = h_s(t) - h_L(t) \tag{5.8}$$

An individual term $h_{Lpq}(t)$ of $h_L(t)$, (5.6c) is approximately given by

$$h_{Lpq}(t) = f_s(t_g) G_{pq}(-\Gamma_1)(1-G_p/T) \tag{5.9a}$$

in which

$$t_g = t - t_o - \frac{h_o}{v_o}\left[(2p-1)\sqrt{\varepsilon_R-(S_o^f)^2} + (2q-1)\sqrt{\varepsilon_R-(S_o^i)^2}\right] \tag{5.9b}$$

$$T = \tan \omega_p t_g, \tag{5.9c}$$

and

$$G_p = [1-G_{pq}(-i\omega_o)/G_{pq}(-\Gamma_1)]/D \tag{5.9d}$$

Thus the factor $(1-G_p/T)$ in (5.9a) represents the distortion of the envelope of $h_{Lpq}(t)$.

6. SURFACE WAVES EXCITED BY INCIDENT PLANE WAVES AND WKB SOLUTIONS FOR THE SURFACE WAVES

The steady state scattered surface wave in db, H_{db} at x = L, y = 0 as a function of the plane wave incident angle θ^i is

$$H_{db} = 20\left|\log H_z(L,0)/H_{zm}^o\right| \tag{6.1}$$

where $H_z(L,0)$ is given by (2.21). The normalization coefficient is $H_{zm}^o = H_z^o(\theta^i = \theta_m^i)$ in which $H_z^o = H_z(L,0)$ for $\delta = 0$ and θ_m^i is the angle at which H_z is maximum. The plane wave at an angle of incidence θ^i is assumed to be excited by a magnetic line source $\bar{J}_m(\bar{r},t)$ (2.27). Using (2.11d), (2.11e), and (2.7), it follows that

$$H_m^i(2\pi/\omega\varepsilon_o) = -K(\pi v_o/2\omega_o\rho_o)^{\frac{1}{2}} \exp(i\pi/4)\exp(-i\omega t_o) \tag{6.2}$$

here $t_o = \rho_o/v_o$ is the time required for the signal to travel the distance ρ_o (Fig. 1) and $K(\pi\, v_o/2\omega_o\rho_o)^{\frac{1}{2}} = 1$.

The steady state WKB solutions for the surface waves given by (2.27) are evaluated for an observation point at x = L, y = 0 and a line source at x_o = L, y = 0 and by setting the intensity of the line source K = 2.

The response to transient excitations is obtained by following the same procedures used to evaluate the scattered radiation fields (5.6).

7. ILLUSTRATIVE EXAMPLES

Unless otherwise specified the values of parameters used in illustrative examples presented in this section are as follows:

$$L = 5000 \text{ meters} \qquad \Delta = -1 \text{ degrees} \qquad h_o = 100 \text{ meters}$$

$$\varepsilon_R = 8 \qquad \varepsilon_I = 0 \qquad Z_s = 0 \text{ ohms}$$

$$f_o = 3\times10^5 \qquad f_p = f_o/40 \qquad c = 10\, f_p \qquad \theta^i = 85^o \qquad (7.1)$$

and the number of terms of the series (2.11b) is taken to be 15, $(p-q \leq 6)$.

The response is normalized such that $H_z(\omega_o)$ in (5.16) is evaluated for $\Delta = 0^o$ and $\theta^f = \theta^i$ for the scattered radiation field and $\theta^i = \theta^i_m$ for the scattered surface wave.

The shape of the envelope depends strongly upon the incident and observation angles θ^i and θ^f. The envelope of the individual terms of the field expansions closely resemble the shape of the input Loran C pulse except for values of θ^f very near the minima of $H_{pq}(\theta^f)$. The minima of H_{pq} for different values of p and q do not occur for the same values of θ^f (unless $\Delta = 0^o$), and the envelope of the total field is not necessarily distorted only when the envelope of an individual term is distorted. The envelope of the response is usually distorted most strongly in the neighborhood of a minimum of $H_{db}(\theta^f)$. In Fig. (3) $|h_{LN}| \simeq |h_{sN}|$ is plotted for $\Delta = -1^o$, $\varepsilon_I = .5$ with $\theta^f = 44^o$, 45°, 46°, and 47°. Major distortion of the envelope occurs when $\theta^f = 45^o$-46°. In this case $H_{11}(\theta^f)$ is a minimum when $\theta^f = 44.6^o$ and $H_{db}(\theta^f)$ is minimum when $\theta^f = 46^o$.

In Fig. (4) $|h_{LN}| \simeq |h_{sN}|$ is plotted for $\Delta = -1^o$ with $\theta^f = 46^o$. In an earlier comparison of the full wave steady state solutions with one derived using a geometrical optical approach it was pointed out that there are n terms for which p + q - 1 = n (n,p,q = 1,2,3...) in the full wave series expansion (2.11b), and associated with these n terms there

exists only one term in the corresponding geometrical optical solution [3],[4]. The envelopes of the individual terms h_{pq} (5.21a) for $n = p + q - 1 \leq 3$ together with the sum of only these six terms are also given in Fig. (4). The time of arrival of the n terms associated with $p + q - 1 = n$ progressively increases as n increases. These n terms of the series correspond to waves that are reflected at the overburden-substrate interface n times before they emerge above the overburden. This particular property of the full wave solution assures that the reciprocity relationships in electromagnetic theory are satisfied.

The computed value of $|h_{LN}|$ for $p + q \leq 6$ (15 terms of the series 2.11b) is approximately equal to the sum obtained by taking $p + q \leq 4$. Notice that while the envelopes of the individual terms of the series are not double humped, the total response $|h_{LN}|$ is very distorted. In this case the minimum of $H_{db}(\theta^f)$ (which occurs at $\theta^f = 46^o$) is the result of the destructive interference between the individual terms.

In Fig. (5) $|h_{LN}| \simeq |h_{sN}|$ and its significant terms are plotted for $\Delta = -.45^o$, $\theta^f = 57.9^o$. Due to the increased damping of the higher order terms when $\varepsilon_I = 10$, $|h_{LN}|$ is approximately equal to $|h_{LN11}|$.

The individual terms of the total response for θ^i near the Brewster angle are illustrated in Fig. (6) for $\Delta = -1^o$, $\theta^i = 70^o$, $\theta^f = 71.19^o$ (where $H_{11}(\theta^f)$ is minimum. Here $|h_{LNpq}| << |h_{LN}|$ for $p + q > 2$ since both R^i_{o1} and R^f_{o1} and R^f_{o1} are small.

In Fig. (7) the envelopes of the scattered surface waves h_{LN} and h_{LNpq} ($p + q \leq 4$) are plotted for $f_o = 1x10^5$ Hz, $\varepsilon_I = 5$. $\Delta = 1^o$, $\theta^i = 38.32^o$. In this case $H_{11}(\theta^i)$ is minimum for the value of θ^i chosen. The relative contributions of higher order terms increases as the overburden skin depth increases.

BIBLIOGRAPHY

[1] Bahar, E., Radio Sci., 5, pp. 1069-1075, 1970.

[2] Bahar, E., J. Geophys. Res., 70, pp. 1921-1928, 1971.

[3] Bahar, E., and G. Govindarajan, J. Geophys. Res., 78, pp. 393-406, 1973.

[4] Bahar, E., Radio Sci., 6, pp. 1109-1116, 1971.

[5] Beckmann, P., and A. M. Spizzichino, The Scattering of Electromagnetic Waves, Pergamon, London, and Macmillan, New York, 1963.

[6] Beckmann, P., The Depolarization of Electromagnetic Waves, Golem Press, Boulder, Colorado, 1968.

[7] Richmond, H. W., J. London Math. Soc., 19, pp. 31-38, 1944.

[8] Brigham, E. Oran, The Fast Fourier Transform, Prentice-Hall Inc., Englewood Cliffs, New Jersey, 1974.

[9] Johler, J. R., and S. Horowitz, Office of Telecommunications Report 73-20 (Superintendent of Documents, U.S. Government Printing Office, Washington, D.C. 20402), 1973.

ACKNOWLEDGMENTS

This work was sponsored by the U.S. Army Research Office, Grant. No. DAHC04-74-G-0074. The computations were performed by M. Fitzwater and the manuscript was prepared by E. Everett.

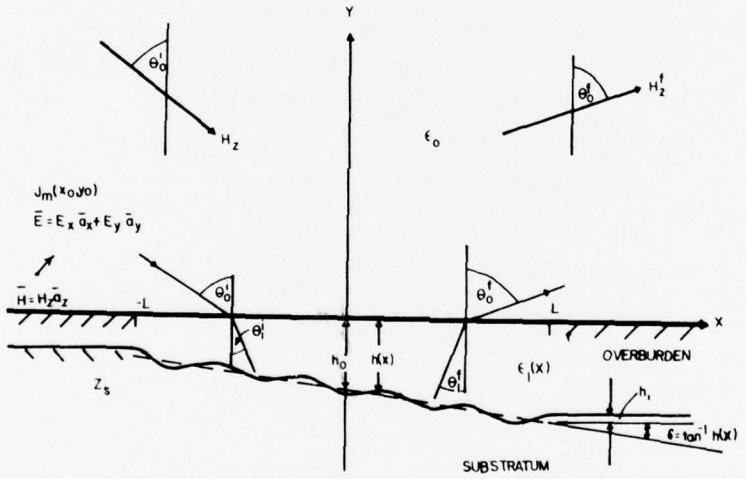


Fig. 1 Line source over a nonuniform overburden
$h(x) = h_o + \delta x + h_1 \cos \alpha x, \; -L < x < L$

BEST AVAILABLE COPY

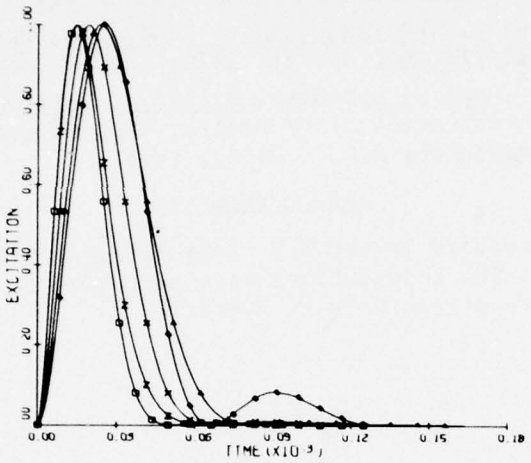


Fig. 2 Loran C pulse excitation
(□) $f_p = f_o/30$, $c = 10f_p$; (△) $f_p = f_o/50$, $c = 10f_p$;
(X) $f_p = f_o/40$, $c = 10\ f_p^{\frac{1}{2}}$ (◇) $f_p = f_o/40$, $c = 5f_p$;
(Z) $f_p = f_o/40$, $c = 15f_p$

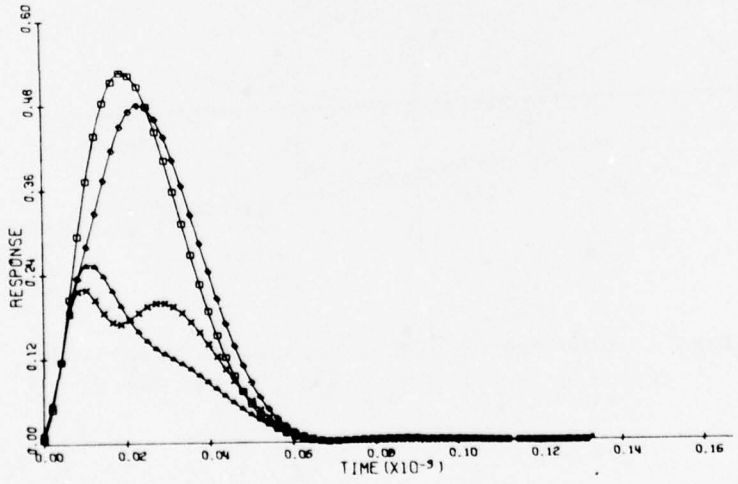


Fig. 3 The envelope of $h_{LN}(t'')$ for $\varepsilon_I = 0.5$,
(□) $\theta^f = 47^o$, (△) $\theta^f = 46^o$, (X) $\theta^f = 45^o$, (◇) $\theta^f = 44^o$

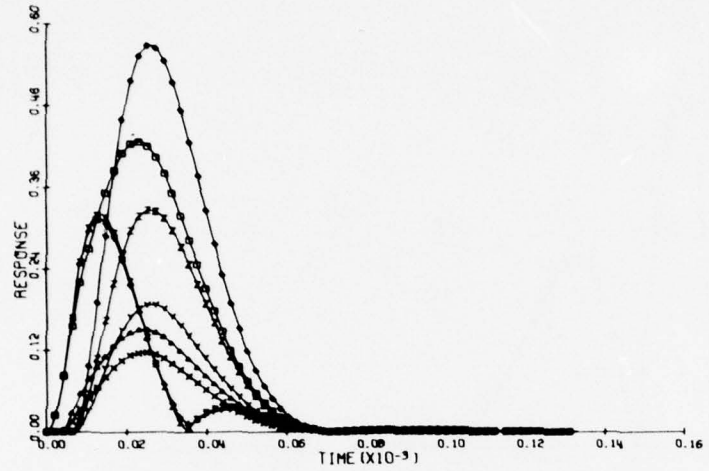


Fig. 4 The envelopes of (□) $h_{LN11}(t")$; (△) $h_{LN12}(t")$; (X) $h_{LN21}(t")$; (◇) $h_{LN13}(t")$; (Z) $h_{LN22}(t")$; (Y) $h_{LN31}(t")$; (⊠) $h_{LN}(t")$, $p + q \leq 6$; (+) $h_{LN}(t")$, $p + q \leq 4$ for $\theta^f = 46^o$

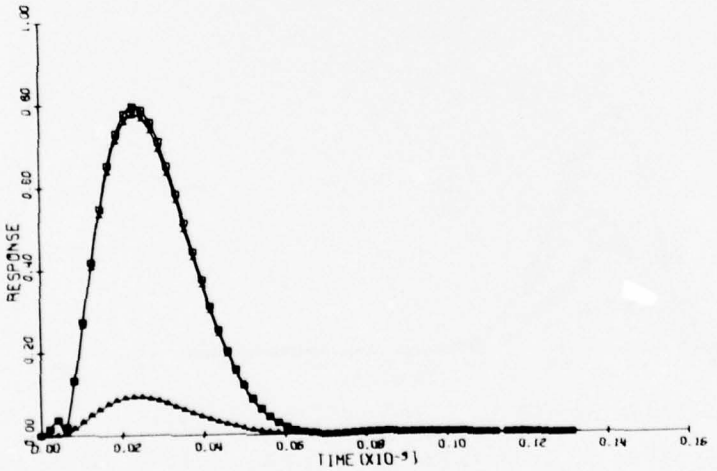


Fig. 5 The envelopes of (□) $h_{LN11}(t")$; (△) $h_{LN12}(t")$, (⊠) $h_{LN}(t")$, $p + q \leq 6$ for $\Delta = -0.45^o$, $\theta^f = 57.9^o$, $\varepsilon_I = 10$, $Z_s = 10\ (1 + i)$ ohms

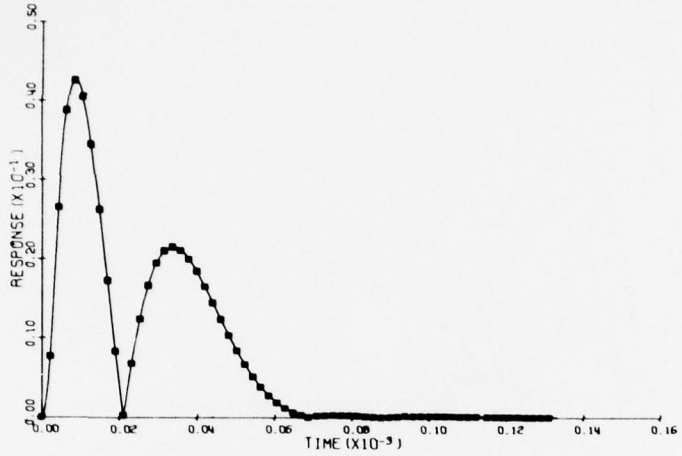


Fig. 6 The envelopes of

(□) $h_{LN11}(t")$; (X) $h_{LN}(t")$, $p + q \leq 6$ for $\theta^f = 71.19^o$, $\theta^i = 70^o$

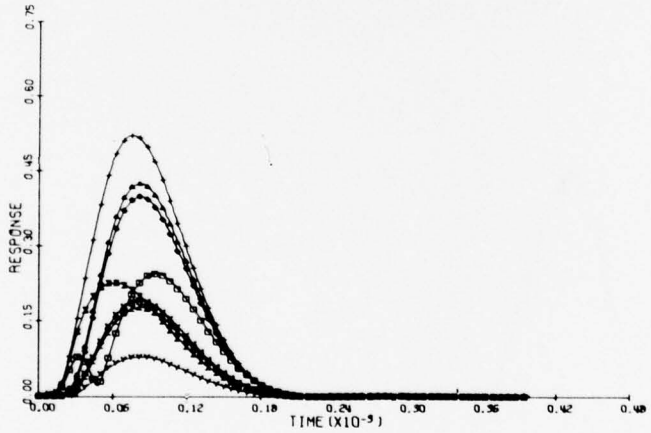


Fig. 7 The envelopes of (□) $h_{LN11}(t")$; (△) $h_{LN12}(t")$;
(X) $h_{LN21}(t")$; (◇) $h_{LN13}(t")$; (Z) $h_{LN22}(t")$; Y $h_{LN31}(t")$; (X) $h_{LN}(t")$;
(+) $\sum_{pq}(t")$, $p+q \leq 4$ for $f_o = 1x10^5$ Hz, $\varepsilon_I = 5$, $\Delta = 1^o$, $\theta^i = 38.32^o$

DR. REDER:

You have applied this to underground structure actually?

PROF. BAHAR:

This example here was for a non-uniform overburden. That means the earth's crust's thickness is changing, but we are now applying it also to the case where you simply have a hill or a valley without any layers to it.

DR. REDER:

How deep does the wave go in? What is your thickness?

PROF. BAHAR:

This is only 100 meters.

DR. REDER:

Is there any energy 100 meters down for Loran frequencies?

DR. BAHAR:

If you have seen the cases where I said the higher conductivity of the earth is, in those cases we had practically only one term, so the conductivity of the overburden is large, as in many cases, and indeed there is only one term, the dominant term, but, we have also examined the cases where the overburden conductivity is not large, in which case the 100 meters would be of the order of a skin depth, and then the high order terms are appreciable in their effect.

DR. REDER:

I do hope that you two gentlemen get together and maybe the theory of Professor Bahar can be applied to Mr. Roll's experimental data and vice versa.

TEST OF LOW-COST OMEGA NAVIGATION OVER ALASKAN AIRWAYS

Robert Moore, Department of Transportation, Federal Aviation Administration, NAFEC, Atlantic City, New Jersey

ABSTRACT

An airborne survey of OMEGA signal coverage along major airways in the state of Alaska produced records of reception at 10.2 KHz from Hawaii, Japan, Norway, and North Dakota in May, 1975. A low cost OMEGA receiver for general aviation was tested at minimum airway altitudes and relatively high speed, both in and out of clouds of ice crystals. Received signals were monitored and performance measured in terms of accuracy along course and at waypoints.

INTRODUCTION

The Federal Aviation Administration has been testing airborne navigation equipment which receive and process signals in the very low frequency band. The test and evaluation of such equipment poses unique problems due to the characteristics of propogation in VLF, the band of frequencies and the velocity of the test aircraft. Standard test factors such as accuracy and reliability take on new meaning when operating at high-speed over long ranges in a VLF propogation environment. In order to perform such tests aircraft, which are instrumented for testing OMEGA navigation equipment, should also be instrumented for simultaneous airborne monitoring of VLF signals. Combining such data with more readily available static monitor information contributes greatly to the development of performance standards and and to the verification of computed models of VLF propogation.

The purpose of this paper is to describe a series of flight probes, that were flown over Alaska, with a prototype model of a low cost OMEGA Navigation receiver. Alaska became the test site for the following reasons: it has a harsh and varied terrain; it is only partially covered by conventional navigation aids; and, it must somehow support the rapidly expanding use of civil aircraft as a primary mode of transportation. The flight probes were designed to gather preliminary information concerning the quality of OMEGA signal reception along major air routes throughout the state.

PRECEDING PAGE BLANK-NOT FILMED

Six major test flights were conducted between May 10-18, 1975. The routes were designed to include varied terrain, over-water legs, and the maximum number of established airways. Three additional unscheduled flights were made. Signal outages and malfunctions in the test aircraft interrupted three of the planned flights so that nine flights were made in all.

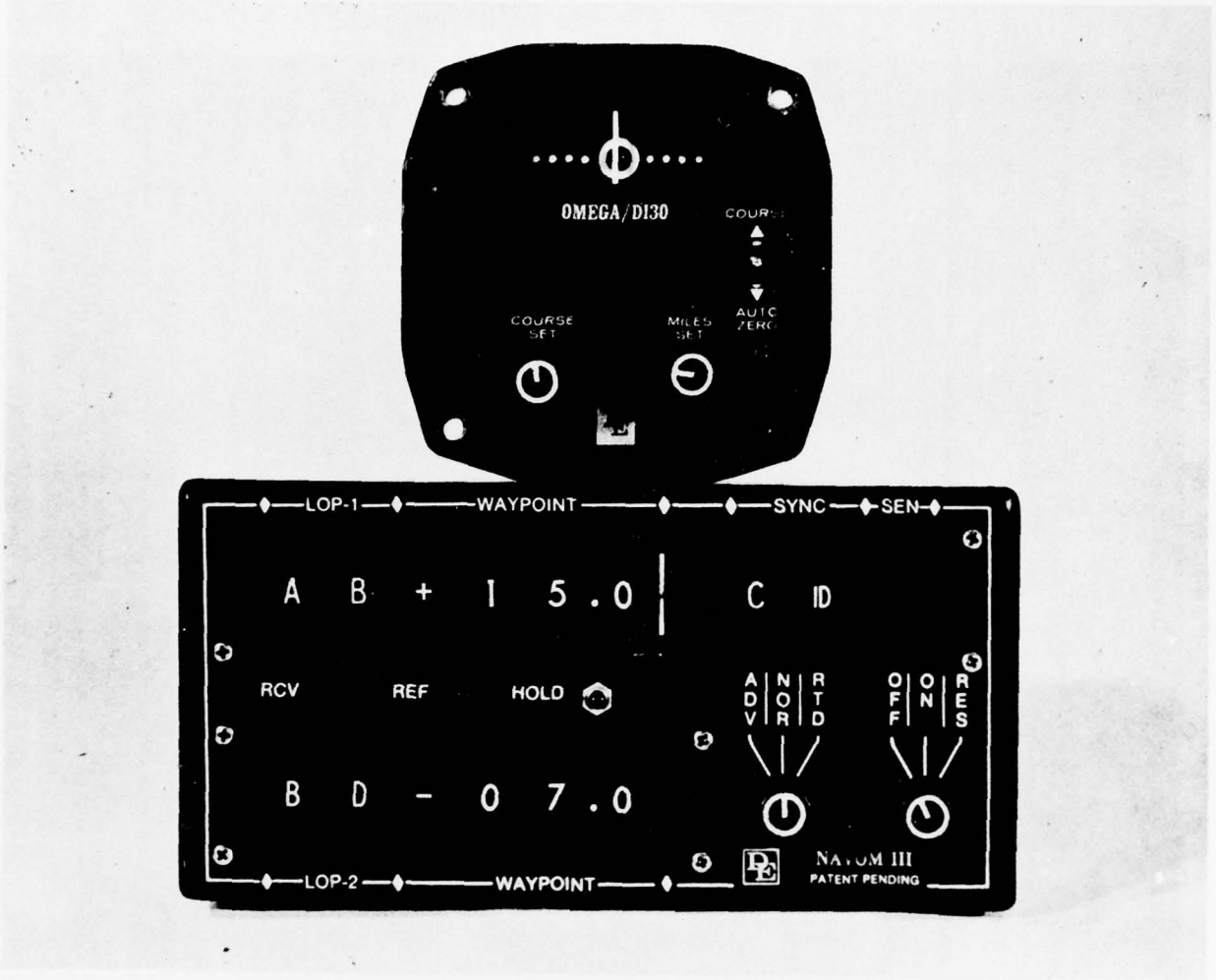
OMEGA Equipment--See Specifications

A low cost OMEGA navigation receiver, which was procured for these tests, was the Dynell Corporation Mark III OMEGA Navigation Set. The equipment is a prototype model that was designed for general aviation operations at maximum speeds of 400 knots under optimum signal conditions. The major units, receiver and indicator, were designed and packaged to standard form factors and cost the Government approximately $3000. The indicator contained a constant sensitivity crosspointer, digital distance display, to/from flag and course/distance set controls.

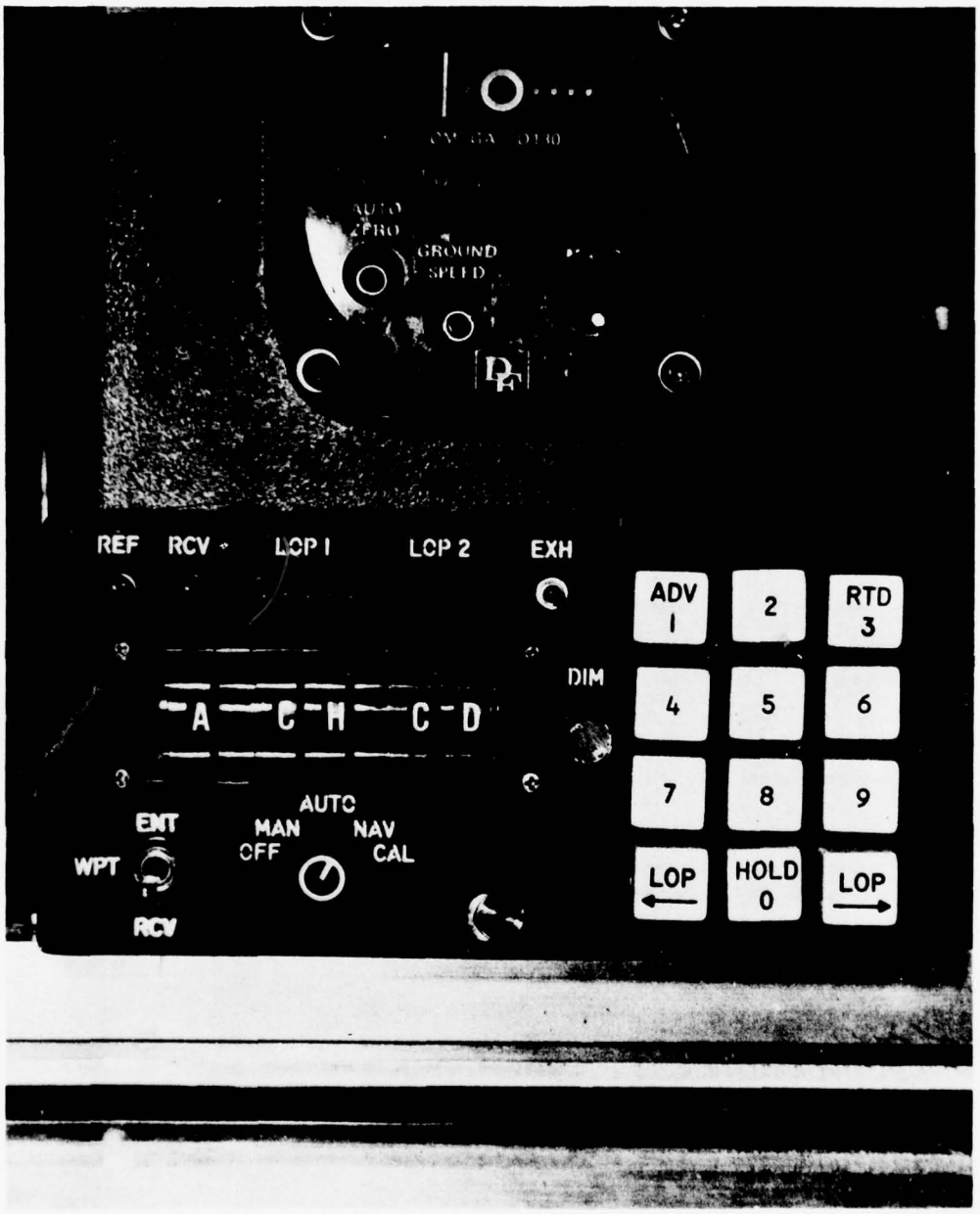
The receiver panel contained all programming switches, synchronization and reset controls. This unit housed three subsystems. These included clock generation and synchronization, phase tracking and error-signal processing circuits.

The Dynell Mark III accepted only single frequency, 10.2 KHz OMEGA navigation signals and did not have provisions for rate-aiding inputs such as compass heading or true airspeed. The system was coupled to an E-field antenna for signal reception. Normally the ADF sense long wire on an aircraft would be coupled to such an equipment in parallel with other avionics. Because of its relatively simple design, the Dynell Mark III was applicable to lower performance aircraft of the general aviation category and not to high performance types. The Dynell receiver did not contain circuitry for diurnal-shift compensation while enroute. The vendor's suggested method of diurnal compensation for large shifts enroute was to modify the manually computed lane crossing on inputs during preparation for each flight. The result of such a refinement would be a flight path, which was not quite linear, but with a minimized end point error. This procedure was not employed for any of the Alaskan test flights.

Operation of the Dynell set was fairly simple. Before flight the receiver was synchronized automatically. The desired destination



PROTOTYPE-DYNELL MARK III OMEGA NAVIGATION RECEIVER



PRODUCTION MODEL-DYNELL MARK III OMEGA NAVIGATION RECEIVER

in terms of OMEGA lanes was inserted by operating thumbwheel switches; the Enroute Deviation Indicator (CDI) was zeroed; and known the miles to the destination was set into the digital readout. The entire process, excluding trip computation, took approximately 2 minutes. Simple pre-flight computations established the number of lanes to be traversed for two selected station pairs. The calculated number of lane crossings was the difference between the OMEGA coordinates of the destination and the origin.

In flight the pilot maintained the CDI at zero deflection and the mileage display counted down. When the destination was reached, a flag appeared on the indicator. Simply stated the operation involved synchronizing the receiver to OMEGA transmissions, zeroing all counters, generating a vector, and applying a mileage-scaling factor and end point to the vector. The crosspointer served as a null meter to help the pilot maintain the vector.

TEST BED

Initial planning for flight tests of the low-cost receiver in Alaska had specified installation of the Dynell receiver and related data collection devices in an FAA aircraft, the Douglas Model DC-6B. This aircraft had been selected because of its operating range, relatively low operating speed (240 knots) and the fact that it had long wire E-plane antennas available for OMEGA reception. Flights were conducted in the vicinity of NAFEC and between NAFEC and Anchorage, Alaska, during January 1975. However, the planned flight tests in Alaska had to be cancelled due to a shutdown of the OMEGA Hawaii transmitter. Alaskan tests were rescheduled in May. Unfortunately, the DC-6 was not available and the entire test system had to be reconfigured and installed in another FAA aircraft Convair Model 880. This jet aircraft was found acceptable after insuring that it could be flown at speeds as low as 250-300 knots during actual test operations in Alaska. Aboard this aircraft there was an inertial navigation system, Litton Model LTN-51. It was used as an onboard positioning reference.

The antennas available on the CV-880 included an ADF E-plane plate sensor, and an active E-plane blade. The blade antenna was selected for all tests in Alaska on the basis of performance comparisons made while enroute to the test area from NAFEC. The primary test



FAA CONVAIR 880 (N-42)

installation which was mounted on a rack in the airplane, consisted of the Dynell Mark III prototype OMEGA navigation receiver, recording interface and incremental magnetic tape recorder. Additional instrumentation included an OMEGA signal monitor and analog pen recorder, a VOR/DME recording console and a camera installation on the flight deck for photographing the LTN-51 INS position reference. A production version of the Dynell Mark III receiver was also installed on the CV-880. This was to safeguard the mission to Alaska and would have been tested in the event of failure of the prototype Mark III receiver. The indicator of the prototype Mark III system was remotely installed for viewing at the pilots position. Some additional test instrumentation was mounted on test racks on the project test area.

TEST METHODS

Several operational procedures which are described below, were followed for all test flights in Alaska.

All flights except numbers 24, 25 and 26 began and terminated with an overflight of the Anchorage Vortac to secure a datum for data processing. Data collection was terminated and restarted on two occasions when a fuel stop became necessary part way through a planned flight.

The LTN-51 INS and the feasibility model OMEGA receiver were programmed with the same waypoint coordinates inserted in their own respective language. The INS was programmed prior to flight and the OMEGA receiver was programmed with track change information at every waypoint. This information consisted of lane crossing numbers retaining the point of flight origin as reference in the majority of instances.

The pilot flew the test routes using OMEGA course deviation and distance-to-go for aircraft guidance. The only exceptions to this procedure were, made just prior to waypoint passage and where OMEGA navigation was not possible. A constant heading was maintained prior to approaching a waypoint in order to allow time to insert new lane information into the OMEGA receiver. Waypoint passage was marked by conventional navigation aids. At this point a track change was made in the OMEGA receiver.

All flights were flown in standard air routes at published minimum enroute altitudes and at ground speeds of approximately 300 knots.

All flights were accomplished during daylight hours, commencing at approximately 1000 local time. Anchorage time in May was GMT−9 hours.

FLIGHT ROUTES

Dynell Flight 21 (AL Test #1) May 10, 1975

Airway to	Waypoint	Distance, nmi	M. E. A. ft.
V438/456	Big Lake	26	2000
V456	Gulkana	133	10000
V456	Northway	109	11000
V444	Big Delta	121	8000
V444	Fairbanks	77	5000
V438	Big Lake	202	10000
V438/456	Anchorage	26	2000

This initial relatively short flight in the southeast central portion of the state demonstrated operation and signal reception over high ranges and deep valleys. The legs from Northway to Fairbanks were flown in a valley with high ranges between the aircraft and the coastline. Close observations were made of the signal received from Norway in order to detect any degradation as the flight proceeded eastbound toward the Canadian Border. This flight was flown with only team members aboard in order to shakedown equipment and optimize team effort. Signal reception from OMEGA Stations A, C, D and H was recorded.

Dynell Flight 22 (AL Test #2) May 12, 1975

Airway to	Waypoint	Distance, nmi	M. E. A., ft.
V440	McGrath	187	11000
V440	Nome	273	8000
V506	Bethel	242	8000
V506	King Salmon	198	8000
V456	Kenai	204	13000 to 5000
V456	Anchorage	43	2000

During this flight to the western portion of the Alaskan mainland, reception of OMEGA signals A, C, D and H was verified over and adjacent to high ranges and along and over the water segment. There were no indications of RF interference. The airways flown along the west coast of the mainland were on the edge of the VOR/DME network.

Dynell Flight 23 (AL Test #3 May 13, 1975

Airway to	Waypoint	Distance, nmi	M. E. A., ft.
V436	Talkeetna	69	3000
V436	Nenana	141	10000
V504	Bettles	152	7000
V504	Dead Horse	211	10000 to 7000
A15	Pt. Barrow	177	-6000 Actual
	Cape Lisburne	240	-6000 Actual
	Kotzebue	143	-6000 Actual
V498	Galena (fuel)	192	8000

Dynell Flight 23 (AL Test #3) May 13, 1975 (continued)

Airway to	Waypoint	Distance, nmi	M. E. A., ft.
V498	McGrath	112	6000
V440	Anchorage	187	10000

This flight was the longest one of the series requiring a fuel stop at Galena. The flight covered most of the North Slope area after crossing over the Brooks Range. Some areas did not have Navaids other than non-directional beacon (NDB) equipment. Signal coverage from OMEGA A, C, D and H was monitored with A signals displaying a dramatic increase in quality as we progressed northbound.

OMEGA Demonstration Flight May 14, 1975

Airway to	Waypoint	Distance, nmi	M. E. A., ft.
V438/456	Big Lake	26	2000
V438	Fairbanks	202	10000
V438	Big Lake	202	10000
V438/456	Anchorage	26	2000

This flight was a demonstration of OMEGA navigation for the Director, Alaskan Region, and members of his staff. Operation of low cost OMEGA and all related systems onboard were demonstrated and explained. Multiwaypoint operations and functions of the controls were examined. OMEGA signals A, C, D and H were monitored.

Dynell Flight 24 (AL Test #4) May 15, 1975

Airway to	Waypoint	Distance, nmi	M. E. A., ft.
V456	Kenai	43	2000
V456	King Salmon	204	13000
V456	Cold Bay	287	14000
	Adak	536	14000

This test provided information on OMEGA signal coverage in the Aleutian Chain between Cold Bay and Adak. A 536 nmi. course was flown over water originating at Cold Bay and terminating at Adak. The Tacan at Adak was inoperative during the test period.

Dynell # Flight 25 (AL Test #5) May 16, 1975

Airway	to	Waypoint	Distance, nmi	M. E. A., ft.
		Approx. 300 nmi NE of Adak		13000 actual
		Return to Adak		13000 actual

This flight was planned to provide a single leg that was 793 nautical miles long for navigation testing over the Bering Sea enroute to Anchorage. The flight was aborted when a problem developed in the LTN-51 reference. A turn of 180 degrees was initiated in the OMEGA test systems. Proper operation of OMEGA during the inbound leg was confirmed by Adak Radar at a distance of 50 nmi. The LTN-51 problem was resolved after landing and the test flight was reinitiated.

Dynell Flight #26 (AL Test 5A) May 16, 1975

Airway	to	Waypoint	Distance, nmi	M. E. A., ft.
		King Salmon	793	13000
V456		Kenai	204	13000
V436/456		Anchorage	43	2000

This flight, the fifth of the planned series, demonstrated operation of a low-cost OMEGA on a single-leg that was 793 nmi. flight over water. OMEGA signals A, C, D and H were monitored and/or utilized for Dynell navigation.

Dynell Flight #27 (AL Test #6) May 18, 1975

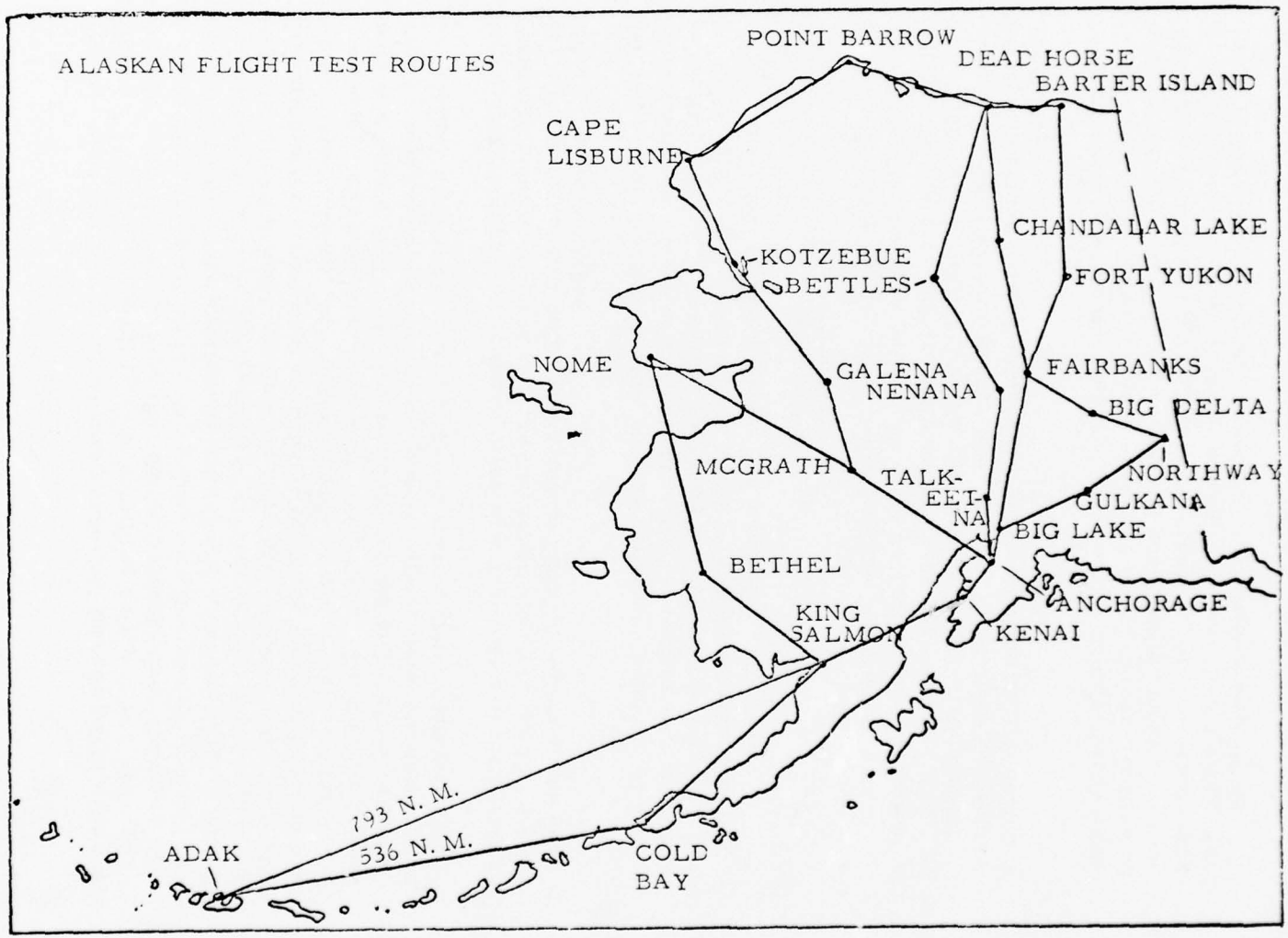
Airway	to	Waypoint	Distance, nmi	M. E. A., ft.
V438/456		Big Lake	26	2000
V438		A point approx. 100 nmi. north of Anchorage		10000

This flight was aborted approximately 100 nmi. north of Anchorage because of an unscheduled outage of the OMEGA Station at Hawaii. Rather than lose data legs enroute, while waiting for Hawaii to resume transmission, an unknown factor, the test was terminated. Prior to turning back to Anchorage, pilot confirmed that enough flight time remained on N-42 to repeat the test. Signals from Hawaii were received again prior to landing at Anchorage. Telephone contact was made with OMEGA Hawaii which confirmed that approximately 30 minutes outage had been due to component failure. The test was rescheduled next day; the planning included the alternate selection of station pairs in case that Hawaii should again prove unreliable.

Dynell Flight #28 (AL Test #6A) May 19, 1975

Airway to	Waypoint	Distance, nmi	M. E. A., ft.
V438/456	Big Lake	26	2000
V438	Fairbanks	202	10000
V347	Chandalar Lake	164	11000
A15	Dead Horse	163	10000
	Barter Island	98	10000 act.
B26	Fort Yukon	217	12000
V438	Fairbanks	127	8000
V438	Big Lake	202	10000
V438/456	Anchorage	26	2000

This test was the last of the planned series conducted in Alaska. The course was designed to traverse the remainder of the North Slope east of Prudhoe Bay and the airway roughly paralleling the Canadian border between Barter Island and Fairbanks. In addition, this route provided a repeat leg over V438 between Fairbanks and Anchorage for data comparison.


ALASKAN FLIGHT TEST ROUTES
POINT BARROW
DEAD HORSE
BARTER ISLAND
CAPE LISBURNE
CHANDALAR LAKE
KOTZEBUE
BETTLES
FORT YUKON
NOME
GALENA
NENANA
FAIRBANKS
BIG DELTA
MCGRATH
TALK-EET-NA
NORTHWAY
GULKANA
BIG LAKE
BETHEL
ANCHORAGE
KING SALMON
KENAI
193 N. M.
536 N. M.
ADAK
COLD BAY

DATA COLLECTION TECHNIQUES

The low-cost OMEGA receiver was connected interfacing it to an incremental digital tape recorder. The sampling rate was 1.3 seconds Records were synchronized to the OMEGA transmission format. A delay after the start of the "A" pulse was introduced in order to secure records of the relative amplitudes of received OMEGA signals. Unfortunately, a defective integrated circuit in the recorder prevented collection of amplitude information and LOP 1 lane counts. Other parameters were recorded successfully. These included course deviation, distance-to-go, LOP 2 lane counts, weak signal warning, to/from flag, and reset/auto zero switch functions. Despite the loss of magnetic tape signal data a permanent record of received relative signal amplitude was obtained by monitoring the detected envelope of the OMEGA receiver continuously with a strip chart recorder.

Stop action photography was employed at a 1 minute sampling rate to record present position in latitude and longitude from the INS display while the aircraft was being navigated by OMEGA steering and distance to go information.

VOR/DME position information was recorded continuously whenever signals were available at a flight inspection recording console. This data was gathered to describe coverage available with the conventional navaid systems and to maintain a check on the performance of the LTN-51 inertial navigation system as a position reference.

DATA PROCESSING TECHNIQUE

The total process for reducing and compiling the data collected during the Alaskan tests will include the following: total usage of all INS present position samples for position reference purposes, correlation of VOR/DME data with OMEGA/INS samples, correction factors to compensate for INS drift error and referral to published announcements concerning station outages and anomalies during the period of test flights.

Total processing and analysis of all information gathered in Alaska was not complete at this writing. In order to provide an approximate measure of low-cost OMEGA accuracy under good signal reception conditions in Alaska random samples of data were processed and are expressed here in terms of comparative cross-track and along-track errors. Cross-track error information was developed by first

converting a sample of CDI deflection voltage to nautical miles, offsetting the INS present position for that time frame and finally comparing the resultant position to a computed great circle track from waypoint to waypoint. Along-track error is the difference between the reading of OMEGA distance-to-go and the computer distance between the corrected present position and the destination waypoint.

DATA SAMPLES

Alaska Test #1 May 10, 1975

GMT	Waypoint	OMEGA Distance	Comparative Error nmi Cross-track	Along-track
	Anchorage			
193756		14.0	2.0R	-1.1
	Big Lake			
194756		101.0	1.2R	2.6
195256		77.0	0.7R	1.5
195756		51.0	0.8R	-0.1
200256		28.0	2.8R	0.2
	Gulkana			
201656		70.0	1.1R	-0.3
202156		47.0	0.0	1.2
202656		22.0	0.0	0.0
	Northway			
203756		93.0	0.2R	0.1
205356		9.0	1.2L	0.9
	Big Delta			
205956		53.0	2.4L	-2.9
	Fairbanks			
211756		172.0	0.4R	-0.3
212256		150.0	2.8R	2.2
212756		127.0	5.4R	2.3
213256		102.0	2.7R	0.5
213756		81.0	3.5R	3.2
214256		57.0	2.0L	3.7
214856		25.0	1.7R	1.1
215156		11.0	2.0R	1.9

Alaska Test #2 May 12, 1975

GMT	Waypoint	OMEGA Distance	Comparative Error nmi Cross-track	Along-track
	Anchorage			
194659		51.0	0.2L	1.0
194959		35.0	0.0	-0.9
195159		26.0	0.9R	0.5
	McGrath			
201159		192.0	6.0R	1.2
201559		174.0	7.0R	2.8
202559		127.0	6.7R	5.9
	Nome			
205558		221.0	0.2L	-2.1
210058		194.0	1.7R	-4.2
211058		139.0	6.8R	-9.0
211558		112.0	7.7R	-10.5
	Bethel (reset)			
214358		187.0	0.8R	6.2
214958		151.0	0.5R	-0.2
215458		121.0	0.0	-5.5
215958		93.0	6.6L	-8.8
220458		78.0	1.1R	1.1
220958		50.0	1.7R	-3.1
221558		17.0	1.8R	-8.1
	King Salmon (reset)			
223658		139.0	1.7R	-2.7
224158		115.0	2.9R	3.5
224657		92.0	2.5R	2.9
225157		69.0	2.5R	2.7
225657		44.0	4.8R	1.0
230057		22.0	2.7R	1.4

Alaska Test #3 May 13, 1975

	Anchorage			
193357		7.0	0.5L	0.3
	Talkeetna			
194557		91.0	2.0L	3.4
200057		19.0	3.3L	3.7

Alaska Test #3 (continued)

GMT	Waypoint	OMEGA Distance	Comparative Error nmi Cross-track	Along-track
	Nenana			
201557		102.0	0.9L	4.4
205757		76.0	0.3L	3.5
202557		53.0	0.1R	6.0
203157		23.0	0.5L	6.1
	Bettles			
204157		186.0	3.7L	8.5
205557		115.0	5.9L	4.9
210556		69.0	6.4L	5.7
211556		21.0	6.5L	3.4
	Dead Horse			
213556		102.0	2.7R	3.9
214556		55.0	3.7R	6.4
215356		14.0	2.0R	4.6
	Point Barrow			
220956		169.0	8.4R	-7.6
222056		114.0	8.4R	-7.6
222556		91.0	8.5R	-5.7
223556		42.0	9.0R	-4.3
224056		17.0	8.7R	-5.2
	Kotzebue (reset)			
233156		116		-1.4
233556		97		-2.0
234056		75		-0.6
225556		21		6.0
	Galena			
012450		93		6.0
013050		64	.05L	-4.7
013550		40	1.3R	0.6
014050		14	2.0R	-0.3
	McGrath			
015050		153	1.0L	-0.2
015550		134	0.13L	4.8
020550		86	1.0R	3.7
022150		9	1.6R	-0.4

Alaska Test #4 May 15, 1975

GMT	Waypoint	OMEGA Distance	Comparative Error nmi Cross-track	Along-track
	King Salmon (reset)			
201600		280.0	1.3R	5.5
205500		81.0	5.0R	0.6
	Cold Bay (reset)			
211500		515.0	0.3L	2.1
212500		461.0	1.5R	0.7
214500		350.0	0.0	-6.9
223000		120.0	1.8L	-1.5

Alaska Test #5A May 16, 1975

	Adak (reset)			
002848		793.0	0.2L	5.7
004748		706.0	0.5R	8.7
025139		73.0	5.1R	2.7
	King Salmon (reset)			
031539		156.0	2.9L	4.4
033539		57.0	0.7R	4.6
	Anchorage			
190356		11		-4.7
190656		6		-5.0
	Big Lake			
190956		200.0		-2.2
191255		183.0		-5.1
191555		168.0		-5.9
192055		142.0		-6.8
192555		116.0		-7.0
	Abort 100 mi north of Anchorage			

Alaska Test #6 May 18, 1975

Alaska Test #6A May 19, 1975

	Anchorage			
191255		9.0	1.1L	-0.8
	Big Lake			
192855		129.0	3.7L	1.3
194055		66.0	0.2L	1.3
	Fairbanks			
200155		121.0	0.9L	6.8
202055		26.0	0.1R	5.5

Alaska Test #6A (continued)

GMT	Waypoint	OMEGA Distance	Comparative Error nmi Cross-track	Along-track
	Chandalar Lake			
202555		163.0	0.6R	6.3
	Dead Horse			
211055		33.0	0.8R	-0.9
	Barter Island			
213055		150.0	0.45R	1.9
215055		46.0	3.8R	1.3
	Fort Yukon			
220555		105.0	3.5L	6.5
221555		56.0	4.4L	6.1
	Fairbanks			
223055		181.0	0.3L	5.0
224555		106.0	0.7L	5.7
225555		60.0	2.2L	8.4

DATA ANALYSIS

In general reception of signals from OMEGA stations transmitting from Norway, Hawaii, North Dakota and Japan were of high quality during VFR conditions on all flights in Alaskan airspace. The Norwegian Station was unusable from west of a line through White Horse, Canada, to another line passing south of the Yakatut-Sitka area along the Pacific Coast. Station pairs AD and AC were processed on all flights for programming Dynell Mark III navigation alternate pairs CH and CD were considered but the reliability of Japan's station had not yet been established. As expected, recordings during flight through snow showers and dense clouds were characterized by high noise levels and impaired signal reception. The effect on OMEGA Navigation depended upon the density of the snow or clouds and aircraft speed. These effects, characteristic of operation with E-plane antennas, would have been less noticeable had the tests been conducted in a test bed of performance more nearly representative of the more numerous types of general aviation aircraft flown in Alaska.

The low-cost OMEGA set performed well considering the severity of the demands made on it for navigation. Although some trip initializations were performed enroute (transfer of origin) over waypoints, the majority of test flights retained Anchorage as origin. This resulted

in long duration legs with many waypoint calibrations enroute. The manual waypoint calibrations are a source of human errors which tend to accumulate. Errors in the distance along the track appeared more likely to be long than short of actual distance and more likely to occur than errors in course deviation indication.

Dynell Flight 21 (AL Test #1)

The flight was initiated and terminated over the Anchorage Vortac with six waypoints enroute. The westward portion indicated a decrease in Norway signals but had not affected the OMEGA navigation. The flight through the clouds near Gulkana did not impede OMEGA navigation. The end point error at Anchorage was less than 1 nmi. on distance and course deviation pointer.

Dynell Flight 22 (AL Test #2)

Heavy snow showers and ATC diversions were encountered after leaving Anchorage. The distance error was 8 nmis. approaching McGrath. The error increased to 20 nmi. by the time we flew over Bethel. Several cloudy areas were encountered enroute. The course deviation indicator remained usable from Anchorage to Bethel. A reset (transfer of ORIGIN) was initiated over King Salmon for flight to Anchorage. The end point error was approximately 20 nmi. in distance and crosspointer. Some of this error is attributed to the quality of the airborne mark over King Salmon.

Dynell Flight 23 (AL Test #3)

OMEGA navigation from Anchorage to Cape Lisburne was satisfactory. Waypoint marks indicated minimal accumulated error. The leg from Lisburne to Kotzebue was unusable because of difficulty in marking Cape Lisburne. A reset was accomplished over Kotzebue for flight to Galena. The end point error was 10 nmi. and approximately 1 nmi. on crosspointer. Heavy snow showers were encountered enroute. A reset was initiated at Galena for flight to Anchorage. The end point error was less than 1 nmi. on distance and crosspointer.

Dynell Flight 24 (AL Test #4)

Heavy clouds with signal reception problems prevented OMEGA navigation between Anchorage and King Salmon. Resets were

accomplished at King Salmon and Cold Bay. The end point error at Adak was approximately 4 nmi. in distance and 2 nmi. on cross-pointer.

Dynell Flight 25 (AL Test #5)

The flight originated and terminated at Adak. OMEGA reception and navigation was excellent throughout flight. The end point error was 1 nm. in distance and crosstrack.

Dynell Flight 26 (AL Test #5A)

Severe signal drop out was experienced 190 nmi. out from Adak. Signals returned but project power was interrupted shortly after. An airborne restart over an INS checkpoint enabled OMEGA navigation for the last 270 nmi. to King Salmon. Error at this point was approximately 2 nmi. in distance and 1 mile in crosstrack.

Dynell Flight 27 (AL Test #6)

The flight was aborted 100 nmi. north of Anchorage due to an unscheduled outage of OMEGA Hawaii.

Dynell Flight 28 (AL Test #6A)

error was 10 nmi. in distance and 3 nmi. on crosstrack. Some of this error was accumulated during waypoint operations ; clouds were encountered for a short period of time. The detected signal recording also indicated two Hawaii signal problems for periods of less than four OMEGA epochs while on the North Slope.

SUMMARY

The low-cost OMEGA receiver is relatively simple to operate. Pre-flight planning by the user is necessary but not excessively time consuming. The equipment appeared to be adequate as a VFR ONLY supplemental enroute system when operated in the CV-880 test bed. It is likely that signal interference, due to penetration of ice clouds and snow showers when using an E-plane antenna, would be substantially decreased or avoided during flights at lower airspeeds typical of light aircraft. However, the antenna seems to remain the weak link in low-cost OMEGA navigation avionics.

Careful placement on the aircraft of new types of E-plane plates or noise cancelling antenna units may be expected to help solve this problem.

OMEGA signal reception from Norway, Hawaii, North Dakota and Japan provided adequate coverage of Alaska with respect to geometry. For all practical purposes the world-wide OMEGA system was found to be complete in Alaska since there were several station pairs available for primary and alternate use. Station outages appear to be a deminishing problem based on these and previous OMEGA test efforts. Signals received during all test flights were usable except after penetrating dense clouds or when a station outage occurred. The test series flown can only be considered a minimal probe in assessing the characteristics and reliability of OMEGA signals. Continuous monitoring at various points in Alaska would provide more thorough and complete information regarding OMEGA propogation and the natural phenomena which affect it.

Mark III OMEGA Airborne Navigation System Specifications

Dimensions	
Receiver Unit (DR-30)	6"W x 3"H x 13"D
Indicator Unit (DR-30)	3.5"Dia. x 5"D
Weight	
Receiver Unit	4.5 lbs.
Indicator Unit	1.5 lbs.
Prime Power (total)	+12 Vdc, 1A
Operating Temperature	-20°C to +60°C
Maximum Aircraft Speed	Approximately 400 knots
Navigation Range	
Single Leg Flight	Approximately 1000 nmi.
Multiwaypoint Flight	Unlimited
Navigation Readouts	
CDI Meter	Sensitivity nominally 4 files full scale
Miles to go	3 digit display to 999 nmi.
To/from Flag	Indicates designation arrival
On Ground Setup Time	Approx. 2 minutes with destination number predetermined
Antenna Coupler	Provided as required

QUESTION AND ANSWER PERIOD

MR. SAKRAN:

Charley Sakran, Navy.

Could you describe briefly how the problem of diurnal propagation corrections is accounted for in this set?

MR. MOORE:

I can be very brief about that. There is no diurnal compensation built into this set. I neglected to mention that. It is mentioned in the paper, though. The only method prescribed by the vendor to compensate for diurnals expected enroute would be to offset your preliminary computations to account for the changes expected during a flight. This would produce a flight path that would be slightly non-linear, but would reduce your end point error.

MR. SAKRAN:

Thank you. Could you also describe how you decided what an adequate signal was during the flight? What criteria was used?

MR. MOORE:

The equipment had a weak signal indicator, and we were monitoring with some Tracor equipment, doing some tracking of the pair selected, and the indications on the Omega receiver would correspond to slewing or would break track. The distance to go would freeze. This induced the 20 mile error. I believe that occurred in two snow cloud periods over a period of quite a bit of time. The end point error was 20 miles, or approximately two lanes. The correspondent did not seem to be affected as much. I believe it just goes dead when it loses signal, and you get a red light telling you you don't have any more signals left.

MR. SAKRAN:

Was there any indication of interfering noise, other than precipitation static, specifically onboard-aircraft-generated noise with the E-Field antenna?

MR. MOORE:

No, sir. Our problem appeared to be mainly a charge buildup. There were noticeable increases in noise level for very short periods of time after takeoff, which did not affect Omega navigation. The effects of cloud penetration were obvious. They appeared and disappeared when the visibility decreased and increased. I didn't notice any problems with onboard equipment. The equipment -- by the way, I didn't mention it -- is a 12-volt system and draws about one ampere of power, so I didn't notice any interference on the aircraft.

MR. BARSZCZEWSKI

Barszczewski, National Research Council.

In Canada we have some data on operation in the eartern part of Arctic and Omega. We have been operating there for the last five years, and it is just not there. In particular, on low level. If you go below 5000 feet with Greenland completely masking Norway, we get Foresport, that is about the only thing we get there.

Do you have any data on signal strength versus altitude?

MR. MOORE:

No, sir. All of the flights in Alaska were flown at the minimum enroute altitudes for the benefit of the type of aircraft we were testing for, and one of the ideas of flying at low levels was to get into the depressions in Alaska, for instance between Norway and Fairbanks there is quite a valley of depression area. The peaks to the right and left were higher than the altitude of the aircraft. I have no information to correlate altitude with signal strength at this time.

I can say that a subsequent flight flown in September at jet speeds in the same aircraft using an automatic Omega set at altitudes far above the minimum enroute altitudes produced approximately the same signal coverage results.

DR. REDER:

I would like to make two comments; in fact, part of it the gentleman already answered, and that is the effect of Greenland, as we all know, is that it cuts off Omega signals practically completely. That is how he lost it on the way

down. But, as far as Alaska is concerned, you don't have any problems, and there is another advantage for Alaska and that is that the diurnal shift of most of the Omega signals being used there is relatively small. In summer you have almost none; in winter you have almost none; and the paths from Hawaii and Japan are short. So this is one advantage of Alaska, probably the only one.

Oh, excuse me. I forgot the oil.

MR. MOORE:

All of the test flights flown in Alaska were started at approximately 1000 local time. That is GMT minus 9, so I believe the diurnal shift effects were minimal at that time.

DR. REDER:

On the precipitation static, if one could use ferite loop sticks, or loops anyway, that will drastically reduce precipitation noise.

MR. BARSZCZEWSKI:

Regarding your loops, now there is a set built by Canadian Marconi, and they started to operate with the loop. What happens, you pick up tremendous noise from the aircraft engines, from spark plugs, and so on, and so they went to the E-antenna just for that reason. So you can have one or the other, but you can't have them both.

DR. REDER:

Well, maybe the airplanes should be changed. What altitude did you fly?

MR. MOORE:

The minimum altitudes ranged from 6,000 feet on the north slope to 13,000 feet east of Anchorage.

INFLIGHT WORLDWIDE VLF EXPERIENCE USING GLOBAL NAVIGATION GNS-500

William R. Tymczyszyn
Global Navigation Incorporated
Torrance, California

ABSTRACT

Throughout five years and thousands of hours of operation, many of the advantages and disadvantages originally envisioned for VLF navigation were borne out by practical experience with commercially available equipment utilizing both VLF Communications and OMEGA Navigation stations. Global Navigation Incorporated proved it possible to design, manufacture and market reliable low-cost equipment which is low in weight and power input requirements. The equipment exhibits excellent long term accuracy with reception unaffected by altitude or terrain. Expected disadvantages to VLF navigation have been experienced as well, and can be grouped into five major areas: reception, signal ambiguity, propagation anomalies, station network geometry, and transmitter reliability. This paper remarks on the positive aspects and details the gravity of the negative aspects as they have proven inflight to be a problem, along with methods used to minimize their detrimental effects. Prospects for truly redundant worldwide signal coverage utilizing either the present VLF Communications Network or the proposed fully implemented OMEGA Navigation chain are analyzed independently, based on both actual experience and computer generated predictions. It is suggested that a combination VLF Comm/OMEGA system is one way to achieve the degree of coverage required.

INTRODUCTION

In 1970, flight testing began on what was to become the first commercially available navigation system based on a worldwide VLF Communications network. This prototype system proved the feasibility of such a base for navigation, and was developed into the Model GNS-200 by

PRECEDING PAGE BLANK-NOT FILMED

Global Navigation Incorporated. The GNS-200 gained acceptance in many parts of the world but was hampered by the need for increased capability and a computer to ease pilot operating workload. Nevertheless, the operational experience gained in navigating on the VLF Comm signals and OMEGA unique frequencies with this system proved invaluable in developing the next generation system, GNS-500. During and after this time, hundreds of thousands of flight hours have shed more light on the problems which must be dealt with in the development of any VLF Comm or OMEGA navigation system. This paper begins with the GNS-500, as much has been published about the Model 200.

GNS-500 DESCRIPTION

Theory of Operation

The GNS-500 derives navigation information from VLF signals by a phase measurement technique. As all the Comm signals and OMEGA unique frequencies are transmitted on different frequencies, receiver boards must be provided for each of the stations to be received, but decommutation is not necessary. That is, if only these two types of inputs are used, the fact that they are all on different frequencies automatically tells the computer which station just sent which signal. These various frequencies are measured simultaneously and then converted to a common frequency for comparison and processing. As there are so many frequencies being received, position fixing in the OMEGA sense is impossible because signal processing ratios become too complicated.

The GNS-500 is a Rho-Rho system rather than hyperbolic, meaning that lines of constant phase are circles instead of hyperbolas. Each receiver must be initialized and calibrated at the time it first phase locks with a reliable signal. Five times each second the computer measures the phase angle and calculates the distance to each station (whether received or not). These changes in phase angle are accumulated and converted to a change in latitude and longitude from the last computed position. The accuracy of this fix is based solely on the accuracy of the position inserted by the pilot before flight, and any error accumulation after that time.

Use of Frequency Standards

The phase of each received signal is compared with a stable frequency reference carried in the GNS-500. If this reference is of sufficient stability, navigation can be conducted with only two stations being received (assuming a reasonable angle at the receiver position). If the standard is not stable enough for the degree of accuracy required, a third station is necessary to navigate, it in effect acting to stabilize the onboard standard.

The GNS-500 includes both a highly stable Rubidium Atomic Frequency Standard (about one part in ten to the tenth) and a separate quartz crystal local oscillator. Under normal operation, the Efratom FRK Rubidium Standard is used solely to stabilize the less accurate local oscillator and thus allow for navigation on as few as two received signals. This design philosophy of including two types of standards was chosen to allow for navigation before the Atomic Standard has warmed up, or to allow navigation to continue in the Rho-Rho mode despite a failure of the Atomic Frequency reference, provided three suitable signals are present in these cases. This scheme takes maximum benefit from the Rubidium Standard in areas where good navigation depends on it, and in effect releases the system from this dependence when enough signals are otherwise available.

Equipment Description

The GNS-500 is made up of four main boxes. These include:

1. The Control Display Unit (Figure 1) includes the numeric displays, data input keyboard, data selector switch, power and operating mode controls. Physical dimensions of this unit were made to conform with Arinc specifications, and operation of the unit was designed to closely match that of popular inertial navigation systems.
2. The Receiver Computer Unit (RCU) is the heart of the system, containing all of the VLF Comm and OMEGA receivers, the entire microprocessor and memory, boards for interfacing inputs from outside sources and formatting outputs to the aircraft into standard forms, the quartz crystal local oscillator, and the system power supply. The RCU comprises a 3/4 ATR

short box mating with standard Arinc rack and connector.

3. The Optional Equipment Unit (OEU) contains the Rubidium Atomic Frequency Standard and a battery pack to sustain the entire system in the event of short power input loss.

4. The Antenna (Figure 2) is a high speed blade design E-field type which includes a preamplifier in the base. It was chosen as the standard system antenna in lieu of a loop because of higher gain and ease of determining a location for mounting. Although a loop antenna is preferable in conditions producing precipitation static, it is more susceptible to aircraft-generated disturbances, many time necessitating a skin-mapping of the aircraft before installation. In some cases an ADF sense antenna has been used successfully with the GNS-500 through a signal splitter.

The entire system described above weighs 36 pounds and requires 3.7 amps of 28 volts DC, with no requirement for AC power. It is certified for operation to 45,000 feet unpressurized, through a normal operating temperature range of -54 to +55 degrees Centigrade, and for installation in an explosive environment.

VLF STATIONS AND THEIR CHARACTERISTICS

VLF Communications Stations - General

Table 1 - VLF Communications Stations

Ident	Location	Abbrev. on Fig. 3	Frequency kHz
NSS	Annapolis, Maryland	A	21.4
NAA	Cutler, Maine	M	17.8
NBA	Balboa, Panama Canal Zone	P	24.0
NLK	Jim Creek, Washington	W	18.6
NPM	Lualualei, Hawaii	L	23.4
NWC	Northwest Cape, Australia	S	22.3
GBR	Rugby, England	G	16.0
NDT	Yosami, Japan	J	17.4
JXN	Helgeland, Norway	O	16.4
GQD	Anthorne, England	R	19.0

Although the primary mission of the VLF Comm stations is communication, the signals which they radiate are well-suited for navigation as well. Operating between 16 and 24 kHz, they are phase stable to one part in ten to the twelfth or better, and radiate up to 1000 kilowatts of power, many times that of the OMEGA signals. Communication is carried out on these frequencies by frequency shift keying with the transmitter "on frequency" about 50% of the time. The combination of this high density duty cycle and tremendous radiated power provides extremely long reception range and a strong signal-to-noise ratio at the receiver. Even in high-speed maneuvering aircraft, the receiver need not be rate-aided, as the signals received from the Comm stations are effectively continuous.

With all the apparent advantages to navigation on Comm signals come some disadvantages, too. One of the most evident is the weekly maintenance schedule which puts each station off the air for about four to six hours per week. Two of the stations shut down daily (Table 2).

Table 2 - VLF Station Maintenance Schedule

Ident	Day	Time (GMT)
NAA (M)	Monday	1400-1800
NPM (L)	Monday-Tuesday	1700-0200
GBR (G)	Tuesday	1000-1400
NBA (P)	Tuesday	1200-1800
NWC (S)	Wednesday	0000-0400
NSS (A)	Wednesday	1300-1900
NLK (W)	Thursday (1st and 3rd of month)	1700-2200
NDT (J)	Daily	2300-0750
JXN (O)	Daily	0400-0500
		1000-1100
		1600-1700

In addition to scheduled maintenance, some of the Comm stations shut down or shift off frequency for a few minutes every other hour just prior to the even GMT hours (e.g., 0954Z, 1557Z, etc.). Almost all of the Comm stations do this within ten minutes prior to midnight GMT.

OMEGA Navigation Stations - General

One of the most comforting aspects of the OMEGA Network is the peace of mind which comes from knowing one is using stations dedicated to navigation. Although they were dreadfully slow in coming on the air, there are five transmitting today with reasonable regularity.

OMEGA stations transmit 10 kilowatts of power when fully commissioned. Presumably, this level is kept low to limit transmission distance and avoid confusing a receiver which might otherwise pick up the same station from several pathways around the globe.

OMEGA is a time-shared phase system using three different frequencies in a commutation pattern to fix position, and their processing ratios to expand positional ambiguity. It is not possible to utilize any of the three regular navigation frequencies in a pure phase measurement machine such as the GNS-500 without commutation of the signals to figure out which station just sent that last burst of signal. For this reason, the only part of the OMEGA signals which have previously been utilized have been the unique frequencies transmitted for three or five segments out of eight segments from Hawaii, North Dakota, and formerly from Trinidad and Norway. (The newly released Model GNS-500A does commutate the OMEGA navigation signals before phase comparison.)

In our experience using unique frequencies, transmission for three segments of every eight segments seems to be about the minimum acceptable duty cycle density for a non-rate-aided receiver doing phase measurement in a high speed aircraft. The remaining empty segments can be thought of as pure noise during which time the receiver must calculate a phase angle in anticipation of the next signal burst. This tracking task is aggravated in a noisy environment such as precipitation static conditions so that the first stations to drop out are usually the OMEGAs, before the higher power and longer duty cycle Comm stations.

Nevertheless, the capability of utilizing stations which have no regularly scheduled maintenance periods or bi-hourly outages would seem to be a nice supplement to a pure VLF Comm system, if only to sustain navigation during these outage periods in areas where necessary. Unfortunately, even the fully commissioned OMEGA stations must be

maintained. This is exemplified by the one month outages for antenna maintenance of both North Dakota and Japan beginning on 2 September and 15 October, respectively. Fortunately, these periods did not overlap.

VLF Comm and OMEGA Signal Reliability

A study was done by the Collins Radio Company to determine signal availability and signal failure duration for both the VLF Comm and OMEGA stations. Data was compiled from all the "Daily Phase Values and Time Differences" bulletins (TSA-4) issued by the U.S. Naval Observatory during one year, beginning September, 1973. The analysis was directed at answering the following two significant questions:

1. What is the probability of having usable transmitted signals for flights of various time duration?
2. When a station fails, how long and with what probability will it stay off the air?

Results of the analysis of actual VLF Comm and OMEGA operating data are summarized below:

Table 3
Probability of Signal Availability (percent)

Flight Time (hours)	2	4	6	8	10
VLF Comm	98.9	98.0	97.2	96.3	95.5
OMEGA	98.2	96.6	95.2	93.8	92.5

Table 4
Probability of Failure Duration (percent)

Failure Duration (minutes)	2	5	10	60
VLF Comm	91.9	75.8	55.9	6.4
OMEGA	92.1	36.3	17.4	4.5

Table 3 shows that 98.0 percent of all four hour long flights will be completed with complete VLF Comm coverage. On the remaining 2.0 percent of four hour flights, when signal outage does occur, 75.8 percent of the time it will last for five minutes or more. Similarly, for OMEGA navigation, signals were available for 96.6 percent of all four hour flights, with 36.3 percent of the outages

lasting five minutes or more. (This is the interpretation made by Collins of their data, but it is not clear what minimum number of signals are required by the represented VLF Comm or OMEGA equipment to retain defined "signal availability".)

VLF NAVIGATION CHARACTERISTICS AND PHENOMENA

To produce a truly useful system, OMEGA and Comm navigation system designers must understand and cope with characteristics sometimes peculiar to VLF navigation alone. Those noted inflight to be significant include the following:

A. Antipodal or multipath susceptibility.
B. Signal ambiguities and operation without signals - dead reckoning.
C. Reception geometry dependence.
D. Diurnal phase shift error.
E. Sources of signal attenuation.
F. VLF Comm and OMEGA signal coverage.

Antipodal or Multipath Susceptibility

An example of carrying a good thing too far is the problem which exists when VLF signals reach around the world from different directions. Propagational antipoles are created which are areas of confusion from the receivers' point of view. Figure 4 depicts regions where receivers have been adversely affected by this phenomenon, and the particular Comm stations involved. It has also been noted that these areas change position between night and day. Other areas probably exist in addition, but have not been confirmed in the field. The GNS-500 protects itself from this occurrence by disregarding the position determination from a station which is separated from the receiver by a given maximum distance.

Areas can also exist far from the geographic antipoles where multipath signals will be received under certain conditions. The inherent ability of the receiver to determine the dominant mode plays a part in safeguarding against a detrimental effect on the system. When this safeguard breaks down and an erroneous phase is locked by the receiver, the computer must become involved in ferreting out the guilty signal. As multipath signals normally reveal themselves in the receiver as very high rates of

change of position, the GNS-500 computer disregards the input from any station which claims the aircraft has an unreasonable groundspeed, i.e., over a given maximum limit.

Signal Ambiguity and Operation Without Signals - Dead Reckoning

Signal ambiguity is present in a radio frequency carrier primarily because one signal cycle is identical to the next. However, positional ambiguity is resolved up to a 72 mile lane size with three frequency OMEGA by processing the ratios between these frequencies. Indeed, one of the most attractive capabilities of the OMEGA system is its ability to reposition itself in a lane following a signal outage, provided the aircraft remains within the lane. Severe ambiguities occurring in a multi-frequency phase system make minimum signal retention of prime importance to designers. Nevertheless, signal loss can occur (the GNS-500 requires a minimum of two suitable inputs), and position must then depend on a sophisticated form of dead reckoning in order to reacquire a correct position after the return of signals.

Dead reckoning in the GNS-500 employs magnetic heading from the aircraft compass and True Airspeed input either from an air data system or manually inserted by the pilot on the CDU keyboard. These are used together with the last computed wind direction and speed to navigate during periods of signal loss. As these periods are usually of short duration and the dead reckoning reasonable, error accumulated is normally quite acceptable.

There are two conditions most likely to cause dead reckoning. They are heavy precipitation static where the signals are lost in noise, and operation in areas of marginal VLF Comm or OMEGA coverage, usually aggravated by poor station geometry and transmitter shutdowns.

Reception Geometry Dependence

The number of stations received by a VLF Comm or OMEGA navigation system is of importance only if the direction of reception is considered as well. From the Saudi Arabian peninsula, for example, the Comm stations in Great Britain (2), Norway, Maine, Annapolis, Panama, and Washington are all received within a 23 degree angle at the

receiver position. This multitude of stations is little better than two transmitters forming the same angle, and the result (assuming there are no other inputs) is minimum acceptable navigation. Figure 5 shows a similar occurrence with OMEGA stations where the area included within the 22.5 degree angle in the Southeast United States is unnavigable with an OMEGA system requiring three stations, even when Japan, North Dakota, and Hawaii are on the air. For OMEGA systems capable of Rho-Rho navigation on two stations, this area is unnavigable with only Japan and North Dakota transmitting.

Diurnal Phase Shift Error

VLF signals are propagated in a waveguide formed by the earth and the ionosphere, so changes in the earth or ionosphere will result in changes in signal parameters such as phase velocity. Diurnal phase shift is the most pronounced variation affecting the signals, being caused by the rise and fall of the reflecting layer. Because this shift is essentially repeatable and predictable, corrections are applied by an analytical model in the computer. The pilot inserts Greenwich Mean Time and the date on the keyboard which are converted to the sun zenith angle, to continuously compute the light and dark portion of the path between the receivers and each station.

Correction in OMEGA systems is more critical than VLF Comm systems because of the lower frequencies used by OMEGA. An error shift of one cycle at 10 kHz involves twice the distance as one cycle at 20 kHz. This frequency dependence is true also of sudden ionic disturbances (SIDS) and other unpredictable changes.

Sources of Signal Attenuation

The usable range of VLF Comm and OMEGA signals is affected by physical factors. A signal will have greater range when traveling over salt water, in an Easterly direction, or on a pathway in darkness. Attenuation of signals occurs over large land masses or frozen areas, in a Westerly direction, and on daylight pathways.

One of the most striking sources of signal attenuation is the island of Greenland. This mass of nonconducting fresh water ice which exceeds 10,000 feet of thickness in the center attenuates all VLF signals crossing it, creating

shadows on the opposite side from the transmitter. These shadows have surprisingly well-defined borders as shown in Figure 6 for the Comm stations in Great Britain, Japan, and Australia.

VLF Comm and OMEGA Signal Coverage

Actual results of Comm station usability measured and flown around the world over the last six years are shown in Figure 7. Station symbols depicted in capital letters over an area are considered prime navigable stations. Those shown in small case are weaker secondary stations which are of benefit at night or of limited use midday. It should be noted that at this time (November, 1975) Hawaii Comm (L) is off the air for maintenance and Annapolis (A) is transmitting on a special format, removing them from the picture at present. (A modified Annapolis receiver has been made to track the minimal shift keying format now being experimented with, but is not at present in the field.)

Figure 7 shows, for most areas of the world, more than minimum Comm coverage even during station maintenance. In fact, this has been the experience of the GNS-200 and GNS-500 and one reason for their commercial success. It has been proven beyond a doubt that navigation is easier on signals which are available, although not dedicated to navigation, than with stations not yet commissioned.

"Omega 10.2 kHz Signal Coverage: Local Noon", Figure 8, comes from a report entitled "OMEGA Signal Coverage Prediction" written by representatives of the Analytic Sciences Corporation of Reading, Massachusetts, and the OMEGA Navigation System Operations Detail of the U.S. Coast Guard. The figure is a composite diagram on which all the -20 dB signal-to-noise ratio contours are plotted for the planned full OMEGA network.

Several assumptions were made. OMEGA coverage was defined to exist where the signal-to-noise ratio is -20 dB or better in a 100 Hz bandwidth. Under these conditions, a well designed receiver is capable of making an accurate phase measurement, and in fact, the experience gained by OMEGA tracking of the GNS-500A affirms many of these contours. Each coverage limit line is labeled by the appropriate station with an arrow in the direction of the usable signal.

Figure 9 depicts world areas to expect three OMEGA station reception, this diagram being simply a compilation of the information contained in Figure 8. As three stations is the minimum number of signals that some OMEGA systems are designed to operate with, and this study has assumed that all eight of the stations are operating, it is seen that areas of the world will be lacking if any one station is shut down.

The next figure shows areas to expect two OMEGA station reception with all eight at full power. These will be areas of minimum acceptable navigation for those systems capable of Rho-Rho fixing from only two stations, and will be areas of dead reckoning for systems requiring three stations. Given the assumptions that Liberia and La Reunion come up as scheduled, that the South Pacific station finds a home and begins transmitting, that none of the eight stations ever leave the air for maintenance as have North Dakota and Japan recently, then Figures 9 and 10 should be the best OMEGA coverage situation that the world should expect.

CONCLUSIONS

The U.S. Navy and Department of Defense seem to lack the desire to accept a dual mission for their VLF Comm stations to include navigation. The signals are on the air as they have been for years, they are high powered, phase stable, and suitable for navigation. The DOD has at least stated recently that they do not intend to shut down the Comm stations, but offers no blessing to users or the FAA. Even so, the free availability of such signals should be considered a valuable national resource, and treated as such.

Navigation on VLF Comm or OMEGA has advantages and disadvantages. Figure 11 shows the VLF Comm signals usable in areas of two and three station OMEGA reception. The OMEGA Network is just what the doctor ordered for supplementing VLF Comm navigation, or it can be said that the Comm stations can provide help where the OMEGA is lacking. There are many methods open to system designers, many ways to place emphasis. Through the experiences gained in all types of VLF navigation with the GNS-200 and GNS-500, the Model GNS-500A has evolved as Global Navigation's answer, and the first VLF system to receive up to sixteen stations.


33 48.0 N 118 20.0 W
LEG CHG
01 1
WPT DEF
VLF DR
FR TO
DIS/ETE
DA/GS
BRG/VAR
TK/TKD
WPT
XTK/SX
POS
/IND
GMT/DATE
TAS
OFF
M
A
C
ENTER
DIM
L 1
N 2
R 3
W 4
5
E 6
7
S 8
9
HOLD
0
BACK
VLF·OMEGA
GLOBAL NAVIGATION INC.

Figure 1

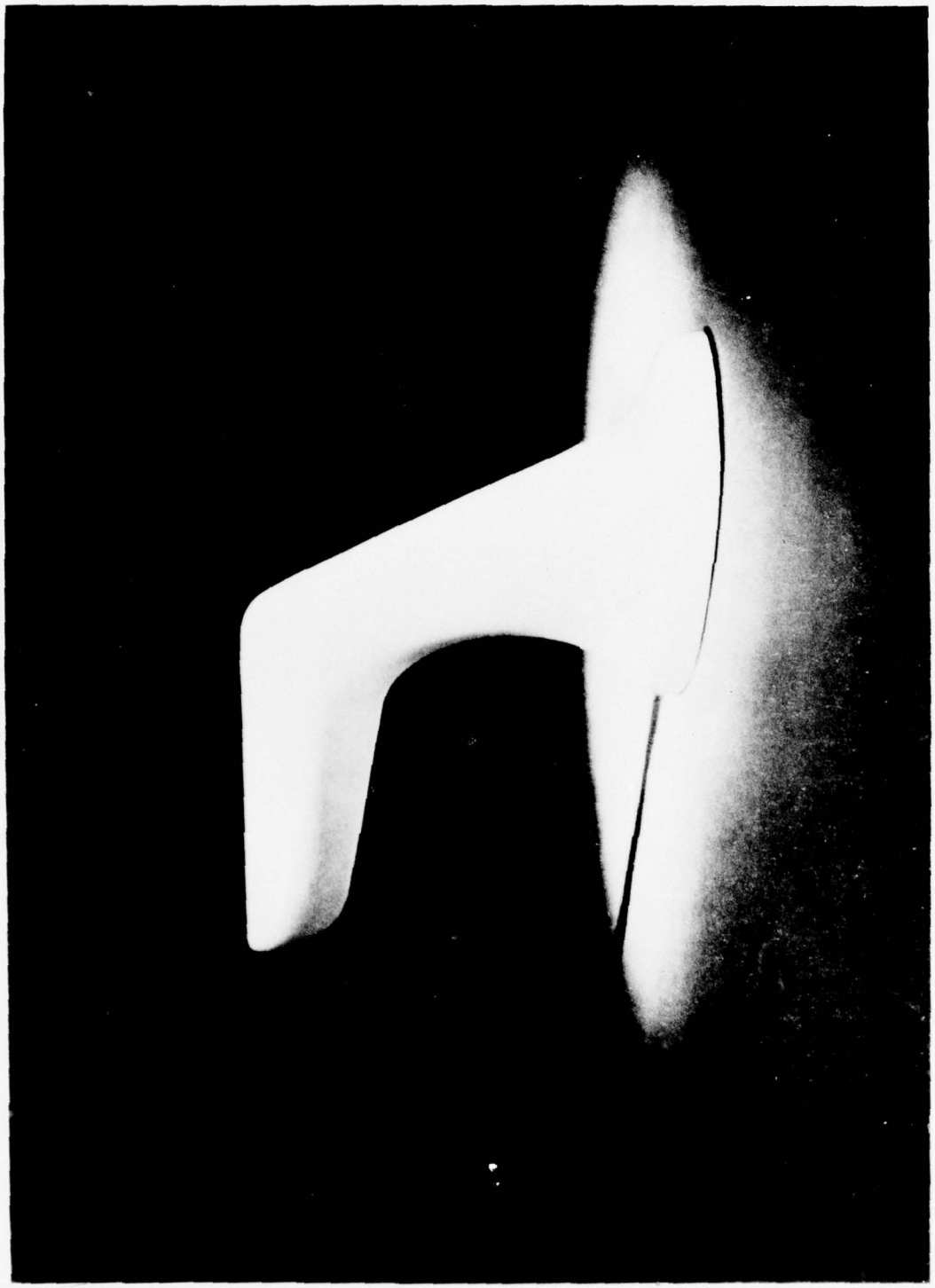


Figure 2

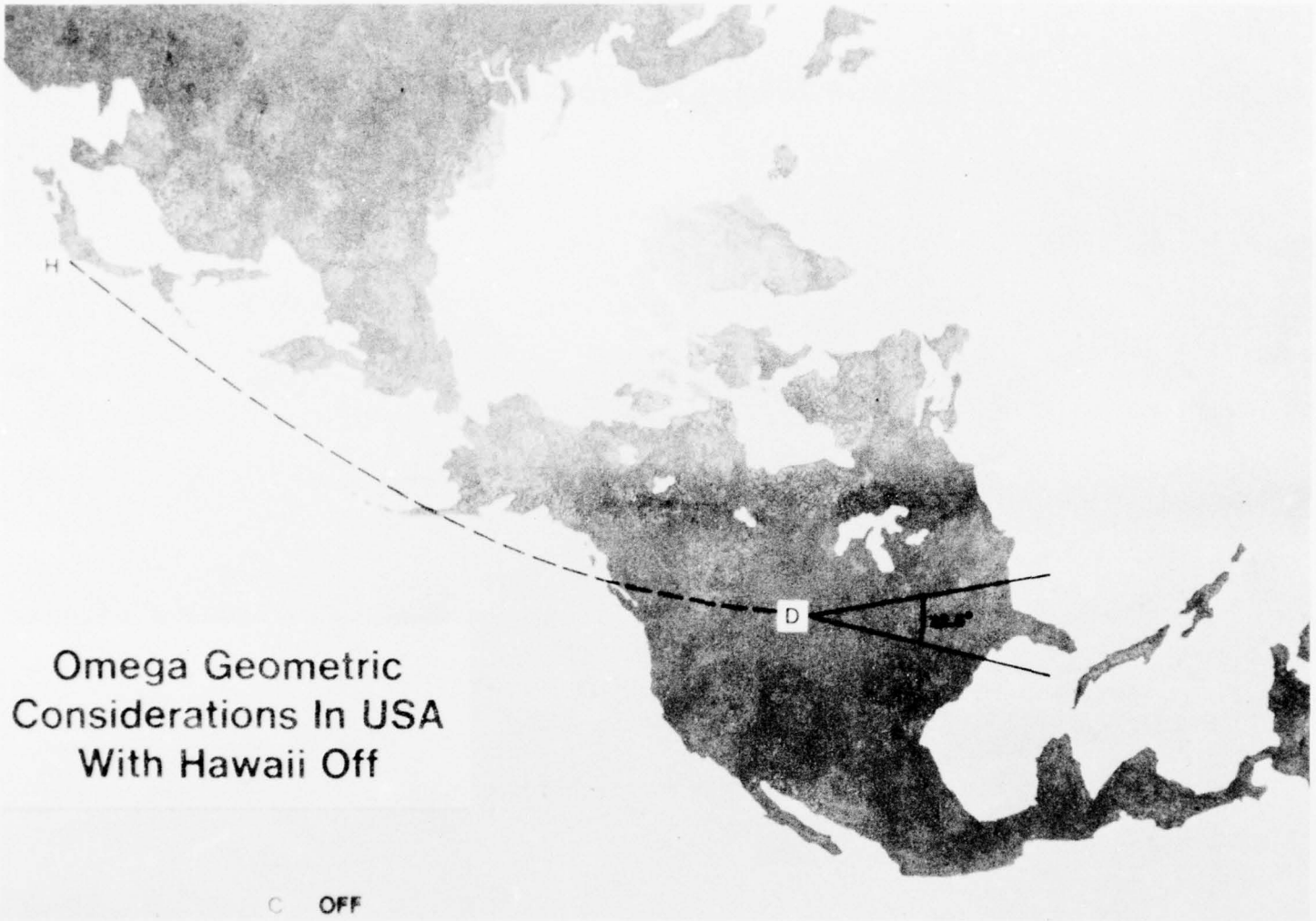


Worldwide VLF Comm/Omega Network Used by GNS-500A

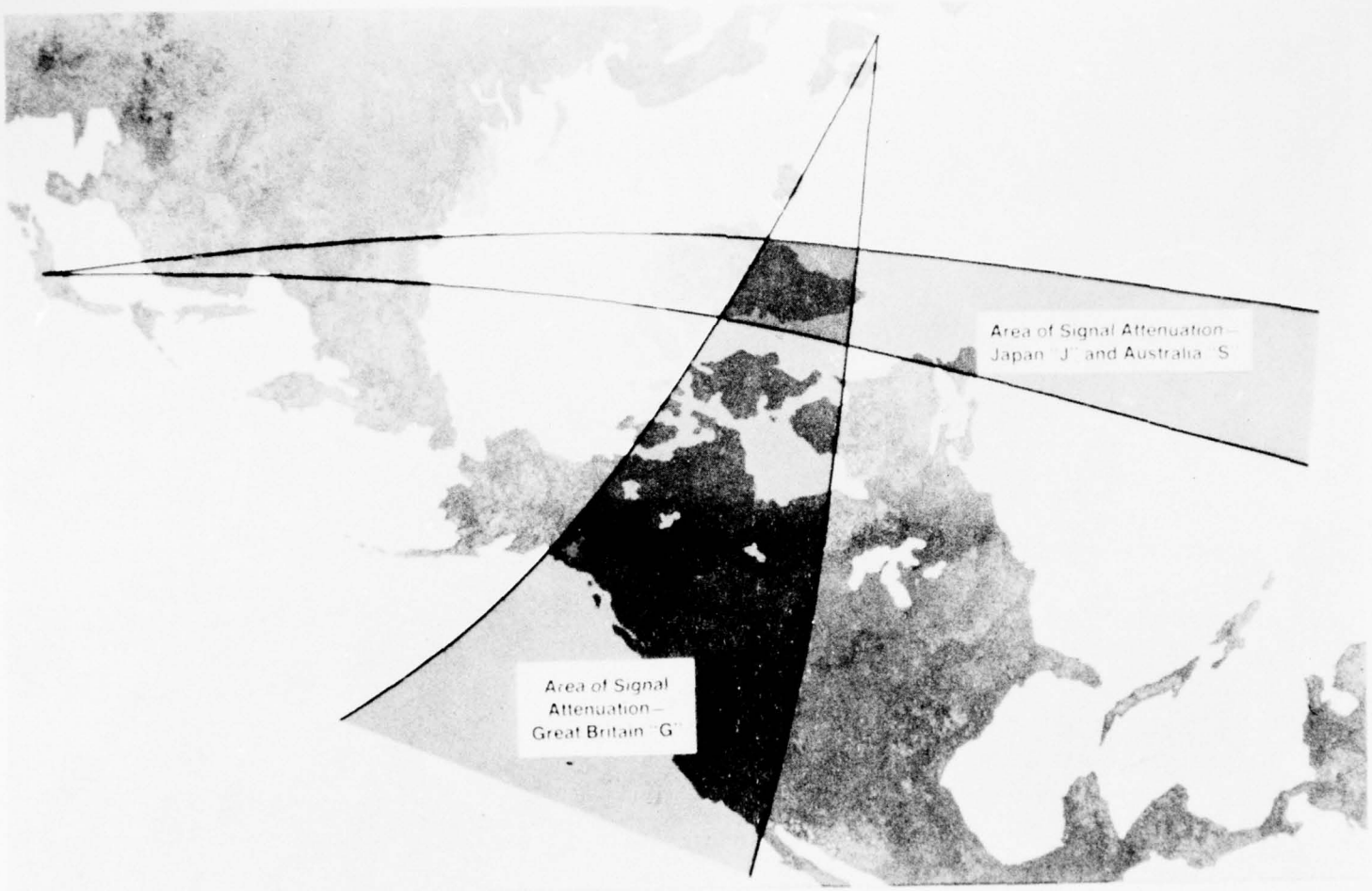
Figure 3



Areas Where Antipodal Or Multipath Activity
Has Been Experienced Inflight

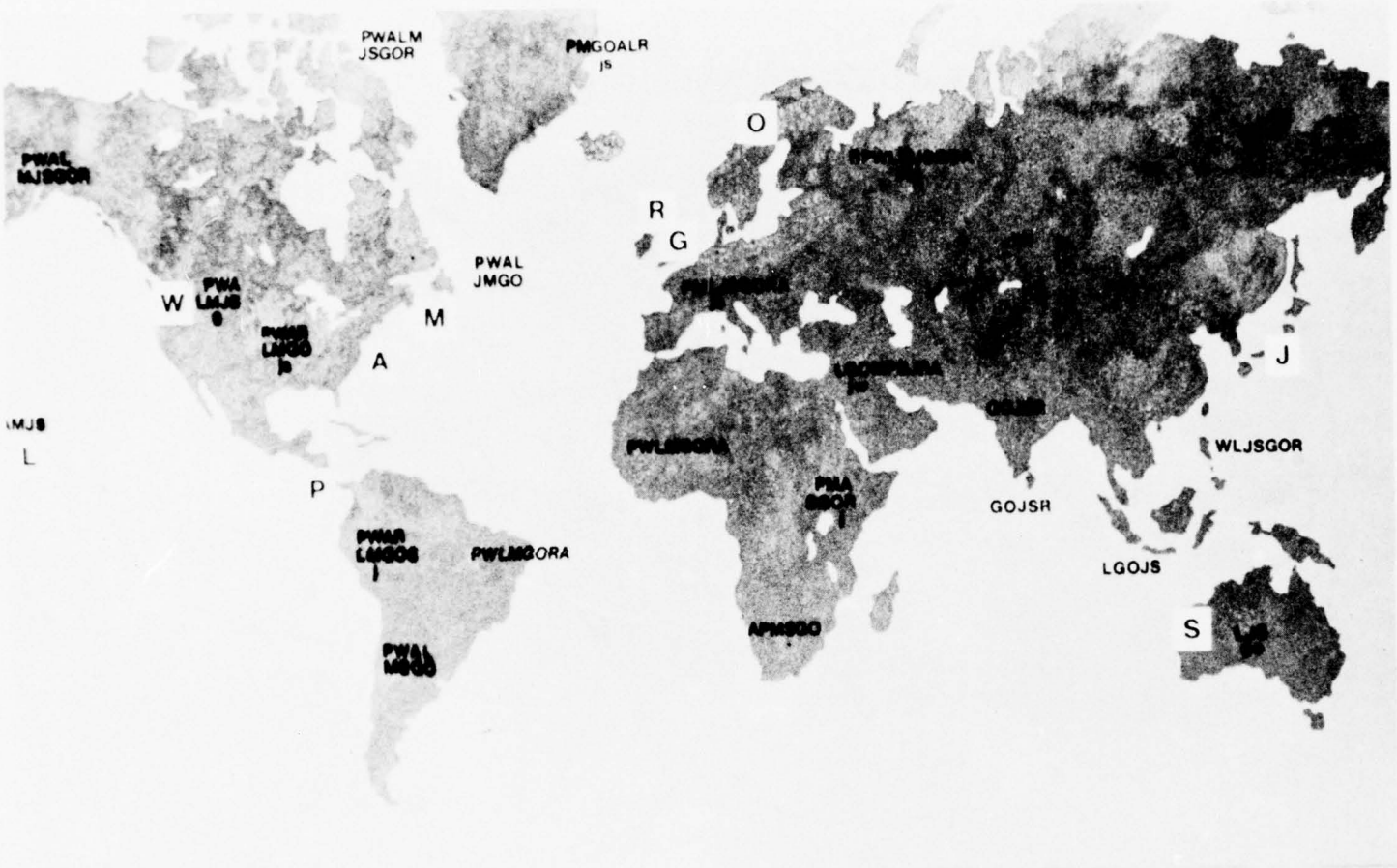


Omega Geometric
Considerations In USA
With Hawaii Off



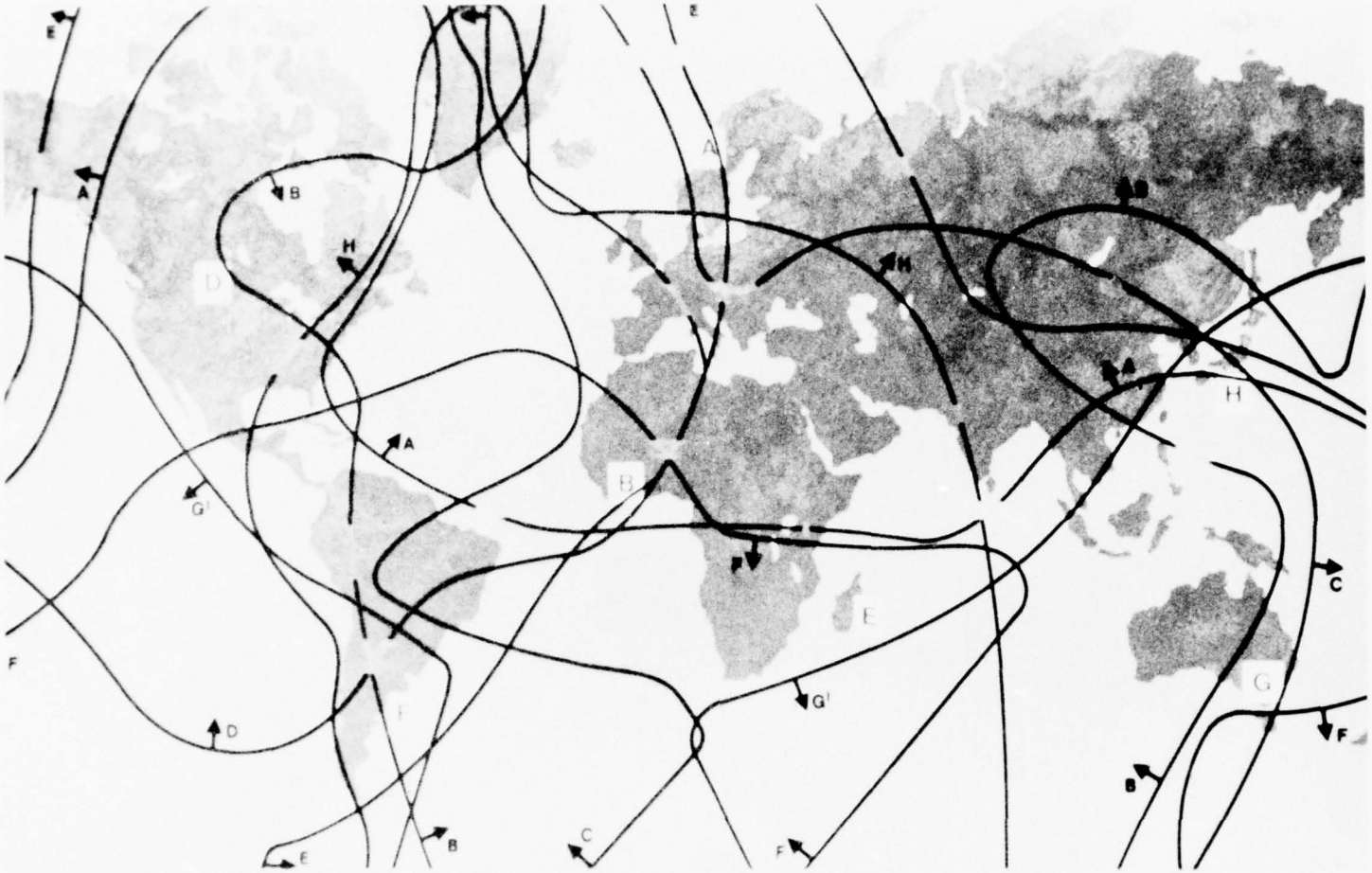
Effect Of Greenland On VLF Propagation

Figure 6



Primary Secondary VLF Comm Usability

Figure 7



Omega 10.2 KHz Signal Coverage Local Noon

Figure 8



World Areas To Expect Three Omega Stations At Local Noon
Assuming All Eight Operating

Figure 9



World Areas To Expect Two Omega Stations At Local Noon
Assuming All Eight Operating

Figure 10

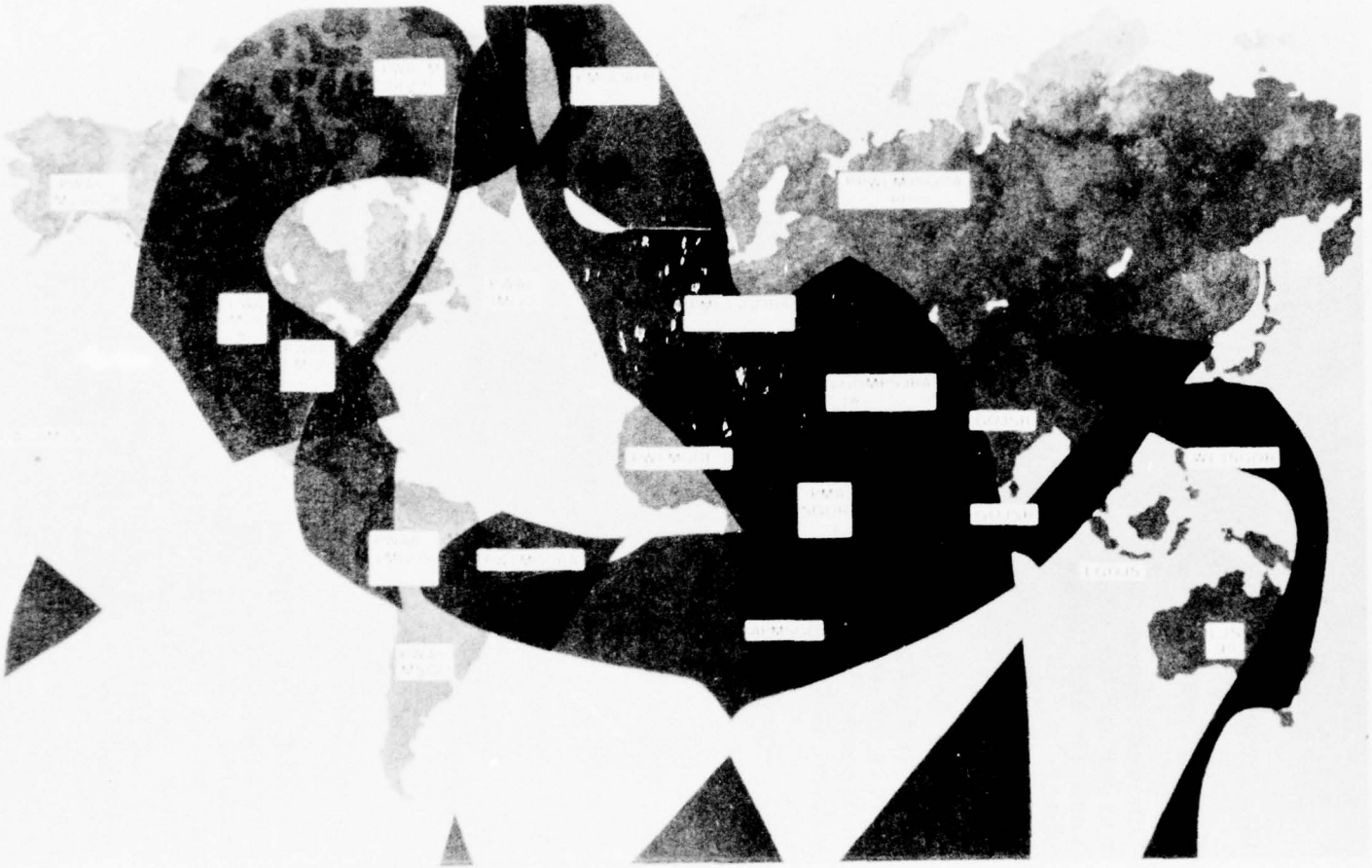


Figure 11

QUESTION AND ANSWER PERIOD

MR. STONESTREET:

Bill Stonestreet, Draper Laboratory.

You mentioned that you have a commutator in the Omega receiver or in your VLF receiver, that commutates or synchronizes to the Omega transmission. Would you care to expand on that?

MR. TYMCZYSZYN:

What we do is, we use a 10.2 frequency, and it takes the computer about three minutes in the beginning after you switch it on to commutate if you are receiving at least two stations, including 10.2. Then it uses the 13.6 phase angles actually to navigate with.

MR. STONESTREET:

Is it an amplitude correlation or is it done in phase?

MR. TYMCZYSZYN:

I am sorry. I can't answer that. I don't know.

MR. STONESTREET:

Okay, fine. I would also like to say that I like your test pattern.

MR. BARSZCZEWSKI:

Barszczewski, National Research Council.

I would just like to make a comment. First of all, all VLF Omega navigation systems are only 99.5 or whatever proof, because you have other anomalies like sudden disturbances and polar cap absorption, whatever gives, that makes sometimes the data quite unreliable, and as far as the coverage, I think there is some excellent publication by NRL quite recently by a gentleman named Houser, that gives excellent predictions: signal-to-noise ratio and signal strength for VLF stations worldwide, and this particular thing is very useful to me. We have spotchecked a couple of times, and it verifies very nicely.

MR. TYMCZYSZYN:

I would like to see that report. I in my own experience have found that a few of those lines have matched the ability of our receivers to receive the Omega. Of course, anytime besides local noon, I have had better results. In fact, on a flight recently in California, I was receiving 13 stations. That was 8 Comm stations and 5 Omega stations, but we have to assume that some of our customers want to fly at local noon.

DR. REDER:

There are two areas according to our experience with VLF monitoring which are a big problem no matter what the prediction says. One is the area around Australia because of the problem of Omega signals from Haiku, due to mode interference; and No. 2 is the area around the Indian Ocean and Madagascar. The reason there, is antipolar inter ference. For instance, Japan Omega to Madagascar is very heavily contaminated by antipolar interference.

It is interesting to note that NDT, which is in the link, Japan-to-Madagascar, is mixed with antipolar signals, but the same signal over the same pathlinks, just with the slightest different angle going down towards La Reunion -- that is a French Island a little further south -- is not mixed. So it just shows how important the angles in the magnetic field are.

DR. WINKLER:

Unless somebody else has something to say to the question of why the Navy does not want to sanction or bless the use of the VLF communication signals for navigation; I would like to clarify that. There are a variety of reasons why the communications service cannot accept responsibility for the consequences of the use of these signals other than communication. However, I can assure you that there is a sufficient interest in the department of defense to assist any user as much as possible with this information, and it is for that reason that the Observatory Bulletins and also messages and the telephone service, which is an answering service, will provide improved information on the availability of these signals and down times as much as it can.

One of the reasons why a responsibility for navigational use cannot be accepted is that indeed, as has been mentioned before, some of the stations will begin testing with other

modes of operations, and minimum shift keying is one of them. Also, in view of the use of these stations for priority communications, there is a possibility of rather short notice on frequency changes or unannounced frequency changes, but if you look at the record over the last ten years, these have been less so than any other service.

MR. TYMCZYSZYN:

If I might make a comment, we have had excellent relations with the Navy. They have been very good at giving these reports, not only to us, but to our customers, and we have had a little more trouble with the Department of Defense. In fact, one of our customers wrote a letter to the Department of Defense, a general inquiry, saying I am using your system and on and on, just to put in another point for us. He got a very stern letter back, and he called us up and read us this letter, and said, "Boy, the Department of Defense doesn't seem to be on your side. By the way, I would like two more GNS Systems next month."

DR. REDER:

But, Mr. Tymczyszyn, don't you know that the Navy is a part of the Department of Defense?

Well, isn't it really that they don't want to bind themselves, because they cannot guarantee that they won't go off the air? I think that is the most important thing.

DR. WINKLER:

I am not disputing anything which has been said, but the requirements for the communications are practically identical. Communication signals must stay on the air, and every possible measure is taken to assure that. I think the real reason is one of keeping one's liberty to make changes in an emergency must be preserved, but fortunately that has never been used in the past, not yet.

DR. REDER:

Before we go to the next paper, I just would like to mention one thing. We had oodles and oodles of VLF phase and amplitude recording at Fort Monmouth. Dr. Winkler has the same amount, almost, of VLF phase recordings in Washington. If you need any information, please contact us. The stuff is all available.

DR. REDER:

Before we go to the next paper, I just would like to mention one thing. We had oodles and oodles of VLF phase and amplitude recording at Fort Monmouth. Dr. Winkler has the same amount, almost, of VLF phase recordings in Washington. If you need any information, please contact us. The stuff is all available.

One more comment to what was mentioned about the PCA's of polar cap absorptions, I think the PCA problem is probably the least worrisome, for the simple reason that protons are very bad, but they have one very nice feature -- they come in such a mass that actually phase stability during the PCA is rather good on this northern path, and it is one that has started, more or less predictable of what will happen in the next couple of days, which you cannot say for solar x-ray flares. The worst things are solar x-ray flares No.1; and No. 2, in certain areas, electron precipitation from the belts.

Fortunately, this area is rather limited, but this is the worst, because they are very poorly predictable.

GEOMAGNETIC STORMS AND ASSOCIATED PHASE ANOMALIES OF A VLF RADIO WAVE AT MIDLATITUDES

Tadayoshi Hara and Koji Horiai

International Latitude Observatory of Mizusawa, Japan

ABSTRACT

Sudden phase anomalies (SPA's) were investigated by data obtained from the reception of NLK during 25 months from August 1970 to December 1973 with the point of view of associating SPA's with geomagnetic storms. We will express the amount of SPA by a phase deviation with respect to a monthly mean value and use the horizontal component of geomagnetism observed at Memanbetsu (Japan) together with the Ap-index published regularly in the J. Geophys. Res. as an index of intensity of a geomagnetic storm. The results obtained for nocturnal periods at midlatitudes are:
a) Phase of the NLK wave is advanced by 10 μs in the case of moderately large storms (i.e. around 70 γ).
b) Phase change occurs 2 hours later than the main phase of a geomagnetic storm and continues for about 2 days, but a weak effect continues for about 5 days.

SPA's are observed at noon when the solar zenith angle is about 70° and observed also during extremly large storm periods even with a solar zenith angle of 30°.

INTRODUCTION

Precise time comparisons are attained with a stability of the order of 0.1 microseconds by using the Loran-C system within the ground wave region. But this area is limited to the restricted region of the northern hemisphere. The VLF navigation system and especially Omega is effective for global frequency calibration or for navigation purposes. But VLF signals which are received during nocturnal periods show frequent phase fluctuations by as much as 8 microseconds and those fluctuations correspond to a position error of more than one nautical mile. VLF signals which propagate for a long distance are explained by the wave guide mode theory [1], and the reflection height in daytime may be

PRECEDING PAGE BLANK-NOT FILMED

arounded 70 km (electron density may be 300 cm^{-3}) [2]. A reflection height of 85 km at night can be assumed from the reflection height in daytime and by amounts of diurnal phase variations. This height corresponds to the upper D-region. Electron density in the D-region is strongly disturbed by the radiation of electromagnetic waves and high energy particles from the Sun. In daytime, electron density increase is caused by sudden enhancement of X-ray fluxes whose wave length is less than 8 Angstroms during the solar flare periods. In night time, the flux of Lyman-α which is the main ionization source in the D-region extremly decreases, then the ionization by precipitations of high energy particles is effective. The marked ionization by high energy particles is observed in the polar cap region. Also in the midlatitude region, the possibility of ionization by precipitations of high energy particles has been discussed in association with geomagnetic storms. But there is no association between this phenomena and Polar Cap Absorption (PCA) events. About half of the propagation path (7300 km) from the NLK transmitter (Jim Creek, Washington, USA, geographic coordinates, 121°35'W, 48°05'N, geomagnetic latitude 54°N) to Mizusawa (geographic coordinates, 141°08'E, 39°08'N, geomagnetic latitude 29°N) goes near the polar cap region and SPA's (Sudden Phase Anomalies) are often observed during geomagnetic storms. The association of the SPA's of the NLK (18.6 KHz) radio signal at Mizusawa with geomagnetic storms is examined in this report.

SPA'S DURING NOCTURNAL PERIODS

Cesium frequency standards are equipped at both receiving site and transmitting site but slight frequency differences were observed and a constant frequency off-set was removed by using the daytime data. Twenty four month's data were obtained during the periods of August 1970 to July 1971, September 1971 to October 1971, April 1972 to October 1972, and August 1973 to December 1973. We will express the amount of SPA by deviation of phase with respect to a monthly mean value and will exclude strongly disturbed days. A negative sign means the phase of the received signal is advanced. Phase data were taken with a Tracor Model 599E VLF Tracking Receiver every 15 minutes to a resolution of 0.1 microseconds but there could be an instrument error of 0.5 microseconds. Standard deviations of a single observation are ±0.5 microseconds for the best condition (i.e. in the daytime in summer) and are ±8 microseconds in the night time. Calibrations of the receiving system are made monthly by suppling a synthesized signal to the loop antenna. Data of geomagnetism at the Memanbetsu Magnetic Observatory, Japan were used. Associations of SPA's with geomagnetic disturbances were examined when disturbances of the horizontal component were greater than 100 gammas. Belrose and Thomas [3] called the SID (Sudden Ionospheric Disturbance) which accompanied the main phase of geomagnetic storm, the 'primary storm effect' and the one which begins three or four days after the onset of storms and continues for several days, the 'storm after-effect'.

We designate the SPA which occurs immediately after the main phase, the PSE and the one which occurs after the PSE, the SAE. Correspondences of geomagnetic storms and associated PSE's and SAE's were summerized in three groups as follows.

Table I - a)

Geomagnetic Storms at Memanbetsu, Japan,
and Associated Phase Disturbances of
NLK Signal Received at Mizusawa, Japan.
'Primary Storm Effect' was Observed in these SPA's.

Date of onset of SPA's			Time of ssc		Deviation of H-component	Duration of 'storm after effect'
Year	Month	Day	Day	Hour(U.T.)	(γ)	(day)
1970	8	17	16	2204	280	2
	11	7	7	0046	149	1
	11	21	21	0622	132	2
	12	14	14	0154	284	4
1971	1	27	27	0430	117	5 - 8
1972	4	28	27	13.3	132	3
	8	9	9	0037	241	4
1973	10	29	28	7.5	187	3

Table I - b)

'Storm After Effect' was observed but
'Primary Storm Effect' was not
observed in these SPA's.

Time of ssc				Deviation of H-component	'Primary storm effect'	Duration of 'storm after effect'
Year	Month	Day	Hour (U.T.)	(γ)		(day)
1970	10	16	0917	138	?	5
1971	4	9	0428	174	?	2
	4	14	1243	184	Day time	4
	5	6	2.0	101	?	3
	9	17	1125	108	Day time	2
1972	6	17	0628	290	Day time	1
	8	4	0119	520	Day time	4
1973	9	22	3.0	162	?	2 - 4
	10	2	4.3	119	?	1 - 3

Table I - c)

Neither 'Primary Storm Effect' nor
'Storm After Effect' was observed
for these Magnetic Storms.

Time of ssc				Deviation of H-component	'Primary storm effect'	'Storm after effect'
Year	Month	Day	Hour (U.T.)	(γ)		
1970	11	18	1225	141	Day time	?
1971	4	3	2139	102	?	No
	5	17	0629	112	?	?
	9	24	1430	119	?	?
1972	5	15	1849	187	No	No
1973	10	16	0520	101	?	?
	11	24	10.7	109	No	?

a) The case of the PSE's and SAE's which are detected in the NLK signal at Mizusawa is tabulated in Table I - a).

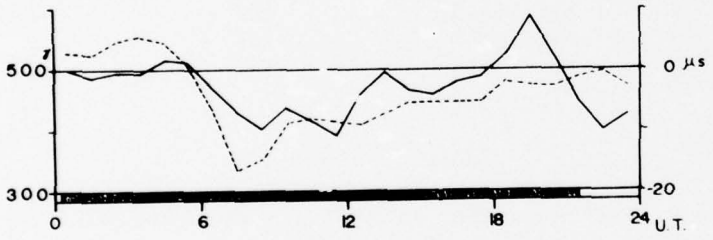


Fig. 1-The solid line shows an anomalous phase change of NLK at Mizusawa on 14 December, 1970. The dotted line shows hourly mean value of the geomagnetic horizontal component. All the propagation path is day time for 22h to 0h U.T. and night time for 10h to 15h U.T.. The remaining periods contain the transition region.

These eight storms are moderately large and bay like patterns are easy to distinguish such as the example shown in Fig. 1. Correspondences of decrease of the horizontal component in advance of the received signal can be clearly seen from Fig. 1. An averaged correspondence is depicted in Fig. 2 for storms of 17 August, 7 November, 21 November, and 14 December, 1970 which are similar in bay like patterns. In this case epochs of each storm were fixed to coincide in the main phase.

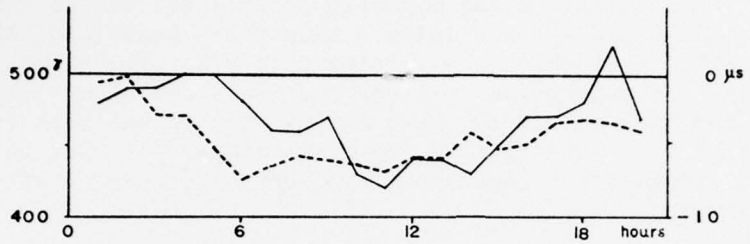


Fig. 2-The dotted line shows the geomagnetic horizontal component averaged for four events in 1970. The solid line shows the corresponding phase change of the NLK signal at Mizusawa.

The feature of PSE of VLF radio waves which propagate in the midlatitude in night time shows us that the phase of VLF signal advances after two hours of a main phase of a storm by the amount of 8 microseconds for a decrease of 70 gammas of the hourly mean horizontal component. An example of SAE is shown in Fig. 3 for the storm of 14 December, 1970.

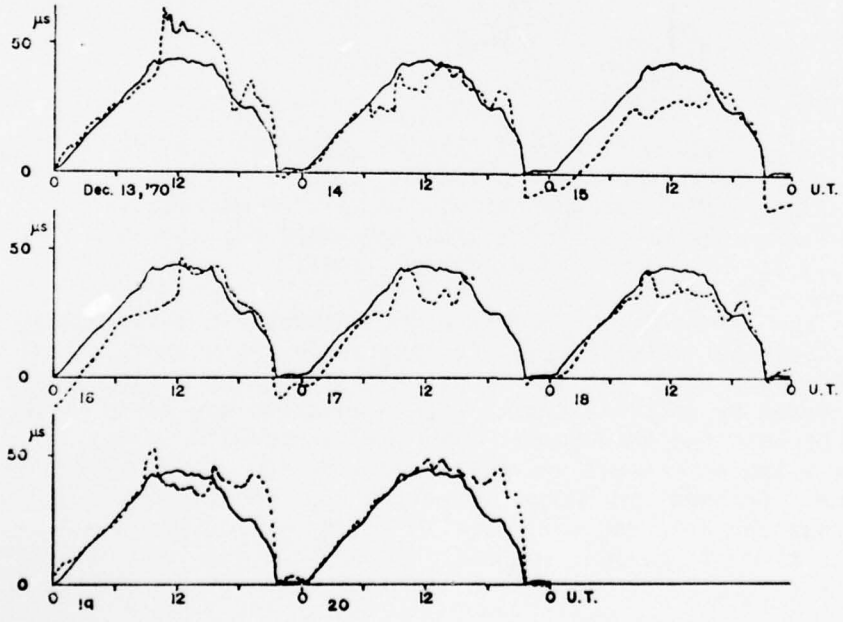


Fig. 3-The solid line shows monthly mean value of the diurnal phase change. The dotted line shows day-to-day phase variation associated with the geomagnetic storm of 14 December, 1970 (main phase is around 6h U.T.). A large phase advance continued for two days and the small effect continued for four days.

The sudden commencement of the magnetic storm (ssc) was at 0154 U.T. on 14 December, 1970 and 4 hours later a main phase began and SAE occured on 15 and 16 December which was greater than PSE. To see how long the SAE persists, the superposed Ap-index and SPA's are shown together in Fig. 4 for the same storms as shown in Fig. 2. It has been said that SAE persists for 10 days or more for large storms [3], but it may be said that a large effect continues for 2 days and a small effect for 5 days in our case.

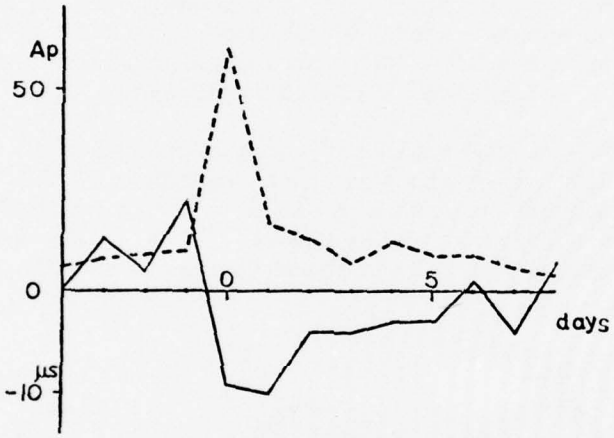


Fig. 4-The solid line shows the day-to-day variations in the mean phase of NLK at Mizusawa and corresponding mean geomagnetic disturbances are represented by the Ap-index (dotted line).

b) SAE's are detected but PSE's are not observed in these cases, which are tabulated in Table I - b). In this table the 9 examples are included as SPA's which can not be distinguished from abnormal ionizations aroused by an X-ray burst. Examples shown are cases of no SPA effect, because the geomagnetic disturbances occured in day time and cases in which we can not say that storms caused obvious SPA's even in nighttime. Berlose and Thomas summarize the subject of the SAE by noting that the greatest increases in ionization occurs 2 - 4 days after the time of maximum magnetic disturbance [3]. In our case, it may be said from Figs. 3 and 4 that the time lag of the SAE is one day.

c) In table I - c) 7 storms are shown which do not cause either PSE or SAE. These storms were not so large except for the one which occured on 15 May 1972.

SPA'S IN DAYTIME

It may be said that the anomalous ionization changes in the D-region associated with geomagnetic storms are not significant in daytime. And storm after effect has been observed only in the m.f. absorption data in daytime. On our NLK - Mizusawa propagation path, SPA's were observed 3 times in daytime. Two SPA's were detected on 14 December and on 21 November in the winter of 1970 where solar zenith angles were between 60° and near 80° and they were pretty large even at noon. An example of anomalous phase advance can be seen in Fig. 3, where daytime mean phase advances were 13 μs and 4 μs for storms of 14 December and 21 November, 1970 respectively. Another SPA was observed on 4 August, 1972 when the solar zenith angle was small but this storm was exceptionally large and caused a phase advance of 8 μs averaged during the daytime period from 1930 U.T. to 0300 U.T.. An X-ray burst was observed on 4 August by the SOLARD10-Explorer44 but the X-ray flux of 1 to 8 Angstroms calmed down by 1800 U.T. of the same day. So the SPA may not include ionization by X-ray radiation.

DISCUSSION

Using l.f. absorption Lauter and Knuth investigated the storm after-effect which is the main feature of the D region at midlatitudes [4]. They made clear that the storm after-effect is observed mainly after storms with Ap>60. In our case, however, the storm after-effect was observed after storms with Ap>30. This fact might be due to the unusual propagation path which follows the precipitation region for about 3000 km and also might be due to the method of phase comparison which is sensitive to ionization changes.

In accordance with the position of the radiation belt over Europe, Lauter and Knuth found that there is a strong decrease in number and intensity of absorption effects with latitude south of 53°N. The storm after-effect might be aroused in the region of geomagnetic latitudes of 55°N in which the NLK - Mizusawa circuit is parallel to the geomagnetic L shell 3 at 100 km altitude. It may be made clear, however, which region affects the SPA by comparing cases where the region in question is either in day time or night time when the main phase of a storm begins.

CONCLUSIONS

Correlations between disturbances of the D-region and geomagnetic storms were examined by the phase data of VLF radio signals which propagate in midlatitude. SPA's were aroused in nighttime by 70% of geomagnetic storms whose disturbances had a horizontal component greater than 100 gammas. SID's caused by X-ray burst persist for a relatively

short time and these SPA's are easy to identify but SPA's associated with geomagnetic storms continue for long periods and great care must be taken when using these signals for navigation and frequency comparison purposes. During the moderately large storm of 21 April,1970 a direct measurement of precipitation fluxes was made and showed that this ionization is in competition with the total of all other daytime ionization sources for the midlatitude D-region [5]. It may be expected that extremly large storms will then cause an anomalous phase advance even in the daytime. Actually, in the storm of 4 August, 1972, an 8 μs phase advance was observed. In winter the solar zenith angle has the large value of 70° even in daytime for the NLK - Mizusawa circuit, and SPA's were observed as a SAE in moderately large storm periods. The cause of differnces between predicted and measured diurnal phase was mentioned above and this discrepancy amounts to about 10 microseconds. In addition to SPA's associated with geomagnetic storms, anomalous phase retardations were observed chiefly in September and October and might be due to local disturbances of propagation [6]. These retardations are cancelled out by storms and they then advance and become stable in advanced phase.

ACKNOWLEDGEMENTS

The authers wish to express their hearty thanks to Prof. H. Oya, because this investigation was made according to his suggestion and was evaluated with his advice. We are indebted also to Mr. B. McCune who read through this manuseript and improved some expressions.

REFERENCES

[1] WAIT, J. R. : Electromagnetic Waves in Stratified Media. Pergamon Press, (1962).

[2] NICOLET, M. and AIKIN, A. C. : The Formation of the D Region of the Ionosphere. J. Geophys. Res. 65, 5, (1960), 1469-1483.

[3] BELROSE, J. S. and THOMAS, L. : Ionization changes in the middle latitude D-region associated with geomagnetic storms. J. Atmosph. Terr. Phys., 30, (1968), 1397-1413.

[4] LAUTER, E. A. and KNUTH, R. : Precipitation of high energy particles into the upper atmosphere at medium latitudes after magnetic storms. J. Atmosph. Terr. Phys., 29, (1967), 411-417.

[5] GOUGH, M. P. AND COLLIN, H. L. : Energetic electron precipitation as a source of ionization in the night-time D-region over the midlatitude rocket range, South Uist. J. Atmosph. Terr. Phys., 35, (1973), 835-850.

[6] BATES, H. F. and ALBEE, P. R. : General VLF Phase Variations Observed at College, Alaska. J. Geophys. Res., 70 (1965), 2187-2211.

QUESTION AND ANSWER PERIOD

PAPER NOT PRESENTED ORALLY, THEREFORE, NO QUESTIONS AND ANSWERS.

SOME ASPECTS OF PROJECT SPECKLED TROUT

W. J. Klepczynski
U.S. Naval Observatory

Major W. L. Bertino, USAF
Andrews Air Force Base

ABSTRACT

Project Speckled Trout concerns itself with the evaluation of navigation systems for the Air Force on a continuing basis. Four classes of navigation systems are currently being evaluated and intercompared:

1. Inertial
2. Omega
3. VLF, using both Omega and communication signals
4. Area.

In this paper, the results of a number of test flights will be presented. Frequency stability requirements as a function of navigational accuracy for the VLF navigation system will briefly be covered.

Finally, a few remarks on deriving PTTI information from electronic navigation systems will be made.

I. PROJECT SPECKLED TROUT

Project Speckled Trout is an ongoing program to operationally evaluate navigation equipments for the U. S. Air Force. The evaluation of off-the-shelf hardware is an essential part of the overall supply picture. Knowledge of existing capability can greatly reduce expenses and maximize the cost effectiveness of equipment purchases. In addition, utilizing knowledge of state-of-the-art equipment, realistic design and system specifications can be set down for future equipment development with a reasonable assessment of the risk involved.

Currently, four types of navigation systems are being evaluated on the Speckled Trout aircraft:

a. Inertial Navigation Systems (INS);
b. Omega Navigation Systems;
c. VLF Navigation Systems; and
d. Area Navigation (RNAV) Systems.

By way of introduction, Table I lists some of the general characteristics of the navigation systems carried on board Speckled Trout during the test flights. Four inertial navigation systems were in operation: two LTN 51's, an LTN 72 (manufactured by Litton Industries) and an INS 61B (manufactured by the Collins Radio Group of Rockwell International). The inertial navigation systems are self-contained, completely passive devices. An INS senses accelerations along a set of axes defined by a gyroscope aligned with the Earth's axis of rotation. Position is obtained by a double integration of the accelerations. Any errors in the measurement of the accelerations or the alignment of the measurement axes will also be integrated twice and will produce time divergent errors.

Only one Omega set was on board during this period. It was an ARN-115, manufactured by the Canadian Marconi Co. Omega navigation errors, although they are sometimes functions of time of day, can normally be considered as bounded. Usually, the navigation errors are associated with the propagation errors of VLF transmissions.

Two VLF navigation systems, the Ontrack II manufactured by the Communication Components Corp. and the GNS-500 manufactured by Global Navigation Systems, Inc., were carried. However, there were some periods when each was off the aircraft for maintenance. The errors associated with VLF navigation systems are either bounded or unbounded depending on the mode of operation of the particular set. In the hyperbolic mode, two pairs of phase measurements are being compared as in conventional Omega navigation; therefore, the errors will exhibit the same character as Omega errors. However, in the rho-rho mode, the errors associated with the VLF navigation systems are not bounded. In the rho-rho mode, since a phase comparison between the received signal and the signal from a local on-board oscillator is made, any uncompensated drift rate or calibration error of the local oscillator will be directly translated into a position error as a function of time. Both VLF navigation sets operated in the rho-rho mode.

Area Navigation (RNAV) Systems combine and filter navigational data from several sources and display that information to the flight crew. The error associated with the dis-

played position reflects the error of the input source. Two different navigation systems provided input to the RNAV system on board the Speckled Trout: the INS 61B and the standard VOR/DME system, which is the primary source of air navigation data throughout the U.S. On those flights outside the VOR/DME network, the primary navigational data being supplied to the RNAV system is inertial data. In this case, the position error is unbounded. However, when within VOR/DME coverage, the displayed position should not be in error by more than the error associated with the VOR/DME system.

II. SUMMARY OF RESULTS OF SPECKLED TROUT FLIGHTS

Reports which list the results of the various test flights are issued at fairly regular intervals. Each report contains for each flight during the covered period, flight path, duration of flight, the navigational data obtained on each system by manufacturer's name, and any notes of interest. The navigational data consists of the error for each of the navigation systems at the end of the flight. The error is defined as the difference between the system readout for some well-defined point on the airport at touchdown and the coordinates for that point obtained from C-5 Airfield Diagrams and/or Jeppesen Airport diagrams. The navigational error is listed in latitude/longitude offsets in nautical miles (nm) from the assumed position as well as radial error. The radial error is divided by the duration of the flight to derive a radial error rate/hour.

Listing the data contained in each of the reports for each flight is a little impractical for this paper. Therefore, it was decided to list summaries of the data contained in two of the more recent reports considered representative of the flights. The two reports selected were Report No. 75-09 and Report No. 76-01. These reports contain data from 39 flights throughout Europe, the Mid-East, the Pacific, and the U.S. The flights lasted between 1 and 9 hours. Table II lists simple averages of the data from each of the two reports and an average of all the data contained in these two reports. Column 1 lists the report from which the data presented was computed. The second column lists the months when the flights contained within each report were flown. The next four columns list the average radial error rate in nm/hr for each of the four inertial navigation systems flown during the test period. The next two columns list the average radial error rate for each of the two VLF navigation systems. Please note that no mention of specific manufacturer's equipment is made in this table so that the results listed here can in no way be interpreted as an endorsement

of any one product.

The data listed for the one Omega navigation set in the next column are not the average radial error rates, but the average radial error in nautical miles. The last column lists the radial error for the RNAV system operated during this time frame. Radial error rather than radial error rate is listed here because the mode of operation of the Omega and RNAV systems was such that the errors should be bounded and not functions of time.

The results indicate that the four inertial units performed reasonable well throughout the test period. One of the inertial units, Set #1, performed exceptionally well exhibiting an average radial error rate of only 0.4 nm/hr.

The VLF navigation systems exhibited average radial error rates of 1.5 nm/hr and 2.6 nm/hr. If one attributes these error rates solely due to the unmodeled drift rate of the local oscillator with respect to the oscillators governing the VLF transmissions, then one obtains 2.6 parts in ten to the ninth and 4.4 parts in ten to ninth, respectively, for the unmodeled drift rates.

It should be noted that the VLF navigation sets in addition to exhibiting the unbounded error growth with time should also reflect to some degree the bounded error of the Omega navigation system, i.e., reflect some of the navigational error caused by propagation variations in the VLF transmissions. The average radial error of the Omega navigation set tested here was 2.3 nm. If we assume that the VLF navigation systems were affected, on the average, by the same constant error of 2.3 nm, we could then adjust the radial error by this amount and recompute a new average radial error rate. On doing this, the new average radial error rates for the two VLF navigation systems become 1.85 nm/hr and 0.71 nm.hr, respectively. These rates would correspond to an unmodeled fractional frequency difference or drift rate of 3.1 and 1.2 parts in ten to the ninth, respectively. These numbers are a little larger than expected considering that rubidium frequency standards were used on both these sets. The expected error rate is less than 0.1 nm/hr, corresponding to a drift rate of about 1 part in ten to the tenth. Tymczyszyn (1975) at this conference has reported on improvements in one of these systems which should remove the deficiency noted above. The improved system now accounts for propagation path variations during the calibration of the frequency prior to take-off.

III. SOME SPECULATION ON PTTI AND FUTURE NAVIGATION SYSTEMS

The VLF navigation sets discussed earlier seem to represent the future trend in navigation sets. Future navigation systems will contain either an atomic frequency standard or high precision crystal oscillator. Within the same dust cover, one can and most likely will find a powerful microprocessor. In addition, some systems will have the capability to receive and process a mixture of signals from VLF, LF, and VHF to UHF. The potential flexibility that some current and most future navigation systems will exhibit is staggering. It does not seem likely that future navigation equipment will need distinctions such as Loran-C or Omega. Most systems will process the best available signal or combination of signals in the most efficient mode to derive the best possible position fix.

In the past, PTTI information has usually been extracted from navigation systems through specially developed receivers. These receivers are usually cheaper than the equivalent navigation receiver for that system. The PTTI information derived from the navigation system can be either relative information or absolute information depending on whether the system has been calibrated. However, it appears that in the future it should be possible to derive absolute PTTI information from most electronic navigation systems using off-the-shelf navigation receivers with modified software. The trend of the future for PTTI seems to be a trade-off of hardware development for software development.

In the literature, several articles already have appeared with suggestions on how to extract both time and time interval from navigation systems. Future navigation receivers will most likely have the hardware and computing capability to implement these schemes.

With respect to the LF navigation system Loran-C, Ryerson (1969) indicated how the simultaneous use of Loran-C in both the hyperbolic and rho-rho mode could be used to extract absolute time and time interval provided there is a local oscillator at the receiver. Kelley (1969) and Uttam and Palsson (1975) discussed the use of Loran-C in a rho-rho mode for timing. All schemes involving clock calibration require deducing the distance to three or more stations. Two stations are required for the navigational fix; the third is used for calibrating the clock. Most Loran-C chains operate with four transmitting stations. Therefore, sufficient redundancy is already built into the system.

Experiments by Chi and Wardrip (1973) using Omega indicate that a timing precision of better than ± 5 μs is now attainable. However, knowledge of the accurate position of the receiver is presumed. Gaon (1974) incorporates the technique of composite Omega as put forth by Papousek and Reder (1973) to derive PTTI information from the Omega system. Smith (1974) and Burch and Sakran (1974) report on the Northrop ARN-99(V)2 Omega navigation set which operates in the rho-rho mode using a crystal oscillator as the basis for its timing.

It seems that Omega, utilizing the composite frequency technique in combination with the navigation signals being processed in both the hyperbolic and rho-rho mode, might offer the most precise way to get absolute PTTI information into the field. This conjecture is based on the fact that the composite frequency technique seems to offer the best way to minimize propagation effects.

IV. CONCLUSIONS

The reports of Project Speckled Trout are a valuable source of information. They will most likely be the basis for a number of studies. The deficiency of the VLF systems noted in this report seems now to be corrected. Future reports should verify this.

The signal processing techniques employed by the VLF navigation systems, if applied to future navigation receivers, seem to indicate that absolute PTTI information should be easily extracted from navigation systems. However, the mixing and matching of the various navigational signals in different operational modes will necessitate improved synchronization between all navigation systems.

REFERENCES

1. Burch, P.B. and Sakran, F.C. 1973, "Flight Tests of Two Airborne Omega Navigation Systems", Proceedings of the National Radio Navigation Symposium, 146, published by the Institute of Navigation, Suite 832, 815 15th Street, N.W., Washington, D.C. 20005.

2. Chi, A.R. and Wardrip, S.C. 1973, "Clock Synchronization Experiments Using Omega Transmissions", Proceedings of the 5th PTTI Planning Meeting, 369.

3. Gaon, B.N. 1975, "Hand Held Calculator Technology

Applied to an Advanced Omega Receiver", Navigation, Vol. 22, No. 4, 302.

4. Kelley, C.T. 1969, "Use of Loran in the Range-Range Mode", Navigation, Vol. 16, No. 4, 390.

5. Papousek, W. and Reder, F.H. 1973, "A Modified Composite Wave Technique for Omega", Navigation, Vol. 20, No. 2, 171.

6. Ryerson, J.L. 1969,"Derivation of Circular Fixes in Hyperbolic Navigation Systems", Navigation, Vol. 16, No. 4, 382.

7. Smith, E.J. 1974, "Flight Test of ARN-99(V)2 Omega Navigation Set in F-4 Aircraft", Proceedings of the 2nd Omega Symposium, 139, published by the Institute of Navigation, Suite 832, 815 15th Street, N.W., Washington, D.C. 20005.

8. Tymczyszyn, W.R. 1975, "Inflight Worldwide VLF Experiment Using Global Navigation GNS-500", Proceedings of the 7th PTTI Planning Meeting.

9. Uttam, B.J. and Palsson, T. 1975, "Calibration of Reference Time Errors in Direct Ranging Loran-C Navigation", Proceedings of the ION National Marine Meeting - 14-15 October 1975, published by the Institute of Navigation, Suite 832, 815 15th Street, N.W., Washington, D.C. 20005.

System	Error Properties	Operational Mode	Type of Operation	Sensing System
Inertial	Unbounded		Self-Contained	Acceleration
Omega	Bounded	Hyperbolic	Relies on Omega Transmitters (Passive)	Phase Comparison
VLF	{Bounded / Unbounded}	{Hyperbolic / Rho-Rho}	Relies on Omega Transmitter and/or VLF Communication Transmitter (Passive)	Phase Comparison
RNAV	Bounded	Rho-Theta	Primarily Relies on VOR/DME Stations (Active)	Pulse

Table I - *Synopsis* of Navigation Systems Being Tested on Speckled Trout

Report	When Flights Made	Inertial				VLF		Ω	RNAV
		#1	#2	#3	#4	#1	#2		
		nm/hr	nm/hr	nm/hr	nm/hr	nm/hr	nm/hr	nm	nm
75-09	Mar-May 75	0.4	0.5	0.5	0.7	1.9	1.1	2.6	0.8
76-01	Jun-Jul 75	0.4	0.5	0.8	0.8	3.3	1.8	1.9	0.5
Averages		0.4	0.5	0.7	0.8	2.6	1.5	2.3	0.7

Table II - Synopsis of Navigation Data from Speckled Trout

QUESTION AND ANSWER PERIOD

MR. BARSZCZEWSKI:

Barszczewski, NRC.

Again, there are a few points I would like to make. First of all, on this bounded and unbounded rate of error with VLF and Omega, if you talk of Omega and VLF you should talk in the same sets of units. I mean, if you operate hyperbolically, then the error is bounded by propagation, and there is no increase in an error rate.

Now, personally, I have no beef against either choice of VLF, Omega, Loran C, or whatever it is. We operate in the Arctic, and we take what we can get. The magnetic compass is no good. The VLF signals are there. You usually have a coverage of three stations, sometimes more. The coverage is quite good. There are strong signals, and so on.

Now, most of navigation systems will be, aided and of course the best aid is to have a competent navigator at the clock and air speed indicator. That is ultimate, but if you go by the electronic systems, you will probably use some sort of air speed indication and some heading. We have been using sort of a hybrid system like that for several years. We use a minicomputer to keep track as we go along, and we always manage to return, but we have had some problems with loss of information, generally due to failure of electronics.

Now, as far as the future, there is one little point I would like to make. I would like to see some of the beacons, LF beacons in particular, to be put on cesium frequency control because that would be an additional input that could be used for navigation.

SATELLITE-TO-SATELLITE TRACKING SYSTEM AND ORBITAL ERROR ESTIMATES

P. E. Schmid
P. D. Argentiero
F. O. Vonbun
NASA-Goddard Space Flight Center

ABSTRACT

Satellite-to-satellite tracking and orbit computation accuracy is being evaluated on the basis of data obtained from near Earth spacecraft via the geostationary ATS-6. The near Earth spacecraft involved are Apollo-Soyuz, GEOS-3 and NIMBUS-6. In addition ATS-6 is being tracked by a new scheme wherein a single ground transmitter interrogates several ground based transponders via ATS-6 to achieve the precision geostationary orbits essential in satellite-to-satellite orbit computation. Also one way Doppler data is being recorded aboard NIMBUS-6 to determine the position of meteorological platforms. Accuracy assessments associated with the foregoing mission related experiments are discussed.

1.0 INTRODUCTION

Orbit determination accuracy of Earth orbiting spacecraft is primarily a function of the:

- knowledge of the Earth's gravity field, atmospheric drag, solar pressure, solar and lunar gravity effects,
- tracking system performance and validity of atmospheric refraction corrections, and
- tracking geometry and station location accuracy.

The tracking system makes measurements such as range, range rate, angles and direction cosines to a spacecraft relative to a given tracking station. This data, typically on magnetic tape, is preprocessed (i.e. edited, pre-smoothed, changed to metric units, combined with calibration constants and so on) prior to being used as input to an orbit computation computer program. The quantity of tracking data required to achieve a desired orbital accuracy is directly linked with the spacecraft-to-tracking station relative geometry and dynamics. The orbit computation program is a means of mathematically providing a "best fit" (usually in a least-squares sense) of the measured tracking data to the physical laws of orbital mechanics.

The span of data used for an orbit determination may be as short as a few minutes, such as during critical launch or injection maneuvers, or data sampling over a period of several days may be used during high eccentricity earth orbits and planetary trajectories.

Assuming reasonable tracking geometry the accuracy of spacecraft position and velocity determination will be primarily limited by tracking system performance for any computation spanning the data collection interval. That is, if continuous tracking is provided from a set of well surveyed stations the computation is essentially one of geometry. On the other hand the accuracy of orbit prediction based on an initial spacecraft vector determination will be degraded as a function of time in direct relation to the accuracy to which physical parameters are modeled. This modeling includes gravitational fields, atmospheric drag and refraction effects, solar pressure, station location determination and so on. The most critical of these modeling parameters in terms of orbit determination accuracy is the gravity field model which at present is generally expressed in terms of a spherical harmonic expansion.

The question to be answered is what does one mean by "accuracy" and how is it to be measured? For the tracking system the accuracy of measurement is usually determined by means of static collimation tower tests where known distances, angles, and zero Doppler conditions are predictable to the limit of physical survey, time delay measurement, and frequency measurement. Predicting tracking system performance under dynamic conditions is usually accomplished by observing the behavior of associated sub-systems under simulated signal conditions. Experience has shown that the tracking system accuracy can be specified, implemented and verified with a high degree of confidence (ref. 1). On the other hand it is much more difficult to verify the accuracy of the complex modeling required to predict orbits. There is a continuing effort underway to improve our knowledge of such fundamental modeled parameters as the Earth's mass, the universal gravitational constant, speed of light, drag coefficients and so on. For it is easily shown that assuming perfect modeling the propagated (i.e. predicted) orbit errors due to tracking system uncertainties can invariably meet all current operational requirements for navigation, telemetry acquisition and satellite based Earth platform location. In this regard it is well established that satellite position errors of tens of meters will propagate into kilometers after only one or two weeks of orbit prediction. Such errors can only be reduced by increasing the number of tracking observation periods or improving the Earth's gravitational field modeling.

This paper presents a number of orbit error assessments as derived from satellite-to-satellite tracking and orbit computation involving the geostationary ATS-6 and the near Earth GEOS-3, Apollo-Soyuz, and NIMBUS-6.

2.0 TRACKING SYSTEM PRINCIPLES

All of NASA's range and range rate radio satellite tracking systems consist of narrowband phase modulated signals where several ranging tones are sequentially modulated onto the carrier to provide a degree of range measurement ambiguity resolution. Once the ambiguity is resolved only the highest frequency tone is transmitted to assure maximum resolution. The high resolution range tone extends from 20kHz to 500kHz depending on the specific tracking system under consideration. The range observation is basically a propagation time delay measurement from ground station to satellite and back. In the case of the current NASA satellite-to-satellite tracking experiments (e.g. ground station to the geostationary ATS-6 to near Earth satellite) four distinct propagation links are involved.

The range rate relative to a given tracking station is generally observed by counting cycles of carrier Doppler where each cycle of Doppler corresponds

to a half wavelength change in total path length at the operating frequency. All satellite-to-satellite tracking is currently conducted at a nominal carrier frequency of 2GHz and hence each cycle of two way Doppler corresponds to 7.5CM of path length change. Strictly speaking the basic measurement is one of range change and only becomes a range rate when averaged over the Doppler counting interval.

The foregoing is depicted in simplified form in Figure 1 which is appropriate for the satellite-to-satellite tracking associated with the geostationary ATS-6 tracking of GEOS-3, Apollo-Soyuz and NIMBUS-6. Satellite-to-satellite tracking permits the computation of near Earth satellite orbits by means of a single tracking station. NASA is implementing an operational tracking system of this type in the 1980 time frame by means of the geostationary Tracking and Data Relay Satellite System (ref. 2).

BASIC MODULATION SCHEME

$S(t) = \cos(2\pi f_o t + \beta \sin 2\pi f_m t)$

$\beta = 0.5$ RADIANS

$f_o = \frac{C}{\lambda_o} = 2000$ MHz

$f_m = 100$ KHz



FREQUENCY SPECTRUM

BASIC RANGE RATE DETERMINATION

AVERAGE DOPPLER $= f_D = \frac{-2\dot{\bar{R}} f_o}{C} = \frac{-\dot{\bar{R}}}{\lambda_o/2} = \frac{N}{T}$ Hz

N = INTEGRAL NUMBER OF CYCLES

T = ELAPSED MEASUREMENT TIME
(0.2 TO 10 SECONDS)

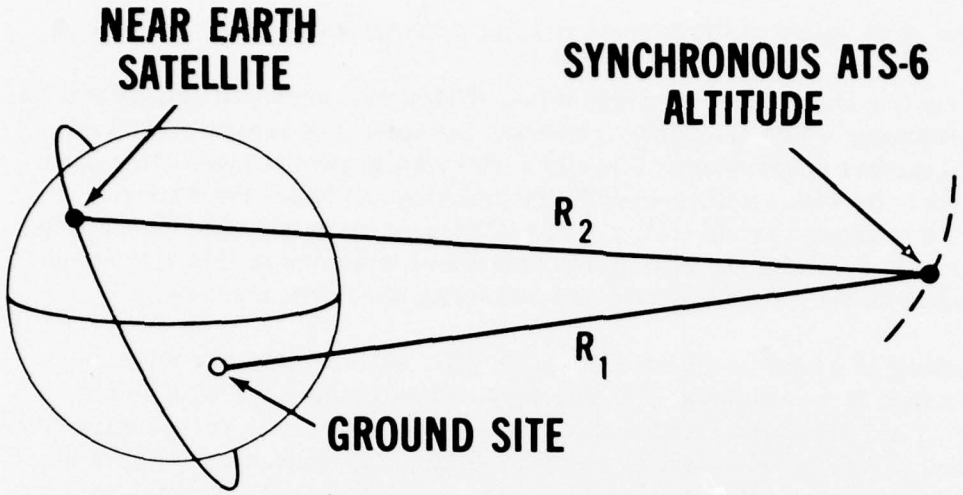
Figure 1. Structure of Tracking Signal

2.1 TWO WAY SATELLITE-TO-SATELLITE TRACKING

In two way tracking a signal is transmitted from a well surveyed ground station to a transponder which frequency translates the signal for re-transmission either to another spacecraft or directly back to the ground station. This paper deals primarily with satellite-to-satellite tracking and hence the ATS-6/ NIMBUS-6 tracking system (ref. 3 & 4) will be used as an example. Except for minor details involving the near Earth spacecraft transponder this discussion also applies to the ATS-6/GEOS-3 and ATS-6/Apollo-Soyuz tracking.

The tracking of a near Earth satellite via a geostationary satellite might be accomplished in a number of different ways. For example, tracking signal generation and data demodulation might be performed directly at the synchronous satellite and sent by telemetry to a ground station. The advantage of such a scheme is that inter-satellite measurements (synchronous to low satellite) can be separated from the total path delay. The principal disadvantage is that the relative complexity of a total ground station must be placed in orbit. Another possibility which is easier to implement electronically is the "bent pipe" concept where tracking signals between ground station and near Earth satellite are relayed back and forth via the geostationary satellite. In this scheme all tracking data demodulation, digitizing and recording is performed at the ground station. The disadvantages is that total path delay is combined into a single measurement which in turn adds a degree of complexity to the orbit determination program. It might be thought that the geostationary satellite motion is negligible over the observation interval, however this is not the case. The reason is that geostationary satellites, are generally not maintained at zero degrees inclination. Nominal values of inclination maintained for current NASA geostationary spacecraft extend from 1.5° to 6°. Such synchronous orbits are apparently more stable than zero degree inclination orbits. As a result the slant range relative to an observing ground station typically undergoes a sinusoidal variation of several hundred kilometers over a 24 hour period. This effect will also be reflected in the corresponding ground to geostationary satellite range-rate (Doppler) measurement as tens of meters per second.

The "bent pipe" scheme has been implemented for all NASA satellite-to-satellite tracking and orbit computation to date. The geometry of such tracking is shown in Figure 2. This concept has also been used in a "trilateration tracking" scheme (ref. 5) as indicated by Figure 3 to pinpoint ATS-6 while stationed over the U.S.A. at 94°W Longitude. Recent experience indicates that the success of satellite-to-satellited orbit determination is to a large measure dependent on the accuracy of the a priori estimates used for the geostationary satellite. Conventional one or two station tracking of geostationary satellites, while perfectly suitable for most meteorological image registration and data acquisition



MEASUREMENT TYPE	RESOLUTION	APPLICABLE FREQUENCY
RANGE $(R_1 + R_2)$	2 METERS	100 KHZ
DOPPLER $(\dot{R}_1 + \dot{R}_2)$	0.05 cm/sec	2000 MHZ

Figure 2. Basic Tracking Geometry

purposes, is not generally adequate for satellite-to-satellite applications. Trilateration tracking provides the geometry and tracking data resolution which results in geostationary satellite a priori estimates at the 100 meter or better level.

The same scheme is being used to track ATS-6 at its current position of 35°E Longitude with interrogation from the Madrid site and transponders at Madrid, Ascension Island and Johannesburg.

- SYSTEM DESCRIPTION

ATS-6 is in an earth-synchronous orbit at 35,800km.

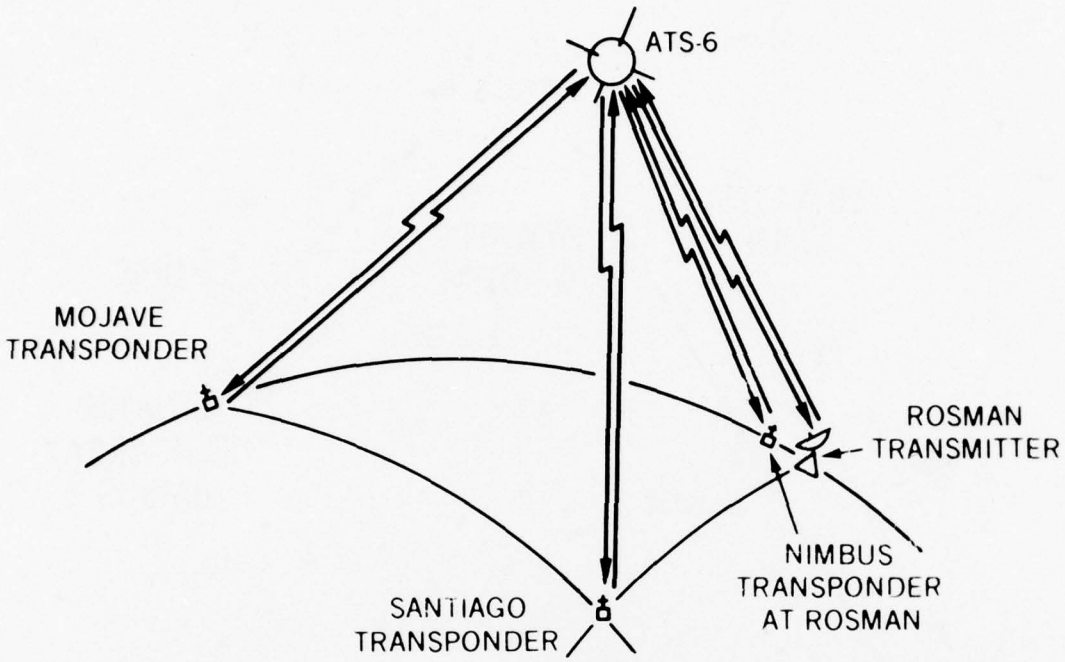
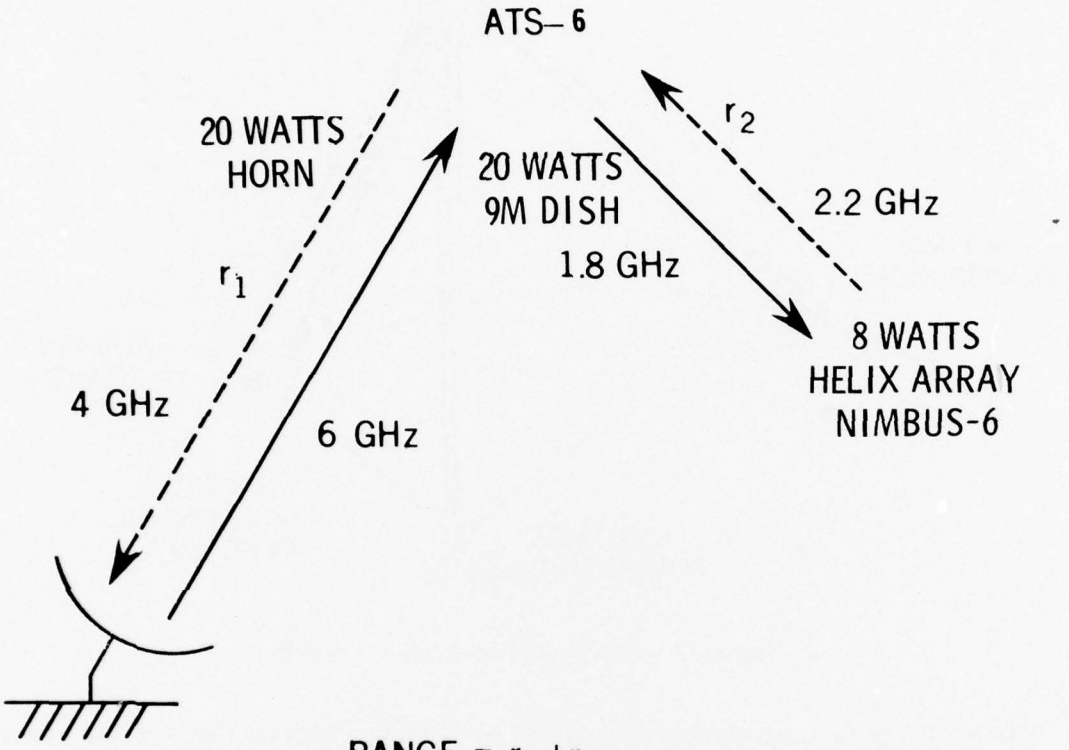


Figure 3. ATS-6 Trilateration Tracking

NIMBUS-6 is in a sun-synchronous orbit at 1100km. Figure 2 shows this basic geometry and the location of a ground tracking station.

The vital ATS elements for tracking Nimbus and relaying Nimbus experiment data to the ground are a communications transponder and a 2-GHz nine-meter parabolic antenna. The transponder translates 6 GHz ground station signals into 2 GHz signals sent to Nimbus and also translates the 2 GHz signals from Nimbus into 4 GHz signals which are sent to the ground. Figure 4 shows these frequency links between Nimbus, ATS, and the ground. The antenna has a nominal beam width of 1.4 degrees and a gain of 36 dB. It can be electronically scanned ±5 degrees off boresight, and has monopulse capability to track the Nimbus satellite. However, the primary ATS antenna pointing mode for the tracking experiment is for the ground station to program the ATS with computed pitch and roll commands based upon ATS and Nimbus ephemeris data.

Nimbus observes ATS by means of an up-looking 2 GHz antenna array which has a nominal gain of 15 dB corresponding to a 3 dB beam width of 25 degrees. The system consists of the gimbaled antenna assembly, the gimbal drive electronics, the power amplifier, transponder, and the digital electronics. The



$$\text{RANGE} = r_1 + r_2$$

$$\text{DOPPLER} = -\frac{2f_t}{c}\left[(a_1+a_2)\dot{\bar{r}}_1 + a_2\dot{\bar{r}}_2\right]$$

Figure 4. Tracking Signal Power Levels and Pointing

gimbaled high-gain antenna is directed to ATS by programmed activation of an X/Y mechanical mount. The antenna is located on the top of the Nimbus spacecraft.

The tracking data recorded at the ground station consists of range and Doppler measurements in terms of time delays. The range data is elapsed radio wave propagation time. The Doppler data, which is a function of range rate, is recorded as the time required to count a fixed number of cycles of two-way Doppler.

Figure 5 illustrates the overall tracking data processing required for this experiment.

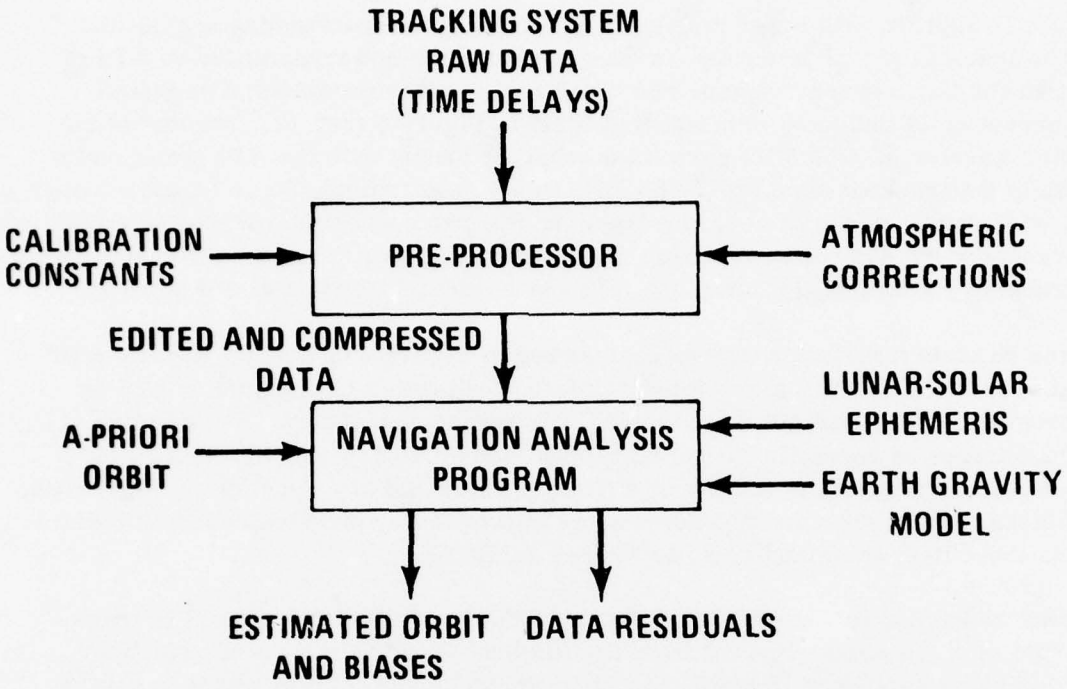


Figure 5. Data Processing for Satellite-to-Satellite Orbit Computation

The overall ranging measurement consists of a measurement of the total round trip signal delay and involves:

- The interrogation station located at Rosman, North Carolina (or currently from the transportable site at Madrid, Spain)
- The phase-locked ATS translation transponder and S-Band parabolic antenna, and
- The Nimbus crystal-controlled transponder used in conjunction with the programmed S-Band helical antenna array (phase-locked transponder for GEOS-3 and Apollo)

The rate of range change ("average range rate") is observed as a Doppler shift and necessarily involves the relative motions of the two spacecraft and the ground station.

The ground station typically will transmit at a 2 kw (CW) level, although it is capable of transmitting up to 10 kw. The highest resolution range

tone is 100KHz with lower ambiguity resolving tones used during acquisition. The tracking signal generated at the ground station and transmitted to ATS is used for the coherent Doppler and tone ranging measurements. The signal generation is indicated in simplified form in Figure 6 (ref. 6). The use of the pilot carrier at 6150 MHz permits a coherent lockup with the ATS transponder, while the tracking signal (6137.85 MHz in the case indicated) can be varied over a wide range to permit coherent tracking of other spacecraft or ground located transponders without reacquiring ATS in the frequency domain. The coherent tracking signal translation by the ATS transponder is indicated in Figure 7.

The Nimbus translation transponder shown in Figure 8 is interrogated by ATS at 2062.85 MHz. The four-element antenna subsystem is directed to ATS by programmed activation of a gimbaled X/Y mechanical mount. The pointing information is normally loaded into the Nimbus memory via VHF radio link when the spacecraft is in view of a Nimbus command site such as the Fairbanks, Alaska, STDN. The antenna can also be controlled by direct access and control via the ATS-6 command relay to Nimbus (S-Band).

With reference to Figure 8 the incoming Doppler-shifted ATS signal is translated by a frequency derived from the Nimbus 37.550 MHz crystal oscillator. This same reference is multiplied up to S-Band (2253.0 MHz) where it serves as the carrier for the Nimbus-to-ATS eight-watt link. The translated ATS-to-Nimbus signal is phase modulated onto the 2253.0 MHz carrier at a nominal modulation index of 1.5 radians. This system is based on the Goddard Range and Range Rate concept, where a crystal-controlled relatively broadband (several hundred KHz) transponder is employed. This system is made equivalent to coherent (i.e., phase-locked transponder) operation by proper ground station processing of the transmitted carrier which is coherent with the onboard reference oscillator. The advantage of using such a transponder is that no frequency swept acquisition is required by the interrogating signal. The frequency excursion at 2 GHz due to one-way Doppler often approaches ±50 KHz, since the linear speed of near-earth spacecraft is typically 8 km per second.

Doppler data is the most accurate form of tracking data available for purposes of orbit computation because one cycle of Doppler is recorded for every half wavelength the spacecraft moves radially relative to the interrogating station.

The group delay of the Nimbus transponder has been carefully calibrated over a wide range of frequency and temperature. Measured group delay repeatability is within ±20 nanoseconds with a nominal delay of 2.6 microseconds. Systematic one-way ranging errors introduced by the Nimbus transponder are thus expected to be less than ±3 meters.

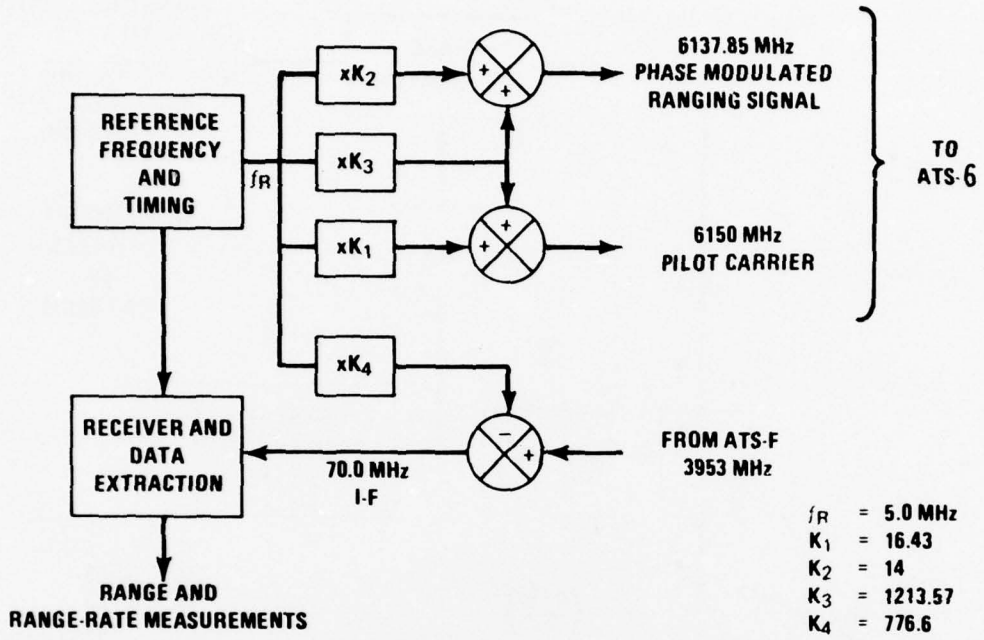


Figure 6. Ground Station Signal Generation to ATS-6

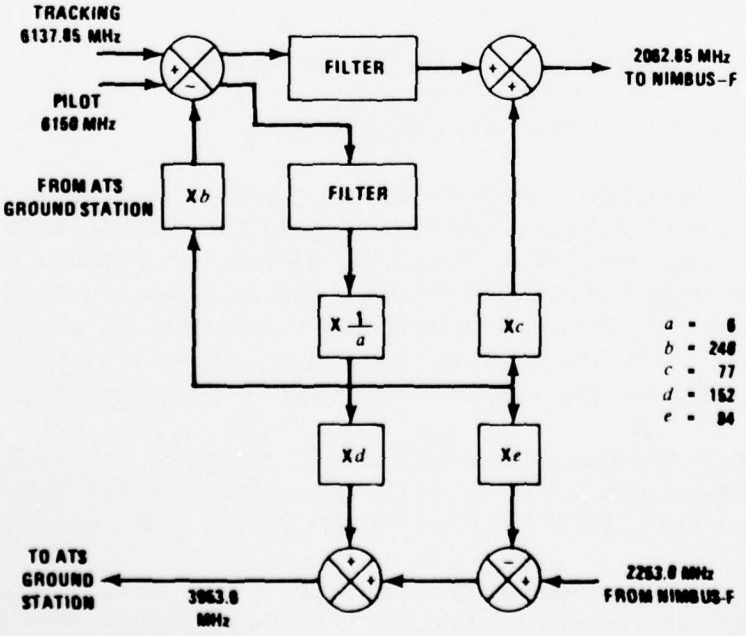


Figure 7. Signal Translation by the ATS-6 Transponder

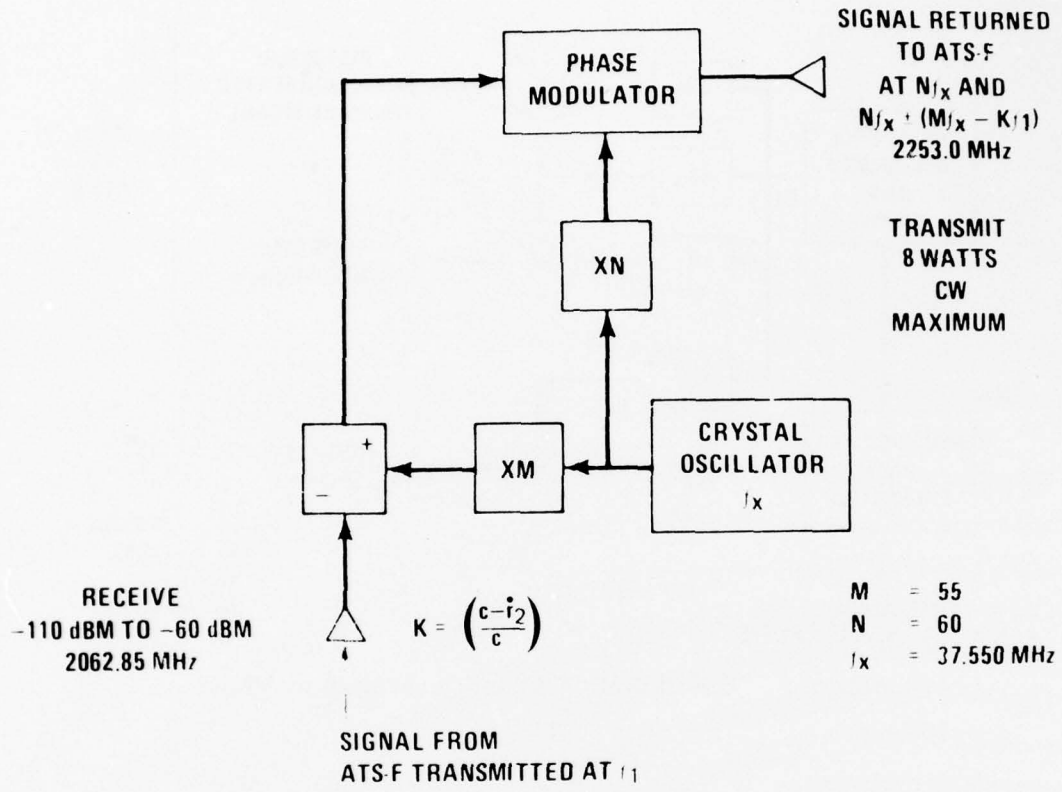


Figure 8. NIMBUS-6 Transponder

- TRACKING MEASUREMENT INTERPRETATION

The "range" measurement is performed by comparing transmitted and received tone zero crossings, the highest resolution tone frequency in this case being 100KHz. The "range rate" measurement is performed by counting a predetermined constant number of Doppler cycles and recording the time required to receive these cycles. Thus, both "range" and "range-rate" are recorded in terms of elapsed time. The raw data actually lists elapsed cycles of a 100 MHz clock; consequently the time readout is quantized to 10 nanoseconds.

The highest resolution ranging tone used in this experiment is 100 KHz. Lower frequency tones are sequentially used during acquisition for ambiguity resolution. The lower tones are at 20 KHz, 4 KHz, 800 Hz, 160 Hz, 32 Hz, and 8 Hz.

The tone ranging measurement is quite straightforward. However, its accuracy depends chiefly on the quality of preflight calibration of both the ATS and Nimbus

AD-A040 774 NATIONAL AERONAUTICS AND SPACE ADMINISTRATION GREENB--ETC F/G 14/2
PROCEEDINGS OF THE ANNUAL PRECISE TIME AND TIME INTERVAL (PTTI)--ETC(U)
DEC 75

UNCLASSIFIED NASA-GSFC-X-814-76-45 NL

7 OF 8
ADA040774



transponder group delay. Such preflight calibration data have been taken over a range of frequencies and temperatures. Indications are that with careful calibration the total systematic delay error in the ranging measurement can be held to a few meters of equivalent one-way range.

The electronics for ATS-6 satellite-to-satellite tracking have been so configured that the Doppler output is approximated by the following equation:

$$f_d = \frac{-2 f_t k}{c} [a_1 \bar{\dot{r}}_1 + a_2(\bar{\dot{r}}_1 + \bar{\dot{r}}_2)] \quad (1)$$

where f_d measured average Doppler frequency

f_t = uplink frequency = 6137.85 MHz

k = 0.336

a_1 and a_2 are scalar constants determined by equipment frequency multiplications

$\bar{\dot{r}}_1$ = average range-rate ATS to ground site

$\bar{\dot{r}}_2$ = average range-rate ATS to Nimbus, Apollo, or GEOS-3

A detailed discussion of Doppler factors in satellite-to-satellite tracking is given in ref. 7. A description of the observations, data formats and system parameters associated with NASA-GSFC satellite-to-satellite tracking is given in ref. 8.

In order to permit range-rate direction determination a fixed bias frequency (500 KHz) is added to the observed Doppler at the Doppler extractor. Thus the system counts the time, T_c, required to accumulate N cycles of Doppler, f_d, plus bias, f_b. That is:

$$T_c = \frac{N}{f_b + f_d} \text{ (seconds)} \quad (2)$$

where N is given in Table 1.

Table 1
NIMBUS Doppler Cycle Count

N	Data Sample Rate
31995	8 per second
63990	4 per second
127980	2 per second
255960	1 per second
2559600	6 per minute

The GEOS-3 tracking uses a continuous Doppler count such that an accumulation of Doppler cycles over a count time T is given by:

$$N_2 - N_1 = T(f_b + 100 f_d) \tag{3}$$

and the bias frequency is 2×10^7 Hz. For GEOS-3 the Doppler equation in the form of equation (1) is given by:

$$f_d = 2.247 \times 10^9 \left[-\frac{2}{c}\right] \left[\left(1 + \frac{1.700}{2.247}\right) \dot{r}_1 + \dot{r}_2\right] \tag{4}$$

Here the scalars 2.247 and 1.700 are exact and c is the speed of light.

- ATMOSPHERIC EFFECTS

The range and Doppler measurements will also be biased by the Earth's troposphere and ionosphere. Measurement biases of meters in range and tens of cm/sec in range rate can be expected at 2GHz. Atmospheric refraction effects can to a large extent be modeled out. Some of the work done in this area at NASA-GSFC is indicated in references 9, 10, and 11.

The atmospheric range bias is frequency independent through the troposphere and inversely proportional to frequency squared through the ionosphere. The range rate bias, in addition to the foregoing, is proportional to the rate of scan through the atmosphere as well as to the magnitude of horizontal gradients.

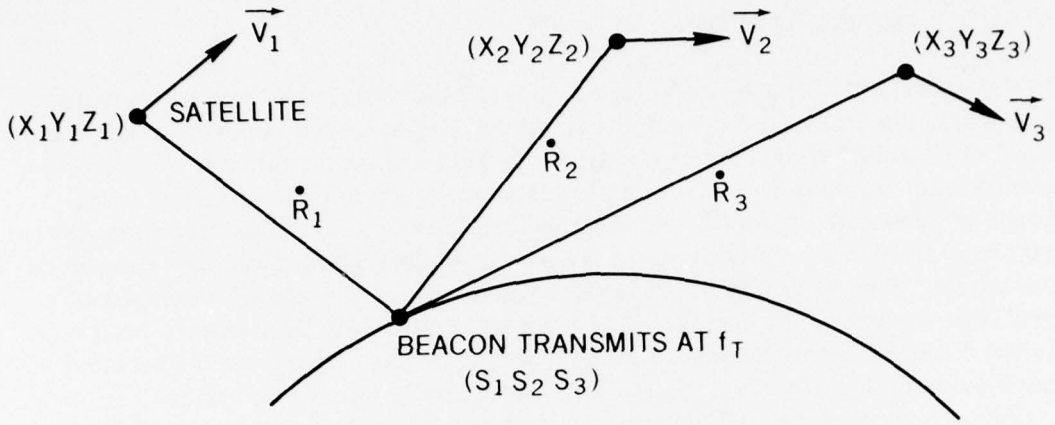
• ORBIT DETERMINATION

In the actual orbit determination program (NASA-GSFC Navigation Analysis Program) the four radio propagation paths are considered separately and the final orbit solution arrived at iteratively. This analysis program is a generalized least squares parameter estimation program designed to accept and process numerous types of tracking observations, and includes algorithms for rigorous treatment of single or multi-satellite time delay and delay rate measurements. The geopotential model can be selected from any of a number of available gravity field models. One such field currently used in this program is the Goddard Earth Model-2 (GEM-2) which is given in terms of spherical harmonics up to order and degree 22. Lunar and solar perturbations are provided by means of the JPL ephemeris residing on permanent disk file at the NASA-GSFC IBM 360/95 computer facility.

Studies have shown (ref. 12 & 13) that Earth gravitational anomalies should be observable in near Earth satellite-to-satellite Doppler data. Preliminary analysis of ATS-6/Apollo-Soyuz data bears out the conclusions of these early studies (ref. 14).

2.2 NIMBUS-6 ONE WAY DOPPLER TRACKING

One way Doppler measurements are being made aboard NIMBUS-6 in conjunction with the satellite balloon and buoy tracking and meteorological experiment entitled "The Tropical Wind Energy Conversion and Reference Level Experiment (TWERLE). On the daylight portion of each orbit, when the NIMBUS is within range of the meteorological balloons (several hundred up at present) the Random Access Measurement System (RAMS), which is the space-borne segment of TWERLE, detects, demodulates and stores the one way Doppler shifted signal and sensor data transmitted by each platform (ref. 15). The power level of the beacon is on the order of 600 milliwatts at a nominal carrier frequency, f_0, of 401.2MHz. The expected uncertainty in this frequency is ± 5kHz and the maximum one way Doppler shift at NIMBUS as calculated from $-\dot{r}/c\ f_0$ is ± 10kHz. The onboard double conversion receiver derives successive translation frequencies of 345.6MHz and 55.575MHz from the NIMBUS 1.6MHz clock and consequently operates at a nominal intermediate frequency (IF) of 25kHz. The IF operating range is from 10 to 40kHz (ref. 16). Figure 9 indicates the principle of operation of the RAMS system. The NIMBUS operational orbit is computed by the NASA tracking network and the ephemeris (X, Y, Z and $\dot{X}$, $\dot{Y}$, $\dot{Z}$) is used as computational input at the ground based computing center. Frequency offset (i.e. departure from nominal 401.2MHz Doppler) is solved for along with the beacon position coordinates S_1 S_2 S_3. Position can be determined in a single



$$R^2 = (X-S_1)^2 + (Y-S_2)^2 + (Z-S_3)^2$$

$$\dot{R} = \frac{\partial R}{\partial X}\dot{X} + \frac{\partial R}{\partial Y}\dot{Y} + \frac{\partial R}{\partial Z}\dot{Z} = \frac{(X-S_1)}{R}\dot{X} + \frac{(Y-S_2)}{R}\dot{Y} + \frac{(Z-S_3)}{R}\dot{Z}$$

$$\text{DOPPLER SHIFT AT SATELLITE} = -\frac{\dot{R}}{C} f_T$$

NOTE: GEOCENTRIC CARTESIAN
EARTH FIXED COORDINATES
$C = 2.997925 \times 10^8$ METERS/SEC

Figure 9. One Way Doppler Location of Beacon

satellite pass. Balloon velocity is estimated from two successive passes (ref. 17). The software developed for satellite-to-satellite orbit computation (i.e. Navigation Analysis Program) has also been applied to the solution of the one way beacon problem and consistently recovers such parameters as frequency offset, timing bias and beacon location. The fixed reference platform used in experimenting with this data type (apart from the normal TWERLE Balloon operations) is located at the NASA Fairbanks, Alaska tracking station.

3.0 EXPERIMENTAL RESULTS

The following presents some recent results in the areas of satellite-to-satellite tracking, geostationary satellite trilateration and one way Doppler Earth fixed beacon location from a near Earth satellite.

3.1 SATELLITE-TO-SATELLITE ORBITS

The geostationary ATS-6 spacecraft launched on 30 May 1974 has been the relay satellite for all NASA satellite-to-satellite tracking to date involving GEOS-3 (launched 9 April 1975), Apollo-Soyuz (15 July - 24 July 1975), and NIMBUS-6 (launched 12 June 1975).

The expected error for the NASA range and range rate satellite-to-satellite tracking system is a function of many controlled parameters such as range tone frequency, sample rate, bandwidth settings, signal-to-noise spectral density ratios, spacecraft dynamics and so on (ref. 6). However the system is generally used with what might be termed a standard set of options such as; 100kHz maximum range tone frequency, signal levels such that system is not thermal noise limited, 1 per second or 6 per minute data rate, and a 25Hz range tracking loop two-sided noise bandwidth. Table 2 lists the theoretical system performance for the foregoing selected options. Doppler averaging time is approximately one half the sample time interval for NIMBUS tracking and equal to the sample interval for Apollo and GEOS tracking.

For averaging times, T, up to about 10 seconds the noise decreases as $1/T$. The principal Doppler noise contribution comes from receiver voltage controlled crystal oscillators and the analog to digital conversion. For longer integration times the Doppler noise is also influenced by noise falling off as $1/\sqrt{T}$ (Fig. 10). This effect is attributed to the phase jitter in the transmitter reference signal used at the Doppler extractor. It should be pointed out that the least significant range bit recorded is 1.5 meters which is consistent with the best expected one way performance of 1.7 meters resolution.

Table 2 indicates the predicted satellite-to-satellite tracking system measurement resolution.

Table 2
Tracking System Measurement Resolution

Range (Meters)		Range Rate (Cm/Sec)	
Systematic	Random	Systematic	Random
1.2	1.2	Negligible	0.03
		NOTE: 10 Sec. Averaging	

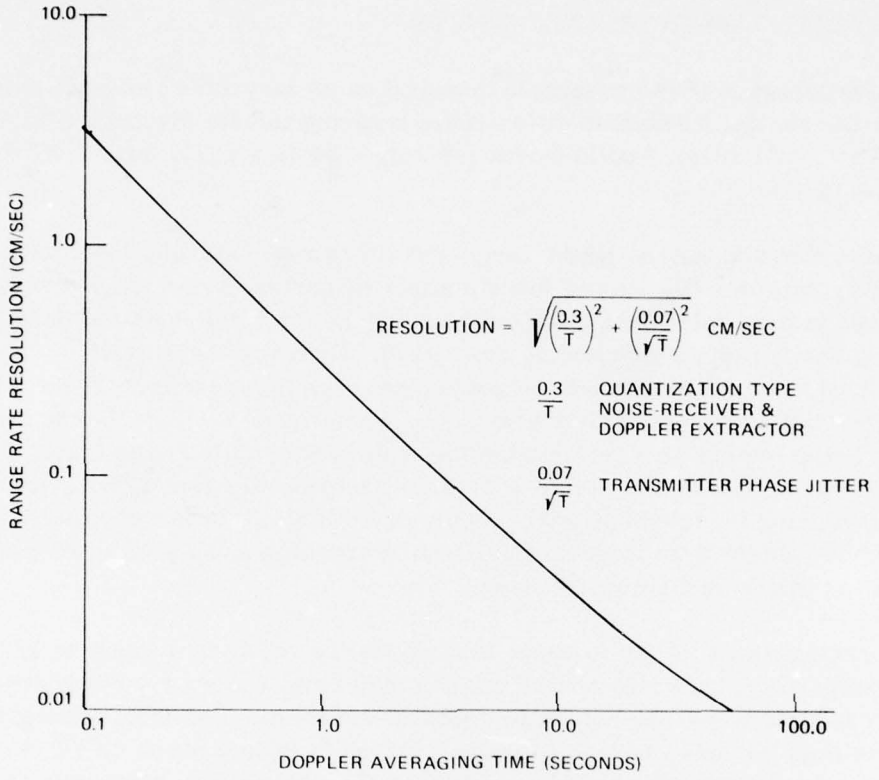


Figure 10. Range Rate Resolution

Measured results indicate close agreement with expected system performance. System random errors or "noise" are generally observed by the least squares fitting of short data spans (i.e. 1 to 10 minutes) with polynomials of at least 5th degree to account for spacecraft dynamics. Care must be taken such that the polynomial itself does not introduce apparent error. (ref. 18). If the data is from a static or collimation tower test a least squares straight line fit is appropriate.

Once an orbit is computed one indication of valid results is the difference between observed and calculated parameters over the data span. Such differences are often referred to as "orbit residuals". When the data is compared with the calculated orbit over one or more revolutions the results will be indicative of uncertainty in modeled parameters such as imperfect gravitational field harmonics and so on. It is clear that in order to improve such modeling through orbit solutions the basic orbit determination uncertainty introduced by tracking system errors must be less than the perturbation being solved for. Another

test of validity is the independent determination of two or more orbits of a given spacecraft for the same time span epoch and differencing the position and velocity components. Differencing independently determined orbits for a given spacecraft over the same time span is often referred to as "orbit overlap analysis" (ref. 19).

If independent tracking data sets are used to overlap the same orbit interval over which the overlap comparison is made the differences generally reflect tracking system performance, tracking geometry, data quantity, station location uncertainty and computational accuracy. However if one orbit is computed from a given data set and then predicted or "propagated" several days or more to overlap an orbit computed with a new data set, the orbit errors will be primarily due to uncertainties in gravitational field modeling. Orbit determination errors can thus be assessed either near the time of data observation or after orbit propagation.

Finally, another measure of accuracy is the closeness of recovery of the same parameter or orbit using two or more independent means of comparison such as; ground tracking by lasers versus satellite-to-satellite tracking, or using different orbit computation programs to recover the same parameter and so on. Again the differences in results provide some measure of accuracy. One must be careful in interpreting such results since such comparisons usually imply one tracking system and/or computer program can be referred to as a "standard".

- ATS-6/GEOS-3 ORBIT DETERMINATION

Satellite-to-satellite tracking and trajectory computation analysis has been underway for approximately 6 months. ATS-6/GEOS-3 tracking provided the first example of this new data type. Preliminary indications are that the accuracy of the a priori position used for the geostationary satellite (ATS-6 in this case) is a very critical factor in achieving orbit solution convergence. The most effective procedure for two-way satellite-to-satellite orbit determination appears to be as follows:

(A) acquire satellite-to-satellite range sum and range sum rate data over several successive low satellite passes

(B) obtain a reasonably accurate (i.e. position within several hundred meters) geostationary orbit by means of, for example, trilateration tracking

(C) obtain an approximate near Earth satellite a priori vector based on operational predictions

(D) solve for both geostationary and near Earth satellites simultaneously.

In this manner a 34 hour arc starting May 2 - 2300 Hours UT and ending May 4 - 0900 Hours UT consisting of ten passes of range sum and range rate sum satellite-to-satellite tracking data was processed to estimate the GEOS-3 orbit, the ATS-6 orbit, range data bias and solar radiation coefficients for each satellite. A priori estimates of each satellite epoch states were obtained from ground based tracking. Data rates were 6 per minute. The GEM-1 geopotential field was selected for this particular solution since this field has been most widely distributed to the user community. Orbit propagation studies are also currently being pursued using ATS-6/GEOS-3 satellite-to-satellite data in conjunction with evaluation of the GEM-1 through GEM-8 geopotential fields. The a posteriori residuals of the fit were 1.3mm/sec R.M.S. for range rate sum residuals and 16 meters for range sum residuals (Fig. 11 & 12). The optimal weights for a priori estimates of states have not yet been determined. A solution when the ATS-6 satellite state is totally constrained yields larger residuals than the solution above. An unconstrained solution fails to converge. Preliminary overlap tests indicate that satellite-to-satellite tracking can produce orbits comparable to that derived from ground based tracking (ref. 19). For example the 34 hour arc just described was used to produce two GEOS-3 orbits which were then overlapped. One orbit was computed from the first 24 hour data span and the second based on the last 24 hour span 2nd the overlap consisted of 12 hours. Comparison of the two GEOS-3 orbit vectors thus generated resulted in a minimum position difference of 10 meters and a maximum difference of 30 meters.

These orbital differences represent the very first result of overlap as applied to satellite-to-satellite tracking. Each of the two overlapped orbits was derived from data acquired during only three GEOS-3 revolutions.

- ATS-6/APOLLO-SOYUZ ORBIT DETERMINATION

The possibility of using high resolution satellite-to-satellite Doppler data in a short arc orbit computation to detect gravitational anomalies led to the Apollo-Soyuz Geodynamics Experiment (ref. 14). The purpose of this experiment was to demonstrate the feasibility of detecting and recovering high frequency components of the Earth's gravity field by observing Doppler data from the near Earth (200KM altitude) Apollo satellite via the geostationary ATS-6 satellite.

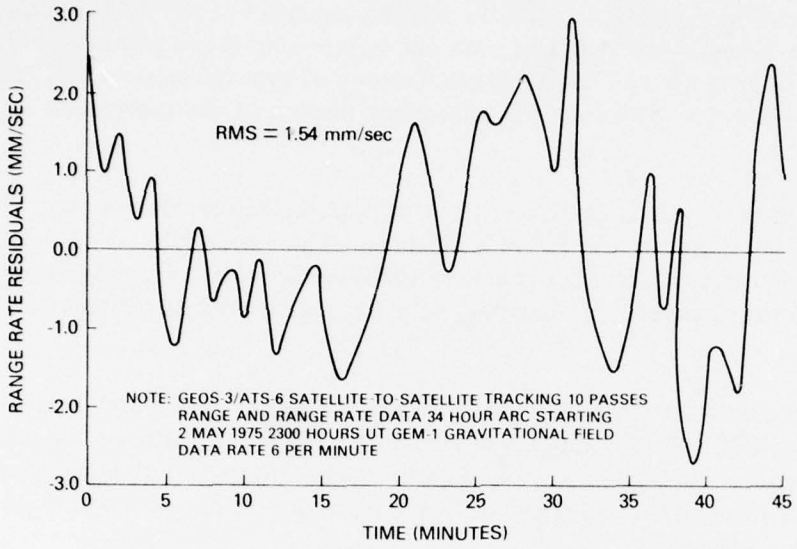


Figure 11. Typical GEOS-3 Per Pass Orbit Residuals

RMS OBSERVED MINUS CALCULATED

PASS NUMBER	RANGE-RATE (MM/SEC)	RANGE (METERS)
1	1.4	–
2	1.3	–
3	*	13.7
4	1.8	–
5	1.5	16.5
6	*	16.5
7	1.1	–
8	0.4	–
9	*	16.8
10	1.3	19.0

NOTE: 34 HOUR ARC STARTING AT 2300 HOURS UT 2 MAY 1975
ATS-6/GEOS-3 SATELLITE-TO-SATELLITE TRACKING
* DOPPLER INVALID
– NO RANGING PERFORMED

Figure 12. GEOS-3 Residual Summary

Detectability has been demonstrated through an analysis of the residual patterns in the satellite-to-satellite tracking data and comparing these patterns with previously predicted signatures due to perturbations of gravity anomalies. The recoverability objective involves the actual estimation of the magnitude of these anomalies.

The prime area of experiment data collection was the Indian Ocean Depression centered at 5° N. Latitude and 75° E Longitude. The experiment data collection phase was very successful. All data were obtained for the originally requested 28 experiment revolutions. In addition, data were collected on 79 unscheduled revolutions.

Preliminary results show that the detectability objective of the experiment has been demonstrated in the Indian Ocean Depression (Figure 13) area as well as over several other anomalous areas. Further analysis is required to demonstrate the possibility of actual recovery or estimation of the magnitude and distribution of the anomalies.

It should be pointed out that because of the short arc - typically 35 minute - orbit solutions used to detect anomalies, the results are essentially "independent" of the particular spherical harmonic gravity field used. The GEM-1 field was used during the analysis which produced Figure 13.

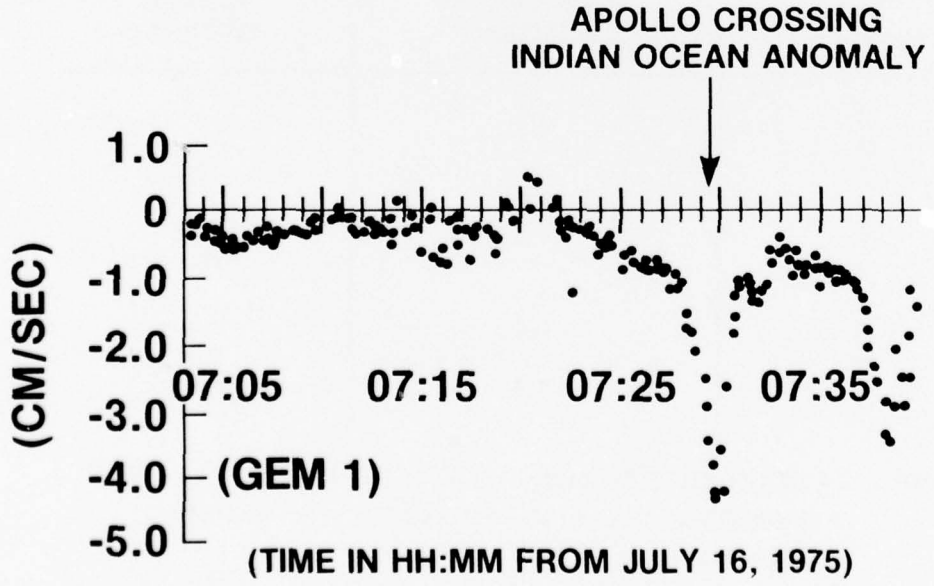


Figure 13. Apollo/ATS-6 Satellite-to-Satellite Range Rate Residual

3.2 ATS-6 TRILATERATION ORBITS

Experience to date indicates that well converged satellite-to-satellite orbit determination requires an a priori geostationary satellite position to an accuracy of a few hundred meters. This might be achieved by means of three or more widely spaced tracking stations. However a much more efficient means for accurate geostationary orbit computation has been established wherein a single station sequentially interrogates a number of widely deployed transponder via the geostationary satellite. The same station then records the tracking data in exactly the same manner as during satellite-to-satellite tracking. Weekly trilateration tracking of ATS-6 is now being performed in support of the satellite-to-satellite tracking involving GEOS-3 and NIMBUS-6. The following ATS-6 trilateration tracking test was conducted during the checkout phase of the satellite-to-satellite tracking system.

Geostationary Satellite Trilateration

On 4 November 1974 a 24 hour ATS-6 trilateration tracking test (Fig. 3) was run using the tracking stations at Rosman N. C. and Mojave, California. The availability of essentially 2 separate data sets (Mojave and Rosman) covering the same 24 hour period made this test extremely valuable in assessing orbit computation accuracy since the prime transmit-receive sites (i.e. Rosman & Mojave) could be expected to contribute the major tracking measurement uncertainty. The transponders were located at Rosman, Mojave, NTTF Greenbelt, Maryland and Santiago, Chile. Each data stretch was approximatedly 5 minutes long and the data rate was one sample per 10 seconds. Over the 24 hour period each station sequentially tracked the transponders via ATS-6. Rosman and Mojave tracked over alternate 2 hour periods. The data noise was at the system resolution level (Figure 14). The two position vectors calculated from the Mojave and Rosman data sets were overlapped and were in agreement to within 20 meters at the center of the data span (Figure 15). It is reasonable that the center of the span should represent maximum accuracy since this point in time is bracketed by equal quantities of data providing maximum information regarding higher order time derivatives of position. As a matter of interest the effectiveness of the ATS-6 solar pressure modeling is indicated in Figure 16.

3.3 NIMBUS-6 DOPPLER BIAS RECOVERY

A one way Doppler satellite-to-satellite system clearly would be much simpler to implement that the two way system described in this paper. The primary disadvantage of the one way Doppler system is that the near Earth satellite

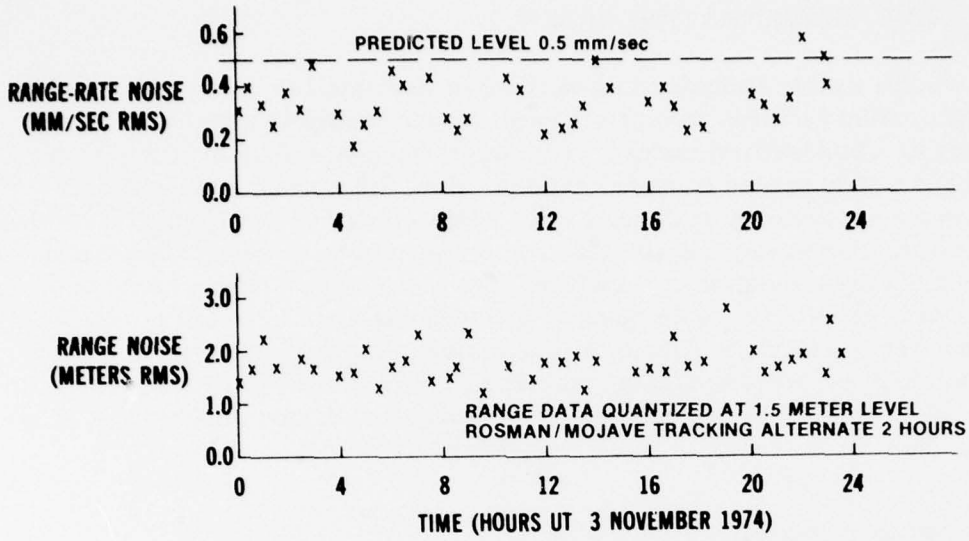


Figure 14. Tracking System Noise

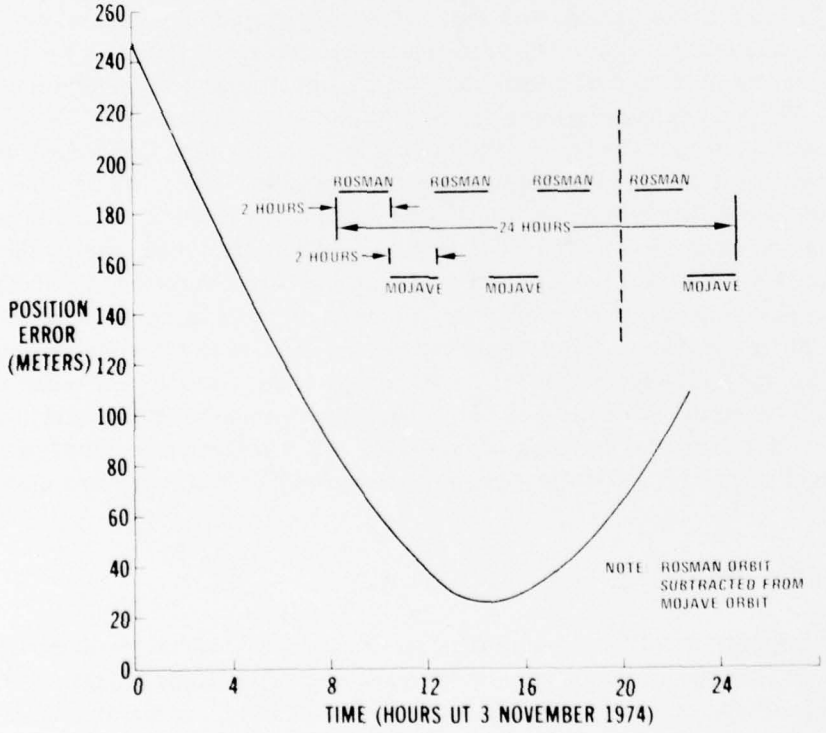


Figure 15. ATS-6 Total Position Error

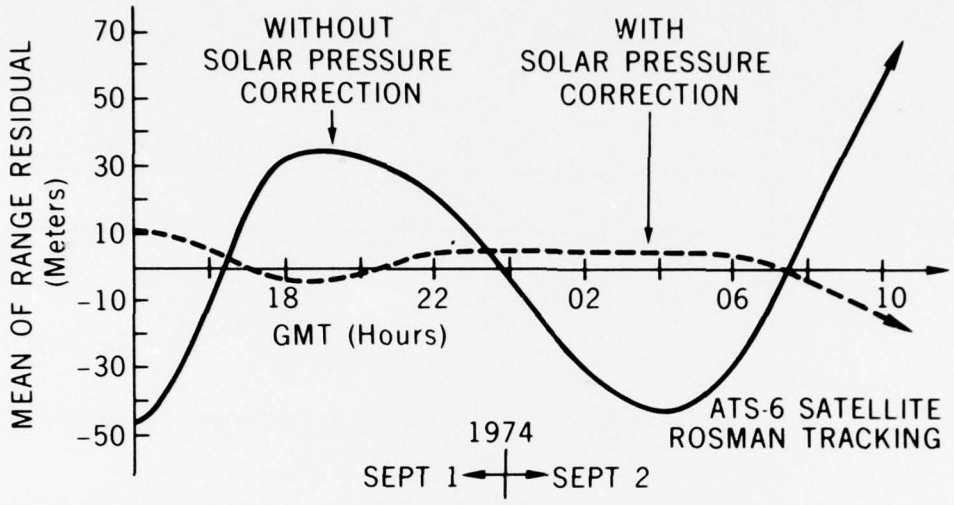


Figure 16. Effect of Solar Pressure on Geostationary Orbits

transmission frequency must somehow be accurately determined without direct measurement. Once the offset from nominal frequency has been determined one way Doppler satellite-to-satellite orbit solutions are possible. In all one way Doppler tracking systems used for position determination it is necessary to determine this offset between the nominal and actual transmitting frequency. The one way Doppler as recorded aboard NIMBUS-6 at 401.2 MHz has permitted an assessment of how well this frequency offset can be recovered in a single 15 minute data pass.

The NIMBUS-6 one way Doppler beacon location capability is being investigated in terms of Search and Rescue Applications. Single satellite passes over the Fairbanks, Alaska station are being analyzed. One question of interest is the recoverability of the frequency bias introduced by uncertainty in the ground beacon and spacecraft translation oscillators. Figure 17 indicates a typical Doppler pass. Figure 18 suggests that a frequency bias is quite observable in that one test using four distinct methods of calculation resulted in agreement to within 0.4Hz for a system with an expected measurement accuracy of ± 1Hz (ref. 16). The NIMBUS project calculation uses the algorithm described in ref. 17. The GTDS program is the principal NASA-GSFC operational orbit computation program. The NAP program is used primarily for orbital analysis. The geometric solution consisted of programming the observational equation indicated in Figure 9 and solving for the frequency offset along with the unknown position S_1 S_2 S_3. All four cases used the same unadjusted NIMBUS-6 ephemeris which had been computed independently.

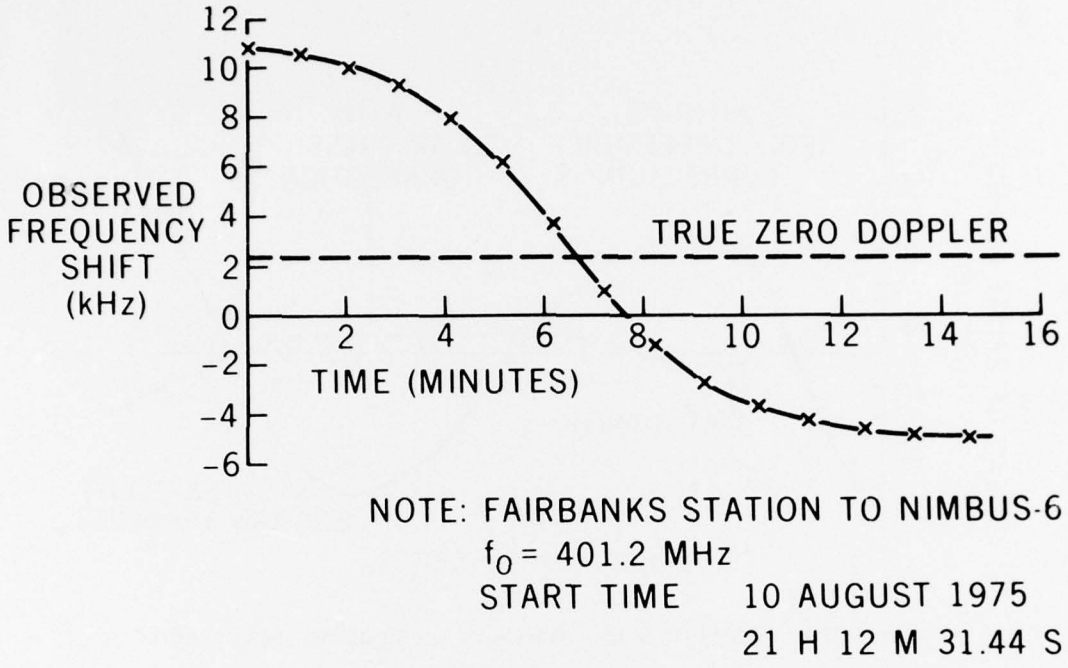


Figure 17. Typical One Way Doppler Measurement

- **FAIRBANKS ALASKA BEACON**
- **NOMINAL 401.2 MHz**
- **NIMBUS-6 RECEIVER**
- **SINGLE PASS RECOVERY**

NIMBUS PROJECT	**3098.5 Hz**
GTDS PROGRAM	**3098.7**
NAP PROGRAM	**3098.7**
GEOMETRIC	**3098.3**

Figure 18. One Way Doppler Bias Recovery

4.0 CONCLUSIONS

Satellite-to-satellite tracking system measurement resolution is predictable and readily verified. The resolution of the system described in this paper is 0.05 cm/sec in range rate and 2 meters in range.

A long arc (34 hour) GEOS-3 satellite-to-satellite derived orbit displayed RMS observed minus calculated values of 0.13 cm/sec in range rate and 16 meters in range. Over the same arc the GEOS-3 orbit position differences as obtained from a 12 hour 3 pass overlap computation are 30 meters or less.

The Apollo-Soyuz Geodynamics Experiment demonstrated that short arc satellite-to-satellite orbit solutions readily detect gravity anomalies. The Indian Ocean anomaly Doppler signature (observed minus orbit calculation) was at the expected level of 5 cm/sec.

Experience to date indicates that successful satellite-to-satellite orbit determination is to a large extent dependent on the accuracy of the a priori geostationary orbit. Trilateration geostationary satellite tracking to consistently reduce ATS-6 position errors to less than a few hundred meters is being performed regularily in support of all ATS-6/GEOS-3 and ATS-6/NIMBUS-6 satellite-to-satellite tracking currently being performed.

REFERENCES

1. Data Evaluation Branch, "Apollo 14 MSFN Metric Tracking Performance Final Report", NASA-GSFC X-832-71-175, May 1971.

2. Vonbun, F. O. and J. T. Mengel, "Tracking and Communications for Planetary Manned Mission", J. Spacecraft, Vol. 5, No. 7, pp. 863-865, July 1968.

3. Vonbun, F. O., "The ATS-F/NIMBUS-E Tracking Experiment", pp. 112-120, "Rotation of the Earth", P. Melchior & S. Yumi (eds), D. Reidel Publishing Co., Dordrecht, Holland, 1972.

4. Schmid, P. E. and F. O. Vonbun, "The ATS-F/NIMBUS-F Tracking and Orbit Determination Experiment" 1974 IEEE INTERCON, New York City.

5. Schmid, P. E. and J. J. Lynn, "Results of the 3 November 1974 Applications Technology Satellite-6 (ATS-6) Trilateration Test", NASA/GSFC X-932-75-104, April 1975.

6. Jones, C. E., ATSR Receiver Modification, Report Number R-71-033, General Dynamics, Electro Dynamic Division, San Diego, California, September 1971.

7. Marini, J. W., "Doppler Factors in Satellite-to-Satellite Tracking", NASA-GSFC X-932-74-93, April 1974.

8. Bryan, J. W., J. J. Lynn and A. O. Hinely, "A User's Guide for Satellite-to-Satellite System Observations and Data Formats", NASA-GSFC X-932-75-78, March 1975.

9. Schmid, P. E., R. B. Bent, S. K. Llewellyn, G. Nesterczuk, and S. Rangaswamy, "NASA-GSFC Ionospheric Corrections to Satellite Tracking Data", NASA-GSFC X-591-73-281, December 1973.

10. Marini, J. W., "Correction of Satellite Tracking Data for an Arbitrary Tropospheric Profile", Radio-Science Volume 7, Number 2 pages 223-231, February 1972.

11. Marini, J. W., "Tropospheric Range-Rate Tracking Data Correction", NASA-GSFC X-551-72-277, August 1972.

12. Vonbun, F. O., "Geodetic Satellite Mission and GEOS-C Spacecraft", pp. 457-467, Space Research XI, Akademie-Verlag Berlin, 1971.

13. Vonbun, F. O., "Earth and Ocean Physics Applications Program", pp. 239-245, "Astronautical Research 1972", L. G. Napolitano et al (eds) D. Reidel Publishing Co. Dordrecht-Holland, 1973.

14. Vonbun, F. O., W. D. Kahn, J. W. Bryan, P. E. Schmid, W. T. Wells and T. J. Conrad, "Gravity Anomaly Detection from ATS-6/Apollo-Soyuz", 1975 Fall Annual AGU Meeting (also to be published) December 1975.

15. Cote, C. and P. Julian, "The Tropical Wind Energy Conversion and Reference Level Experiment (TWERLE)" as presented in "The NIMBUS-6 User's Guide" NASA-GSFC February 1975.

16. Texas Instruments, Inc., Equipment Group Hb103-Eg73, "Random Access Measurement System (RAMS)", Instruction and Maintenance Manual, Under NASA Contract NAS5-21702, 15 May 1974.

17. T. Green, "Satellite Doppler Data Processing for Platform Navigation", p. 28-38 IEEE Transactions on Geoscience Electronics Vol. GE-13, Number 1, January 1975.

18. Grenchik, T. J., and C. W. Murray, Jr., "Smoothing of Functions of Range and Range Rate Measurements from Earth Orbiting Satellites", NASA-GSFC X-551-72-385, October 1972.

19. Vonbun, F. O., "Satellite Trajectory Determination and their Expected Errors OGO-IV, GEOS-1", in "Dynamics of Satellites" (1969) COSPAR Symposium Pragne, Editor B. Morando, Springer-Verlag/Berlin, 1970.

QUESTION AND ANSWER PERIOD

MR. RUEGER:

I would like to make some comments about this paper. This is a very elegant way of taking advantage of new technologies of very precise tracking of satellites and using a synchronous satellite to do the job of a large global network, and it looks to me as if it should have applications of reducing the cost of doing many of the experiments that one might want to do, and that you are, however, cascading the errors of two sets of orbits, and that is unfortunate but if you can get the accuracy in the initial orbit, then this one satellite can handle the job of a number of satellites in lots of orbits.

The accuracies he is showing us here today are really frontier type of work. Could you tell us what the contribution of the errors of your gravitational model might contribute to this?

MR. SCHMID:

Right. Well, during the short arc, of course, the gravity field is not the predominant factor, but over a week of time our uncertainty in GM which is the universal gravitational constant and the earth's mass will contribute up to 2 to 3 kilometers in a week to the synchronous satellite position, and that is the most critical. This means you have to update your orbit once a week.

What we are trying to do now, because of the observability, we are trying to recover a better value for this universal constant times the mass. I think we can do it.

MR. RUEGER:

How many coefficients do you have in your polynomial of the gravitational field?

MR. SCHMID:

In the spherical harmonic expansion, it is roughly a 21 by 21 field.

DR. REDER:

Reder, Fort Monmouth.

How much contribution would the satellite have to a timing error from orbit error?

MR. SCHMID:

There are two things. Most of the measurements I was presenting were time interval measurements. The Doppler is counted with 100 megahertz clock, and the same clock is used in clocking out the ranging signal, so in that case our timing is limiting the resolution of the system, but the resolution is on the order of half a millimeter every second, so that is not a limiting problem.

On the other hand, I believe you are asking me what is the error, propagation error that one would expect due to satellite uncertainty, and I think that that would be related to the uncertainty of the speed of light and also the uncertainty in the absolute measurement to the synchronous satellite which I indicated would be no better than say 20 meters or 10 meters perhaps. Of course, you have the propagation effects; I haven't even begun to mention the ionosphere and the troposphere effects on propagation.

DR. REDER:

The ionosphere is not being mentioned these days.

MR. SCHMID:

Well, for one thing, the two satellites I had were above the major part of the ionosphere. This is one advantage of this type of tracking, you get out of the atmosphere, and the only length that is critical then is from the geostationary satellite to ground, but that is predictable because that is more or less going through the same portion of the atmosphere. We are operating at 6 HGz.

DR. REDER:

So the guy who needs it is down on the earth.

MR. SCHMID:

That is right.

NASA TRACKING SHIP NAVIGATION SYSTEMS

John J. McKenna
NASA/Goddard Space Flight Center

ABSTRACT

The Ship Position and Attitude Measurement System that is installed aboard Goddard Space Flight Center's tracking ship VANGUARD will be described. An overview of the entire system will be given along with a description of how precise time and frequency is utilized. The instrumentation will be broken down into its basic components. Particular emphasis will be given to the inertial navigation system. What it is, how it works, and the requirement for precise time will be described. Each navigation system used, a Marine Star Tracker, Navigation Satellite System, Loran C and OMEGA in conjunction with the inertial system will be described. The accuracy of each system will be compared along with their limitations.

INTRODUCTION

Ladies and Gentlemen, I have come before you today for the purpose of introducing you to the Ships Position and Attitude Measurement System (SPAMS). This system is used on NASA's Tracking ship VANGUARD. Its function is to provide on a continuous basis attitude data (roll, pitch, and heading), velocity data (velocity North, velocity East and total velocity), and position (latitude and longitude) to the Ship's Central Data Processor where it is used for directing the tracking antennas.

During the Apollo program, the assumption was made that the only source of error in the data was due to the ship's position. Requirements were placed on the VANGUARD instrumentation such that the overall accuracy (i.e., error budget for both Navigation and Tracking antennae) would appear to be no more than 0.75 nautical miles in position and angle data would appear to be no more than 0.4 mils (0.023 degrees). Therefore, the error budget for the SPAMS with respect to its navigation and attitude data must be well within the overall accuracy assigned to the ship's instrumentation.

PRECEDING PAGE BLANK-NOT FILMED

Before discussing the SPAMS, a few definitions are needed. The geoid is the figure of the earth as defined by the undistrubed surface of the waters of the oceans over the entire surface of the earth. Because the direction of gravity is not everywhere perpendicular, the geoid is not quite an ellipsoid of revolution. Most navigation systems relate to a model of the earth that is defined by an ellipsoid of revolution (spheroid). On that ellipoid is then imposed a grid that we call Latitude and Longitude. There are a number of definitions for latitude

1) Terrestrial latitude is the angular distance from the equator measured northward or southward through 90°.

2) Astronomical latitude is the angular distance between the direction of gravity and the plane of the equator and,

3) Geodetic latitude is the angular distance between the plane of the equator and a normal to the spheroid.

Longitude has similar definitions but is measured from an adopted reference point or prime meridian and is measured eastward or westward through 180°.

Dead reckoning or deduced position is the determination of position by advancing a previous position for courses and distances.

INTEGRATED NAVIGATION SYSTEM

Figure 1 shows that the Integrated Navigation System (INS) is really made up of two systems; a Marine Star Tracker (MST) and Ships Inertial Navigation System (SINS). Figure 2 shows photographs of each component in the system. The binnacle contains the inertial platform on which four gyros and three PIPA's are located.

The SINS is a dead reckoning system and is composed of an inertial platform which is stabilized by three (3) single-degree-of-freedom gyros; three accelerometers, which sense acceleration in the level (x and y) and vertical (z) directions; a gimbaling system to isolate platform motion from ship's motion, and associated electronics and hardware (torquer motors, servos, pickoff sensors, etc.). Also contained, as part of the MK3 Mod 5 SINS, is a monitor system composed of a fourth gyro and accelerometer which are mounted on a separate platform. This separate platform, with monitor gyro and monitor accelerometer, is mounted on the main (inertial) platform, and it has freedom of motion in the level (x-y) and (z) direction plane. The monitor system provides the capability for internal calibration of the gyros and accelerometers. Fig. 3.

The SINS is an analog/digital computer. Besides a timing input it requires a damping signal which is provided by a Electro Magnetic (EM) log, an azimuth reference, and position fix information that is provided by a Marine Star Tracker, Navigation Satellite System, LORAN-C, and OMEGA.

Here we must speak of Navigation. Dutton defines Navigation as the art or science of determining a ship's or aircraft's position at any time and of conducting a ship or aircraft from one postion to another Science is involved in developing the instrumentation to accomplish this purpose. The application, the interpretation of information received, and its analysis constitute an art requiring both skill and experience.

No one Aid to Navigation or combination of such Aid's provides all the information to give a perfect fix, that is an exact Latitude and Longitude. Each Aid to Navigation has unique advantages and disadvantages which must be considered by the user. It is then possible to make a reasonable estimate of one's Latitude and Longitude. Even then results differ depending on which ellipsoid is used as the reference ellipsoid.

The primary mode of navigation for the Integrated Navigation System is the Stellar-Inertial mode. In this mode up to six preselected stars can be tracked by the Marine Star Tracker. This instrument is an electronic sextant. It measures observed elevation and azimuth angle to the selected stars and transmits this data to the MINDAC computer where in conjunction with precise time, star ephermis and besselian day number, a position fix is calculated at six minute intervals. The period of one complete circuit of the fictitious mean sun in right ascension beginning at the instant when the right ascension is 18H 40M is known as the Besselian solar year. This position fix provides Latitude, Longitude and a reference azimuth which can be either automatically inserted into the Sperry Kalman Optimal Reset (SKOR) filter at six minute intervals or manual control can be affected at the operator's discretion. Fig 4.

Unlike normal celestial navigation where a good horizon available during twilight periods (or a bubble Sextent) is required to obtain a fix using the stars, the Marine Star Tracker can be used day or night. It has an accuracy under ideal conditions for a single fix in the neighborhood of 0.05 NM.

The limitations on its accuracy are many. First, it is not possible to track when it is overcast, second refraction and other parameters are not always constant, third there are system calibration errors, and fourth there is an error due to a deflection of the vertical. The deflection of vertical is the difference between the actual geoid and

the reference ellipsoid.

NAVIGATION SATELLITE SYSTEM

The Navigation Satellite System utilizes knowledge of the position and velocity of a satellite to obtain a geographic fix. The orbit parameters or ephemeris of the satellite are transmitted by the satellite. The range from the observer to the satellite is determined by measuring the doppler frequency shift in the transmitted radio signals. This doppler frequency shift is dependent upon the transmitted frequency, position and velocity of the satellite, and position and velocity of the observer. The time reference and satellite ephermeris are transmitted from the satellite at two minute intervals. Fig. 5.

To obtain a fix, an observer assumes a set of positions for the two minute intervals at which doppler frequencies were recorded. From these positions and orbit data he computes set of doppler frequencies. The computed doppler frequencies are then compared to the observed doppler frequencies on an iterative basis to obtain a best fit. When this fit is obtained a fix is generated. Fig. 6.

The accuracy of this system is dependent on

a) the geometry of the pass

b) accuracy to which the satellite orbit is known

c) accuracy to which the doppler frequency can be determined

d) accuracy of the computational methods utilized.

The degree to which doppler frequency measurement changes in an observer's position is a function of the observer's position relative to the satellite orbit. An observer in the satellite orbit plane sees no velocity normal to the orbit plane; therefore, the longitude of the fix is very poor. Similarly the satellite-observer velocity change is very small when on the horizon of the observer. For best results the observer to satellite elevation should be greater than 15 degrees and less than 45 degrees; however, satisfactory results can be obtained at elevations of 70 degrees.

Orbit parameter predictions are transmitted from the satellite's memory on a continuous basis at even two minute intervals. The information contained in the satellite's memory is inserted at periodic

intervals with updated orbit parameter predictions by a ground station. Any errors in these computations and any perturbations in the satellite orbit will be reflected as an error in the fix that is determined by the observer.

In addition to the orbit parameter predictions there are uncertainties in doppler frequency measurements which result in errors in the fix. There are refraction effects, frequency variation, and observer velocity prediction errors.

Ionospheric refraction effects cause a path length distortion of the radio signal transmitted from the satellite. To reduce this error the Navy Navigation Satellite System utilizes a two frequency satellite transmission and a linear approximation of the frequency-refraction relationship as a correction to the doppler frequency measurement. Fig. 7.

The navigation satellite system is a doppler frequency measurement system. An instability in the reference frequency will cause an error in the position fix. On the VANGUARD, the AN/SRN-9 Navigation Satellite Systems are directly interfaced with the instrumentation timing system which has greater long and short term stability than those freqency standards normally supplied with navigation satellite receivers.

To reduce error in time measurement the satellite transmits a time signal with an accuracy of approximately 50 us as part of its data transmission. The observer receives the signal, corrects it for propagation and then can use it to correct the ship's clock.

During a satellite pass, an error in the observer's velocity and the effects of wind and current will result in a error in the position fix. To minimize this error source the VANGUARD uses the inertial system which is independent of the effects of wind and current. At least half of the total error can be attributed to this source.

There are other sources of error such as noise, altitude of observer and signal propagation. These are negligible in effect and will not be discussed.

There are many opinions as to the accuracy of this system. On the VANGUARD where an inertial system is used to correct for the observer's velocity, individual satellite fixes of 0.05 to 0.1 nautical when compared to LORAC have been obtained. LORAC is a high accuracy short-range hyperbolic navication system that is used for test purposes. The inertial system's SKOR (Sperry-Kalman Optimal Reset) routine serves as a filter to either eliminate or compensate for satellite fixes which do not conform to the historical movement of the vessel. Without

an inertial system or Loran 'C' to dead reckon during a pass, the velocity error and the effects of wind and current will degrade system accuracy. When a gyro compass and log are utilized for dead reckoning during a pass only 0.5 to 1 nautical mile accuracy can be expected.

The primary disadvantages of this system are the fix period, the reliance on pass geometry for accurate fixes, and the requirement for accurate dead reckoning during a pass. The fix period is such that only an average of ten usable satellite passes can be obtained during a twenty four hour period. Some of these usable passes are not of optimum altitude for maximum accuracy, that, between 20° and 45° from the horizon.

LORAN C and OMEGA

The next systems to be described are Loran "C" and OMEGA. They are similar only in that they are radio navigation aids and that they can be utilized either in the hyperbolic or in the rho rho (range) mode of operation. When applied to tracking ship navigation, they can be very useful aids. Unfortunately due to a lack of data reduction capability, the VANGUARD makes only limited use of them. Therefore, I shall describe how these systems could and should be used to determine the geographic position of the ship and for monitoring the operation of the inertial navigation system.

While not as accurate in determining position as either the Marine Star Tracker or the Navigation Satellite System, they have two (2) useful characteristics viz.. they provide fixes on a continuous basis and the fixes are repeatable. In the case of Loran "C" this repeatability is to within fifty (50) feet. While OMEGA does not exhibit the same repeatability as Loran "C" it does provide a significant improvement in the determination of the ship's geographic position. By correlation of the repeatability characteristics of Loran "C" and OMEGA with the accuracy of the Marine Star Tracker and Navigation Satellite System it should be possible to achieve, within the groundwave range of a Loran "C" chain the determination of the ship's geographic position to an accuracy of less than 0.05 nautical miles, and while in an OMEGA environment an accuracy to within 0.25 nautical miles. The inertial system monitoring provided by these systems makes it possible to detect such problems as gimbal servo oscillations or Schuler loop oscillations.

Loran "C" is a pulsed hyperbolic radionavigation system that operates in the frequency range 90 to 110 kilo-hertz. The United States Coast

Guard is responsible for the operation of the Loran "C" chains. That agency plans to expand the present coverage so that the entire U.S. Coastal Confluence Zone out to two hundred (200) nautical miles is covered with an accuracy of 0.25 nautical miles.

The Loran 'C' derives its accuracy from the time difference measurements of the pulsed signals and the inherent stability of low frequency propagation. Hyperbolic navigation systems operate on the principle that the difference in distance from the point of observation to each of the stations. The locus of all points having the same observed difference in distance to a pair of stations is a hyperbola, called a line of position (LOP). The intersection of two (2) or more LOP's defines the position of the observer. Figure 8.

A Loran "C" chain consists of a master transmitting station and two (2) or more secondary or slave transmitting stations. These stations are located in geographic positions so that the master and two (2) secondary stations can be received throughout the desired coverage area. The transmitting stations transmit groups of pulses at a specific group repetition intervals (GRI). The pulse has the shape indicated in Figure 9 and is transmitted on a 100 KHz carrier.

A minimum GRI is selected of sufficient length so that it contains time for transmission of the pulse group from each station plus time between each pulse group so that signals from two (2) or more stations cannot overlap in time anywhere in the coverage area. Thus with respect to time of arrival of the master, a secondary station will delay its own transmission for a specified time called the secondary coding delay.

Skywaves are echoes of the transmitted pulses which are reflected from the ionosphere. These skywaves may arrive at the receiver between 35 us to 1000 us after the groundwave thus overlapping either its own groundwave or the groundwave of the succeeding pulse. To eliminate the problems of the early arriving skywave the time measurement is made on the first part of the pulse. To eliminate the problem of the late arriving skywave the phase of the 100 KHz carrier is changed in each pulse group in accordance with a predetermined pattern.

Like all navigation systems the Loran "C" system is subject to errors. The sources of error include the following:

a) Receiver limitations due to noise and interference.

b) Short-term inconsistency of the propagating medium.

c) Synchronization of the transmitted signals.

d) Error in location of the transmitting antenna.

e) Propagation effects due to ground conductivities (Secondary Phase).

f) Velocity changes of the signal.

g) Distortion of the grid due to ground anomalies.

h) Wave-front distortion with altitude.

Continuous calibration of the time difference for each master-secondary pair is provided by the Coast Guard by the maintenance of a system area monitor. Cesium frequency standards are used at each transmitting station.

The OMEGA navigation system is a world wide hyperbolic navigation system. It can also be operated in the rho-rho mode, where in conjunction with a precise and stable internal oscillator, accurate distance measurements to the transmitter can be made.

Navigation by the OMEGA system depends on the phase stability of VLF signal propagation and the ability to predict the phase difference at any time of day.

The OMEGA navigation system is similar to LORAN "C" only in that they are both hyperbolic radio navigation systems. To cover the globe a total of eight (8) transmitter stations are planned. Of the eight (8), five (5) are operational. Two (2) are either under construction or testing. A specific geographic location has not been selected for the last station. Fig. 10.

The eight (8) stations are designed to transmit in a time-multiplexed sequence in the Very Low Frequency (VLF) range of 10 to 14 kilohertz over a 10 second period. The frequencies used are 10.2 KHz, 11 1/3 KHz and 13.6 KHz. The stations are phase locked to a common standard of time to the order of a few parts in 10^{12}. Therefore, the signal field phase is stationary at any measureable point. The relative phase angle between any two transmitters is dependent upon the distance between the receiver and the transmitter. The same phase angle is observed at all points that have the same difference in distance from the transmitting stations. The locus of all such points is a contour of constant phase (isophase) fixed on the surface with respect to the transmitters. These isophase contours represent a family of hyperbolic lanes. A single line of position (LOP) is defined by a pair of stations. A second line of position (LOP) is required to

determine a fix. Fig. 11.

In rho-rho operations, the phase of the received signal is compared to phase generated by the observors cesium frequency standard. Only two (2) stations with appropriate LOP's are required but the departure point and continuous operation are a necessity.

Two (2) significant problems with the OMEGA navigation system are its overall accuracy which is in the order of 1 to 2 nautical miles and the lane ambiguity problem.

The sources that contribute to error of the OMEGA navigation system are:

(a) Diurnal Effect - The diurnal effect is caused by the sun's position which effects the height and shape of the ionosphere which by day lowers the height of the ionization region thereby increasing the phase velocity. The converse takes place at night. The diurnal effect is seasonal and non-linear during transition.

(b) Ground Conductivity - The conductivity of the earth directly affects the phase velocity of OMEGA signals. This is especially true where the signal path is through polar regions where the attenuation through ice is high and there is a subsequent slowing of the phase velocity.

(c) Frequency - The use of the different frequencies result is errors because the propagration in the VLF spectrum is non-linear.

(d) Earth's Magnetic Field - The earth's magnetic field effects the attenuation rate and relative phase velocities.

OMEGA lattice tables and OMEGA propagation correction tables are issued by the Defense Mapping Agency Hydrographic Center.

The lane ambiguity problem stems from the nature of the OMEGA system. A pair of transmitters set up standing waves between the two (2) transmitters. Zero phase contours represent one half wavelenghts at the transmitted frequencies. Because the LOP can lie between any consecutive zero phase contours or lane the identification of the proper lane becomes necessary. This can be accomplished by maintaining a continuous OMEGA lane count, by alternate means of obtaining position fixes, or by multiple frequency operation. The maintenance of a continuous lane count over long period of time is difficult, if not

impossible. Weak signal strength of the transmiiter at the observer's position, malfunction of the receiver or of the transmitter, change from one pair of stations to another, or atmospheric noise all tend to cause loss of proper lane count. Alternate means of obtaining position fixes are available on the VANGUARD but most commercial vessels depend on the sextant, chronometer, and tables to determine an accurate fix. Weather conditions may preclude the obtaining of such a fix for long periods of time. With only one frequency (10.2 KHz), the user must know his position to within ±4 nautical miles. When the 10.2 KHz frequency is ued in conjunction with the 13.6 KHz frequency, constant lane contours appear at every fourth zero phase for the 13.6 KHz frequency and every third contour for the 10.2 KHz. This results in a wide lane three times the single lane width. By comparison of the LOP for the two (2) frequencies, a unique LOP is defined within the wide lane. A known position to ±12 nautical miles is then required to initiate OMEGA lane counting. This same technique can be expanded using 11 1/3 KHz where the unambigious lane width of 72 nautical miles thus requires the navigator to know his position within ±36 nautical miles. Fig. 12.

TIME and FREQUENCY

Before concluding, let me review how time and frequency are used in the SPAMS. The SINS utilizes 1 PPS and 10 PPS from the timing system in order to synchronize the MINDAC with the ship's instrumentation. Provision is made to automatically switch to the computer's internal clock should there be any failure of the ship's timing system.

Star Fixes require an accurate knowledge of real time. Because one second of time is equivalent to fifteen seconds of arc, real time must be known to an accuracy of fifty milliseconds if position errors due to time are to be less than one second of arc. The MINDAC receives two pulse trains from the timing system 100 PPS IRIG B and 2 PPM. The IRIG B is not used directly but instead utilizes the basic 100 PPS rate to provide the basic source of real time. The 100 PPS rate provides a resolution of 10 milliseconds in real time. The 2 PPM is used as the repetition rate for counting the 100 PPS pulses.

The Navigation Satellite System uses a basic 5 MHz signal source for the doppler counting function in the receiver. Any error in this signal source will result in a position error. A frequency standard with an accuracy of a few parts in 10^{10} is required.

Loran 'C' and OMEGA require the accuracy of a crystal frequency standard when used in the hyperbolic mode. In the rho-rho or range mode, a Cesium frequency standard is required.

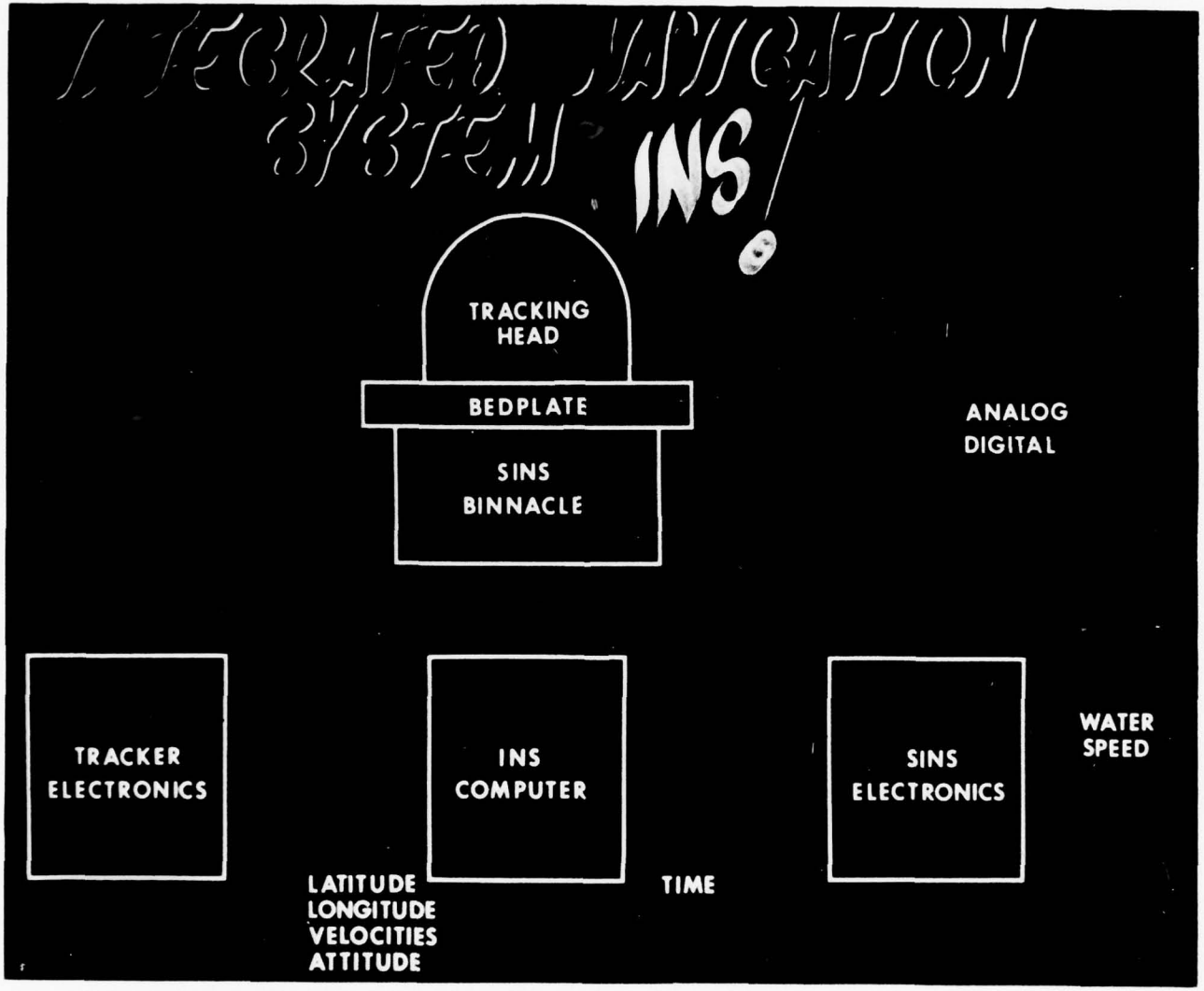
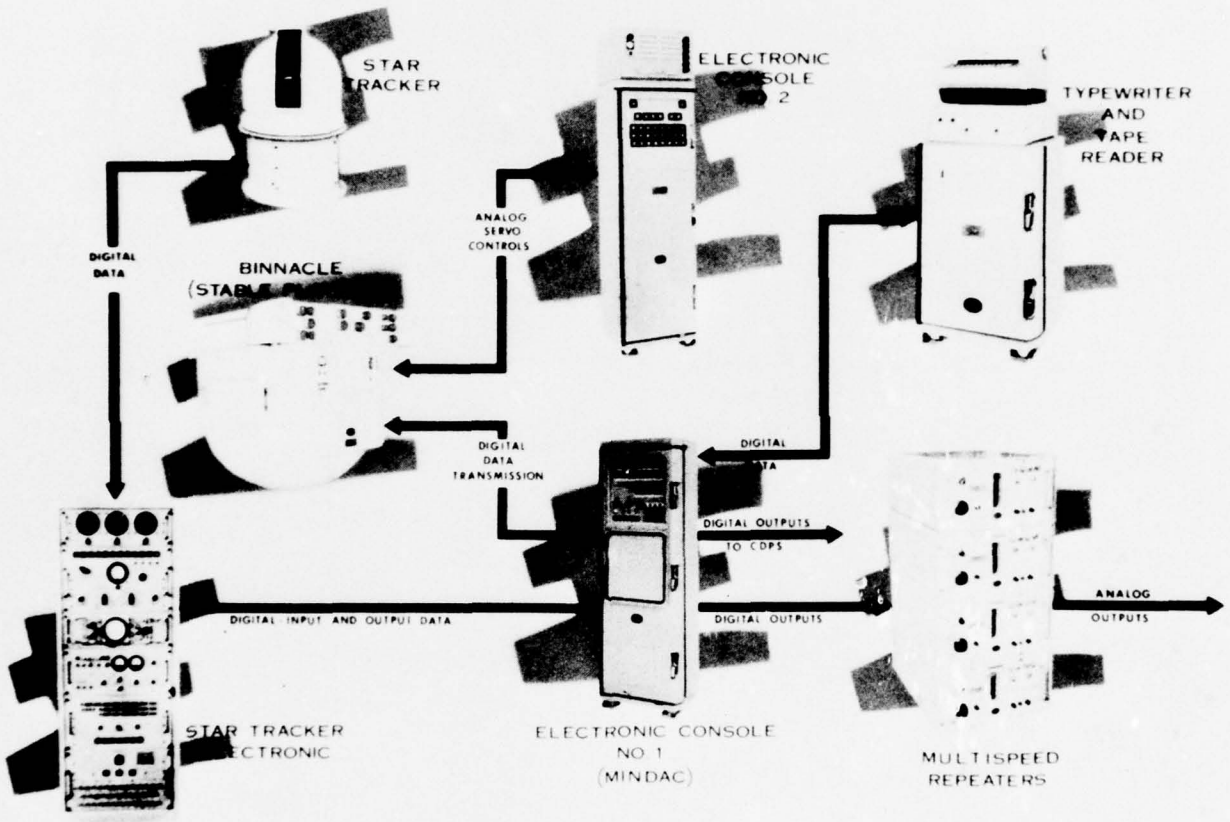

INTEGRATED NAVIGATION SYSTEM
INS
TRACKING HEAD
BEDPLATE
SINS BINNACLE
ANALOG
DIGITAL
TRACKER ELECTRONICS
INS COMPUTER
SINS ELECTRONICS
WATER SPEED
LATITUDE
LONGITUDE
VELOCITIES
ATTITUDE
TIME

Figure 1

INTEGRATED NAVIGATION SYS.



SINS MK 3 MOD 5

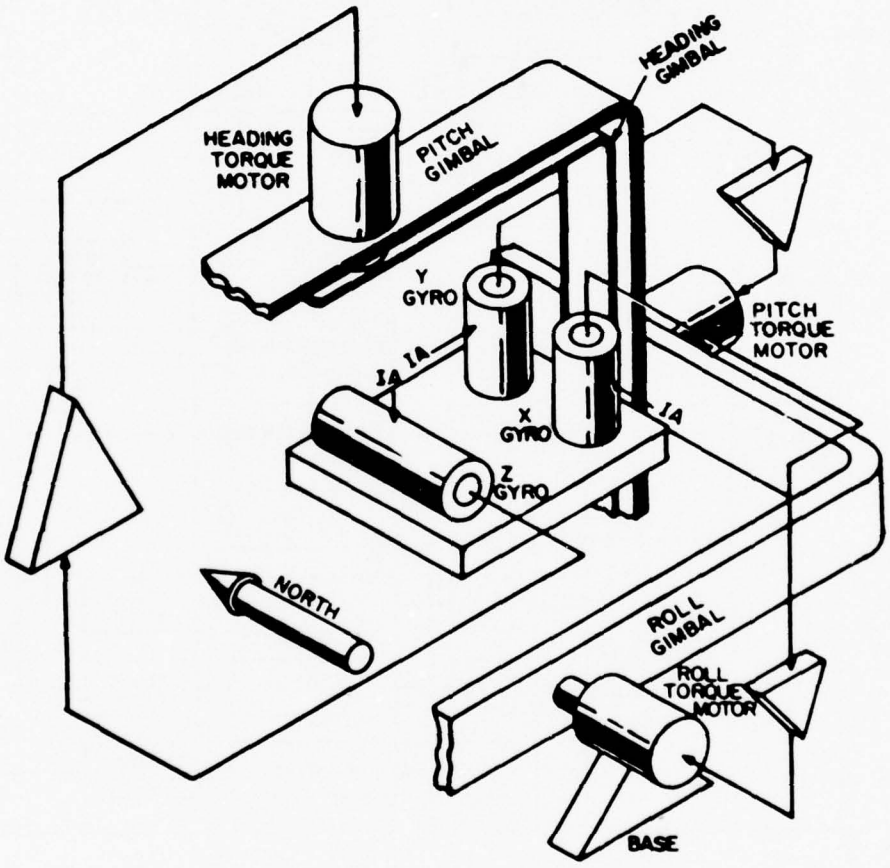


Figure 3. Three Axis Stabilization

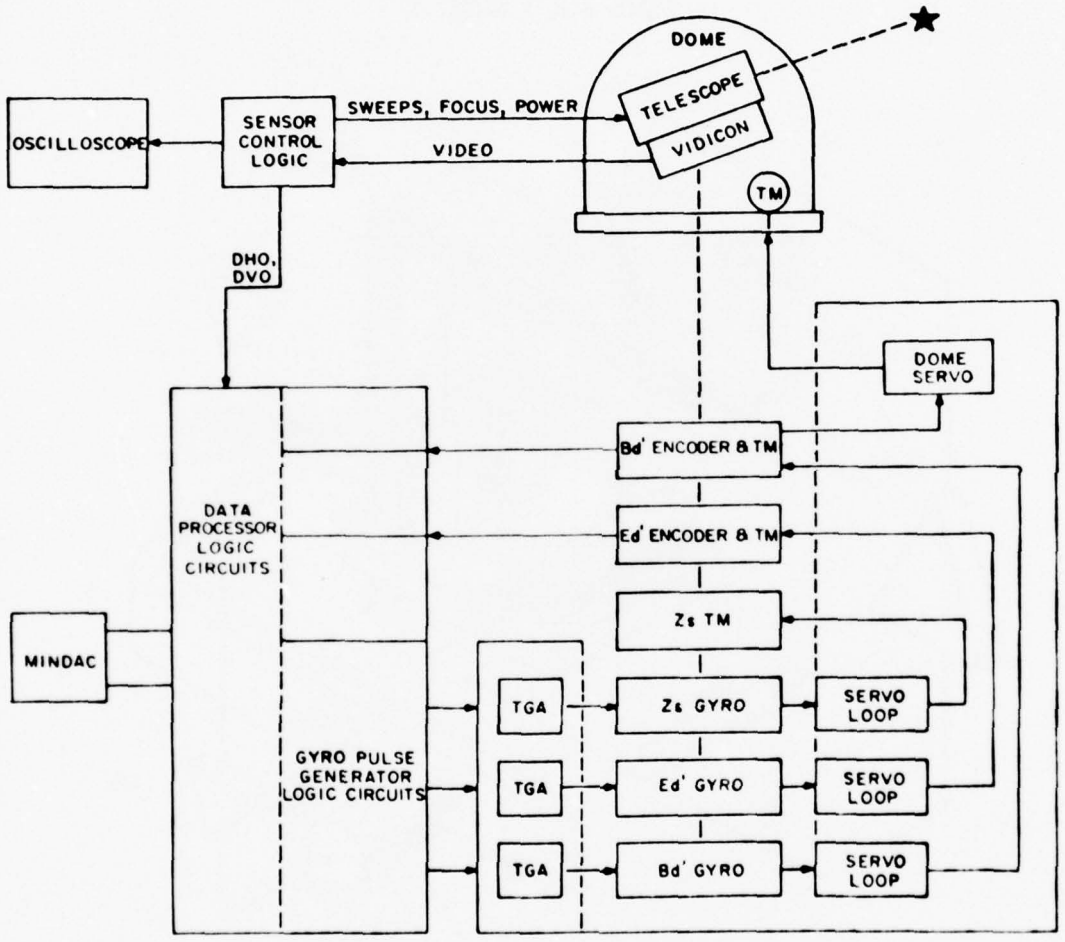


Figure 4. Marine Star Tracker Simplified Block Diagram

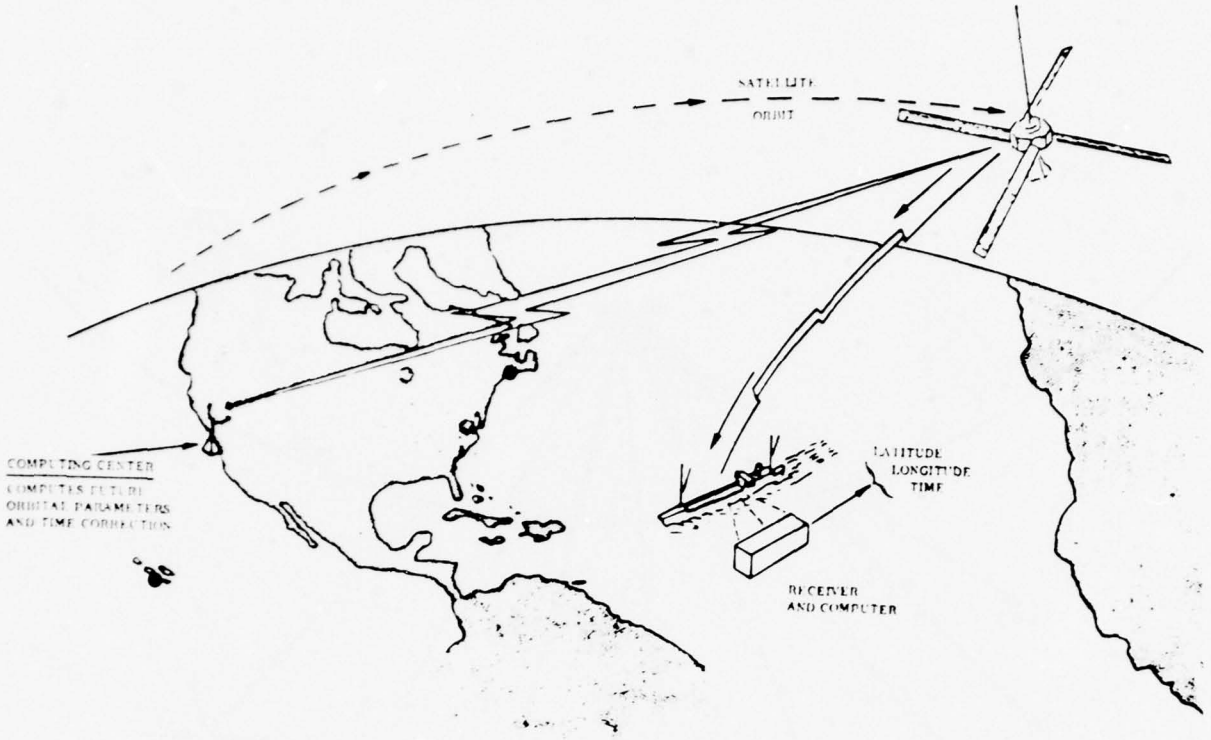


Figure 5. The Navy Navigation Satellite System

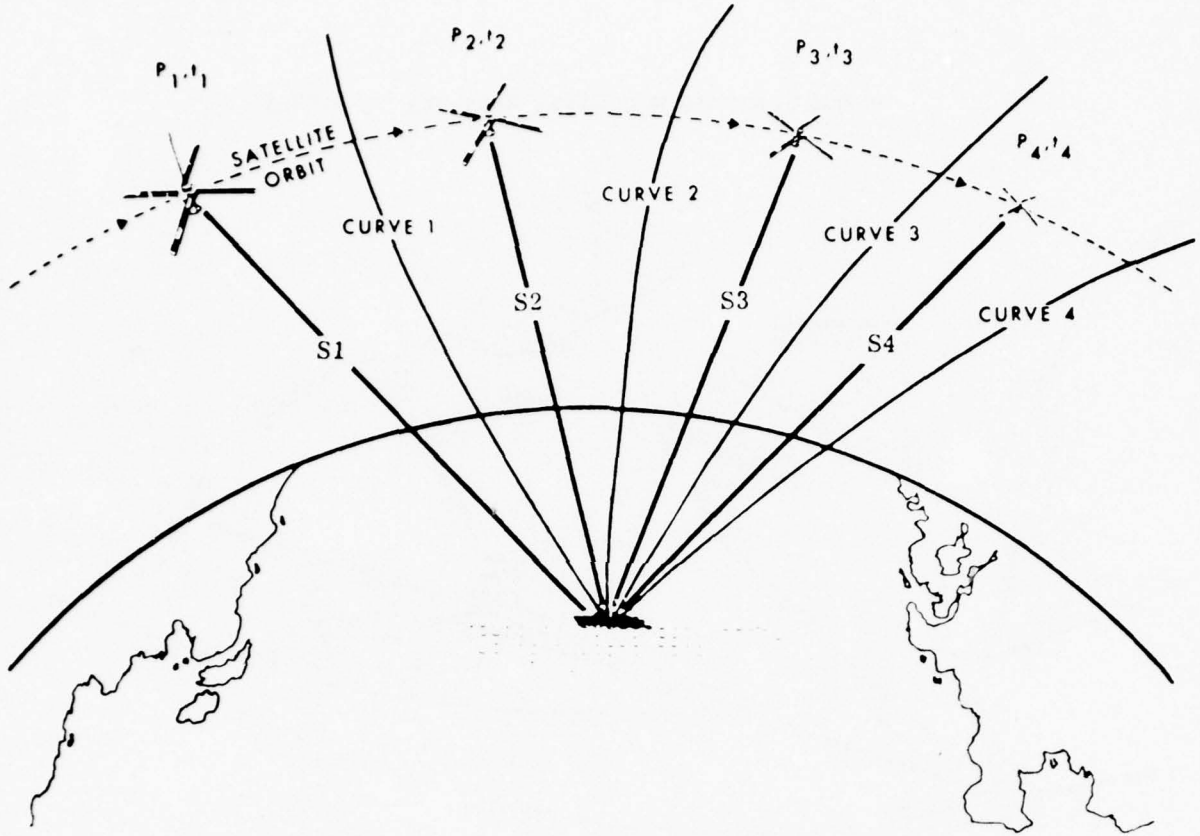


Figure 6. Obtaining a Position Fix Using Satellite Navigation Equipment

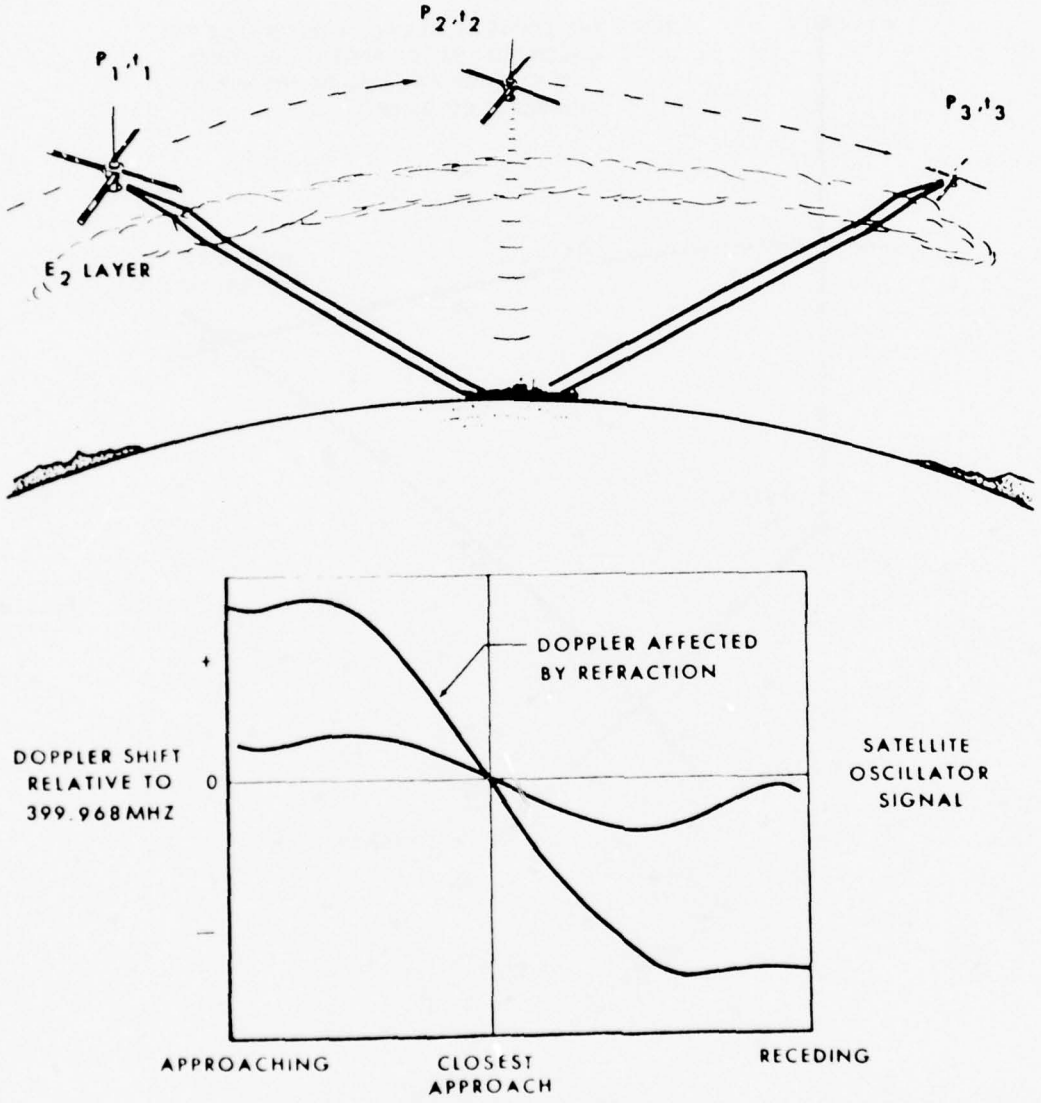
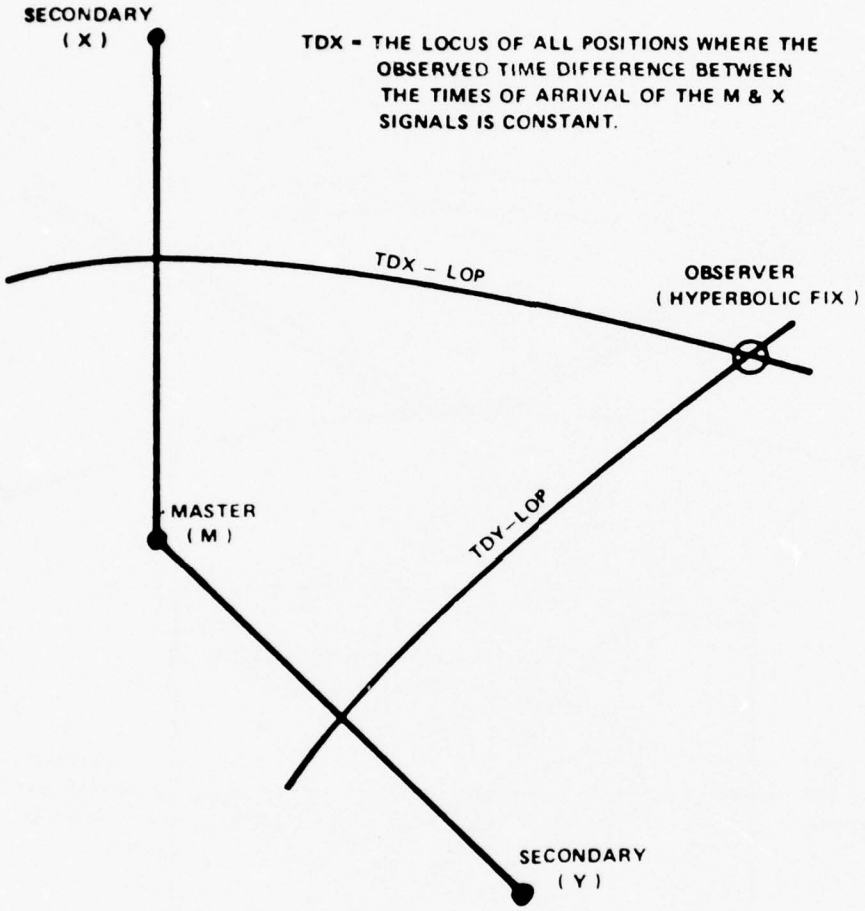
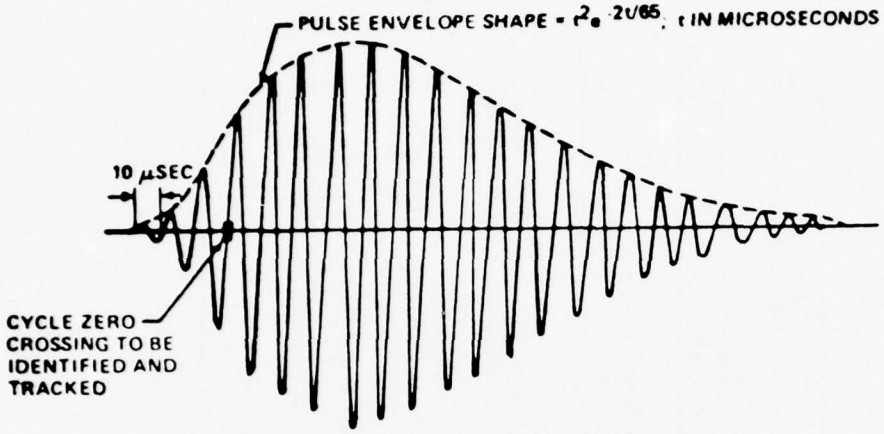


Figure 7. Satellite 400 MHz Signal Subjected to Refraction

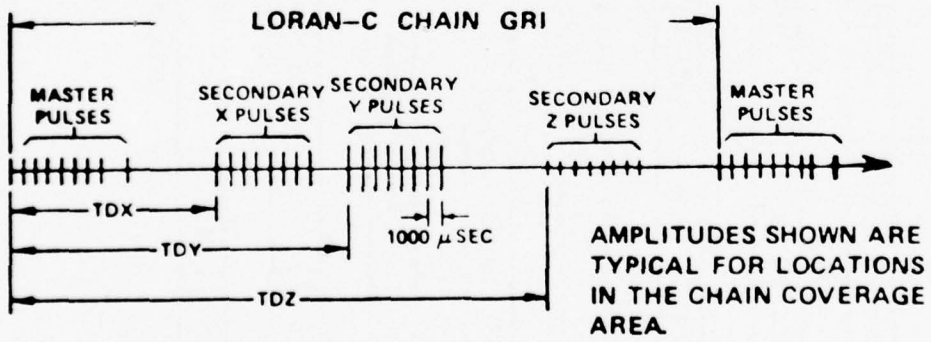


HYPERBOLIC FIX GEOMETRY

Figure 8

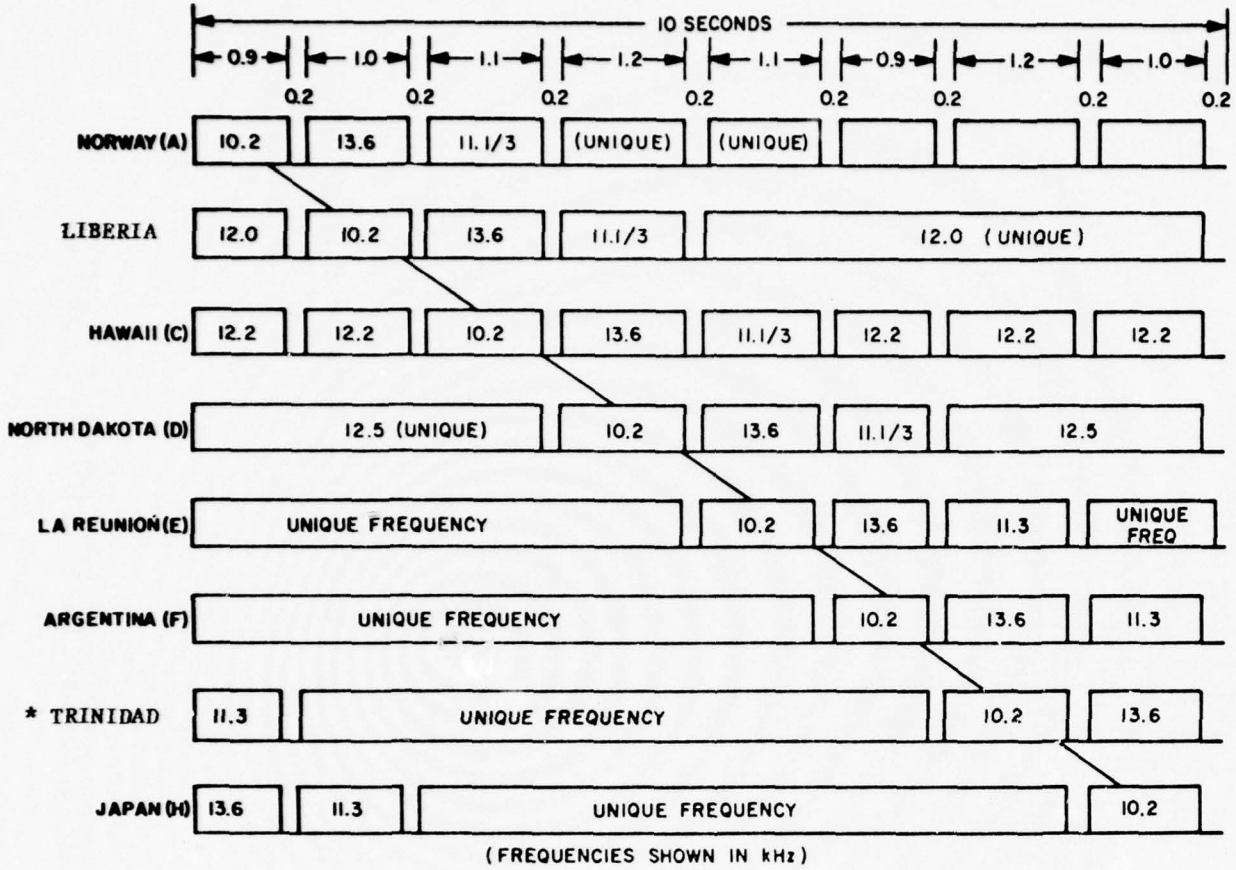


LORAN–C PULSE



EXAMPLE OF RECEIVED LORAN–C SIGNAL

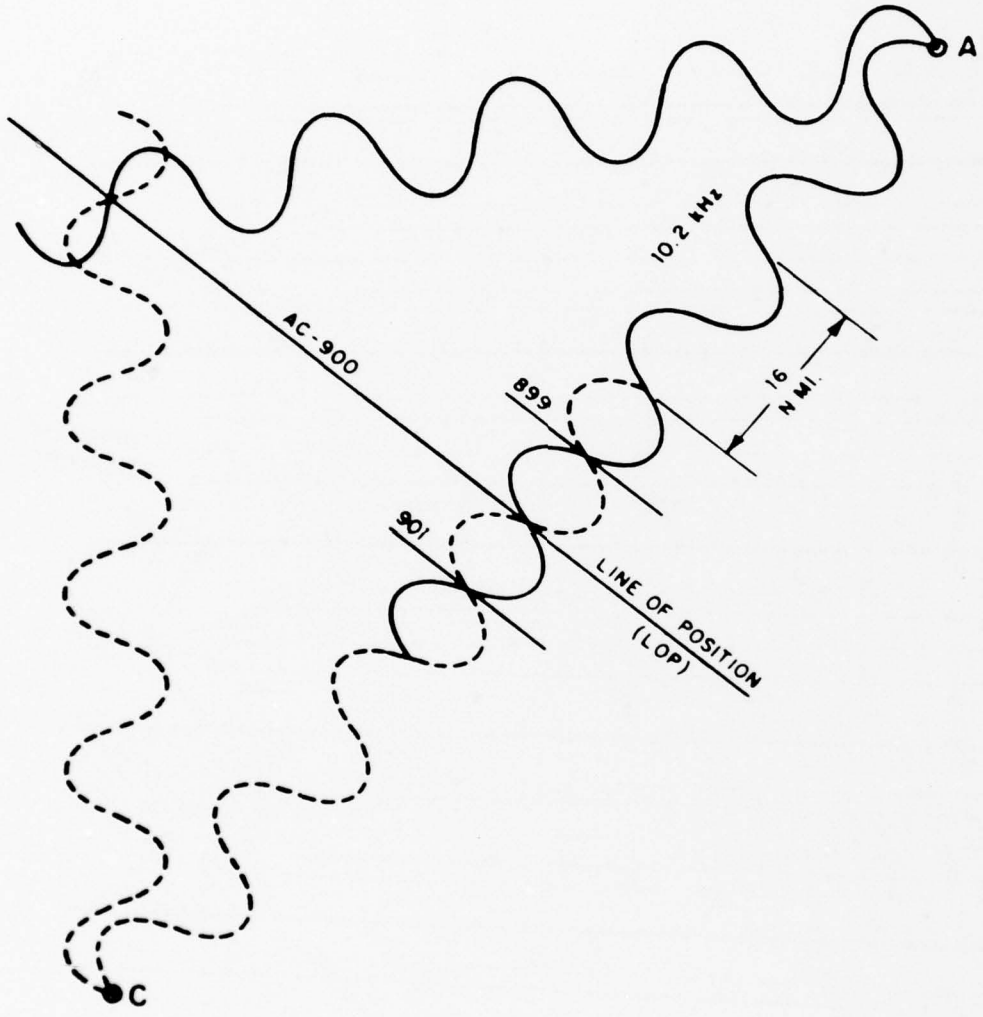
Figure 9



* Temporary

Omega Signal Format

Figure 10



Omega Lines of Position

Figure 11

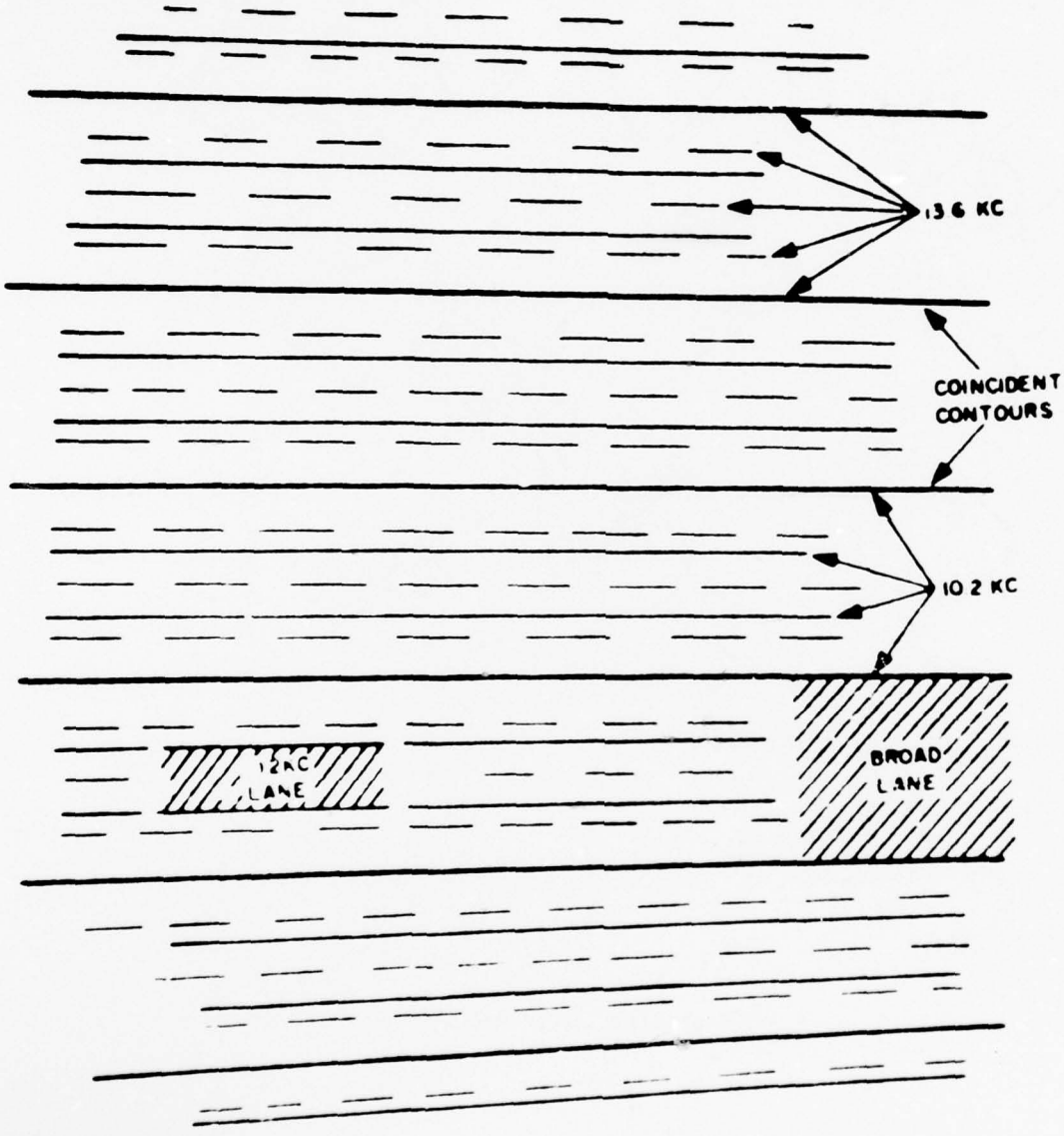


Figure 12. Principles of Lane Resolution

QUESTION AND ANSWER PERIOD

MR. RUEGER:

I would say you have had a very thorough rundown of all the navigation aids that are available today on a modern ship.

DR. REDER:

You listed frequency dispersion as an error for the Omega system. I say this dispersion is a blessing because if the dispersion did not exist, you could not eliminate propagation errors by receiving two frequencies, so long live dispersion, and I think it should be taken out of your sources of error.

MR. McKENNA:

No comment on that one.

MR. CHI:

Chi, Goddard Space Flight Center.

In the case of Omega navigation system, I think probably it should be pointed out that it is VLF, however, there is a diurnal problem involved for navigation, but the long range property should be brought out. That is the superior property for the navigation system as compared to other techniques.

MR. MC KENNA:

Well, the advantage of Omega is that it is worldwide. Loran C is limited in geographic area. There are other systems, like differential Omega to improve your accuracy. Let me get into differential Omega. Actually it is merely a bias. If you have some local means of obtaining position on the ship itself, like Navsat or the Star Tracker, you can actually determine what your propagation bias is.

Normally, when people think of differential Omega, they think of a land-based station which transmits a biased or a propagation bias for the user. It is a good system, but it has limitations, especially if you lose lane count.

DR. COSTAIN:

Costain, NRC.

I enjoyed very much this comparative study of these systems. I would like to suggest inclusion of another system. I suffered a momentary disappointment in confusing nanometers and nautical miles, so I hope the metric system will be included before too long.

MR. MC KENNA:

I learned nautical miles.

DR. KLEPCZYNSKI:

I have a question on the Star Tracker. You quoted errors there of about 0.5 nautical miles. Is that system design error, or actually have you tried to use it to get that accuracy?

MR. MC KENNA:

It is in use presently, and we get accuracies of 0.5 nautical miles. The system is operational.

DR. KLEPCZYNSKI:

Okay. I have a question then. Do you account for DUT-1? How do you get it or make use of it?

MR. MC KENNA:

I am not familiar with the DUT-1.

DR. KLEPCZYNSKI:

That is the difference between, say, the uniform or universal time coordinated and the actual time of the rotation of the earth, DUT-1, which I assume you must be referring your angular measures of the star system to.

MR. MC KENNA:

We use the ship's timing system. We are using the ship's timing system for all our timing references.

MR. RUEGER:

You failed to mention the area of operations of Vanguard, I believe. Can you identify in what part of the world you want to operate?

MR. MC KENNA:

The Vanguard operates in all parts of the world. At the present time, it is in the Indian Ocean, and has been for about six months.

MR. RUEGER:

You mentioned the deflection of the vertical. I wondered if you had good enough data in that part of the world to do the Star Tracking to this accuracy.

MR. MC KENNA:

Actually, it is one of the errors we don't know. The error generally is about the accuracy of about 30 seconds, but really it does not significantly enter the picture. I could, and it does where we run into the situation where the ship is near a land mass. You can actually tell by what happens to the inertial system that the ship is going over a sea mountain or something of that nature. We have to recalibrate the sins because of it.

MR. RUEGER:

In order to meet the requirements you laid out of a .75 nautical mile, by what method can you justify to yourself that you have realized this performance in all points of the world?

MR. MC KENNA:

We have run tests with the Vanguard and off the Florida Coast. There are two Loran networks down there, the A net and the B net. Periodically we do check out all the systems to see that they are working properly, and we do achieve that accuracy. As a matter of fact, most of our accuracy is less than .5 nautical miles.

MR. RUEGER:

That is rather a local geographical region. I wonder if

you can extrapolate that well.

MR. MC KENNA:

I think we can. The deflection of the vertical is going to cause an error, but it will cause an error like .1 nautical miles, something of that nature.

ANALYSIS OF THE IMPACT OF SATELLITE NAVIGATION SYSTEM RECEIVER OSCILLATOR ERRORS ON USER NAVIGATION PERFORMANCE*

Gregory L. Mealy
The Analytic Sciences Corporation
Reading, Massachusetts

ABSTRACT

This paper considers a satellite-based passive radio navigation system that is capable of providing highly accurate navigation fixes to properly equipped users. For the user to access such a system he must be equipped with a receiver that includes a local oscillator which maintains a time base and generates frequency information required for signal acquisition and for pseudo-range and pseudo-range-rate measurements. This paper examines the impact of receiver quartz crystal oscillator errors on user navigation performance. A model is developed which describes environmentally-induced oscillator errors. This error model is incorporated into a simulation to assess the impact of environmentally-induced oscillator errors on user navigation performance. The analysis considers both basic oscillator performance and the effect of environmentally induced errors including: oscillator warm-up, temperature, vibration and acceleration sensitivities and the effect of a shock to the oscillator. Methods are presented with which the receiver software may be designed to reduce the impact of the significant error sources.

---

*This work was performed in support of the Air Force Avionics Laboratory under Contract No. F33615-75-C-1112. The program was funded by the U.S. Army Satellite Communications Agency.

INTRODUCTION

Recent advances in technology have demonstrated the feasibility of a satellite-based passive radio navigation system that will be capable of providing highly accurate navigation fixes to properly equipped users (Ref. 1). For the user to access the satellite navigation system he must be equipped with a receiver that includes a local oscillator which maintains a time base and generates frequency information required for signal acquisition and for pseudo-range and pseudo-range-rate measurements. A relative phase offset between the user clock and the satellite clocks will lead to pseudo-range errors while a frequency offset in the user oscillator introduces pseudo-range-rate errors. This paper examines the impact of quartz crystal oscillator errors on user navigation performance for such a satellite navigation system.

In order to properly assess the impact of environmentally-induced quartz crystal oscillator errors on navigation performance a comprehensive model of the oscillator error behavior must be developed. The complete error model will include a description of the intrinsic instability of the oscillator as well as the environmentally-induced errors. The model for intrinsic instability follows directly from a consideration of the frequency stability of a specific oscillator and has been developed previously (Ref. 2). This paper presents the development of an error model which describes the effects of the environment on a quartz oscillator. The error model is then utilized to assess the degradation in navigation performance for an airborne user which arises from the use of the receiver oscillator in a realistic (non-ideal) environment.

QUARTZ CRYSTAL OSCILLATOR ERROR MODELING

The prototype for the quartz crystal oscillator error model to be considered is shown in Fig. 1 with

$\delta\phi(t)$ = total clock phase error in seconds at time t

$\delta\phi(t_0)$ = initial phase error (seconds)

$\delta f(t_0)$ = initial fractional frequency offset (dimensionless)

$\dot{\delta f}(t_0)$ = initial fractional frequency drift or "aging" (seconds^{-1})

q_f = spectral level of white noise driving the flicker noise model (dimensionless)

δf_{env} = environmentally-induced fractional frequency error

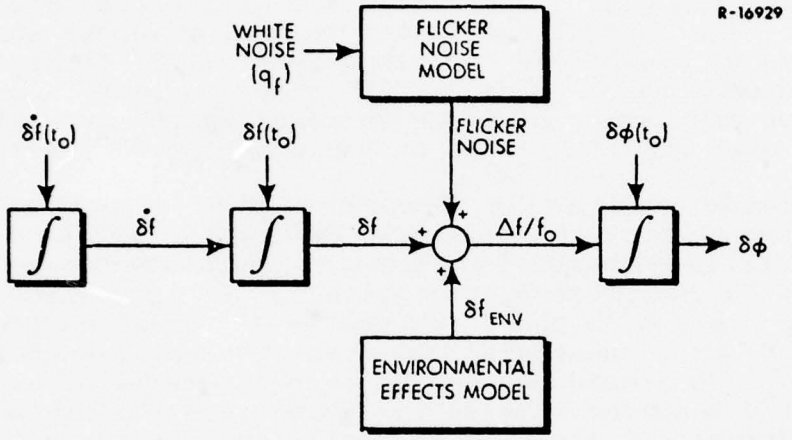


Fig. 1 Prototype Quartz Crystal Oscillator Error Model

As mentioned above, the methodology for constructing the basic oscillator model has been presented in an earlier paper (Ref. 2). This paper will deal only with the development of an environmental effects model for a quartz oscillator. A completely general error model for environmental effects would be prohibitively complex. However, if certain assumptions are made about the form and number of environmental influences, then an environmental effects model can be developed for a specific device. In the following paragraphs the effects of temperature, warm-up, acceleration, vibration and shock on a quartz crystal oscillator will be discussed.

Temperature - A quartz oscillator responds to a change in ambient temperature with a shift in frequency. The relationship between this frequency shift and the temperature change varies from oscillator to oscillator and may be quite nonlinear. When the oscillator is incorporated into the navigation system receiver, a linearized coefficient relating the frequency shift to a temperature change can be obtained.

For temperature excursions about a nominal receiver operating temperature (assumed to be $\simeq 60^{o}C$) the assumed linear temperature drift coefficient for this study is $K_{tv} = 1 \times 10^{-10}/^{o}C$.

The frequency shift, which results from a temperature change, does not occur instantaneously due to a "thermal lag" inherent in the oscillator. The temperature-regulating oven surrounding the quartz crystal is the main contributor to this lag. The typical oscillator thermal response shown in Fig. 2 can be adequately described by a simple first-order system as depicted in Fig. 3. The time constant, τ_{tv}, depends upon the number of ovens surrounding the crystal. For a single oven device τ_{tv} is on the order of 80 minutes.

The error model shown in Fig. 3 represents the response of the crystal oscillator to an arbitrary temperature variation. In order to utilize this model the input temperature variation must be described quantitatively. It is obvious that differing users will encounter vastly different environmental conditions. These dissimilar environmental scenarios will result in mission-dependent temperature fluctuations outside the receiver. These variations are not transmitted instantaneously to the crystal oscillator due to the moderating influence of the receiver thermal mass. Assuming random temperature variations, the ambient temperature surrounding the crystal oscillator is reasonably modeled as a

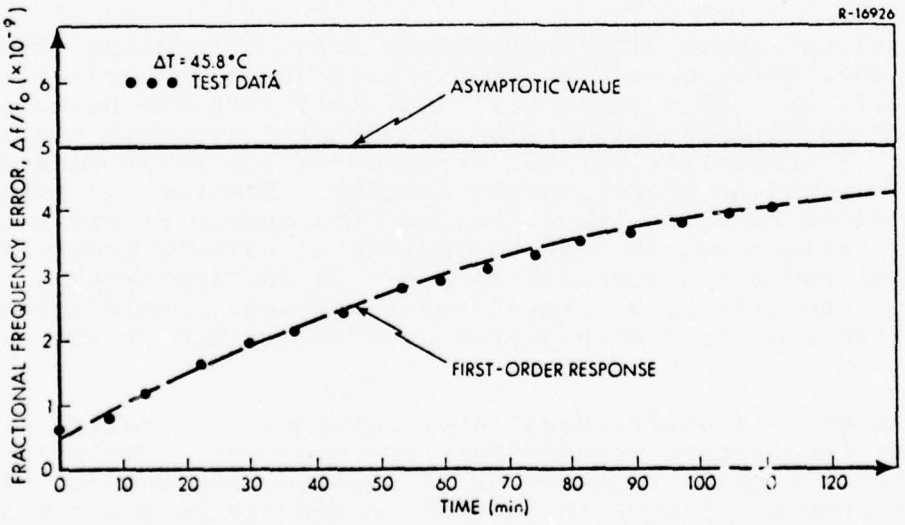


Fig. 2 Response of Crystal Oscillator Frequency to a Step Ambient Temperature Change

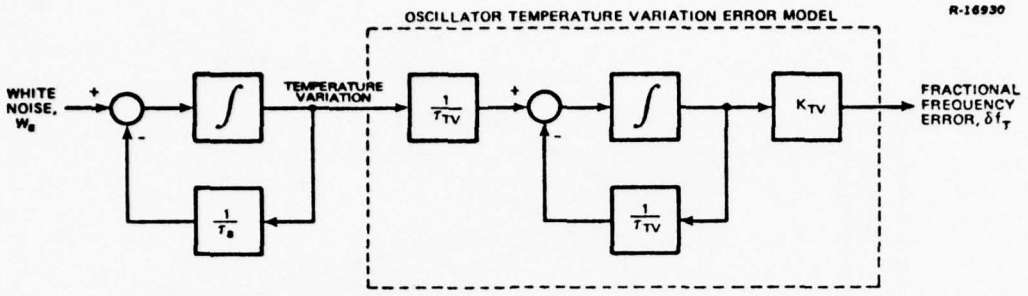


Fig. 3 Quartz Crystal Thermal Error Model

first-order Markov process. The parameters of the process, rms value and time constant, must be chosen to reflect the temperature variations outside the receiver and the moderating effect of the receiver. For a typical receiver the rms value of the temperature fluctuations near the crystal oscillator is expected to be on the order of $3^{o}C$ with a time constant (τ_a) of 100 minutes.

Warm-up - Figure 4 shows the fractional frequency error versus warm-up time characteristics of three quartz crystal oscillators. The three oscillators exhibit vastly different behavior which is not amenable to direct analysis. The dashed line in the figure describes an exponentially decaying envelope (the plot is semi-log) which can be viewed as a statistical bound on the frequency error. The warm-up fractional frequency error variance ($\sigma^2_{\delta fw}$) for this exponential model is

$$\sigma^2_{\delta fw} = \sigma^2_w \, e^{-2t/\tau_w}$$

with $\sigma^2_w = 1 \times 10^{-10}$ and $\tau_w \simeq 100$ seconds.

Acceleration - A constant acceleration introduces a frequency offset in a quartz oscillator proportional to the magnitude of the acceleration, i.e., $\delta f_a = K_g |\underline{a}|$. The coefficient of proportionality, K_g, is dependent upon the orientation of the acceleration vector with respect to the crystallographic axes of the quartz crystal. A worst case value is $K_g = 1 \times 10^{-9}/g$.

Vibration - Vibration introduces sidebands (at the vibration frequency) into the spectrum of the signal from a quartz crystal oscillator. These sidebands produce a frequency error which is dependent upon the oscillator sensitivity at the vibration frequency. Figure 5 presents the results of measurements of the fractional frequency error (averaged over a 10-second interval) arising from the lateral (sinu-

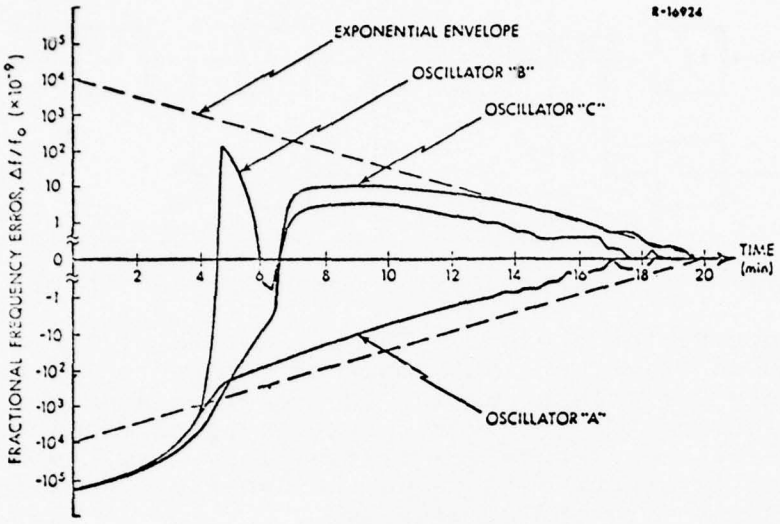


Fig. 4 Warm-up Characteristics of Three Quartz Crystal Oscillators

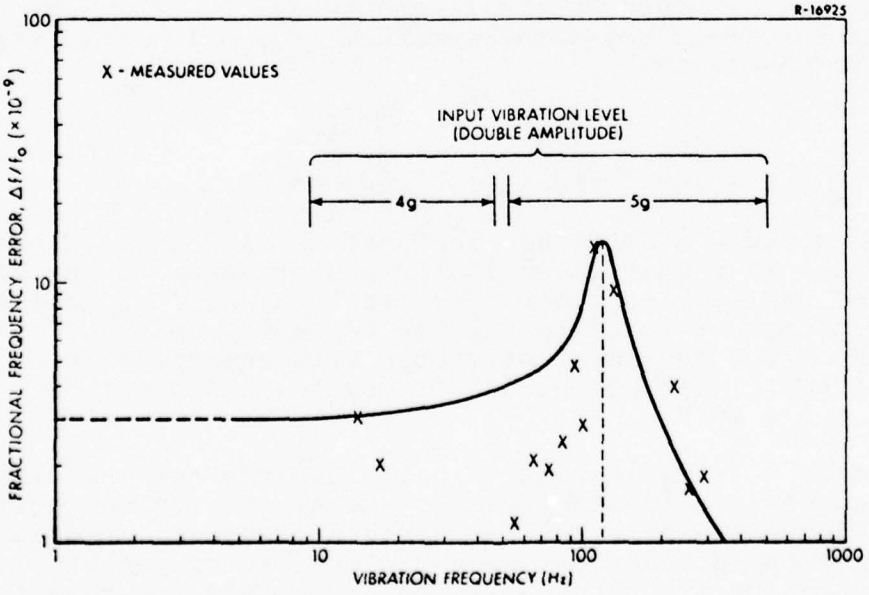


Fig. 5 Frequency Error as a Function of Vibration Frequency

soidal) vibration of a quartz crystal oscillator. The worst case response is adequately modeled by the resonant second-order curve which is superimposed upon the data. In lieu of a well-defined spectrum for the vibration in an operational environment the baseline model will assume a white noise input with spectral level

$$q_v = 0.02\ g^2\ \text{sec.}$$

The model representing the frequency error due to vibration, δf_v, is shown in Fig. 6. The parameters of the model are obtained from Fig. 5. The resonant curve in the figure corresponds to a natural frequency, ω_n, of 754 rad/sec and a damping ratio, $\zeta = 0.1$. The constant K_v is the lateral vibration drift coefficient with a value of $6 \times 10^{-10}/g$ from Fig. 5. As expected, the vibration coefficient K_v is very close to the g-sensitive drift coefficient K_g.

Shock - When a quartz crystal oscillator is subjected to a shock, a permanent frequency offset results. No specific values are available (at this time) for the magnitude of this offset during the shock but step fractional frequency shifts on the order of 1×10^{-9} have been observed following shocks of 15g to 60g. A reasonable model for the effect of a shock of short duration ($\simeq$1 msec), occuring at time t_s, is a step fractional frequency shift ($\delta f_s|_{t_s}$) of 1×10^{-9}.

In the previous paragraphs models were developed to describe the frequency errors which arise from perturbations in the oscillator's environment. The total fractional fre-

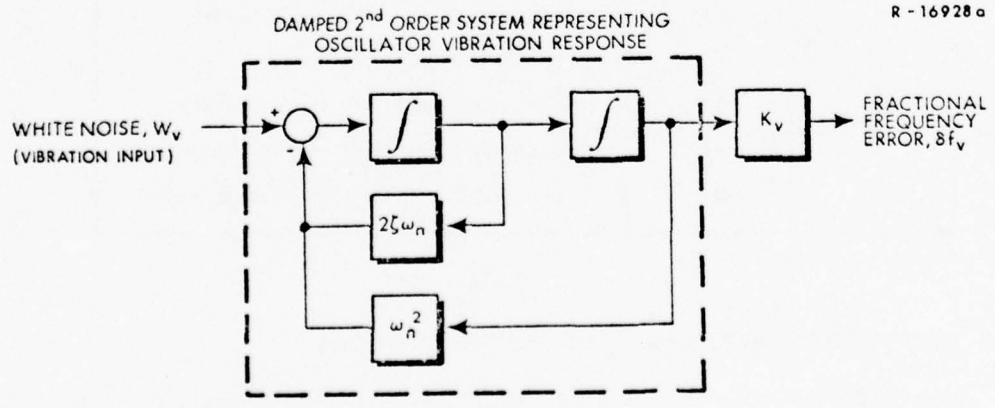


Fig. 6 Crystal Oscillator Vibration Error Model

quency error due to environmental effects, δf_{env}, is the sum of the individual errors resulting from temperature changes, oscillator warm-up, acceleration, shock and vibration effects, viz,

$$\delta f_{env} = \delta f_t + \delta f_w + \delta f_a + \delta f_s|_{t_s} + \delta f_v$$

The environmental effects model can be combined with the intrinsic instability model of the quartz oscillator as shown in Fig. 1. The error state vector for the quartz crystal oscillator error model is given in Table 1. Two error sources are not included explicitly in the state vector. The error arising from the acceleration of the oscillator (i.e., $\delta f_a = K_g|\underline{a}|$) is more appropriately modeled as an additive quantity. The second error source, which will remain unmodeled, is the effect of an impulsive shock to the oscillator. Although it is unmodeled, the impact of such an unanticipated shock will be examined in this paper.

TABLE 1

QUARTZ CRYSTAL OSCILLATOR
ERROR MODEL STATE VECTOR

STATE	SYMBOL	DESCRIPTION
1	$\delta\phi$	Phase Error
2	δf	Frequency Error
3	$\delta\dot{f}$	Frequency Rate Error
4	x_{1f}	Flicker Noise
5	x_{2f}	Intermediate Flicker Noise State
6	δf_t	Frequency Error (Thermal Model)
7	x_t	Temperature Variation
8	δf_w	Frequency Error (Warm-up Model)
9	δf_v	Frequency Error (Vibration Model)
10	x_v	Intermediate Vibration Error State

USER EVALUATION SCENARIO AND ERROR MODELS

The analysis of the airborne user performance employed a simulation program developed at TASC in order to investigate the effects of environmentally-induced errors. The airborne

user (helicopter) trajectory is illustrated in Fig. 7. The user initially processes one minute of measurements while stationary to calibrate the receiver clock. After takeoff the helicopter makes turns at a maximum of 15 deg/sec, accelerates at a maximum of 2.5 mps/sec and changes altitude at a maximum of 3.0 mps.

An inertial navigation system (INS) is included in the user formulation to provide accurate short-term navigation between measurements. A barometric altimeter is also included to bound the vertical channel of the INS. The measured altitude is used in a closed-loop fashion to damp the altitude errors. For the airborne user performance analyses considered in this paper, pseudo-range and pseudo-range-rate measurements are obtained simultaneously from four of the satellites in view every 10 seconds.

Two error models are required for the generation of user performance projections. The first is a model describing the "real world" errors. This model would ideally be a complete description of all significant error sources which impact upon user navigation performance. The second model, which is a deliberately simplified description of the "real world" errors, is implemented in the user Kalman filter.

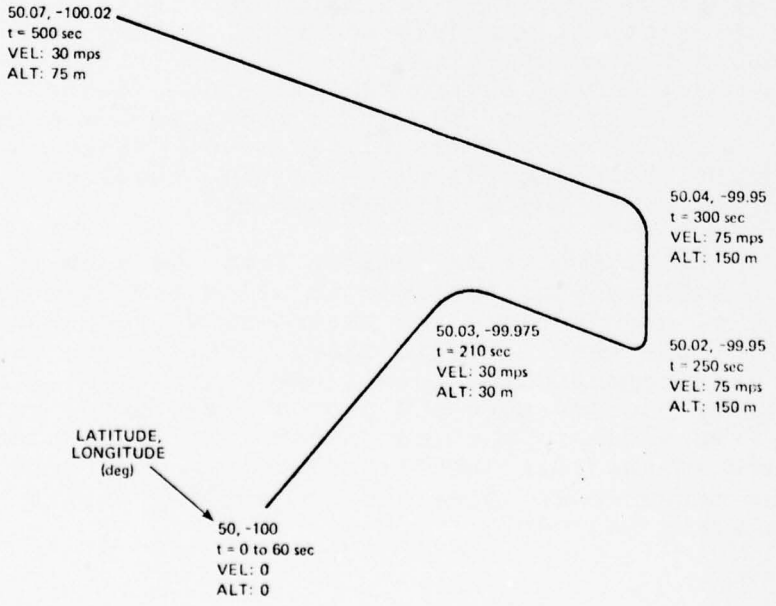


Fig. 7 Airborne User Trajectory

The "real world" error model includes a description of the satellite navigation system errors, the user INS errors and a user clock error model. The satellite navigation system errors, as implemented in the simulation program, include satellite clock and ephemeris errors, signal propagation delays (ionospheric, tropospheric and multipath), and receiver noise and quantization.

The user clock error model was developed above. The 10-state clock error model includes a description of the effects of temperature, warm-up and vibration. Errors which arise from acceleration and shock are not explicitly included in the error state vector (see Table 1). However, these two error sources are included in the description of the "real world" and their effects on user navigation performance will be evaluated.

The user Kalman filter (Ref. 3) estimates the 20 user navigation and clock errors summarized in Table 2. The user position and velocity errors are referenced to a locally level [north (n), east (e) and down (d)] coordinate system located at the instantaneous user position. As indicated in Table 2, INS errors are characterized by gyro drift (with bias and random walk components) and accelerometer bias error terms. This model will provide a reasonable description of INS errors during the short ($\simeq$8 minute) mission under consideration. Since the purpose of this paper is to discuss the effect of user clock errors, a more detailed INS error model would be undesirable. The user filter does not include a model of any environmentally-induced errors in the user clock. In addition, the state modeling the effects of aging has been deleted in the filter model since the total mission duration is shorter than the time required for the effects of aging to become significant.

The user filter formulation assumes that the user is equipped with a multichannel receiver to allow the simultaneous processing of pseudo-range and pseudo-range-rate information from four of the satellites in view. The filter-assumed receiver measurement noise levels are 7.5 m (rms) and 0.15 mps (rms) for pseudo-range and pseudo-range-rate, respectively. Errors due to the ionospheric and tropospheric effects are assumed (in the filter) to be compensated to within the measurement noise and are not correlated with the other error sources.

TABLE 2

STATE DESCRIPTIONS FOR 20-STATE
AIRBORNE USER FILTER

STATE NUMBER	SYMBOL	DESCRIPTION
1	δR_n	North Position Error
2	δR_e	East Position Error
3	δh	Altitude Error
4	δV_n	North Velocity Error
5	δV_e	East Velocity error
6	δV_d	Down Velocity Error
7	ψ_n	Platform Misalignment About North
8	ψ_e	Platform Misalignment About East
9	ψ_d	Platform Misalignment About Down
10	δs_a	Barometric Altimeter Error
11	ε_n	North Gyro Drift
12	ε_e	East Gyro Drift
13	ε_d	Down Gyro Drift
14	μ_n	North Accelerometer Bias Error
15	μ_e	East Accelerometer Bias Error
16	μ_d	Down Accelerometer Bias Error
17	$\delta\phi$	Phase Error
18	δf	Fractional Frequency Error
19	x_{1f}	Flicker Noise
20	x_{2f}	Intermediate Flicker Noise State

USER PERFORMANCE PROJECTIONS

This section will present user performance projections which predict the impact of environmentally-induced receiver clock errors on user navigation performance. The results are given in the form of user estimation errors and the rms estimation error envelope (standard deviation boundary) predicted by the user Kalman filter. Each error source modeled above is introduced into the "real world" error model separately and its effect on user navigation performance is assessed by comparing the resultant navigation errors with those of a baseline run in which environmentally-induced errors were deleted. The following paragraphs discuss the impact of the various error sources.

Baseline - The baseline performance of the airborne user is indicative of the navigation errors which arise from navigation system errors (satellite ephemeris and clock errors, signal propagation errors, etc.) and user dependent errors (INS error sources and the nonenvironmentally-induced clock errors). This performance is illustrated in Fig. 8 for the trajectory of Fig. 7. The peak in horizontal velocity error at the first turn is due to a residual heading error which couples the acceleration experienced during the turn into the horizontal velocity error. This makes the heading error highly observable, such that pseudo-range-rate measurements during the turn calibrate the heading error.

Temperature and Vibration - The impact of the oscillator temperature and vibration sensitivities on user navigation performance was minimal for the assumed levels of random inputs. In both cases the projected user performance was indistinguishable from the baseline values. It should be noted, however, that a strong sinusoidal vibration near 120 Hz (see Fig. 5) would result in a large frequency error and could lead to a degradation in user navigation performance.

Warm-up - The impact of quartz crystal oscillator warm-up on user navigation performance is considered next. It was assumed that the oscillator had been turned on 12 minutes prior to the start of the flight. The 12-minute period was chosen to be compatible with a 5-minute coarse gyrocompass and 420-second fine-align of the INS.

Figure 9 illustrates the effects of oscillator warm-up when it is not modeled in the user filter. The frequency offset present during warm-up appears directly as the predominant contributor to frequency estimation error. This large frequency offset results in an increase in velocity error since

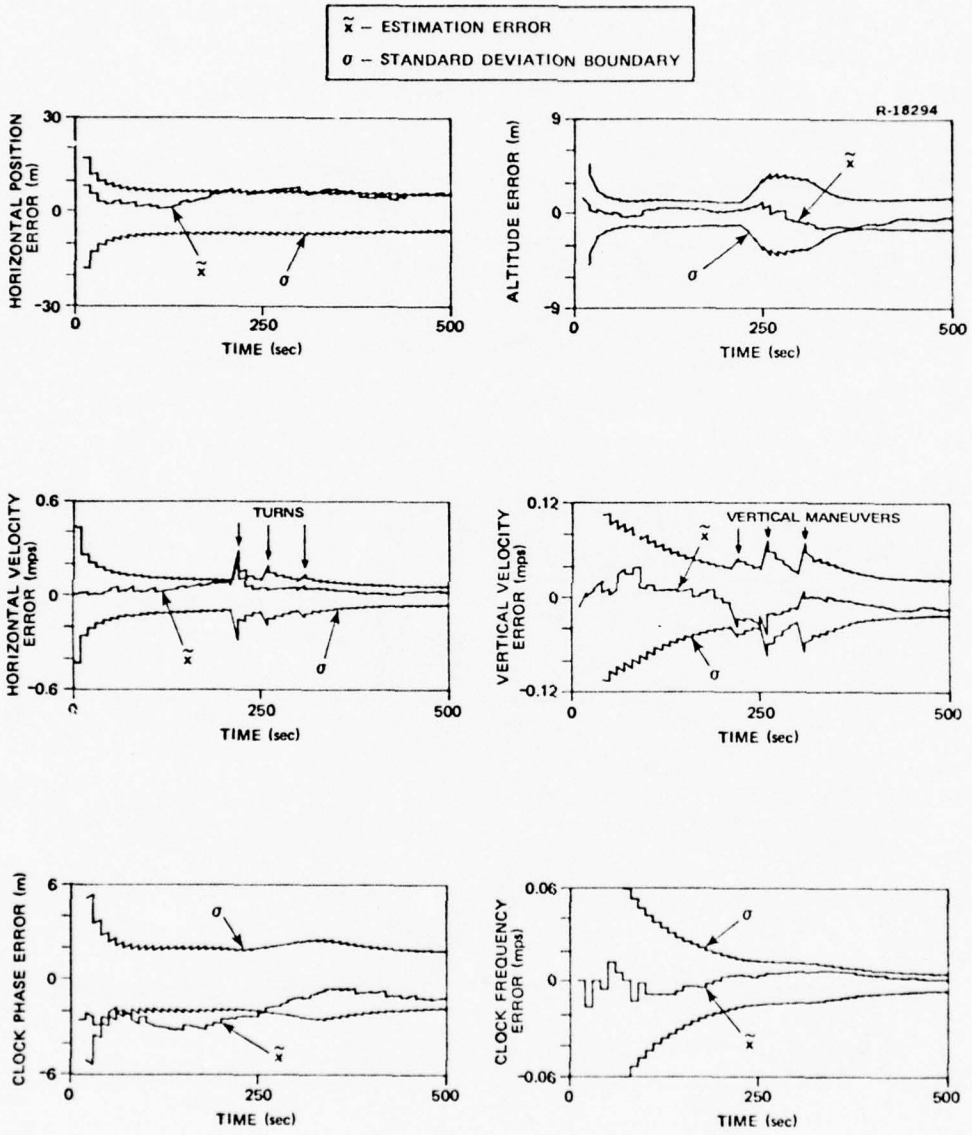


Fig. 8 Airborne User Errors - Baseline

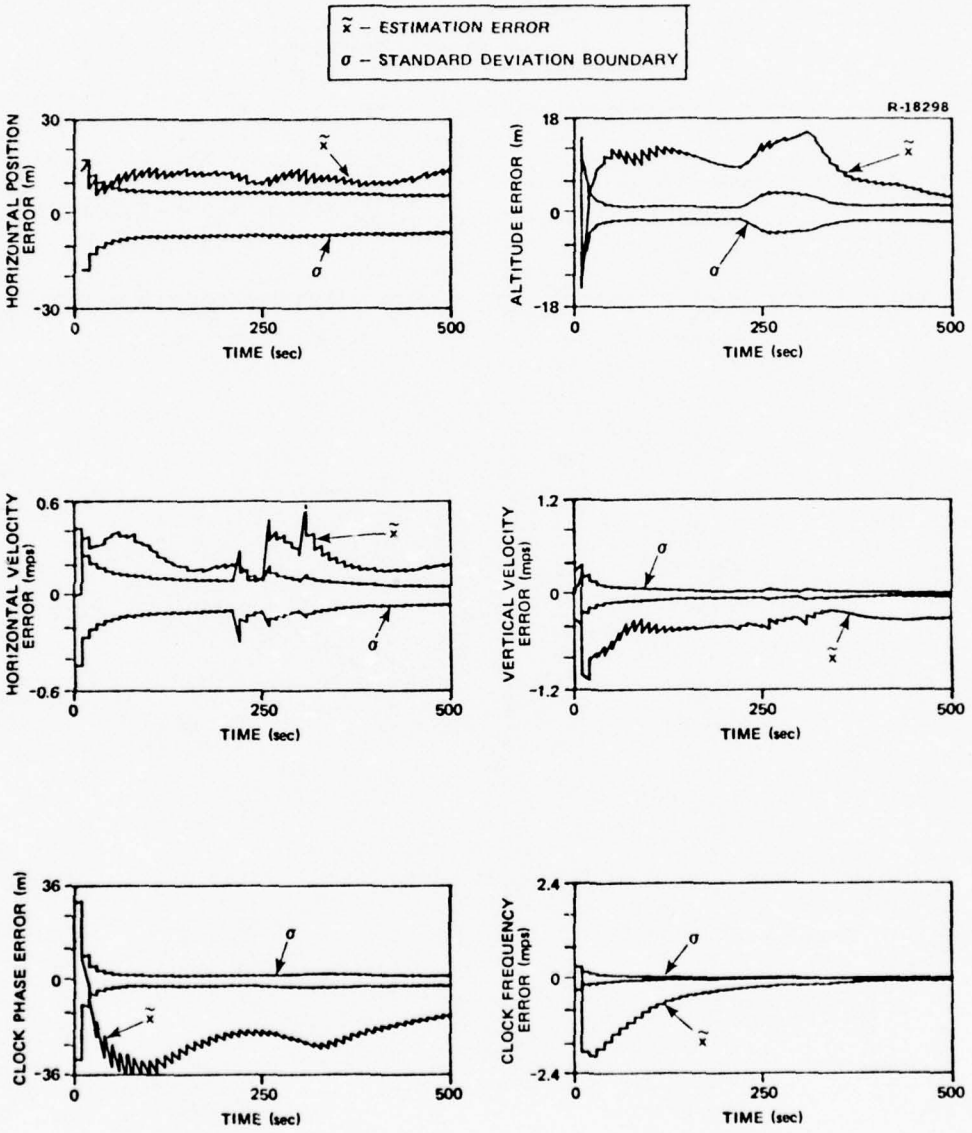


Fig. 9 Airborne User Errors - Warm-up (Not Modeled in User Filter)

the filter cannot properly allocate the large pseudo-range-rate measurement residual. The clock phase error also increases due to the warm-up induced frequency offset and consequently user position errors are increased.

The use of warm-up initial conditions at 12 minutes after oscillator turn-on is arbitrary; however, it is consistent with the time frame imposed by the calibration of the INS. If the oscillator were turned on at a point in time closer to the start of the flight, the frequency offset would be larger and consequently user navigation performance would be degraded. Conversely, if a longer warm-up period were allowed, user navigation errors would tend to be closer to their baseline values.

Acceleration - The effects of acceleration of the user clock on navigation performance are shown in Fig. 10. The frequency error arising from the g-sensitivity of the quartz oscillator is readily apparent as the airborne user traverses the trajectory of Fig. 7. The impact of this frequency error is manifest in the horizontal and vertical velocity errors. When the user resumes straight and level flight following the third turn, the frequency error is reduced through processing of pseudo-range-rate measurements. Since the filter model does not contain any information about the acceleration sensitivity, the filter gains are small at this point and do not weight the pseudo-range-rate measurements heavily enough to remove the residual frequency error entirely. One consequence of this residual frequency error is the large residual velocity error which remains after straight and level flight is resumed.

The clock phase error grows to a maximum value of 200 m as the user proceeds through the turns and begins to recover during the straight and level portion of the flight. However, since the filter gains are small (the filter has no information about the large clock phase error), the phase error is not reduced rapidly. The large horizontal velocity error ($\simeq$1 mps) drives the horizontal position error to 60 to 70 m. The altitude error results from the misallocation (by the filter) of the large pseudo-range measurement residual which is due to the clock phase error (these errors are highly correlated).

Shock - The effects on user navigation performance of a shock to the receiver crystal oscillator are shown in Fig. 11. The sharp jump in frequency error is quite evident as is the rapid growth in clock phase error due to this frequency shift. These errors are subsequently reduced through

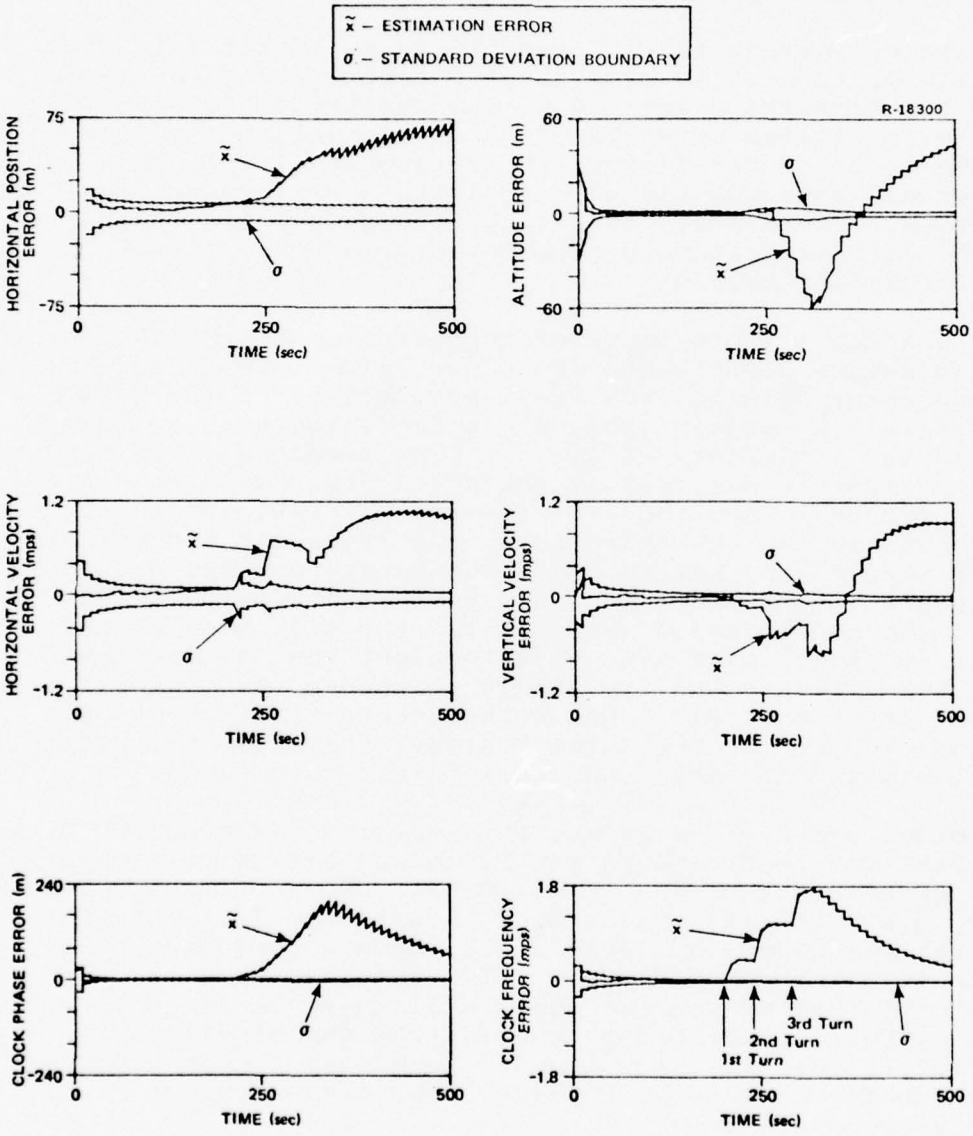


Fig. 10 Airborne User Errors - Acceleration (Not Modeled in User Filter)

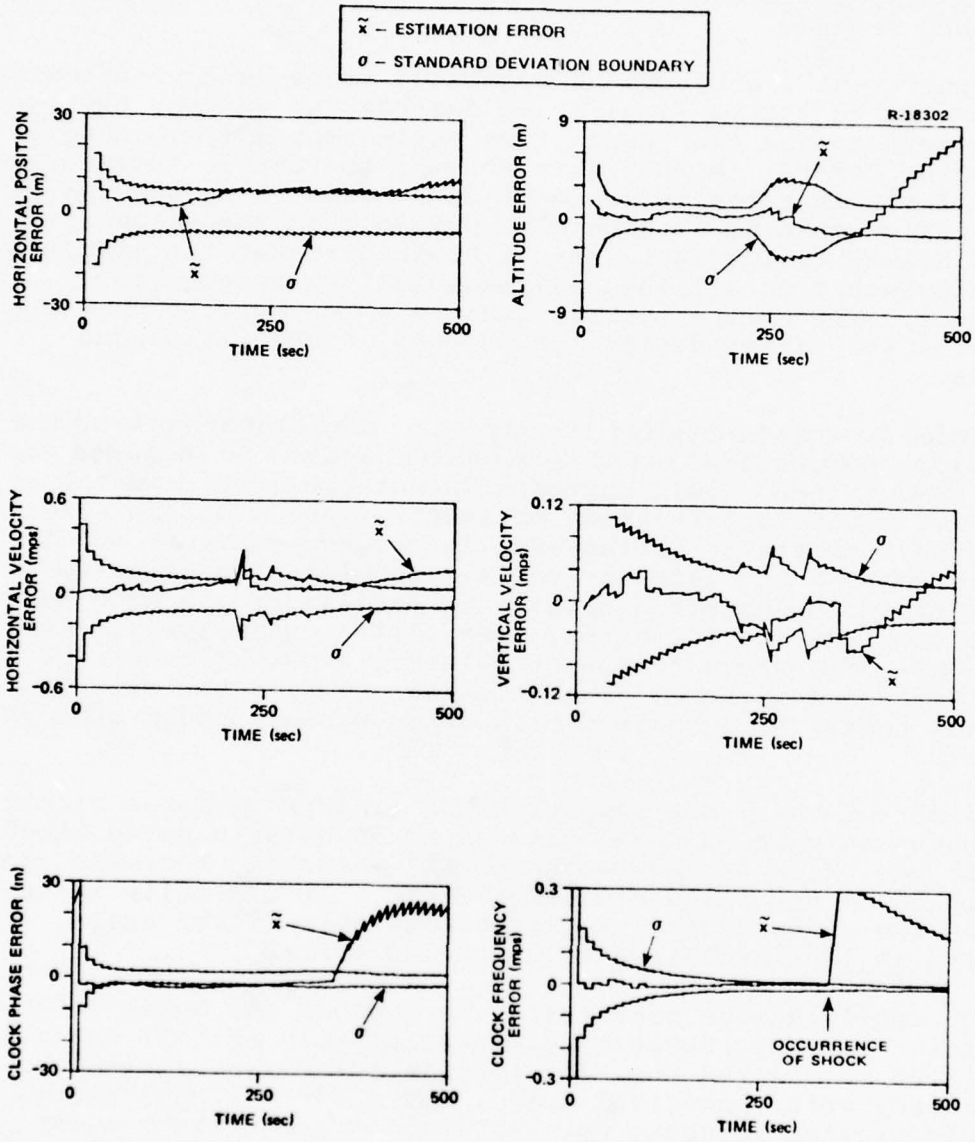


Fig. 11 Airborne User Errors - Shock (Not Modeled in User Filter)

processing of pseudo-range and pseudo-range-rate measurements; however, the recovery is not rapid since the filter gains are small during this latter portion of the flight, and the position and velocity errors appear to diverge after t = 350 seconds.

The performance projections presented above have graphically demonstrated that a significant degradation in user navigation performance can result from environmentally-induced oscillator errors. Rather than attempt to further isolate the oscillator from its environment as a means to reduce the navigation errors, it should be possible to reformulate the user Kalman filter such that it "acknowledges" the simultaneous presence of all the environmentally-induced error sources. The dominant error sources which must be considered in the filter design are warm-up, acceleration and shock.

In order to compensate for the impact of oscillator warm-up the decaying exponential model developed above may be included in the user filter. This approach is not applicable in the case of either acceleration or shock since, for the acceleration sensitivity of the oscillator, any explicit model would require knowledge of vehicle acceleration relative to the crystal orientation within the oscillator - a much too complex situation for a real time filter. Similarly, for the case of a shock to the oscillator, a priori knowledge of the time of occurrence of a shock is unlikely and such behavior cannot be described by a Gauss-Markov random process model.

In light of this one simple method of improving the filter's response to unknown accelerations or an unanticipated shock is to add white process noise to the filter to increase the variance of the frequency error state. This results in an increased uncertainty associated with this filter state, making it less sensitive to unmodeled errors.

Thus, modifying the user filter to include the model of oscillator warm-up [decaying exponential with initial variance of $(3.05 \text{ mps})^2$] and the additional white noise driving the frequency error [spectral level, $q = 1.83 \times 10^{-3} (\text{mps})^2/\text{sec}$], should provide adequate user navigation performance under all environmental conditions. This performance is indeed realized as shown in Fig. 12. For this run all of the environmental error sources discussed individually in the preceding paragraphs were included in the "real world" clock model. The horizontal position and velocity errors are indistinguishable from their values in the baseline run (in

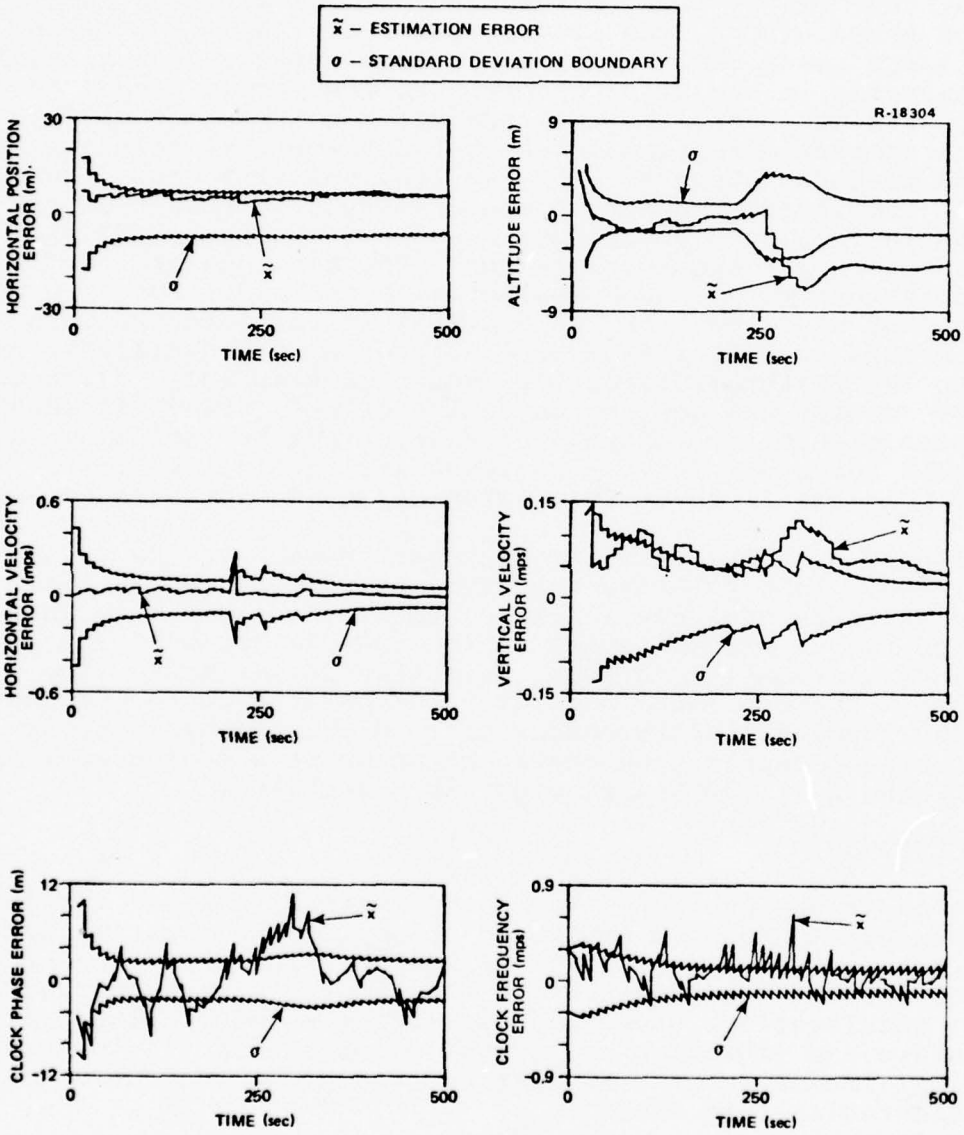


Fig. 12 Airborne User Errors - Modified User Filter (All Environmental Error Sources Present)

which it was assumed that no environmentally-induced errors existed). The increase in altitude error during the second turn is a result of the unmodeled phase error growth in the turn. Due to the high correlation between altitude and clock phase errors, the filter cannot distinguish between the large phase error and the altitude errors, thus causing an increase in the altitude error at the pseudo-range update. Following the turn, the altitude error settles out at 4 to 5 m. A similar situation arises between vertical velocity and clock frequency errors. The vertical velocity error increases at the pseudo-range-rate measurement as a result of the jumps in frequency error but is reduced to about 0.05 mps during straight and level flight. The altitude and vertical velocity errors are much smaller with the modified filter than they would be with the original filter (compare with the errors resulting from acceleration of the oscillator prior to the filter modification, shown in Fig. 10). Although filter design was not the objective of this study, it should be possible to further reduce these errors by including white process noise driving the altitude and vertical velocity states in the filter. This alternative was not pursued here.

It should be noted that this approach does have its disadvantages. In a relatively benign environment (e.g., small accelerations, no unanticipated shocks, etc.), the inclusion of additional process noise in the user filter will lead to a minor degradation in user navigation performance. The tradeoff between improved filter performance in the presence of environmental disturbances must be weighed against any performance degradation which may arise in a benign environment when a filter design study is undertaken.

CONCLUSIONS

This paper has presented the development of a model for environmentally-induced errors in a satellite navigation system receiver quartz crystal oscillator. The error sources, which proved to be dominant in an airborne user scenario, were acceleration, shock and oscillator warm-up. The temperature and vibration sensitivities of the oscillator had minimal impact on user navigation errors for the environment considered in this study.

The environmental error sources have direct impact upon the oscillator phase and frequency errors. Due to the high correlation between clock errors and vertical channel errors, large unmodeled phase and frequency errors tend to increase altitude and vertical velocity errors at filter updates, i.e., the filter cannot properly attribute the large pseudo-

range and pseudo-range-rate measurement residuals to the clock states alone and thus "divides" the large residual between clock and vertical channel errors. The horizontal position and velocity errors are insensitive to all but extreme environmentally-induced errors (e.g., acceleration).

A simple modification of the user filter to model oscillator warm-up and the effects of acceleration and shock substantially improves user navigation performance if these error sources are present. However, in the absence of these errors the modified filter introduces some degradation in user navigation performance. Careful "tuning" of the user filter or an adaptive filtering mechanization could reduce this sensitivity.

ACKNOWLEDGEMENT

The author wishes to express his appreciation to Dr. Erich Hafner of the U. S. Army Electronics Command and to personnel of the Hewlett Packard Corporation for the provision of data inputs for the error modeling portion of this work.

REFERENCES

1. Shoemaker, H., "NAVSTAR Global Positioning System," Proc. IEEE 1975 National Aerospace and Electronics Conference, June 1975, pp. 351-354.

2. Mealy, G.L. and Vander Stoep, D.R., "Time Standard Error Modeling with Applications to Satellite Navigation," Proc. 29th Annual Symposium on Frequency Control, May 1975, pp. 417-424.

3. Gelb, A., ed., Applied Optimal Estimation, M.I.T. Press, 1974.

QUESTION AND ANSWER PERIOD

MR. RUEGER:

Where did you come by the acceleration numbers? Are those experimentally determined by your people?

MR. MEALY:

No, we don't do it. Dr. Hafner at ECOM provided some of it.

MR. RUEGER:

I was going to say that our experience has been factors of 4 higher than that in the coefficients that you might use. I don't know that it doesn't create a problem.

MR. MEALY:

It is a factor of 4 higher, or a factor of 4 worse is what it amounts to, so we haven't treated those.

DR. REINHARDT:

In your first slide, you seemed to indicate that you had a model for generating flicker noise from white noise. Was that true?

MR. MEALY:

Yes.

DR. REINHARDT:

And what kind of model is that?

MR. MEALY:

It is described in a paper I gave last May at the Frequency Control Symposium. It is a transfer function that I can discuss with you if you would like. It does work fairly well. It is a shaping filter that works in the frequency domain, such that you shape the spectrum of the white noise to follow $\frac{1}{f}$ behavior.

DR. REINHARDT:

Does it work in a finite domain?

MR. MEALY:

This was all generated using discrete time. It is a continuous formulation, but can be converted to a discrete time formulation.

DR. REINHARDT:

But does it work in a finite or infinite frequency domain?

MR. MEALY:

Oh, finite frequency range, but the limits are arbitrary.

PRECISION SATELLITE TIME DETERMINATION FOR APPLICATION TO GEOS-3 DATA

F. M. Boykin
NASA - Wallops Flight Center

R. E. Dwyer
Computer Sciences Corporation

ABSTRACT

The Geodynamics Experimental Ocean Satellite (GEOS-3) was launched on April 9, 1975, to perform experiments in the geosciences discipline (e.g., solid earth physics and oceanography). The primary experimental instrument, a dual mode radar altimeter, is being applied to oceanographic objectives which include mapping the topography of the ocean surface and determining the ability of the altimeter to measure wave height. Precise time correlation of the altimetric measurements to UTC (within an accuracy of ±600 μsec) is required in the application of the data. A special timing system is employed which is independent of the timing data recorded on analog telemetry tapes at the NASA - Spacecraft Tracking and Data Network (STDN), and ultimately serves to identify the time of each altimeter transmitted pulse to the required accuracy. The timing system begins in the GEOS-3 spacecraft where both the altimeter pulse repetition frequency and the telemetry bit rate frequency are coherently derived from a clock divider driven by an ultra - stable 5 MHz oscillator. The telemetry format is programmed to uniquely identify each major and minor telemetry frame over an unambiguous period extending more than one year. Approximately once each day, a STDN station is scheduled to detect the time of arrival (relative to station time) of a selected bit in the telemetry frame synchronization patterns over the duration of the pass. Approximately 600 data points consisting of time and major and minor frame identifications are transmitted to the GEOS-3 control center located at Goddard Space Flight Center (GSFC) along with station pre- and post-pass delay measurements. At the control center the data is processed to account for spacecraft system delay, propagation delay, ground systems delay, and discrepancies between station time and UTC. Within a matter of minutes a report is generated providing UTC time (at the spacecraft) for uniquely identified major frames of telemetry. Indications as to the quality of the data are also provided. The timing reports

PRECEDING PAGE BLANK-NOT FILMED

are transmitted to the Wallops Flight Center, where all GEOS-3 altimeter data is processed. Using the daily timing reports and interpolating between each report, a time base is established to allow precise time tagging of each GEOS-3 frame of data. Subsequently, as telemetry data arrive at Wallops on magnetic tape, the frames of data are simply identified and appropriately time tagged. The UTC time of each altimeter measurement telemetered within a given frame is then identified by applying known time relationships between telemetry frame time and the time of the altimeter transmitted pulse(s) from which the telemetered altimetric measurement was derived.

INTRODUCTION

GEOS-3 Mission:

The Geodynamics Experimental Ocean Satellite (GEOS-3) was launched on April 9, 1975, from the Western Test Range by a two-stage Delta Vehicle, thrust augmented with four first-stage solid propellant motors. A near perfect 844 km circular orbit was obtained with an inclination of 115 degrees and a period of 101.8 minutes. These orbit parameters were chosen to provide orbit traces that cover the earth's surface in a prescribed grid work pattern.

The GEOS-C Mission Objectives in order of priority are:

To perform an in-orbit satellite altimeter experiment to: (1) determine the feasibility and utility of a space-borne radar altimeter to map the topography of the ocean surface with an absolute accuracy of ±5 meters, and with a relative accuracy of 1 to 2 meters, (2) determine the feasibility of measuring the deflection of the vertical at sea, (3) determine the feasibility of measuring wave height, and (4) contribute to the technology leading to a future operational altimeter satellite system with a 10-centimeter measurement capability.

To further support the calibration of NASA and other agencies' ground C-band radar systems by providing a space-borne coherent C-band transponder system, to assist in locating these stations in the unified earth-centered reference system, and to provide tracking coverage in support of the radar-altimeter experiment.

To perform a satellite-to-satellite experiment with the ATS-6 satellite using an S-band transponder subsystem to directly measure the short period accelerations imparted to the spacecraft by the gravity field and to determine the position of the spacecraft. The satellite-to-satellite system is also used for altimeter telemetry data relay through ATS-6.

To further support the intercomparison of new and established geodetic and geophysical measuring systems including: the radar altimeter, satellite-to-satellite, C-band, S-band, Laser, and Doppler tracking.

To investigate solid-earth dynamic phenomena such as polar motion, fault motion, earth rotation, earth tides, and continental drift theory with precision satellite tracking systems.

To further refine orbit-determination techniques, the determination of interdatum ties, and gravity models.

To support the calibration of S-band sites in the STDN to assist in positioning the network stations in the world reference system, and to assist in evaluating the system as a tool for geodesy and precise orbit determination.

GEOS-3 Spacecraft

The GEOS-3 Spacecraft, shown in Figure 1, was designed and fabricated by the Johns Hopkins University/Applied Physics Laboratory. The structure consists of a rigid box in the form of an octahedron topped by a truncated pyramid. The octahedron measures 1.37 meters across the flats. A 6.46 meter rigid boom supporting a 46.2 Kg end mass provides gravity gradient stabilization for the spacecraft. Total spacecraft weight is 345.9 Kg. The system block diagram is shown in Figure 2.

The experiment package consists of five basic instruments as follows:

1. Radar Altimeter

2. C-band Transponders

3. S-band Transponder

4. Laser Retroreflector

5. Doppler Transmitters

The basic objectives of the radar altimeter experiment are to demonstrate the feasibility of utilizing an on-board altimeter to measure the time varying behavior of the ocean's surface and the departure of the sea-surface from the geoid, as well as to investigate altimeter instrumentation technology. The basic measurement goals established for the altimeter are:

Precision: Short pulse mode 30 centimeters
Long pulse mode 60 centimeters

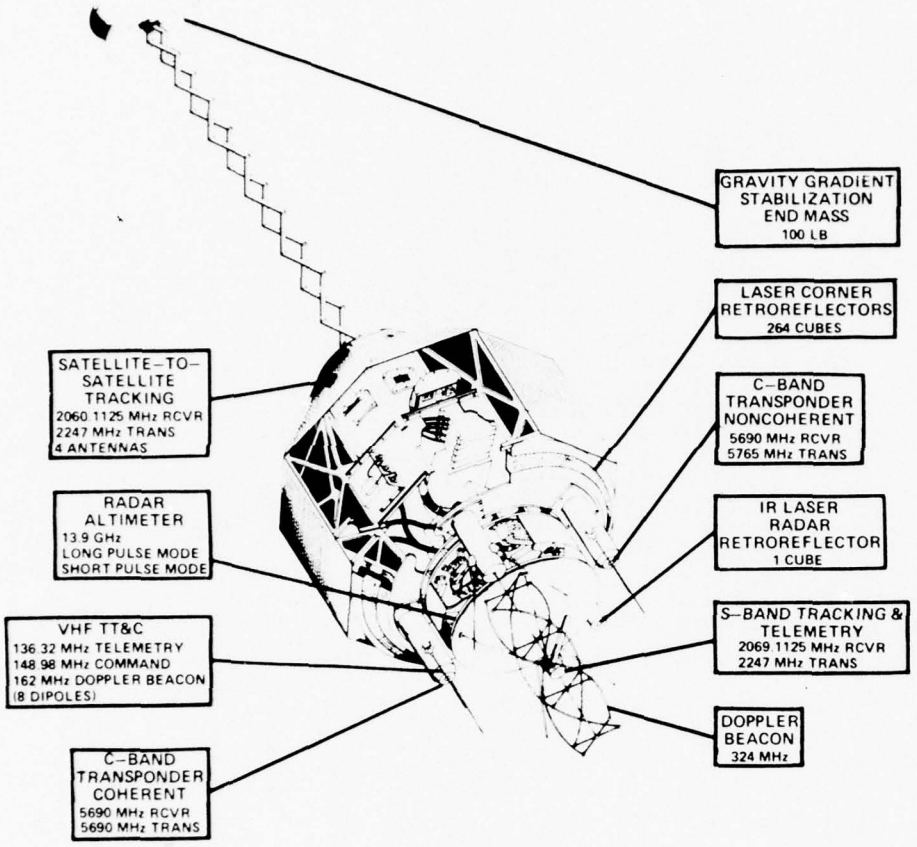


Figure 1 GEOS-3 Spacecraft Cutaway

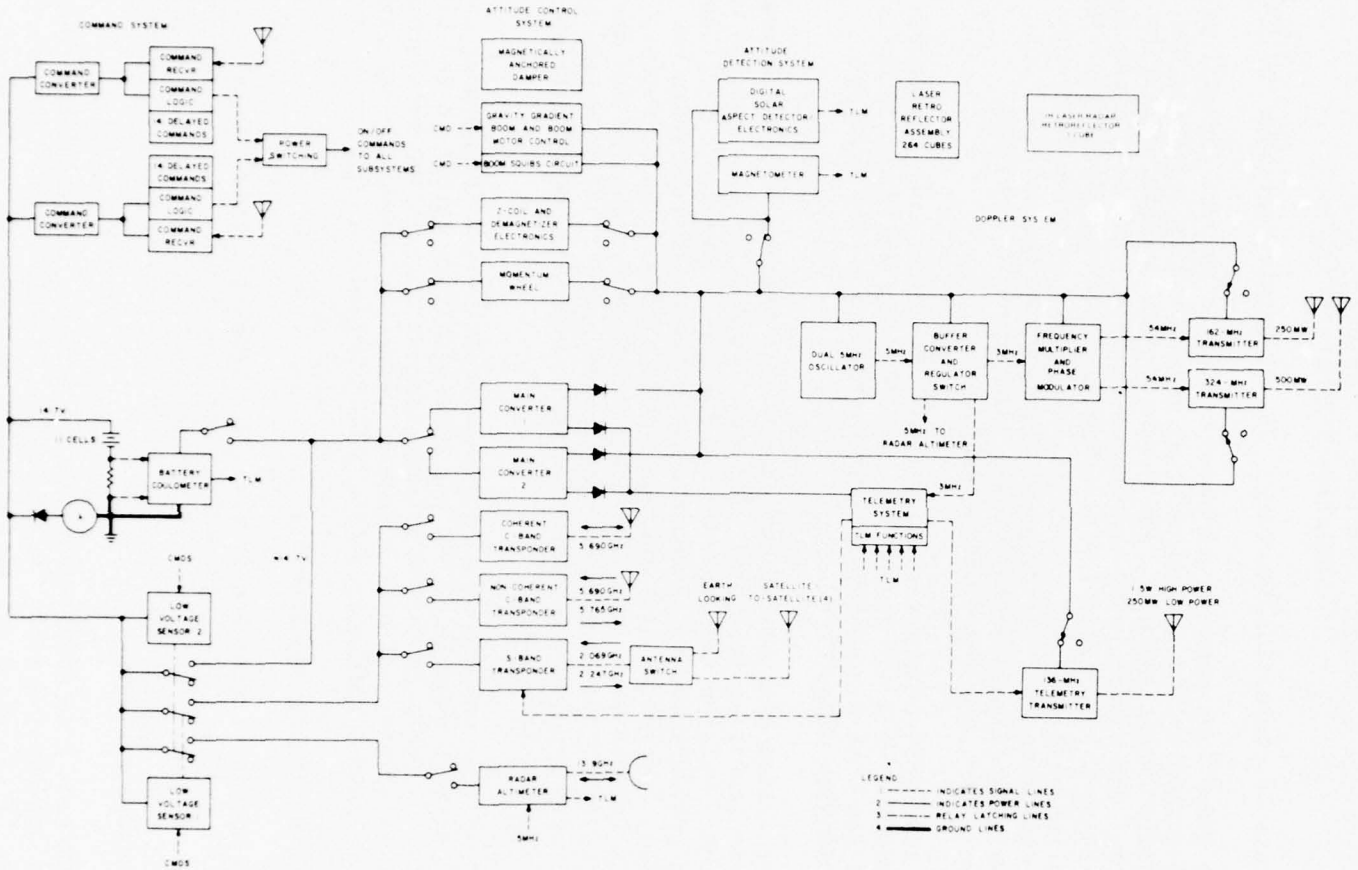


Figure 2 - GEOS-3 Spacecraft Systems Block Diagram

Geoid Recovery Accuracy: Absolute ± 5 Meters
Relative ± 2 Meters

Sea State Determination Accuracy: 25% of Significant Wave Height

Two C-band radar transponders are incorporated to support the altimeter and C-band system calibration as well as geometric, gravimetric, and other geodetic investigations. The C-band system consists of the two transponders (one coherent and one noncoherent) and the associated ground tracking C-band radars. The noncoherent transponder, operating in conjunction with existing ground radar systems, provides range and angle measurements. The coherent transponder, operating in conjunction with existing coherent ground radar systems, provides range, range rate, and angle measurements.

The laser retroreflector array consists of 264 quartz cube corner reflectors mounted on a 45° conic frustum. The retroreflector is utilized in conjunction with ground-based laser systems to obtain precise satellite ranging data.

The Doppler System consists of two space-borne transmitters and ground base doppler receiving stations. The dual frequencies (162 and 324 MHz) are coherently related and derived from the 5-MHz spacecraft oscillator, which also provides the basis for the altimeter Pulse Repetition Frequency (PRF), telemetry rates and spacecraft timing. The difference frequencies between the higher and lower received frequencies and the station oscillator are combined in the proper proportions to obtain both the first-order ionospheric refraction correction and the refraction corrected doppler frequency.

The S-band system consists of a single coherent S-band transponder and an antenna network capable of two-way communications direct to the STDN ground stations or to the ATS-6 ground stations through the geosynchronous ATS-6 satellite. In either mode of operation coherent range-rate, ranging, and GEOS-3 telemetry data can be provided.

GEOS-3 Mission Timing Requirements

The GEOS-3 Mission Timing Requirements are segmented into two categories: (1) tracking station requirements associated with the various tracking instrument types, and (2) spacecraft timing requirement associated with time tagging the data of the space-borne tracking instrument, the radar altimeter.

Tracking station time requirements are satisfied by conventional techniques and are not the topic for discussion in this paper. The tracking station timing goals are listed below:

Instrument Type	Timing Accuracy Goal
Laser	± 8 μsec
S-band:	
Direct-to-Ground	± 25 μsec
Through ATS-6	± 11 μsec
Coherent C-band	± 10 μsec
Non-Coherent C-band	± 50 μsec
Doppler	± 100 μsec

Relative to satellite altimetry, the purpose of the ground tracking systems is to provide data for precise orbit determination in position and time. With the orbit established, the radar altimeter data must be time tagged commensurate with its ranging precision. The requirement is to time tag the range data to an accuracy of ±600 μsec. With a maximum radial range rate of 100 meters per second due to the combined effects of orbit eccentricity and geoid undulation, a 600 μsec timing error would produce a range error of six centimeters. The altimeter precision is estimated to be 50 centimeters at a measurement rate of 10 samples/second. A one-second average yields a precision of about 20 centimeters.

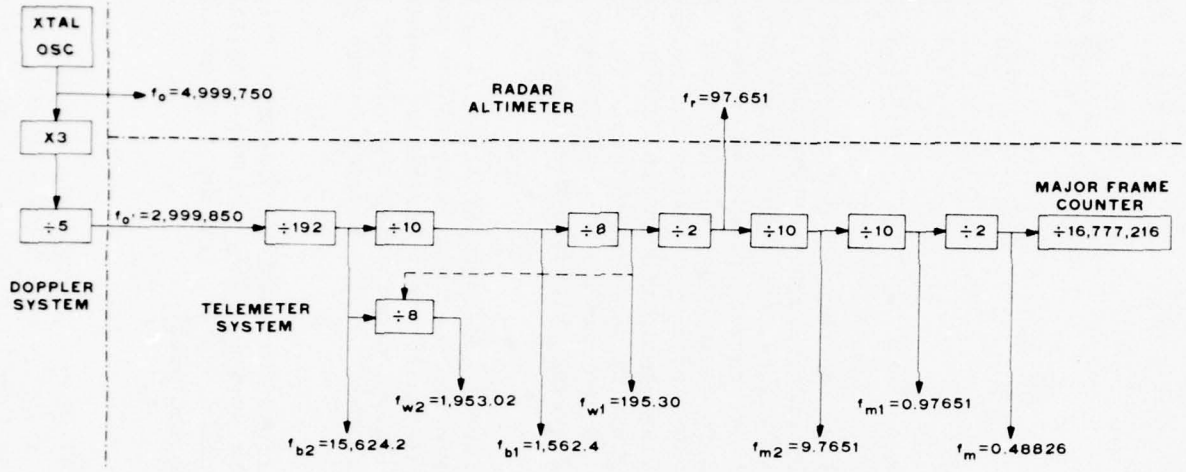
Since the altimeter is a spacecraft-borne radar with all of the associated tracking functions performed in-orbit, a means was sought to satisfy the time tagging requirement. This necessitates determining spacecraft time, and, specifically, determining the time of the radar altimeter transmitted pulse(s) that is incorporated in any given range measurement.

The system implemented to perform this task is discussed relative to the three main portions of the system. They are the satellite system, the ground station time detection system, and the data processing system. Sample results are also included.

SPACECRAFT SYSTEM

In the spacecraft, both the altimeter PRF and the telemetry bit-rate frequencies are derived from a stable crystal oscillator operating nominally at 4999,750 Hz. The timing network is given in Figure 3 and supplies the clock for (1) two telemetry bit rates detailed in Table 1, (2) the altimeter PRF, and (3) a major frame counter referred to as the Time Code Generator (TCG). The altimeter transmitted pulse time relationships are very similar for either telemetry bit rate. Therefore,

TIMING NETWORK FOR DUAL RATE TELEMETER SYSTEM



NOTES:
- f_b DENOTES BIT RATE
- f_m DENOTES MINOR FRAM RATE
- f_M DENOTES MAJOR FRAME RATE
- f_o DENOTES ALTIMETER REFERENCE FREQUENCY
- $f_{o'}$ DENOTES TELEMETER REFERENCE FREQUENCY
- f_r DENOTES ALTIMETER REPETITION RATE
- f_w DENOTES WORD RATE

ALL RATES AND FREQUENCIES IN Hz. SECONDARY SUBSCRIPTS 1 AND 2 DENOTE LOW AND HIGH DATA RATES, RESPECTIVELY.

Figure 3

TELEMETRY PARAMETERS

- FREQUENCY — 136.32 MHz
- TYPE — PCM-SPLIT PHASE/PM
- INDEX — ONE RADIAN
- BIT RATES — 1562 Hz AND 15624 Hz
- POWER (MIN.) — .25 WATTS AND 1.5 WATTS

659

FORMATS

	LOW RATE	HIGH RATE
WORD (BITS)	8	8
MINOR FRAME LENGTH (WORDS)	100	100
MAJOR FRAME LENGTH		
• MINOR FRAMES	4	64
• PERIOD (SECONDS)	2.05	3.28

Table 1

for clarity sake only the low bit rate telemetry mode (i.e., 1562 bps) is discussed in this paper.

Table 2 is a sample of a GEOS-3 minor telemetry frame in the low bit rate. As noted in Table 1, four of these minor frames constitute a major frame with each major frame identified by a specific TCG count. The TCG increments in a binary count on every major frame up to a maximum of 2^{24} and then turns over to zero and begins counting again. The four minor frames within a major frame are identified by the FFID which increments in a 2 bit field from 00 binary to 11 binary. Therefore, with the combination of TCG and FFID (See Table 2) each minor frame is unambigiously identified throughout more than one year.

The radar altimeter transmitted pulses have a known relationship to the telemetry frame. As shown in Figure 4, a transmit clock occurs one word time (5120.2 μsec) + 224 μsec = 5344.2 μsec before the beginning of the frame. The actual altimeter transmit pulse is generated 25.6 μsec after the clock (a value derived through tests). Therefore, the altimeter pulse precedes the frame start time by 5318.6 μsec. This pulse is the last included in the referenced altitude accumulation (See Figure 4) with the altitude result subsequently read-out into the telemetry stream in words 11, 13, 15, and 17 (See Table 2). The altimeter transmitted pulse time for subsequent altitude results are derived in a similar manner and are all referenced in the beginning of a telemetry frame.

The actual telemetry frame start time used as a reference in the foregoing is delayed by a constant during the process of developing the split-phase Pulse Code Modulation (PCM) waveform. Figure 5 shows this relationship. The spacecraft delay of 336 μsec is accounted for in the time correlation data processing to be discussed later in this paper.

To summarize the spacecraft system, the following has been established:

1. The time relationship of the telemetry frame and the altimeter transmitted pulses.

2. The unambigious identification of any telemetry minor frame for more than a one-year period.

3. A spacecraft delay constant to be applied in time correlation data processing.

GROUND STATION TIME DETECTION SYSTEM

Selected STDN stations detect the time of arrival of the leading edge of the first bit in the telemetry synchronization pattern with respect

MODE 1 TELEMETRY FORMAT

Word	Function	Word	Function	Word	Function	Word	Function	Word	Function
0	$SYNC_a$	20	NCSS	40	ASC0 (4 + B)	60	ASC0 (8 + B)	80	ASC0 (12 + B)
1	$SYNC_b$	21	FFID	**41**	**TCG_a**	**61**	**TCG_b**	**81**	**TCG_c**
2	$SYNC_c$	22	NCRR	42	ASC1 (4 + B)	62	ASC1 (8 + B)	82	ASC1 (12 + B)
3	**FFID**	23	CP	43	$DSAD_a$	63	$DSAD_b$	83	Spare
4	RTP	24	ASC0 (1 + B)	44	ASC0 (5 + B)	64	ASC0 (9 + B)	84	ASC0 (13 + B)
5	AS	25	AS	45	AS	65	AS	85	AS
6	ANG	26	ASC1 (1 + B)	46	ASC1 (5 + B)	66	ASC1 (9 + B)	86	ASC1 (13 + B)
7	Spare	27	DSC (A)	47	DSC (1 + A)	67	DSC (2 + A)	87	DSC (3 + A)
8	ARG	28	ASC0 (2 + B)	48	ASC0 (6 + B)	68	ASC0 (10 + B)	88	ASC0 (14 + B)
9	IPG	29	IPG	49	IPG	69	IPG	89	IPG
10	APG	30	ASC1 (2 + B)	50	ASC1 (6 + B)	70	ASC1 (10 + B)	90	ASC1 (14 + B)
11	**$CALT_d$**	31	$CALT_d$	51	$CALT_d$	71	$CALT_d$	91	$CALT_d$
12	AASG	32	ASC0 (3 + B)	52	ASC0 (7 + B)	72	ASC0 (11 + B)	92	ASC0 (15 + B)
13	**$CALT_c$**	33	$CALT_c$	53	$CALT_c$	73	$CALT_c$	93	$CALT_c$
14	CCSS	34	ASC1 (3 + B)	54	ASC1 (7 + B)	74	ASC1 (11 + B)	94	ASC1 (15 + B)
15	**$CALT_b$**	35	$CALT_b$	55	$CALT_b$	75	$CALT_b$	95	$CALT_d$
16	CCRR	36	ASC2 (A)	56	ASC2 (1 + A)	76	ASC2 (2 + A)	96	ASC2 (3 + A)
17	**$CALT_a$**	37	$CALT_a$	57	$CALT_a$	77	$CALT_a$	97	$CALT_a$
18	RAGC	38	RAGC	58	RAGC	78	RAGC	98	RAGC
19	RSE	39	RSE	59	RSE	79	RSE	99	RSE

Table 2

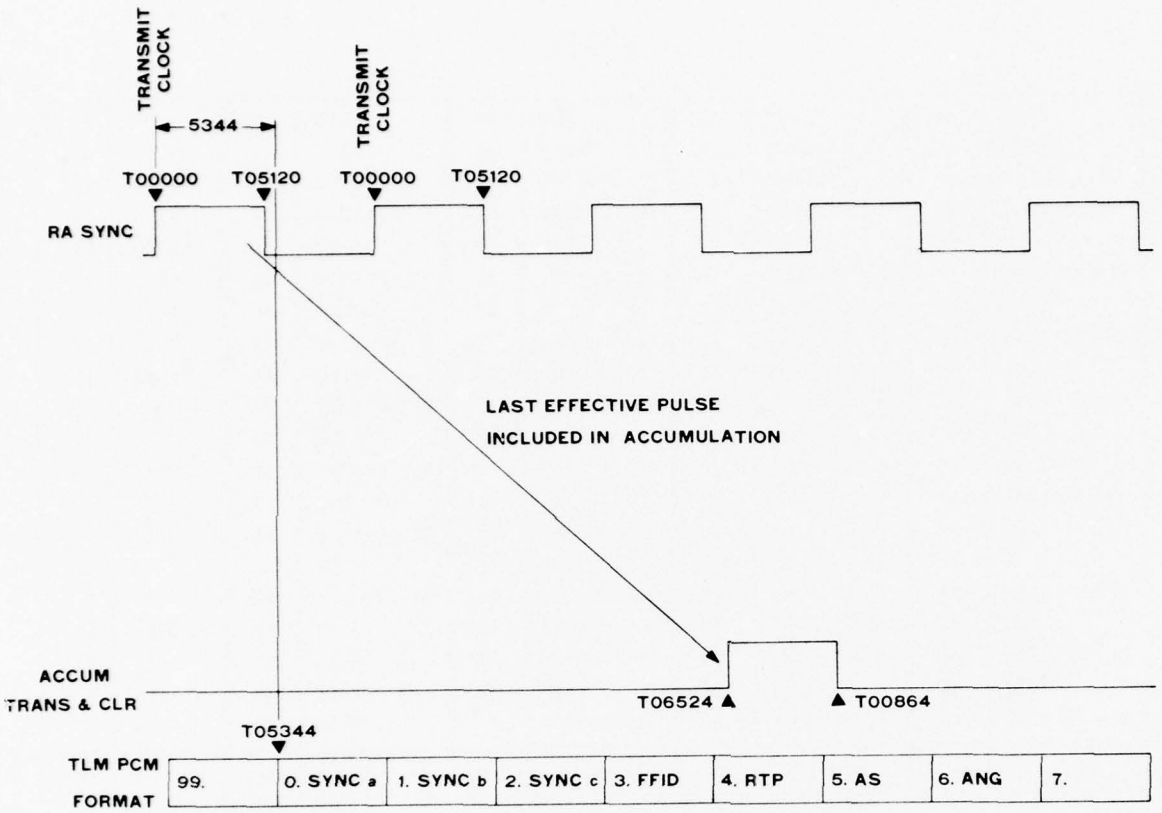


Figure 1 - GEOS-3 Timing Diagram

PCM WAVEFORMS

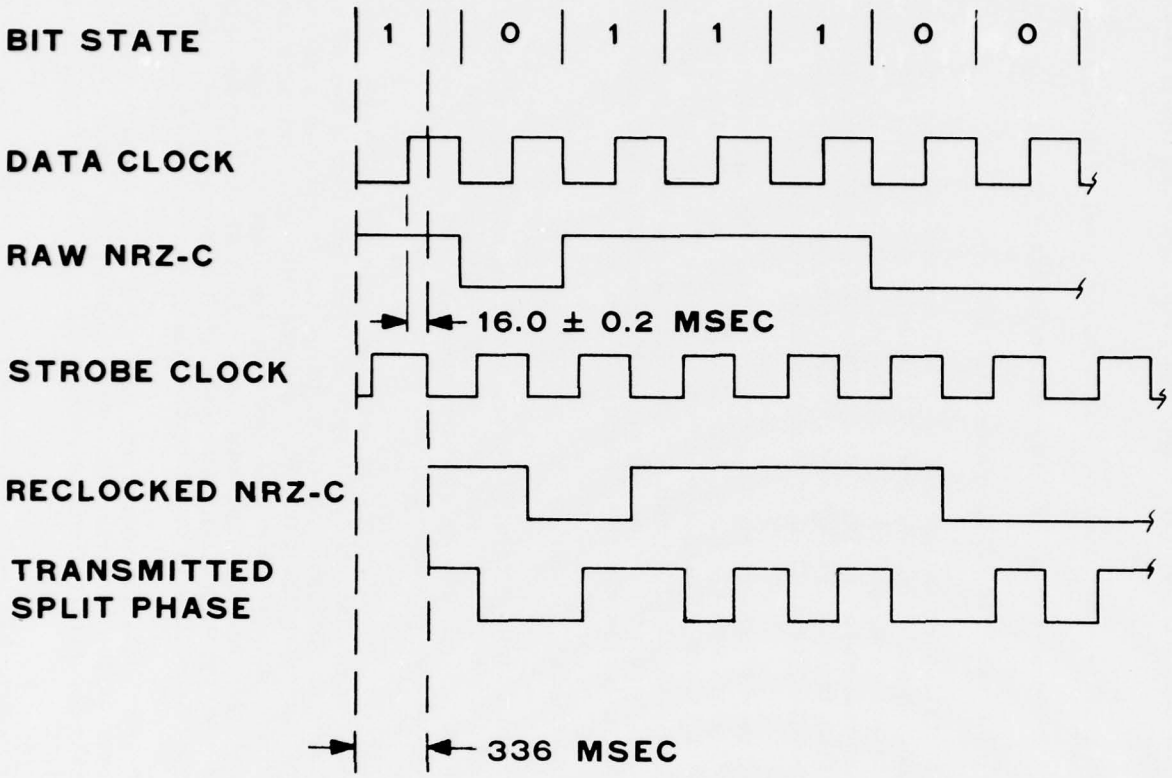


Figure 5

to station time. This is performed at a rate of once every other frame with GEOS-3 in its low data rate. A nominal ten-minute pass yields about 600 data points. Each data point contains the following information:

(1) Station hour, minute, second (major time) of the detected frame.

(2) Microsecond (minor time) of the detected frame.

(3) TCG and FFID of the detected frame.

The station equipment used is a PCM decommutation system known as the Manned Space Flight Telemetry Processor (MSFTP-3). In addition to the data points described above, pre- and post-pass delay constants are measured by generating test patterns and timing their delay through the system as shown in Figure 6. This reported ground system delay is also accounted for in time correlation data processing.

During the satellite pass at the station, the data points are stored for post-pass formatting and transmission to the GEOS-3 control center. The data are formatted as shown in Figure 7 with each 1200 bit block containing 12 data points. A maximum of 50 blocks can be stored (i.e., 600 data points) requiring slightly more than eight seconds for transmission to the control center.

DATA PROCESSING SYSTEM

For each time correlation pass, a maximum of 600 data points are transmitted to the GEOS-3 control center located at Goddard Space Flight Center. These data points are read into the control center SDS-930 computer for processing.

Initially, the data points are grouped in sets of sixteen (16) as shown in the input data set of Figure 8. This provides a set of data at a rate of approximately one data point per second over a period of approximately 16 seconds. This provides the basis for data averaging and makes it consistent with a common major frame start time in both the spacecraft low and high data rates. Each of the sixteen points is then adjusted by subtracting multiples of the nominal minor frame rate to translate each data point to the common major frame boundary.

The input data represents the time of arrival of GEOS-3 telemetry frames at the receiving station. To establish actual frame start time in the spacecraft, four correction factors are applied to each data point:

(1) Station Time Versus UTC Correction - This is a constant derived from knowledge of the difference between station clock and UTC time

TIME DELAY TEST CONFIGURATION

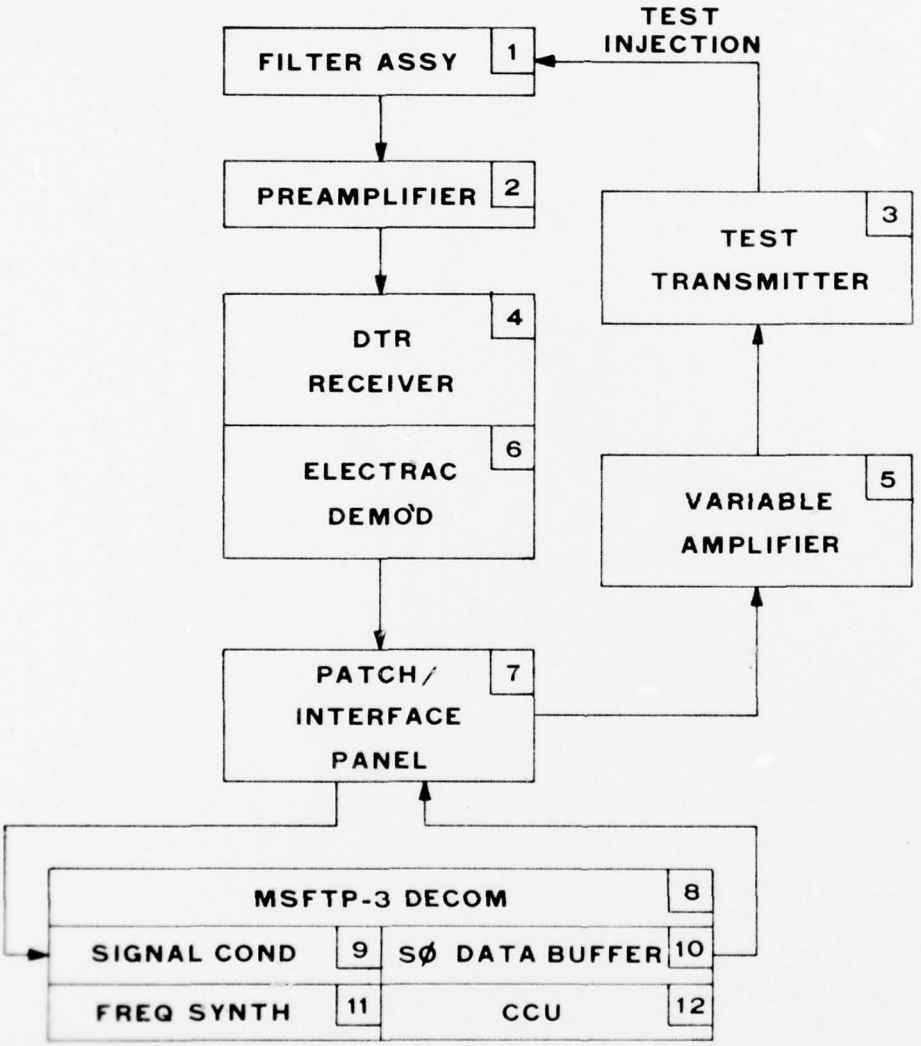
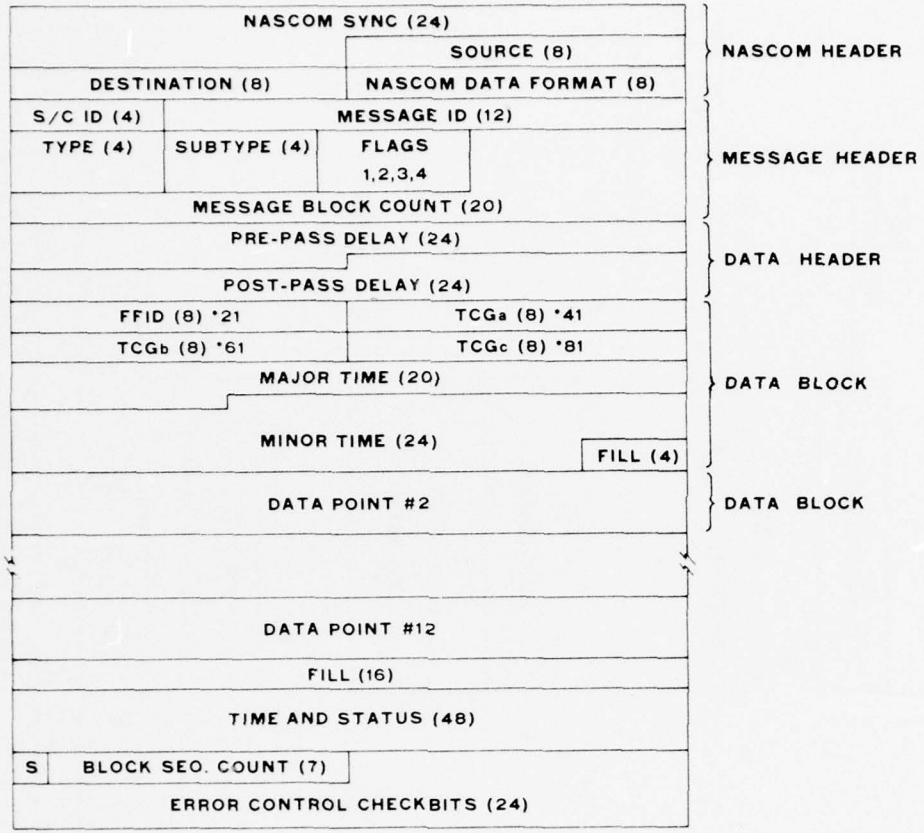


Figure 6

COMMUNICATIONS BLOCK



TOTAL STORAGE = 50 BLOCKS/3750 WORDS

BLOCK SIZE 75 - 16 BIT WORDS = 1200 BITS

Figure 7

32 16 27 -7.921856 23406155 0140
32 16 27 -7.921850 23406155 0142
32 16 27 -7.921852 23406156 0140
32 16 27 -7.921848 23406156 0142
32 16 27 -7.921857 23406157 0140
32 16 27 -7.921847 23406157 0142

INPUT DATA SET 16 SAMPLES

32 16 28 14.318970 23406160 0140
32 16 28 14.340963 23406160 0142
32 16 28 14.365033 23406161 0140
32 16 28 14.389083 23406161 0142
32 16 28 14.413162 23406162 0140
32 16 28 14.437217 23406162 0142
32 16 28 14.461287 23406163 0140
320 16 28 21.485345 23406163 0142
32 16 28 21.509417 23406164 0140
32 16 28 21.533474 23406164 0142
32 16 28 21.557543 23406165 0140
32 16 28 21.581602 23406165 0142
32 16 28 21.605671 23406166 0140
32 16 28 21.629730 23406166 0142
32 16 28 21.653802 23406167 0140
32 16 28 21.677859 23406167 0142

DATA SAMPLES USED 16 SAMPLES

32 16 28 14.306660 23406160 0140
32 16 28 14.306663 23406160 0142
32 16 28 14.306669 23406161 0140
32 16 28 14.306664 23406161 0142
32 16 28 14.306672 23406162 0140
32 16 28 14.306662 23406162 0142
32 16 28 14.306668 23406163 0140
320 16 28 14.306661 23406163 0142
32 16 28 14.306664 23406164 0140
32 16 28 14.306662 23406164 0142
32 16 28 14.306669 23406165 0140
32 16 28 14.306663 23406165 0142
32 16 28 14.306668 23406166 0140
32 16 28 14.306663 23406166 0142
32 16 28 14.306670 23406167 0140
32 16 28 14.306662 23406167 0142

INPUT DATA SET 16 SAMPLES

32 16 28 21.7 1932 23406170 0140
32 16 28 21.725991 23406170 0142
32 16 28 21.750062 23406171 0140
32 16 28 21.774118 23406171 0142
32 16 28 21.798190 23406172 0140
32 16 28 21.822250 23406172 0142
32 16 28 21.846318 23406173 0140
32 16 28 21.870381 23406173 0142
32 16 28 21.894453 23406174 0140
32 16 28 21.918509 23406174 0142

Figure 2

and is applied to each data point with the proper sign to correct station time to UTC time.

(2) Ground System Delay - This is a constant for the pass being processed which is derived as the average of the reported pre- and post-pass delay calibration. This constant is subtracted from each data point. If the pre-to-post-pass delay varies more than 25 microseconds, the data is flagged.

(3) Propagation Delay - This is a variable which is derived from station to spacecraft predicted slant ranges. The predicted range is calculated at the time of each input data point and a corresponding propagation delay is subtracted from the data point.

(4) Spacecraft System Delay - This is the constant delay discussed in the spacecraft system portion of this paper and is subtracted from each data point.

The resultant data set is shown with the corrections applied in the "Data Samples Used" portion of Figure 8. All times as reported by the station are corrected to spacecraft time and the sixteen points are translated to the beginning of the common major frame. The eight octal bit TCG field and four octal bit FFID field is also displayed.

A report is then formatted as shown in Figure 9. The mean time of each data set is calculated and reported with the corresponding TCG number. Quality indicators detailing the number of samples in each data set, the number of samples used, and the standard deviation of the used samples are also reported.

The timing correlation data print is also outputted on paper tape and transmitted via teletype to Wallops Flight Center. At Wallops, the time reports are used in the altimeter data processor to establish the spacecraft telemetry frame time base from which all altimeter data time tagging is derived.

One time correlation report per day provides sufficient data to model the spacecraft oscillator drift. Linear interpolation between these daily data points provides frame time for any of the frames of interest occurring between the daily reports.

TIMING CORRELATION DATA PRINT

MEAN UTC TIME				TCG NUMBER	NUMBER OF SAMPLES	SAMPLES USED	STANDARD DEVIATION
DOY	HH	MM	SS.SSSSSS				
32	16	18	+.883+371	5114712	14	14	000035
32	16	18	47.272870	5114720	16	16	000004
32	16	19	13.607574	5114728	16	16	000006
32	16	19	38.932407	5114736	16	16	000005
32	16	19	+0.377213	5114744	16	16	000005
32	16	20	0.752036	5114752	16	16	000009
32	16	20	19.146858	5114760	16	16	000005
32	16	20	46.531670	5114768	16	16	000004
32	16	20	51.916501	5114776	16	16	000008
32	16	21	+.3 1314	5114784	16	16	000004
32	16	21	24.686127	5114792	16	16	000008
32	16	21	+1.072957	5114800	16	16	000005
32	16	21	37.458770	5114808	16	16	000007
32	16	22	13.843585	5114816	16	16	000008
32	16	22	30.228404	5114824	16	16	000004
32	16	22	+0.613223	5114832	16	16	000004
32	16	23	2.998047	5114840	16	16	000007
32	16	23	19.374851	5114848	16	16	000005
32	16	23	35.759678	5114856	16	16	000010
32	16	23	52.145510	5114864	16	16	000005
32	16	24	+.530302	5114872	16	16	000008
32	16	24	24.914128	5114880	16	16	000005
32	16	24	41.3 3959	5114888	16	16	000008
32	16	24	57.683786	5114896	16	16	000009
32	16	25	+.073585	5114904	16	16	000006
32	16	25	+.458402	5114912	16	16	000006
32	16	25	46.843258	5114920	16	16	000015
32	16	26	3.228066	5114928	16	16	000010
32	16	26	19.612867	5114936	16	16	000004
32	16	26	35.997704	5114944	16	16	000011
32	16	26	52.382562	5114952	16	16	000010
32	16	27	8.767361	5114960	16	16	000009
32	16	27	25.152174	5114968	16	16	000005
32	16	27	+1.537028	5114976	16	16	000013
32	16	27	7.921858	5114984	16	16	000008
320	**16**	**28**	**14.306665**	**5114992**	**16**	**16**	**000004**
32	16	28	+.811432	5115000	16	16	000005
32	16	28	47.076323	5115008	16	16	000008

Figure 9

QUESTION AND ANSWER PERIOD

MR. RUEGER:

You have just heard one of the results of a very complicated satellite that is spewing out data by the carloads, working for seven months in orbit.

They are keeping track of every pulse of the radar in its time relationship to 600 microseconds, and cataloguing this data.

MR. DWYER:

I failed to mention that the requirement is 600 microseconds, but we feel the system is doing much better than that. It is a quantum jump from trying to correlate time on tape to data on tape. It is a quantum jump once you go to a system like this. You go down much better than the 600 micro-seconds. We evaluated about 50 microseconds.

SPACEBORNE RUBIDIUM FREQUENCY STANDARD FOR NAVSTAR GPS

D. E. Ringer, J. Gandy (Rockwell International)
E. Jechart (Efratom)

ABSTRACT

The Navstar Global Positioning System is a multi-service navigation system with the Joint Program Office at SAMSO. This system utilizes a passive navigation system (one way signals from satellite to user) with a frequency standard stability (σ_y) of better than 10^{-12} at one day for the initial phase of the program and a stability of better than 10^{-13} at one day for the operational system. This paper describes the development and test of the miniature Rb gas cell atomic clock built by Rockwell International for the initial Navstar GPS satellites. This small clock provides the timing signal for the dual frequency PRN Navigation System. This 170 cubic inch atomic clock weighs 8.8 pounds and operates on 24.5 watts DC. This Frequency standard features two modes of operation (open loop and closed loop) with remote frequency adjust capability in either mode. The frequency standard utilizes two crystals and operates at a submultiple of the navigation system carrier frequencies, 10.23 MHz.

INTRODUCTION

The GPS satellites require frequency standards which are small, lightweight and ruggedized to meet launch requirements and are sufficiently reliable to meet 5 years of on-orbit service. Stability of the frequency standard must be such that precise timing is maintained between the periods of satellite update. The frequency standard to be utilized for the GPS concept validation phase (Phase I) is a Rockwell built Rubidium (Rb) device shown in Figure 1.

Rb Frequency Standard Development Program

The specific requirements placed upon each of the spaceborne frequency standards to ensure the performance of its portion of the NAVSTAR GPS function are given by Table 1 and Figures 2 and 3.

After conducting a survey of available frequency standards, it was decided to undertake a development program based upon a commercial Rb frequency standard produced by Efratom Inc. The Efratom model FRK Rubidium frequency standard was selected because its size, weight,

power and stability met the GPS criteria and it had previously flown on NRL's satellite, NTS I. After comparing this unit with the space-borne frequency standard requirements Rockwell International concluded that the following modifications and additions were required:

1. Substitute MIL parts for commercial parts.
2. Analyze and revise circuits for optimum performance.
3. Repackage to meet shock and vibration requirements.
4. Improve thermal design for vacuum operation.
5. Characterize the "C" field.
6. Shield for natural radiation.
7. Add 10.23 MHz synthesizer circuit with power amplifier.
8. Add digital tuning circuits for both C-field and varactor frequency adjustment capability.
9. Redesign power supply to accommodate the additional circuits.

In this paper we will review the miniaturization techniques utilized by Efratom in their Rb frequency standard and briefly look at the major additions incorporated by Rockwell. The major additions consist of the 10.23 MHz synthesizer, digital tuning and repackaging as shown by figure 4.

Rb Miniaturization Techniques

The first Efratom step towards a compact design of their commercial unit was the reduction in size of the optical package. This was accomplished by abandoning the optical filter and by combining the filter function with the resonance function in the Rubidium gas cell. This "integrated cell" design is achieved by using suitable isotope mixtures in the lamp as well as the gas cell. This also has the advantage of placing the lamp much closer to the cell and thus makes more efficient use of the lamp radiation.

The efficient application of the 6.83.....GHz magnetic field to the gas cell was also a variation from the classical approach. The cell is contained inside a microwave cavity which must be excited in a mode that possesses a magnetic field component along the optical axis. With conventional designs this requirement is satisfied by exciting the cavity in the TE 011 mode. Unfortunately this mode requires at 6.83.....GHz a minimum cavity diameter of about 2-3/4 inches and it is not possible to reduce this size substantially by using a dielectric

filling. Therefore this type of cavity is not suited for miniaturization, particularly since there is also a mismatch between its size and that of the much smaller gas cell.

To overcome this problem a new cylindrical cavity was developed which is excited in the TE 111 mode. Its diameter is only 1.1 inches, however, its length would have been excessive. To reduce the length, two adjustment screws have been inserted which project into the region of maximum electric field intensity inside the cavity. This results in an overall length of only 1.57 inches. The gas cell, which is fitted snug inside the cavity, is provided with two recessed funnels (see figure 5) to permit insertion of the adjustment screws. This design made it actually possible to increase the size of the gas cell and at the same time reduce the overall size of the resonance assembly.

The adjustment screws also serve the purpose of increasing the magnitude of the RF magnetic field component in the direction of the optical axis. Since in the TE 111 mode this component is strongest on the periphery of the cavity the photo detector has been increased in size to almost the diameter of the cavity to permit interception of the perimeter radiation. The photo cell is sandwiched between the cavity and the gas cell and thus covers the cell's entire face. This design has the added benefit of intercepting most of the available optical radiation.

10.23 MHz Frequency Translation Loop

Because the output of the Efratom frequency standard is at 10.0 MHz, there exists a need to convert the Rubidium loop frequency to the GPS requirement of 10.23 MHz. This function could be accomplished economically by direct digital synthesis but the existing commercial unit has marginal phase noise performance from 1 to 10 hertz from the carrier. Therefore a decision was made to incorporate a secondary loop which would serve the dual purpose of frequency translation and improvement of spectral purity. The strategy behind this secondary loop is to use a very pure oscillator in the secondary loop and then to set the loop bandwidth such that there is an attenuation of primary loop phase noise in the region above 0.1 Hertz from the carrier and then have the primary loop take over very close (0.1 Hertz) to the carrier.

The secondary VCXO consists of a crystal oscillator within a stainless steel Dewar flask. The temperature inside the flask is precisely controlled by two proportional ovens. The quartz crystal within the oscillator is a Premium 'Q' type which has excellent radiation resistance. The method used for phase locking the secondary loop consists of heterodyning the 10.0 MHz against the 10.23 MHz oscillator

output and then using the difference frequency as an error frequency input (see figure 6).

Table 2 is a tabulation of the pertinent performance characteristics of the secondary loop. The phase noise from the primary loop is attenuated by an order of magnitude at 1 Hertz with an additional order of magnitude at 10 Hertz. At approximately 25 Hertz a 3 pole filter increases the attenuation by 18 db/octave. This second filter attenuates the 20 KHz sidebands generated in the 230 KHz synthesizer.

Digital Tuning

The remote tuning technique is similar in concept to the tuning of the Efratom unit in the laboratory. This method increases or decreases the current to the resonator C-field. Also, in the event of Rb circuit failure, the 10.23 MHz VCXO can be operated independently of the Rb loop and the frequency can be remotely tuned by adjusting the VCXO control voltage. The frequency control requirements are as follows:

1. Provide a fixed current source to induce a magnetic field for an absolute frequency.

2. Provide a tunable current source to induce a controlled magnetic field change.

3. Provide a tunable voltage source to induce a controlled change in the output frequency of the 10.23 MHz VCXO when operating in the back-up mode (VCXO only).

The Rb frequency control consists of a fixed current source of approximately 7.5 ma which sets the frequency output near 10.23 MHz. This fixed current source is parallelled by a current source which is variable from 0 to 2.2 ma. The sum of these two sources determine the total C-field current and, thus, the output frequency. The tuner specification requires a total range of 4×10^{-9} with steps no larger than 4×10^{-12}. Data developed on typical Rb physics packages indicates that a one micro-ampere current change will result in a frequency change of 2 ± 0.4 parts in 10^{12}. If the 2.2 ma variable current is divisible into 4096 parts, we have a minimum current change of approximately 0.5 microamperes per step. This corresponds approximately to a minimum step change of one part in 10^{12} a total range of 4096 (1×10^{12}) or 4×10^{-8}. The VCXO tuner has a specified tuning range of 4×10^{-7} with steps no larger than 2.5×10^{-10}.

This tuning technique is implemented as shown by figure 7. A serial output from the command decoder (TTL output) is interfaced with the digital tuning system. The TTL word is translated to C-MOS levels and loaded into a serial to parallel register and then into a holding

register. The 12 bit D to A converter then provides a voltage output (0 to 10 volts) to bias the tunable current and voltage sources.

Repackaging

The major repackaging considerations included the magnetic and thermal effects of the frequency standard in the spacecraft environment.

Magnetic Shielding

To insure that the clock frequency is not affected by the expected one gauss change in magnetic field near the frequency standards three shields are utilized (figure 8). The resonator is first shielded from the electronics with a 0.050 inch thick mumental shield. The total physics package is then contained within a 0.030 thick mumetal shield. Finally, to shield the entire frequency standard from external fields it is covered by a 0.050 thick mumetal cover and a 0.030 thick mumetal base shield.

Thermal Control

To maintain the necessary temperature control of the clocks temperature sensitive components a total of six heaters are used. The 10.23 MHz crystal is temperature controlled within a double oven, whereas the 10 MHz crystal is kept near its turn-around point with a single heater. To generate the correct vapor pressure the Rb lamp is kept at approximately 109°C with a heater as shown by figure 9. Two heaters are also used to control the resonator assembly temperature. One heater is wrapped around the resonator assembly and is maintained at 75°C. This assembly is then contained within a copper oven which is controlled to 68°C.

Thermal Dissipation

Heat is transferred from the individual frequency standard components through the clock's aluminum frame and baseplate to the spacecraft structure. First, all heat sources were identified (heaters and electrical components); then, heat paths between the heat sources and base plate were identified. For those cases where the heat paths were not sufficient additional measures were taken to increase the capacity for heat flow as shown by figure 10. The techniques used to enhance the heat transfer were high conductivity bonding material between beryllium oxide insulators and circuit boards, thermal compound between mating surfaces (of the physics package, the 10.23 MHz oscillator, and the 10 MHz crystal interface). Also, torque requirements were established for the mounting screws used to secure the circuit boards. RTV was also added at the mounting edges of the circuit boards. And finally, the shield at the baseplate was bonded

with a thermally conductive adhesive. Although the operating temperature of the frequency standard is predicted to be from 20 to 35°C on orbit, a component temperature analysis was performed with the base plate at 45°C (worst case). This analysis demonstrated that components were operating well within their specified temperature range.

Development Testing

To verify design concepts and analysis, one prototype and three Engineering Models (EM) were built for purposes of being subjected to development tests. The major development test results are presented here.

Stability - One of the first tests conducted on the prototype unit was long term stability in a vacuum with the baseplate at 28.4°C. Stability of this unit, as shown in figure 11, was 3.4×10^{-13} at a tau of 10^5 seconds. This unit also displayed drift of 3.5 parts in 10^{13} per day. More recent stability data for EM2 was taken at ambient temperature and pressure conditions out to a tau of 3×10^4 seconds; a stability of 2×10^{-13} was demonstrated.

Phase noise - Two engineering units (EM1 & EM2) were tested for phase noise from 1 to 1000 Hertz from the carrier. Both units were at least 10 db better than specification requirements (see figure 12).

Power Demand - A test of power vs baseplate temperature was conducted on EM2 in a vacuum. The test was conducted at three voltage levels. As shown in figure 13, at the expected on-orbit temperature of 35°C and the nominal voltage of 26.5 VDC the power required for operation was 24.5 watts. For the worst case test at the coldest expected temperature of 20°C and a maximum voltage of 28 VDC the power demand was 28 watts.

Frequency change with Temperature - The EM1 test unit was placed in a vacuum and stabilized at 46°C. The temperature was then reduced to 24.6°C in less than 1-1/2 hours. After stabilization, the frequency change was measured to be 2 parts in 10^{12} as shown on figure 14.

Cold Start - To verify the ability of the unit to start after being subjected to low temperatures EM2 was stabilized at -30°C (10°C lower than worst case spececraft temperature). The unit then responded to the turn-on command and the power output was measured to be well within the 17 to 20 dbm specification requirement as shown by figure 15.

Magnetic Susceptibility - The EM2 test unit was placed in a magnetic field which was controlled with a helmholtz coil as shown in figure 16. After several unsuccessful attempts to determine frequency changes with a magnetic field change of less than one gauss the unit was subjected

to a 5 gauss change. The test resulted in a frequency change of less than 2×10^{-13} per gauss in the most sensitive axis (optical axis).

Shock and Vibration - In addition to the test data included here the units have successfully completed pyrotechnic shock and vibration tests. The vibration testing included a test at 0.35 g^2/Hz and 0.5 g^2/Hz. This latter level is far in excess of the levels expected during launch.

Future Tests - Presently, the units do not meet electromagnetic interference requirements. Therefore, modifications and testing will continue in this area. Also, a long term stability test is planned to be conducted with the unit in a vacuum and the baseplate temperature being cycles 4°C. This test will closely simulate the expected on-orbit conditions.

TABLE 1 - FREQUENCY STANDARD REQUIREMENTS

- PERFORMANCE

OUTPUT FREQUENCY	10,229,999.99545 Hz
PRIMARY MODE	DIGITAL TUNING CONTROL OF RUBIDIUM "C" FIELD 4×10^{-12} $\Delta f/f$ STEPS ($\pm 2 \times 10^{-9} \Delta f/f$ RANGE)
BACKUP MODE	DIGITAL TUNING CONTROL OF 10.23 MHz VCXO $2.5 \times 10^{-10} \Delta f/f$ STEPS ($\pm 2 \times 10^{-7} \Delta f/f$ RANGE)
DRIFT	$1 \times 10^{-12} \Delta f/f$/DAY
RF OUTPUT POWER	+17 dBM TO 20 dBM

- ENVIRONMENTAL

OPERATING TEMPERATURE RANGE	+20°C TO +45°C 4°C/DAY MAXIMUM EXCURSION 5°C/HOUR MAXIMUM RATE OF CHANGE
RANDOM VIBRATION	QUALIFICATION 0.35 G^2/Hz
PYROTECHNIC SHOCK	1400 G's MAXIMUM 10 kHz MAXIMUM
TRANSIENT MAGNETIC FIELD	ONE GAUSS, ONE SECOND

AD-A040 774 NATIONAL AERONAUTICS AND SPACE ADMINISTRATION GREENB--ETC F/G 14/2
PROCEEDINGS OF THE ANNUAL PRECISE TIME AND TIME INTERVAL (PTTI)--ETC(U)
DEC 75

UNCLASSIFIED NASA-GSFC-X-814-76-45 NL

8 OF 8
ADA040774



END

DATE
FILMED
7-77

TABLE 2 - 10.23 MHz SYNTHESIZER

WORST CASE	LOOP ANALYSIS
GAIN MARGIN	42 dB
ϕ MARGIN	58°
OPEN LOOP GAIN	86 dB
BANDWIDTH	0.1 Hz
SETTLING	11.2 SECONDS
DAMPING RATIO	0.62
STEADY STATE ERROR	$2.93 \times 10^{-12} \Delta f/f$
HOLD IN-PULL IN RANGE	$+2 \times 10^{-7} \Delta f/f$
MAXIMUM SWEEP LOCKRATE	1.02 RAD/SEC^2
LOCKIN RANGE	1.88 RAD/SEC^2
VCXO CONTROL NOISE REJ	24 dB/OCT AT > 25 Hz

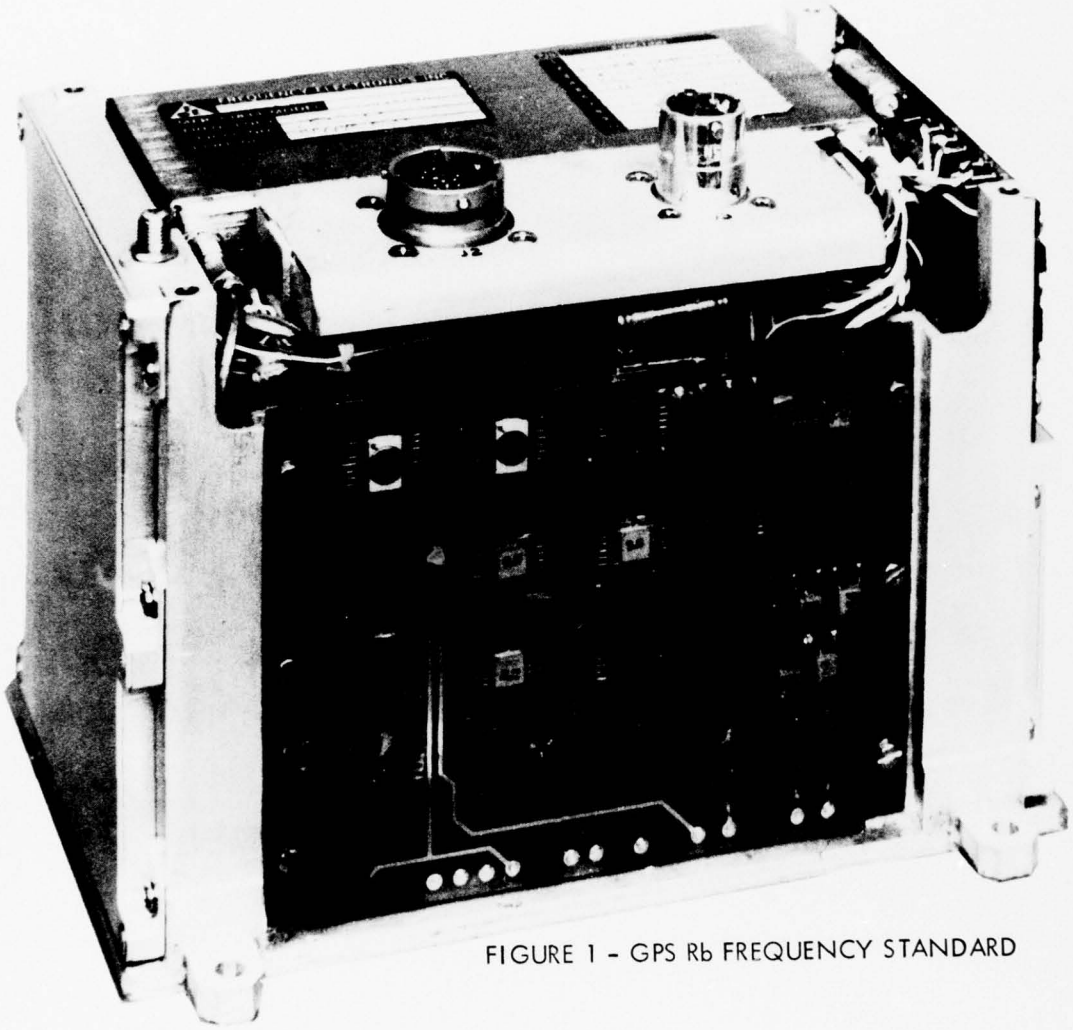


FIGURE 1 - GPS Rb FREQUENCY STANDARD

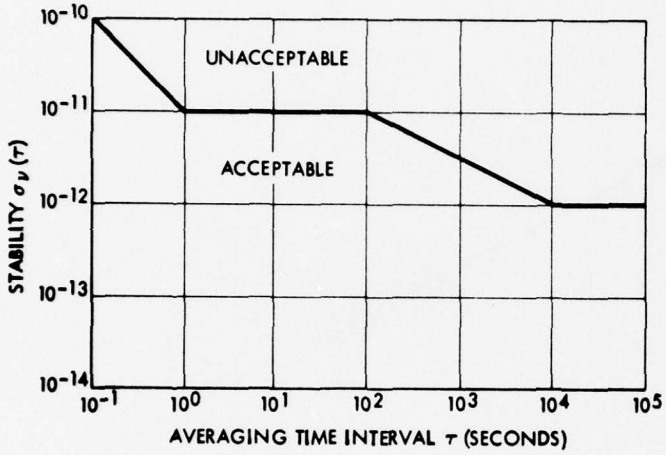


FIGURE 2 - STABILITY REQUIREMENTS

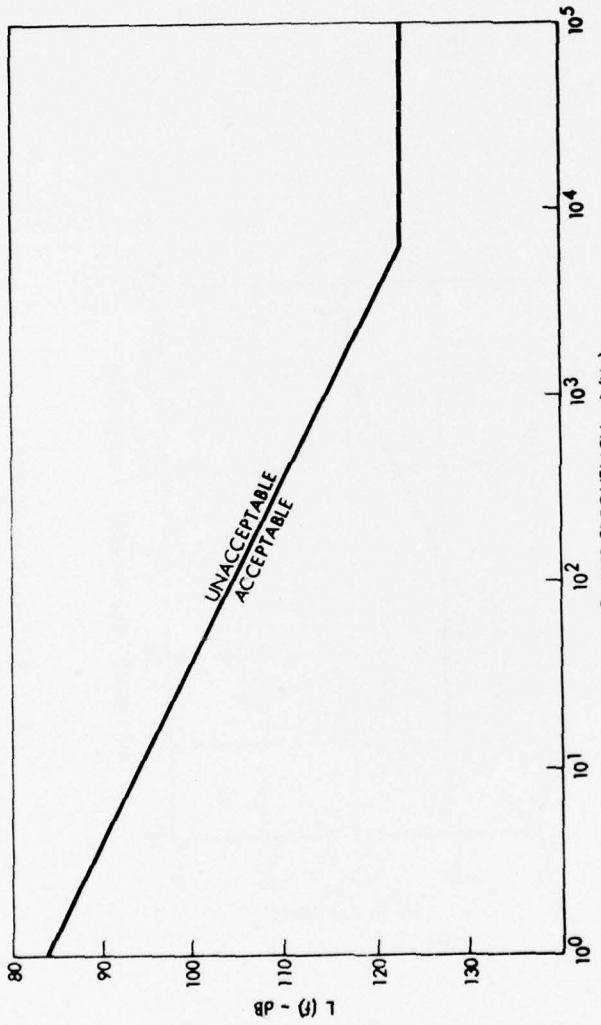


FIGURE 3 - PHASE NOISE REQUIREMENTS

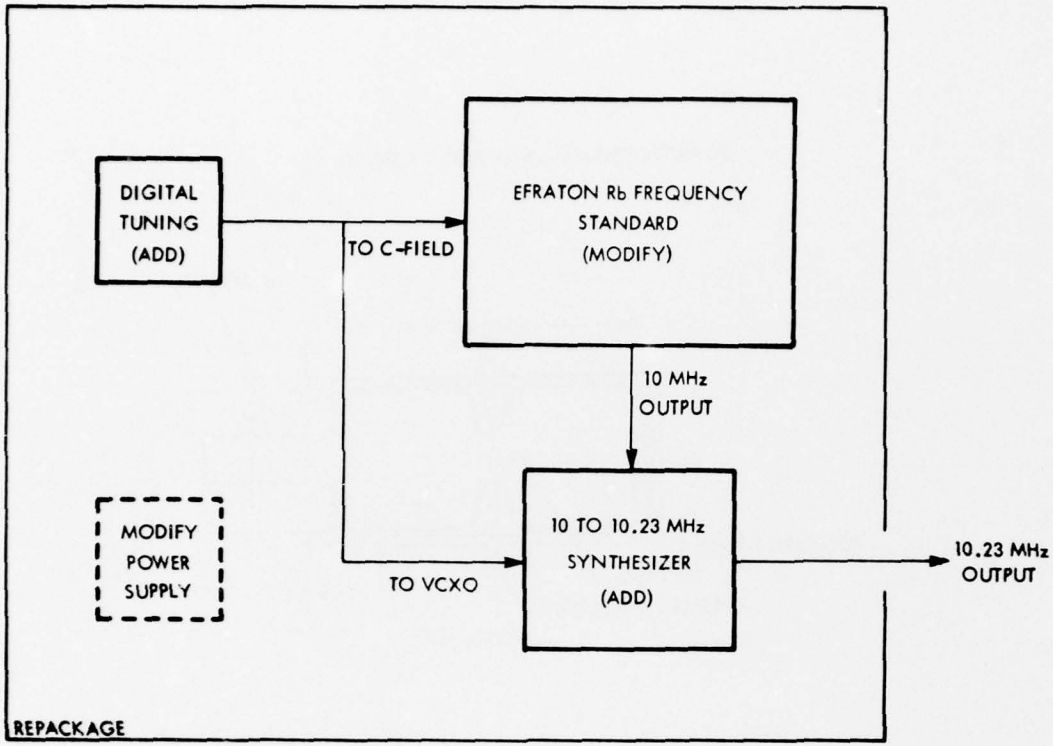


FIGURE 4 - GPS Rb CLOCK MODIFICATIONS AND ADDITIONS

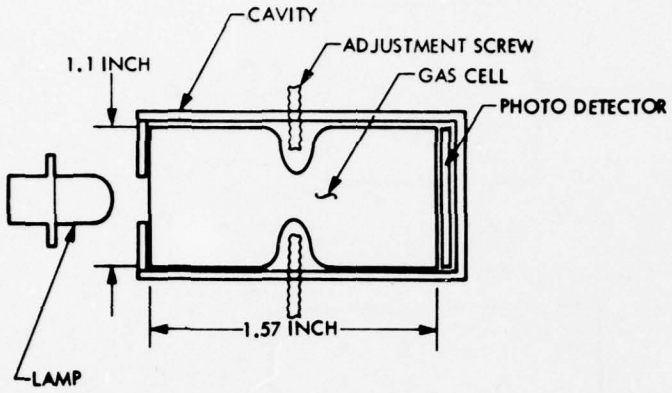


FIGURE 5 - MINIATURE PHYSICS PACKAGE

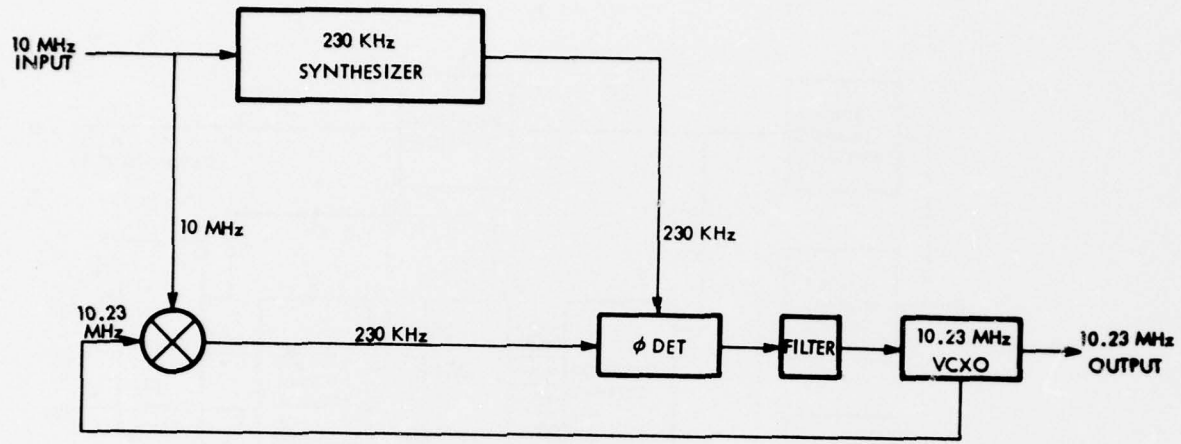


FIGURE 6 - 10.23 MHz SYNTHESIZER

DIGITAL TUNING BLOCK DIAGRAM

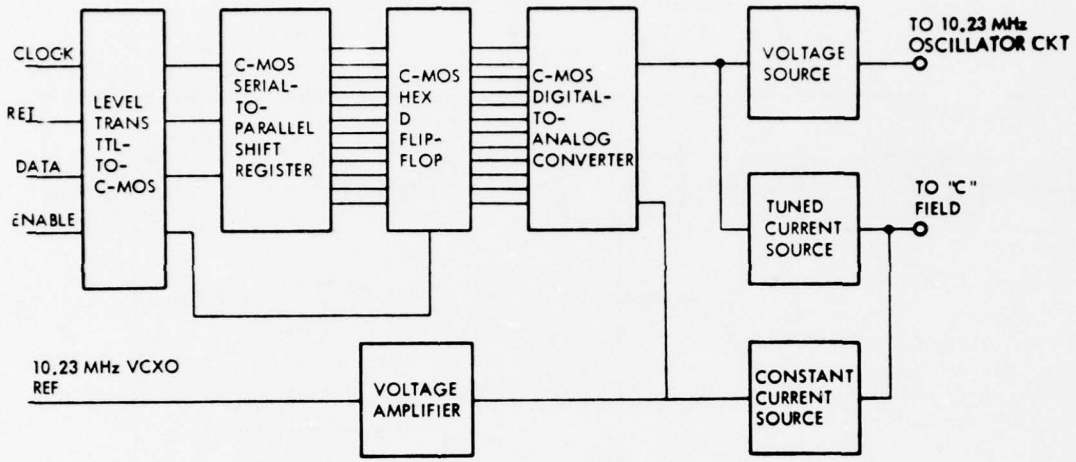


FIGURE 7 - DIGITAL TUNING BLOCK DIAGRAM

MAGNETIC SHIELDING (MUMETAL)

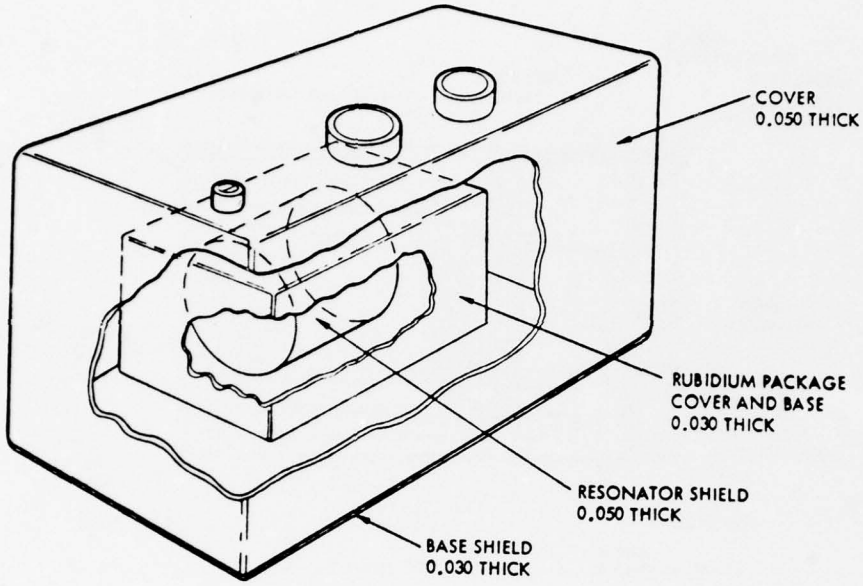


FIGURE 8 - MAGNETIC SHIELDING

RUBIDIUM PACKAGE CROSS SECTION

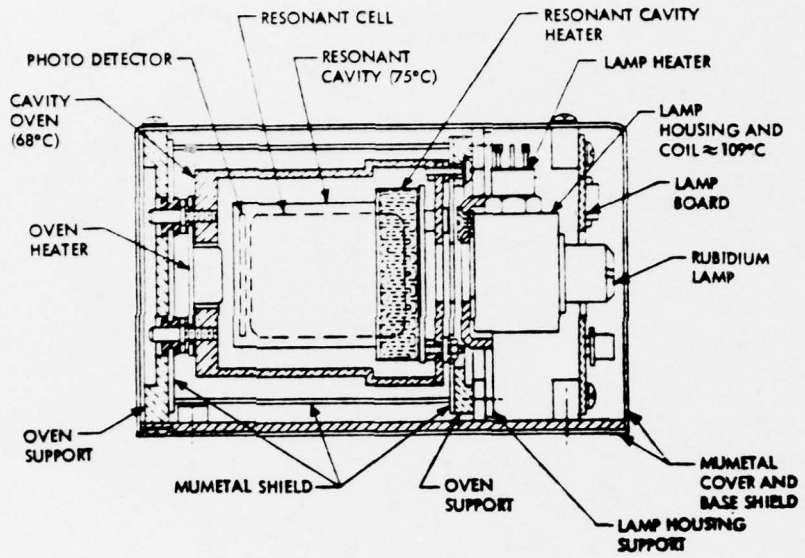


FIGURE 9 - Rb HEATERS

TYPICAL THERMAL FLOW

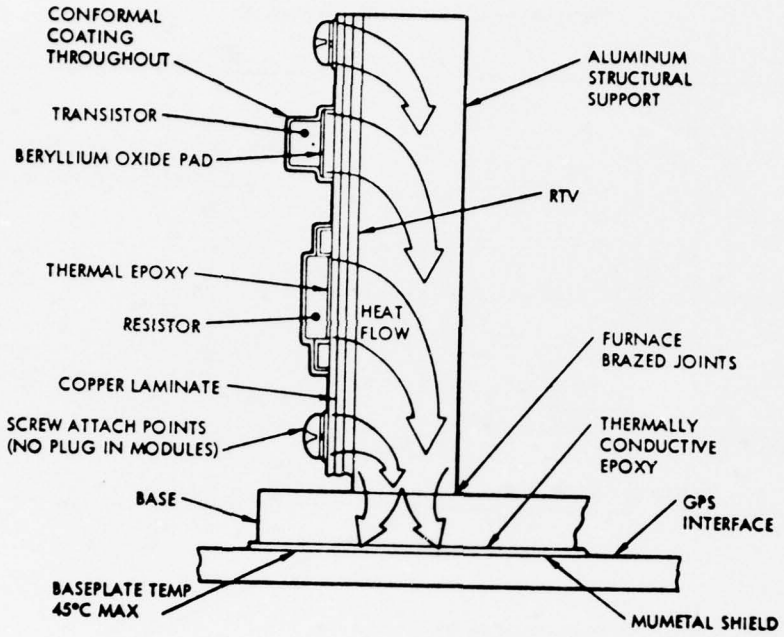


FIGURE 10 – THERMAL FLOW

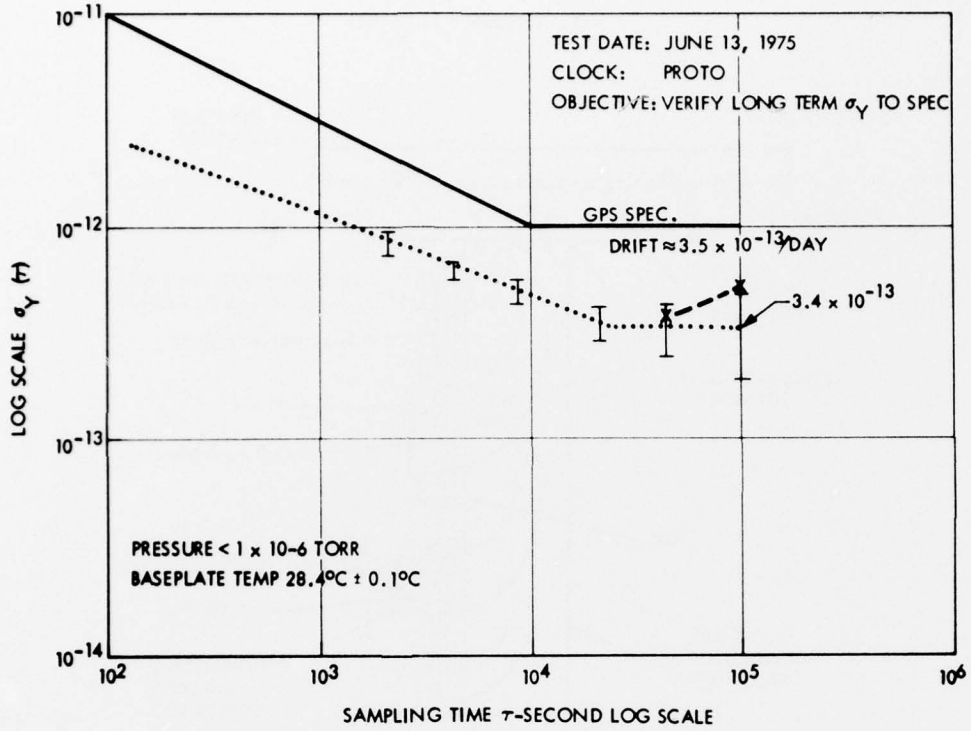


FIGURE 11 - LONG-TERM STABILITY DATA

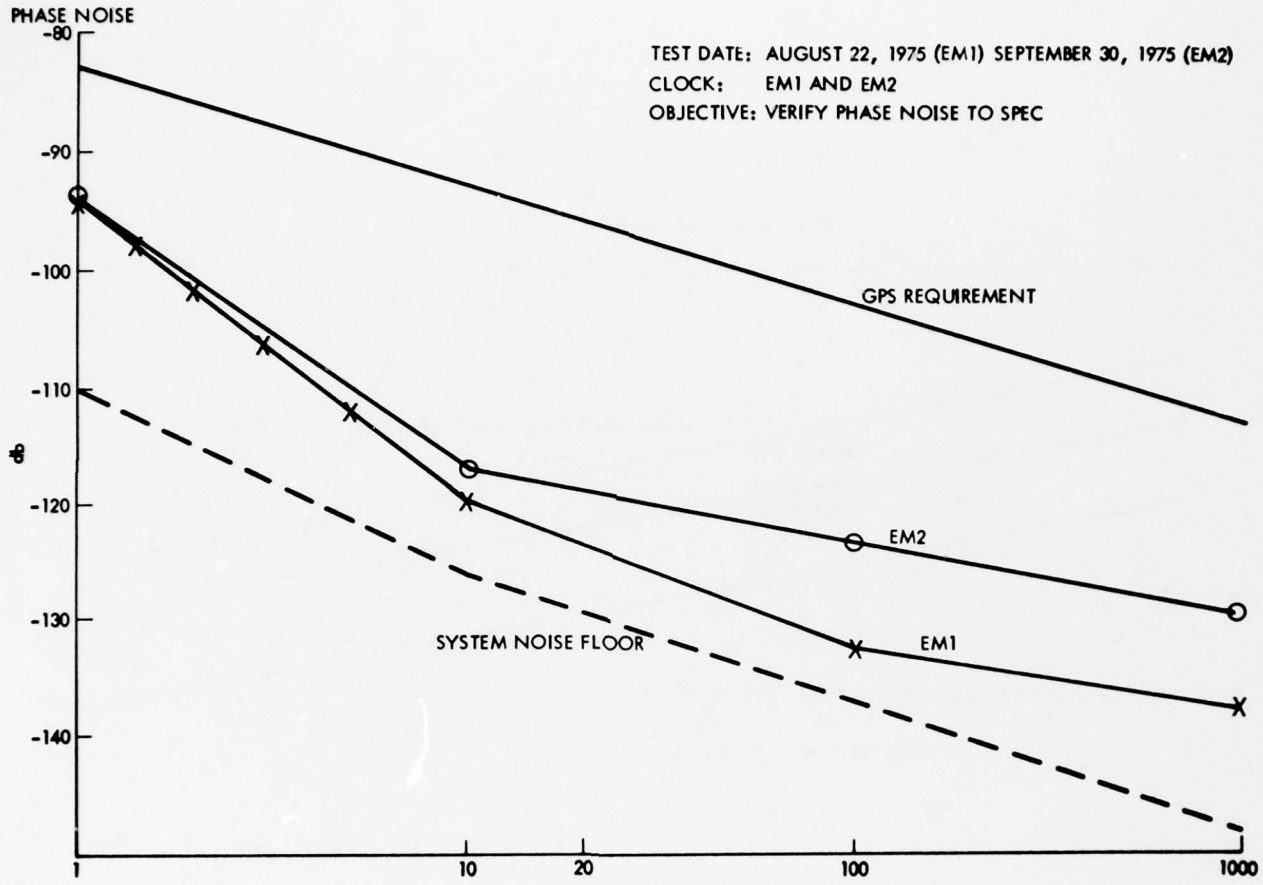


FIGURE 12 - PHASE NOISE DATA

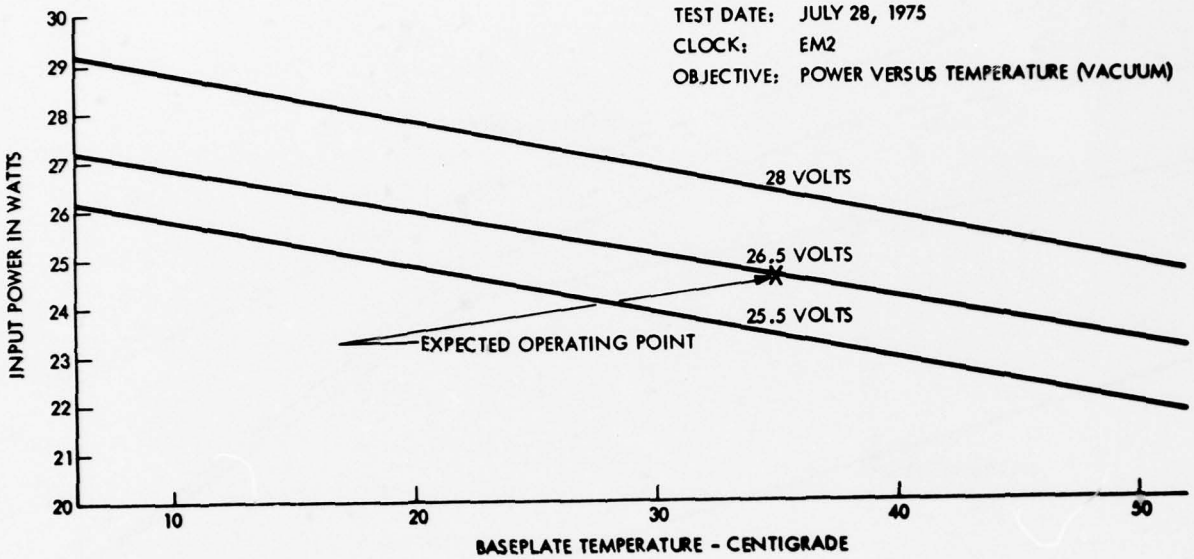


FIGURE 13 - POWER DEMAND DATA

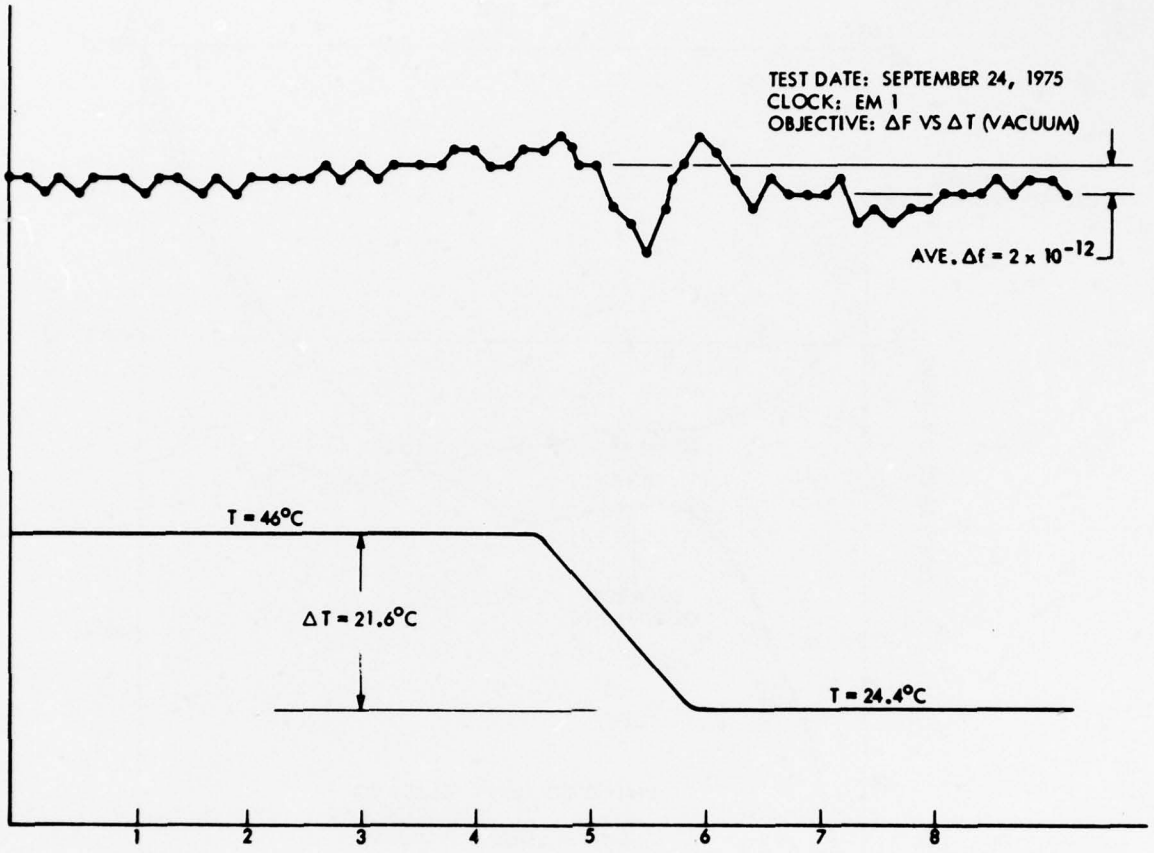


FIGURE 14 - ΔF VERSUS ΔT

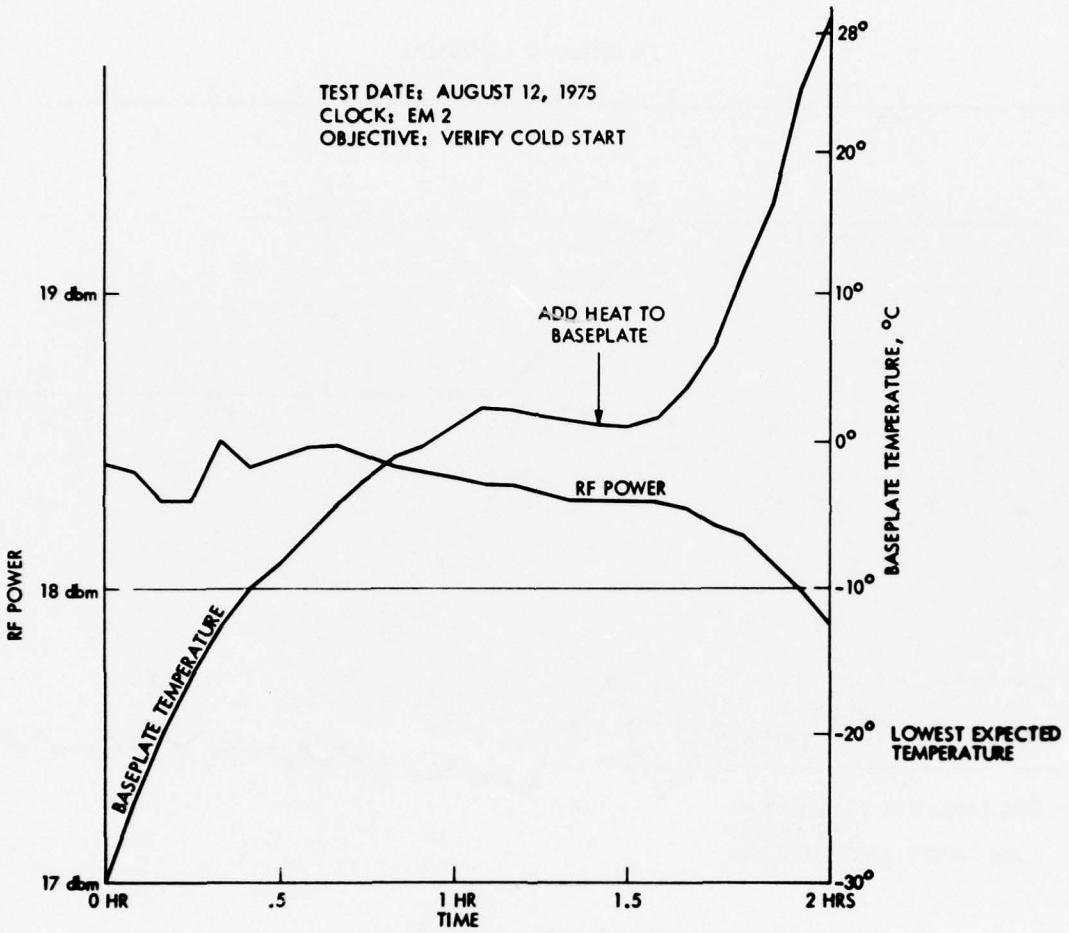


FIGURE 15 - COLD START DATA

- TEST CONFIGURATION
- OBJECTIVE
  - DETERMINE Δf VS ΔB
- TEST PARAMETER
  - $B = \pm 2.5$ GAUSS AT RFS
  - $\Delta B = 5$ GAUSS
- TEST RESULTS
  - $\Delta f/\Delta B = 2 \times 10^{-13}$/GAUSS IN MOST SENSITIVE AXIS

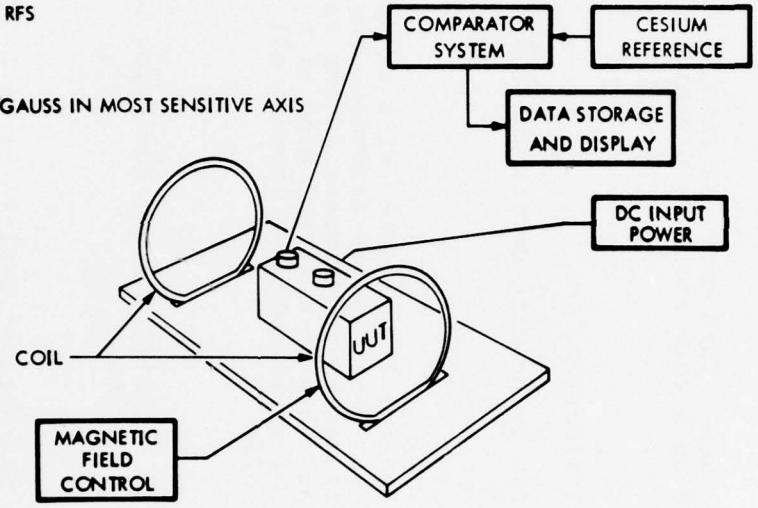


FIGURE 16 - ΔF VERSUS ΔB TEST

QUESTION AND ANSWER PERIOD

MR. RUEGER:

Thank you very much. This shows an example of a very fine engineering job on a very simplified rubidium type standard.

MR. McDADE:

McDade, General Electric.

Were you required to operate during the shock and vibration tests?

MR. RINGER:

We only monitored for the presence of a signal and we monitored current input only to determine any catastrophic failures. There was no requirement during either the shock or the vibration tests to meet any kind of a frequency stability, and of course when we launch, all the clocks will be turned off.

SPEAKER:

On your frequency stability plot, could you tell me what you measured it against?

MR. RINGER:

This plot here was against Hewlett-Packard 5061 cesium. Since then we have purchased 5061, with a high performance capability and all of our further tests will be done with the high performance unit.

MR. RUEGER:

This looked a little bit more noisy than what you normally expect from a rubidium standard. Do you feel that was mostly the reference you were measuring against?

MR. RINGER:

Later data shows that we get down to our flicker floor much quicker using the 004 standard, so I think this long-term stability data here, as much as anything, was a measure of the HP cesium.

APPENDIX

LIST OF ATTENDEES AND REGISTRANTS

7th PTTI PLANNING MEETING

Goddard Space Flight Center

December 2-4, 1975

LIST OF ATTENDEES AND REGISTRANTS

Allan, David W.
Department of Commerce
National Bureau of Standards
325 Broadway, Room 2035
Boulder, Colorado 80302

Allen, Ralph T.
U.S. Navy
Naval Electronic Systems Command
Washington, D. C. 20360

Alpert, Arnold
Newark AFS
Newark, Ohio 43055

Andren, Carl S.
Navigation Systems Inc.
8841-43 Monard Drive
Silver Spring, Maryland 20910

Babitch, Daniel
Hewlett Packard
5301 Stevens Creek Boulevard
Santa Clara, California 95050

Bahar, Ezekiel
University of Nebraska
Electrical Engineering Department
Nebraska Hall W194
Lincoln, Nebraska 68508

Barnaba, James F.
U.S.A.F.
Newark AFS, Ohio 43055

Barszczewski, Andrew
National Research Council
N.A.E.
Ottawa, Canada

Bartholomew, C. A.
Naval Research Laboratory
Code 7962
Washington, D. C. 20375

Beard, R. L.
Naval Research Laboratory
4555 Overcook Avenue, S. E.
Washington, D. C. 23075

Beaty, James S.
FAA/NAFEC
ANA-140
Atlantic City, New Jersey 08405

Beehler, Roger E.
National Bureau of Standards
Section 277.06
Boulder, Colorado 80302

Benavente, Jose
Spanish Naval Observatory
Observatorio De Marina
San Fernando, Cadiz, Spain

Bertino, William L.
U.S.A.F.
4024-3 Ashwood Circle
Andrews AFB, Maryland 20035

Bloch, Martin B.
F.E.I.
3 Delaware Drive
New Hyde Park, New York 11040

Bowerman, Jack C.
NAVELEX
11804 Mentone Road
Wheaton, Maryland 20906

PRECEDING PAGE BLANK-NOT FILMED

Bowman, John A.
Naval Research Laboratory
Code 5424
Washington, D. C. 20375

Braff, Ronald
The Mitre Corporation
1820 Dolley Madison
McLean, Virginia 22101

Britney, O. L.
Canadian Defence Staff
2450 Massachusetts Avenue, N. W.
Washington, D. C. 20008

Bruhl, Keith R.
Beukers Labs/Washington
3110 Faber Drive
Falls Church, Virginia 22044

Buisson, James
U.S. Naval Research Laboratory
7714 Martel Place
Springfield, Virginia 22152

Burpee, Lee E.
Arbiter Systems Inc.
1402 Norman Firestone
Goleta, California 93017

Burridge, Malcolm, R.
Australian Department of Defence
Embassy of Australia
1601 Massachusetts Avenue
Washington, D. C. 20036

Byron, Ernest
Johns Hopkins/APL
1100 Johns Hopkins Road
Laurel, Maryland 20810

Canfield, Roger A.
Army Metr. & Cal. Center
Building 5435
Redstone Arsenel, Alabama 35809

Casey, Clifford F.
Computer Sciences Corporation
6565 Arlington Boulevard
Falls Church, Virginia 22046

Casselman, Fred L.
GTE Sylvania
189 B Street
Needham, Massachusetts 02194

Cauffman, James A.
Naval Electronic Systems Command
Washington, D. C. 20360

Chapman, William H.
U.S. Geological Survey
3802 Howard Street
Annandale, Virginia 22003

Chi, Andrew R.
NASA-GSFC
Code 810
Greenbelt, Maryland 20771

Chronister, Richard D.
AF Weapons Laboratory
Kirtland AFB, New Mexico 87118

Clarke, Randolph T.
Naval Observatory
Washington, D. C. 20390

Coates, Robert J.
Goddard Space Flight Center
Code 900
Greenbelt, Maryland 20771

Cole, Bella
Goddard Space Flight Center
Code 582.3
Route 1, Box 8722, Belle
Indianhead, Maryland 20640

Collie, Jimmie B.
NAVELEX
6341 Route 29
Columbia, Maryland 21046

Comstock, Robert H.
C. S. Draper Laboratory
224 Albany Street
Cambridge, Massachusetts 02139

Costain, Dr. C. C.
National Research Council
Ottawa, Canada

Cox, Dr. Duncan B., Jr.
C. S. Draper Laboratory
MS 92, 224 Albany Street
Cambridge, Massachusetts 02139

Damerow, R. A.
Sandia Laboratories
Albuquerque, New Mexico 87115

Dennison, Bearl F.
Hughes Aircraft Company
6926 S. Spruce Drive W.
Englewood, Colorado 80110

Dermanis, Athanasios
Department of Geodetic Science, OSU
1958 Neil Avenue #404
Columbus, Ohio 43210

Doepke, Lawrence B. A.
DMA Aerospace Center
St. Louis AFS, Missouri 63118

Donaldson, R. W.
Westinghouse
P. O. Box 1897, MS 935
Baltimore, Maryland 21203

Doran, Pete Mac
Jet Propulsion Laboratory
4800 Oak Grove Drive
Pasadena, California 91103

Doubt, Randolph J.
DMA - HC
Code NVEZ
Elect. Nav. Div.
Washington, D. C. 20390

Dwyer, Robert E.
Computer Sciences
6565 Arlington Boulevard
Falls Church, Virginia 22046

Easton, Roger L.
Naval Research Laboratory
Code 7960
Washington, D. C. 20375

Emmons, Donald A.
Frequency & Time Systems Inc.
182 Conant Street
Danvers, Massachusetts 01923

Enck, William
Sperry Systems Management
Great Neck, New York 11020

Enstrom, Roger D.
U.S. Coast Guard
CCGD14, 677 Ala Moana
Honolulu, Hawaii 96813

Fehlner, Leo
Applied Physics Laboratory
Johns Hopkins Road
Laurel, Maryland 20810

Fisher, Laura
U.S. Naval Observatory
34th & Massachusetts Ave., N. W.
Washington, D. C. 20390

Flanagan, Terry
IRT Corporation
P. O. Box 80817
San Diego, California 92138

Fosque, Hugh S.
NASA Headquarters Code TS
600 Independence Ave., S. W.
Washington, D. C. 20003

Frensch, Theo
Hewlett-Packard
5301 Stevens Creek
Santa Clara, California 95050

Friend, Charles W.
AFAL DHM
Wright-Patterson AFB, Ohio 45433

Fullerton, Les
U.S. Coast Guard
Washington Radio Station
7323 Telegraph Road
Alexandria, Virginia 22320

Gagnepain, Jean Jacques
Ecole Nationale Superieure de
Chronometrie
La Bouloie, Route de Gray
25030 Besancon
Cedex, France

Galitzen, Mike J.
Jet Propulsion Laboratory
4800 Oakgrove Avenue
Pasadena, California 91103

Gardner, L. M.
Sperry Systems Management
Great Neck, New York 11020

Gilchrist, M. R.
JMR Institute
1210 Villamay Boulevard
Alexandria, Virginia 22309

Gillett, George R.
U.S. Coast Guard
7323 Telegraph Road
Alexandria, Virginia 22310

Girnius, A.
Smithsonian Astrophysical Observatory
60 Garden Street, P-349
Cambridge, Massachusetts 02138

Goldberg. Edwin A.
RCA Corporation
P. O. Box OX800
Princeton, New Jersey 08540

Goldman, Simon
11622 Sourwood Lane
Reston, Virginia 22091

Greck, John A. De
National Security Agency
Ft. Meade, Maryland 20755

Hacker, Henry
Magnavox
2131 S. Coliseum Boulevard
Fort Wayne, Indiana 46804

Hall, R. Glenn
U.S. Naval Observatory
Washington, D. C. 20390

Hanson, Wayne
National Bureau of Standards
325 South Broadway
Boulder, Colorado 80302

Hayes, N. J.
TRW Systems Group
One Space Park
Redondo Beach, California 90278

Heinz, Badura
Efratom California Inc.
3303 Harbor Boulevard
Costa Mesa, California 92626

Hellwig, Helmut
Department of Commerce, National Bureau of Standards
325 Broadway
Room 2035
Boulder, Colorado 80302

Henriksen, Soren W.
NOAA/NOS
2863 Beechwood Circle
Arlington, Virginia 22207

Herman, Bruce
NSWC
Astronautics DK-11
Dahlgren, Virginia 22448

Hyatt, Ron
Hewlett-Packard Company
5301 Stevens Creek
Santa Clara, California 95050

Hynson, Richard W.
Bendix Field Engineering
Columbia, Maryland 21043

Ilyn, Vladimir
Gosstandart U. S. S. R.
9 Leninsky Avenue
Moscow, U. S. S. R.

Imbier, Edward
SAO
60 Garden Street
Cambridge, Massachusetts 02138

Inouye, Tadao
National Research Laboratory of Metrology
10-4 Kaga-1, Itabashi
Tokyo, Japan

Jechart, Ernst
Efratom California Inc.
3303 Harbor Boulevard
Costa Mesa, California 92626

Joglekar, Dr. Anil
The Mitre Corporation
1820 Dolley Madison
McLean, Virginia 22101

Johnson, Andrew C.
Naval Observatory
3400 Massachusetts Avenue, N. W.
Washington, D. C. 20390

Jones, A. Edward
Navigation Systems, Inc.
8841 Monard Drive
Silver Spring, Maryland 20910

Jones Leon
Navigation Systems Inc.
8841 Monard Drive
Silver Spring, Maryland 20910

Kartaschoff, Peter
SWIS PTT R&D Division
Centre Technique
CH3000 Bern 29
Switzerland

Kaufmann, Donald C.
Goddard Space Flight Center
NASA
Code 814
Greenbelt, Maryland 20771

Kern, Robert H.
Frequency & Time Systems, Inc.
182 Conant Street
Danvers, Massachusetts 01923

Kies, LCdr. Phillip J.
U.S. Coast Guard
Loran Station
Box L
Carolina Beach, North Carolina 28428

Kittler, Capt. Dittmar
SAMSO/YEEK
P. O. Box 92960
Worldways Postal Center
Los Angeles, California 90009

Klepczynski, W. J.
U.S. Naval Observatory
Washington, D. C. 20390

Kodama, Archer, F.
Control Data Corporation
901 S. Highland Street
Arlington, Virginia 22204

Kovacs, Robert M.
Kentron Hawaii Ltd.
Box 1207
APO San Francisco, California 96555

Kriegsman, Bernard A.
C. S. Draper Laboratory
75 Cambridge Parkway
Cambridge, Massachusetts 02173

Krutenat, Robert A.
Naval Torpedo Station
Keyport, Washington 98345

Kudell, Philip D.
Defense Mapping Agency
12310 Glen Mill Road
Potomac, Maryland 20854

Lance, A. L.
TRW Systems Group
One Space Park
Redondo Beach, California 90278

Lanham, Noel
SAO
60 Garden Street
Cambridge, Massachusetts 02138

Lanphear, J. L.
General Radio Company
P. O. Box 842
Gaithersburg, Maryland 20760

Lavanceau, Jean-Damiel
U.S. Naval Observatory
Massachusetts Avenue & 34th Street, N. W.
Washington, D. C. 20390

Lawrence, Robert E.
Vitro Laboratories
14000 Georgia Avenue
Silver Spring, Maryland 20910

Lawson, Jim
University of Oklahoma
Earth Sciences Observatory
P. O. Box 5
Leonard, Oklahoma 74043

Leeb, Len
Hewlett-Packard Company
5301 Stevens Creek
Santa Clara, California 95050

Lester, Vestal R.
Hughes Aircraft Company
19631 Strathern Street
Reseda, California 91335

Lieberman, Theodore
NAVELEX
5001 Treetop Lane
Alexandria, Virginia 22310

Lipschultz, Lionel
Johns Hopkins/APL
Johns Hopkins Road
Laurel, Maryland 20810

Luck, John M.
Division National Mapping, Aust.
589 Stinchcomb Drive #4
Columbus, Ohio 43202

Lukac, Carl F.
Time Service Division
U.S. Naval Observatory
Washington, D. C. 20390

Luzier, Harmon
Audichron Company
3620 Clearview Parkway
Atlanta, Georgia 30340

Lynch, Donald W.
Naval Research, Laboratory
Washington, D. C. 20375

Lyons, Lloyd F.
Frequency & Time Systems, Inc.
182 Conant Street
Danvers, Massachusetts 01923

McCarty, Thomas A.
Johns Hopkins/APL
Laurel, Maryland 20810

McCaskill, Thomas B.
U.S. Naval Research Laboratory
Code 7965
Washington, D. C. 20375

McCormick, Ben F.
Naval Avionics
6100 - 21st Street
Indianapolis, Indiana 46218

McCreary, Terrence J.
Vitro Laboratories
14000 Georgia Avenue
Silver Spring, Maryland 20910

McDade, James C.
General Electric
French Road
Utica, New York 13503

McKenna, John J.
Goddard Space Flight Center
12604 Cedarbrook Lane
Laurel, Maryland 20811

Mattison, Edward
Smithsonian Institution
60 Garden Street
Cambridge, Massachusetts 02138

Mawson, R. R.
E M A Inc.
11501 Huff Court
Kensington, Maryland 20795

Mealy, Gregory L.
Analytic Sciences Corporation
6 Jacob Way
Reading, Massachusetts 01867

Medvedev, P.
U. S. S. R. Embassy
1125 - 16th Street, N. W.
Washington, D. C. 20036

Merrion, Arthur B.
DMA Hydro Center
Suitland, Maryland 20390

Melbourne, W. G.
Jet Propulsion Laboratory
4800 Oak Grove Avenue
Pasadena, California 91103

Merritts, Robert S.
WATC Patuxent River
Box 305 NAS
Patuxent River, Maryland 20670

Miller, H. Gilbert
The Mitre Corporation
1820 Dolley Madison
McLean, Virginia 22101

Miller, Richard B.
Jet Propulsion Laboratory
4800 Oak Grove Avenue
Pasadena, California 91103

Milne, C. R.
British Embassy
3100 Massachusetts Avenue, N. W.
Washington, D. C. 20008

Mitchell, Don
Kentron Hawaii Ltd.
Box 1207
APO San Francisco, California 96555

Monger, Don R.
U.S. Naval Observatory
P. O. Box 757
Perrine, Florida 33157

Moore, Robert
FAA NAFEC
Atlantic City, New Jersey 08405

Moore, Robert B.
Naval Research Laboratory
Code 7962
Washington, D. C. 22375

Mueller, Ivan I.
Department of Geodetic Science
Ohio State University
Columbus, Ohio 43210

Murray, James A., Jr.
Naval Research Laboratory
Code 5461
Washington, D. C. 20375

Nesmith, Willie R.
Bendix Kokee Kauai
Box 538
Kauai, Hawaii 96796

Nichols, Stephen
Naval Research Laboratory
Code 7962
Washington, D. C. 20375

Noël, Fernando
Universidad De Chile
Casilla 36D
Santiago De Chile

Nugent, Michael J.
National Security Agency
Fort George G. Meade, Maryland 20755

Olson, Trevor
Naval Observatory
Time Service Division
Washington, D. C. 20390

Ostrowski, Joseph J.
USAF PTF
Newark AFS
Newark, New Jersey 43055

Parker, H. C.
RCA
8501 Greenbelt Road
Greenbelt, Maryland 20770

Percival, D.
Naval Observatory
34th & Massachusetts Avenue, N. W.
Washington, D. C. 20390

Perfetto, Henry A.
Booz Allen Research
4733 Bethesda Avenue
Bethesda, Maryland 20014

Peters, Harry E.
Consultant
Box 607
Seabrook, Maryland 20801

Petrey, H. E.
DMA Topographic Center
Apt. 394
2600 S. 13th Road
Arlington, Virginia 22204

Phillips, David H.
Naval Research Laboratory
Code 5424C
Washington, D. C. 20375

Phillips, Ruth E.
Naval Research Laboratory
Code 5424C
Washington, D. C. 20375

Piasecki, Stanley
Navigation Systems Inc.
8841-43 Monard Drive
Silver Spring, Maryland 20910

Pitsenberger, John W.
Strategic Systems Project Office
Department of Navy
Washington, D. C. 20376

Potts, LCdr. C. E.
U. S. C. G. Activities Europe
Box 50
FPO New York 09510

Pritt, Dewey L.
Naval Research Laboratory
4555 Overlook Avenue
Washington, D. C. 20375

Puckett, Eric L.
NAVSEC Mechanicsburg Division
Mechanicsburg, Pennsylvania 17055

Putkovich, Kenneth
USNO
34th & Massachusetts Avenue, N. W.
Washington, D. C. 20390

Raines, Marilyn
U.S. Naval Observatory
34th & Massachusetts Avenue, N. W.
Washington, D. C. 20390

Rait, Howard
NAVELEX Englenwash
Navy Yard
Washington, D. C. 20374

Ramon, Eduardo
Observatorio Naval
Buenos Aires, Argentina

Ransom, James R.
Computer Sciences
6565 Arlington Boulevard
Falls Church, Virginia 22046

Reder, Fritz H.
Army Electronics Command
AMSEL-NL-RH
Ft. Monmouth, New Jersey 07740

Reinhardt, Victor
NASA/Goddard Space Flight Center
Code 814
Greenbelt, Maryland 20771

Repass, Donald J.
Naval Avionics
6100 E. 21st Street
Indianapolis, Indiana 46218

Ringer, Dale E.
Rockwell International
2214 Lakewood
Downey, California 90240

Roll, Ronald G.
Johns Hopkins/APL
Johns Hopkins Road
Laurel, Maryland 20810

Rueger, Lauren J.
Johns Hopkins/APL
Johns Hopkins Road
Laurel, Maryland 20810

Sakran, F. C.
Code AT41
U.S. Naval Air Test Center
Navigation
Patuxent River, Maryland 20670

Sazhin, Vladislav V.
Gosstandant, U. S. S. R.
9 Leninsky Avenue
Moscow, U. S. S. R. 147049

Scavullo, Joseph J.
FAA ANA-3310
NAFEC Building 301
Atlantic City, New Jersey 08406

Schmid, J. G.
USAF AFSC Samtec
ROKSE
Vandenberg AFB, California 93437

Schmid, Paul E.
NASA/Goddard Space Flight Center
8703 Westwood Drive
Vienna, Virginia 22180

Seher, Chris C.
FAA/NAFEC
Building 201, ANA 511
Atlantic City, New Jersey 08405

Shapiro, Irwin I.
MIT
Room 54-622
Cambridge, Massachusetts 02139

Shepard, Leonard F.
ILC Industries Inc.
856 Schoolhouse Lane
Dover, Delaware 19901

Sims, Ted
NSWC
Astronautics
Code DK11
Dahlgren, Virginia 22448

Skujins, Romans
Defense Command Agency
1860 Wiehle Avenue
Reston, Virginia 22090

Sleeper, Capt. S. J. USN
Naval Observatory
Washington, D. C. 20390

Smith, Arthur E.
U.S. Government
Pacific Missile Test Center
Point Mugu, California 93042

Smith, Humphry
Royal Greenwich Observatory
Herstmonceux Castle
Hailsham, Sussex, England

Souza, Victorio De
Naval Observatorio
Buenos Aires, Argentina

Speight, John J.
Defense Mapping Agency
3413 Valley Drive
Alexandria, Virginia 22302

Spellman, Marc I.
Harris Electronic Systems
Melbourne, Florida

Stonestreet, William
Draper Laboratory
224 Albany Street
Cambridge, Massachusetts 02139

Stover, Dr. Harris A.
DCA/DCEC
1860 Wiehle Avenue
Reston, Virginia 22090

Strain, John
REI
651 Lofstrand Lane
Rockville, Maryland 20850

Strand, K. A.
Naval Observatory
Washington, D. C. 20390

Strucker, Peter P.
Metrology Engineering Center
1675 W. Mission Boulevard
Pomona, California 91766

Taylor, E. A.
NOAA
4815 Eades Street
Rockville, Maryland 20853

Tewksbury, David L.
Smithsonian Institution
Astrophysics Observatory
60 Garden Street
Cambridge, Massachusetts 02138

Tomlin, James W.
Hughes Aircraft
503 Nile Street
Aurora, Colorado 80010

Toms, Jimmie L.
T. E. Corporation
701 E. Gude Drive
Rockville, Maryland 20850

Tymczyszyn, William R.
Global Navigation
24701 Crenshaw Boulevard
Torrance, California 90254

Vessot, Robert F. C.
Smithsonian Observatory
60 Garden Street
Cambridge, Massachusetts 02138

Vetter, J. R.
Johns Hopkins/APL
Johns Hopkins Road
Laurel, Maryland 20810

Wang, Harry T. M.
Hughes Research Laboratories
3011 Malibu Cynwood Road
Malibu, California 90265

Ward, Samuel C.
NASA
Jet Propulsion Laboratory
4800 Oak Grove Drive
Pasadena, California 91103

Wardrip, S. Clark
Goddard Space Flight Center
Code 814
Greenbelt, Maryland 20771

Wasserman, R., Pres.
Datametrics, Inc.
340 Fordham Road
Wilmington, Massachusetts 01887

Wheeler, Paul J.
USNO
Washington, D. C.

White, Joe
Naval Research Laboratory
4555 Overlook Avenue
Washington, D. C. 20375

Wilcox, Dwight L.
Wiltronix, Inc.
5504 Waterway
Rockville, Maryland 20853

Wiley, Randall E.
Navelel Syscom
9517 Vandola Court
Burke, Virginia 22015

Williams, Lindsey, W.
Quest Research Corporation
6845 Elm Street, Suite 407
McLean, Virginia 22101

Wilson, John
Naval Electronics Laboratory Center
Code 2400
San Diego, California 92152

Winkler, Gernot M. R.
Naval Observatory
Washington, D. C. 20390

Wright, C. R.
Federal Aviation Administration
Atlantic City, New Jersey 08405

Youskites, Ed
Beta Technology Inc.
94 Verdi Street
Farmingdale, New York 11735

Zemlin, Gerald D.
ITT Avionics Division
500 Washington Avenue
Nutley, New Jersey 07110

Zorzy, Plato
Timing Systems Inc.
P. O. Box 384
Marblehead, Massachusetts 01945

Schlueter, Bernard & Wavre, Andre
Oscillo Quartz
c/o Wosic
600 Fifth Avenue
New York, New York 10020